ACTA UNIVERSITATIS SZEGEDIENSIS

ACTA PHYSICA ET CHEMICA

NOVA SERIES

TOMUS XXXI FASCICULI 1—2

AUSHAF 31 (1—2) (1985)

HU ISSN 0324—6523 Acta Univ. Szeged
HU ISSN 0001—6721 Acta Phys. et Chem.

SZEGED, HUNGARIA
1985

Adiuvantibus

M. BARTÓK, M. BÁN, K. BURGER, L. CSÁNYI, J. CSÁSZÁR, P. FEJES, P. HUHN, E. KAPUY, I. KETSKEMÉTY, F. SOLYMOSI, L. SZALAY et F. SZÁNTÓ

Redigit

PÁL FEJES

Edit

Facultas Scientiarum Universitatis Szegediensis de Attila József nominate

Editionem curant

J. ANDOR, I. BÁRDI, Á MOLNÁR, K. SZATMÁRY et Á. SÜLI

Nota

Acta Phys. et Chem. Szeged

Szerkeszti

FEJES PÁL

A szerkesztő bizottság tagjai:

BARTÓK M., BÁN M., BURGER K., CSÁNYI L., CSÁSZÁR J.,FEJES P., HUHN P., KAPUY E., KETSKEMÉTY I., SOLYMOSI F., SZALAY L. és SZÁNTÓ F.

Kiadja

a József Attila Tudományegyetem Természettudományi Kara (Szeged, Aradi vértanúk tere 1.)

Szerkesztő bizottsági titkárok:

ANDOR J., BÁRDI I., MOLNÁR Á., SZATMÁRY K., és SÜLI Á.

Kiadványunk rövidítése:

Acta Phys. et. Chem. Szeged

Zeocat '85 Siófok Hungary

PROCEEDINGS
OF THE INTERNATIONAL SYMPOSIUM
ON ZEOLITE CATALYSIS

Siófok (Hungary) May 13—16. 1985.

Responsible for the contents: The Authors
(Their ready-for-copy manuscripts have been printed without corrections)

1985 by Acta Physica et Chemica Szegediensis
Szeged
Printed: Petőfi Nyomda, Kecskemét (43726)
ISBN 9630162598

PREFACE

Since the previous national conference on zeolite catalysis in Szeged, Hungary, in September 1978, the intense research that has characterized activity in the zeolite field in recent decades has not lost its momentum. This is vividly seen from the fact that two symposia were held in our immediate neighbourhood in 1984, the first in Prague in May, the second in Portorose in September, both being real successes as regards the scientific levels of the papers submitted and also the number of participants. The initial successful steps of Hungarian zeolite research, which led to the first national symposium in Szeged, have now inspired the organization of the second one, this time in Siófok, at Lake Balaton, with the unchanged topic: "zeolite catalysis".

From among the more than 120 submitted papers, the Paper Selecting Committee accepted roughly 60 for oral presentation, the invited papers included, and another 22 as posters. The Organizing Committee decided that both types of manuscripts should be included in the Symposium Volume. The prerequisites for the acceptance of papers were originality, a satisfactory level of English, and their presentation in camera-ready form. In a few cases the last two conditions were not fulfilled, but the rejection of otherwise excellent papers would have been unfounded. In these cases we decided to accept the papers for oral or poster presentation but to withhold their publication. The resulting Symposium Volume is an impressive tome, with some 700 pages.

400 copies will appear in paperback form, folded specially as preprints of the symposium, while another 400 will comprise an extraordinary issue of Acta Chimica et Physica Szegediensis, intended to be distributed on an exchange basis.

As far as the papers are concerned, it is not an easy task to summarize their contents. The authors of the invited papers have presented overviews of the "state of the art" in the different fields of research. The Organizing Committee is indebted to all these persons, specifically, P. A. Jacobs, Kh. M. Minachev, Y. Ben Taarit, W. O. Haag, G. Schulz-Ekloff, H. Bremer, J. Weitkamp and

K. K. Steinberg, for their generosity in having accepted the request of the Organizing Committee to cope with the plenary lectures.

Thanks are also due to the members of the International Scientific Advisory Board for their participation in the preparatory work of the symposium and for their help in the solving of some of the scientific and technical difficulties.

As concerns the scope of the symposium, the most interesting and numerous contributions deal with questions of the structures and modifications of zeolites. The pentasil-type zeolites have remained at the centre of interest. A wide variety of transformations are considered from the conversion of methanol into hydrocarbons to the alkylation of aromatics. This interest is fully warranted by the simplicity of their syntheses, as well as by their excellent stabilities and adaptability. Further subsessions are devoted to the problems of alkylation, transformation of alkyl aromatics, cracking, hydroisomerization and the conversion of methanol to hydrocarbons. The subsession dealing with metal and metal-complex containing zeolites presents novel trends through the introduction of inclusion compounds into the repertoire of promising catalysts.

This wide pattern of topics is supplemented with lectures on the dehydrogenation, oxidation, synthesis and decomposition of organic compounds containing heteroatoms, CO hydrogenation and coke formation. This last subsession seems to be a very important one, for deactivation through coke formation is a major disadvantage of the use of nearly all zeolitic materials in the petroleum industry.

In conclusion, we sincerely hope that the work of the Paper Selecting Commitee will enable the participants of the ZEOCAT symposium to acquire a realistic picture about the different fields of current zeolite research and thereby to benefit from the contents of this volume.

February 1985.

P. Fejes
Applied Chemistry Department,
József Attila University, Szeged

D. Kalló
Central Research Institute,
Hung. Acad. Sci., Budapest

CONTENTS

STRUCTURE AND MODIFICATION

PENTASIL ZEOLITES

METAL AND METAL COMPLEX CONTAINING ZEOLITES

ALKYLATION

TRANSFORMATION OF ALKYL AROMATICS

CRACKING OF HYDROCARBONS

HYDROISOMERIZATION AND HYDROCRACKING

DEHYDROGENATION, OXIDATION

CONVERSION OF METHANOL TO HYDROCARBONS

SYNTHESIS AND DECOMPOSITION OF ORGANIC COMPOUNDS WITH HETERO ATOMS

CO HYDROGENATION

COKE FORMATION

ART1/043

ISOMORPHIC SUBSTITUTION IN ZEOLITES : ITS POTENTIAL CATALYTIC IMPLICATIONS

M. Tielen, M. Geelen, P.A. JACOBS
Laboratorium voor Oppervlaktechemie, Katholieke Universiteit Leuven
Leuven, Belgium.

I. INTRODUCTION

Isomorphic substitution in high-alumina zeolites : the first generation materials

The replacement of isomorphous elements in a crystalline lattice, i.e. of elements with similar cationic radii and coordination requirements, has also been reported for the class of synthetic zeolites. When the term isomorphic substitution is used for these compounds, it refers to replacements of T-atoms, i.e. atoms tetrahedrally coordinated to oxygen atoms. Commonly encountered T-atoms are silicon and aluminum. In the early literature, reviewed by Breck [1], as potential candidates are described for substitution in tetrahedral sites : Ga^{3+}, P^{5+}, Ge^{4+} and Fe^{3+}. The existence of Zr-, Ti- and Cr-silicate "zeolites" has been claimed as well. By the same author it was stated that " at this stage boron incorporation in a zeolite had not been achieved". All this work refers to substitution in so-called first-generation zeolites with low silicon content. The main arguments that proof the existence of the replacement of T-atoms by isomorphic ions are :

i) the change of the unit cell dimensions with the degree of substitution. In faujasite-type zeolites, the contraction of the cubic unit cell seems to be correlated linearly to the degree of substitution of Al for Si [2]. The same kind of relation was shown to hold when in an A-type aluminosilicate structure, phosphorus was incorporated : at increasing degree of P incorporation, the unit cell was also found to contract [3].

ii) the gradual shifts of the lattice vibrations with the degree of substitution. This correlation has been established by Flanigen [4] for faujasites with different Si/Al ratios. Depending on the particular nature of the normal vibration, the susceptibility of its frequency to shifts is different.

The existence of a general equation, describing the unit cell parameters as a function of the Al content of the framework has been discussed. Indeed, Dempsey et al. [22] have reported discontinuities in this relation at 80,64 and 52 Al atoms per unit cell. Smith [23] argued about the statistical reliability and accuracy of

the chemical analysis of the data of Dempsey et al. [22]. Kühl, [24], however, reported the synthesis of gallosilicate faujasites with no aluminum and with a number of gallium ions per unit cell varying between 49 and 80, approximately. With the larger gallium ion (compared to aluminum) even more distinct breaks are observed in the relationship. The lattice parameters of the high-silica faujasites (less than 54 Ga/U.C.) deviate from this relation, as a result possibly of the presence of amorphous silica. In a recent publication Beyer et al. [25] showed that when the Breck-Flanigen equation is extrapolated to low Al contents, the regression line is parallel to their equation used to fit the a_0 - Al content data for $SiCl_4$-treated NaY :

$$a_0 = 8.68\ 10^{-4}\ N_{Al} + 2.425$$

in which N_{Al} is the number of Al atoms per unit cell and a_0, the cubic lattice constant in nm.

These substitutions have all been realized during synthesis, and in case of the replacement of Al for Si, the degree of substitution is rather limited. For other metallosilicates, as zirconium and titanosilicates, the degree of substitution of Al was complete but in agreement with Breck [1] we believe that their characterization was insufficient to proof univocally that the claimed material was also obtained in reality. The isomorphic replacement of silicon by germanium is another reported and proved example in which the substitution was complete and the characterization sufficient [5-7]. Materials with different structure but low silicon content were obtained (faujasite and philipsite). It should be stressed that only the germanium equivalent of zeolite X has been synthesized but never a material with enhanced germanium content, equivalent to Y-zeolite could be made.

A third example of isomorphic replacement consists in the synthesis of aluminoberyllosilicates. Such materials have been reported with the faujasite [26] as well as the mordenite [27] structure. In Fig. 1 the contraction of the cubic unit cell of faujasite is plotted for such samples, at two different Al/Be ratios. This figure shows that the regression lines for the two families of materials change in an almost parallel way with the Al content. The effect of the Be content of the faujasite is much less pronounced. This is not unusual since Be^{2+} and Si^{4+} have similar ionic radii (see later). Possible substitution mechanisms are [26] :

$$2(AlO_2)^- = (BeSiO_4)^{2-}$$

$$(AlO_2)^- = |BeO(OH)|^-$$

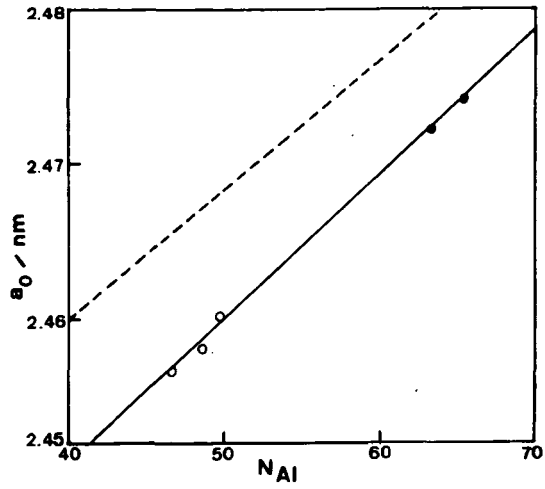

FIG. 1. Unit cell contraction of aluminoberyllosilicates with faujasite structure with different Al and Be concentrations. The open points refer to samples with $BeO/Al_2O_3 \cong 0.40$, the full points to BeO/Al_2O_3 ratios of 0.20, approximately. The experimental data are from ref. 26, exs. 1-5, the dashed line corresponds to the Breck and Flanigen correlation [2] for aluminosilicates with faujasite structure.

Arguments which point to the incorporation of Be in the faujasite lattice are :

i. the different a_0 values obtained for alumino- and aluminoberyllosilicates with the same structure (Fig. 1), the a_0 value being lowest for the Be-containing zeolite.

ii. the possibility to synthesize easily faujasites with high Si/Al ratio in presence of Be. Values above the critical BeO_2/Al_2O_3 ratio of 6 can be obtained in the Be-Al-Si-system [26].

Recently, Beyer and Belenykaya [8] were able to show that by the following solid state replacement reaction, faujasite structures with Si/Al ratios varying between 2.5 and infinity could be obtained easily :

$$Na_x (AlO_2)_x (SiO_2)_y + SiCl_4 \rightarrow Na_{x-1} (SiO_2)_{y+1} + NaAlCl_4$$

The contraction was again described by a regression line parallel to the ones given in Fig. 1 [25]. Preparation of aluminum-deficient faujasites and mordenites can be achieved by a wide variety of methods, giving materials with variable properties, as far as crystallinity, and concentration of defect sites is considered. This particular matter has been the subject of a recent review [9] .

Only in case of $SiCl_4$ [8] and $(NH_4)_2SiF_6$ aqueous solutions [10], the substituting element is of extra-lattice origin. All the classical dealumination methods, such as hydrothermal treatment of NH_4Y [11], reaction with chelating agents [12], acids [13] or treatment with F_2 gas [14] or combinations of these methods, in a first step seem to form defect sites, consisting of hydroxyl nests. In suitable reaction conditions these holes, have to be filled up with silicon atoms originating from amorphous parts of the zeolite lattice. In this way defectuous structures have to be formed, mainly characterized by the occurrence of a secondary porosity and the generation of a bidisperse pore size distribution [15].

Isomorphic substitutions in high silica-medium pore zeolites : the second generation materials.

In this new generation of zeolites with medium pore size and high silica content, extensive substitution of aluminum for silicon seems also possible. The existence of a series of ZSM-5 zeolites with continuously varying Si/Al ratios in the framework structure has been proven and gives the so-called ZSM-5 substitutional series [16]. Even the aluminum-free structure types, can be synthesized and give rise to the existence of crystalline silica polymorphs with a zeolitic structure type. Silicalite 1 [17], silicalite 2 [18] and TEA-silicate [19] belong to this family of new materials. They all can be obtained by direct synthesis. Further variation of their composition can occur by the classical dealumination methods as steaming. Realumination of such structures with aluminum halides seems to be possible via an aluminum insertion during a high-temperature gas-solid reaction [20,21], at least to a limited extent [21]. The opposite reaction of this alumination was shown to be possible with fluorosilicate solutions as driving force [10].

In the recent patent literature a whole variety of metallosilicates with medium pore size and high silica content has been claimed. A non-exhaustive enumeration of such materials is given in Table 1.

Table 1 shows that apparently numerous possible substitutions can occur in these high silica structures with medium pore sizes. Generally speaking these new materials are claimed based upon their novel chemical composition or XRD spectrum or both. This novelty doesnot necessarily mean that the new materials contain the new element, or at least part of it, substituted in the zeolite framework. As far as we are aware, only in the case of boron substitution sound proof is available for its presence in the zeolite lattice :

i. the unit cell volume of these zeolitic borosilicates was found to decrease monotonously with the degree of B-substitution [44]. The phenomenon can be described by the following theoretical regression line [44] :

$$V_B = V_{Si} - {}_{Si}\left[1-(d_B/d_{Si})^3\, x\right]$$

TABLE 1

Survey of different metallosilicates claimed in patent literature

NATURE OF SILICATE	Si/Me	Si/Al	REMARKS	REF.
AMS-1B borosilicate	52.3	1410	Specific XRD	28,ex.1
ZBH borosilicate zeolite	48.8	-	Pentasil-type	29,ex.1
Boroaluminosilicate	4.5	1667	Offretite-type	30,ex.1
Boralite	120.0	-	Various structures	31,ex.1
Gallosilicate	68.3	-	THETA-1	32,ex.1
Chromesilicate zeolite	86.8	275.1	MFI	33,ex.1
TRS-27 : beryliumsilicate	12.0	-	-	34,ex.1
TRS-66 : zincsilicate	15	-	-	34,ex.3
TRS-64 : titaniumsilicate	3	-	-	34,ex.6
TRS-48 : vanadiumsilicate	17	-	-	34,ex.7
Titanoaluminosilicate	21.3	87.0	MFI	35,ex.1
Zirconoaluminosilicate	28.6	76.9	MFI	36,ex.1
AMS-1 Cr chromosilicate	32.6	1515.2	AMS	37,ex.4
Zincosilicate	0.8	-	Zeolite A	38,ex.2
Zincaluminumsilicate	13.4	94.5	-	39,ex.1
Arsenesilicate	207.3	375.2	Zeolite structure	40,ex.1
Organosilicate containing tin	7.6	1787.0	Zeolite	41,ex.1
Iron-silicate	200	0.0	Zeolitic	42,ex.7
Iron-alumino-silicates	23.0	163.1	MFI	43,ex.1

in which V_{Si} and V_B stand for the unit cell volume of the silicate and B substituted form, respectively and x corresponds to the B fraction of the T-atoms.

ii. a discrete boron NMR signal is found in such materials and has been assigned to tetrahedrally coordinated boron in the structure [45,46].

Third generation molecular sieve zeolites.

The recent discovery of a new family of zeolites shows that isomorphic substitution in the $(Si_x\ Al_y\ P_z)O_2$ system is possible over a very wide range [47,48]. They are denoted as SAPO-n in which n refers to a particular structure-type. Up to 13 tridimensional microporous frameworks have been reported till now [48]. In contrast to these SAPO's, the AlPO family of aluminophosphate molecular sieves [49,50] consist of tridimensional $(Al\text{-}P)O_2$ frameworks. As a result of the valency of the cations (Al^{3+}, P^{5+}), these materials do not contain any excess of negative charge in tetrahedral coordination with oxygen. These materials have therefore no exchange capacity and have to be classified as molecular sieves instead of as zeolites. SAPO zeolite structures are considered to be derived from the corresponding aluminophosphate framework by substitution of silicon for phosphorus or by simultaneous substitution of 2 silicons for one aluminum and one phosphorus [48].

After this short review of the state of the art in matters of isomorphic substitution in zeolites, an attempt will be made to predict the effect of this substitution on catalyst activity and selectivity, using general and basic chemical principles more in particular the MFI-structure type will be considered and the general rules will eventually be illustrated with literature or new experimental data.

II. ATTEMPT TO PREDICT THE CATALYTIC IMPLICATIONS OF ISOMORPHIC SUBSTITUTIONS IN ZEOLITES USING GENERAL CHEMICAL PRINCIPLES

Possible types of isomorphic substitutions

When in a crystalline microporous silica polymorph with zeolite framework, ions of different valency state are substituted, the following possibilities exist :

i. for a substitution with a tetravalent ion the framework remains electrically neutral;

ii. for every trivalent ion incorporated in such a structure, a negative charge will have to be compensated for;

iii. with the incorporation of a bivalent ion, the creation of two negative charges is associated if tetrahedral coordination is strictly obeyed; otherwise oxygen defect sites will make the lattice electroneutral;

iiii. when a pentavalent ion is incorporated an excess positive charge exists. In order to behave as a cation exchanger, T-atoms with formal charge of 2 or lower, have to be present at the same time. Potential sites formed in this way, with protons as charge compensating ions, can be schematically represented as follows :

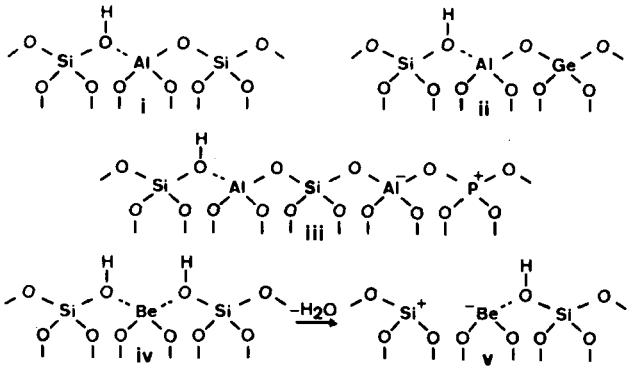

——— : chemical bond; ---- : formal coordination link

The scheme shows that incorporation of Me^{2+} forms two silanol groups in close proximity (iv), which are expected to be very susceptible to dehydroxylation (v) and result possibly in elemination of $Me\text{-}O_x$ and structural rearrangements. Incorporation of pentavalent ions generates a SAPO-type structure with a relatively high Al and low proton content.

Substitution with Me^{3+} T-atoms gives an increased number of Brønsted sites (i), the strength of which can be varied by substitution with Me^{4+} of different nature (ii). These qualitative considerations already suggest that SAPO-type materials for an identical number of Brønsted sites will contain a lower Si/Al ratio than the corresponding aluminosilicate and since Brønsted acid strength decreases with increasing aluminum content [51], they will show lower Brønsted activity. This is also experimentally observed in the cracking of n-butane [48]. The effect of the nature of the T^{4+}-atom on the Brønsted acid site strength was confirmed for the silicon- and germanium analogues of zeolite X : in the dehydration of tertiary-butanol, the former material - all other factors remaining the same - was by far the more active [52]. In some particular reactions, because of the low uniform Brønsted acidity, secondary reactions and coke formation are suppressed on the germanium-substituted faujasite [52].

Requirements for tetrahedral coordination

Stable tetrahedral coordination of the substituting elements will be determined by the size of the T-atoms. A possible measure for this can be the ionic radius. Ionic radii from several literature sources for pertinent ions are given in Table 2.

TABLE 2

Ionic radii of elements susceptible for substitution in a zeolite framework and their minimum radius ratio "R", in a Me-O matrix

ION	PAULING[a]	GOLDSCHMIDT[b]	SCHANNON[c]	R[e]
Si^{4+} d	0.41	0.38	0.40	0.37
Ge^{4+} d	0.53	0.54	0.53	0.43
Cr^{4+}	-	-	0.55	-
Ti^{4+}	0.68	0.60	0.56	0.55
Sn^{4+}	0.71	0.71	0.69	0.55
Zr^{4+}	0.80	0.77	0.73	0.62
Hf^{4+}	-	-	0.72	-
B^{3+} d	0.20	0.2	0.25	0.20
Al^{3+} d	0.50	0.45	0.53	0.41
Fe^{3+}	-	0.53	0.63	0.45
Cr^{3+}	-	0.55	-	-
Ga^{3+} d	0.62	0.60	0.61	0.46
Be^{2+} d	0.31	0.30	0.41	0.25
Mg^{2+}	0.65	0.65	0.71	0.47
Zn^{2+}	0.74	0.69	0.74	0.50
As^{5+}	-	-	0.475	0.40
P^{5+} d	-	-	0.31	0.34
V^{5+}	-	-	0.495	0.50
Cr^{5+}	-	-	0.485	-

a, ref. 53; b, ref. 54; c, ref. 55; d, for these ions there exists firm experimental evidence that they can be incorporated in a zeolite matrix (see introduction); a, radii in octahedral and c, in tetrahedral coordination; e, derived from ref. 53.

Based on this table and the evidence mentioned in the introduction, elements with ionic radii between 0.020 and 0.061 nm are potential candidates for incorporation into a framework, and most of the claimed elements possibly fit as T-atom in a zeolite matrix.

A more accurate estimate of the potential of given cation to be tetrahedrally coordinated in an oxygen matrix of anions is available. Pauling defined for this the concept of minimum radius ratio, R, which determines the stability of various coordination polyhedra or the preferred ligancy of a cation [56]. According to Pauling stable tetrahedral coordination can be formed for $0.225 < R < 0.414$. Using this criterion it is obvious that B^{3+} will prefer trigonal coordination in a zeolite matrix. It follows that the B-analogue of species i will be relatively unstable. B-substitution may therefore give rise easily to the formation of defect sites in which trigonal coordination is favoured.

Using the minimum radius rate concept, it can be understood that upon substitution of P for Si the unit cell volume of zeolite A decreases [3], as well as when Si is substituted for Al in faujasite frameworks [2]. It also explains that boralites show a decreased unit cell volume when boron is incorporated in a silicious zeolite [44]. Neglecting the contribution of differences in T-O-T bond angles upon substitution, the unit cell contraction of a given structure will be determined by R. In Fig. 2 are shown the change of the unit cell volume when elements with suitable R are substituted in the framework of a silica polymorph.

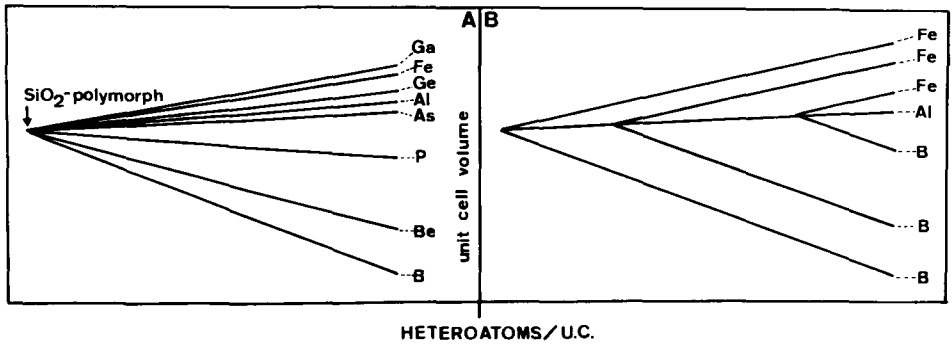

Fig. 2 Schematic representation of the changes in the unit cell volume of a silica polymorph upon isomorphic substitution of Si for one (A) or two different (B) elements.
The slope of the lines is proportional to $(R_{Si-O} - R_{Me-O})$.

Fig. 2 further shows that a wide range of changes in the volume of a unit cell may be achieved when judiciously selected elements are incorporated. It explains why AMS-1B zeolites show high p-xylene yields [57] in alkylation or isomerization reactions. The absolute value of these contractions is expected to be dependent on the structure type but it is clear that even subtle changes in the effective size of medium pore zeolites may induce pronounced changes in reaction selectivity. Typical examples of such effects are reported when the MFI-structure type is changed for the MEL-structure type [58].

In conclusion, it may be stated that many elements which on pure chemical grounds are claimed to be occluded in medium pore silica zeolites, are susceptible for being substituted in such frameworks as can be derived from the argumentation of this paragraph. Substitution of selected elements can also induce predictable changes in the unit cell dimensions and affect reaction selectivity.

Isomorphic substitution and changes in Brønsted acid strength

Changes in Brønsted acidity upon isomorphic substitution in aluminosilicates can be rationalised in terms of the average Sanderson electronegativity [51]. In fact, in this picture the acid strength of an OH group vibrating in a zeolite pore is then determined by the chemical composition of the environment. This relation holds only for an homologous series of materials, as e.g. a silica polymorph with the MFI structure in which different elements are substituted. In Fig. 3 is shown, therefore, the change of the average Sanderson electronegativity, S, when different elements are incorporated, which according to the coordination requirements are susceptible to substitution.

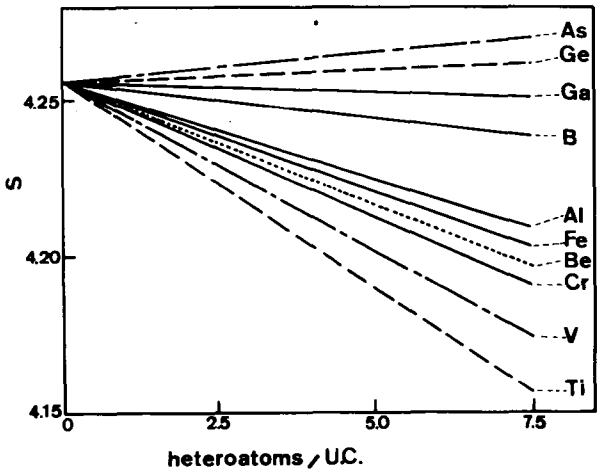

Fig. 3 Change of the Sanderson electronegativity, S, of a silicon polymorph with a MFI-structure in which foreign elements are substituted to different extents.

The figure shows that depending on the nature of the substituent and its amount incorporated, the Sanderson electronegativity and consequently the overall Brønsted acidity of such a material which contains protons, can be varied over a wide range. It follows also that given their higher S values, boron and galliumsilicates should exhibit stronger acidity than the corresponding aluminumsilicates. There is at least one example in literature which experimentally indicates an opposite trend : the boralite family of zeolites in the decomposition of methyltertiary butylether (MTBE) is found to be less acidic than ZSM-5 [44].

Since most reactants to prepare silica polymorphs contain impurity elements, as e.g. Al, changes in S were also calculated for the case of a silica polymorph with MFI structure containing 5 heteroatoms as well as for a material containing 5 aluminum next to 5 heteroatoms. The effect of these substitutions in MFI can be followed in Fig. 4.

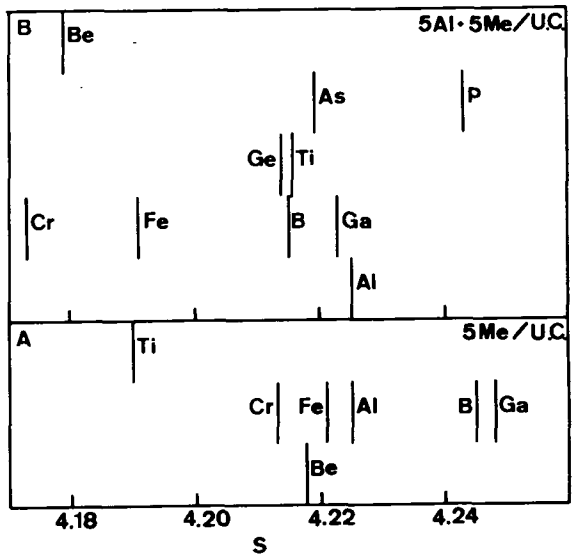

FIG. 4. Effect on the average Sanderson electronegativity, of isomorphic substitution in a silica polymorph with a MFI-unit cell : A, incorporation of 5 heteroatoms per unit cell; B, substitution of 5 Al next to other heteroatoms.

When two kinds of heteroatoms are present, the average S now decreases from the aluminosilicate to the aluminoborosilicate system. This is in line with the results obtained from the MTBE reaction [44]. From a selection of the literature on heteroatom incorporation into such systems [22-44], it is evident that each

material has residual Brønsted catalytic activity. However, no systematic comparison has been made of the effects of these substitutions.

We decided to synthesize therefore several MFI-type metallosilicates containing the following heteroatoms : Al, Al + B, Al + Fe, and Al + Be, covering in this way a relatively wide change in S, as well as in unit cell contraction. The changes in catalytic properties of these solids were followed in the n-decane isomerisation-hydrocracking reaction. The activity of a catalyst in this reaction can be rationalised in terms of its S value [51] and the selectivity is affected by minor changes in the pore sizes and void structure [59].

III. n-DECANE HYDROCONVERSION OVER MFI ZEOLITES WITH VARIOUS HETEROATOMS

The experimental procedure to follow the n-decane isomerization-hydrocracking reaction has been described in extenso [59]. ZSM-5-type zeolites were synthesized according to the diluted method described by Von Ballmoos [60]. Al, Be, Fe were added as nitrates, B as H_3BO_3. Changes in the OH^-/SiO_2 ratio provoked this way were compensated with NaOH. The samples contained each 0.20 $\pm$ 0.08 Al atoms per unit cell. The Me content measured after washing and NH_4-exchange was 1.6 $\pm$ 0.2 Me atoms, assuming that they all are substituted in the framework. The conversion of these NH_4-(Me)-ZSM-5 zeolites into bifunctional catalysts containing 1 % Pt is also described in earlier work [59,60]. The samples will be further denoted by the nature of the heteroatoms followed by their concentration in the solid as possible heteroatoms per unit cell. The crystals in each case have an hexagonal shape of 6 x 10 μm, approximately.

Influence of substitution on the activity

The overall activity of the $Al_{1.6}$, $B_{1.6}$ - $Al_{0.2}$, $Fe_{1.6}$ - $Al_{0.2}$ and $Be_{1.6}$ - $Al_{0.2}$ samples is given in Fig. 5A, together with that of an $Al_{0.2}$ sample. A series of parallel curves is obtained, displaced with respect to each other on the temperature ascis. The data allow to make two general statements :

i. there has been incorporation of B, Fe or Be in the MFI-structure. Indeed, the overall activity is definitely higher than due to the presence of residual aluminum.

ii. the activity sequence :

Al > B > Fe > Be

is the one predicted by the Sanderson electronegativity of such systems (Fig. 4).

Another proof for the incorporation of these elements in the structure and for their relative stabilizing such environment can be derived from the change in catalytic activity after high temperature calcination of the samples (Fig. 5B).

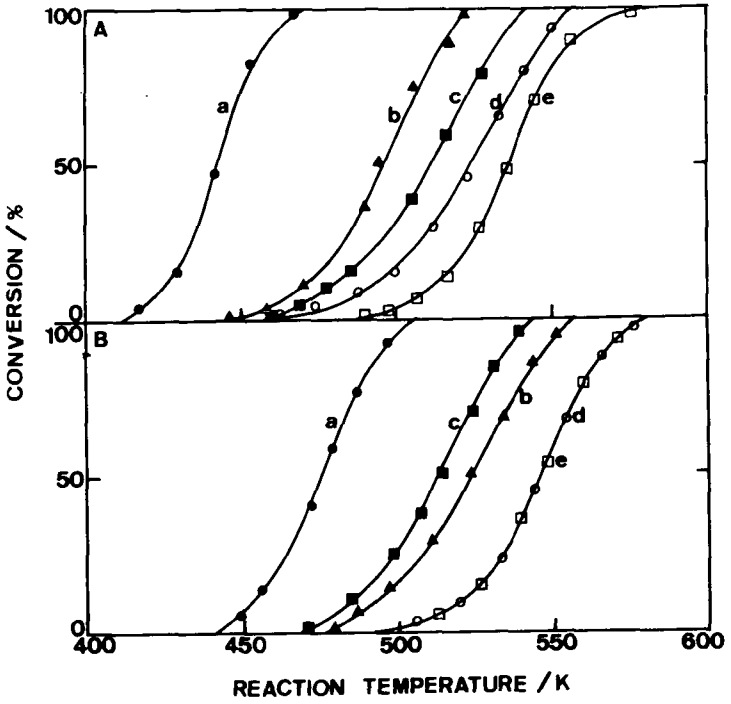

Fig. 5. Overall hydroconversion of n-decane on Me-containing zeolites of the MFI-structure type. A, samples precalcined at 823 K and B at 973 K : a, $Al_{1.6}$; b, $B_{1.6} - Al_{0.2}$; c, $Fe_{1.6} - Al_{0.2}$, d, $Be_{1.6} - Al_{0.2}$ and e, $Al_{0.2}$.

After calcination at 973 K, the activity of the Be-sample has decreased to the level of the reference Al-sample. This probably indicates that under such severe conditions all lattice Be has been removed. When the behaviour of the B, Be and Fe samples is compared, it can be derived that the stability of the respective ions in the tetrahedral coordination of the MFI-structure should decrease as follows :

Fe > B > Be

This same sequence could have been derived using the general concepts on which has been elaborated in previous section.

The overall isomerisation-hydrocracking selectivity in the bifunctional conversion of n-decane is also governed by acid strength [51]. All other factors, as competitive sorption-desorption, remaining equal, the Brønsted acid strength will determine the life-time of the carbocation intermediates. For longer

life-times, caused by stronger acidity, the probability for cracking will increase with respect to isomerization. The selectivity towards feed isomerization is therefore expected to increase as follows (Fig. 4) :

Al > B > Fe > Be

That this is observed in actual reaction conditions is illustrated in Fig. 6 for the two extremes of this series of materials.

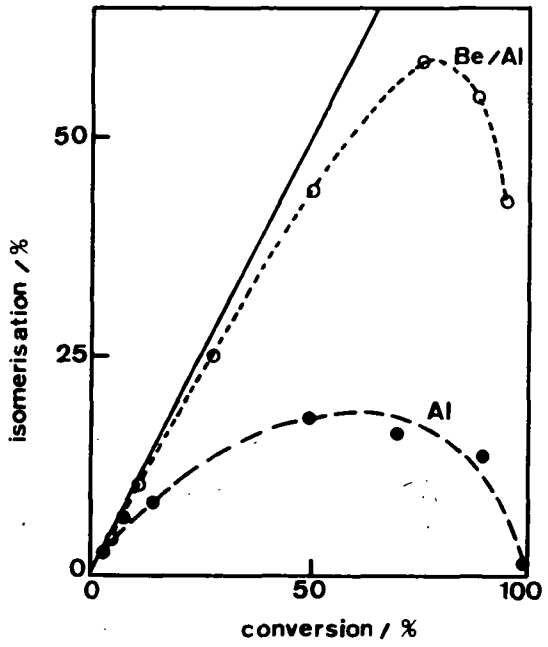

Fig. 6. Isomerisation-hydrocracking selectivity in the conversion of n-decane over $Al_{1.6}$ and $Be_{1.6}$ - $Al_{0.2}$ substituted MFI-structure types.

Effect of isomorphic substitution on product selectivity

It has been shown that hydrocracked products are formed via a consecutive β-scission reaction on multibranched isomers [61]. Central cracking is most probable on highly branched isomers, preferentially with branchings in α,α,γ -positions. It follows that in case of n-decane, the amount of isopentane formed will be strongly dependent on the nature of the intermediate isomers in the inner void structure in a particular zeolite. These isomers not necessarily desorb. Therefore the absolute yield of isopentane formed will be very susceptible to small

changes in the zeolite pore size [59]. In the present case, this yield is expected to decrease when lattice contraction occurs. The data of Fig. 7 confirm this again with experimental data.

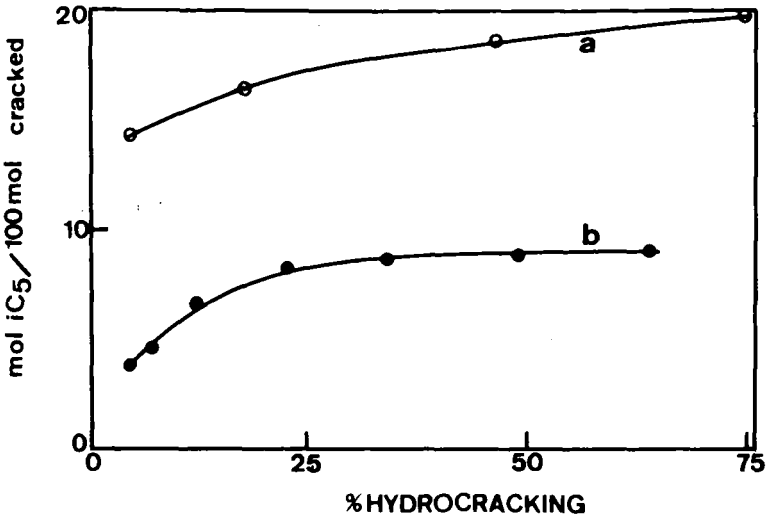

Fig. 7. Absolute yield of isopentane formed from n-decane at increasing hydrocracking conversion : a, $Al_{1.6}$ and b, $Be_{1.6} - Al_{0.2}$ samples.

The decreased isopentane yield on the $Be_{1.6} - Al_{0.2}$ sample compared to the $Al_{1.6}$ ZSM-5 zeolite, can be interpreted as a decrease in unit cell volume upon replacement of Si by Be, just as predicted by the general considerations developed earlier.

IV. CONCLUSIONS

Literature as well as new experimental data confirm the conclusions on isomorphic substitution of foreign elements in zeolite aluminosilicates. Based on general principles the nature of the ions which are potential candidates for substitution has been determined. Such replacement has consequences for the size of the unit cell of a zeolite and for the strength of Brønsted acid sites. This has implications for both catalytic activity and selectivity. A judicious selection of several elements for substitution in zeolite frameworks may give a zeolite with a tailor-made porosity and acid site strength. Much remains to be done in the area before it will be possible to advance further generalization.

V. ACKNOWLEDGMENTS

P.A.J. acknowledges a permanent research position from N.F.W.O. Support for this research was recieved in the frame of a concerted action on catalysis, sponsored by the Belgian Government (Wetenschapsbeleid).

REFERENCES

1. Breck, D.W., "Zeolite Molecular Sieves", J. Wiley, New York, 1974, p. 320.
2. Breck, D.W. and Flanigen, E.M., "Molecular Sieves", Soc. Chem. Ind., London, 1968 p. 47.
3. Flanigen, E.M. and Grose, R.W., Adv. Chem. Ser. 101 (1971) 76.
4. Flanigen, E.M., in "Zeolite Chemistry and Catalysis". J.A. Rabo, Ed., ACS Monogr. 171 (1976) 80.
5. Lerot, L., Poncelet, G. and Fripiat, J.J., Mat. Res. Bull. 9 (1974) 979.
6. Poncelet, G. and Lauriers, M., Mat. Res. Bull. 10 (1975) 1205.
7. Lerot, L., Poncelet, G., Dubru, M.L. and Fripiat, J.J., J. Catal. 37 (1975) 396.
8. Beyer, H.K. and Belenykaya, I.M., Stud. Surf. Sci. Catal. 5 (1980) 203.
9. Scherrer, J., ACS Symp. Ser. 248 (1984) 157.
10. Skeels, G.W. and Breck, D.W., Proceed. 6th Int. Conf. Zeolites, Olson, D. and Bisio, E., eds., Butterworths, 1984, p. 87.
11. McDaniel, C.V. and Maher, P.K., "Molecular Sieves", Soc. Chem. Ind., London, 1968, p. 186.
12. Kerr, G.T., J. Phys. Chem. 72 (1968) 2594.
13. Scherrer, J., J. Catal. 54 (1978) 285.
14. Lok, B.M., Gortsema, F.P., Messian, C.A., Rastelli, H. and Izod, T.P.J., ACS Symp. Ser. 218 (1983) 41.
15. Lohse, U., Stach, H., Thamm, H., Schirmer, W., Isirikjan, A.A., Regent, N.I. and Dubinin, M.M., Z. Anorg. Allg. Chem. 460 (1980) 179.
16. Olson, D.H., Haag, W.O. and Lago, R.M., J. Catal. 61 (1980) 390.
17. Flanigen, E.M., Bennett, J.M., Grose, R.W., Cohen, J.P., Patton, R.L., Kirchner, R.M. and Smith, J.V., Nature (London) 271 (1978) 512.
18. Bibby, D.M., Milestone, N.B. and Aldridge, L.P., Nature (London) 280 (1979) 664.
19. Grose, R.W. and Flanigen, E.M., U.S. Patent 4, 104, 294 (1978), assigned to Union Carbide Corp.
20. Jacobs, P.A., Tielen, M., Nagy, J.B., Debras, G., Derouane, E.G. and Gabelica, Z., Proceed. 6th Int. Conf. Zeolites, Olson, D. and Bisio, A., eds., Butterworths, 1984, p. 783.

21. Chang, C.D., Chu, C.T.W., Miale, J.N., Bridger, R.F. and Calvert, R.B., J. Am. Chem. Soc. 106 (1984) 8143.
22. Dempsey, E., Kuehl, G.H. and Olson, D.H., J. Phys. Chem. 73 (1969) 387.
23. Smith, J.V., Adv. Chem. Ser. 101 (1971) 171.
24. Kühl, G.H., J. Inorg. Nucl. Chem. 33 (1971) 3261.
25. Beyer, H.K., Belenykaya, I.M., Hange, F., Tielen, M., Grobet, P.J. and Jacobs, P.A., JCS Faraday I, to be published.
26. Marosi, L., Ripperger, W. and Schwarzmann, M., G. Offenl.. 2, 256, 450 (1974), assigned to BASF.
27. Stabenow, J., Marosi, L. and Schwarzmann, M., G. Offenl. 2, 325, 228 (1974), assigned to BASF.
28. Klotz, M.R., U.S. P 4, 269, 813 (1981), assigned to Standard Oil.
29. Hoelderich, W., Mross, W.D. and Schwarzmann, M., G. Offenl. 3, 143, 045 (1983), assigned to BASF.
30. Baltes, H., Leupold, E.I., Litterer, H. and Wunder, F., G. Offenl. 3, 134, 316, (1983) assigned to Hoechst.
31. Perego, G., Fattore, V. and Taramasso, M., G. Offenl. 3, 316, 488 (1983), assigned to Snamprogetti.
32. Barri, S.A.I. and Young, D., E.P.A. 106, 478 (1983), assigned to BP.
33. Marosi, L., Stabenow, J. and Schwarzmann, M., G. Offenl. 2, 831, 630 (1980), assigned to BASF.
34. Taramasso, M., Manara, G., Fattore, V. and Notari, B., U.K.P.A. 2, 024, 790 (1980), assigned to Snamprogetti.
35. Baltes, H., Litterer, H., Leupold, E.I. and Wunder, F., E.P.A. 77, 522 (1982), assigned to Hoechst.
36. Baltes, H., Litterer, H., Leupold, E.I. and Wunder, F., G. Offenl. 3, 141, 285 (1983), assigned to Hoechst.
37. Klotz, M.R., U.S.P. 4, 405, 502 (1983), assigned to Standard Oil.
38. McAnespic, P., Dyer, A. and Mehta, J.B., U.S.P. 4, 329, 328 (1980), assigned to National Res. Dev. Corp.
39. Weisser, J., Scharfe, G., Grolig, J. and Waldmann, H., E.P.A. 71, 136 (1982), assigned to Bayer.
40. Marosi, L., Stabenow, J. and Schwarzmann, M., G. Offenl. 2, 830, (1980), assigned to BASF.
41. Dwyer, F.G. and Jenkins, E.E., U.S.P. 3, 941, 871 (1976), assigned to Mobil Oil.
42. Boersma, M.A.M., Nanne, J.M. and Post, M.F.M., U.S.P. 4, 337, 176 (1982), assigned to Shell Oil.
43. Marosi, L., Stabenow, J. and Schwarzmann, M., E.P.A. 10, 572 (1980), assigned to BASF.
44. Taramasso, M., Perego, G. and Notari, B., in Proceed. 5th Int. Conf. Zeolites, Rees, L.V.C., ed., Heyden, London, 1980, p. 40.

45. Gabelica, Z., Debras, G. and Nagy, J.B., Stud. Surf. Sci. Catal. 19 (1984) 113.
46. Gabelica, Z., Nagy, J.B., Bodart, P. and Debras, G., Chem. Lett. (1984) 1059.
47. Lok, B.M., Messina, C.A., Patton, R.L., Gajek, R.T., Cannan, T.R. and Flanigen, E.M., U.S.P. 4, 440, 871 (1984), assigned to Union Carbide.
48. Lok, B.M., Messina, C.A., Patton, R.L., Gajek, R.T., Cannan, T.R. and Flanigen, E.M., J. Am. Chem. Soc. 106 (1984) 6092.
49. Wilson, S.T., Lok, B.M., Messina, C.A., Cannan, T.R. and Flanigen, E.M., J. Am. Chem. Soc. 104 (1982) 1146.
50. Wilson, S.T., Lok, B.M., Messina, C.A., Cannan, T.R. and Flanigen, E.M., ACS Symp. Ser. 218 (1983) 79.
51. Jacobs, P.A., Catal. Rev. Sci. Eng. 24 (1982) 415.
52. Poncelet, G., Dubru, M.L., Somme, O., Lerot, L., Jacobs, P.A., Tielen, M. and Uytterhoeven, J.B., Acta Phys. Chem. 24 (1978) 273.
53. Pauling, L., "The Nature of the Chemical Bond", Cornell Univ. Press, 3rd. ed., 1960, p. 514.
54. Cotton, A. and Wilkinson, G., Advanced Inorganic Chemistry, Interscience, New York, 2nd ed., 1966, p. 45.
55. Shannon, R.D., Acta Crystallogr. 32 (1976) 751.
56. Pauling, L., "The Nature of the Chemical Bond", Cornell Univ. Press, 3rd. ed., 1960, p. 545.
57. Fox, J.L., Science 227 (1985) 35.
58. Jacobs, P.A. and Tielen, M., Proceed. 8th Int. Cong. Catal., Verlag Chem., Weinheim 1984, p. 357.
59. Martens, J.A., Tielen, M., Jacobs, P.A. and Weitkamp, J., Zeolites 4 (1984) 98.
60. Von Ballmoos, R., Diss. ETH 6765, Verlag Sauerländer, Argau, 1981, p. 71.
61. Martens, J., Parniente, J. and Jacobs, P.A., this volume and references therein.

NATURE AND PROPERTIES OF ACIDIC SITES IN ZEOLITES REVEALED BY QUANTUM CHEMICAL AB INITIO CALCULATIONS

J. SAUER
Central Institute of Physical Chemistry, Academy of Sciences,
DDR-1199 Berlin, German Democratic Republic

ABSTRACT

Molecular models for Brönsted and Lewis sites are proposed. For bond lengths and angles empirically corrected theoretical values are used. To reveal differences between various sites, binding energies of the H_2O molecule on the respective models are considered.

INTRODUCTION

There has been continuous interest in the nature and properties of acidic sites, both Brönsted and Lewis, of zeolites. Recent stimulation of research in this field came from the development of highly efficient catalytic materials such as ZSM-5 zeolites. Nonempirical quantum chemical methods proved to be a valuable tool for making predictions of local structures and properties of minerals provided that suitable molecular models were used [1]. This is also true for active sites in zeolites [2-5]. While in a previous paper [3] local structures, vibrational properties and deprotonation energies of bridging and terminal hydroxyls were compared, in this work we construct molecular models that are appropriate for Brönsted and Lewis sites. These models are to be used to obtain reliable energies for the interaction of adsorbed molecules with active sites. Here, we report first results for the H_2O molecule. Some of them can be compared with the outcome of a related study by Geerlings et al. [4].

SPECIFICATION OF MODELS AND LOCAL STRUCTURES OF ACTIVE SITES

While there is no doubt that bridging hydroxyls are the source of Brönsted acidity [3], the existence and nature of Lewis sites in zeolites is debatable. We investigate in this study the threefold coordinated framework aluminium site and the Al^{3+} cation as possible candidates for Lewis sites. However, the AlO^{+} species or the $Al^{3+}(H_2O)_n$ and $AlO^{+}(H_2O)_n$ complexes may be more realistic models than

the free Al^{3+} cation and will be considered in forthcoming studies. Figure 1 shows molecular models that we propose for bridging hydroxyls (B-O) and threefold coordinated aluminium atoms (L-O). There are two possibilities for choosing the geometry parameters: (i) theoretical results which are obtained by optimization for the particular molecule serving as model, and (ii) realistic values which are inferred from all that is known from theory and experiment for the active sites and related molecules. While Geerlings et al. [4] adopt the first possibility, we strive for realistic models which reflect as closely as possible the local structure of the sites considered. To this end, use is made of empirically corrected theoretical geometries for bridging and terminal hydroxyls as well as for nonprotonated $\gtrless Si\text{-}O\text{-}Al^{\ominus} \lesssim$ framework sites (Table 1), which were taken from previous studies [3,7,8]. The results of the quantum chemical calculations were corrected for (empirically) known systematic errors and limitations of models. The justification of the procedure is outlined in Ref.3. Table 1 shows all the values used in this work. The models T-O for terminal hydroxyls and L-O for Lewis sites (Figure 1) retain the values of the B-O model for the geometry parameters.

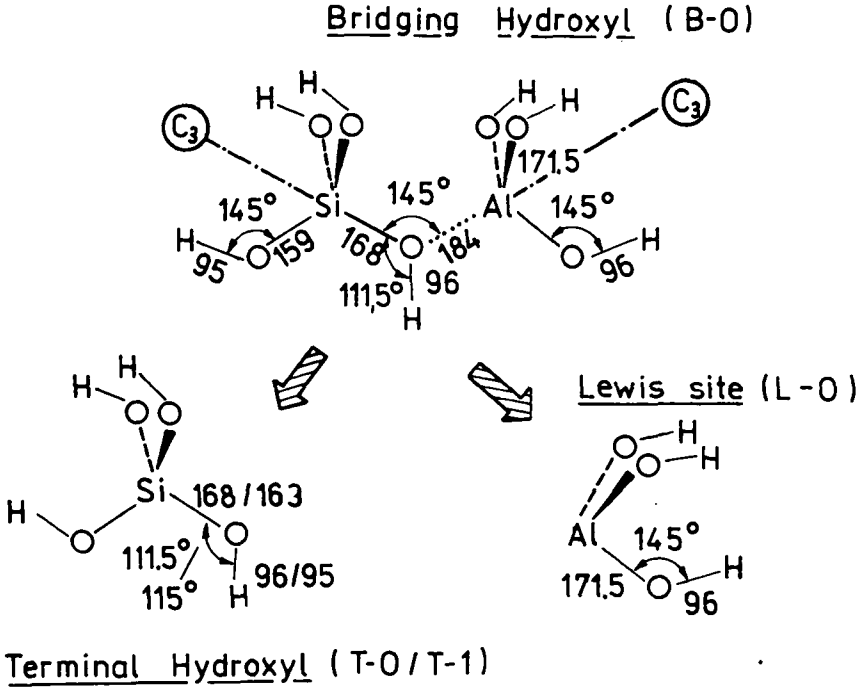

Fig. 1. Molecular models of active sites and values of bond lengths (in pm) and angles (in degree).

Table 1

Values of bond lengths and angles for molecular models of active sites in zeolites (cf. Figure 1)

Parameter	Value [a]	Source
	(i) models B-O, T-O, and L-O	
Si-O(H)	168	Values recommended for bridging hydroxyls [3]
(Si)O-Al	184	
(Si)O-H	96	
∢ Si-O-H	111.5	
Si-O	159	Values recommended for nonprotonated ≥Si-O-Al⊖≤ bridges [3,7]
Al-O	171.5	
∢ Si-O-Al	145	Typical value from X-ray results, may be subjected to variations
∢ Si-O-H	145	These are models of Si-O-Si and Al-O-Si bridges and, therefore, the same value as above is adopted
∢ Al-O-H	145	
(Si)O-H	95	STO-3G results for Si(OH)4 and [Al(OH)4]⊖ [7], empirically corrected by -3pm (see Tab. IV of Ref. 3)
(Al)O-H	96	
	(ii) model T-1	
Si-O(H)	163	Values recommended for terminal hydroxyls [3,8]
(Si)O-H	95	
∢ Si-O-H	115	

[a] Distances in pm, angles in degree

CALCULATIONS

Interaction energies are obtained within the "supermolecule" approach by means of ab initio calculations of SCF energies for the models M, the H_2O molecule and the complexes M-H_2O:

$$\Delta E^{SCF}_{M\text{-}H_2O} = E_{M\text{-}H_2O} - (E^{SCF}_{M} + E^{SCF}_{H_2O}).$$

Corrections are made for the basis set superposition error. The MINI-1 basis set is used which proved to be particularly suitable for calculating complexes, both of hydrogen-bonded and ionic type [6]. It yields more reliable absolute values of interaction energies than the 3-21 G basis set employed in Ref.4. Details of the computational procedure can be found in Ref. 6.

RESULTS AND DISCUSSION

Figure 2 shows the approach of the H_2O molecule towards the models of active sites. It was found by step-by-step optimization of the six intermolecular degrees of freedom. The hydrogen bonds are virtually linear, and the H_2O molecule is within the plane of the $\geq$SiOH group. Table 2 shows the optimum distances and binding energies (defined as the negative interaction energy at the optimum structure) for the complexes of H_2O with different sites. For comparison, the results of the hydrogen-bonded H_2O dimer [6] are included. Note, that contributions due to dispersion interaction are not yet considered

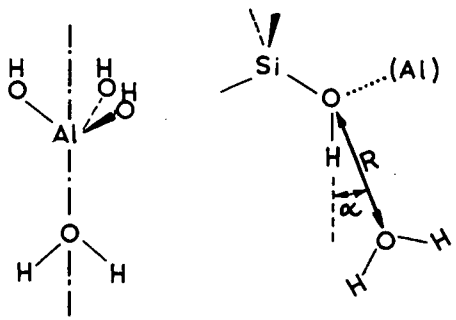

Fig. 2. Structure of complexes of different models with H_2O

Table 2

Optimum distances [a] and binding energies [b], $-\Delta E$, for complexes of H_2O with different models for active sites in zeolites

Site (Model)	R(pm) [a]	$-\Delta E$(kJ/mol)
Bridging hydroxyl (B-O)	259[c]	58.4
Terminal hydroxyl (T-O)	288[c]	16.4
Siloxan bridge ($(HO)_3SiOSi(OH)_3$)[d]	325[c,d]	10.1±0.3[d]
H_2O [e]	288[c,e]	20.1
Threefold coordinated Al (L-O)	191[f]	194
Al^{3+} [e]	176[f,e]	791[e]

[a] Cf. Fig. 2. [b] SCF energies corrected for the basis set superposition error. [c] Linear hydrogen bond (α =0), R=R(O,O). [d] Ref. 10. [e] Ref. 6. [f] R=R(Al,O).

and that, therefore, the final values of the binding energy may be larger by 5-10 kJ/mol. This, however, will not affect the conclusions reached below.

For bridging hydroxyls a binding energy is obtained which is 2.9 times the value of the H_2O dimer, while the previous estimate was 2.0 times this value [4]. In order to understand the substantial difference between the binding energies of bridging hydroxyls (about 60 kJ/mol, this work) and terminal hydroxyls (about 25 kJ/mol, [9]) the T-O model has been investigated. In this model the ≥SiOH group has exactly the same geometry as in bridging hydroxyls (B-O model). The binding energy for the B-O model is 3.5 times that of the T-O model (Table 2). Two effects may contribute to this result: (i) the additional direct interaction of the H_2O molecule with the $Al(OH)_3$ part of the B-O model and (ii) the enhanced acidity of the ≥SiOH group due to its polarization by the neighboring $Al(O-)_3$ group. This polarization is reflected (Figure 3) by changes of net charges when passing from the T-O (values in parenthesis , Figure 3) to the B-O model. Ref. 4 provides a detailed discussion. While we observe the same increase of the negative charge on the oxygen atom as the authors of Ref. 4, the increase of the positive charges on the acidic hydrogen atom and, in particular, on the silicium atom that we obtain is larger.

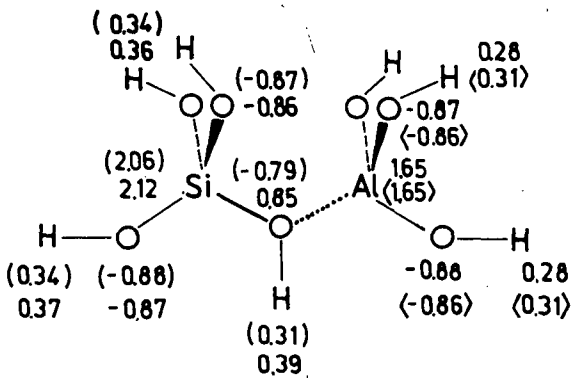

Fig. 3. Atomic net charges for the B-O model (bridging hydroxyls) compared to those of the T-O (in parenthesis) and L-O models in brakets .

Siloxan bridges, ≥Si-O-Si≤, are the constituents of microporous silica. The energies of binding for H_2O on these groups amount to only a fraction of that of bridging hydroxyls. This finding supports the view (see, e.g., [11]) that in siliciumrich molecular sieves bridging

hydroxyls act as hydrophilic sites within an environment of hydrophobic siloxan bridges.

Finally we comment on tentative models of Lewis sites. The huge stabilization energy of the H_2O-Al^{3+} complex makes it very unlikely that the Al^{3+} cation exists in noncoordinated form in zeolites. Even threefold coordinated framework aluminium sites bind H_2O with a three times larger energy than bridging hydroxyls do. We conclude that this type of sites may act as defect sites which are strongly preferred by H_2O molecules on adsorption in zeolites.

ACKNOWLEDGEMENT

Thanks go to Prof. W. Schirmer for promoting these studies, to Dr. W.J. Mortier for sending a preprint of Ref. 4 and to M. Urban for the help with the calculations.

REFERENCES

1. Sauer, J., Zahradník, R., Int. J. Quantum Chem. 26, 793 (1984).
2. Sauer, J., Haberlandt, H., Schirmer, W., in: P.A. Jacobs et al. (Eds.), Structure and Reactivity of Modified Zeolites (Studies in Surface Science and Catalysis, 18), Elsevier Sci. Publ. Co., Amsterdam, 1984, p. 313.
3. Mortier, W.J., Sauer, J., Lercher, J.A., Noller, H., J. Phys. Chem. 88, 905 (1984).
4. Geerlings, P., Tariel, N., Botrel, A., Lissillour, R., Mortier, W. J.: The Interaction of Surface Hydroxyls with Adsorbed Molecules. A Quantum Chemical Study, in preparation.
5. Kazansky, V.B., in: see Ref. 2, p. 61.
6. Hobza, P., Sauer, J., Theoret. Chim. Acta (Berl.) 65, 279 (1984); Sauer, J., Hobza, P., Theoret. Chim. Acta (Berl.) 65, 291 (1984).
7. Sauer, J., Engelhardt, G., Z. Naturforsch. 37a, 277 (1982).
8. Sauer, J., Chem. Phys. Lett. 97, 275 (1983).
9. Sauer, J., Schröder, K.-P., Z. physik. Chem. (Leipzig), in press.
10. Sauer, J., Morgeneyer, C., Schröder, K.-P., J. Phys. Chem., in press.
11. Nakamoto, H., Takahashi, H., ZEOLITES 2, 67 (1982).

THE SYNTHESIS AND PROPERTIES OF THETA-1, THE FIRST UNIDIMENSIONAL MEDIUM PORE HIGH SILICA ZEOLITE

A.G. Ashton[a], S.A.I. Barri[a], J. Dwyer[b]
BP Research Centre, Sunbury-on-Thames, Middlesex, TW16 7LN, England (a)
Department of Chemistry, UMIST, Manchester, England (b)

ABSTRACT

The novel high silica zeolite, Theta-1, is synthesised from hydrogel systems containing organic 'templates' of the general formula:

$$HX\text{-}CH_2CH_2\text{-}Y\text{-}CH_2CH_2\text{-}ZH$$

where X, Y and Z are oxygen and/or NH groups. Crystallisation is carried out at 150° - 175°C under autogeneous pressure. The formation of Theta-1 is found to be primarily dependent on the SiO_2/Al_2O_3 molar ratio, the hydroxyl to water ratio and the crystallisation time.

The zeolite is characterised by X-ray powder diffraction, electron microscopy and adsorption measurements. The structure and channel system of Theta-1 and the shape-selective properties are discussed. The alkylation of toluene with methanol is used as the test reaction and the results obtained compared with those over ZSM-5.

INTRODUCTION

Theta-1 is a novel medium-pore high silica zeolite distinguished by its unique X-ray diffraction pattern. The structure of Theta-1, which has been published elsewhere (1-3), is the first example of a new, topologically distinct, structure-type. It has been proposed to designate this new zeolite as TON (1).

Recently, a number of zeolites (KZ-2 (4), Nu-10 (5), ZSM-22 (6) and ISI-1 (7)) have been reported which have X-ray diffraction patterns consistent with that of Theta-1.

Theta-1 has been synthesised in a pure crystalline form using a number of templates. The product was characterised by X-ray powder diffraction and pore volume determination. Catalysts prepared from Theta-1 were tested for the alkylation of toluene with methanol and activities and selectivities compared with those of ZSM-5 type zeolites.

EXPERIMENTAL

Synthesis. Zeolite syntheses were generally carried out as described previously (2). A clear aluminate solution consisting of sodium aluminate, sodium hydroxide and water was prepared. The templating agents which had the formula:-

$$HX-(CH_2-CH_2)-Y-(CH_2-CH_2)-ZH$$

where X, Y and Z are oxygen and/or NH groups were added to the aluminate solution followed by Ludox AS 40 silica sol (containing 40 per cent by weight silica). The addition took ca. 10 - 45 min. The resultant hydrogel was stirred for a further 10 - 30 min and then crystallised at 150° to 175°C in a stainless steel pressure vessel. In the case of a small scale synthesis (ca. 100 g gel), a 200 cm^3 pressure vessel was used which was rotated in an oven. The pressure vessel was half filled with gel in order to ensure thorough mixing during crystallisation. In the case of a large scale synthesis (ca. 2000 g gel), a 3 litre autoclave was used which was rocked in a jacket furnace at the required temperature. At the end of the crystallisation period the pressure vessel was cooled and the zeolite filtered, washed and then dried at 100°C.

The H-form of the zeolite was prepared by (a) calcining the zeolite at 550°C for 60 h (shallow bed ca. 5 mm in depth) to remove organics, (b) refluxing the zeolite in an aqueous solution of ammonium nitrate (1 M) for 4 h (100 cm^3 of solution/10 g of zeolite), and (c) calcining as in step (a) for 12 h to remove ammonia.

The ZSM-5 zeolite used in comparison was synthesised as reported before (8).

Characterisation. The zeolites were characterised first by X-ray powder diffraction using a Philips PW 1050 vertical diffractometer (9) and CuKα radiation. The Si/Aℓ ratio was determined by X-ray fluorescence spectroscopy and particle sizes estimated by electron microscopy. The pore volumes of the zeolites were determined by nitrogen adsorption using the BET method. The relative diffusivity of ortho- and para-xylenes was estimated using an electronic microbalance (C.I. Electronics). Samples were degassed under vacuum (10^{-5} torr) at 400°C and sorption experiments were carried out at 120°C with a xylene partial pressure of 5.8 mbar. Relative diffusivities were estimated by measuring increases in sample weight with time.

Catalyst Preparation and Testing. Catalysts were prepared by mixing the H-form of the zeolite with Ludox AS 40 (containing 40 per cent silica; 1 g of zeolite: 2 g of Ludox). Water was added to the mixture to form a paste which was mixed thoroughly and dried at 60°C. The solid was then broken and sieved to form granules (12 - 30 mesh BSS).

A reactor (10 mm ID) was packed with beads (25 cm^3, preheat section) and catalyst (5 cm^3) which was activated by heating in a flow of air at 650°C for 4 h and then purged with nitrogen. A feed of toluene and methanol (2:1 molar) was passed over the catalyst at a liquid hourly space velocity (LHSV) of 1 h^{-1}. Liquid products were collected over 30 min periods and analysed by gas chromatography.

RESULTS AND DISCUSSION

Synthesis. Zeolite Theta-1 was sythesised in a pure crystalline form using the templates, diethanolamine, N-(2-aminoethyl)ethanolamine, 2-(2-aminoethoxy)ethanol or digol. Some typical hydrogel compositions are given in Table 1. As can be seen, Theta-1 can be synthesised using various alkali metals and organic templates, but the crystallisation time varies. Optimum time of crystallisation may also be dependent on the hydrogel composition (eg SiO_2/Al_2O_3 ratio, hydroxyl/water ratio, etc). For a given gel long times may result in the decline in the quantity of Theta-1 and the formation of α-cristobalite. By optimising the time of crystallisation for each gel a pure crystalline form of Theta-1 was obtained.

Characterisation. Figure 1 shows a typical diffraction pattern of zeolite Theta-1. A more detailed report on the X-ray powder diffraction analysis of Theta-1 is being published (9). The unit cell is C-centred orthorhombic with dimensions:- a = 13.836 ± 0.003, b = 17.415 ± 0.004 and c = 5.042 ± 0.001 Å and the space group of $Cmc2_1$.

The Si/Al ratio of the zeolite produced was generally close to the ratio used in the preparation of the hydrogel. The higher the OH/H_2O in the hydrogel, the higher was the difference between the Si/Al ratio of the zeolite and the hydrogel. The Si/Al ratio of the Theta-1 zeolite used in the characteristion and catalytic testing was 32 (atomic). The ZSM-5 zeolite used in comparison tests had a Si/Al ratio of 19.

The electron micrographs of Theta-1 and ZSM-5 are shown in Figure 2. The crystals of Theta-1 were rod-like in shape and were approximately 0.5 μm in length as compared to 2 - 5 μm for ZSM-5.

The pore volume determined for Theta-1 was 0.10 ± 0.01 $cm^3\ g^{-1}$ which is the maximum expected based on the structure (1) and is smaller than that of zeolite ZSM-5 (0.20 ± 0.01 $cm^3\ g^{-1}$).

The Structure of Theta-1. The framework of Theta-1 along the c-axis is shown in Figure 3. The structure can be made entirely from complex 5-1 T secondary building units. This places the structure of Theta-1 in the mordenite group of materials (10) which includes the zeolites: mordenite, ferrierite, dachiardite, epistilbite and bikitaite. It is proposed to designate the new zeolite as TON according to the recommendation of IUPAC (11).

The structure of Theta-1 comprises a zig-zag arrangement of 5-T ring chains along the a-direction giving a repeat of 13.8 Å (Figure 4). These chains are linked by alternating 6-T and 10-T rings giving a repeat of 17.4 Å in the b-direction. The same structure projection is found in ferrierite, ZSM-5 and ZSM-11 (12), though with different lattice parameters and specific topologies. The b-c projection of Theta-1 (Figure 5) is very similar to the a-b projection in bikitaite which consists of interlinking 6-T rings giving ~5 Å repeat. Thus in Theta-1 the 10-T ring channel is unidimensional along the c-axis.

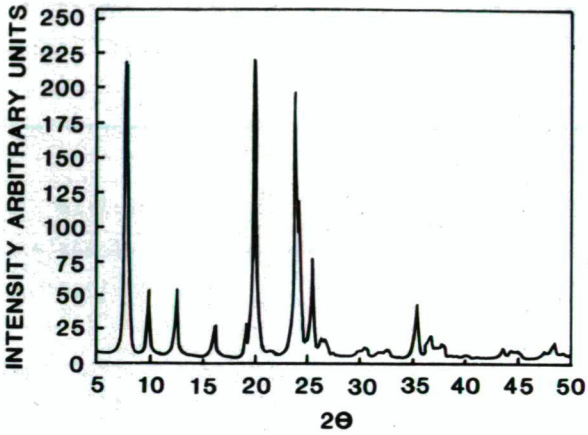

FIG 1
TYPICAL X-RAY DIFFRACTION PATTERN
OF THETA-1 ZEOLITE

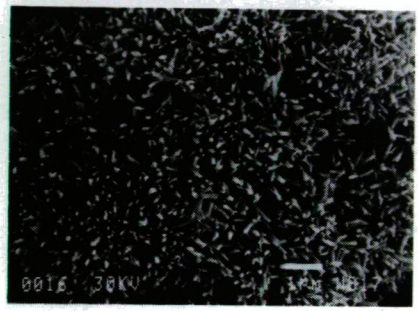

(a)

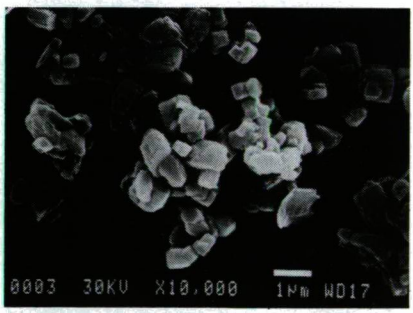

(b)

FIG 2 ELECTRON MICROGRAPHS
OF (a) THETA-1 AND
(b) ZSM-5 CRYSTALS

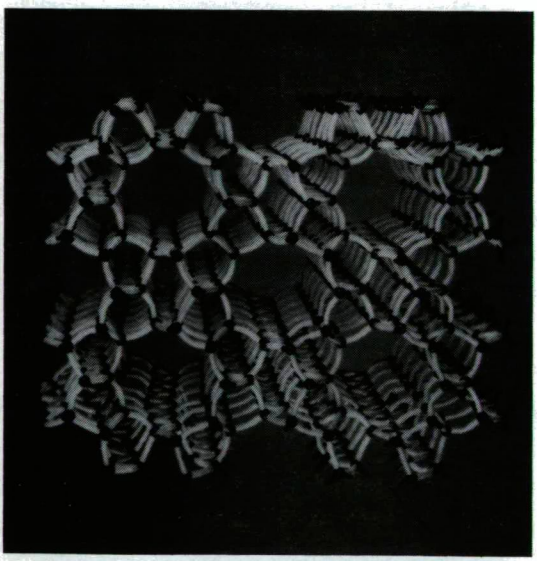

FIG 3 THETA-1 FRAMEWORK
VIEWED DOWN THE c-AXIS,
SHOWING THE 10-T RING
UNIDIMENSIONAL CHANNELS

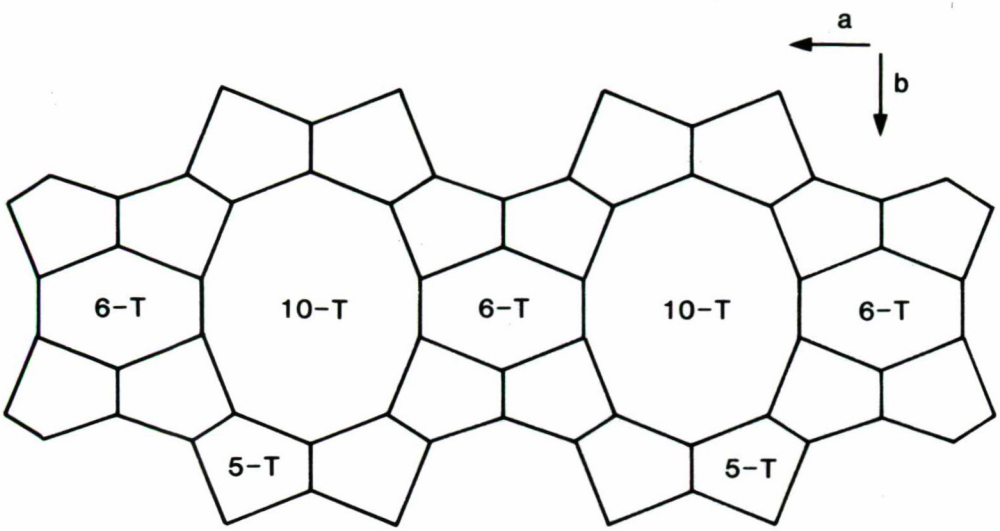

FIG 4 PROJECTION IN THE a-b PLANE OF 5-5-T AND 6-T RINGS TO SHOW THE ELLIPTICAL 10-T RING CHANNELS IN THE c-DIRECTION

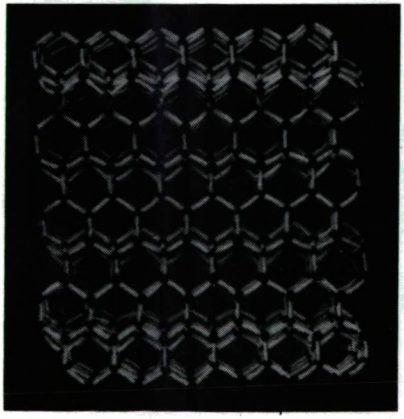

c-DIRECTION

FIG 5 THETA-1 FRAMEWORK VIEWED DOWN THE a-AXIS, SHOWING INTERLINKING 6-T RINGS TO PRODUCE 5 Å REPEAT ALONG THE c-AXIS. THIS PROJECTION IS COMMON WITH THE a-c PROJECTION IN THE ZEOLITE BIKITAITE

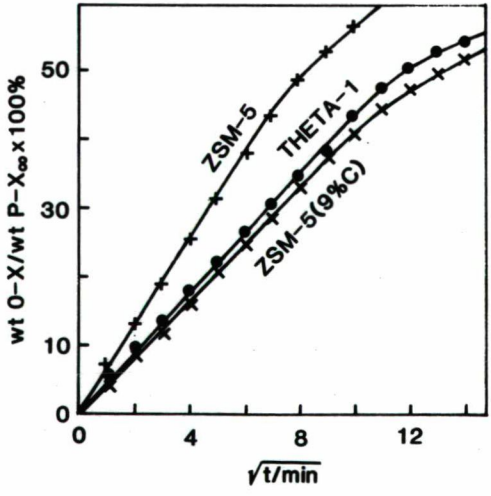

FIG 6 RELATIVE RATE OF INGRESS OF ORTHO-XYLENE OVER THETA-1 AND ZSM-5

Table 1

Hydrogel compositions and conditions used in the synthesis of Theta-1 zeolites

Organic 'Template' (TEM)	Hydrogel composition moles/mole of Al_2O_3					Nucleation/crystallisation		Approximate composition by X-ray powder diffraction
	Na_2O	K_2O	TEM	SiO_2	H_2O	Temp °C	Time h	
$(OHCH_2CH_2)_2NH$	2.5	-	30	54	720	175	40	Theta-1
	3.5	-	40	75	990	175	24	Theta-1
	1.1	1.4	30	55	740	170	24	Theta-1
	3.0	-	34	65	860	175	16	Theta-1
	3.0	-	34	65	860	175	44	Theta-1 + 20% α-cristobalite
	1.1	1.4	36	57	750	170	28	Theta-1 + 20% α-cristobalite
$(OHCH_2CH_2)NH(CH_2CH_2NH_2)$	4.9	-	36	85	1840	170	72	Theta-1 + 30% α-cristobalite
	10.4	-	90	210	4600	170	72	Theta-1 + 80% α-cristobalite
$(OHCH_2CH_2)O(CH_2CH_2NH_2)$	4.9	-	36	85	1840	175	96	Theta-1
$(OHCH_2CH_2)_2O$	5.1	-	45	105	1860	175	72	Theta-1
	6.4	-	60	140	2480	175	72	Theta-1 + 40% α-cristobalite

Table 2

Product compositions from the alkylation of toluene with methanol over ZSM-5 (MFI) and Theta-1 (TON)

		H-TON	H-MFI	H-TON	H-MFI	H-MFI
Conditions						
Temperature	°C	550	550	650	650	600
TOL/MeOH	molar	2/1	2/1	2/1	2/1	2/1
LHSV	h^{-1}	1	1.2	1	1.2	4.8
Time-on-stream	h	0.75	0.75	0.75	0.75	1.5
Conversion	%					
Toluene		23.9	37.9	27.2	46.5	31.8
Methanol		100	100	100	100	100
Liquid Product	%wt					
Benzene		0.7	9.4	1.3	13.8	3.4
Toluene		70.8	56.0	67.3	54.2	67.0
Para-xylene		10.2	7.3	12.1	6.7	11.1
Meta-xylene		6.5	15.5	8.4	13.9	11.1
Ortho-xylene		6.0	7.1	7.4	6.1	4.6
1,3,5-trimethylbenzene		0.4	1.1	0.3	1.3	0.2
1,2,4-trimethylbenzene		4.3	3.3	3.2	3.0	2.4
1,2,3-trimethylbenzene		N/D	0.1	N/D	0.5	N/D
Total		98.9	99.8	100.0	99.5	99.8
Xylene Composition	%					
Para		44.9	24.4	43.4	25.2	41.4
Meta		28.6	51.8	30.1	52.0	41.4
Ortho		16.4	23.8	26.5	22.8	18.2

Both the pore structures of Theta-1 and ZSM-5 have sets of straight 10-T elliptical channels; however they differ in that ZSM-5 has a second set of sinusoidal channels also consisting of 10-T rings intersecting with the straight channels to create channel intersections nearly 9 Å in diameter (13). Theta-1 has no such channel intersections giving it specific structural properties.

The Shape-Selective Properties of Theta-1. In the last decade, several workers have used the alkylation of toluene with methanol as a test reaction for probing the shape-selective properties of zeolite catalysts (14-15). An estimate of shape-selectivity can be obtained from the observed distribution of xylene isomers produced. Catalysts which show no initial shape-selectivity produce xylene isomers in a ratio close to that calculated for the equilibrium mixture; p:m:o = 24:52:24 per cent weight (14). Materials which show a high degree of shape-selectivity form para-xylene in a proportion greater than 24 per cent weight.

Shabtai (16) has suggested a simple model based on restricted transition-state selectivity (17) for predicting selective para-alkylation of monoalkylbenzenes. For para-alkylation to predominate, the main requirement is for a near-cylindrical channel with lengthwise orientation of the alkylbenzene along it:

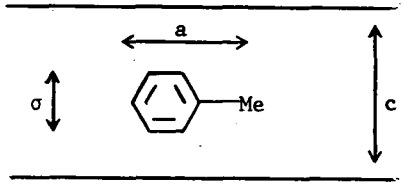

This alignment is preferred if $a > c > \sigma$. If such a model applies, then the approach of the electrophile to the ortho- and meta-positions of the orientated substrate is sterically hindered, while the para-position remains exposed to substitution.

Theta-1, when used as catalyst gave a high selectivity to p-xylene production and it fulfills the requirement of the Shabtai model. Results for the alkylation of toluene with methanol are shown in Table 2. The results confirm the above observation predictions with the proportion of para-xylene in the xylene fraction being significantly in excess of that for the equilibrium mixture.

Table 2 also shows results for alkylation over ZSM-5 (Si/Al = 19) under the same conditions. At short times-on-stream (<1 h), ZSM-5 produces xylenes with a distribution close to that calculated for the equilibrium mixture. ZSM-5 and Theta-1 have channels of similar size but differ in that Theta-1 has elliptical channels which run in only one direction whereas ZSM-5 has two sets of channels which create 'cage-like' channel intersections. The presence of channel intersections in ZSM-5 represents a deviation from the idealised Shabtai model. The larger space available at the intersections may facilitate attack of the electrophile at both the ortho- and meta-positions leading to a lower intrinsic shape-selectivity for ZSM-5 compared with Theta-1.

Kaeding et al (14, 18) have also observed an equilibrium distribution of xylene isomers for unmodified ZSM-5 at short times-on-stream. Kaeding has rationalised this result on the basis of rapid secondary isomerisation of the outwardly diffusing xylene isomers to produce the equilibrium mixture. The preservation of a high proportion of para-xylene over Theta-1 implies that the ratio of the rate of alkylation to that for isomerisation is greater over Theta-1 than ZSM-5. The lower isomerisation activity of Theta-1 compared with ZSM-5 has been confirmed in separate experiments (19).

High selectivity to para-xylene can also be due to 'product-selectivity' (17). The xylene isomers formed at sites located within the internal zeolite structure can only be observed in the products if they can diffuse out of the crystal structure. If the outward diffusivity of the para-isomer is sufficiently greater than that of the other isomers, then its relative concentration in the internal reaction volume is reduced. Under these circumstances, isomerisation occurs to maintain the thermodynamic equilibrium so that para-xylene is formed at the expense of the other isomers.

The degree of shape-selectivity introduced by 'product-selectivity' can be gauged from measurements of the relative rates of uptake of ortho- and para-xylene. Haag et al (20) have shown that the time ($\tau_{0.30}$) taken for ortho-xylene to sorb to 30 per cent of the equilibrium sorption capacity for para-xylene increases as the selectivity of the catalyst to para-xylene production increases. Figure 6 shows a $\sqrt{t}$ min$^{-\frac{1}{2}}$ plot for ortho-xylene adsorption over unmodified ZSM-5 and Theta-1. The time, $\tau_{0.30}$, for ZSM-5 is ca. 25 min as compared with 50 min for Theta-1. The sorption results show, therefore, that Theta-1 should be more selective to para-xylene than ZSM-5 (see Table 2) and the experimental results confirm this observation.

Although ZSM-5 shows no initial selectivity to para-xylene, there is a significant increase in the proportion of the para-isomer with increased time-on-stream as coke is deposited on the catalyst (14, 19). Thus for a sample of ZSM-5 coked for 90 min by toluene alkylation at 600°C (coke content 9 per cent w/w; Table 2), the time, $\tau_{0.30}$, for ortho-xylene uptake is similar to that for pure Theta-1 (Figure 5). The proportion of para-isomer produced by the ZSM-5 sample modified by a deposit of 9 per cent weight carbon is about 41 per cent (Table 2). There is good agreement, therefore, between the observed initial selectivity for alkylation over Theta-1 and the calculated selectivity from sorption measurements (Table 2).

The alkylation of toluene with methanol over Theta-1 and ZSM-5 also produces trimethylbenzenes. The ratio of 1,2,4-trimethylbenzene/1,3,5-trimethylbenzene is around 11 for Theta-1 compared with 3 for ZSM-5. This is a further illustration of the greater shape-selectivity of Theta-1 compared with ZSM-5. The greater selectivity to the 1,2,4 isomer over Theta-1 can be attributed to both restricted

transition-state selectivity (absence of channel intersections) and enhanced product selectivity (the smaller kinetic diameter of the 1,2,4 isomer favours its outward diffusion relative to the larger 1,3,5 isomer).

In the alkylation of toluene with methanol over ZSM-5 at short times-on-stream and at reaction temperatures greater than 500°C there is generally a significant amount of benzene in the liquid product (14, 19) (see Table 2). The benzene is mainly produced by secondary bimolecular disproportionation of toluene which is thought to form via a large 1,1-diphenylalkyl transition-state (18). For zeolites with small pore-sizes, bimolecular disproportionation is minimised because of restricted-transition-state selectivity (21). Since Theta-1 does not contain any of the channel intersections found in ZSM-5 it is reasonable to assume that Theta-1 would have a lower activity for toluene disproportionation than ZSM-5. Reference to the product distributions shown in Table 2 are consistent with this assumption. The lower disproportionation activity of Theta-1 compared with ZSM-5 has been confirmed in separate experiments (19).

CONCLUSIONS

The synthesis of zeolite Theta-1 from hydrogels containing various organic templates has been delineated. Knowledge of the structural and sorptive properties of Theta-1 compared with those of ZSM-5 enables the shape-selective properties to be explained. Thus in the alkylation of toluene with methanol, Theta-1 shows greater selectivity to para-xylene than is observed with ZSM-5 and secondary reactions (eg, disproportionation) are minimised. This enhanced selectivity can be attributed to the differences in framework structures and the increased transition state-selectivity of Theta-1.

ACKNOWLEDGEMENT

We thank Dr W.J. Ball, Miss S.M. Church, Mr B.H. Stringer, Mr D.M. Thornley, Dr D. White, Mr D. Wood and Dr D. Young for valuable contributions and BP International p.l.c. for permission to publish.

REFERENCES

1. Barri, S.A.I., Smith, G.W., White, D., Young, D., Nature, 1984, 312, 533.
2. European Patent No 0 057 049.
3. Published European Patent Application 0 104 800.
4. Parker, L.M., Bibby, D.M., Zeolites, 1983, 3, 8.
5. Published European Patent Application No 0 065 400.
6. Published European Patent Application No 0 102 716.
7. Published European Patent Application No 0 087 017.
8. European Patent No 0 030 811.
9. Highcock, R.M., Smith, G.W., Wood, D., Acta Cryst., to be published.

10. Barrer, R.M., Hydrothermal Chemistry of Zeolites, Academic Press, London, 1982, 18.
11. Chemical Nomenclature and Formulation of Composition of Synthetic and Natural Zeolites, Special International Union of Pure and Applied Chemistry (IUPAC) Commission under the Chairmanship of R.M. Barrer. IUPAC yellow booklet, 1978.
12. Meier, W.M., Olson, D.H., Atlas of Zeolite Structure Type, Structure Commission of the International Zeolite Association, 1978.
13. Derouane, E.G., Gabelica, Z., J. Catal., 1980, 65, 486.
14. Kaeding, W.W., Chu, C.C., Young, L.B., Weinstein, B., Butter, S.A., J. Catal., 1981, 67, 159.
15. Yashima, T., Sakaguchi, Y., Namba, S., Proc. 7th Int. Congr. Catal., (T. Seiyama, K. Tanabe, Eds), Elsevier, Tokyo, 1981.
16. Shabtai, J., La Chimica El'Industria, 1979, 61 (10), 735.
17. Csicsery, S.M., in Zeolite Chemistry and Catalysis, J. Rabo, Ed, (ACS 171, Washington), 1976, 680.
18. Kaeding, W.W., Chu, C.C., Young, L.B., Butter, S.A., J. Catal., 1981, 69, 392.
19. Ashton, A.G., PhD Thesis, UMIST, Manchester, 1984.
20. US Patents Nos 4 117 026 and 4 097 543.
21. Haag, W.O., Dwyer, F.G., in Aromatice Processing with Intermediate Pore Size Zeolite Catalysts, Am. Inst. Chem. Eng. Annual Meeting, Boston, Massachusettes, 1979.

ON THE STRUCTURE AND CATALYTIC PROPERTIES OF SILICA-ALUMINA

K.-P. WENDLANDT[a], H. BREMER[a], M. JANK[a], M. WEBER[b], P. STARKE[c], D. MÜLLER[c]
Technical University "Carl Schorlemmer" Leuna-Merseburg, Merseburg, GDR (a)
VEB Leuna-Werke "Walter Ulbricht", Leuna, GDR (b)
Central Institute of Inorganic Chemistry, Academy of Sciences of the GDR (c)

ABSTRACT

From basic, neutral and even weakly acidic solution, amorphous sodium aluminosilicates are obtained. During the thermal treatment of the corresponding ammonium form, obtained by ion exchange from the sodium form, most of the aluminium is removed from the tetrahedral positions, accompanied by a strong increase of the condensation degree of the silica fragments in the solid. Structure and catalytic properties of such silica rich silica-alumina closely resemble those of hydrothermally treated zeolites possessing a large amount of extra lattice aluminium.
Silica-alumina samples of equal composition but precipitated at different pH values may widely differ in their properties. Under certain preparation conditions an alumina rich sample may even reach an acidity and catalytic activity as high as that of a silica rich sample.

INTRODUCTION

Silica-alumina still continues to be of interest as catalyst component for the processing of high-boiling petroleum fractions. Fripiat et al. concluded /1/ that at low alumina contents (30 wt %) silica-alumina consists of a zeolite-type network structure. The nature of the Brönsted sites at the silica-alumina surface accordingly should correspond to that of the acidic OH groups in H-zeolites. This conception of the silica-alumina structure, however, turned out to be incompatible with results obtained by other authors /2-4/. Pott /2/ concluded from X-ray phosphorescence studies that the

H-form of amorphous aluminosilicates is unstable and that tetrahedrally coordinated Al is probably absent in silica-alumina; his experimental evidences, however, did not remain uncontradicted. Independently of the sample preparation, a maximum of the catalytic activity as a function of sample composition was found /5-7/ at about 15–40 wt % Al_2O_3. Existence and position of this maximum is explained /6/ by the isomorphous incorporation of Al into the silica matrix up to 30 wt % Al_2O_3. At higher alumina content, part of the Al is present in separate alumina phases, or bound in mullite-type structures /6/.

The present work is directed on the existence and stability of the H-form of X-ray amorphous aluminosilicates. The impact of sample preparation and composition on the catalytic properties of silica-alumina is emphasized.

EXPERIMENTAL

Sample preparation. SiO_2-Al_2O_3 samples were prepared by continuous precipitation from a sodium aluminate solution (4 wt % Al_2O_3) and water glass (4 wt % SiO_2). The pH value of the precipitation suspension was adjusted by adding sulphuric acid. The gels were filtered, washed and dried at 390 K. By subsequent ion exchange with 1 m aqueous solution of ammonium sulphate the residual sodium content was decreased to 0.02 wt %.

Sample series A, B. Samples of different composition were obtained by varying the flow rate of the partial streams (aluminate, water glass, sulphuric acid), the pH value was adjusted to 9 in the series A and to 6 in the series B. Thermal activation of the NH_4^+ exchanged samples was carried out prior to catalytic investigation in a stream of oxygen at 780 K.

Samples I-IV. Sample NaI (atomic ratio Si/Al = 1.1) was precipitated from a solution of the composition 2.3 SiO_2·1.0 Al_2O_3·3.4 Na_2O·170 H_2O; the gel was aged under the mother liquor for 6 hrs at 355 K. Samples NaII (Si/Al = 2.8), NaIII (Si/Al = 4) and NaIV (Si/Al = 4.2) were precipitated from a solution of 9 SiO_2·1.0 Al_2O_3·3.7 Na_2O·120 H_2O, with a pH value of 12 (NaII), 10 (NaIII) and 6 (NaIV) being adjusted by sulphuric acid. The gels were filtered after 5 min stirring. The corresponding H-forms HI-HIV were obtained by ammonium ion exchange and subsequent thermal deammonization.

Characterization methods used in this work (cumene cracking,

IR, DTA, NMR and the molybdate reaction) have been described in detail in references /8-10/.

RESULTS AND DISCUSSION

Formation and stability of the H-form of X-ray amorphous aluminosilicates

The X-ray amorphous precipitates NaI - NaIV are true amorphous aluminosilicates: the Na/Al atomic ratio is 1, the Na^+ ions are susceptible to nearly complete and stoichiometric cation exchange, and no structure sensitive bands characteristic of zeolites appear in the IR spectra.

The amount of tetrahedrally coordinated Al (Al^{IV}) strongly affects the asymmetrical T-O valence vibration band ($\tilde{\nu}_{asym}$; T = Si, Al) in the IR-spectra. As is evident from Figure 1, nature and magnitude of this functional relationship between the position of the $\tilde{\nu}_{asym}$ band and the amount of Al^{IV} correspond to the relationship known from zeolites /11/. Hence, the amount of Al^{IV} can be determined from the position of this band for silica-alumina just as in the case of partially dealuminated zeolites.

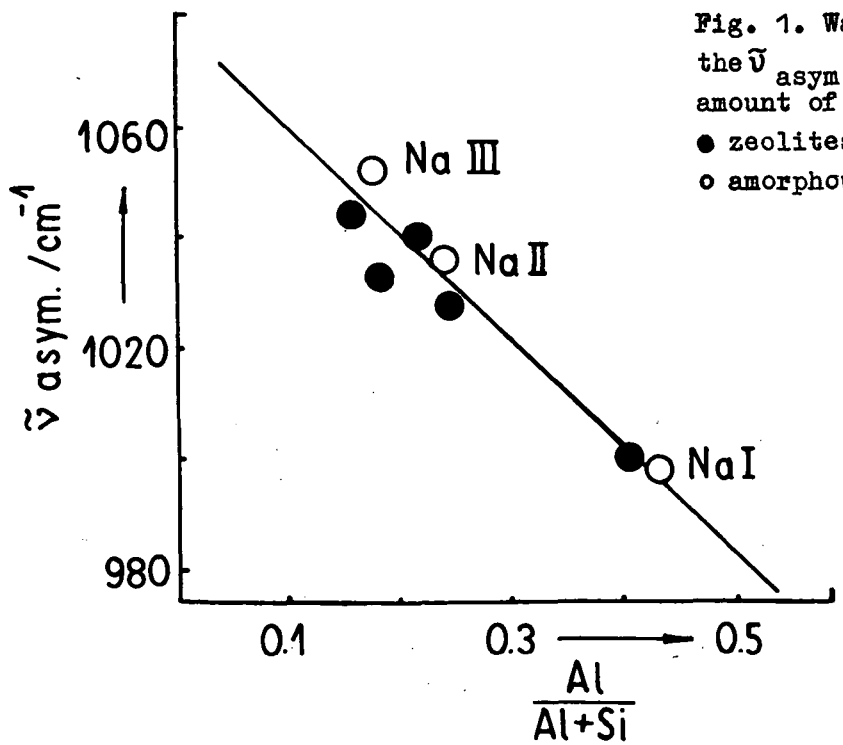

Fig. 1. Wave number of the $\tilde{\nu}_{asym}$ IR band and amount of Al^{IV}.
● zeolites Y /11/,
o amorphous samples.

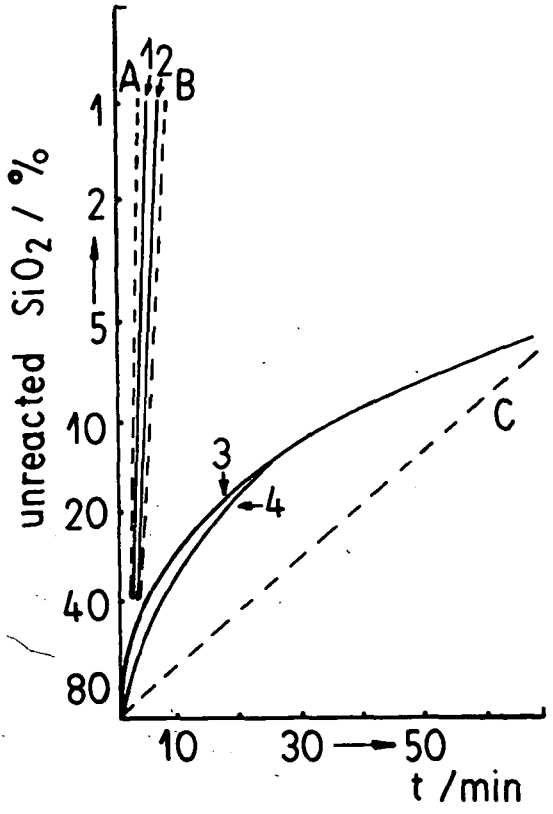

Fig. 2. Molybdate reaction curves.
A-monosilicic acid,
B-disilicic acid,
C-polysilicic acid,
1-NaI. 2-NaI, tempered at 775 K, 3-NaII,
4-NaII, tempered at 775 K.

The isomorphous incorporation of Al into a silica matrix decreases the number of directly interconnected $SiO_{4/2}$ tetraedra that is the condensation degree of the silicate fragments present in the solid. As a consequence the reaction rate of the solid with molybdate yielding β-dodecamolybdato silicic acid increases. Figure 2 presents the reaction curves obtained by the molybdate method for samples NaI and NaII. The reaction curves of the mono- and disilicic acid as well as of a polysilicic acid are added for comparison. The slopes of the curves represent the first order reaction rate constants of the formation of the coloured silicomolybdato complex. The comparison reveals that sample NaI mainly contains monosilicate fragments, whereas in sample NaII (Si/Al = 2.8) also fragments of a higher condensation degree exist. A thermal treatment at 390 and 780 K scarcely affects the condensation degree in the case of the Na-samples; the slight increase (which is paralleled by a decrease of the 920 cm^{-1} band in the IR spectra) is caused by condensation of terminal silanol groups.

By contrast with the Na samples, thermal treatment of NH_4^+ exchanged samples results in a marked increase of the silicate

condensation degree (cf. Fig. 3b).

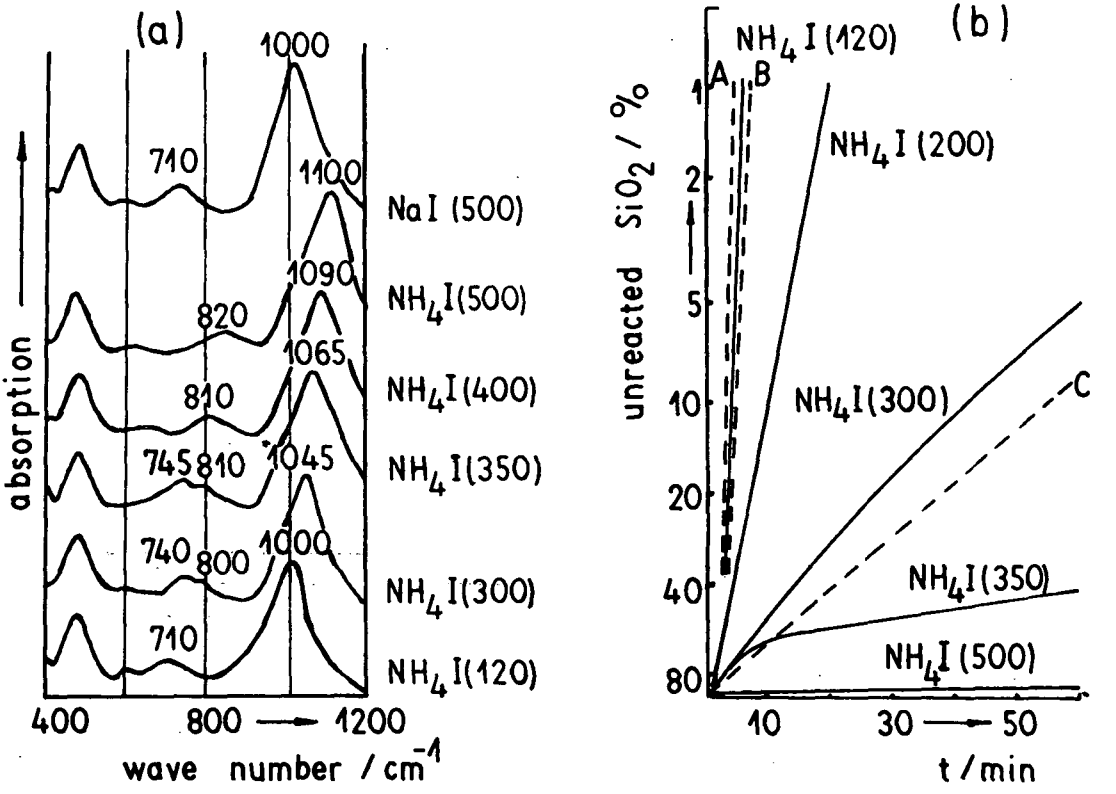

Fig. 3. IR spectra (a) and molybdate reaction curves (b) of samples NaI and NH_4I after thermal pretreatment at the indicated temperatures.

After a pretreatment at 770 K the condensation degree is so high that the reaction rate with molybdate is scarcely perceptible. New Si-O-Si bonds are formed along with changes in the IR spectra (Fig. 3a), which are in agreement with a removal of Al from 4-fold coordinated sites: shift of the $\tilde{\nu}_{asym}$ band to higher wave numbers, development of the $\tilde{\nu}_{sym}$ band at 820 cm^{-1} at the expense of the 740 cm^{-1} band.

The information obtained by various methods about the structure of sample NaI and the corresponding acidic form are summarized in Figure 4. In the Na form (as well as in the uncalcined NH_4 form) all Al is present in tetrahedral sites. In the ^{27}Al MAS NMR spectrum a single signal appears with a chemical shift of 52 ppm due to Al in $AlO_{4/2}$ tetrahedra ($AlCl_3$ in aqueous solution as external standard) /10/ /12/. Because there are no direct Si-O-Si bonds as derived from

the molybdate reaction, and taking into account the sample composition (Si/Al~1), the validity of the Loewenstein rule can be assumed for this sample. This is in accordance with the appearance of only one signal in the ^{29}Si NMR spectrum /13/. The pure H form is not obtained. In accordance with the results of the molybdate method and IR spectroscopy, ^{29}Si NMR proves the formation of new Si-O-Si bonds. In the ^{27}Al NMR spectrum, the intensity of the 52 ppm line is drastically reduced. The amount of Al remaining in tetrehedral sites is small, but still sufficient to account for the Brönsted acid sites. The signal at 0 ppm is due to unstrained AlO-octahedra. The structure-less broad background signal indicates that part of the Al is present in strained Al-O-polyhedra.

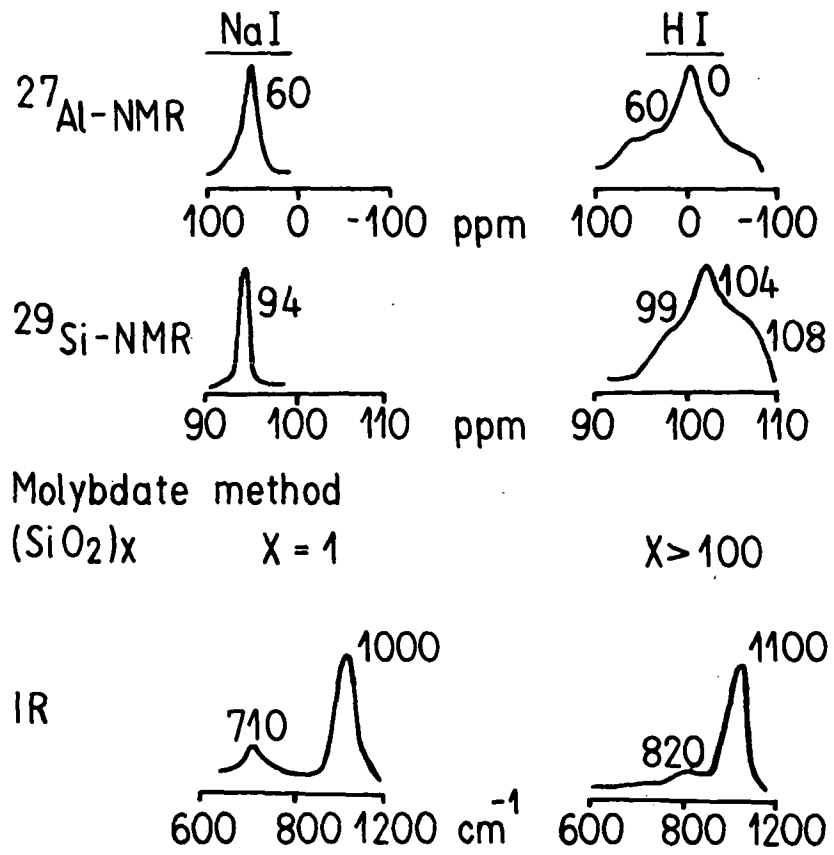

Fig. 4. Results obtained by different methods on the structure of samples NaI and HI.

Silica-alumina and zeolites

SiO_2-rich silica-alumina can be regarded as true aluminosilicates possessing a highly dealuminated lattice and a large amount of extra lattice Al. In this respect, it is comparable to hydrothermally ultrastabilized zeolites. This is emphasized by the resemblance between the ^{27}Al NMR spectra of sample HIV and of a zeolite US (w), given in Figure 5a. The US (w), prepared from an NH_4Y zeolite by a 3 hrs vapor treatment at 1090 K /14/, contains 90% of the Al in extra lattice positions. Strength ($H_R \approx -16$) and concentration ($\approx 10^{-5}$ mequ./m^2) of acid sites in both samples are of comparible magnitude. Structural acidic OH groups in silica-alumina resembling those in silica-rich zeolites have been proved by IR /15/.

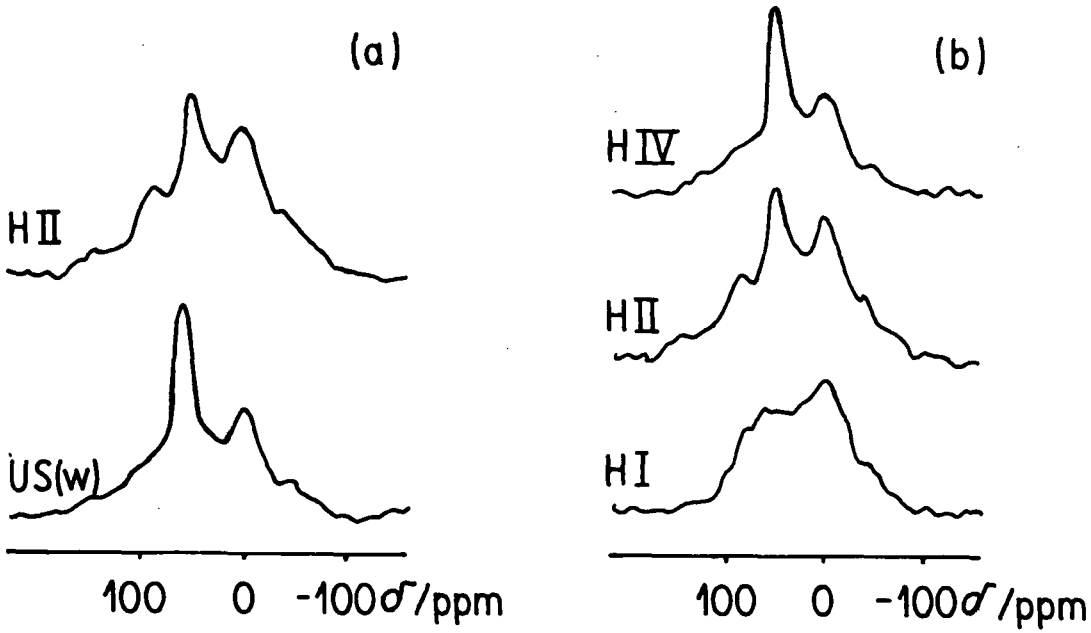

Fig. 5. ^{27}Al MAS NMR spectra of a) samples HI and US (w) and b) samples HI (Si/Al = 1.1), HII (Si/Al = 2.8) and HIV (Si/Al = 4.2).

Such OH groups can be formed by dissociative adsorption of water on extra lattice Al /16/, as it is known for zeolites loaded with polyvalent cations. This may explain the reversible transformation of Lewis into Brönsted sites in silica-alumina upon addition of water /17/. The higher Lewis site concentration explains the stronger tendency of silica-alumina for coking in hydrocarbon conversions.

The selectivity in some complex reactions, e. g. toluene methylation, may be considered as typical for highly dealuminated aluminosilicates /18/.

Effects of composition and preparation

Comparison of the ^{27}Al NMR spectra of samples HI, HII and HIV in Figure 5b suggests that the distribution of the Al over different coordination sites is affected by the Si/Al ratio: In samples HIV (Si/Al = 4.2) and HII (Si/Al = 2.8), which are richer in Si, the intensity of the 52 ppm line (Al^{IV}) is more strongly marked than is sample HI (Si/Al = 1.1) containing less Si.

The simultaneous effect of composition and preparation on the catalytic activity is demonstrated in Figure 6 with the samples of series A and B in the cumene cracking.

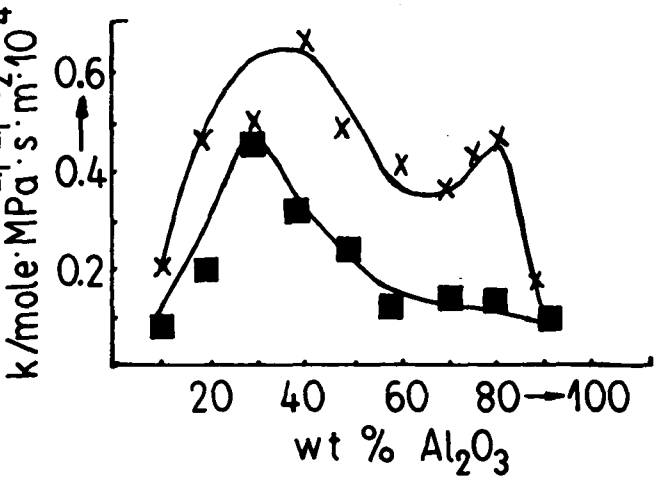

Fig. 6. First order rate constant k of cumene cracking at 675 K on silica-alumina of series A (■) and B (✕).

At a given composition, samples B exhibit a higher activity than samples A. Apart from the maximum at 40 wt %, a marked local maximum appears at 80 wt % Al_2O_3 in series B. The sequence of activity of

the various samples correspond to their sequence of acid site concentration, only samples of series B with about 80 wt % Al_2O_3 are characterized by a particularly high concentration of weakly acidic sites /8/.

Obviously, the interaction between the both components alumina and silica is stronger in samples B than in samples A. These differences cannot be levelled by subsequent tempering, as is evident from different tendencies for mullite formation, considerably more pronounced in samples B /8/. The nature of the amorphous alumina phase in the alumina-rich samples of series B appears to be related to that of the amorphous oxide phase formed by the extra lattice Al on the crystallite surface of zeolites at prolonged hydrothermal treatment /14/. This phase is very reactive, and is rapidly attacked by diluted acids, moreover, it appears to play a special role as adsorption sites in catalytic hydrocarbon reactions /19/.

CONCLUSION

Structure and properties of silica-alumina can be compared to those of highly dealuminated zeolites containing a large amount of extra lattice aluminium.

ACKNOWLEDGMENT

The authors thank Dr. U. Lohse, Central Research Institute for Physical Chemistry of the Academy of Sciences of the GDR, for the US (w) sample referred to in this work. The assistance of Dr. G. Scheler, Friedrich-Schiller-University Jena in the Al NMR investigation is gratefully acknowledged.

REFERENCES

1. Fripiat, J.J., Léonard, A., Uytterhoeven, J.B., J. Phys. Chem. 69, 3274 (1965).
2. Pott, G.T., Proc. 6th Intern. Congr. Catal., London 1970, Vol.1, p. 195.
3. Peri, J.B., J. Catal. 41, 227 (1976).
4. Miesserov, K.G., J. Catal. 13, 169 (1969).
5. Sato, M., Aonuma, T., Shiba, T., Proc. 3rd Intern. Congr. Catal., Amsterdam 1964, p. 396.
6. Léonard, A., Suzuki, S., Fripiat, J.J., De Kimpe, C., J. Phys.

68, 2608 (1964).
7. Damon, J.P., Delmon, B., Bonnier, J.M., J. Chem. Soc., Faraday Trans. I 73, 372 (1977).
8. Bremer, H., Jank, M., Weber, M., Wendlandt, K.-P., Z. anorg. allg. Chem. 505, 79 (1983).
9. Bremer, H., Jank, M., Fahlke, B., Starke, P., Wendlandt, K.-P., Z. anorg. allg. Chemie 500, 51 (1983).
10. Müller, D., Starke, P., Jank, M., Scheler, G., Bremer, H., Wendlandt, K.-P., Z. anorg. allg. Chem. 517, 167 (1984).
11. Lohse, U., Alsdorf, E., Stach, H., Z. anorg. allg. Chem. 482, 49 (1981).
12. Müller, D., Hoebbel, D., Gessner, W., Chem. Phys. Lett. 84, 25 (1981).
13. Heidemann, D., Z. anorg. allg. Chem. in press.
14. Lohse, U., Dissertation B, Berlin 1981.
15. Kazansky, V.B., Kustov, L.M., Borovkov, V.Yu., Zeolites 3, 77 (1983).
16. Hunger, M., Dissertation, Leipzig 1984.
17. Basila, M.R., Kantner, T.R., Rhee, K.H., J. phys. Chem. 68, 3197 (1964).
18. Wendlandt, K.-P., Bremer, H., Proc. 8th Intern. Congr. Catal., Berlin (West) 1984, Vol. IV, p. 507.
19. Bremer, H., Weber, M., Vogt, F., Wendlandt, K.-P., this book.

ON THE CHARACTER AND CATALYTIC ACTIVITY OF DEFECTS FORMED BY γ-IRRADIATION OF H- AND AlH-ZEOLITES

B. WICHTERLOVÁ[a], S. Beran[a], J. Nováková[a] and Z. Prášil[b]
J. Heyrovský Institute of Physical Chemistry and Electrochemistry, Czechoslovak Academy of Sciences, CS-121 38 Prague, Czechoslovakia (a)
Institute for Research, Production and Applications of Radioisotopes, CS-102 27 Prague, Czechoslovakia (b)

ABSTRACT

It has been found that various defects are formed by the γ-irradiation of zeolites, depending on the type of the original zeolite. With the HY and HZSM-5 zeolites, skeletal defects consist of an electron hole on a skeletal oxygen atom sharing one Si and one Al skeletal atom (Si-O-Al), as well as an electron hole delocalized on several skeletal oxygens $(-O-)_n^{\cdot}$. With the AlHY and Al_xO_yHZSM-5 zeolites containing extralattice Al, electron holes on oxygen atoms neighbouring two Al atoms (Al-O-Al defects), along with some delocalized $(-O-)_n^{\cdot}$ defects, have been detected. These conclusions are based on the ESR spectra measurements and on model quantum chemical calculations. A considerable activity of the γ-irradiated zeolites in the D_2-H_2 exchange was observed at room temperature. While the skeletal Si-O-Al and $(-O-)_n^{\cdot}$ defects are quenched by hydrogen, the Al-O-Al defects are rather stable. For this reason the γ-irradiated zeolites containing extralattice Al exhibit higher and very stable activity in the D_2-H_2 isotopic exchange compared to H-zeolites.

INTRODUCTION

Since the appearance of the first paper by Stamires and Turkevich dealing with the paramagnetic resonance absorption of γ-irradiated zeolites (1), the structure of the defects formed has been studied in detail (2-6). A positive effect of the irradiation on zeolite catalytic activity in the cracking reaction and CO_2 methanation has also been observed (7,8).

EPR studies have shown that the low temperature γ-irradiation of HY zeolites is connected with the formation of V center type defects and that the ejected electrons are trapped either by H^+ ions (creating H atoms entrapped within zeolite structure) or in the insulator material (5). The V center represents an electron hole localized in lone pair orbitals of skeletal oxygen atoms sharing two skeletal silicon atoms and/or one silicon and one aluminum skeletal atom. The stability of the centers is assumed to be strongly dependent on the electron scavengers. An electron hole lo-

cated on an oxygen atom sharing two aluminum atoms in stabilized Y as well as AlHY zeolites was detected (2,3). This result was taken as evidence that stabilized zeolites contain some dimers of aluminum species which have never been observed in pure γ-irradiated γ- and η-alumina.

Because of a complete lack of the data in literature on the relationship between the structure of defects in irradiated zeolites and their stability and reactivity this problem is considered here by studying various defects in H- and Al-Y and ZSM zeolites. For these purposes ESR spectroscopy, quantum chemical model calculations and measurements of catalytic activity in D_2-H_2 exchange were employed.

EXPERIMENTAL

The starting NH_4Y (70 % of exchange) and ZSM-5 zeolites were supplied by the Institute for Oil and Hydrocarbon Gases, Czechoslovakia. Prior to the ionic exchange of the ZSM-5 zeolite with 0.5 m HNO_3 at 298 K for 24 hours (HZSM-5), the zeolite was calcinated in an oxygen stream at 870 K for 6 hours. Extralattice Al was introduced into the HZSM-5 zeolite cavities by supporting an $Al(NO_3)_3$ solution followed by the zeolite calcination in an oxygen stream at 770 K for 5 hours. Extralattice Al was incorporated into the NH_4Y zeolite by ion exchange with 0.1 m $AlCl_3$ solution at pH 4 at 360 K. The composition of the zeolites was determined by AAS after disolution of the samples (Table 1).

Table 1

Composition and Ar sorption capacity of zeolites

irradiated zeolite	Si/Al total	Si/Al latt.	sorption capacity* (Ar, mmol/g) prior irr.	after irr.
HY	2.17	2.17	10.7	10.6
AlHY	1.86	2.17	9.6	9.7
HZSM-5	13.6	13.6	5.3	5.5
Al_xO_yHZSM-5	5.08	13.6	5.2	5.1

*Sorption capacity ($1.33.10^4$ Pa of Ar at 80 K) was measured on samples evacuated at 670 K and related to 1 g of dry zeolite

The preservation of the zeolite structures after the introduction of extralattice Al as well as after the zeolite irradiation was controlled by testing the sorption capacity for argon (see Table 1) and using the IR spectra of skeletal vibrations. Before irradiation the zeolites (placed in an EPR tube and/or in a reactor) were treated in a vacuum of 10^{-3} Pa at a temperature of 670 K and sealed off. The ESR spectra and the reactivity of the zeolites were measured immediately after the γ-irradiation without exposure to the air.

The γ-irradiation of zeolites was performed at 298 K in a ^{60}Co cell for doses of about 10^5 Gy. The X-band ESR spectra were recorded at 80 K on an ERS-220 spectrometer (Academy of Sciences, Berlin) with a modulation frequency of 100 kHz. The magnetic field was measured by proton magnetometer related to a Mn^{2+} standard.

The catalytic activity of the irradiated zeolites was tested by measuring the rate of isotopic exchange of the mixture of D_2 and H_2 molecules at room temperature. The irradiated zeolite (0.1 g) was allowed to react with $2x10^2$ Pa of hydrogen isotopes in a static apparatus (volume, 700 cm^3). A negligible amount of gases was linked directly to a mass spectrometer (MCH 1302, USSR). No exchange between the gaseous deuterium and the zeolitic OH groups was observed at this temperature. The exchange rate R (atoms $g^{-1}min^{-1}$) was evaluated using the equation

$$R = - \frac{N}{mt} \ln \frac{[HD]_\infty - [HD]_t}{[HD]_\infty - [HD]_0}$$

where N is the number of gaseous atoms, m zeolite weight (g), and $HD_{\infty,t,0}$ is concentration of HD molecules at the given time t (min).

RESULTS AND DISCUSSION

As the isotopic exchange reaction was measured at a temperature of 298 K, the γ-irradiation of zeolites was also carried out at 298 K to obtain defects sufficiently stable at this temperature. Therefore, H atoms which might be formed by the interaction of ejected electrons with H^+ ions necessarily recombined and were not detected.

ESR studies on the structure and stability of defects in γ-irradiated zeolites

HY zeolite. The ESR spectrum of zeolite in hydroxylated form (Fig. 1A) exhibits a wide signal of ΔH=38 G with 7 hyperfine lines. An analogous spectrum has already been published with the parameters g_1=2.002, c_1=7.5 G, g_2=2.005, c_2=8.0 G, g_3=2.045 (6). It has been ascribed to skeletal Si-O-Si and Si-O-Al defects, the hyperfine splitting (hfs) corresponds to the interaction of the unpaired electron with the Al nucleus (I_n=5/2), the 7th line is coming from the anisotropic g factor. The assignement of the signal with the hfs to the Si-O-Al defects agrees with our interpretation. However, the presence of the localized Si-O-Si defects seems to be unprobable. Theoretical consideration supports the assumption of an unpaired electron delocalized over the lone pair orbitals of several skeletal oxygens denoted $(-O-)_n^{\cdot}$ in such a way that no hfs interaction of this electron with the Al nucleus is observed. Interaction of zeolite with hydrogen ($1.33.10^4$ Pa at 298 K, also for the zeolites described below) caused decrease of the complex signal and only a sharp low intensity signal close to the free electron value was retained. The latter signal corresponds probably to the ejected electron stabilized within the zeolite matrix and is found in all irradiated zeolites. Analogous behaviour of defects present in γ-irradiated silica containing Al impurities with respect to hydrogen was observed by Parijsky et al (9).

HZSM-5 zeolite. The ESR spectrum of the hydroxylated zeolite exhibits a wide

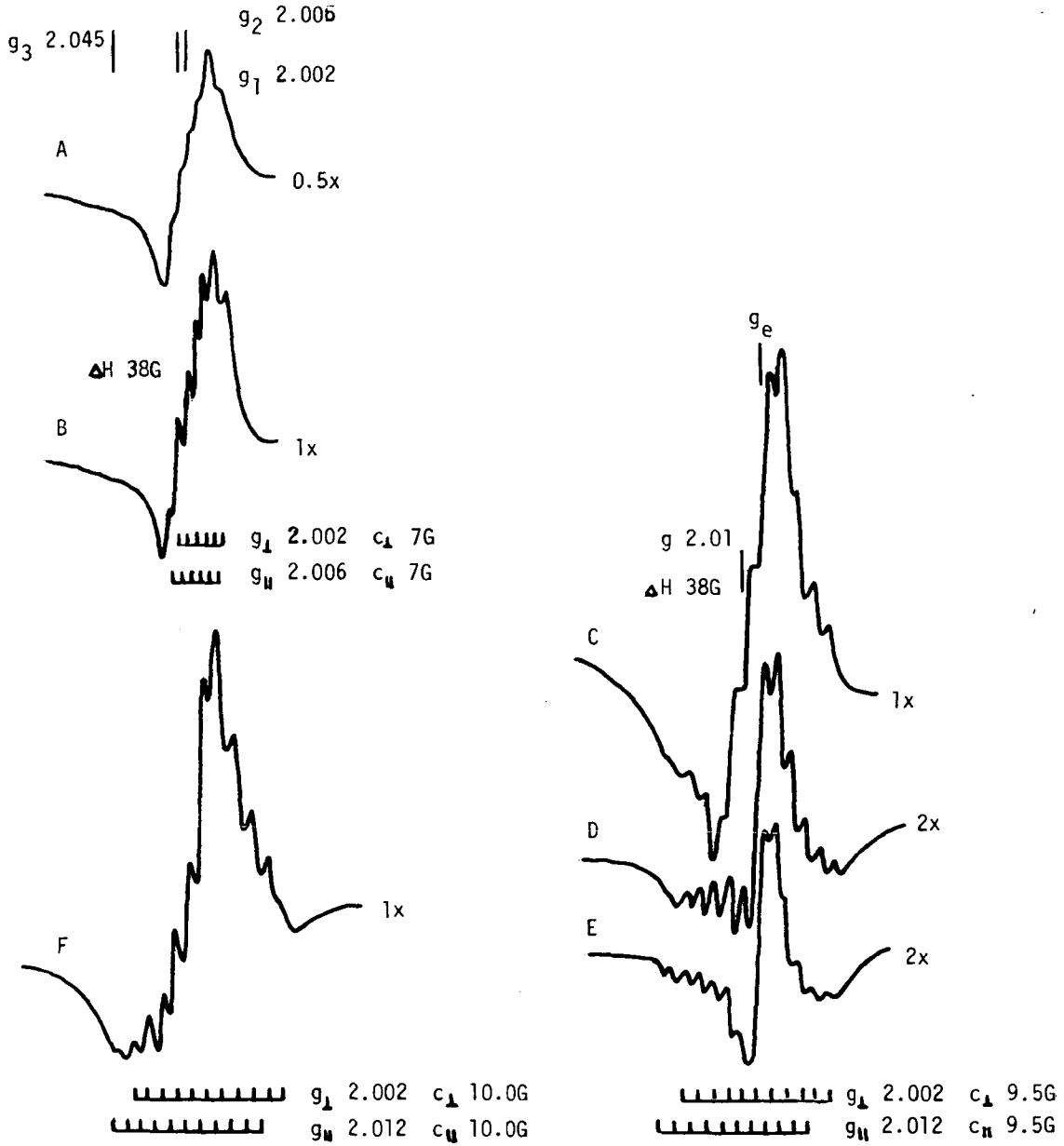

Fig. 1. X-band ESR spectra of γ-irradiated zeolites at 298 K recorded at 80 K A) HY, B) HZSM, C) AlHY, D) AlHY + $1.33.10^4$ Pa of H_2 for 15 minutes, E) AlHY + + $1.33.10^4$ Pa of H_2 for 24 hours, F) Al_xO_yHZSM-5

signal of ΔH=38 G with hyperfine splitting of 7 well resolved lines with the parameters given in Fig. 1B. This complex signal can be analogously attributed to the skeletal Si-O-Al and $(-O-)_n^{\cdot}$ defects. The better resolution of the hfs lines for HZSM compared to the HY zeolite may be a result of the low amount of Al in the skeleton of the HZSM-5 zeolite, as well as the higher degree of localization of defects arising from its lower structural symmetry. After treatment of the zeolite in hydrogen, the complex signal vanished and a signal close to g_e and a low intensity signal with 12 lines appeared. The latter signal is likely due to some additional defects on oxygen neighbouring extralattice Al (for comparison, see below) as such Al has been found in trace amounts in HZSM-5 zeolite using the IR spectra of pyridine adsorption (10).

AlHY zeolite. The zeolite with Al in the cationic sites (extralattice) and in the zeolite skeleton exhibits a broad signal with 12 hyperfine lines. The spectrum and its parameters are given in Fig. 1C. Treatment of the zeolite with hydrogen resulted in a decrease in the broad signal and in retention of the signal with 12 hfs lines and of the signal close to g_e (Fig. 1D). The intensity of the signal at g_e was constant, while the intensity of the splitted signal decreased slowly with time (Fig. 1E).

It is, therefore, evident that the spectrum of the irradiated zeolite consists of three particular signals: i) the sharp signal close to the g_e value (already mentioned), originating from the ejected electrons trapped within the zeolite material; ii) the signal with hfs of 12 lines (9.5 G) corresponding to an electron hole on an oxygen atom interacting with two Al atoms (12 lines being due to uniaxial symmetry of the g factor, cf. ref. 3, see Fig. 1C), iii) the broad signal which originates from the skeletal $(-O-)_n^{\cdot}$ defects already described for H-zeolites. Localized spin density on Si-O-Al defects is not present probably because of the easier formation of Al-O-Al defects in which one skeletal and one extralattice Al atom participate (cf. Fig. 2 model C). Then it is quite understandable that there is nearly zero probability of the creation of two defects close together.

Al_xO_yHZSM-5 zeolite. This zeolite with extralattice Al in the form of Al^{III} supported in the zeolite cavities again exhibits a complex broad signal with 12 well resolved hfs lines (10.0 G), indicating that, in addition to skeletal defects, the Al-O-Al defects are formed as a result of zeolite irradiation (Fig. 1F). Analogously as for the AlHY zeolite, the presence of hydrogen did not cancel the signal with 12 hfs lines. It can be assumed that in this zeolite, extralattice Al should exhibit various forms. It may possess a charge-balancing character or it may correspond to alumina species coordinate to the zeolite skeleton (cf. various species e.g. of Fe^{III} supported in zeolite (11)).

As for the stability of the V defects in γ-irradiated zeolites the ESR signal intensity of defects in HY zeolites was stable for several hours at 298 K, while that for AlHY and Al_xO_yHZSM-5 for several weeks. However, the signal intensity for HZSM-5 was slightly more stable than that for the HY zeolite. The total number of all

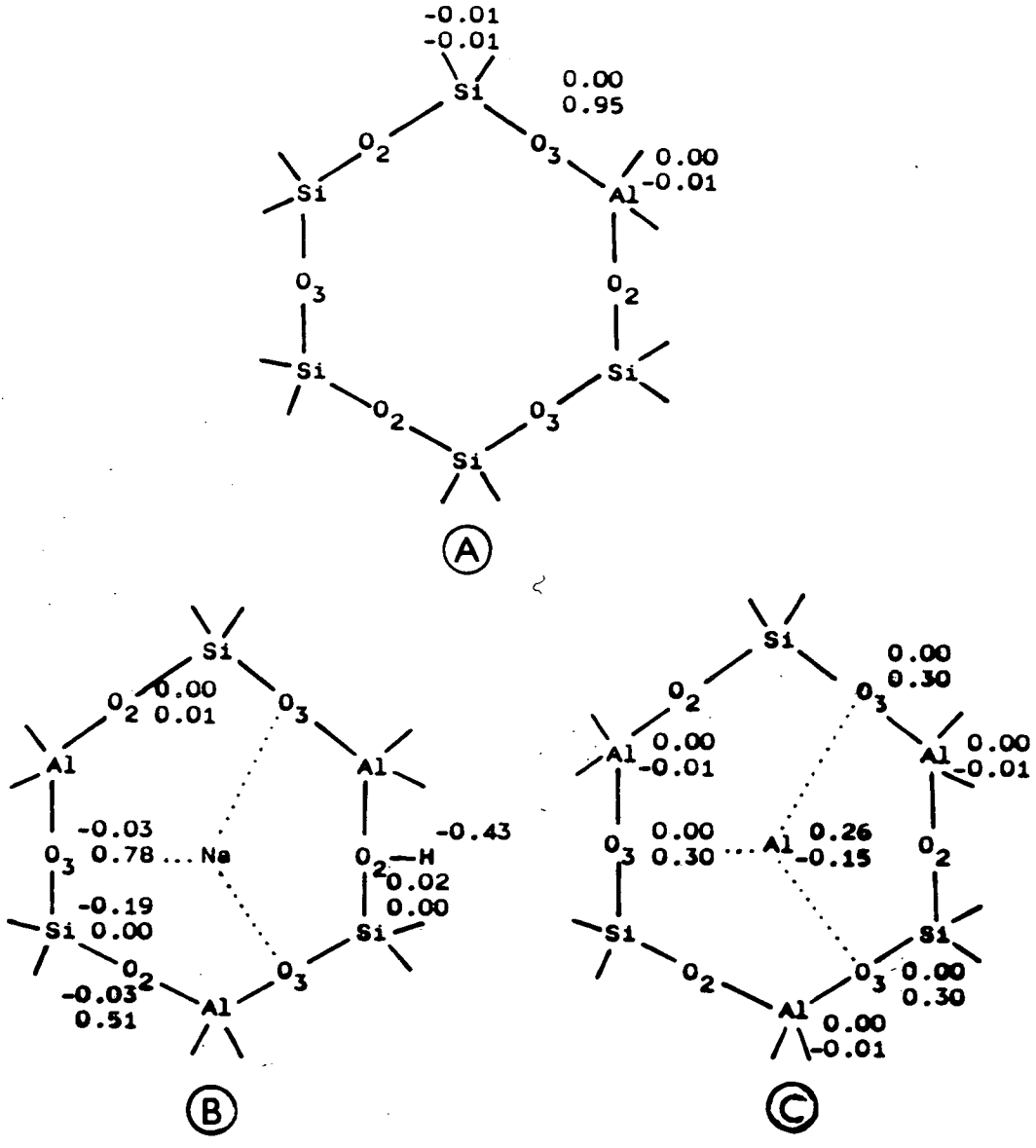

Fig. 2. Schematic depiction of the clusters studied with indication of spin densities (higher or equal than 0.01) in the s atomic orbital (upper value) and in the p atomic orbital (lower value) on individual atoms. Positive values stand for α spin densities and negative for β spin densities.

defects is of the order of 10^{19}, i.e. it is substantially lower than the number of sites available for their formation. This is understandable from the point of view of the low stability of these defects as well as of the ejected electrons trapped in the zeolite material. The number of the individual defects is difficult to estimate because of the signal overlap.

Model quantum chemical calculations on defects in γ-irradiated zeolites

Localization of anunpaired electron in the H- and Al-forms of faujasites was also investigated by means of model quantum chemical calculations. The standard version of the UHF CNDO/2 method (12) with an s,p base for Si and Al atoms was employed (13) in the calculations. The zeolites were then modelled using the following cluster models: i) The $Si_5AlO_6(OH)_{12}^-$ cluster, representing a six-member zeolitic window facing the large cavity (Fig. 2A); ii) The $Si_3Al_3O_6(OH)_{12}NaH^\cdot$ cluster, depicting the same window with the Na cation coordinated in the S_I cationic position and the skeletal hydroxyl group formed by the O_2 type of oxygen (Fig. 2B); iii) The $Si_3Al_3O_6(OH)_{12}Al^\cdot$ cluster, modelling the same window with an Al cation again situated in the cationic position (Fig. 2C). The models were terminated by H atoms and their geometry characteristics were taken from X-ray data (14).

The values of α- and β-spin densities calculated for the clusters studied are listed in Fig. 2. From these values it follows that: i) If no cations or protons are bonded to the zeolitic skeleton, the unpaired electron is mainly located in the lone pair orbital of the skeletal oxygen atom bonded to the Al and Si atoms. The remaining part of the α-spin density is delocalized over the whole cluster. Only a very small amount of β-spin density is also situated on the Si and Al atoms adjacent to the O atom bearing the major part of the unpaired electron. ii) If, in addition to the Na cation, a proton is bonded to the skeletal O_2 atom, the α-spin density is again located in the lone pair orbital of the skeletal O atoms. Simultaneously, however, a relatively large amount of the β-spin density is found on the H atom forming this OH group. iii) When an Al cation is coordinated in the cationic position, the unpaired electron is mainly located on the Al cation and in the lone pair orbitals of the O_3 atoms coordinating this cation. A very small amount of the β-spin density is also situated on the skeletal Al atoms.

Catalytic activity of defects in the γ-irradiated zeolites in D_2-H_2 exchange

The activity of irradiated zeolites can be ascribed to the defects formed by their irradiation, as original zeolites listed in Table 2 did not exhibit any D_2-H_2 exchange activity at 298 K. While the defects formed in the HY zeolite exhibit relatively low activity which completely disappears after the zeolite treatment in hydrogen at low pressure, the zeolites with extralattice Al possess substantially higher and very stable activity. The activity of the Al_xO_yHZSM-5 zeolite was stable even after exposure of the zeolite to 10^5 Pa of hydrogen for 1 hour. The higher and stable activity of ZSM-5 compared to the Y zeolites can be accounted for in terms of

Table 2

Rate of the D_2-H_2 exchange on irradiated zeolites at 298 K

Irradiated zeolite	HY	AlHY	HZSM-5	Al_xO_yHZSM-5
$R.10^{-19}$ atom/min.g	0.2	3.9	6.1	19.8
$R^a.10^{-19}$ atom/min.g	0	2.4	6.1	19.8

[a] after zeolite treatment in 4.10^{19} molecules of hydrogen at 298 K for 1 hour

the structural differences together with the presence of some extralattice Al, which is always present in small amounts in the HZSM-5 zeolite (see above and ref. 10).

CONCLUSIONS

The results given indicate that γ-irradiation of zeolites may produce electron holes located at various sites of the zeolite structure, depending on the type of zeolite. With H-zeolites not containing extralattice Al, electron holes are mainly localized in lone pair orbitals of the skeletal oxygen atoms. A small amount of spin density is also situated on the adjacent Al atom. Therefore, they correspond to the skeletal Si-O-Al and $(-O-)_n^{\cdot}$ defects. On the other hand, if the zeolite contains extralattice Al species (either in the cationic form or supported in the zeolite cavities) then, in addition to the Si-O-Al and $(-O-)_n^{\cdot}$ defects, it exhibits an electron hole on an oxygen atom neighbouring two Al atoms (Al-O-Al). These defects seem to be formed by a skeletal oxygen bonded to one skeletal and one extralattice Al atom. Moreover, a substantially larger amount of spin density appears to be located on the Al atoms compared to the Al-O-Si defects. Nevertheless, the presence of Al-O-Al defects formed by two extralattice Al atoms cannot be fully excluded, but their existence seems to be less probable as they have never been observed in pure γ-irradiated aluminas. Much higher stability of the Al-O-Al defects compared to the remaining observed defects in a hydrogen atmosphere is understandable, as the latter defects are capable of capturing hydrogen and formed OH groups. On the contrary, supposing that the Al-O-Al defects consisted of a skeletal oxygen sharing one skeletal and one extralattice Al atom, then the lone pair orbitals of this oxygen are saturated by the extralattice Al and, therefore, it can bond an additional H atom only with difficulty.

In this way it is also possible to explain different activities of γ-irradiated H- and Al-zeolites in D_2-H_2 exchange. All irradiated zeolites exhibit very high activity even at a low temperature at which the original zeolites are quite inactive. Particularly the presence of Al-O-Al defects substantially increases and stabilizes the zeolite activity. The reactivity of the Al-O-Al, Al-O-Si and $(-O-)_n^{\cdot}$ defects in the

D_2-H_2 exchange cannot be simply compared, as the latter two defects are quickly annihilated by the interaction with hydrogen. For Si-O-Al defects, this process seems to be consistent with the following scheme

$$\dot{\text{Si}}\text{-O-Al} + H_2 = \text{Si-}\underset{\text{H}}{\text{O}}\text{-Al} + H^+$$

explaining both annihilation of the $\dot{\text{Si}}$-O-Al defects and limited D_2-H_2 exchange. The delocalized $(\text{-O-})_n^{\cdot}$ skeletal defects are probably eliminated in a similar way.

REFERENCES

1. Stamires, D.N. and Turkevich, J., J, Amer. Chem. Soc. 86, 757 (1964).
2. Wang, K.M. and Lunsford ,J.H., J. Catal. 24, 262 (1972).
3. Vedrine, J.C., Abou-Kais, A., Massardier, J. and Dalmai-Imelik G., J. Catal. 29, 120 (1973).
4. Vedrine, J.C. and Nacchache, C., J. Phys. Chem. 77, 1606 (1973).
5. Abou-Kais, A., Vedrine, J.C., Massardier, J. and Dalmai-Imelik, G., J. Chem. Soc., Faraday Trans. 1, 70, 1039 (1974) and refs. therein.
6. Abou-Kais, A., Vedrine, J.C. and Massardier, J., J. Chem. Soc., Faraday Trans. 1, 71, 1697 (1974).
7. Garibov, A.A. and Melikadze, M.M., Zhur. Fiz. Chim. 54, 2607 (1980).
8. Gupta, N.M., Kamble, V.S. and Iyer ,R.M., J. Catal. 66, 101 (1980).
9. Parijsky, G.B., Mischenko, Yu.A. and Kazansky, V.B., Kin. Katal. 6, 625 (1965).
10. Novakova, J., Kubelkova, L., Habersberger, K. and Dolejsek, Z., J. Chem. Soc., Faraday Trans. 1, 80, 1457 (1984).
11. Novakova, J., Kubelkova, L., Wichterlova, B., Juska, T. and Dolejsek ,Z., Zeolites 2, 17 (1982).
12. Pople, J.A. and Beveridge, D.L. , Approximate Molecular Orbital Theory, Mc Graw-Hill, New York, 1970.
13. Beran, S. and Dubsky, J., J. Phys. Chem., 83, 2538 (1979).
14. Eulenberger, G.R., Schoemaker, D.P. and Keil, J.G., J. Phys. Chem. 71, 1812 (1976).

INFLUENCE OF BASICITY OF NITROGEN BASES ON THE HEAT OF THEIR PROTONATION ON THE SURFACE OF HNaY ZEOLITE

YU.D. PANKRATIEV, E.A. PAUKSHTIS, V.M. TURKOV, E.N. YURCHENKO
Institute of Catalysis, Novosibirsk 630090, USSR

ABSTRACT

The heats of protonation of ammonia, butylamines, triethylamine, pyridine and a series of its derivatives on HNaY zeolite have been measured by calorimetric method. The heat of protonation has been shown to depend primarily on proton affinity of the base and on the number and strength of hydrogen bonds between ions and oxygen atoms on the zeolite surface.

INTRODUCTION

One of the key problems of heterogeneous acid catalysis is elucidation of the principles that determine the capability of acid centers to protonate probe and reagent molecules. Accumulated numerous experimental data indicate that the interaction of nitrogen bases with protic catalytic centers leads to the formation of ions. In this work the heats of protonation of ammonia and a series of amines that differ in their basicity (primary, secondary and tertiary butylamines, triethylamine, pyridine, 2-chloropyridine, 2,3- 2,5- and 3,5-dimethylpyridines and 2,4,6-trimethylpyridine) on HNaY zeolite were measured by calorimetric method. The molecule of ammonia as the simplest one of the above molecules was used for the analysis of the specificity of the interaction between ions and the surface. The use of other bases was necessitated by the elucidation of all factors determining the protonation heat.

EXPERIMENTAL

The 2.2 wt.% Na zeolite with SiO_2/Al_2O_3=4.8 was used. Prior to IR spectroscopic experiments, the zeolite was pressed into tablets (8-12 mg/cm^2) and calcined in vacuum at 723 K for 2 hr. Adsorbates were dried with the NaA zeolite and outgassed by repeated freezing out. Adsorption was performed at room temperature at a pressure of saturated vapors (10 mm Hg for ammonia) for 15-30 min. Spectra were

taken at room temperature (at 77 K for ammonia) using a UR-20 spectrometer immediately after adsorption, as well as after evacuation at 298, 423, 523, 623 and 723 K for 1 hr.

Prior to adsorption-calorimetric measurements, the zeolite samples were treated either in vacuum or in pure helium at 723 K for 3 h. The adsorption of ammonia was examined at 423 K in a volumetric system.

The adsorption of organic bases was studied at 373-473 K in a flow system containing a gas chromatograph furnished with an integrator (see Fig. 1). Such simple construction provides measurements of the quantity of the adsorbate at the inlet and outlet of the calorimetric cell filled with a catalyst. The difference between these quantities allows of the determination of the adsorption value, provided that no blowing out of the adsorbed substance by the carrier-gas occurs. With adsorption heats of 40-80 kJ/mol the blowing out is observed at low surface coverages of the catalyst by the substance under study.

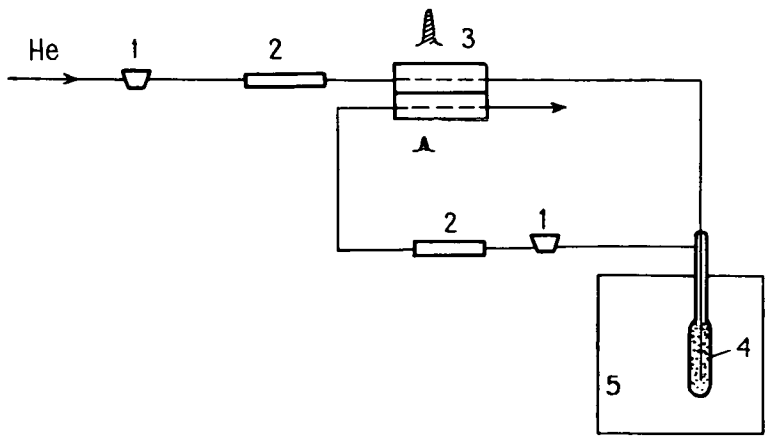

Fig. 1. Flow-adsorption system:
1 - vaporizer,
2 - chromatographic column,
3 - heat-conducting detector,
4 - calorimetric cell filled with the catalyst,
5 - Tian-Calvet-type calorimeter

Dozing of the adsorbates was made by microsyringe. All parts of the system were heated up to 400-423 K to prevent vapor adsorp-

tion on its walls. Purified helium (content of impurities was no more than 1 ppm) was used as carrier-gas, its flow velocity being 30 cm^3/min. Adsorption heat measurements were stopped with the first signs of blowing out of the adsorbed substance from the catalyst surface.

RESULTS AND DISCUSSION

1. As shown by IR data, during the adsorption of all bases used in the work the intensity of the ν_{OH} 3640 cm^{-1} absorption band ascribed to OH-groups localized in large cavities of the zeolite framework decreases. This decrease is proportional to the quantity of the adsorbed base. In the case of ammonia, the intensity of the ν_{OH} 3550 cm^{-1} absorption band, corresponding to OH-groups in small zeolite cavities, also decreases. The variations in both line intensities were nearly the same. One may suppose that the difference in the behavior of OH-groups with respect to ammonia and organic amines is due to their different accessibilities. During the course of desorption over the temperature range from 423 to 723 K the line intensities of the adsorbed bases decrease and the line intensities of hydroxyl groups are reduced in a similar way. Spectra of amines themselves on the HNaY zeolite considerably differ from spectra of liquid bases and those physically adsorbed on NaY and silica, as well as from spectra of amines on alumina. They are similar to the corresponding spectra of hydrochlorides. To our opinion, these facts provide a sufficient evidence for the protonation of amines during their interaction with the HNaY zeolite surface producing BH^+ ions.

2. Adsorption heats of ammonia, pyridine and its derivatives, butylamines and triethylamine on HNaY zeolite at 373, 423 and 473 K are shown in Figs. 2-4. For ammonia, the adsorption heat almost linearly falls with a coverage increase at the initial period of time, then reaches a minimum (25 kJ/mol) at adsorption about 2500 μmol/g and further remains constant. In the region of the adsorption heat constancy the equilibrium pressure of ammonia over the sample increases almost linearly with coverage. It is reasonable to suppose [1] that this linear region is the part of the Henry isotherm of ammonia adsorption, which is characterized by an adsorption heat of 25 kJ/mol. Unfortunately we failed to strictly identify the nature of these adsorption sites.

By subtracting the linear component from the total adsorption isotherm we have obtained curve 2, which seems to describe the interaction of ammonia with the most acidic hydroxyl groups of the zeolite

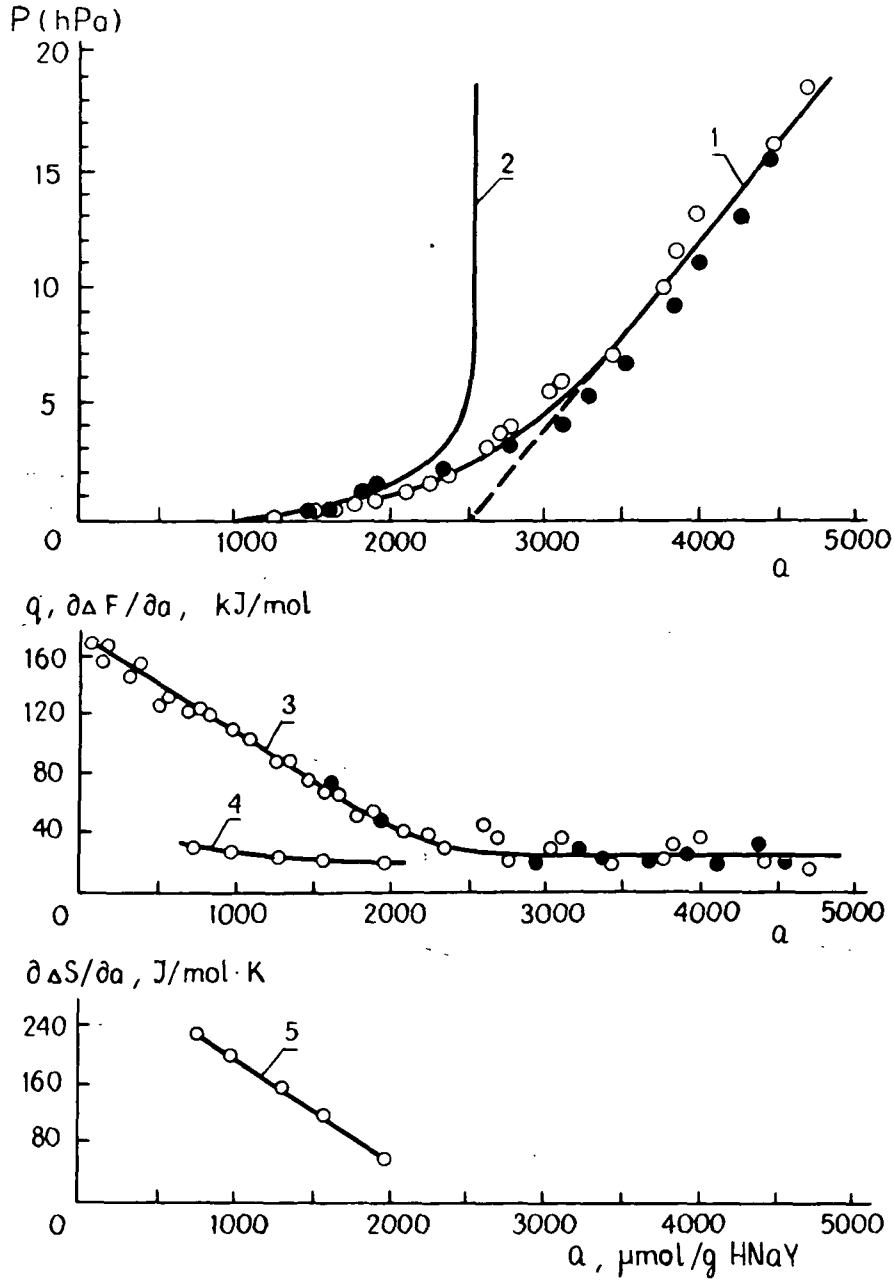

Fig. 2. Equilibrium pressure (1), differential values of heat (3), free energy (4) and entropy (5) of ammonia adsorption on HNaY zeolite at 423 K versus adsorption (light points - adsorption, filled points - desorption)

surface. For the range of surface coverages from 750 to 2000 μmol NH_3/g HNaY, within which the equilibrium pressure of ammonia increases from 0.017 up to 1.6 hPa, from curve 2 we have calculated the dependence of the integral free energy of NH_3 protonation ($\Delta F(a) = -RT \ln K(a)$, where $K(a) = a/p(a^{max} - a)$) and the differential free energy (curve 4). As is seen, in contrast to the adsorption heat, the free energy of ammonia protonation changes slightly with coverage variations, i.e. nearly complete compensation effect occurs. The adsorption entropy (curve 5) is close to the total entropy of gaseous ammonia at the temperature of experiment when the surface coverage does not exceed 1000 μmol NH_3/g HNaY. This indicates a very rigid binding of NH_3 molecules to the zeolite surface at these coverages. The molecules thus lose all translational and rotational degrees of freedom.

Fig. 3 shows the adsorption heats of pyridine and its derivatives on HNaY measured by successive delivery of the substances on the same zeolite sample. It is seen that the chemical nature and the number of substituents reveal a strong effect on the base adsorption heat. The adsorption heats of butylamines, triethylamine and pyridine measured on different zeolite samples over a wide range of surface coverages are presented in Fig. 4. Noticeable dependence of the adsorption heats on coverage is observed only for pyridine and triethylamine.

3. The protonation heat of bases on the catalyst surface can be defined as a sum of three terms [2]: $q_{H^+} = PA^B - PA^a + q_B$, where PA^B and PA^a are affinities to proton of the base and acid residue, respectively; q_B is the energy of BH^+ binding to the surface. In turn, q_B can be described as a sum: $q_B = q_x + nq'$, where q_x in the first approximation is the electrostatic component of the bond and q' is the energy of the hydrogen bond formation. For HNaY q_x was found to be constant for all bases. Thus, we obtain $(q_{H^+} - nq') = PA^B - (PA^a - q_x)$, i.e. the protonation heat of bases on HNaY (after subtraction of the energy of formation of hydrogen bonds) is linearly dependent on their proton affinities. In order to find q', it is possible to use a known formula: $q' = 1.3(\nu^0_{NH} - \nu^{c.g.}_{NH} - 40)^{0.5}$, which relates the heat of formation of H-complexes with the shift of the NH-bond stretching band [3].

For all studied bases, except for ammonia and butylamines, a single hydrogen bond is formed during the adsorption. In the case of ammonia and butylamines, the formation of two or even three hydrogen bonds seems to be possible. This supposition is supported by

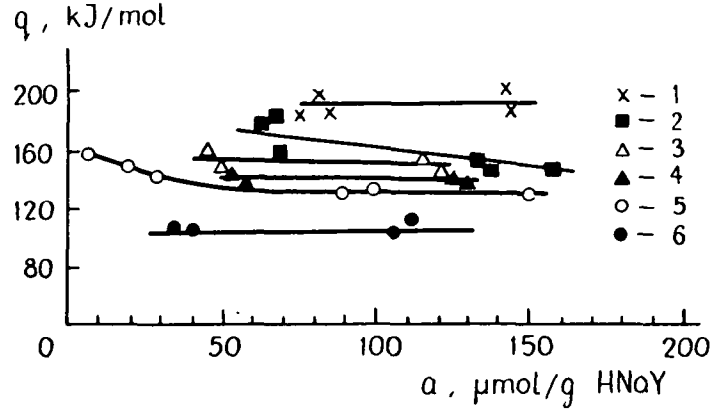

Fig. 3. Adsorption heats of pyridine and its derivatives on HNaY zeolite at 473 K: (1) 2,4,6-trimethylpyridine, (2) 3,5-dimethylpyridine, (3) 2,3-dimethylpyridine, (4) 2,5-dimethylpyridine, (5) pyridine, (6) 2-chloropyridine

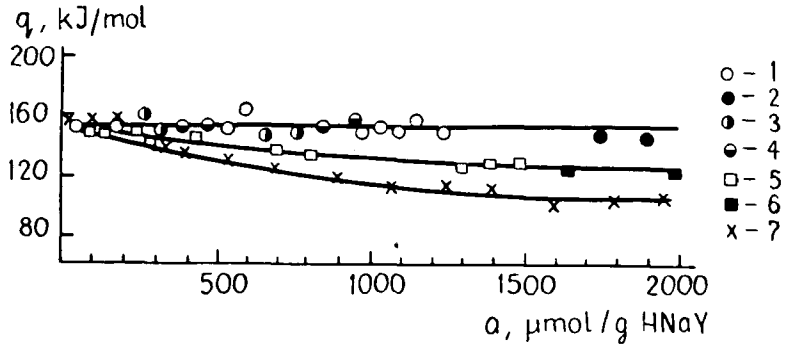

Fig. 4. Adsorption heats of primary butylamine at 423 (1) and 373 K (2); secondary (3) and tertiary (4) butylamines at 423 K, triethylamine at 423 K (5) and 373 K (6), pyridine (7) at 423 K on HNaY zeolite

the above data on entropy variations during ammonia adsorption on the HNaY zeolite, as well as by the analysis of IR spectra in the region of deformation vibrations. At 90-100 K in the range 1300-2000 cm^{-1} the bands at 1370, 1433 and 1490 cm^{-1}, and also at 1690 and 1850 cm^{-1} were observed. The former bands are attributed to the splitted components of antisymmetric deformation vibration of the free ion, while the latter bands correspond to the splitted components of symmetric deformation vibration of the same ion. According to the calculations made by E.B. Burgina, for the ion bound to the zeolite surface only via one hydrogen bond one can expect

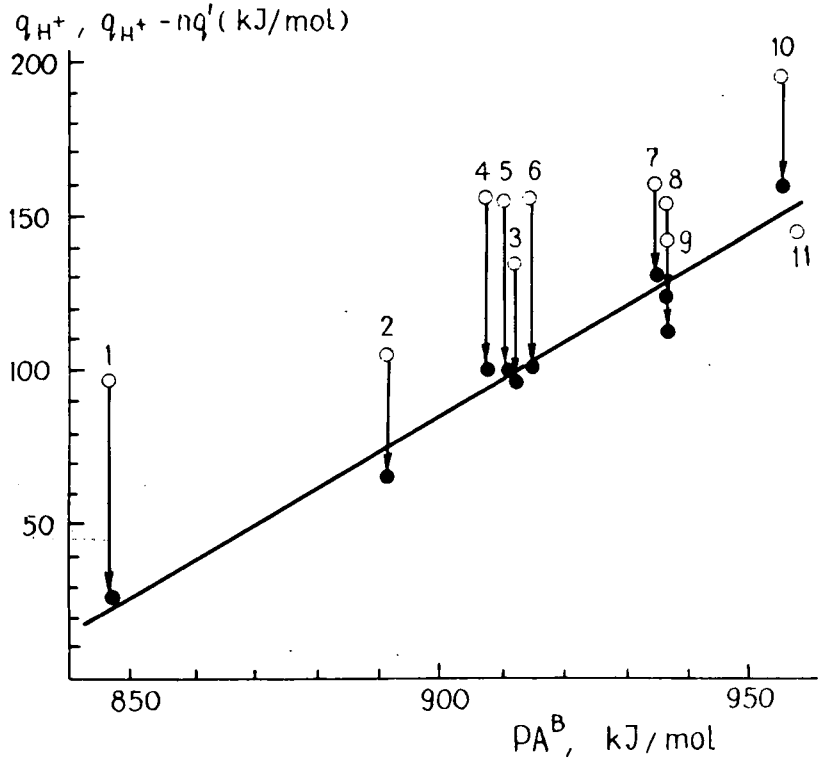

Fig. 5. Comparison of integral heats of protonation of bases on the surface of HNaY zeolite (light points) and theirfrom calculated values of (q_{H^+} - nq') (filled points) with proton affinity of adsorbed molecules (PA^B): (1) ammonia, (2) 2-chloropyridine, (3) pyridine, (4) primary butylamine, (5) secondary butylamine, (6) tertiary butylamine, (7) 3,5-dimethylpyridine, (8) 2,3-dimethylpyridine, (9) 2,5-dimethylpyridine, (10) 2,4,6-trimethylpyridine, (11) triethylamine

the same number of components in the range from 1300 to 2000 cm^{-1}. However, the splitting values between them seem to be much smaller.

A comparison of measured integral heats of protonation of the bases on the HNaY zeolite surface and theirfrom calculated values of (q_{H^+} - nq') with proton affinities PA^B is shown in Fig. 5. If one assumes that in the case of ammonia and butylamines n=2, i.e. during the adsorption of each molecule two hydrogen bonds are formed, there is a good correlation between (q_{H^+} - nq') and PA^B. Low value of the heat of triethylamine protonation may be accounted for by steric hindrances during its adsorption on the zeolite [4].

REFERENCES

1. Garrone, E., Ghiotti, G., Giamello, E., Fubini, B., J.C.S. Faraday Trans. I, 77, 2613 (1981).
2. Paukshtis, E.A., Yurchenko, E.N., Usp. Khim. 52, 428 (1983).
3. Iogansen, A.V., Dokl. Akad. Nauk SSSR 184 , 610 (1965).
4. Jacobs, P.A., Theng, B.K.G., Uytterhoeven, J.B., J. Catalysis 26, 197 (1972).

FLUORINE MODIFICATION OF ZEOLITE CATALYSTS

K. A. BECKER[a], K. FABIANSKA[a], S. KOWALAK[b]
Fritz-Haber-Institut der Max-Planck-Gesellschaft, Berlin (West), F.R.G. (a)
A. Mickiewicz University, Poznan, Poland (b)

ABSTRACT

The introduction of fluorine into the zeolite phase can significantly change the catalytic activity of the zeolite. The dependence of the catalytic activity of modified samples on the fluorine content was determined for acidic-type reactions. In addition, the acidic centers in the fluorinated zeolites were studied using microcalorimetric measurements of the heat of ammonia adsorption. For ZSM 5-type zeolites the influence of an assumed ordered center distribution on the activity is discussed.

INTRODUCTION

Fluorine is often used as a component and a modifier of catalysts [1]. During the last few years some fluorine modifications of zeolites have been described.

Araya et al. [2] studied zeolites containing occluded salt molecules, introduced to the inner zeolite structure by means of heating in molten salts. They found that unlike samples containing Cl^- and NO_3^-, only some of the occluded F could be removed by water elution from the zeolite phase. The authors suggested that two different fluoride species had been incorporated into the lattice.

Sariev and coworkers [3-5] reported on their modifications of zeolite catalysts with diluted HF aqueous solutions. Normally the catalytic activity of the samples was increased after a mild fluorination. However, introduction of larger amounts of fluorine caused a decrease in catalytic activity and usually in crystallinity. The authors considered the possibility of bonding fluorine to the framework Al atoms or to the cations present in the zeolite.

Lok et al. [6, 7] used diluted gaseous fluorine at nearly room temperature for zeolite fluorination. They found that the properties of the fluorine-modified zeolites can be controlled by the fluorination

conditions and the post-treatment conditions. Under severe treatment conditions zeolites usually showed high dealumination, hydrophobicity of the surface, reduction in catalytic activity and changes in crystalline structure. Under mild conditions catalytic activity for n-butane cracking was significantly enhanced.

We also found in our earlier investigations a significant influence of fluorine presence on the catalytic activity of zeolites [8-12]. The samples of AlY zeolites fluorinated using NH_4F solution without prior calcination showed a considerable increase in catalytic activity for cumene cracking. A sample preheated before fluorination showed low activity and poor crystallinity. We believe that fluorine reacts mainly with Al-bearing cations yielding the catalytically active products still present in the inner zeolite structure [8, 9].

According to our experiments [10] fluorination of HY zeolite usually brought about a reduction of both crystallinity and catalytic activity. HY zeolites modified with Al cations before fluorination, however, showed a good crystallinity and high activity for cumene cracking [11].

Fluorination of H-mordenite by means of NH_4F aqueous solution or by treatment with gaseous CHF_3 resulted in a significant increase of activity for cumene cracking. The maximum increase of activity was observed for the sample containing about 0.4 wt. % of fluorine. A further increase of the fluorine content caused a decline of activity. Calorimetric measurements of the heat of ammonia adsorption showed a generation of new stronger acidic centers. We believe that during the fluorination some of the acidic OH groups were substituted with fluorine. The number of the hydroxyl groups was reduced, but the strength of the remaining ones was enhanced due to the inductive effect of fluorine [12].

The aim of the following study is to determine the influence of fluorination on the catalytic properties of ZSM 5-type zeolites. The samples were prepared by BASF according to its patent [13].

The patent authors have found that polyamines as templating agents can produce ZSM-type zeolites of well-ordered Al atom distribution. Such a structure can be obtained if the SiO_2/Al_2O_3 ratio has a specified value dependent on the templating amine used. In these so-called "isotactic" forms the distances between the Al atoms should be similar to those of the NH_2 groups in the amine molecules. We have some evidence that this well-ordered Al distribution stimulates a "geometric" selectivity in catalytic reactions of appropriate molecules. Therefore, it seemed interesting to check the influence of fluorination on this kind of selectivity.

EXPERIMENTAL

Samples of ZSM-5 zeolites, supplied by BASF and labeled as ZBM 10/4 and ZBM 12/1, were taken as starting materials. 1,6-diaminohexane and 1,3-diaminopropane, respectively, were used as templates during the preparation. The respective silica to alumina rations of the initial samples were 32.2 and 25.3. These values correspond to those of an isotactic structure.

The samples were calcined at 500° C to remove the remainders of the template. Samples labeled ZBM 10/4F1, -F2, -F3, and ZBM 12/1F1, -F2, -F3, were modified with fluorine by means of NH_4F aqueous solutions. In the case of sample 10/4FG gaseous CHF_3 was used for fluorination [10, 12, 13]. The conditions of the fluorination procedure and the properties of the samples under study are summarized in Table 1.

Table 1

Sample	Conditions of Modification	F-Content Weight %	SiO_2/Al_2O_3 Ratio
10/4		0	32.2
10/4F1	8g zeolite, 160ml 0.025M NH_4F-solution for 20h at room temperature, 12h at 100°C, 12h at 450°C in air stream	0.18	34.5
10/4F2	8g zeolite, 5x160ml 0.1M NH_4F-solution for 5x12h at room temperature, 12h at 100°C, 12h 450°C in air stream	0.23	36.4
10/4F3	8g zeolite, 160ml 0.1M NH_4F-solution for 20h at room temperature, 12h at 100°C, 12h at 450°C in air stream	0.25	36.5
10/4FG	8g zeolite, calcined in He-stream at 450°C, treated with 500ml CHF_3 (diluted with He) at 260°C for 6h	0.30	
12/1		0	25.3
12/1F1	as for 10/4F1	0.18	35.7
12/1F2	as for 10/4F2	0.53	33.8
12/1F3	as for 10/4F3	0.47	36.7

The crystallinity of the samples was examined by X-ray diffraction The calorimetric measurements of the heat of ammonia adsorption for selected samples were carried out with a Calvet microcalorimeter using a volumetric method for the estimation of the amount of adsorbed ammonia. Results are shown in Figure 1.

The catalytic properties of the modified samples were examined for hexadiene isomerization and cumene cracking. Both test reactions were

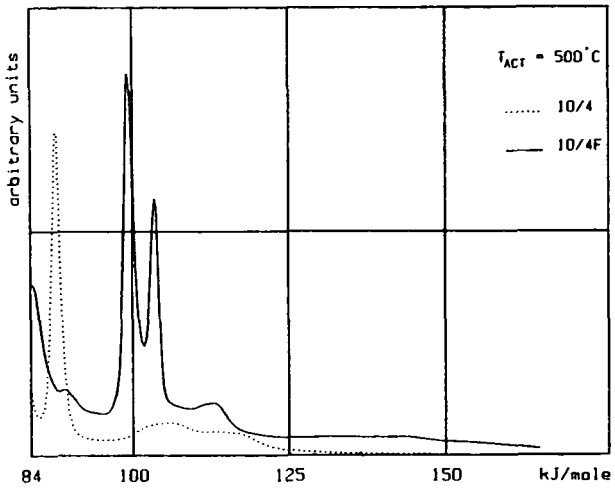

Fig. 1. Section of acidity spectra of ZBM 10/4 and ZBM 10/4F1 (concerning the strongest sites)

carried out using pulse microreactors. 20 mg of the catalyst (particles of 0.125-0.25 mm in diameter) were activated in a helium stream (300 ml/min) for 7 h at 450°C before the reaction. 1 µl pulses of hexadiene isomers (1,3; 1,5 and c1,4) were injected at the reaction temperature of 150°C. For the cumene cracking, 10 mg of powder samples were heated at 450°C for 1 h prior to reaction in a helium stream (80 ml/min). Reaction tests were carried out at 350°C. 10 pulses of 1 µl were injected and in addition pulses at 200° and 250°C were applied. The results are presented in the Figures 2 and 3.

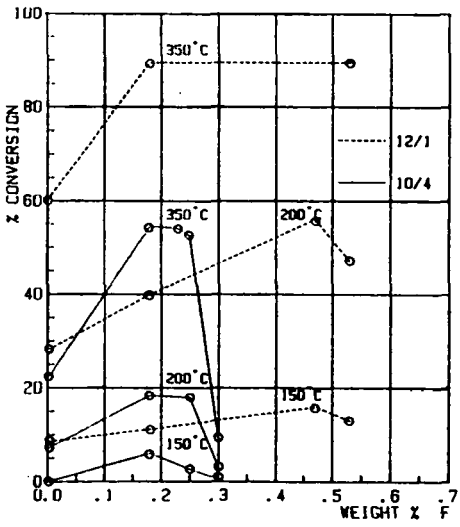

Fig. 2. Correlation between cumene cracking and fluorine content of catalyst

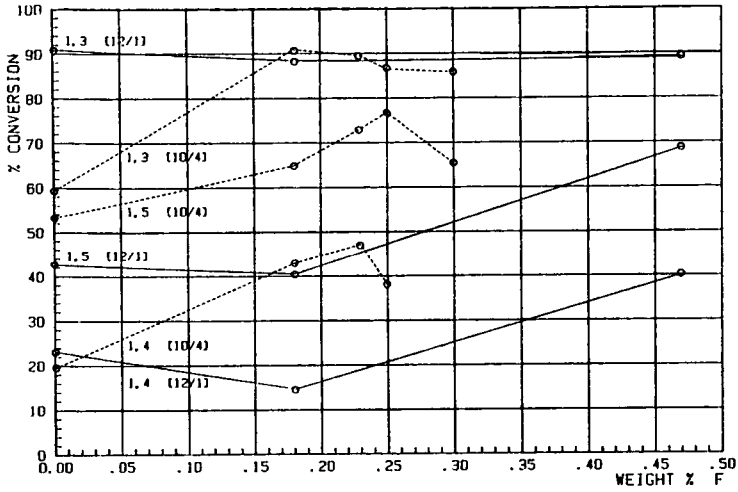

Fig. 3. Correlation between isomerization of hexadienes and fluorine content of catalyst

RESULTS AND DISCUSSION

According to the X-ray diffraction data the fluorine introduced to the ZSM-type zeolite does not affect significantly the crystalline structure. The intensities of the diffraction peaks for the fluorinated samples are similar to those of the initial ones.

The procedure applied for fluorination of ZBM zeolites was very similar to that of H-mordenite [12]. The amounts of fluorine introduced, however, are much smaller. The maximum of fluorine content for the 12/1 zeolite was about 0.5 %, whereas in the case of 10/4 it was only 0.25 % (using NH_4F solution for fluorination). The Si/Al ratio of 10/4 is higher than that of 12/1, but in the case of 12/1 this ratio increases during the fluorination process probably due to dealumination. The comparison of the maximum amounts of fluorine for both ZBM zeolites and H-mordenite leads us to the conclusion that a correlation exists between the Si/Al ration (which corresponds to the number of OH groups in the applied H-forms) and the capability for fluorine incorporation. The higher the framework Al content, the larger the amount of fluorine that can be introduced to the zeolite.

Such a correlation supports our supposition concerning fluorine-modified H-mordenite and suggests that the fluorine is introduced to the zeolite mostly by the substitution of OH groups. In the case of ZSM-type zeolites a similar method of fluorine incorporation is very likely. However, dealumination observed for the 12/1 series probably involves different sites of the zeolites framework for fluorination.

It may be worthwhile to mention that for fluorination with CHF_3

even a temperature as low as 260° C is sufficient to introduce fluorine, although Mc Vicker [14] suggested that the cleavage of a C-F bond is only possible at temperatures higher than 400°C.

The increase of activity is very pronounced in the case of cumene cracking, where strong Brønsted acid sites are involved. The activity of unfluorinated ZBM 12/1 is more than twice as high as that of ZBM 10/4. This difference can result from the higher content of acidic OH-groups in the first sample. Introduction of only 0.18 wt % of fluorine results for both zeolites in a strong increase of cumene conversion, observed even at low temperatures. The further incorporation of fluorine does not considerably change the activity of modfied samples. In the case of ZBM 10/4, however, a very sharp decrease of cumene conversion is seen above 0.25 Wt % of fluorine content whereas the sample 12/1 is still active above 0.5 % of fluorine. Some decrease in activity can be seen only at lower reaction temperatures. In our latest experiments, however, we prepared additionally a fluorine modified sample, containing more than 1 % of fluorine (a sample of ZBM 12/1F3 was fluorinated again with NH_4F). The decrease of activity for cumene cracking was very drastic, similar to the case of the 10/4 series (6 % conversion at 300°C, traces at 200°C, and 0 % at 150°C). Very similar catalytic behavior was observed in our investigation of fluorine-modified H-mordenite [12].

It is interesting to compare the catalytic activity of ZBM 10/4 and ZBM 12/1 for the reaction of 1,3-, 1,4- and 1,5-hexadiene and cumene with regard to the postulated differing distribution of the acidic centers in these zeolites. The comparison relates to the unfluorined forms and samples with the same fluorine content.

According to the concept of Marosi [13], under "isotactic" synthesis conditions such structures will be formed in which a favored arrangement of AlO_4^- tetrahedra is stimulated by the $NH_3^+ \ldots NH_3^+$ distances of the applied diamines. The corresponding acidic centers within the channel structure should show similar distances.

Concerning the isotactic 10/4 and 12/1 zeolites, the distances between the active centers of ZBM 10/4 are comparable to the distance of double bonds in 1,5-hexadiene, whereas for 12/1 a better fitting exists with 1,3-hexadiene. The distance between the double bonds in 1,4-hexadiene is similar to neither the center-to-center distances in the 10/4 nor in the 12/1 structure.

From Figure 4, in which the hydrocarbon conversion for one and the same reaction on both types of catalysts is compared, it is evident that for the non-fluorinated samples the ZBM 12/1 prefers the 1,3-con-

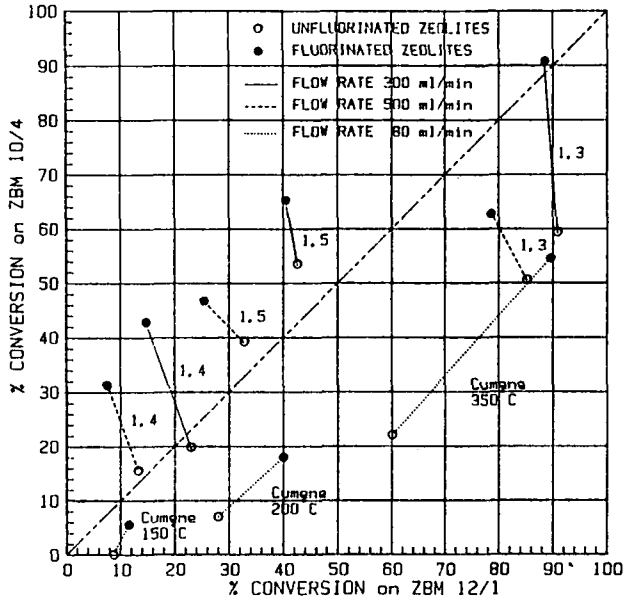

Fig. 4. Comparison of activity of fluorinated and unfluorinated ZSM 5-type catalysts for hydrocarbon reactions

version, whereas the ZBM 10/4 favors 1,5-conversion. Isomerization of 1,4-hexadiene proceeds for both catalysts with about the same yield. Since cracking of cumene involves only one acidic center a higher conversion is achieved with ZBM 12/1 because this type has a higher concentration of acidic centers due to its smaller SiO_2/Al_2O_3 ratio. In the case of cumene cracking the distances between centers are inconsequential.

The 10/4 and 12/1 types behave differently upon fluorination. Whereas ZBM 10/4 shows the expected increase in activity induced by fluorine, a slight decrease in activity occurs with 12/1. Chemical analysis of 12/1 and 12/1F1 (see Table 1), however, shows that in this case the fluorination is associated with dealumination. This probably causes an additional disturbance in the sequence of centers which could explain the observed reduction in the catalytic activity for 12/1. Since cumene cracking is independent of the ordering of the centers, the influence of the increase in acidity due to the fluorine presence dominates so that here an increase in activity results for both ZBM 10/4F1 and ZBM 12/1F1.

The increase in the catalytic activity of the fluorinated zeolites is more pronounced for cumene cracking than for hexadiene isomerization. The acidity spectrum presented in Figure 1 shows a generation of new, much stronger acidic centers after the fluorination. These newly

created centers are involved in catalyzing the cumene cracking, which requires strong acidic sites, and for this reason the fluorination effect on the catalytic activity for the cumene reaction is markedly stronger than that for isomerization.

The explanation of the nature of fluorine-bearing species introduced to the inner zeolite structure needs more extended investigation, including NMR-measurements.

ACKNOWLEDGEMENTS

We are most grateful to Dr. Marosi from BASF for supplying us with the unfluorinated ZBM samples and for helpful discussions. The authors are also indebted to Mrs. Köckeritz and Mr. Kollmitt for their valuable assistance in microcalorimetric and analytical measurements. Miss Wieczorek is acknowledged for fluorine determination. The financial support from the Fonds der Chemischen Industrie is gratefully acknowledged.

REFERENCES

1. Chaudhary, V.R., Ind. Eng. Chem. Prod. Res. Div., 16, 12 (1977).
2. Araya, A., Dyer, A. Zeolites, 1, 35 (1981).
3. Sariev, I.T., Penchev, V., Proc. IV. Int. Conf. Heterog. Catal., Varna, Publishing House of Bulgarian Academy of Sciences, Sofia 1979.
4. Penchev, V., Sariev, I.T., Zhelazkova, M.D., Kinet. Katal. 22, 732 (1981).
5. Zhelazkova, M.D., Sariev, I.T., Koralska, S.A., Heterogeneous Catalysis, Proc. V. Int. Symp., Varna, Publishing House of Bulgarian Academy of Sciences, Sofia 1983.
6. Lok, B.M., Izod, T.B.J., Zeolites, 2, 66 (1982).
7. Lok, B.M., Gortsema, F.P., Messina, C.A., Rastelli, H., Izod, T.B.J., "Intrazeolite Chemistry", ACS Symp. Series 218, 41 (1983).
8. Kowalak, S., React. Kinet. Catal. Lett., accepted
9. Becker, K.A., Kowalak, S., to be published
10. Becker, K.A., Kowalak, S., Kozlowski, M., React. Kinet. Catal. Lett., submitted
11. Fiedorow, R., Kowalak, S., Kozlowski, M., to be published
12. Becker, K.A., Kowalak, S., J.C.S. Faraday, accepted
13. DOS, DE 3006471 (27.08.1981).
14. Mc Vicker, G.B., Kim, C.J., Eggert, J.J., J. Catal. 80, 315 (1983).

MODIFICATION OF ZSM5 TYPE ZEOLITES WITH H_3PO_4

Johannes A. Lercher, Gerd Rumplmayr and H. Noller
Institut für Physikalische Chemie, Technische Universität Wien,
Getreidemarkt 9, A-1060 Vienna, AUSTRIA

ABSTRACT

The effects of H_3PO_4 upon the acidic and catalytic properties of ZSM5 zeolites were investigated. Pyridine and ammonia were found to adsorb on the same sites indicating no sterical constraints for the former. Two desorption states were observed, denoted as α and γ. Comparison of t.p.d. and i.r. spectra suggests that the first desorption rate maximum is due to pyridine (ammonia) desorbing from very weakly acidic sites, the second (γ) is due to molecules desorbing from Bronsted acid sites. The strength of the latter sites decreased with increasing H_3PO_4 loading. Strong Bronsted acid sites have been found to be indispensable for hydrocarbon formation from methanol. Zeolites with 5 and 8 w % H_3PO_4 did not catalyze hydrocarbon formation at a considerable rate. Because the energy of activation for n-hexane cracking increased strongly with H_3PO_4 loading, we concluded that the sites decreased in strength and we could exclude diffusional constraints as cause for reduced activity with increasing P-content.

INTRODUCTION

According to Sanderson's concept of electronegativity (1), oxides of higher intermediate electronegativity should exhibit sites of higher acid strength. Therefore one expects to find also with zeolites higher acid strength with increasing silicon-to-aluminum ratio. Indeed , Kazanskii et al. (2), calculating relative values for the deprotonation energies of bridging hydroxyls in models beeing representative for samples of Si/Al ratios from 1 to 4, found deprotonation energy to decrease with increasing Si/Al ratio, which accords with the results of Jacobs and Mortier (3). These theoretical calculations and the experiments reported by Jacobs et al. (4) are discussed by Mortier et al. (5). Lercher and Noller (6) have shown for silica-alumina-magnesia mixed oxides that, after acetone was adsorbed, the wavenumber of (non Bronsted) terminal hydroxyl groups was displaced the more the higher the intermediate electronegativity of the investigated mixed oxide was. This increase indicates increasing acid strength, i.e. increasing electron pair acceptor (EPA) strength , in the same order (7).

Therefore one would expect that surface treatment of a zeolite with compounds of high electronegativity like H_3PO_4 would increase the acid strength. In contrast, the catalytic experiments reported with phosphorous modified zeolites suggested a decrease in acid strength rather than the reverse (8,9). Derouane et al. also reported (10) that incorporation of boron into tetrahedral sites (substituting Al^{3+}) decreased the acid strength of the resulting zeolite.

In order to study these effects in some greater detail we have prepared a series of ZSM5 zeolite catalysts loaded with increasing amounts of H_3PO_4. The acidic properties of these materials were studied by means of pyridine adsorption and desorption (i.r transmission-absorption spectroscopy and temperature programmed desorption) as well as by reactions with methanol and n-hexane and are compared with those of pure ZSM5 and pure $AlPO_4$-5 molecular sieve (11).

EXPERIMENTAL

Catalysts and reagents. ZSM5 zeolite (Silicalite, 98.76 w% Si, 1.13 w% Al, 0.11 w% Na) was obtained from Union Carbide, Linde Division, New York (LOT # 8496-68). To impregnate the zeolites, 10 g were suspended in 100 ml distilled water and the desired amount of H_3PO_4 was added. This suspension was refluxed for 2 hours and then the water was evaporated under reduced pressure. The remainder was dried at 373 K and tempered at 773 K for 1 hour in air. The resulting catalysts contained 1, 2, 5 and 8 % H_3PO_4 by weight, denoted as ZSM5P1, ZSM5P2, ZSM5P5 and ZSM5P8, respectively in the following. $AlPO_4$-5 (AlPO) was prepared according to (11). The BET surface areas were 365, 304, 287, 295, 230 and 290 $m^2.g^{-1}$ for ZSM5, ZSM5P1, ZSM5P2, ZSM5P5, ZSM5P8 and AlPO, respectively. The crystallinity of all materials was checked by X-ray diffraction analysis and no other lines than those characteristic of ZSM5 or AlPO were observed.

Pyridine, methanol and n-hexane have been obtained from Merck (uvasol grade). All gases used, had at least 99.995 vol% purity.

Infrared measurements. The oxides were investigated by means of the transmission - absorption technique. The i.r. cell was constructed to permit all sample handlings to be done under vacuum and was described previously. For investigation, the zeolites were pressed into thin self supporting wafers ($p=10^8$-3.10^8 Nm^{-2}). The spectra were recorded from 4000 - 1000 cm^{-1} using a Perkin Elmer 325 type i.r. spectrophotometer with 3 cm^{-1} resolution at 3600 cm^{-1}.

Temperature programmed desorption (t.p.d.) measurements. T.p.d. was carried out in vacuum (below 10^{-1} Pa) using a temperature increment of 10 $K.min^{-1}$ in the range between 300 K and 1000 K. The reactor was a quartz glass tube connected with a vacuum pump and a Balzers 311 quadrupole mass spectrometer for detection of the desorbed species. The mass spectrometer was controlled by a Digital MINC computer. For further details see reference (12). The sample (50

mg) was calcined in the t.p.d. reactor at 873 K for one hour, cooled to ambient temperature and contacted with the adsorbent (1.8 kPa pyridine, 2.5 kPa ammonia). Then the sample was evacuated at ambient temperature for 30 to 60 minutes and the t.p.d. started subsequently.

Catalytic measurements. Measurements were carried out in continuous flow mode with methanol at a feed rate of $5.6.10^{-3}$ mol.h^{-1} and a partial pressure of 15.4 kPa and with n-hexane at a feed rate of 7.10^{-3} mol.h^{-1} and a partial pressure of 15.9 kPa. The total pressure was 1 bar and 0.1 g catalyst were used. The products were kept at 400 K and injected into the G.C. column (Chromosorb 102) via a six-port-valve. A Hewlett Packard 5840A gaschromatograph with FID was used. For n-hexane cracking the differential method of data analysis was employed.

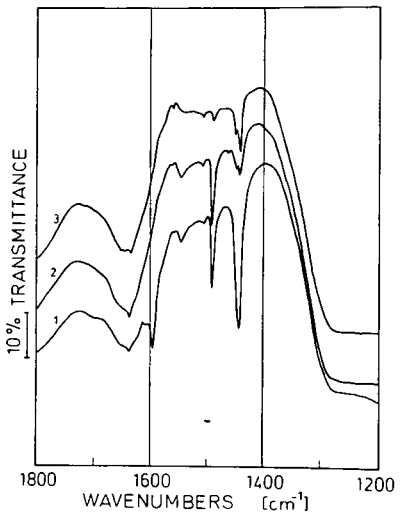

Fig.1. Pyridine on ZSM5
(1) 0.001 Pa, 298K, 1h, (2) 0.001 Pa, 573K, 1h, (3) 0.001 Pa, 773K, 1h

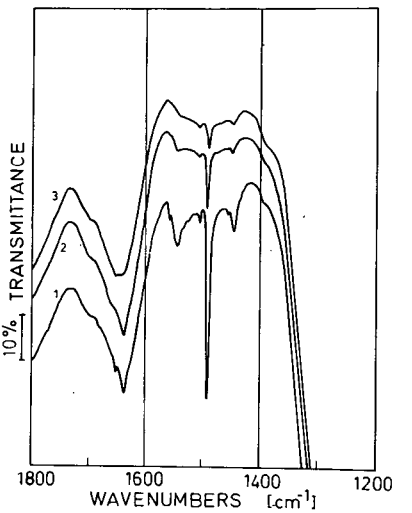

Fig.2. Pyridine on ZSM5P5
(1) 0.001 Pa, 573K, 1h, (2) 0.001 Pa, 573K, 1h, (3) 0.001 Pa, 773K, 1h

RESULTS

I.r. adsorbate spectra of pyridine. The wavenumbers of the 8 a,b and 19 a,b vibrations of pyridine adsorbed on the zeolites are compiled in table 1. Adsorbate spectra with pure ZSM5 and ZSM5P5 can be seen in figure 1 and 2. After admission of 1860 Pa pyridine into the i.r. cell at ambient temperature all adsorbate spectra exhibited intense 19 b bands around 1438 cm^{-1} indicating weak interaction between the surface and the pyridine molecules. Furthermore, it is interesting to note that the relative intensity of the 1540 cm^{-1} band (due to protonized pyridine molecules) is rather low under these conditions. When the i.r. cell was evacuated (10^{-2} Pa) it increased in intensity, while the 19 b band (1438 cm^{-1}) decreased strongly. This could be observed with all zeolites investigated. Two 19 b bands (1450 and 1445 cm^{-1}) were found with pure ZSM5 but

only one (near 1448 cm^{-1}) with H_3PO_4 treated molecular sieves. The relative intensity of this band decreased with increasing H_3PO_4 loading. $AlPO_4$-5 exhibited, however, a rather strong band at this wavenumber. The band at 1540 cm^{-1} (not observed with $AlPO_4$-5) had a markedly lower stability with ZSM5P5 and ZSM5P8 than with the other zeolites (see figure 1 and 2). The wavenumber itself showed no significant variation.

TABLE 1

Wavenumbers (cm^{-1})of 8a,b and 19a,b bands of pyridine adsorbed on ZSM5 samples

	298K, 1.6kPa	298K, ev.	473K, ev.	673K, ev.
ZSM5	1640,1595,1585	1640,1595	1640,1595	1640,1545
	1545,1490,1482	1545,1490	1545,1490	1490,1450
	1443,1438	1443	1450,1443	1445
ZSM5P1	1640,1602,1598	1640,1595	1640	1640
	1585, 1545	1545	1545	1545
	1490,1485,1438	1490,1448	1490,1448	1490,1448
ZSM5P2	1640,1602,1598	1640,1600	1640	1640
	1588,1582,1545	1545,	1545	1545
	1490,1485,1438	1490,1448	1492,1448	1492,1448
ZSM5P5	1640,1602,1598	1640	1640	1640
	1585,1545	1545	1545,1490	1490
	1490,1482,1438	1490,1448	1448	1448
ZSM5P8	1640,1602,1598	1640	1640	1640
	1585,1545	1545,1490	1545,1490	1490
	1490,1482,1438	1448		
AlPO	1609,1577	1610,1577	1620	1620
	1492,1480	1491	1490	1490
	1447,1438	1448	1449	1449

T.p.d. of pyridine. Pyridine desorbed in two steps causing one desorption rate maximum at 373 K and another between 758 K and 778 K. These adsorption states are denoted as α and γ peak in the following in accordance with (13,14). The maxima are compiled in table 2, the plots can be seen in figure 3. While the α peak showed no effect of H_3PO_4 treatment, the γ peak shifted gradually to lower temperatures with increasing H_3PO_4 loading. The lower maximum of the rate of desorption indicates a decrease of the energy of activation of desorption.

T.p.d. of ammonia. The temperatures of the maxima of desorption rate are collected in table 2, the temperature dependence of the desorption rate is

plotted in figure 4. The types of adsorption states are identical with those found for pyridine, the maxima, however, were found at somewhat lower temperatures and the intensity of the α peak was significantly lower than with pyridine. With increasing H_3PO_4 loading the maximum of the γ peak was found at lower temperatures, present only as a weak shoulder with ZSM5P5 and ZSM5P8. No γ peak was detected with $AlPO_4$-5.

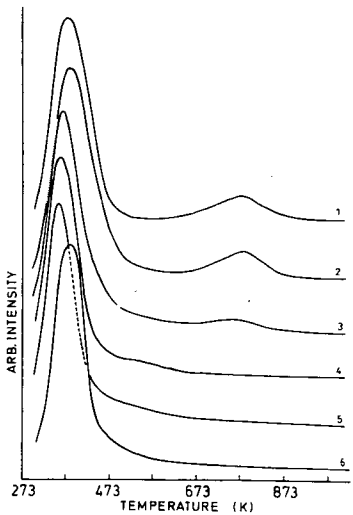

Fig.3. T.p.d. of pyridine

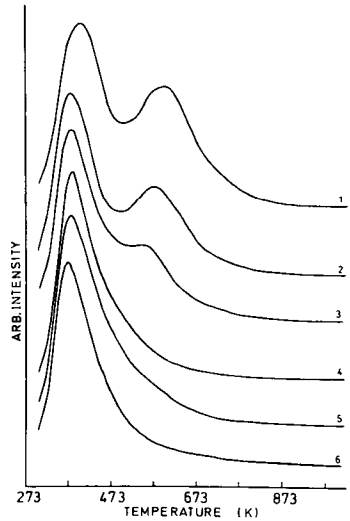

Fig.4. T.p.d. of ammonia

(1) ZSM5, (2) ZSM5P1, (3) ZSM5P2, (4) ZSM5P5, (5) ZSM5P8, (6) AlPO

TABLE 2

Maxima of desorption rates of pyridine and NH_3 (K)

	ZSM5	ZSM5P1	ZSM5P2	ZSM5P5	ZSM5P8	AlPO
Pyridine	383,778	381,778	370,758	367	360	373
Ammonia	383,598	379,580	378,547	383	383	378

Reactions with methanol. Figures 5-7 summarize the main product selectivities and activities of reactions of methanol over ZSM5, ZSM5P1 and ZSM5P5. Under the reaction conditions (15.4 kPa methanol) used, a high preference to olefins is expected and was observed. The conversion to hydrocarbons reached 89.5, 93.6, 4.6 and 0.4 mol % over ZSM5, ZSM5 1, ZSM5P5 and $AlPO_4$-5, respectively. For the latter two zeolites even at temperatures higher than 673 K no significant amounts of hydrocarbons were found, i.e. methanol was completely converted into dimethylether.

In order to establish the nature of active sites the catalyst was partial-

ly poisoned with pyridine. For one set of experiments, pyridine was adsorbed and the temperature was ramped to 673 K with an increment of 10 K per minute. This catalyst converted methanol only to dimethylether. If, however, the temperature was ramped to 873 K the original activity and selectivity of the zeolite was restored.

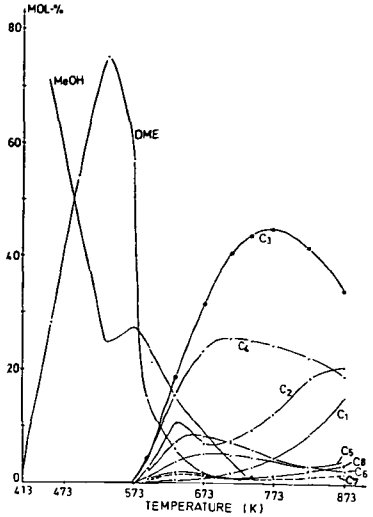

Fig.5. Methanol over ZSM5

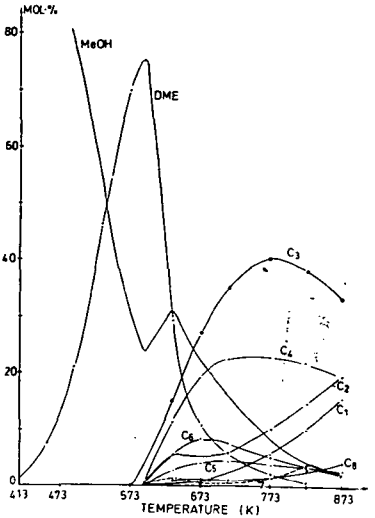

Fig.6. Methanol over ZSM5P1

Cracking of n-hexane. For further characterization of the acidic properties, cracking of n-hexane was performed in a differentially operated continuous flow reactor. The turnover frequencies (TOF) at 673 K (number of molecules n-hexane cracked per second and unit area of the zeolite), the apparent energy of activation and the product distribution are compiled in table 5. The TOF decreases from $1.1 \cdot 10^{15}$ over ZSM5 to $1.9 \cdot 10^{13}$ over ZSM5P5. Furthermore the molar ratio of ethane and ethene reverses from ZSM5P2 to ZSM5P5 indicating a change in mechanism.

TABLE 3

Cracking of n-hexane at 673 K

	TOF	E_a (kJ/mol)	Product distribution				
			C1	C2	C3	C4	C5
ZSM5	$1.1.10^{15}$	78.9	0.79	21.75	48.46	24.25	4.75
ZSM5P1	$8.3.10^{14}$	110.4	0.75	23.36	42.68	27.99	5.22
ZSM5P2	$4.5.10^{14}$	120.1	0.74	27.00	51.16	13.40	7.70
ZSM5P5	$1.9.10^{13}$	170.9	1.54	26.15	33.85	10.77	27.69

DISCUSSION

Adsorption of pyridine reveals two kinds of acid sites with H_3PO_4 modified zeolites, Lewis acid sites and Bronsted acid sites. It was outlined in the introduction that using Sanderson's electronegativity model one expects to find an increase in acid strength upon modification with highly electronegative compounds. The results, however, suggest that the reverse happens.

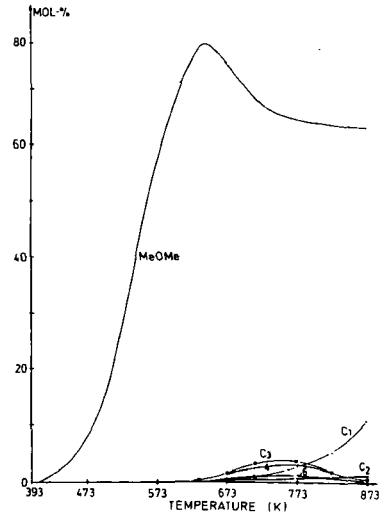

Fig.7. Methanol over ZSM5P5

The strength (the apparent acceptor strength (15)) of the Lewis acid sites was somewhat diminished after the first amounts of H_3PO_4 were deposited on the zeolite. Only one wavenumber of the 19 b vibration (1448 cm^{-1}) was found, instead of two with pure ZSM5 (1450, 1445 cm^{-1}). This indicates a slight decrease of the EPA strength (16) and it may be explained by the better shielding of the phosphorous atom with oxygen compared to Al^{3+}. Once this is achieved (by impregnation with 1 w % H_3PO_4) the wavenumber did not change any further, indicating a similar EPA strength independent of loading. The number of these sites, judged from the relative intensity of the band at 1448 cm^{-1}, decreased with loading.

The relative intensities of the band near 1540 cm^{-1} (due to protonized pyridine molecules) slightly increased with P-content. Hence the density of Bronsted acid sites seems to increase H_3PO_4 is deposited. The thermal stability of the pyridinium ions decreased, however, with increasing loading. This suggests decreasing acid strength.

If these i.r. adsorbate spectra are compared with the rate of desorption during t.p.d., it is possible to correlate the i.r. adsorbate structures with the adsorption states (for details see (14)). The α state is caused by pyridine desorbing from very weakly acidic sites. Adsorption sites for these molecules

certainly include OH groups. For pure ZSM5, a comparison of the i.r. spectra after evacuation at 673 K and 873 K (the temperature intervall of the γ t.p.d. peak) reveals that the intensity of the pyridinium band (1540 cm^{-1}) changes significantly, suggesting that these pyridine molecules desorb from Bronsted acid sites. The absence of a desorption peak around 773 K with zeolites having higher H_3PO_4 loading accords nicely with the lower thermal stability of the pyridinium ion as found by i.r. adsorbate spectra.

Because Topsoe et al. (13) had reported similar adsorption states using ammonia as a probe molecule, but rejected pyridine as not suitable, we also performed ammonia desorption experiments. We found that the estimated amount of NH_3 desorbing from the α state is smaller than that of pyridine and that all desorption rate maxima are shifted to lower temperatures with respect to pyridine. This indicates an overall weaker interaction of ammonia. It also suggests that pyridine is able to adsorb on all sites within the catalyst pore system.

In order to check this, we performed partial poisoning experiments (for details see (14)) by reactivating ZSM5 zeolite (after pyridine adsorption) at 673 K and 873 K, respectively. Over both catalysts methanol was converted. The temperatures were chosen so that in the first experiment pyridine was still adsorbed on Bronsted acid sites, while these sites were accessible in the second. Since hydrocarbons were only found after the latter pretreatment, the experiment shows the necessity of Bronsted acid sites for that reaction and furthermore that pyridine is capable to adsorb on all acidic sites in the channel structure.

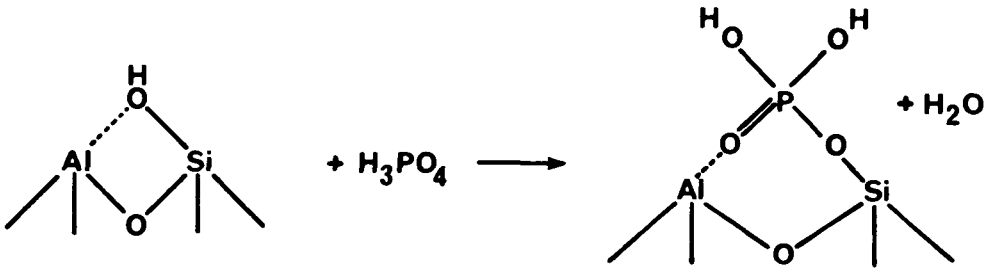

Fig.8. Model of the interaction of H_3PO_4 with Bronsted acid sites

Therefore the selectivities and reactivities found with H_3PO_4 treated ZSM5 zeolites suggest that the strength of all acid sites was diminished and that the weaker Bronsted acid sites found with ZSM5P5 and ZSM5P8 are hardly able to form hydrocarbons from methanol. The decrease in acid strength had (like partial poisoning with pyridine) virtually no influence upon the formation of dimethylether (DME). It indicates that only weak acid sites are needed for DME

formation, but strong for hydrocarbon formation from methanol.

It was reported (17-19) that the modification with H_3PO_4 leads to the modification of the outer and inner surface of the ZSM5 zeolite and that narrowing of the pore mouth and the pores will take place and will cause diffusional constraints. However, the results of cracking of n-hexane show a sharp increase in apparent activation energy with increasing H_3PO_4 loading, which is interpreted as decrease in acid strength and is incompatible with diffusional constraints for n-hexane. In addition, the relative small decrease in BET surface area suggests only small changes of the accessible pore volume of the catalyst. Therefore we are confident that H_3PO_4 entered the catalyst pores.

Since strong Bronsted acid sites could be replaced by rather weak Bronsted acid sites, the place of anchoring the phosphate ions in the zeolite framework should be given by Al^{3+} cations. In another paper, we suggested (in accordance with (20)) that the channel intersections are the most probable locations for these Al^{3+} cations (14).

Speculating, how the phosphate might be anchored (see figure 8) we recognize that the bridging OH group of the zeolite is replaced by two "terminal" hydroxyl groups. Mortier et al.(5) showed that the former type has significantly higher acid strength. Therefore the model proposed, accounts for the decrease in acid strength caused by H_3PO_4 loading.

The effects of H_3PO_4 upon ZSM5 zeolites show again that general relationships, such as Sanderson's electronegativities, have to be used with great care to predict properties of materials. These relationships are very useful to predict the relative strength of a particular group, if neither the type of bonding (as demonstrated here) nor, for the same type of bonding, (shown by Derouane et al. (10)) the bonding geometry has been altered. Both limitations must be handled strictly and are seldom fullfilled, when changing from one class of chemical compounds to another.

ACKNOWLEDGEMENTS

The authors thank J. Lebok, H. Schnait, Ch. Weigel, B. Zeiler and A. Jentys for assistance during measurements as well as the "Fonds zur Förderung der wissenschaftlichen Forschung" for providing the i.r. spectrometer.

REFERENCES

1. Sanderson, R.T.: Chemical Bond and Bond Energy, Academic Press, New York, 1971.
2. Mikheikin, I.D., Abronin, I.A., Zhidomirov, G.M., Kazanskii, V.B., J. Mol. Catal. 3, 435 (1978).
3. Jacobs, P.A., Mortier, W.J., Zeolites 2, 226 (1982).

4. Jacobs, P.A., Martens, J.A., Weitkamp, J., Beyer, H.K., Faraday Discuss. 72, 353 (1981).
5. Mortier, W.J., Sauer, J., Lercher, J.A., Noller, H., J. Phys. Chem. 88, 905 (1984).
6. Lercher, J.A., Noller, H., J. Catal. 77, 152 (1982).
7. Hair, M.L., Hertl, W., J. Phys. Chem. 74, 91 (1970).
8. Chandawar, K.H., Kulkarni, S.B., Ratnasamy, P., Applied Catal. 4, 287 (1982).
9. Young, L.B., Butter, S.A., Kaeding, W.W., J. Catal. 76, 418 (1982).
10. Derouane, E.G., Baltusis, L., Dessau, R.M., Schmitt, K.D. in "Catalysis by Acids and Bases", Elsevier Pub. Co., Amsterdam, 1985.
11. Wilson, S.T., Lok, B.M., Flanigen, E.M., U.S. Patent 4,385,994 (1983) and U.S. Patent 4,310,440 (1982).
12. Latzel, J., Kaes, G., React. Kin. Catal. Lett. 9, 183 (1978).
13. Topsoe, N.Y., Pedersen, K., Derouane, E.G., J. Catal. 70, 41 (1981).
14. Lercher, J.A., Rumplmayr, G., Z. Phys. Chem. NF, submitted.
15. Lercher, J.A., Vinek, H., Noller, H., J. Chem. Soc., Faraday Trans. I 80, 1239 (1984).
Lercher, J.A., Ritter, G., Vinek, H., J. Coll. Int. Sci., in press.
16. Ward, J.W., J. Catal. 10, 34 (1968).
17. Gilson, J.P., Derouane E.G., J. Catal. 88, 538 (1984).
18. Kaeding, W.W., Butter, S.A., J. Catal. 61, 155 (1980).
19. Kaeding, W.W., Chu, C., Young, L.B., Weinstein, B., Butter, S.A., J. Catal. 67, 159 (1981).
20. Babu, G.B., Hedge, S.G., Kulkarni, S.B., Ratnasamy, P., J. Catal. 81, 471 (1983).

CATALYTIC AND PHYSICOCHEMICAL PROPERTIES OF ACID-LEACHED OFFRETITES

F. HERNANDEZ, R. IBARRA, F. FAJULA, F. FIGUERAS

Laboratoire de Chimie Organique et Cinétique Chimique Appliquées - U.A. C.N.R.S. 418 - E.N.S.C.M., 8 rue de l'Ecole Normale - 34075 Montpellier Cedex France.

ABSTRACT

Two series of acid-leached offretites have been prepared by treating synthetic HK and NaK offretites with dilute HCl solution. The solids were characterized by elemental analysis, X-ray diffraction and surface area measurements. Their catalytic activity has been evaluated in the cracking of cyclohexane and the hydration of butenes. Acid treatment induces a simultaneous dealumination and decationization of the parent zeolites and structural modifications. The lattice of HK offretite is progressively destroyed by the acid whereas acid-leached NaK offretites contain mesopores and crystalline zones enriched in silica. For both zeolites the acid strength is enhanced by dealumination. The main conclusion of the study is that acid leached offretites exhibit a catalytic behaviour very similar to that of ZSM-5.

INTRODUCTION

Offretite is a hexagonal zeolite whose structure consists in parallel arrangements of cancrinite cages (cage ε) linked by hexagonal prisms (double six rings) in the c-direction. These ensembles delimit a system of 12-membered oxygen ring channels (free diameter 6.4 Å) along the c-axis intercommunicating through gmelinite cages (openings 3.6 x 5.2 Å) in the a-direction [1].

The porous network of offretite, available for sorbents, is virtually one-dimensional, with free apertures intermediate between those of the pentasil zeolites such as ZSM-5 (5.8 Å) and of the mordenites (6.7 Å), two zeolites types of great commercial importance in the field of catalysis.

In a large majority of cases, the lower the aluminium and residual cation content are of the zeolites, the higher their catalytic activity. With ZSM-5 and mordenite high degrees of decationization (> 95%) are readily achieved by standard low temperature ion-exchange. This is not the case for offretite. Each unit cell contains a non-exchangeable cation located in a cage ε [2, 3]. This cation cannot be substituted by sodium in the synthesis [4, 5] and its extraction at high temperature causes severe disruption of the framework.

On the other hand Si/Al ratios in synthetic offretites rarely exced values of 4. Steam and acid treatments must therefore be performed very cautiously in order to avoid crystal collapse.

Although the litterature dealing with the catalytic properties of offretites is very scarce, recent reports point out the potential of this zeolite for the dewaxing of gas-oils [6]

the cracking of naphtenes [7] and the hydration of olefins [8, 9]. In the above studies, data refer to offretites prepared by standard ion-exchange.

The objective of our study has been to investigate the properties of offretites activated with mineral acids.

In this paper we report our initial results obtained on a series of solids prepared by treating NaK and HK forms of synthetic offretites with dilute solutions of HCl. Some physical properties of the modified offretites are described and their catalytic properties for the cracking of cyclohexane and the hydration of n-butenes are presented and compared to that of other zeolites.

EXPERIMENTAL

Materials. Two samples of synthetic offretite were obtained from Grace Davison :
- a NaK form, of oxide composition : [0.79 K, 0.26 Na]$_2$O, Al_2O_3, 6.54 SiO_2, 3.28 H_2O. Its surface area (180 $m^2.g^{-1}$, Table 1) and cation/aluminium ratio, greater than one, suggested that this sample contained some extra-lattice material.
- a HK form, oxide composition [0.23 K, 0.02 Na, 0.75 H]$_2$O, Al_2O_3, 6.78 SiO_2, 3.9 H_2O, 2.5 wt% residual potassium, 0.1 wt% sodium. Its surface area was 531 $m^2.g^{-1}$. Its constraint index at 450°C, LHSV = 1.9 h^{-1} was constant with time on stream and equal to 3.2. For both samples, zeolite crystals had a prismatic shape with 1 to 1.5 µm length and 0.3 to 0.6 µm width.

Procedures. Acid leaching was achieved by dispersing first one gram of zeolite in 250 ml of deionised water. The HCl solution (50 ml) chosen so that the amount of acid (expressed in meq) per gram of zeolite ranged from 0.1 to 20, was then added dropwise. After five hours at room temperature the equilibrium pH of the suspension was recorded. The solid was recovered by filtration, washed, oven dried and finally calcined in flowing air for 5 h.

The zeolites used in the comparative catalytic studies were a mordenite from the Société Chimique de la Grande Paroisse, a H-ZSM-5 from the Institut Français du Pétrole and a Y-zeolite from Linde. Their characteristics are given in refs 7 and 9.

Characterization studies. The chemical compositions of the samples were determined by atomic absorption after dissolution. Some samples were also analyzed by X-ray fluorescence. X-ray powder diffraction studies were carried out with a CGR theta 60 instrument using CuKα radiation. The crystallinity of the solids was determined as described previously [10, 11] by comparing the sum of the intensities of selected diffraction peaks to that of the area under the background. Nitrogen BET surface areas were measured in a static volumetric device equiped with an integral Barocel pressure transducer.

Catalytic tests. The conversion of cyclohexane was conducted at 450°C in a flow apparatus at atmospheric pressure using 100 mg of catalyst. This reaction was chosen as a test for two reasons. Firstly, the critical dimension of the cyclohexane molecule ($\simeq$ 6 Å) is very close to that of the offretite pores. The reaction will therefore be very sensitive to the alterations of the zeolite porosity. Actually, offretites with stacking faults lead

o inactive catalysts [7]. Secondly, the selectivity towards cracking or isomerization is closely related to the acidity of the zeolite [7].

Hydration of n-butenes was studied at 250°C and 65 atm of pressure with a water to olefin ratio of 4.5 in a batch reactor. It was previously shown [9] that the hydration activity of zeolites is a direct function of the acid strength of the protons attached to their framework, regardless of their structure.

RESULTS AND DISCUSSION

The chemical compositions of the acid leached HK and NaK offretites, expressed as their unit cell contents, are given in Tables 1 and 2 respectively. Treatment of both zeolites with dilute HCl resulted in a parallel dealumination and decationization of the parent material. The mechanism of aluminium extraction by strong mineral acids generally supposes [12] a two step process of hydrogen ion exchange followed by the replacement of an AlO_4 tetrahedron by four OH groups. The fact that with HK offretite the two processes occur simultaneously (Table 1) can be attributed to the difficulty of removal of the potassium cations trapped in the cancrinite cages. By increasing the severity of the acid

Table 1

Unit cell content, XRD crystallinity and surface area of the samples obtained by acid treatment of KH offretites

Sample	Equilibrium pH	Unit cell content	% crystallinity XRD	Surface area $m^2.g^{-1}$
Starting	material	$K_{0.94}Na_{0.08}H_{3.07}[Al_{4.1}Si_{13.9}O_{36}]8H_2O$	100	531
1	2.2	$K_{0.65}Na_{0.03}H_{3.20}[Al_{3.9}Si_{14.1}O_{36}]6.4H_2O$	97	371
2	1.94	$K_{0.62}Na_{0.01}H_{3.07}[Al_{3.7}Si_{14.3}O_{36}]6.6H_2O$	84	-
3	1.5	$K_{0.54}Na_{0.01}H_{2.60}[Al_{3.2}Si_{14.8}O_{36}]6.2H_2O$	71	312
4	1.4	$K_{0.40}Na_{0.01}H_{2.50}[Al_3 Si_{15} O_{36}]7H_2O$	31	171

treatment the residual cation content could be reduced to 0.4 K^+ per unit cell and up to 30 % of the aluminium atoms could be extracted. However this resulted in a severe loss of crystallinity as evidenced by the XRD measurements and the surface areas determinations (last columns of the Tables). At lower pH the zeolite became totally amorphous.

The KNa offretite sample led to somewhat different results (Table 2). Aluminium extraction began before all the readily exchangeable cations had been replaced by protons. The apparent increase of the aluminium content of sample 5 is more probably due to the removal of extra-lattice silica. Even after the extraction of nearly 50 % of the aluminium atoms from the zeolite each unit cell contained one potassium cation. This shows that the acid treatment of KNa offretite did not affect the cationic sites, and consequently the aluminium tetrahedra, associated with the cages ε. Exchange of the sodium ions was, by contrast, rapidly achieved.

A second difference concerns the physical properties of the resulting solids. Although X-ray diffraction revealed a loss of crystallinity very similar to that observed with HK

Table 2

Unit cell content, XRD crystallinity and surface area of the samples obtained by acid treatment of KNa offretite

Sample	Equilibrium pH	Unit cell content	% crystallinity XRD	Surface area $m^2.g^{-1}$
Starting	material	$K_{3.33}Na_{1.16}[Al_{4.21}Si_{13.78}O_{36}]6.7\,H_2O$	100	180
5	2.55	$K_{2.59}Na_{0.26}H_{1.5}[Al_{4.4}Si_{13.6}O_{36}]8.4\,H_2O$	84	377
6	2.47	$K_2\ Na_{0.12}H_2\ [Al_{4.1}Si_{13.9}O_{36}]8.6\,H_2O$	67	400
7	2.37	$K_{1.9}Na_{0.07}H_{1.5}[Al_{3.5}Si_{14.5}O_{36}]8.23\,H_2O$	60	396
8	2.32	$K_{1.2}Na_{0.08}H_{1.6}[Al_{2.9}Si_{15.1}O_{36}]10.9\,H_2O$	37	403
9	2.2	$K_1\ Na_{0.08}H_{1.5}[Al_{2.6}Si_{15.4}O_{36}]10.4\,H_2O$	30	411
10	1.8	$K_{0.9}Na_{0.07}H_{1.4}[Al_{2.4}Si_{15.6}O_{36}]11.3\,H_2O$	24	350

offretite, the surface areas of the acid leached NaK offretites remained high and unmodified within 10 % variation. Moreover while the parent zeolite exhibited a characteristic, well defined, Type I isotherm, the shape of the curves was progressively shifted to a Type IV isotherm, indicating the appearance of a mesoporosity in the range 20-100 Å. This suggests that during the attack, portions of the crystal have been destroyed producing holes. The variations of the a and c parameters of the remaining crystalline zones of samples 5-10 as a function of their aluminium content are presented in Figure 1. As the aluminium content decreased, the a-axis shrank regularly whereas the c-axis expanded first and then remained constant. Such a unit cell contraction is consistent with the formation of new Si-O-Si bonds in the lattice with silicium atoms taking positions in the vacated tetrahedral sites [12].

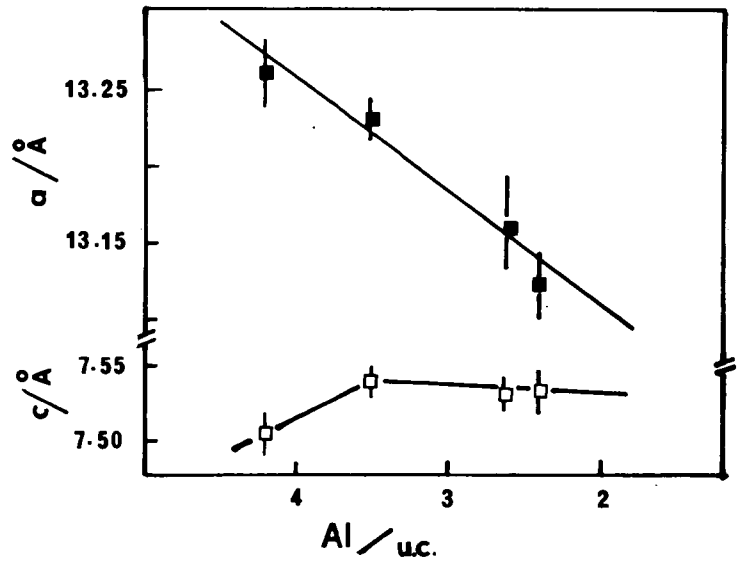

Fig. 1. Variations of the a and c parameters as a function of the aluminium content in acid leached NaK offretite.

Taking into account all these facts the texture of the acid leached NaK offretites can be represented by small crystalline zones, enriched in silica with respect to the starting zeolite, separated by holes. Recent work on the preparation of high silica faujasites by high temperature steaming and acid extraction led to similar solids [13].

There is a clear evidence that, depending on the cationic content of the parent zeolite, the treatment of offretites by dilute HCl leads to different produts.

The relationship existing between the cation content and the sieving properties of offretite have been studied by Aiello et al [14]. The presence of potassium ions in the main channels significantly reduces the penetration of guest molecules as well as the water content. During acid treatment, electrolyte invasion will thus play a dominant role. From our results it can be postulated that because of diffusion limitations, large concentration gradients exist within the crystals of NaK offretite leading to a heterogeneous acid attack.

Catalytic activity of acid leached offretites. For reactions involving all the hydroxyl groups, i.e. reactions catalyzed by the protonic sites regardless of their strength, the catalytic activity is directly correlated to the acid strength [15]. The hydration of olefins is a reaction of this type [9, 16]. The hydration of n-butene was studied on the solids prepared by acid leaching HK offretite (samples 1-4). The data of Figure 2 show that the activity per protonic site was increased by a factor of 3 when the aluminium content per unit cell

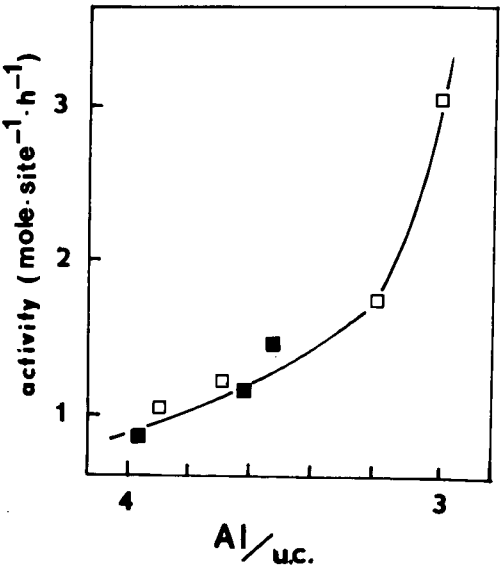

Fig. 2. Correlation between the hydration activity per protonic site and the aluminium content of offretite.

decreased from 4 to 3. On the same figure are reported (full symbols) the results obtained on offretites synthesized with various aluminium contents and then ion exchanged - up to 70 % exchange - using ammonium salts. Clearly, the activity, in other words the acid strength of the protons - is less influenced by the degree of cation exchange (at least in the region

70% - 86% exchange) than by the aluminium content. From a practical point of view, it is interesting to point out that the alcohol yields on a per gram basis increased significantly upon dealumination (Table 3). On this basis, and despite their poor crystallinity, dealuminated offretites exhibited an activity comparable, or even higher, than that of mordenite or ZSM-5 and a selectivity which remained equal to 100 % for alcohol.

Table 3

Hydration of n-butene at 250°C, 65 atm. Activity of various acidic zeolites.

Zeolite structure	Si/Al	% exchange	Alcohol yield, $mmole.g^{-1}.h^{-1}$	% eq[a]
Y	2.5	80	1.1	12
Mordenite	5	85	6.25	66
ZSM-5	49	99	5.73	61
Offretite	3.3	70	1.85	20
Offretite	4.6	83	3.48	37
Offretite	5.01	86	6.02	64

a : percentage of thermodynamic equilibrium.

A further evidence of the enhancement of the acid strength induced by acid treatment was obtained by studying the conversion of cyclohexane on samples 5-10. These solids contained similar amounts of protons (see Table 2) but the reaction rate was increased by one order of magnitude by extracting 50 % of the aluminium (Figure 3). This result also indicated that the channels of the crystalline fraction are not blocked. Moreover, the distribution of the products changed significantly (Table 4). We have shown recently [7] by comparing

Table 4

Product distributions obtained at 10 % conversion during cyclohexane cracking at 450°C.

Catalyst	Selectivity (mole %) C_2-C_5	C_6-C_8 aliphatics	MCP	Benzene	C_7-C_{10} aromatics
Fresh HCeY	31	8.7	15	10.1	35.2
Used HCeY	14.4	15.8	51.3	8.3	10.3
H-ZSM-5	63.5	12.5	4.6	15	3.5
HKO-Sample 5	18.6	16	49.4	10.1	5.9
HKO-Sample 8	36	14	30.2	8.6	11.2
HKO-Sample 10	59.2	9.8	15	6	10

a series of zeolites that isomerization to methylcyclopentane (MCP) was favoured on weakly acidic solids (used HCeY, HK offretites with low Si/Al ratios) whereas cracking requiered strong acidities (Fresh HCeY, H-ZSM-5). After dealumination, the behaviour of offretite is closely related to that of ZSM-5.

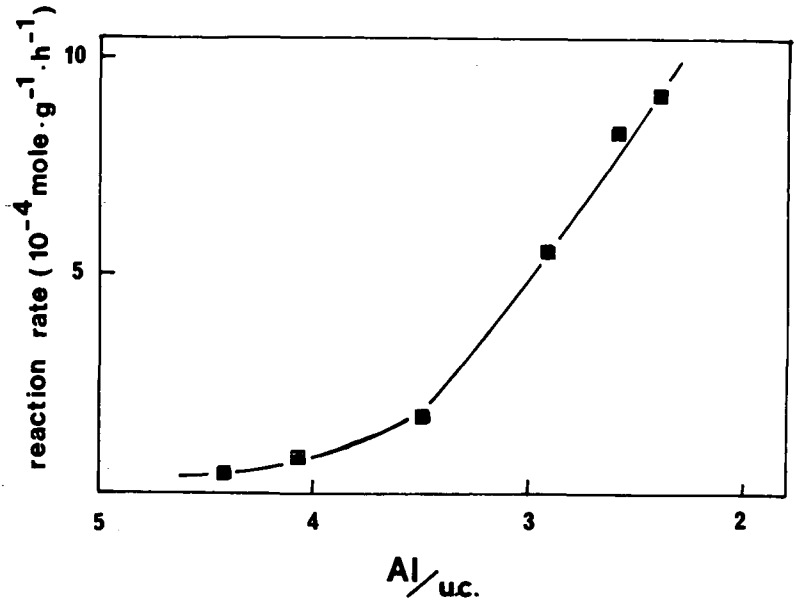

Fig. 3. Rate of cyclohexane conversion at 450°C as a function of the aluminium content in acid leached NaK offretites.

SUMMARY AND CONCLUSIONS

Treatment of synthetic offretites by dilute HCl solutions induces a simultaneous dealumination and decationization of the parent solids. In the case of HK offretite, part of the cations located in the cancrinite cages are extracted and this causes a partial destruction of the lattice. Acid attack occurs in a heterogeneous manner with NaK offretite probably because of diffusion limitations in the channels. The resulting solids contain mesopores and crystalline fractions enriched in silicium. Despite these structural modifications, the acid strength of the dealuminated offretites is greatly enhanced. The main conclusion of this study is that acid leached offretites exhibit a catalytic behaviour very similar to that of ZSM-5 for the hydration of olefins and the cracking of cyclohexane.

REFERENCES

1. Benett, J.M. and Gard, J.A., Nature, **214**, 1005 (1967).
2. Gard, J.A. and Tait, J.M., Adv. Chem. Ser., **101**, 230 (1971).
3. Barrer, R.M. and Harding, D.A., Sep. Science, **9**, 195 (1974).
4. Aiello, R. and Barrer, R.M., J. Chem. Soc. A, 1470 (1970).
5. Moudafi, L., Fajula, F. and Figueras, F., To be published.
6. Chen, N.Y., Schlenker, J.L., Garwood, W.E. and Kokotailo, G.T., J. Catal. **86**, 24 (1984).
7. Hernandez, F., Moudafi, L., Fajula, F. and Figueras, F., Proceedings 8th Int. Congress Catal., Berlin 1984, paper II 447.
8. Gueguen, C., Figueras, F. and Fajula, F., French Pat. Appl. 8307649.

9. Fajula, F., Ibarra, R., Figueras, F. and Gueguen, C., J. Catal, **89**, 60 (1984).
10. Subotic, B., Smit, I. and Sekovanic, L., Proceedings, Fifth Inter. Conf. Zeolites, Ed. L.V.C. Rees, Heyden, 10 (1980).
11. Fajula, F., Moudafi, L., Dutartre, R. and Figueras, F., Nouv. J. Chim. **8**, 207 (1984).
12. Mc Daniel, C.V. and Maher, P.K., Zeolite Chemistry and Catalysis, A.C.S. Monograph 171 (Ed. J.A. Rabo) 285, (1976).
13. Mauge, A., Auroux, A., Gallezot, P., Courcelle, J.C., Engelhard, P. and Grosmangin, J., Int. Sym. "Catalysis by Acids and Basis", Villeurbanne, 1984, Elsevier, In Press.
14. Aiello, R., Barrer, R.M., Davies, J.A. and Kerr, I.S., J. Chem. Soc., Faraday Trans. I, **66**, 1610 (1970).
15. Barthomeuf, D., Zeolites : Science and Technology, NATO ASI Series (Ed. F.R. Ribeiro, A.E. Rodriguez, L.D. Rollmann and C. Naccache), 317 (1984).
16. Boyd, R.H., Taft, R.W., Jr., Wolf, A.P. and Christman, D.R., J. Amer. Chem. Soc. **82**, 4729 (1960).

LATTICE DEFECTS AND SURFACE BARRIERS IN THERMALLY TREATED ZEOLITE Ca A

D. FREUDE, J. Kärger, H. Pfeifer
Sektion Physik der Karl-Marx-Universität,
DDR-7010 Leipzig, German Democratic Republic

ABSTRACT

Novel NMR techniques are applied to study the molecular transport and lattice defects in thermally treated zeolite $Na_{3.2}Ca_{4.4}A$. Mechanisms for the formation of lattice defects and surface barriers are discussed.

INTRODUCTION

With the development of the NMR tracer desorption technique for the first time a method has been found which provides unequivocal information about the existence and the intensity of transport resistances at the surface of molecular sieve crystallites [1,2]. Combining this technique with traditional NMR self-diffusion measurements, it could be demonstrated [2] that in zeolite Na Ca A after different pretreatments, molecular transport of paraffins may significantly be influenced by such surface barriers. However, until now the nature of these barriers and the extend of lattice distortion connected with it are unclear. In the last few years MAS NMR has successfully been applied to the investigation of the lattice structure and of lattice defects in zeolites [3] . Applying these novel techniques and traditional NMR intensity and relaxation measurements, in the present work possible mechanisms for the formation of lattice defects and surface barriers on thermally treated zeolites Na Ca A are discussed.

EXPERIMENTAL

The basic material of all samples is Zeosorb 5 AZ ($Na_{3.2}Ca_{4.4}A$ type zeolite powder with a mean crystallite diameter of about 4 μm) purchased from VEB Chemiekombinat Bitterfeld, GDR. For sample preparation either "deep bed" (DB) or "shallow bed" (SB) conditions have been chosen: Under deep bed conditions the powder is heated in an open glass tube of about 30 mm length at atmospheric pressure by raising the temperature at a rate of 100 Kh^{-1} up to the chosen temperature of activation. After keeping the sample for two hours at this temperature, it is evacuated for twenty hours. Under shallow bed conditions the layer thickness of the zeolite powder is less than 3 mm and the sample is heated in vacuo at a rate of 10 Kh^{-1} up to the final temperature of activation.

In what follows, a sample prepared with a final temperature of 400°C under deep bed conditions is denoted by "400 DB", for example. The samples sealed off under vacuum after the procedures described above are denoted as "dehydrated". One portion was slowly "rehydrated" at room temperature up to about 95% of the saturation value of the adsorption capacity by keeping it for three days in a desiccator over an aqueous NH_4Cl solution. For the self-diffusion and tracer desorption experiments before sealing the adsorbate has been introduced (ethane, about 4 molecules per cavity).

Details of the NMR self-diffusion as well as of the NMR intensity, relaxation and MAS experiments are described in references [2] and [4], respectively.

RESULTS

Tab. 1 shows values for the intracrystalline self-diffusion coefficients D_{intra} and mean life-times τ_{intra} of ethane in different $Na_{3.2}Ca_{4.4}A$ specimens. If molecular desorption is exclusively determined by intracrystalline self-diffusion (i.e. if there is a negligible small transport resistance at the crystallite surface), the intracrystalline molecular mean life time is given by the relation [1,2]

$$\tau_{intra}^{model} = \langle R^2 \rangle / 15 \cdot D_{intra}$$

and may straightforwardly be determined therefore from the mean square crystallite radius $\langle R^2 \rangle$ and D_{intra} (4th column of Tab. 1).

As can be seen from Table 1 the values of τ_{intra} and τ^{model}_{intra} agree reasonably well for the samples 400SB and 200DB so that a significant influence of surface barriers may be excluded. By contrast, for the samples 400DB and 600DB the values of τ_{intra} distinctly exceed that of τ^{model}_{intra}, which clearly indicates the existence of surface barriers.

Table 1

Intracrystalline self-diffusion coefficients D_{intra}, mean life times τ_{intra} and τ^{model}_{intra} for ethane in $Na_{3.2}Ca_{4.4}A$ at 293 K in dependence on the activation procedure of the zeolite

activation procedure	τ_{intra} / ms	D_{intra} / $m^2 s^{-1}$	τ^{model}_{intra} / ms
400SB	1.5±0.3	$(2.0\pm0.6)\cdot10^{-10}$	1.3±0.4
200DB	3.0±0.6	$(1.0\pm0.3)\cdot10^{-10}$	2.7±0.8
400DB	8.0±1.6	$(1.0\pm0.3)\cdot10^{-10}$	2.7±0.8
600DB	8.0±1.6	$(1.0\pm0.3)\cdot10^{-10}$	2.7±0.8

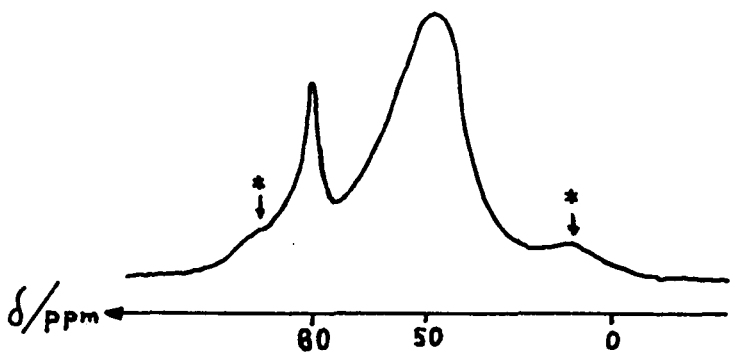

Fig. 1. ^{27}Al MAS NMR spectrum of the 300DB-sample, partially rehydrated, measured at 70 MHz, * denotes spinning side bands.

Fig. 1 shows the ^{27}Al MAS NMR spectrum of the partially rehydrated (6 H_2O per cavity) 300DB sample measured at 70 MHz with a rotational frequency of 3 kHz. The signal of the lattice aluminium atoms with a resonance shift of about 50 ppm referred to $Al(H_2O)_6^{3+}$ is in a good agreement with values given in [3]. A signal at 0 ppm corresponding to $Al(H_2O)_6^{3+}$-cations which has been observed in the ^{27}Al MAS NMR spectra of rehydrated zeolites HY [5] could not be found here. However, an additional signal appears with a resonance shift of 79±1 ppm. According to [6] a signal at 80 ppm must be ascribed to the anion $Al(OH)_4^-$ of aluminates. From the intensity of the signal at 79±1 ppm a concentration of 1.7 aluminate anions per cavity would be determined. This means that after a 300°C deep bed activation at least 1.7 aluminium atoms per cavity are released from the zeolite lattice. The maximum number of extra-lattice aluminium cannot exeed a value of two aluminium atoms per cavity since a greater deficiency of lattice aluminium should be observable by a decrease of the intensity of the line at 50 ppm.

The experimental results of the ^{27}Al MAS NMR measurements can be explained as follows: Extra-lattice aluminium forms $Al(OH)_4^-$-anions and $Al(H_2O)_6^{3+}$ -cations if it is solved in a basic (e.g. zeolite Ca A) or in an acidic environment (e.g. zeolite HY), respectively.

The signal of the aluminate anion could only be observed in Ca A samples activated at temperatures from 200°C up to 600°C under deep bed conditions followed by a rehydration. Samples prepared under shallow bed conditions or deep bed treated dehydrated zeolites did not show any signal at this position. In Table 2, column 4, values for the number of aluminate anions per cavity are given for fully rehydrated samples. The fact that in these cases the concentration does not attain the value of 1.7 measured for the partially rehydrated sample (as described above) may be explained by the lower pH-value in the fully hydrated samples.

The ^1H NMR spectra of the hydrated samples measured at $T_M < 150K$ are characterised by a superposition of a singlet due to hydroxyl protons and a doublet due to water protons. By a separation process both intensities can be determined [7]. The concentration of water in the rehydrated samples has been found thus to be about 25 molecules per cavity. After dehydration this value decreases to a concentration of ca. 10 for the samples 20DB, 20SB and 100DB, to about 4 for the sample 100SB and to less than 1/3 for the samples dehydrated at 200°C and above. Values for the concentration of hydroxylgroups are given in Tab. 2.

Table 2

Concentration of OH groups and of aluminate anions in dependence on the sample preparation.

sample preparation	dehydrated samples, OH groups per cavity	rehydrated samples		
		OH groups per cavity	$Al(OH)_4^-$ per cavity	non-aluminate OH groups per cavity
20DB	1.6±0.6	0.9±0.4	0.0	0.9±0.4
100DB	2.3±0.6	0.9±0.4	0.0	0.9±0.4
200DB	4.7±0.4	3.6±0.4	0.55±0.05	1.4±0.6
300DB	4.4±0.4	3.9±0.4	0.35±0.05	1.5±0.6
400DB	3.0±0.3	3.4±0.4	0.20±0.05	2.6±0.6
500DB	2.1±0.3	2.5±0.4	0.16±0.05	1.9±0.6
600DB	0.8±0.3	3.2±0.4	0.13±0.05	2.7±0.6
20SB	1.5±0.6	0.9±0.4		
100SB	2.6±0.6	1.0±0.4		
200SB	2.0±0.3	1.1±0.4		
300SB	1.5±0.3	1.1±0.4		
400SB	1.1±0.3	1.2±0.4		
500SB	0.6±0.3	1.2±0.4		

The free induction decay (FID) of the dehydrated samples measured at room temperature can be described by a single transverse relaxation time T_2^{FID}. Its value is 70 μs and 50 μs for the 400DB and 400SB samples, respectively. The envelope of Hahn's spin echoes decays with the relaxation times of T_2^{Hahn} = 340 μs and 170 μs for the 400DB and 400SB samples, respectively.

Fig. 2 shows the ^1H MAS NMR spectra of the 300DB and 300SB samples measured at 270 MHz. According to [8] a signal with a chemical shift of 1.8 ppm must be ascribed to isolated SiOH or AlOH groups similar to OH groups at the surface of silica gel or γ-Al_2O_3. A signal at 3.9 ... 5.6 ppm corresponding to bridging OH groups [8] could not be found. However, a signal appears at about 3 ppm, which is weak for shallow bed and strong for deep bed pretreatment.

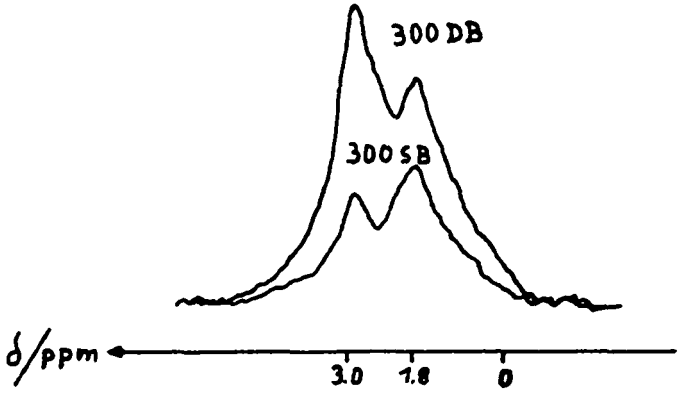

Fig. 2. ^{1}H MAS NMR spectra of dehydrated 300DB and 300SB samples, measured at 270 MHz

DISCUSSION

Combination of the NMR self-diffusion and tracer desorption experiments (cf. tab.1) clearly indicates the formation of surface barriers during the deep bed activation. We shall discuss the following three possibilities of their structural origin:

(i) transformation of the crystallite in the vicinity of the surface from a 5 A- to a 4 A-type structure as a consequence of the formation of monovalent $CaOH^{+}$ cations,

(ii) formation of an amorphous surface layor due to lattice destruction in the vicinity of the surface,

(iii) deposition of extra-lattice species in the cavities in the vicinity of the surface.

Since the surface barrier is resistant to temperatures as high as 600°C (cf. Tab. 1) and since at these temperatures the final stage of dehydroxilation (cf. Tab. 2) will be reached which as well should comprise the reaction $2\ CaOH^{+} \longrightarrow Ca^{2+} + CaO + H_2O$ explanation (i) must be excluded.

The second model presupposes a destruction of the lattice structure at least for a part of the cristallite surface. This implies that a part of the surface is closed for the molecular transport. However, measurements of the activation energy E of τ_{intra} according to the equation $\tau_{intra} = \tau_o \exp\{E/RT\}$ yields an increase of E, wheras for a partially closed surface only an increase of τ_o with E remaining constant would be expected [9]. Therefore we shall confine

ourselves to the discussion of model (iii).

Evidently we have to assume that the deposition of the extra-lattice species predominantly occurs in the surface layer of the crystallites. The blockade of the cavities (or of the windows between them) will then straightforwardly lead to the formation of a surface barrier. It is well-known [10], that during the process of NaY de-alumination extra-lattice aluminium is deposited on the surface. In CaA, the existence of extra-lattice aluminium has been proved by both X-ray [11] and ^{27}Al MAS NMR [12,13] measurements.

We could observe in numerous investigations of A-type zeolites with bivalent cations, a remarkable correlation between the formation of surface barriers and an enhancement of the OH groups concentration. For example, in dehydrated 400DB samples a number of 3.0±0.3 OH groups per cavity could be determined, while for dehydrated 400SB samples (which are characterised by a negligibly small surface resistance - cf. Tab. 1) the value is only 1.1±0.3. On the other hand the value of T_2^{Hahn} = 340 μs as obtained for the 400DB samples is in satisfactory agreement with a theoretical value of 316 μs calculated under the assumption of a statistical distribution of the OH groups (3 per cavity) over the whole crystallite [14]. Therefore it is most likely that the formation of a surface barrier is correlated with a bulk phase process which as well tends to enhance the OH group concentration.

OH groups arise in the process of water dissociation initiated by a temperature enhancement under the influence of the bivalent cations of the zeolite lattice. We shall consider the following models of their formation:

(*) hydration of aluminium oxide species deposited statistically within the zeolite crystals as a consequence of Al_2O_3 excess during zeolite synthesis,

(**) hydroxylation of aluminium atoms released from lattice positions,

(***) formation of $CaOH^+$ cations and bridging OH groups.

Model (*) is based on the fact that chemicalanalysis of the NaA zeolite after synthesis yields a ratio SiO_2/Al_2O_3 = 1.91±0.02 which is not affected by the cation exchange. Since according to the ^{27}Al MAS NMR measurements of the dehydrated samples there are no Al-O-Al bonds in the lattice, the aluminium excess of 4.7 % must be explained by an amount of 0.57 aluminium atoms per cavity on extra-lattice posi-

tions. It may be deposited as aluminium oxide or aluminium hydroxide species. Both in the hydrated NaA 400DB and the Na Ca A SB samples no aluminate could be found. If we assume that under the influence of Ca^{2+} these possibly highly condensed compounds may be transformed into small mobile aluminium hydroxide complexes (e.g. $Al_2O_3 + 3\ H_2O \rightarrow 2\ Al(OH)_3$), these species partially may be concentrated at the surface. With a further temperature enhancement or a decrease of the water pressure these species again may condensate leading to the formation of a surface barrier.

Reaction (**) may be described as follows:

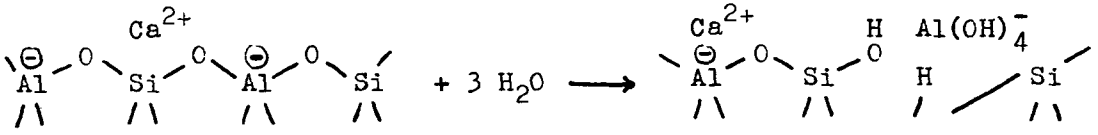

where an aluminium atom is released from its lattice position. After the release of an aluminium from its lattice position in zeolite HY, the site is occupied by a silicon atom and hence the crystal structure is preserved even under the process of dealumination [3]. An analogous reaction in zeolites A would lead to the formation of Si-O-Si bonds. Since in the ^{29}Si MAS NMR spectra of the investigated samples no lines corresponding to Si-O-Si bonds did occur [15], any healing of aluminium defects can be excluded. In the course of the above mentioned reaction also an oxygen atom is released from the lattice, which leads to a distortion of the lattice structure. Via the reaction $Ca^{2+} + Al(OH)_4^- \longrightarrow CaOH^+ + Al(OH)_3$, the aluminate anion may be transformed into aluminium hydroxide. Being uncharged, it has a higher mobility which may lead to the formation of a surface barrier as described above.

According to Planck [16], model (***) might proceed according to the following reaction:

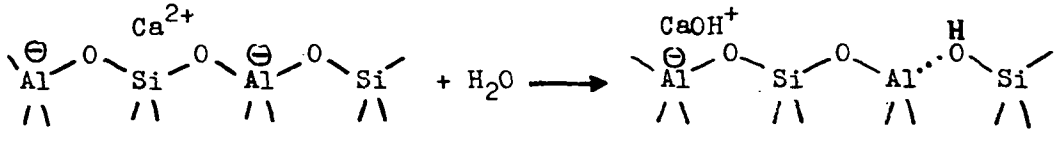

With zeolites CaX and CaY this mechanism could be verified by IR investigations. While two IR bands may be unambiguously attributed to the bridging OH groups, this is not the case for the attribution of the other IR bands to the $CaOH^+$ cations [17,18]. By contrast, in IR investigations of zeolite CaA no IR band is observed which might be attributed to bridging OH groups [19]. Analogously, also in the ^1H NMR spectra (cf. Fig. 2) no acidic OH groups are detected. This experimental finding is in complete agreement with the above stated basic behaviour of zeolite CaA, containing basic aluminates rather than acidic Al^{3+} in $Al(H_2O)_6^{3+}$ complexes. The above reaction cannot be accepted therefore as an explanation for the observed hydroxyl groups and extra-lattice aluminium in zeolite CaA.

Therefore we only have to consider mechanisms (*) and (**). Since the first mechanism permits an amount of extra lattice aluminium of not more than 0.57 per cavity, it must be accompanied by reaction (**). The latter may be considered as a first step of a lattice transformation which may be observed after intense hydrothermal treatment [20]. An unequivocal interpretation of the signal at 3 ppm in Fig. 2 is not yet possible. Perhaps this signal may be attributed to OH groups interacting with additional oxygen atoms. It shall be the task of further investigations, esp. by MAS NMR, to accomplish the proposed model of structural defects in zeolite CaA.

We are obliged to J. Haase, U. Härtel, Dr. G. Scheler (Jena), Dr. R. Seidel (Bitterfeld) and Dr. B. Staudte for discussions and experimental assistance.

REFERENCES

1. Kärger, J., AIChE-Journal 28, 417 (1982).
2. Kärger, J., Pfeifer, H. Heink, W., Proc. 6th Intern. Zeolite Conf. p. 184 (1983).
3. Klinowski, Progress in NMR Spectroscopy 16, 237 (1984).
4. Freude, D., Fröhlich, T., Hunger, M., Pfeifer, H., Scheler, G., Chem. Phys. Letters 98 263 (1983).
5. Freude, D., Fröhlich, T., Pfeifer, H., Scheler, G., ZEOLITES 3, 171 (1983).
6. Müller, D., Gessner, W., Behrens, H.-J., Scheler, G., Chem. Phys. Letters 79, 59 (1981).

7. Oehme, W., Freude, D., Klepel, S., Pfeifer, H., Schmiedel, H., Z. phys. Chemie (Leipzig) 259 1137 (1978).
8. Freude, D., Hunger, M., Pfeifer, H., Scheler, G., Hoffmann, J., Schmitz, W., Chem. Phys. Letters 105, 427 (1984).
9. Kärger, J., to be published.
10. Lohse, U., Mildebrath, M., Z. Anorg. Allg. Chem. 476, 126 (1981)
11. Pluth, J.J., Smith, J.V., J. Am. Chem. Soc. 102, 4704 (1980).
12. Freude, D., Haase, J., Pfeifer, H., Prager, D., Scheler, G., Chem. Phys. Letters (1985).
13. Corbin, D.R., Farlee, R.D., Stuckly, G.D., Inorg. Chem. 23, 2920 (1984).
14. Oehme, W., Freude, D., Schmiedel, H., Z. phys. Chemie (Leipzig) 255, 566 (1974).
15. Klinowski, J., private communication.
16. Planck, C., Proc. 3rd Intern. Congr. Catal. 1, 727 (1964).
17. Ward, J.W., HCS Monograph 171, 118 (1976).
18. Abou-Kais, A., J. Phys. Chem. 81, 397 (1977).
19. Kustov, L.M., Borovkov, V. Yu., Staudte, B, in preparation.
20. Breck, D.W.: Zeolite Molecular Sieves, John Wiley and Sons, N. Y., 1974, p. 488.

SYNTHESIS AND PROPERTIES OF SEVERAL ALUMINOPHOSPHATE MOLECULAR SIEVES

XU QINHUA, Dong Jialu, Yan Aizhen, Jin Changtai
(Department of Chemistry, Nanjing University, Nanjing, China)

ABSTRACT

The $AlPO_4$-5, $AlPO_4$-11, $AlPO_4$-20 and three new family members of aluminophosphate (named CNU-n, n=1,2, and 3, CNU: China, Nanjing University) have been synthesized hydrothermally in the presence of organic amines and quaternary ammonium templates. These samples are characterized by X-ray diffraction patterns and Infrared spectra. It is found that the framework topology of several samples have been changed after calcination. DTA shows no structural collapse below 950°C.

The adsorption properties of water and hydrocarbons on the samples were studied. The results show that the CNU-3 has the largest pore size, and can adsorb 1,3,5-trimethylbenzene but the CNU-1 adsorbs only water vapor. The CNU-2 may adsorb n-hexane but not benzene.

The intracrystalline pore volumes for water on all samples were obtained by TG or adsorption method. All results show that the water pore volumes are usually greater than the hydrocarbon pore volumes, reflecting the presence of additional pore volume accessible to H_2O but not to hydrocarbons.

INTRODUCTION

A novel class of aluminophosphate molecular sieves was discovered by Union Carbide Corporation in 1982.[1] It reperesents the first class of molecular sieves with framework oxide compositions free of silica. $AlPO_4$ molecular sieves can be synthesized hydrothermally in the presence of organic amines and quaternary ammonium templates. The organic template is crucial, and without it no sieves are formed. These $AlPO_4$ molecular sieves exhibit zeolite-like properties. Preliminary findings indicate that this class of molecular sieves will find use as adsorbents, catalyst, and catalyst supports.[1-5]

Up to now, more than 150 types of synthetic zeolites have been obtained, but only about 20 three-dimensional structures of $AlPO_4$ molecular sieves have been reported. One may predict that there will be more new structure types of $AlPO_4$ molecular sieves to appear.

In our work we have synthesized $AlPO_4$-n (n=5,11 and 20) and have found several new family members, named CNU-n (n=1,2 and 3) which were not reported previously. Their properties also have been studied.

SYNTHESIS OF ALUMINOPHOSPHATE MOLECULAR SIEVES

$AlPO_4$-5, -11 and -20 were synthesized by hydrothermal method.[1] The synthesis procedure involved combining equimolar portions of reactive hydrated alumina, phosphoric acid and water. This mixture formed an aluminophosphate gel to which was added an organic amine or quaternary ammonium salt. Generally, the reaction mixture was maintained at temperatures from 150 to 200°C for periods of one day to two weeks. Crystalline products were recovered by filtration, centrifugation and drying. The samples obtained were characterized by X-ray diffraction patterns and were found to be consistent with those of literature.[1]

CNU-1, -2 and -3 were obtained by the same hydrothermal method under the different conditions listed in Table 1. Their X-ray diffraction patterns are shown in Figures 1-3. It is found that they are new family members of aluminophosphate molecular sieves which have not been reported before.

Table 1

The conditions of synthesis

Samples	Compositions of the reaction mixture					Temperature for gel forming, °C	Crystallization		Templating agents
	HCl	R	Al_2O_3	P_2O_5	H_2O		temp. °C	time h	
$AlPO_4$-5	1	1	1		50	room temp.	200	24	TEAOH
$AlPO_4$-11	1	1	1		50	room temp.	200	24	$(i\text{-}C_3H_7)_2NH$
$AlPO_4$-20	1	1	1		50	room temp.	150	70	TMAOH
CNU-1	1	1	1		50	80	150	100	TMAOH
CNU-2	1	1	1		50	40	150	145	TBAOH
CNU-3	0.33	0.67	1		40	60	150	336	TEAOH

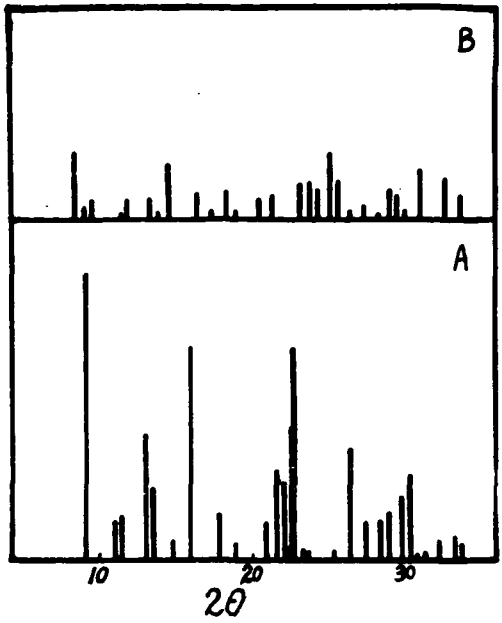

Fig. 1. The X-ray diffraction patterns of CNU-1
A - before calcination
B - after calcination

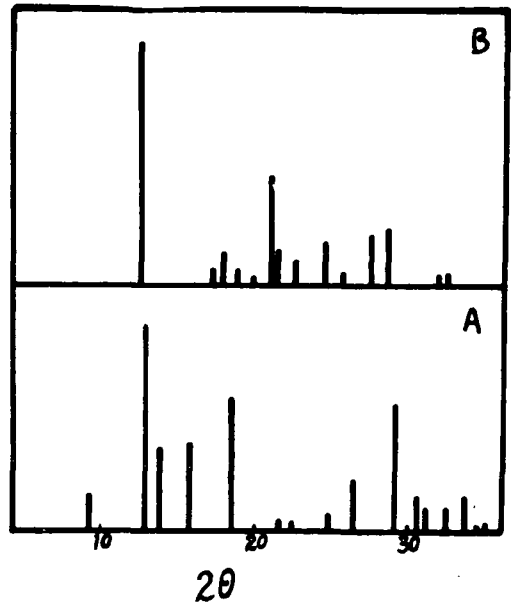

Fig. 2. The X-ray diffraction patterns of CNU-2
A - before calcination
B - after calcination

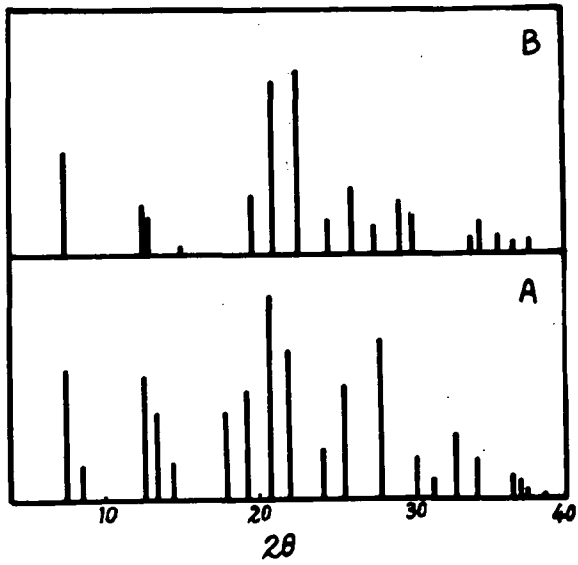

Fig. 3. The X-ray diffraction patterns of CNU-3
A - before calcination
B - after calcination

The results reveal that different family members require different templates, but more than one family members can be obtained using only one kind of templates. In our laboratory, by using the same template (TMAOH) $AlPO_4$-20 and CNU-1 were obtained at different conditions (see Table 1). The scanning electron micrographys of CNU-1, 2, 3 and $AlPO_4$-20 are shown in Figures 4, 5, 6 and 7 respectively.

We also obtained in the experiments that the organic template is crucial; without it no sieves but the dense $AlPO_4$ structures or known hydrates are formed. Therefore, a template is a species which seems to exert a unique structure-directing influence during crystallization of the molecular sieve. The action of a template appears to have both electronic and steric effects in generating pores and cages. In the case of the aluminophosphate molecular sieves all of which have the same composition with Al and P in equimolar proportion, each framework being thus neutral with nil exchanging cation. Therefore, the steric effects of templates seem to predominate.

PROPERTIES OF ALUMINOPHOSPHATE MOLECULAR SIEVES

Stability. The $AlPO_4$ molecular sieves obtained by us exhibit their excellent thermally stable properties, showing no structural collapse below 950°C by DTA method. From Figures 8-11 it can be illustrated that endotherm peaks with a maximum at about 250 to 280°C may be considered as the peaks of the desorption of template agent. Consequently the broad exotherm peaks at temperatures ranging from 300 to 600°C, in which generally there are two peaks may be attributed to the oxidation of nitrogen-containing compound and structure changes. The peak (or peaks) of endotherm below 160°C on the DTA curve is due to dehydration of the samples.

After calcinating the samples to remove the template at 600°C for 2 hours, and then rehydrating it with water, we found that the dehydration peaks generally appear at about 100°C. But the CNU-1 loses water in two steps with a maxima at 48°C and 106°C on the DTA curve. Sample CNU-3 has two dehydration peaks even before calcination. The results may be explained as follows: the water molecules in these samples occupy two different sites within the structure, having two kinds of volatilities. Both before and after calcination, the temperatures of dehydration of all the samples are between those of Faujasite and silicalite. Hence, they exhibit

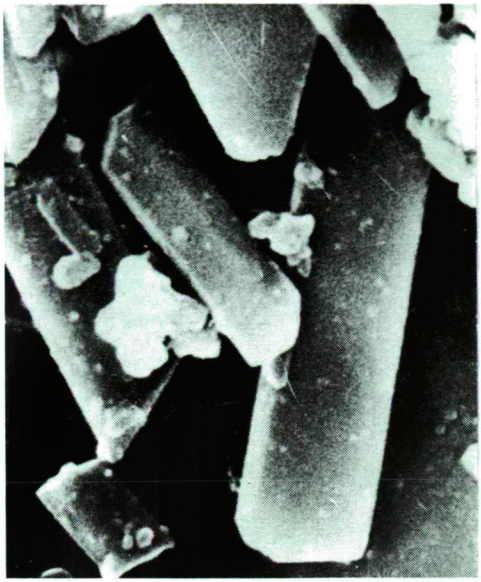

1.0 um

Fig. 4. The SEM of CNU-1

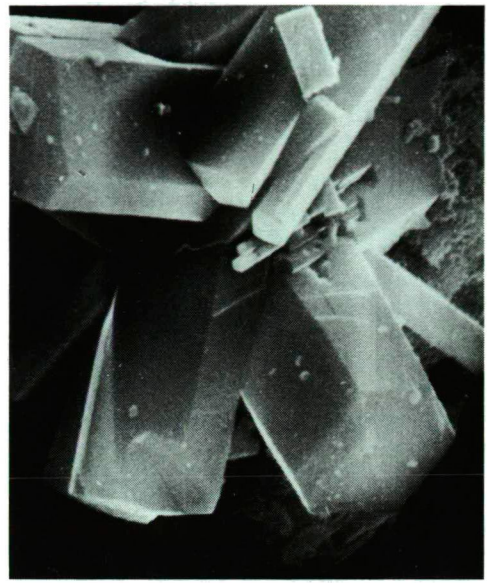

1.0 um

Fig. 5. The SEM of CNU-2

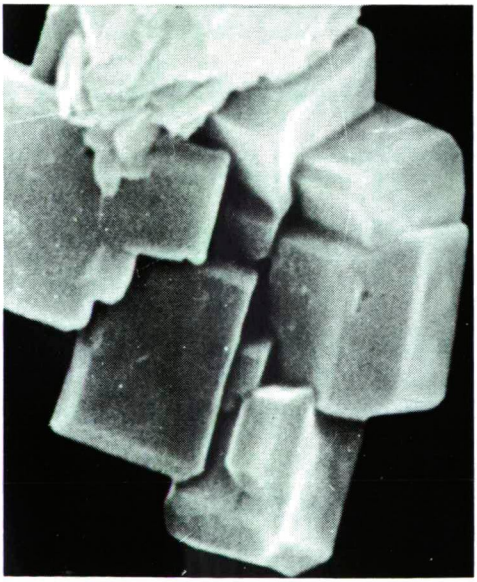

1.0 um

Fig. 6. The SEM of CNU-3

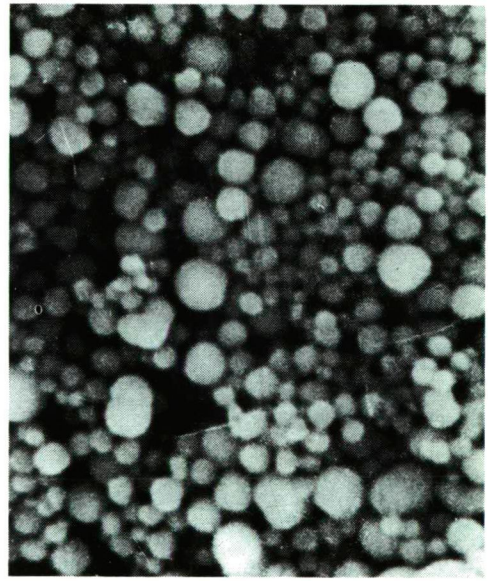

1.0 um

Fig. 7. The SEM of $AlPO_4$-20

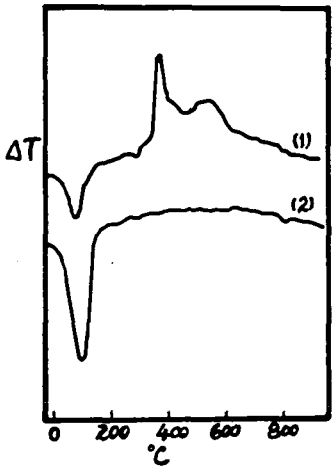

Fig. 8. The DTA curves of $AlPO_4$-5
(1) before calcination
(2) after calcination

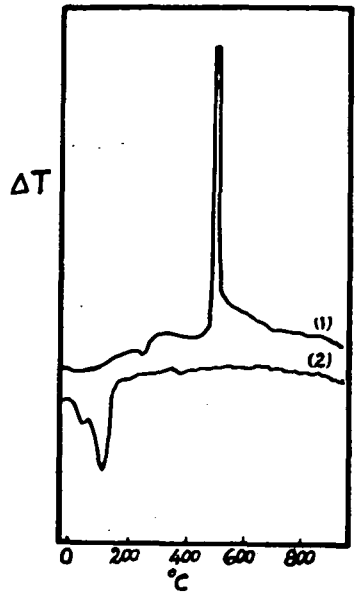

Fig. 9. The DTA curves of CNU-1
(1) before calcination
(2) after calcination

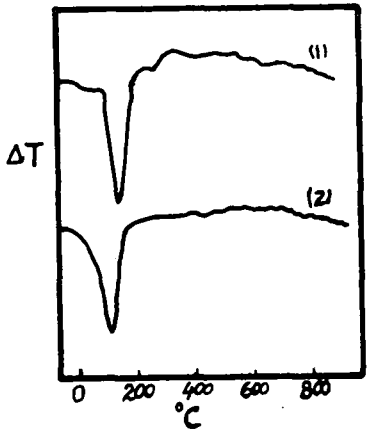

Fig. 10. The DTA curves of CNU-2
(1) before calcination
(2) after calcination

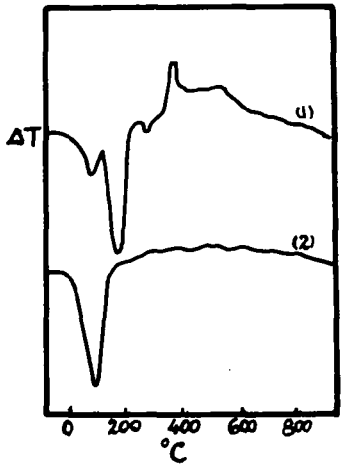

Fig. 11. The DTA curves of CNU-3
(1) before calcination
(2) after calcination

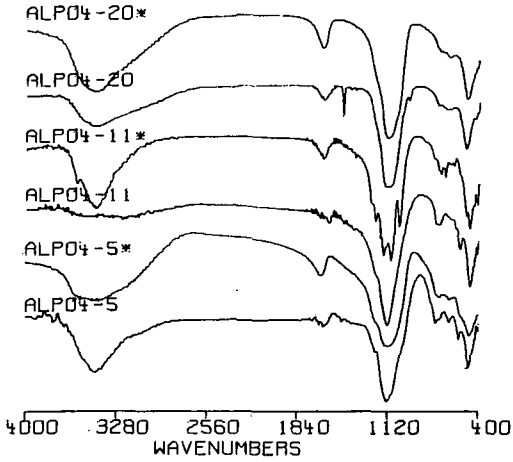

Fig. 12. IR spectra of $AlPO_4$-n
* after calcination

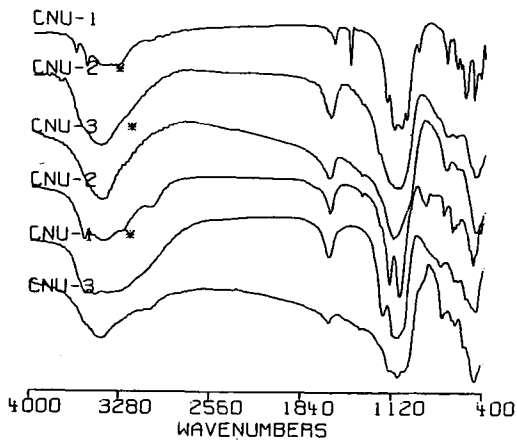

Fig. 13. IR spectra of CNU-n
* after calcination

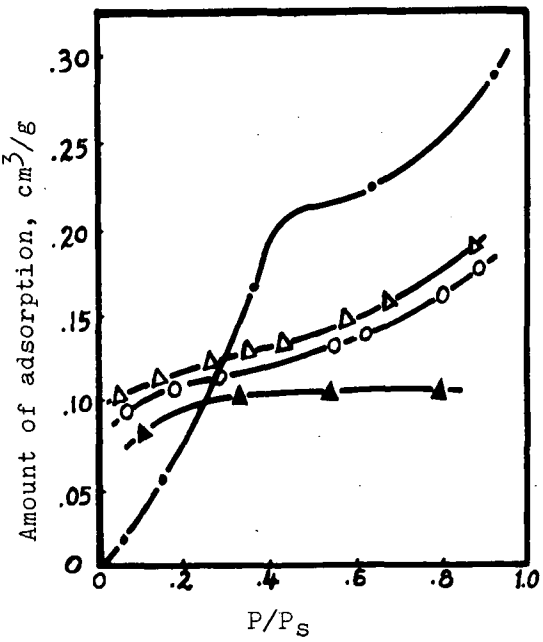

Fig. 14. The adsorption isotherms on $AlPO_4$-5
—●— H_2O, —△— benzene,
—○— cyclohexane
—▲— 1,3,5-trimethylbenzene

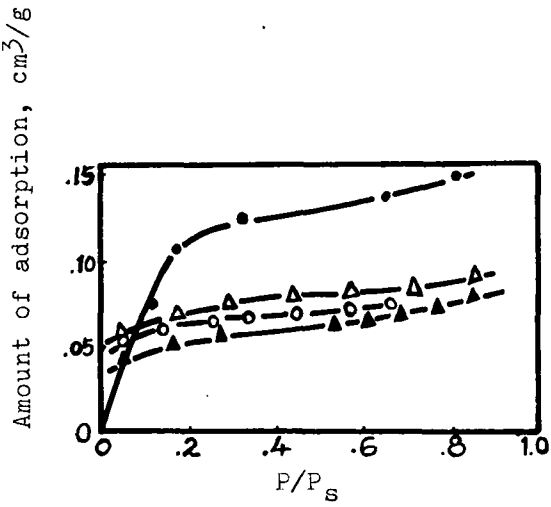

Fig. 15. The adsorption isotherms on $AlPO_4$-11
—●— H_2O
—△— n-benzene
—○— benzene
—▲— cyclohexane

less affinity for H_2O than the hydrophilic Faujasite, but more than the hydrophobic silicalite.

The structure change of the samples after calcination at 600°C for 2 hours and then rehydration of water was examined by the X-ray diffraction and Infrared spectroscopy (see Figures 12 and 13). The X-ray diffraction patterns and IR spectra of $AlPO_4$-5 and $AlPO_4$-20 changed very slightly, which implies that they did not undergo structural changes of framework. But the other samples changed obviously in their framework structures. For $AlPO_4$-11, after calcination, its X-ray pattern changed in accordance with that reported by Flanigen.[1] In our experiment the corresponding IR spectra was found to have changed too. It means that complete dehydration results in irreversible changes in the framework topolgy of $AlPO_4$-11. The behavior of CNU-n is anologous to that of $AlPO_4$-11.

Adsorption. The adsorption isotherms were measured on the samples with water and hydrocarbons by gravimetric method at room temperature. The results show that $AlPO_4$-20 and CNU-1 are small pore molecular sieves that admit only water. The water isotherms for $AlPO_4$-11 and CNU-1 are, roughly, similar to that of Type I, but the other samples are not so. Water sorption on $AlPO_4$-5 and CNU-3 at values of $P/P_s<0.2$ is unusually low, and there is a large increase between $P/P_s = 0.2$ and 0.4. The isotherm shapes of hydrocarbons for all samples are similar to those of Type I. Figures 14-17 show the isotherms of $AlPO_4$-5, $AlPO_4$-11, CNU-1 and CNU-3 respectively. The sample CNU-2 adsorbs water and n-hexane but not benzene. The adsorption properties of $AlPO_4$ molecular sieves are summarized in Table 2.

Table 2

Adsorption properties of $AlPO_4$ molecular sieves

Samples	Pore size (nm)	Intracrystalline pore volume for water cm^3/g	
		from adsorption at $P/P_s = 0.8$	from TG
$AlPO_4$-5	0.8	0.26	0.24
$AlPO_4$-11	0.61	0.15	0.17
$AlPO_4$-20	0.3	0.32	0.25
CNU-1	0.3	0.28	0.25
CNU-2	>0.41	0.19	0.18
CNU-3	0.8	0.21	0.22

From the results we can see that the intracrystalline pore volumes for water obtained by TG are similar to the data obtained by adsorption method. The volume of adsorption with hydrocarbons such as benzene on CNU-3 is about 50% of the volume of adsorption with water at P/P_S=0.5, while on $AlPO_4$-5 and $AlPO_4$-11 they are ~60% and ~80% respectively. In general, the water pore volumes are usually greater than the hydrocarbon pore volumes, reflecting the presence of additional pore volume accessible to water but not to hydrocarbons.

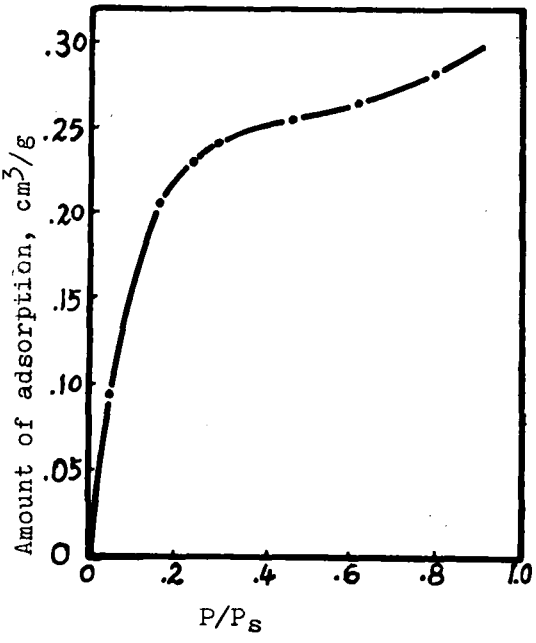

Fig. 16. The adsorption isotherms on CNU-1 with water

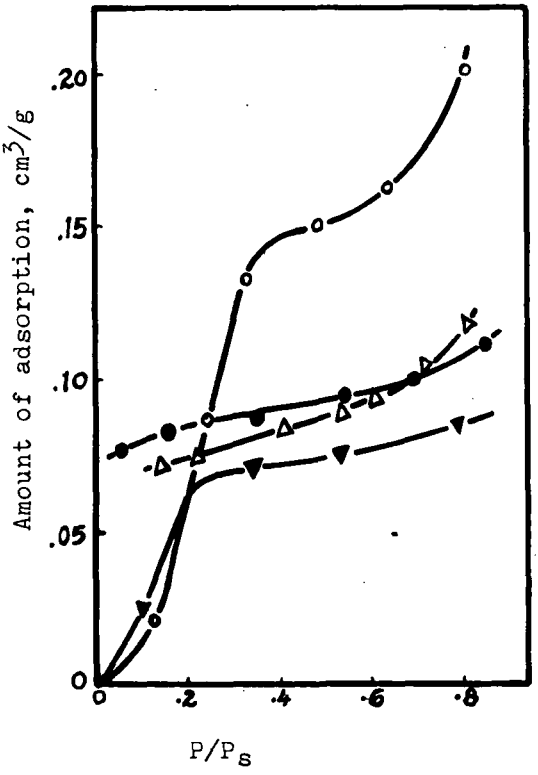

Fig. 17. The adsorption isotherms on CNU-3
—o— H_2O
—△— o-xylene
—●— cyclohexane
—▼— 1,3,5,-trimethylbenzene

Indeed, the samples of CNU-1, -2 and -3 are the new family members of aluminophosphate molecular sieves, as characterized by

the spectra of X-ray diffraction, DTA and IR. They possess the properties of sieves. The pore size of CNU-1 is similar to that of $AlPO_4$-20, CNU-2 can adsorb n-hexane but not benzene, and CNU-3 has large pore size in which 1,3,5-trimethylbenzene may enter.

REFERENCES

1. Wilson, S.T., Lok, B.M. and Flanigen, E.M., U.S.P. 4, 310, 440 (1982).
2. Haggin, J., Chem. Eng. News 60, No. 50, 9 (1982).
3. Haggin, J., Chem. Eng. News 61, No. 25, 36 (1983).
4. Wilson, S.T., Lok, B.M., Messina, C.A., Cannan, T.R. and Flanigen, E.M., J. Am. Chem. Soc. 104, 1146 (1982).
5. Stuck, G.D. and Dwyer, F.G., "Intrazeolite Chemistry", ACS Symposium Series 218, 79 (1983).

FORMATION OF LEWIS ACID SITES IN $NaNH_4Y$ ZEOLITES BY γ IRRADIATION.

A. ABOU-KAIS[a,b], N.N. Abou-Kais[b]
Faculty of Science II, Lebanese University, Mansourieh, Lebanon.(a)
National Council for Scientific Research, Beirut, Lebanon.(b)

ABSTRACT

The thermal heating above 500°C and under vacuum (10^{-5}-10^{-6}torr) of $NaNH_4Y$ zeolite leads to its dehydroxylation with the formation of Lewis acid sites. The same phenomenon occurs upon irradiation with γ rays at room temperature of the same solid preheated to 300°C only.

If the zeolite is preheated above 500°C and irradiated at room temperature, the number of Lewis acid sites formed in the solid is less than when it is simply heated without further irradiation. This decrease is due to the reduction by Compton effect of the strong oxidant sites of this solid keeping the weak sites intact. The electron affinity of the latter increases upon oxygen introduction after irradiation.

INTRODUCTION

It is well known that certain defects are created in solids under the effect of γ irradiation. This causes different physico-chemical modifications in their properties, some of which are more or less durable (1-3). These defects can play an important role in catalysis specially the electron donor and acceptor centers (4,5).

Authors, using different techniques such as infra-red spectrometry (I.R) (6), electron spin resonance (e.s.r.) (7), thermogravimetry (8,9), X-rays diffraction (9,10), etc., agreed that the above centers are formed during the decomposition of $NaNH_4Y$ zeolite by heating. We generally admit that, on one hand, the decomposition of ammonium ions in zeolites is represented by the following reaction:

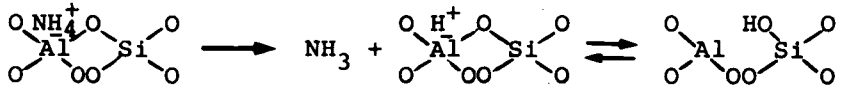

and, on the other hand, the dehydroxylation of zeolites is represented as follows:

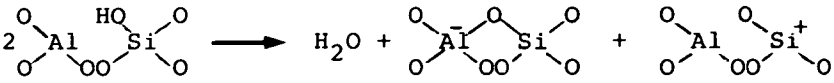

It was shown that the decomposition of NH_4^+ occurs within the range of 200-300°C and produces Brönsted acid hydroxyl groups. The dehydroxylation occurs above 500°C with the formation of Al electron acceptor sites.

EXPERIMENTAL PART

The starting material was NaY zeolite supplied by "Linde Union Carbide". The Na^+ ions were exchanged by NH_4^+ ions by simple treatment with an ammonium nitrate aqueous solution until the required exchanged levels were reached. The exchanged samples were identified by the number of Na^+ ions remaining in the unit cell. Four samples have been prepared: $Na_{56}Y$, $Na_{36,4}(NH_4)_{19,6}Y$, $Na_{16,9}(NH_4)_{39,1}Y$ and $Na_{5,8}(NH_4)_{50,2}Y$.

The samples were placed in an e.s.r. tube surmounted by an equipped ampoule of thin glass which is easily broken by a glass hammer. This allows the contact, under vacuum, of anthracene solution with the preheated and irradiated samples (figure 1).

The samples were heated for 15 hours at a given temperature in 160 torr of oxygen and then evacuated (10^{-5}-10^{-6}torr) at the same temperature for another 20 hours.

The samples were irradiated with doses within a range of 0-20 Mrad at room temperature in a cobalt-60 cell.

After irradiation, the zeolite was poured into a solution of anthracene in benzene (10^{-2}M) prepared in advance. The amount of positive radicals so formed was measured quantitatively by e.s.r. at room temperature using Varian E9 spectrometer. The concentration of the paramagnetic species was measured by comparison with the diphenyl-picryl-hydrazyl (D.P.P.H.) radicals in benzene.

RESULTS AND DISCUSSIONS

When a sample of $NaNH_4Y$ zeolite heated in vacuum at different temperatures and irradiated at room temperature comes into contact with a solution of anthracene in benzene, a dark-yellow coloration is observed due to the formation of positive radicals A^+ after the transfer of an electron from an adsorbed molecule of anthracene to the surface of solid. The e.s.r. spectrum obtained has eleven distinct lines. Such hyperfine structure is attributed to the interaction of an electron with 10 protons of the anthracene molecule. The same e.s.r. spectrum have

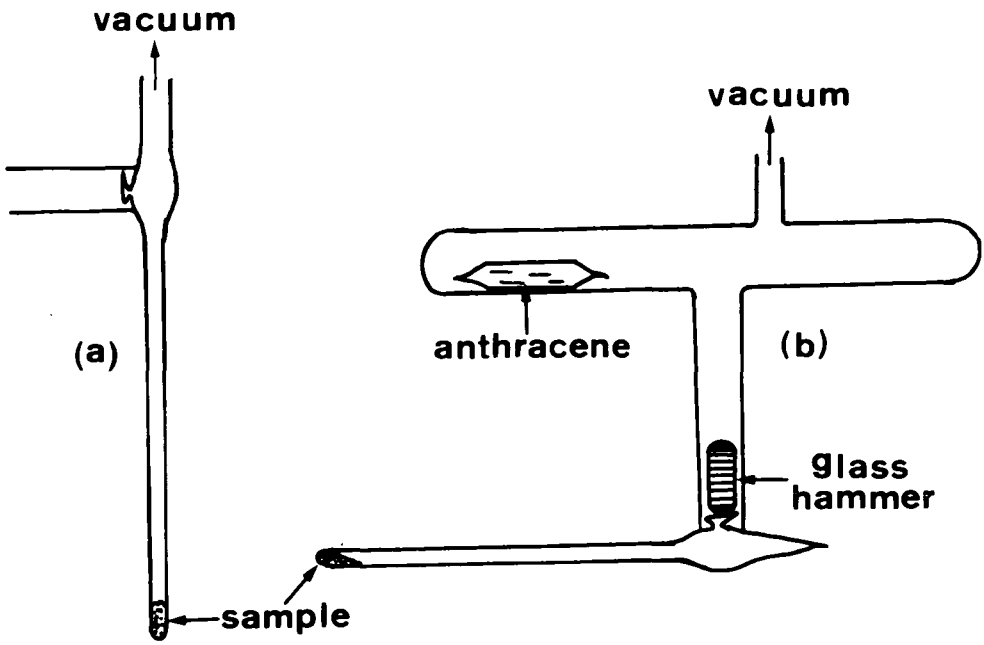

Fig. 1. a) Ampoule used to heat and irradiate the sample under vacuum. b) Ampoule used to introduce the anthracene under vacuum.

been obtained by adsorption of anthracene solution on the non-irradiated zeolite (11).

The curves in figure 2 represent the evolution of the number of positive radicals of anthracene A^+ formed on the irradiated $NaNH_4Y$ zeolite as a function of temperature. We observe that the number of A^+ formed at the irradiated zeolite with a dose of 12 Mrad is different from that at a non-irradiated solid. If the heating temperature is increased, the concentration of A^+ formed on the irradiated samples increases between room temperature and 300°C, remains constant between 300 and 400°C, decreases between 400-500°C and doesn't change if the temperature is increased further on.

When we compare these curves with those obtained from the variation in the loss of weight (thermogravimetry) (8), the intensity of OH groups (infra-red) (6) and the length of unit cell crystal (X-rays diffraction) (9) of $NaNH_4Y$ zeolites as a function of temperature, we notice, on the first hand, that the increase in A^+ number formed on the non-irradiated zeolites and, on the other hand, that the decrease in this number on the irradiated solids are within the temperature range at which the dehydroxylation of zeolites occurs. It seems that the acceptor sites of Al are responsible for the formation of A^+ radicals.

In addition, the number of A^+ formed on an irradiated zeolite

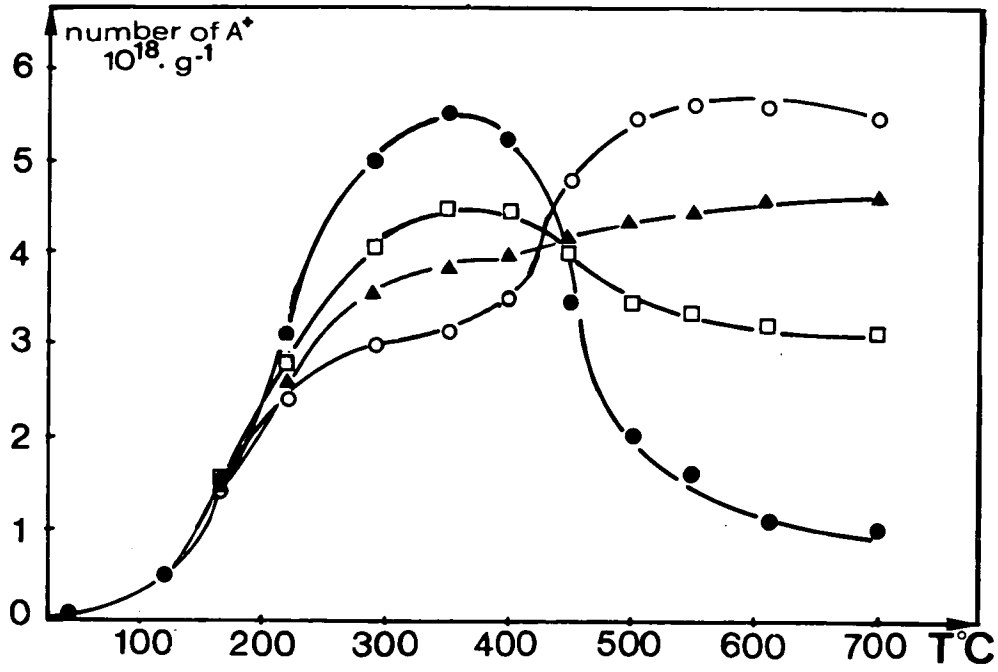

Fig. 2. Evolution of the number of positive radicals of anthracene A^+ formed at the irradiated $Na_{5,8}(NH_4)_{50,2}Y$ zeolite as a function of temperature. ○: 0 Mrad, ▲: 4 Mrad, □: 8 Mrad ●: 12 Mrad.

preheated at a temperature less than 500°C, is more than the number of A^+ formed on a non-irradiated sample preheated at same temperature but equal to this formed on a non-irradiated zeolite preheated at a temperature above 500°C.

On the contrary, the A^+ concentration formed on the irradiated zeolite preheated at a temperature above 500°C is much lower than this obtained on the non-irradiated zeolite preheated at same temperature.

The increase in the number of electron acceptor sites by γ irradiation at a heating temperature less than 500°C may be explained by admitting that the γ rays liberate oxidant sites by dehydroxylation of the solids. The behavior of $Na_{5,8}(NH_4)_{50,2}Y$ zeolite heated at different temperatures and irradiated with doses ranging between 0-20 Mrad have been studied. The number of A^+ formed between 300 and 400°C increases with the dose of irradiation and becomes constant above 12 Mrad. This constant is the same as the number of A^+ formed by heating a solid above 500°C without irradiation (figure 2).

In order to confirm that irradiation replaces heating in dehydroxylation of zeolite, several $NaNH_4Y$ samples having various ratios

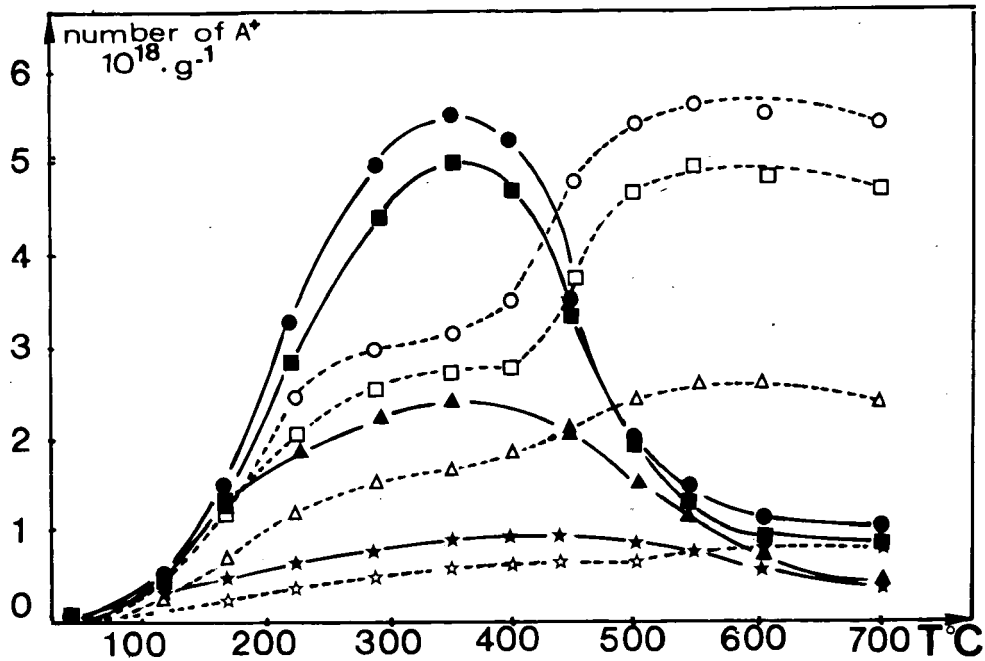

Fig. 3. Evolution of the number of positive radicals of anthracene A^+ formed at the irradiated (——) and non-irradiated (---) $NaNH_4Y$ zeolite as a function of temperature: (★☆) $Na_{56}Y$, (▲△) $Na_{36,4}(NH_4)_{19,6}Y$, (■□) $Na_{16,9}(NH_4)_{39,1}Y$, (●○) $Na_{5,8}(NH_4)_{50,2}Y$.

of Na^+/NH_4^+ have been heated at different temperatures and irradiated by 15 Mrad. We notice that the plateaus obtained between 300 and 400°C increase with the number of NH_4^+ in the unit cell of zeolite and are the same as those formed by the solids heated above 500°C but not irradiated (figure 3).

In addition, we have rehydrated, at room temperature, a sample preheated at 300°C and irradiated with a dose of 15 Mrad. Further treatment at 300°C without irradiation, we observed that the number of A^+ radicals was the same as this obtained from a non dehydroxylated sample. The same phenomenon have been observed with a sample heated at 500°C then rehydrated at room temperature with a further treatment at 300°C. These results confirm that zeolites can be dehydroxylated by γ irradiation.

As an evidence for a probable mechanism of the dehydroxylation of zeolites by irradiation, we suggest that the irradiation will form OH radicals and hydrogen atoms which will combine together to form water. The presence of these entities have been proved in our previous work (12). The suggested mechanism for the dehydroxylation is the

following:

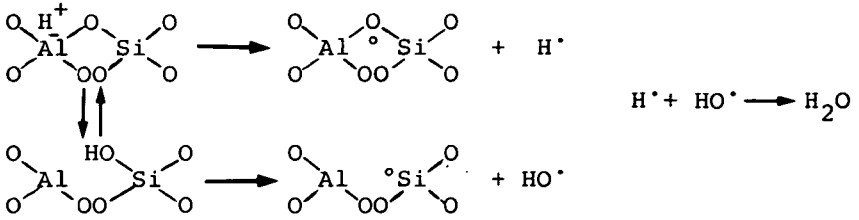

The electron acceptor centers obtained in this mechanism have previously been studied and observed by us (13).

The decrease in the electron acceptor centers under the effect of γ irradiation when a sample is heated above 500°C may be due to modifications in texture and structure of the zeolite. We have proved by X-rays analysis that the structure of the sample is not modified by irradiation (14). In addition, the specific area, determined by B.E.T. method, of $Na_{5,8}(NH_4)_{50,2}Y$ heated at different temperatures and irradiated by 15 Mrad is the same as this obtained from a non-irradiated solid (table 1). So, we can suppose that the reduction of acceptor centers by

Table 1

Comparison of specific area of irradiated and non-irradiated $Na_{5,8}(NH_4)_{50,2}Y$ zeolites

Heating temperature °C	300	400	450	500	600	700
Specific area of non-irradiated zeolite m^2/g	707	724	737	698	700	550
Specific area of irradiated zeolite m^2/g	705	713	740	698	703	558

the ejection of an electron by Compton effect during the irradiation.

To prove that the reduced centers are produced by γ irradiation, we put the irradiated and non-irradiated zeolites in contact with excess oxygen after the adsorption of anthracene. We observe in both cases that a sharp increase in the A^+ number will occur principally for the samples heated at high temperature but this number is less in the case of irradiated zeolite (figure 4) specially at the temperature above 500°C.

To interpret the increase in A^+ number in the presence of oxygen, we suggest two possibilities:

i) The A^+ radicals possess a long spin-lattice relaxation time T_1 which presents a saturated e.s.r. signal. Oxygen which has a short T_1

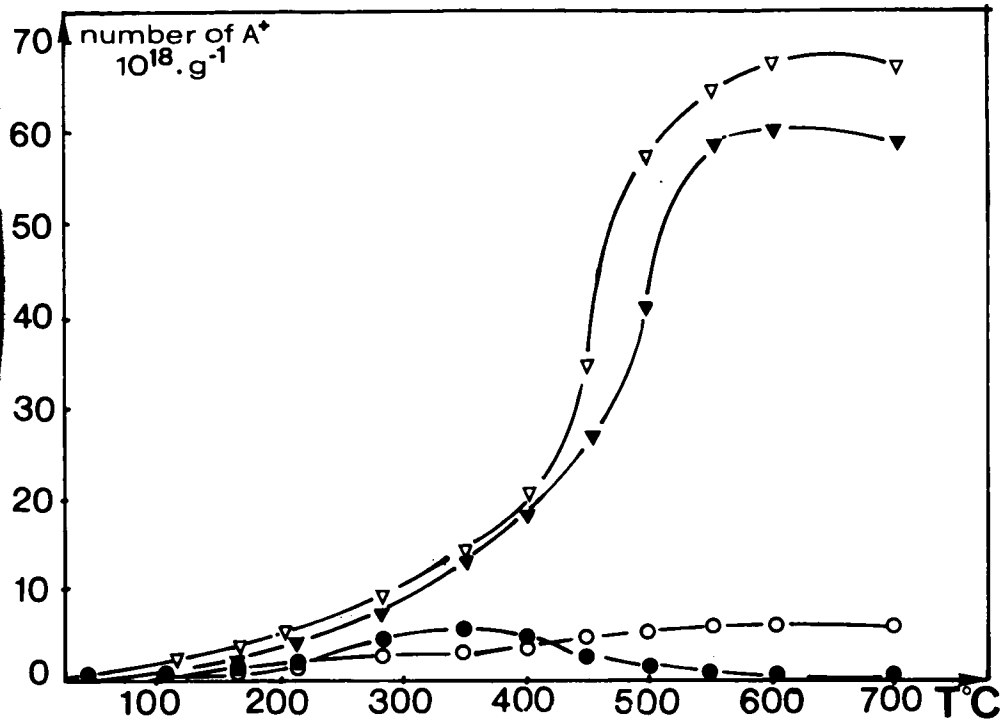

Fig. 4. Evolution of the number of positive radicals of anthracene A^+ formed at the irradiated (●▼) and non-irradiated (○▽) $Na_{5,8}(NH_4)_{50,2}Y$ zeolite under vacuum (●○) and in presence of oxygen (▼▽).

is capable of raising the saturation, thus increasing the intensity of the e.s.r. signal. This increase doesn't correspond to the real A^+ number present in the solid.

ii) Oxygen which possesses an electron affinity can play the role of an electron acceptor center. Thus it contributes to the increase in the electron affinity of some weak sites which will cause the formation of new A^+ radicals. Hall and coll (15) showed that the oxygen used in the reaction of charge transfer is strongly adorbed on the zeolite.

Although, we have recorded the e.s.r. signal at a lower hyperfrequency field to avoid the saturation of signal. It is logical to admit that second possibility is more adequate to interpret the increase in A^+ number in the presence of oxygen.

The difference in the number of A^+ observed on the irradiated and non-irradiated zeolite, after the introduction of oxygen is due to the reduction of strong electron acceptor sites by γ irradiation before oxygen is introduced. The latter is responsible for the increase in

the electron affinity of the weak sites. In the case of the non-irradiated zeolite, the oxygen increases the electron affinity of the weak and strong sites. This explains that the number of A^+ formed on the non-irradiated zeolite is greater than this formed on the irradiated.

CONCLUSION

We conclude from the above study that $NaNH_4Y$ zeolites heated under vacuum, at different temperatures, and irradiated by γ rays, creates weak and strong electron acceptor sites capable of transforming anthracene into a positive radical ion.

The irradiation modifies the number of oxidant sites. It is greater in samples preheated at a temperature below 500°C and afterwards irradiated than on the non-irradiated solids. This number is lower on the solids preheated above 500°C and then irradiated, than obtained on the non-irradiated zeolites.

The γ rays dehydroxylate the zeolite heated below 500°C and reduce the strong oxidant sites formed after dehydroxylation of solid. The weak sites are not modified by γ irradiation but their electron affinity increases in the presence of oxygen then they can ionize anthracene to form the positive radicals.

REFERENCES

1. Emmett, P.H., Livingston, R., Zeldes, H., Kokes, R.J., J. Phys. Chem. 66, 921 (1962).
2. Vedrine, J., Dalmai, G., Imelik, B., J. Chim. Phys. 65, 1780 (1968). Kazansky, V.B., J. Kinet. i Katal. 18, 43 (1977).
3. Aika, K.I., Lunsford, J.H., J. Phys. Chem. 81, 1393 (1977).
4. Abou-Kais, A., Vedrine, J.C., Massardier, J., Dalmai, G., Imelik, B., J. Chim. Phys. 69, 561 (1972).
   Abou-Kais, A., Massardier, J., Dalmai, G., Imelik, B., J. Chim. Phys. 69, 570 (1972).
5. Vedrine, J., J. Chim. Phys. 67, 439 (1970).
6. Uytterhoeven, J.B., Christner, L.G., Hall, W.K., J. Phys. Chem. 69, 2177 (1965).
   Ward, J.W., J. Catal. 11, 251 (1968).
7. Stamires, D.N., Turkevich, J., J. Amer. Chem. Soc. 86, 757 (1964).
   Vedrine, J.C., Massardier, J., Abou-Kais, A., Can. J. Chem. 54, 1678 (1976).
8. Ward, J.W., J. Catal. 9, 225 (1967).
9. Abou-Kais, A., Vedrine, J.C., J. Chim. Phys. 74, 481 (1977).

10. Kerr, G.T., J. Phys. Chem. 73, 2780 (1969).
Bennett, J.M., Smith, J.V., Mater. Res. Bull. 3, 633 and 933 (1968).
11. Ben-Taarit, Y., P.H.D. Thesis, Lyon University, 1970.
12. Abou-Kais, A., Vedrine, J.C., Massardier, J., Dalmai-Imelik, G., J. Chem. Soc. Farad. Trans. I 70, 1039 (1974).
13. Abou-Kais, A., Vedrine, J.C., Massardier, J., J. Chem. Soc. Farad. Trans. I 71, 1697 (1975).
14. Abou-Kais, A., ($3^{ème}$ cycle) Thesis, Lyon University, 1970.
15. Dollish, F.R., Hall, W.K., J. Phys. Chem. 71, 1005 (1967).

DEALUMINATION OF NaX ZEOLITE WITH NITROSYL CHLORIDE

P. FEJES, Gy. Schöbel, I. Kiricsi, I. Hannus
Department of Applied Chemistry, József Attila University, Szeged, Hungary

ABSTRACT

The interaction of nitrosyl chloride with NaX zeolite is described. The reactions observed in a static reactor and an i.r. cell using self-supporting wafers can be divided into two groups: at lower temperatures, an "ion-exchange" process takes place, the Na^+ ions being "exchanged" for the nitrosonium cation stemming from the reactant; at elevated temperatures, NOCl or its surface intermediate, the NO_3^- ion, leads to dealumination of the zeolite. A probable mechanism is proposed for the reactions eventually leading to dealumination.

INTRODUCTION

Since the first publications on "ultrastabilization" in 1966, an increasing number of papers have dealt with dealuminating procedures using different reactants and media, and with investigations of the various physical and chemical properties of the partly or completely dealuminated zeolitic samples [1-17].

A few recent papers describe dealumination procedures in which volatile halogen-containing reactants are used and dealumination is carried out as a gas-solid reaction in the absence of water vapour [18,19].

Some years ago we performed experiments to decrease the aluminium content of zeolites using volatile reagents [20-22]. It turned out that a wide class of chemicals, e.g. volatile metal halides, oxyhalides, thiohalides, acid halides and even metal alcoholates and alkyls, are able to cause dealumination to various extents.

The reactions taking place between a zeolite and some agent from the above classes can be divided into two groups.

The first group involves transformations at ambient temperature or slightly above, where the agent interacts with the exchange cation, resulting in a neutral molecule (which, if non-volatile, remains in

the framework, or, if volatile, leaves it) and in a charged species derived from the agent itself:

$$\{AlO_2^-\}H^+ + MX_n \longrightarrow \{AlO_2^-\}MX_{n-1}^+ + HX \qquad (1)$$

where M is unspecified and X is a halide, alkoxy, alkyl, etc. group. The stability and life-span of the MX_{n-1}^+ ion and its reactivity towar framework ions and extraneous reactants varies between very wide limits, depending mainly on the electronegativity of X.

The second group consists of surface reactions occurring at elevated temperatures between MX_{n-1}^+ and the framework constituents. These transformations have the following common characteristics: one (or two) framework O^{2-} ion(s) from among the nearest neighbours of the aluminium leave(s) the lattice to join MX_{n-1}^+; thereafter, provided X is of sufficient electronegativity (being for example some halide), the X species undergoes rearrangement, leading to the production of an aluminium-oxy-X cluster and an empty nest:

$$\{AlO_2^-\}MX_{n-1}^+ \longrightarrow AlOX + MOX_{n-2} + \{...\} \qquad (2)$$

where the symbol {...} stands for a framework vacancy. As far as MOX_{n-2} is concerned, its chemical identity depends on the valency of M, i.e. on the value of n.

This paper presents recent results on the probable mechanism of dealumination using NOCl as reagent. With M ≡ NO and n = 1, NOCl does not follow in all details the scheme outlined previously, but exhibits a peculiar behavious instead, which may turn out to be characteristic for this class of chemicals.

EXPERIMENTAL

The zeolite used in the experiments was NaX (Union Carbide Co., Linde Div.), as supplied.

The dealumination reactions were carried out in a recirculatory flow reactor and in an i.r. cell.

Both the gaseous products and the solids were analysed.

The surface reactions taking place upon the adsorption of NOCl were followed by i.r. spectroscopy, using self-supporting wafers of appr. 10 $mg \cdot cm^{-2}$ thickness. The adsorptions of the gaseous products of the dealumination (NO_2, NO) were studied separately.

The KBr pressed pellet technique was used for determination of the spectra of the dealuminated zeolites in the structure-sensitive i.r. region.

RESULTS

The gases released in the interaction of NaX zeolite with NOCl were determined in a recirculatory flow reactor. It was found that their molar ratio corresponded to $NOCl:NO_2:NO = 2:1:1$, suggesting an overall reaction in agreement with Eq. (1):

$$2\ \{AlO_2^-\}Na^+ + 2\ NOCl \longrightarrow 2\ \{AlO_2^-\}NO^+ + 2\ NaCl + N_2O_3$$

For investigation of the mechanisms of the reactions taking place between NaX and NOCl in situ, i.r. measurements were performed. Figure 1 shows the spectra recorded upon the adsorption of $3 \cdot 10^2$ Pa NOCl on the pretreated (at 773 K in vacuum) NaX zeolite wafer. After the admission of NOCl at room temperature, three absorption bands appeared, at 2375, 2010 and 1370 cm^{-1}.

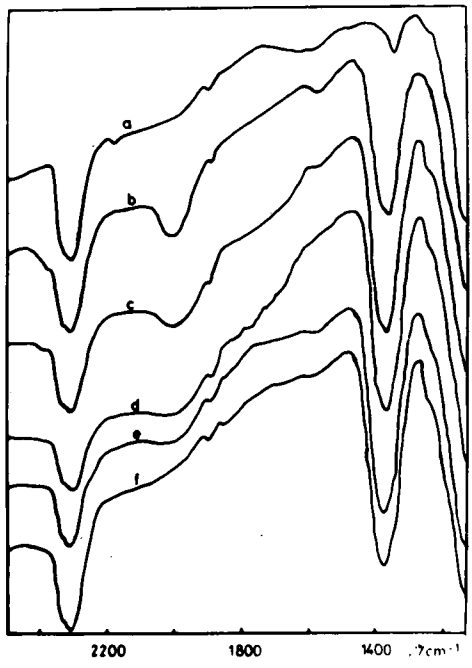

Fig. 1. Infrared spectra of adsorbed NOCl
(a) pretreated NaX
(b) at ambient temperature
(c) 0,5 h at 373 K
(d) 3 h at 373 K
(e) 15 h at 373 K
(f) 0,5 h at 373 K evacuated

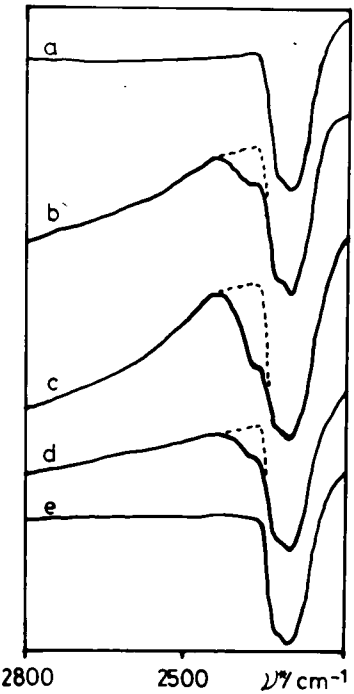

Fig. 2. Infrared spectra of adsorbed NOCl
(a) pretreated NaX
(b) at ambient temperature
(c) 11 h at 273 K
(d) 0,5 h at 373 K
(e) 3 h at 373 K

After heat treatment at 373 K, the intensity of the band at 2010 cm^{-1} decreased. Evacuation at the same temperature led to the complete disappearance of this band. It seems very likely that the absorption at 2010 cm^{-1} is caused by adsorbed NOCl.

The nature of the shoulder at 2375 cm^{-1} was studied in a separate experiment at higher NOCl pressures, for the frequency of this band overlaps with that of the NO^+ ion [23]. The intensity of this band follows a maximum curve as a function of temperature (see Fig. 2), and therefore the species causing this band should be a reaction intermediate.

On elevation of the temperature, the band at 1375 cm^{-1} (probably due to the NO_3^- ion in the zeolite structure [24]) decreases in intensity and two new bands appear, at 1240 and 1630 cm^{-1}, assigned to NO_2^- ions formed in the framework and to adsorbed NO [25], respectively. Heat treatment at 673 K causes a shift in the frequency of the band at 1630 cm^{-1} to 1690 cm^{-1}, and following evacuation it disappears.

From the results of i.r. measurements and reactor experiments it can be concluded that the main gaseous products of the reactions are different nitrogen oxides. In order to assign the bands observed and to acquire a more detailed insight into the reactions taking place in the zeolite framework, separate experiments were carried out with NO_2 and NO, under the same conditions as used with NOCl.

Figure 3 shows the spectra following the adsorption of $4 \cdot 10^2$ Pa NO_2 on NaX zeolite. At room temperature two absorption bands appear, at 1915 and 1370 cm^{-1}. The former band is caused by sorbed NO_2 [26] and the latter can be assigned to the NO_3^- ion. At higher temperatures two other bands develop, at 1690 and 1245 cm^{-1}, while the intensity of the band at 1370 cm^{-1} decreases. The band at 1370 cm^{-1} has the same temperature-dependence as the nitrate band in the case of NOCl adsorption.

Figure 4 shows the absorption bands upon the adsorption of NO on NaX zeolite. The band positions at ambient temperature are 1630, 1240 and 1690 cm^{-1}. It can be seen clearly that, as the temperature is raised the intensity of the band at 1240 cm^{-1} (assigned to NO_2^- ions in the zeolite structure) increases, attains a maximum, and then decreases, provided the sample was exposed to heat treatment at 473 K or above. Simultaneously, the heating gives rise to two new bands, at 1470 and 1410 cm^{-1}.

Figure 5 shows the spectrum of the NaX sample treated with NOCl in the structure-sensitive i.r. region. Comparison of this spectrum with that of the untreated specimen reveals two new absorption bands,

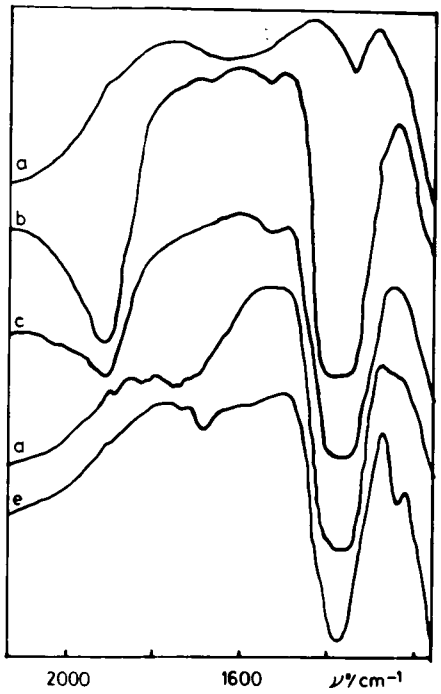

Fig. 3. Infrared spectra of adsorbed NO_2
(a) pretreated NaX
(b) at ambient temperature
(c) evacuated at ambient temperature
(d) 0,5 h at 573 K
(e) 0,5 h at 673 K

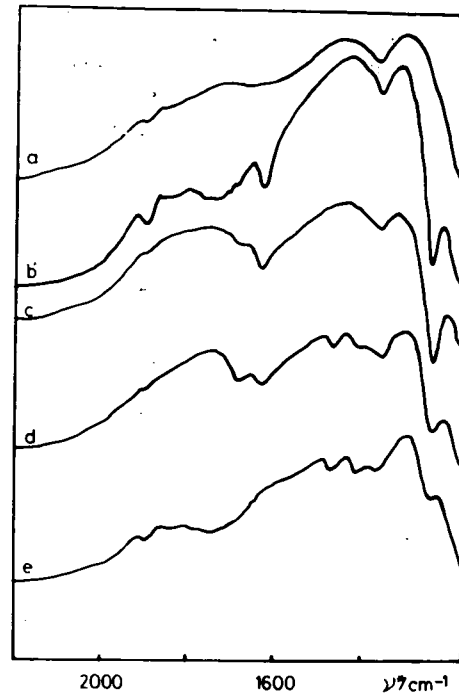

Fig. 4. Infrared spectra of adsorbed NO
(a) pretreated NaX
(b) at ambient temperature
(c) 15 h at 373 K
(d) 15 h at 473 K
(e) 3 h at 573 K

at 1390 and 860 cm^{-1}. The spectrum of NO_3 ions residing in the structure of an NaX sample prepared by the well-known salt occlusion technique exhibits the same characteristics (see Fig. 5, spectrum c).

DISCUSSION

The wavenumbers and the assignments of the bands observed on the adsorption of NOCl, NO_2 and NO on NaX zeolite are listed in Table 1. The spectroscopic changes caused by prolonged adsorption and heat treatment are indicated.

The sequence of reactions taking place during the interaction of NOCl with NaX can be visualized as follows.

At 293 K and above the i.r. absorption developing at 2375 cm^{-1} suggests the formation of NO^+ cations, with the simultaneous formation

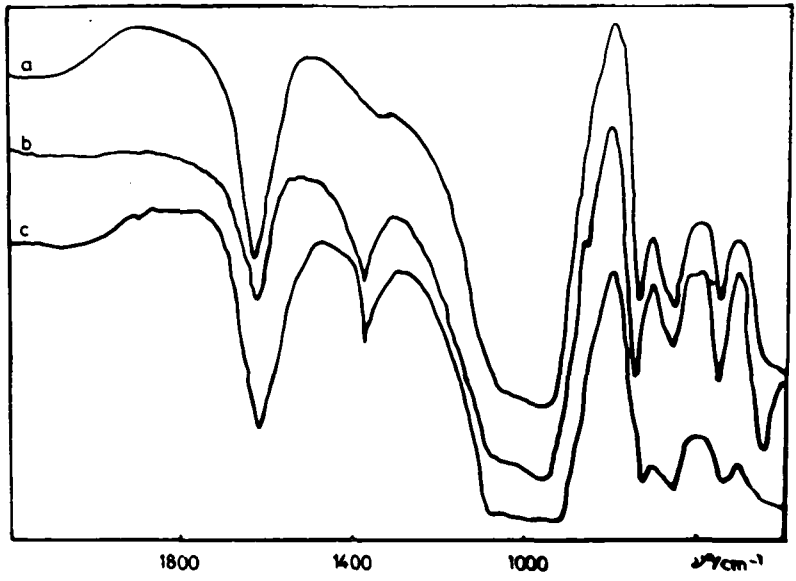

Fig. 5. Infrared spectra of NaX samples in the structure sensitive region
(a) pretreated NaX
(b) NaX treated with NOCl
(c) $NaNO_3$ occluded in NaX framework

of NaCl. It is believed that this reaction is similar to that described by Beattie for the interaction of NOCl and analcite [27]. It is essentially an "ion-exchange", where Na^+ ions are substituted for the NO^+ "ions" of NOCl in agreement with Eq. (1):

$$\{AlO_2^-\}Na^+ + NOCl \longrightarrow \{AlO_2^-\}NO^+ + NaCl$$

At 373 K the band intensity at 2375 cm^{-1} follows a maximum curve, indicating that NO^+ is a surface intermediate and should therefore be involved in successive transformations.

The i.r. absorption at 1370 cm^{-1}, characteristic of the NO_3^- ion, provides evidence that the redox step

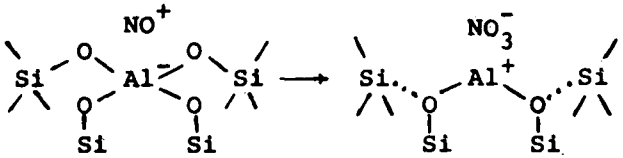

takes place during the elimination of <u>two</u> lattice O^{2-} ions and simultaneous oxidation of the trivalent nitrogen into the pentavalent state. The fate of the two electrons left behind is uncertain at present. After this step the aluminium is presumed to remain bound in the zeolitic lattice.

Table 1

Assignment of the observed bands

Adsorption of	Wavenumber /cm^{-1}				
NOCl	2375	2010	1630	1370	1240
Assignment:	NO^+ ion	adsorbed NOCl	adsorbed NO	NO_3^- ion	NO_2^- ion
Remarks:	maximum curve	decreases in time and with temp. rise	increases	decreases	maximum curve
NO_2		1915	1690	1370	1245
Assignment:		adsorbed NO_2	adsorbed NO	NO_3^- ion	NO_2^- ion
Remarks:		decreases	increases	decreases	increases
NO		1910	1630		1240
Assignment:		adsorbed NO_2	adsorbed NO		NO_2^- ion
Remarks:		decreases	decreases under evacuation		maximum curve

On elevation of the temperature up to 473 K, a strange reversal of the previous redox step takes place: the loosely bound aluminium leaves the lattice and the ($Al^+NO_3^-$) moiety rearranges by charge transfer into $AlONO_2$, where the nitrogen is again present as a trivalent species:

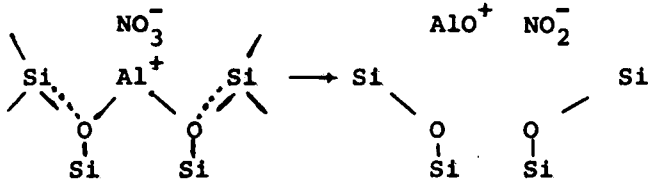

The formation of NO_3^- and NO_2^- ions in the interaction of NOCl with NaX zeolite is corroborated by comparison of the spectra in Fig. 5. The ions reside as stable entities in the structure of the zeolite, unless the reaction temperature exceeds their decomposition temperature. On washing of the treated sample with distilled water, the NO_3^- and NO_2^- ions can be transferred into solution and their concentrations determined by classical analytical methods.

The formation of N_2O_3 is due to the thermal decomposition of the $AlONO_2$ species:

$$2\ AlONO_2 \longrightarrow Al_2O_3 + N_2O_3$$

$$N_2O_3 \rightleftharpoons NO + NO_2$$

The newly formed strained Si - O - Si linkages produce i.r. absorption at 860 cm^{-1}, as shown in Fig. 5. Similar bands could be observed in the case of mordenites dealuminated with phosgene [22].

REFERENCES

1. McDaniel, C.V., Maher, P.K., Soc. Chem. Ind. London 1968, p. 186 Maher, P.K., McDaniel, C.V., US Pat 3 293 192 (1966).
2. Ha, B.H., Guidot, J., Barthomeuf, D., J. Chem. Soc. Faraday Trans. I. 75, 1245 (1979).
3. Ha, B.H., Barthomeuf, D., J. Chem. Soc. Faraday Trans. I. 75, 2366 (1979).
4. Mishin, I.V., Piloyan, G.A., Klachkogurvich, A.L. Rubinstein, A.M., Izv. Akad. Neuk. Ser. Khim. 1, 343, 455 (1973).
5. Eberly, P.E., Kimberlin, C.N., Ind. Eng. Chem. Proc. Res. Dev. 9, 355 (1970).
6. Vuks, T.J., Hillery, H.F., Bolton, A., J. Chem. Soc. Faraday Trans. I. 71, 2051 (1975).
7. Chen, N.Y., J. Phys. Chem., 80, 60 (1976).
8. Wendlandt, K-P., Weigel, W., Hofmann, F., Bremer, H., Z. Anorg. Allg. Chem., 51, 445 (1978).
9. Mishin, I.V., Rubenstein, A.M., Wendlandt, K-P., Z. Anorg. Allg. Chem., 17, 467 (1980).
10. Wendlandt, K-P., Bremer, H., Becker, K., Steinberg, P., Acta Phys. Chem. Szeged, 22, 335 (1978).
11. Koradia, P.B., Kiovsky, J., Asim, M.Y., J. Catal., 66, 290 (1980).
12. Kranich, W.L., Ma, Y.H., Sand, L.B., Weis, A.H., Zwiebel, I., Adv. Chem. Ser., 101, 502 (1970).
13. Bosacek, V., Patzelova, V., Tvaruzkova, Z., Freude, D., Lohse, U., Schirmer, W., Stach, H., Thamm, H., J. Catal., 66, 435 (1980).
14. Kerr, G.T., J. Phys. Chem., 71, 4155 (1967), 72, 2594 (1968), 73, 2780 (1969).
15. Wichterlova, B., Novakova, J., Kubelkova, L., Jiru, P., Proc. Int. 5th Congr. Zeol. Naples, Italy, Hyden, 1980, p. 373.
16. Ione, K.G., Sterpanov, V.G., Mastikhin, V., Paukshtis, V., Proc. Int. 5th Congr. Zeol. Naples, Italy, Hyden, 1980, p. 223.
17. Klinowski, J., Thomas, J.M., Audier, M., Vasudevan, S., Fyfe, C.A., Hartman, J.S., J. Chem. Soc. Chem. Com., 570 (1981).

18. Beyer, H.K., Belenkaja, I., Catalysis by Zeolites, Elsevier, Amsterdam, 1980, p. 203.
19. Klinowski, J., Thomas, J.M., Anderson, M.W., Fyfe, C.A., Gobbi, G.C., Zeolites, 3, 5 1983
20. Fejes, P., Kiricsi, I., Hannus, I., Acta Phys. Chem. Szeged, 28, 173 (1982)
21. Hannus, I., Kiricsi, I., Dékány, I., Fejes, P., Acta Phys. Chem. Szeged, 30, 107 (1984)
22. Fejes, P., Hannus, I., Kiricsi, I., Zeolites, 4, 73 (1984).
23. Little, L.H., Infrared Spectra of Adsorbed Species, Academic Press, London, 1966, p. 84.
24. Rabo, J.A., Zeolite Chemistry and Catalysis, ACS Monograph 171, Washington, 1976, p. 338.
25. Rabo, J.A., Zeolite Chemistry and Catalysis, ACS Monograph 171, Washington, 1976, p. 202.
26. Wada, Y., Otsuka, K., Morikawa, A., J. Catal., 81, 291 (1983).
27. Beattie, I.R., J. Chem. Soc. A. 1957, p. 367.

CATALYTIC PROPERTIES OF ZSM-TYPE ZEOLITES FORMED UNDER DIFFERENT CONDITIONS IN REACTIONS OF CONVERSION OF PARAFFINIC AND AROMATIC HYDROCARBONS

S.P. ZHDANOV[a], N.N. Feoktistova[a], N.I. Kozlova[a], N.R. Bursian[b], S.B. Kogan[b], V.K. Daragan[b], N.V. Aleksandrova[b]

Institute for Chemistry of Silicates, U.S.S.R. Academy of Sciences, Leningrad, U.S.S.R. (a)

All-Union Scientific and Research Institute for Petrochemical Processes, Leningrad, U.S.S.R. (b)

ABSTRACT

Research has been made to compare catalytic properties of H-ZSM-5 type zeolites, H-mordenite (SiO_2:Al_2O_3 = 9-100) and silicalite, in reactions of paraffinic and aromatic hydrocarbons in hydrogen media at P = 3.5 MPa and T = 533-613 K. The H-ZSM-zeolite possesses much higher destruction activity in n-hexane conversion at much lower product isomerization degree which is noticed also with corresponding platinum catalysts. The difference between H-ZSM-zeolites and H-mordenites consists in the different qualitative composition of alkyl benzenes formed by the reaction between n-hexane and benzene. The results demonstrate the variety in chemical nature of n-hexane conversion over the tested zeolites.

INTRODUCTION

On the basis of the previously published data, it might be assumed that zeolites ZSM-5 could be synthesized only in the presence of quaternary ammonium bases or their derivatives. Later it became known that ZSM-5 zeolites might be easily cristallized from aluminosilicate mixtures either containing other organic compounds or without them. It might be expected that the usage of different organic compounds would lead to the formation of ZSM-5-type zeolites distinguished not only by their constitution, but also by their catalytic properties.

EXPERIMENTAL

In the present work, in order to investigate catalytic properties of ZSM-5 zeolites, the samples with various SiO_2:Al_2O_3 ratios

were synthesized. In order to eliminate the possible influence of organic compounds, butyl alcohol was used as organic component in all cases.

Silicalite was also synthesized in the silicate system in the presence of tetrapropylammonium hydroxide.

In all cases, the synthesis was conducted at 423 K in steel autoclaves with teflone inserts. The analytical data on the composition of initial mixtures and crystals are shown in Table 1.

Table 1

Chemical composition of initial mixtures and crystals of ZSM samples

Samples	Moles per 1 mole Al_2O_3					
	Initial mixtures				Crystals[x)]	
	Na_2O	SiO_2	H_2O	C_4H_9OH	Na_2O	SiO_2
ZSM-5	1.28	20	512	34.7	0.87	17
ZSM-5	3.62	60	1453	98.4	0.99	49
ZSM-5	4.10	100	1652	86.2	1.00	97.1

[x)] Incineration losses are to be neglected.
The composition of silicalite crystals corresponds to 0.011 moles Na_2O per 1 mole SiO_2.

ZSM-5 zeolites containing organics are stable to temperatures up to 973-1073 K, their thermostability increases with the increase in SiO_2:Al_2O_3 ratio in crystals. By means of chemical modification of ZSM-5 crystals, their thermostability can be risen up to 1273-1373 K.

In the present work, the properties of pentasiles have been investigated in conditions of paraffin hydrocracking which goes through disproportionation stages resulting mainly in the formation of initial hydrocarbon with the minimum yield of destruction products (C_1-C_2). The similar conversion of n-hexane has been studied over the catalyst on the base of H-mordenite under hydrogen pressure and at the temperature of 593-623 K [1, p. 341;2].

The experiments with mordenites (H-M) were used in this work as reference standards. The sample with silicate modulus 13 (standard), and mordenite obtained by dealuminizing of the standard with a ratio SiO_2:Al_2O_3 = 59 were studied.

Zeolite powdered was formed together with γ-Al_2O_3 (3:1, mass.). The tests were conducted in an ordinary unit of flow-through type. The

amounts of catalyst from 1 to 8 cm^3 with particle size 0.1-0.2 cm were used. Test conditions are listed in notes to Tables 2, 3 and Figures 1-3.

RESULTS AND DISCUSSION

The most significant difference of H-ZSM zeolites as opposed to H-M consists in their much higher destructive activity in conversion of n-hexane at lower (compared with H-M) product isomerization degree (Table 2).

Although the optimum value of silicate modulus approaches 50, the above conclusion is practically true for entire interval of its values (except the low-active silicalite), and also with the changing of conversion degree (10-70%) according to the experimental conditions (T = 533-613 K, LHSV = 4-16 hrs^{-1}).

Table 2

Conversion of n-hexane over H-M- and H-ZSM-type zeolites[x)]

No.	Zeolite/SiO_2:Al_2O_3	Conv. of n-C_6, mass%	Selectivity, %				iso/n		
			C_3	ΣC_4	ΣC_5	ΣiC_6	C_4	C_5	C_6
1	H-M/13	16.5	13.1	13.5	10.5	62.9	2.3	2.8	0.1
2	H-M/59	23.1	7.1	18.7	14.2	59.7	3.4	3.7	0.2
3	H-ZSM/17	33.4	19.8	39.8	25.2	15.2	0.7	0.8	0.1
4	H-ZSM/49	50.6	16.0	40.8	28.1	15.1	0.8	0.9	0.1
5	H-ZSM/100	37.3	15.9	40.3	28.2	15.6	0.8	0.9	0.1
6	Silicalite/~40 000	0.5	6.4	17.0	12.8	63.8	3.0	4.0	0.01

x) T = 573 K, LHSV = 8 hrs^{-1}, P_{H_2} = 3.5 MPa

The increase in conversion degree as a function of modulus (in the interval of 9-49) when passing from mordenite to ZSM is observed for corresponding platinum catalyst with the difference that platinum favours the formation of iso-hexane (in accordance with data [3]) with maximum selectivity for SiO_2:Al_2O_3 = 13 (Pt/H-M, Fig. 1).

The data on the comparison of catalitic activity between H-ZSM- and H-M-type zeolites support the conclusion [4,5] that the decline in number of acidic centers due to decrease in aluminium concentration is followed by the increase in their acidic strength. In the publications, this problem still remains controversial [4-7].

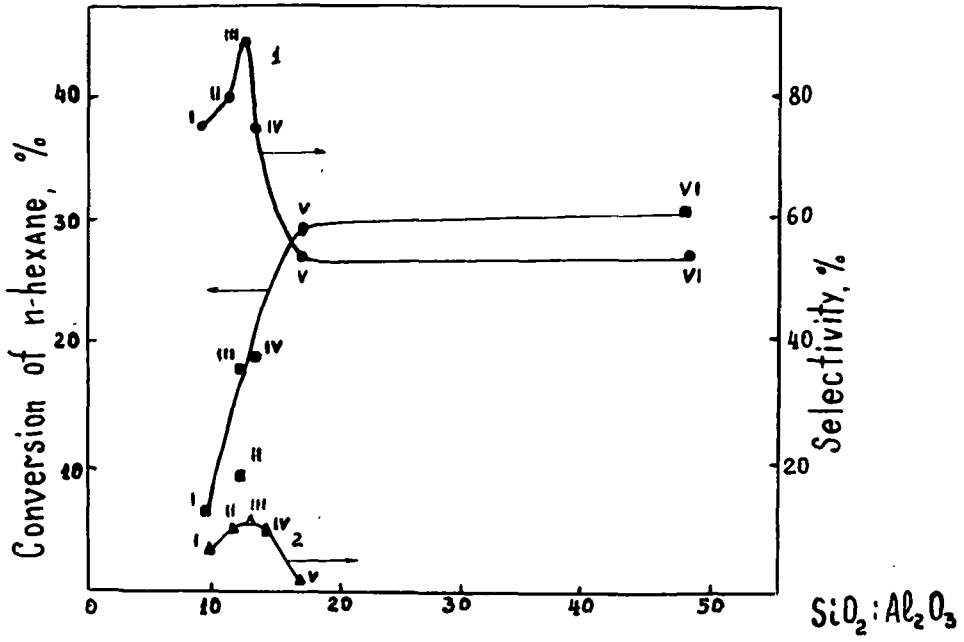

Fig. 1. Conversion of n-hexane over Pt/H-M and Pt/H-ZSM
1 - Selectivity of iso-C_6 formation
2 - Selectivity of 2,2-dimethylbutane formation
I-IV - Pt/H-M
V-VI - Pt/H-ZSM

We have previously shown that, when n-hexane destruction products react with benzene over dealuminized H-M, the main initial product is ethylbenzene [8]. The similar product distribution is observed over standard H-M with modulus equal to 13 (Fig. 2, 1-2).

The zeolites of H-ZSM-type are at the similar conditions characterized by the formation of mainly propylbenzenes along with the formation of higher alkylbenzenes and minimum quantities of ethylbenzene irrespective to conversion degree and silicate modulus (Fig. 2, 3-5).

The conversion of benzene without paraffin at these conditions is negligible, so the composition of alkylbenzenes (if secondary reactions are restricted) depicts the composition of n-hexane distribution products, which are intermediates in the formation of final products, paraffins C_3-C_5. Thus, the prevalence of propylbenzenes over H-ZSM shows the significant difference in chemical mechanisms on n-hexane destruction over H-ZSM and over H-M at the same conditions.

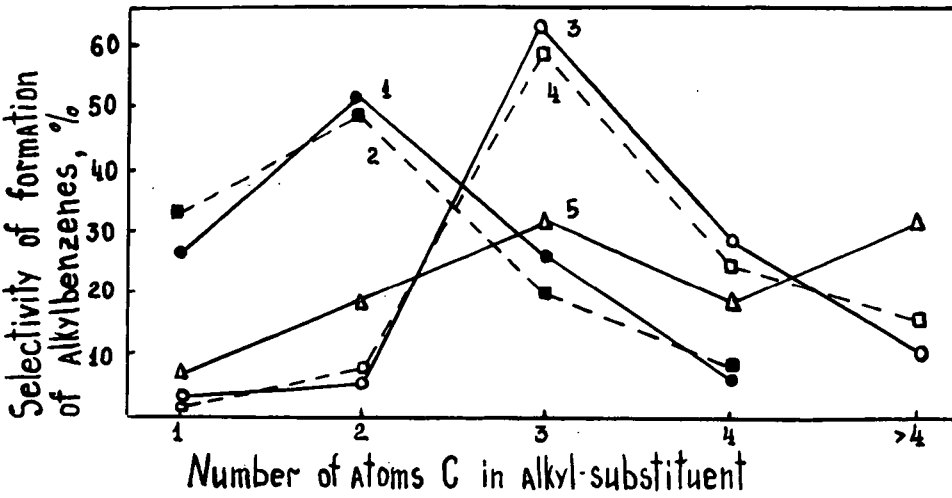

Fig. 2. Distribution of alkylbenzenes in the product of reaction between n-hexane and benzene (86 mole % $n\text{-}C_6H_{14}$ + 14 mole % C_6H_6) over zeolites of H-ZSM- and H-M-type

	$SiO_2:Al_2O_3$	T, K	LHSV, hrs^{-1}	$n\text{-}C_6H_{14}$ conversion, mass %	C_6H_6 conversion, mass %
1 - H-M	13	613	8	18.4	12.1
2 - H-M	59	613	8	28.0	15.0
3 - H-ZSM	17	533	16	20.0	19.4
4 - H-ZSM	49	533	16	22.0	21.7
5 - H-ZSM	17	613	4	70.0	67.2

This effect may be explained by means of the schemes listed below:

I (over H-M):

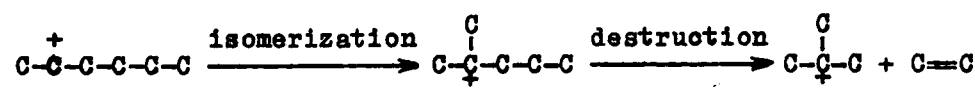

II (over H-ZSM):

It is supposed that the formation of branched structures on H-ZSM-zeolites compared to H-M faces difficulties due to the reduction of effective channel radii in the ZSM structure, which is evidenced by the suppression of 2,2-dimethylbutane formation. At the same time, strong acidic centers of H-ZSM catalyze cleavage with the formation of C_3 fragments (i.e. Scheme II prevails).

It should be noticed that introduction of small amounts of benzene (14%) into the hydrocarbon does not affect the conversion of n-hexane over H-ZSM. Only an excess of benzene (88%) causes some reaction retardation (Table 3).

Table 3

Conversion of n-hexane over zeolites of H-M- and ZSM-type in the presence of benzene[x)]

No.	Zeolite/SiO_2:Al_2O_3	Benzene alkylation degree, mass %	n-Hexane conversion, mass %	Selectivity, %			
				C_3	C_4	C_5	iC_6
	Feedstock: 86 mole% n-C_6H_{14} + 14 mole% C_6H_6						
1	H-M/13	3.8	10.5	10.4	15.4	10.5	63.7
2	H-M/59	6.0	14.6	6.9	13.4	9.2	70.5
3	H-ZSM/17	36.3	34.9	17.4	37.5	25.7	19.4
4	H-ZSM/49	67.5	53.6	15.3	41.1	28.7	14.9
	Feedstock: 12 mole% n-C_6H_{14} + 88 mole% C_6H_6						
5	H-ZSM/17	1.5	29.3	15.4	28.2	22.2	34.2

x) T = 573 K, LHSV = 8 hrs^{-1}

The formation of higher alkylbenzenes is the result of benzene alkylation by the products of oligomerization that also observed in the reaction of benzene alkylation by ethylene on acidic catalysts [1, p. 392].

Actually, in the experiments with mixture containing excess of benzene, there was observed an abrupt decrease in higher alkylbenzen yield with the formation of equal amount of ethylbenzene (Fig. 3).

Therefore, the presence of ethyl- and butylbenzenes in the primary products formed over H-ZSM points to the fact that n-hexane conversion in this case partially follows Scheme (I).

The fact, that ethylene oligomerization at relatively low benzene concentration (12% compared to 88% over H-ZSM) is prevented over H-M, agrees well with the above conclusion that H-ZSM-type zeolites have acidic centers with higher strength.

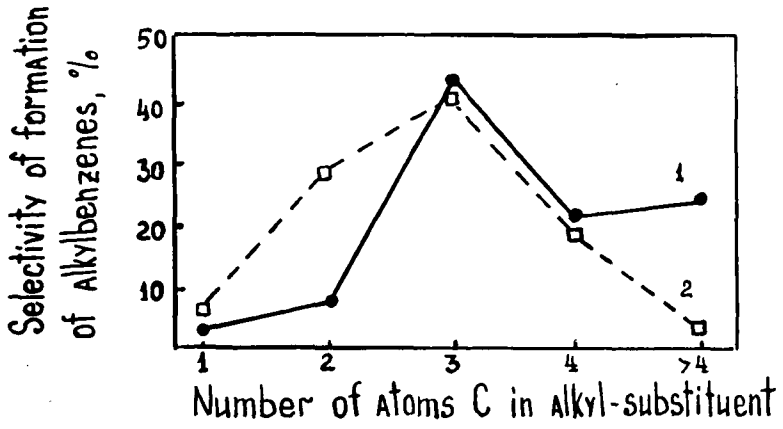

Fig. 3. The effect of bezene concentration on the distribution of alkylbenzenes over H-ZSM zeolite
$SiO_2:Al_2O_3$ = 17, T = 573 K, LHSV = 8 hrs^{-1}
1 - 14 mole % C_6H_6, 2 - 88 mole % C_6H_6

REFERENCES

1. Bolton, A.P. Gidrokreking, izomerizatsiya i drugie promyshlennye protsessy. - In: Khimiya tseolitov i kataliz na tseolitakh. J.Rabo ed. Russ. translation, Kh.M.Minachev ed., Moscow, Mir Publ., 1980, Vol. 2, p. 341, 392.
2. Bursian, N.R., Kogan, S.B., Lastovkin, G.A., Orlov, D.S., Khimiya i tekhnologiya topliv i masel, No. 10, 7 (1981).
3. Sharikhina, M.A., Loginova, A.N., Dyrin, V.G., Levinter, M.E., Nefedov, B.K., Alekseeva, T.V., Neftekhimiya, 23, 485 (1983).
4. Minachev, Kh.M., Kondratiev, D.A., Uspekhi Khimii, 52, 1921 (1983).
5. Kazansky, V.B., Kinetika i kataliz, 23, 1334 (1982).
6. Hidalgo, C.V., Itoh, H., Hattori, T., Niwa, M., Murakami, J., J. Catal., 85, 362 (1984).
7. Vedrine, J.C., Auroux, A., Boles, V., Dejaifie, P., Berg, J.P., van den, J. Catal., 59, 248 (1979).
8. Kogan, S.B., Daragan, V.K., Bursian, N.R., Neftekhimiya, 24, 32 (1984).

STRUCTURE AND CATALYTIC PROPERTIES OF FERRISILICATE ZEOLITES OF THE PENTASIL GROP

P. RATNASAMY, R. B. Borade, S. Sivasanker, V. P. Shiralkar, S. G. Hegde, National Chemical Laboratory, Pune 411008, India.

ABSTRACT

A ferrisilicate pentasil zeolite was synthesised. Its structure was characterised by XRD, ESCA, Mössbauer, ESR and IR spectroscopy, magnetic susceptibility and adsorption techniques. The as-synthesised zeolite contains Fe^{3+} in (1) isomorphous substitution in lattice positions, (2) cation exchange positions and (3) oxide/hydroxide phases. On treatment with nitric acid, the Fe^{3+} ions in non-lattice positions are extracted out. The product is an iron zeolite containing Fe^{3+} and Si^{4+} ions in tetrahedral lattice positions. The temperature-programmed desorption of NH_3 from this zeolite reveals the absence of very strong acid sites in it. Consequently, its catalytic property in the isomerisation of xylenes is different from that of the aluminium analog.

INTRODUCTION

The discovery, manufacture and industrial applications of synthetic crystalline aluminosilicate zeolites has been one of the significant developments in catalysis during the past half century. We now report the synthesis, physicochemical and catalytic properties of a ferrisilicate pentasil zeolite containing both iron and silicon in lattice positions. Even though there are references in the patent literature [1-4] on the

synthesis and catalytic properties of these materials, there are no detailed journal reports on this system. Marosi et al [1,2] claimed the preparation of zeolites with ZSM5 topology and containing iron. No experimental data were provided regarding the location of iron [5].

EXPERIMENTAL

Materials : The iron zeolites (FeZ) were prepared using various sources of Fe, Si, alkali as well as different organic templates [6]. A typical procedure is given below. To 20 g of sodium silicate (8.2% Na_2O, 27.2% SiO_2, 64.6% H_2O)10 ml of water is added to constitute solution A. 2.5 g of tetrapropylammonium bromide is dissolved in 10 ml of water to give solution B. 0.54 g of ferric sulphate (31.2% Fe_2O_3 is added to enough water at 323 K to yield a clear solution C. 1.76 g of H_2SO_4(98%) is diluted in 15 ml of solution to give solution D. Solution B is added to solution A with stirring.Solution C is then added to the mixture with stirring. Solution D is finally added to the resulting mixture dropwise with constant vigorous stirring. A solid gel is formed whose pH is about 10.2. The slurry containing the gel is heated at 423 K in an autoclave under autogenous pressure for 24 hrs. The autoclave is then quenched in cold water. The solid product is filtered, washed with hot water till the filtrate is free from sulphate ions and dried at 393 K for 12 hrs. The material was then calcined in a static air oven at 823 K for 8 hrs to remove the organics. The acid form of the zeolite was obtained by ion exchange (twice) with 5 N ammonium nitrate solution at 363 K for 15 hrs followed by drying and calcination. The non-zeolite iron was finally

extracted out by treatment with nitric acid. The purity of all the reagents and chemicals ued for the adsorption, TPD and catalytic experiments was better than 99%.

Procedures : The instruments and procedures for measuring the X-ray diffraction pattern, temperature-programmed desorption of NH_3, adsorption isotherms and catalytic properties of pentasil zeolites were similar to those described earlier [7-11] for HZSM5 samples. The XPS measurements were performed [12] with a commercial XPS spectrometer (Vaccum Generators, ESCA 3 MK II). The experimental techniques including the calibrations procedures had been described earlier [12].

The ESR spectra were recorded on a Brucker E.R. 100 D spectrometer, at 298 K. The spectrometer was operated at X-band frequency (9.6 GHZ) and calibrated with diphenyl picryl hydrazine (DPPH). The Mössbauer spectra were recorded by Dr. B. Clausen (Haldor Topsoe, Denmark) using a source of ^{57}Co in Rh matrix (Amersham) with the spectrometer in the constant acceleration mode. The spectrometer was calibrated with a thin (12.5 μ m) foil of α- Fe at room temperature. Isomer shifts are given relative to the centroid of this spectrum. 125 mg/cm of sample was used. The magnetic susceptibility data were obtained by the Faraday method at 298 K.

RESULTS AND DISCUSSION

1. Composition and crystal structure : The unit cell composition of a typical sample of iron zeolite (Fe2) in the anhydrous acid form was $Na_{0.04}H_{2.55}[(SiO_2)_{93.41}(FeO_2)_{2.59}]$. Its XRD pattern,that of an aluminium pentasil zeolite ZSM5(Al)

and silicalite are shown in Fig. 1. From the similar X-ray patterns, it is concluded that all the samples of Fig. 1 are pentasil zeolites. This is further supported by the IR framework vibration frequencies of FeZ (Table 1) which are similar to those for HZSM5 [7]

Table 1 : IR frequencies (cm^{-1}) of FeZ and HZSM5(Al)

FeZ : 455,550,590,620,678,730,800,870,888,1040,1100,1230

HZSM5(Ref.7): 450,540,590,620,680,720,790,840,1075,1220

2. Oxidation state and location of iron :

A XPS : That the iron ions in FeZ are in the trivalent state and are indeed situated in lattice positions (and not occluded in the pores) is indicated by the XPS data in Fig. 2, which presents the XPS spectra of iron and oxygen in FeZ (Fig.2) and in a sample of silicalite containing occluded Fe_2O_3. The latter was prepared by impregnation of silicalite with $Fe(NO_3)_3$ followed by drying and calcination. The binding energies of the Fe_{2p} level in the samples (taking a value of 103.3 eV for the Si_{2p} level as the internal standard) were 711.6 (FeZ) and 711.0 (Fe-Sil) indicating Fe^{3+} in both the materials. A $2_{p3/2} - 2_{p1/2}$ splitting of 14.0 eV was observed for both the samples. These results agree with those of Mikusik et al [13] who found a value of 711.1 eV for Fe_2O_3 and 710.5, 711.7 for Fe^{3+} ion exchanged into HY zeolite. However, while only one O_{1s} peak (due to the zeolite lattice oxygen) is observed for FeZ, two peaks at 531.5 and 529.1 eV are seen (Fig. 2) in the case of FeSil. While the peak at 531.5 eV, corresponds to the zeolite lattice oxygen, the other corresponds to the oxygen associated with the occluded Fe_2O_3

phase as could be verified with pure Fe_2O_3 . Stencel et al[14], for a sample of ZSM5 containing occluded Fe_2O_3 had also observed two O_{1s} peaks at 532 and 529 eV, corresponding to oxygen in the zeolite and Fe_2O_3 respectively.

B Mössbauer Spectra : The Mössbauer spectra of FeZ (sodium form) at 300 and 80 K are shown in Fig. 2. These had been computer analysed as a two line and a six-line spectral component to represent the quadrupole doublet and the magnetically split spectrum, respectively. The values of δ (the isomer shift with ref.to Fe) and Δ (the quadrupole splitting) of the quadrupole doublet are given in Table 2. These are typical of Fe^{3+} in high spin state. The Mössbauer spectra of iron ion-exchanged into NaZSM5 (Fig. 5 of ref. 15) are completely different from Fig, 3, supporting our view that Fe^{3+} ions in our samples are in lattice positions and not as countercations. In Ref. 15, iron was present as (1) Fe^{2+} octahedrally coordinated to water molecules (δ = 1.37, Δ 3.27), (2) Fe^{2+} in distorted tetrahedral coordination (δ = 0.75, Δ = 1.28) and (3) Fe^{2+} in tetragonally distorted octahedral symmetry (δ = 1.30, Δ = 3.72). None of these species are present in our sample.

Table 2 : Mössbauer parameters (quadrupole doublet) of of iron zeolite (Na form)

Temp. (K)	δ (mm/s)	Δ (mm/s)	Rel area (%)
300	0.33 + 0.02	8.85 + 0.02	90
80	0.42 + 0.03	1.05 + 0.03	74

In addition to the lattice Fe^{3+}, our spectra (Fig. 3) indicate the presence of small occluded particles of Fe_2O_3 or Fe_3O_4 also. These species, responsible for the magnetically split six line component, are removed by acid extraction porocedures.

C ESR Spectra : The ESR spectra of the as-synthesised zeolite gave evidence for the presence of at least four different kinds of iron sites with g = 4.3, 2.3, 2.0 and 5.3 respectively (Fig. 4). The resonance at g = 4.3 was attributed to high spin Fe^{3+} in the lattice [16] and/or Fe^{3+} in rhombohedrally distorted tetrahedral complexes in cation positions [17]. Since the signal at g = 4.3 was not significantly affected by the level of hydration, treatment in hydrogen or with HNO_3, it was concluded that, in our case, it arises mainly from the presence of Fe^{3+} in lattice. Treatment with HNO_3 decreased drastically the intensity of the signals at g = 2.3, 2.0 and 5.3 indicating that they are due to iron in nonlattice positions. The signal at g = 2.3 is atributed, in agreement with Wichterlova [16], to Fe^{3+} ions in occluded oxide and hydroxides. Similarly, the weak signal at g = 2.0 is due to hexacoordinated Fe^{3+} aquo/oxo complexes located in the cationic sites [16]. The signal at g = 5.3 arises probably from highly distorted tetrahedral complexes of Fe^{3+}.

D Magnetic Susceptibility : The magnetic susceptibility values (cgs units/g) for FeZ and a sample of silicalite containing an equal amount of Fe (as Fe_2O_3) were 4.9 and 3.2 x 10^{-6}, respectively, indicating the larger dispersion of Fe^{3+} in the former (at lattice sites) compared to the latter.

3. Adsorption Properties : The adsorption of H_2O and hydrocarbons in FeZ is shown in Table 3. The values are comparable to those for HZSM5 (Al) published earlier [7]. The shape selective behaviour of FeZ is seen from the large differences in the adsorption of n-hexane and its branched isomers (Table 3).

Table 3 : Adsorption properties of FeZ (Na form)

Absorbate (297 K, Sat.Vap.)	Kinetic diameter, A	Amount adsorbed Molecules/unit cell
H_2O	2.65	26.0
n-Hexane	4.30	7.7
2-Methyl Pentane	5.5	5.8
Cyclohexane	6.0	2.7
2,3-Dimethyl butane	6.1	3.4

4. Acidic Properties : The TPD spectra of NH_3 from FeZ, HZSM5 and silicalite are shown in Fig. 5 (curves denoted by Fe, Al and Si, respectively). The peak at 673 K in HZSM5, due to strongly adsorbed NH_3, is shifted to 610 K in FeZ, indicating that SiOHFe Brönsted acid sites are weaker than those of SiOHAl. The broad, weak peak at 540-673 K in silicalite is due to the presence of Al impurities.

5. Catalytic Properties : In the catalytic conversion of C_8 aromatics over FeZ and HZSM5 (Table 4), the major difference is that at similar conversion of ethylbenzene (EB) and para-xylene approach to equilibrium (PATE), the selectivity of FeZ is higher than that of HZSM5 (lower xylene loss).

Table 4 : Comparison of FeZ and HZSM5 (Al)

Conditions : 713 K, atm.pr., WHSV = 15 hr , H /Oil = 0

Product distribution(wt.%)	Feed	FeZ	HZSM5(Al)
C Aliphatics	2.9	2.7	2.1
Benzene	0.6	9.0	9.9
Toluene	3.0	4.0	5.1
Ethyl benzene	26.5	13.7	14.6
p-Xylene	7.4	14.5	14.4
m-Xylene	55.0	40.1	38.8
o-Xylene	4.6	12.2	12.6
C_9^+ Aromatics		3.8	5.6
EB Conversion % wt.		48.3	45.4
PATE		90.0	94.0
Xylene loss		0.2	4.2

ACKNOWLEDGEMENT : We thank Drs. S. Badrinarayanan and B. Clausen for the XPS and Mössbauer data, respectively.

REFERENCES

1. Marosi, L., Stabenow, J., Schwarzmann, M., Ger. 2,831,611.
2. Marosi, L., Stabenow, J., Schwarzmann, M., Ger. 2,831,630.
3. Dwyer, F., U.S. 3,941,871.
4. Kouwenhoven, H.W., Stork, W. H. J., U.S. 4,208,305.
5. Barrer, R. M., Hydrothermal Chemistry of Zeolites, AP, London, 1982, p. 292.
6. Borade, R.B., Kulkarni, S.B., Hegde, S.G., Kotasthane, A.N., Shiralkar, V.P., Ind. 275/DEL/83.
7. Kulkarni, S.B., Shiralkar, V.P., Kotasthane, A.N., Borade, R.B., Ratnasamy, P., Zeolites, 4, 313 (1982).
8. Babu, G.P., Hegde, S.G., Kulkarni, S./B., Ratnasamy, P.,

J. Catal. 81, 471 (1983).

9. Chandavar, K.H., Kulkarni, S.B., Ratnasamy, P., Appl. Catal., 4, 287 (1982)

10. Borade, R.B., Hegde, S.G., Kulkarni, S.B., Ratnasamy, P., Appl. Catal., 13, 27 (1984).

11. Meshram, N.R., Hegde, S.G., Kulkarni, S.B., Ratnasamy, P., Appl. Catal., 8, 359 (1983).

12. Badrinarayanan, S., Hegde, R.I., Kulkarni, S.B., Ratnasamy, P., J. Catal. 71, 439 (1981).

13. Mikusik,P., Juska, T., Novakova, J.,Kubelkova, L., Wichterlova, B., J. Chem. Soc. Faraday Trans. I.,77, 1179 (1981).

14. Stencel, J. M., Diehl, J.R., Doublas, L. J., Spitler, C.A., Crawford, J.E., Melson, G.A., Colloids and Surfaces, 4, 331(1982).

15. Petrera, M., Gennaro, A., Gherardi, P., Gubitoza, G., Pernicone, N., J. Chem. Soc. Faraday Trans. I., 80, 709 (1984).

16. Derouane, E.G., Mestdagh, M., Vielvoye, L., J. Catal. 18, 90 (1970).

17. Wichterlova, B., Zeolites, 1, 181 (1981).

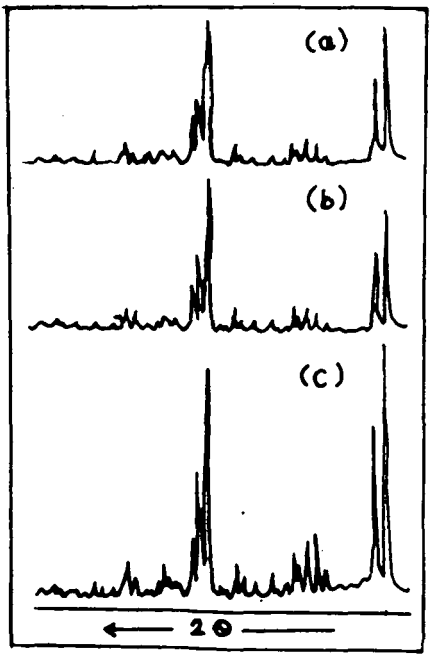

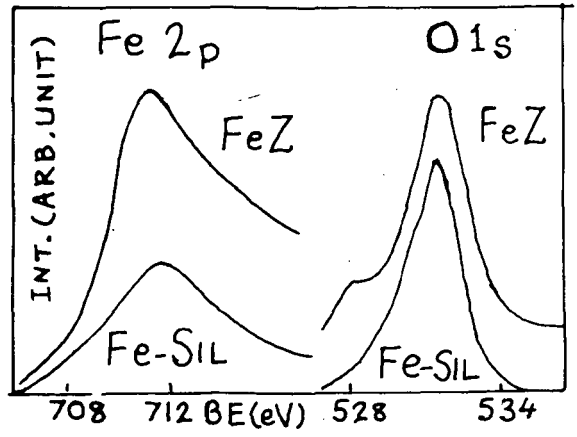

Fig.2: XPS of FeZ and Fe-Silicalite.

Fig.1: XRD Spectra of FeZ, HZSM5 and silicalite (curves a-c).

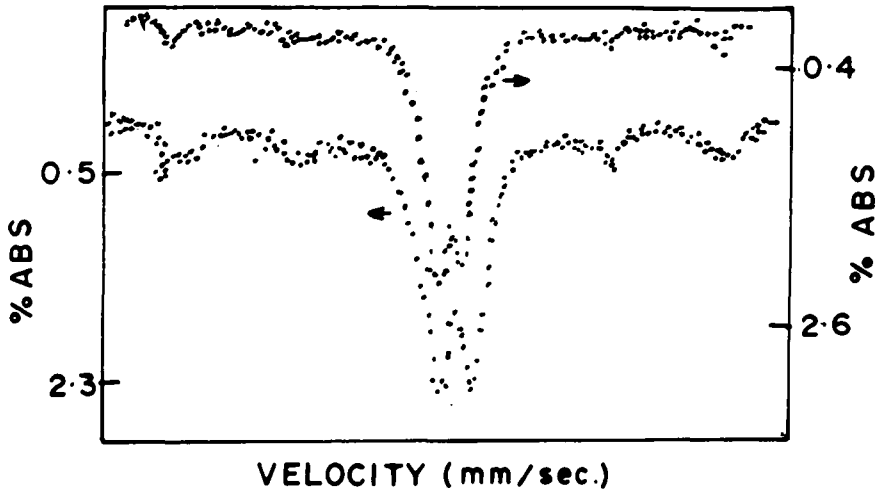

Fig 3:Mössbauer spectra of FeZ at 300(top) and 80K (bottom).

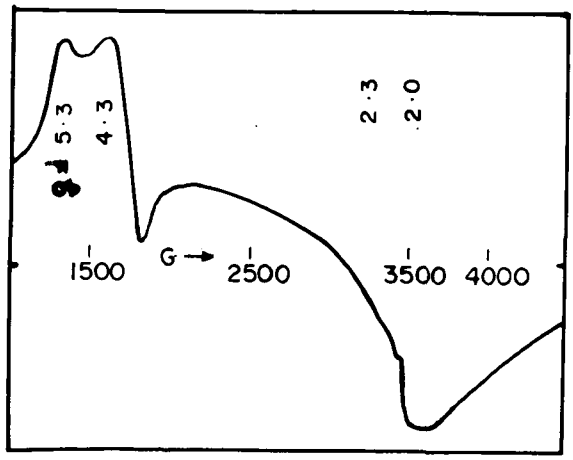

Fig. 4 : ESR Spectra of FeZ .

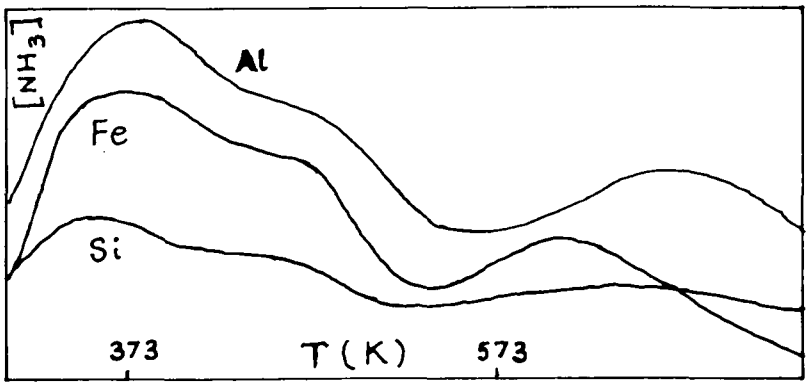

Fig.5 : TPD(NH_3) spectra of HZSM5(Al), FeZ(Fe) and silicalite(Si).

RELAXATION- AND SELF-DIFFUSION MEASUREMENTS OF SOME HYDROCARBONS AND WATER AND METHANOL ON SILICALITE AND ZSM 5 ZEOLITES

H. LECHERT , J. Wienecke , W.D. Basler
Institute of Physical Chemistry, University of Hamburg
Laufgraben 24, 2000 Hamburg 13, Germany

ABSTRACT

The mobility mechanisms of water, methanol, butene, and a series of n-hydrocarbons from butane to dodecane have been studied in silicalite and two samples of ZSM 5 with Si/Al = 18 and 169 by the proton relaxation times T_1 and T_2 and self diffusion measurements. The self diffusion coefficient could be measured only for water and butene in silicalite. Both values are $3*10^{-4}$ cm^2/s at 400 K. The activation energies are 31 resp. 12 kJ/mole.

Water and methanol in silicalite show an almost isotropic reorientation. In ZSM 5 the motion becomes anisotropic, especially in the Na-forms, and the T_1-minima are shifted to higher temperatures. The motion of the hydrocarbons is severely restricted in all samples and strongly anisotropic with rotational reorientation. Butene is bound very tightly with restrictions even of the rotational motions both in Na- and in H-ZSM 5.

INTRODUCTION

The great importance of the ZSM 5 type zeolites for the application lies in the peculiarities of the pore structure causing special selectivity effects in catalysis. The different mechanisms of interaction of the adsorbed molecules with the walls of the channels of the alumosilicate structure and with the cations and the OH-groups have been studied previously by careful sorption experiments /1/.

The present paper shall be devoted to investigations of the mobility of water, methanol, 1-butene and the n-hydrocarbons from butane to dodecane by pulsed NMR-methods. These substances represent the most important types of compounds involved in the wellknown methanol reaction catalyzed preferably by ZSM 5 type zeolites.

As adsorbends two samples of ZSM 5 with Si/Al = 18 and 169 and a silicalite sample are used. In the silicalite sample only the inter-

actions with the silica surface inside the channels is measured and may be compared with the influences originating from the Na-ions and the OH groups in the H-forms of the ZSM 5 samples.

The molecular motion is studied by the H-NMR-relaxation times T_1 and T_2 to obtain the correlation time of the molecular reorientation. This correlation time is the period in which fixed spatial relations of the H-nuclei are given. Therefore, the temperature dependence of T_1 and T_2 gives information about the activation energies and the kind of the molecular motion. In favourable cases the translational motion e.g. the self diffusion can be studied by the pulsed field gradient technique /2/.

The mentioned selectivity phenomena are closely related to the restrictions of the motional freedom of the educts and products in the catalytic process. Therefore, information about molecular motion obtained from NMR-data should give valuable insight into the influences of the pore structure of ZSM 5 zeolites on the kinetics of the catalytic reaction.

EXPERIMENTAL

Samples used. The samples used in the NMR-experiments have been synthesized in our laboratory. In order to obtain large ZSM 5 crystals a batch composition has been used containing Li_2O as described by Nastro and Sand /3/. The batch compositions of the different samples are given in Table 1.

Table 1

Batch compositions of the synthesis of the zeolite samples

Sample	SiO_2/Al_2O_3	Li_2O/Al_2O_3	TPA/SiO_2	NH_4OH/SiO_2	H_2O/SiO_2	t °C
Z18	59	1	0.14	1.28	12.7	180
Z169	168	1	0.14	1.28	12.7	180
S	∞	0	0.06	$NaOH/SiO_2$ 0.03	10.5	95

TPA means the tetrapropylammonium ion.

The samples are characterized by Z for ZSM 5 and by S for silicalite. The number behind the Z gives the Si/Al-ratio of the final product. The analyses of the final products were done by AAS. The Z-samples contained no Li and had Fe-contents of 220 ppm for Z169 and 70 ppm for Z18. The S-sample had 220 ppm Fe-impurity.

The crystallinity was checked by X-ray measurements. All samples showed good crystallinity. Z18 could be shown to consist of needles of an average length of 25 µm, Z169 consists of needles of 10 µm.

The S sample had crystals of a nearly spherical shape with a diameter of 10 µm.

After calcination in air at 500°C the H- and Na-ZSM 5 were obtained by treating the samples with 0.1 M HCl or 0.1 M NaCl solution.

The dehydration of the samples was done at 400°C at a vacuum of 1 mPa for 12 hours. The degree of dehydration was checked gravimetrically. The sorbates water and methanol were purified from air by several freeze-pump-thaw cycles. The gases butane and butene were taken from Merck "minicans" without any purification. The sorption was performed via the gas phase. The amount of sorbed substance was checked gravimetrically and is given in the legends of the figures.

The NMR experiments were carried out with a BRUKER BKR 322 spectrometer at 60 MHz. T_1 was obtained using the 180°-90°-pulse sequence. T_2 less 1 ms were taken from the free induction decay, longer T_2 from the Carr-Purcell-sequence.

The self diffusion coefficients have been measured by the pulsed field gradient technique /4/.

RESULTS

In Fig.1 the temperature dependence of T_1 and T_2 of water, methanol, butane, and butene in silicalite is given. All four substances show motional narrowing of T_2, and T_1-minima. For water a broad T_1-minimum near 200 K is observed. The T_1-minimum of methanol is near 230 K and more pronounced. T_1-minima of butane and butene are found near 260 K. The absolute values of T_1 of several milliseconds indicate interaction with paramagnetic Fe-impurities. Low temperature T_2 at 160 K of water, methanol, and butene are are about 30 µs which is three times longer than the expected rigid lattice value of nearly 10 µs. In contrast, T_2 of butane is 100 µs at 160 K. This indicates at least narrowing of the intramolecular H-H-interaction by rotational motion even at 160 K, especially in case of butane.

Because at least in case of T_2 the contribution of the H-H- and the H-Fe-interaction may vary with temperature no reliable activation energies can be obtained from the slope of log T_2 vs. inverse temperature.

In Fig.2 the results for butene in Na-Z169 and butane in Na- and H-Z169 are shown. The values of butene in Na- and H-Z18 are nearly identical with those in H-Z169, the values of butane in Na- and H-Z18 and in H-Z169 with those in Na-Z169, and therefore not shown.

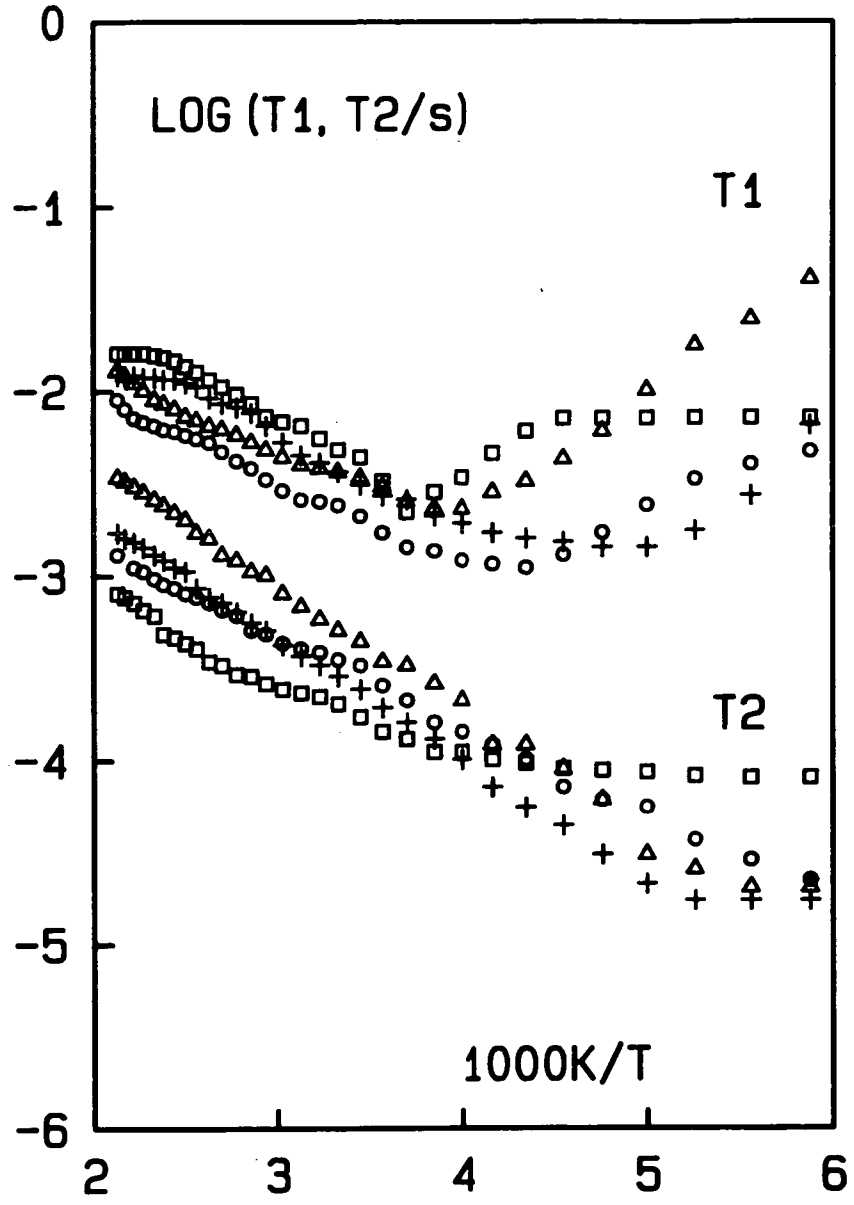

Fig. 1. Temperature dependence of the longitudinal (T_1) and transverse (T_2) proton relaxation times of + 4.0 mmol water, ● 3.5 mmol methanol, ■ 1.3 mmol butane, and ◀ 1.9 mmol butene per g silicalite.

T_2 of butene increases to about 1 ms only in Na-Z169 but remains constant at 30 µs in all other samples. The T_1-minimum of butene is near 290 K in Na-Z169 and shifted to 330 K in H-Z169. In all samples the T_1 minima of butane are near 290 K and all T_2's increase from 0.1 ms at 160 K to 0.5 ms at 470 K.

In Fig.3 water and methanol Na-Z18 and Na-Z169 are compared. Similar results were found for H-Z18 resp. H-Z169 and are not shown. Whereas all T_2's are increasing with temperature only T_2 of water in Na-Z169 is constant at 0.2 ms between 160 and 350 K and then increasing. All T_1-minima are broad and in the range of 250 to 300 K.

The coefficient of self diffusion of water and butene in silicalite, determined the NMR pulsed field gradient technique is given in Table 2.

Table 2

Self diffusion of water and butene in silicalite

T/K	360	380	400	420	
$D/10^{-8}m^2/s$	1.2	1.7	3.0	4.8	water
	2.2	2.8	3.2	4.0	butene

The corresponding activation energy of diffusion is 31±2 kJ/mole for water and 12±2 kJ/mole for butene.

DISCUSSION

The wellknown hydrophobic character of silicalite /5/ can be clearly seen by the relaxation times (Fig.1) and the self diffusion (Table 2). The T_1-minima, where the correlation time of molecular reorientation is about 10^{-9} s, are increasing in the order water-methanolbutene-butane from 200 to 260 K. For comparison the T_1-minimum of water in Na-faujasite is near 260 K. The self diffusion of water can be extrapolated to $2*10^{-9}$ m^2/s at 300 K which is nearly the value of the pure liquid and ten times faster than in Na-X faujasite /6/.

Butene ($D = 10^{-9}$ m^2/s at 300 K) is hundred times more mobile in silicalite than in Na-X /7/. No significant difference between the temperatures of T_1-minima of butane and butene could be observed (Fig.1). Both observations can be explained by the fact that there are no cations in silicalite for specific interaction with the π-bond of butene.

Methanol which has both hydrophobic and hydrophilic parts in its molecule show a behaviour intermediate between water and the hydrocarbons.

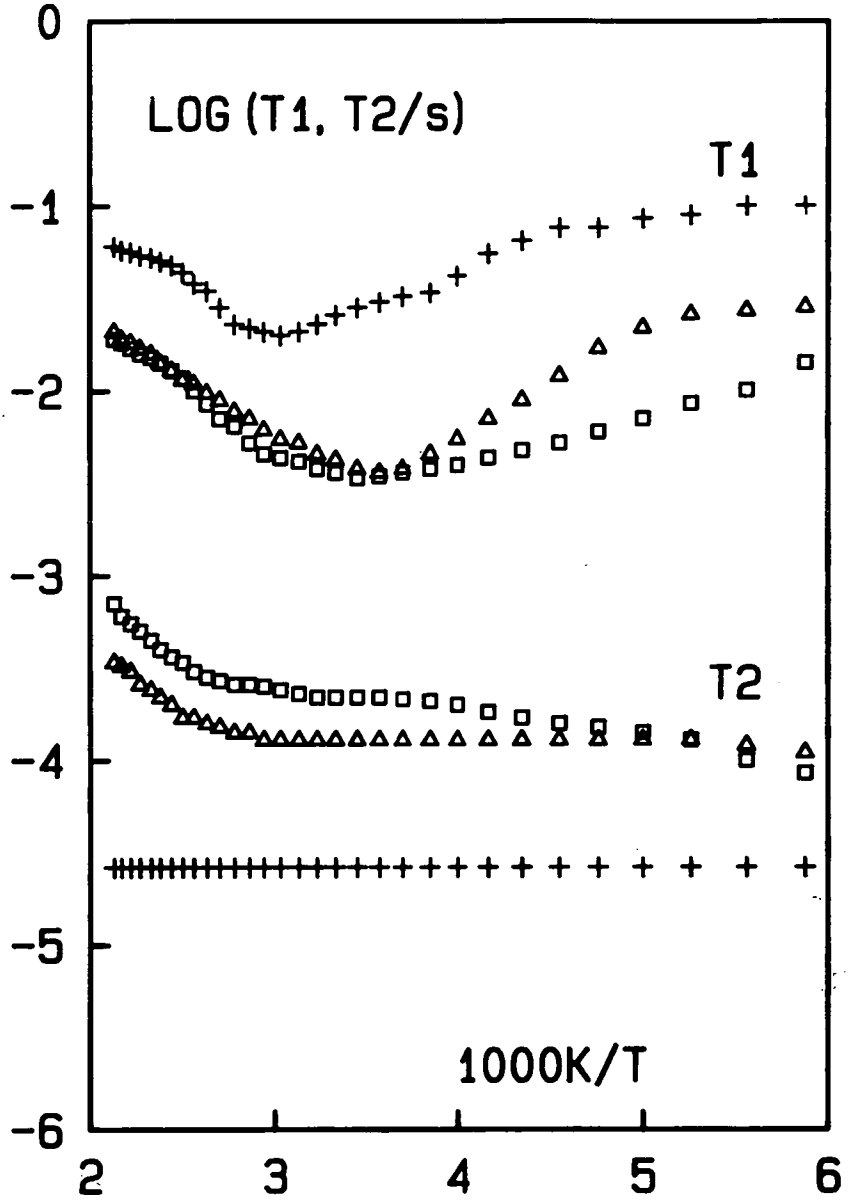

Fig. 2. Temperature dependence of the longitudinal (T_1) and transverse (T_2) proton relaxation times of butane and butene in ZSM 5 with Si/Al = 169 (Z169): ▲ 1,0 mmol butane/g Na-Z169, + 1.0 mmol butene/g H-Z169, and ◘ 1.4 mmol butene/g Na-Z169.

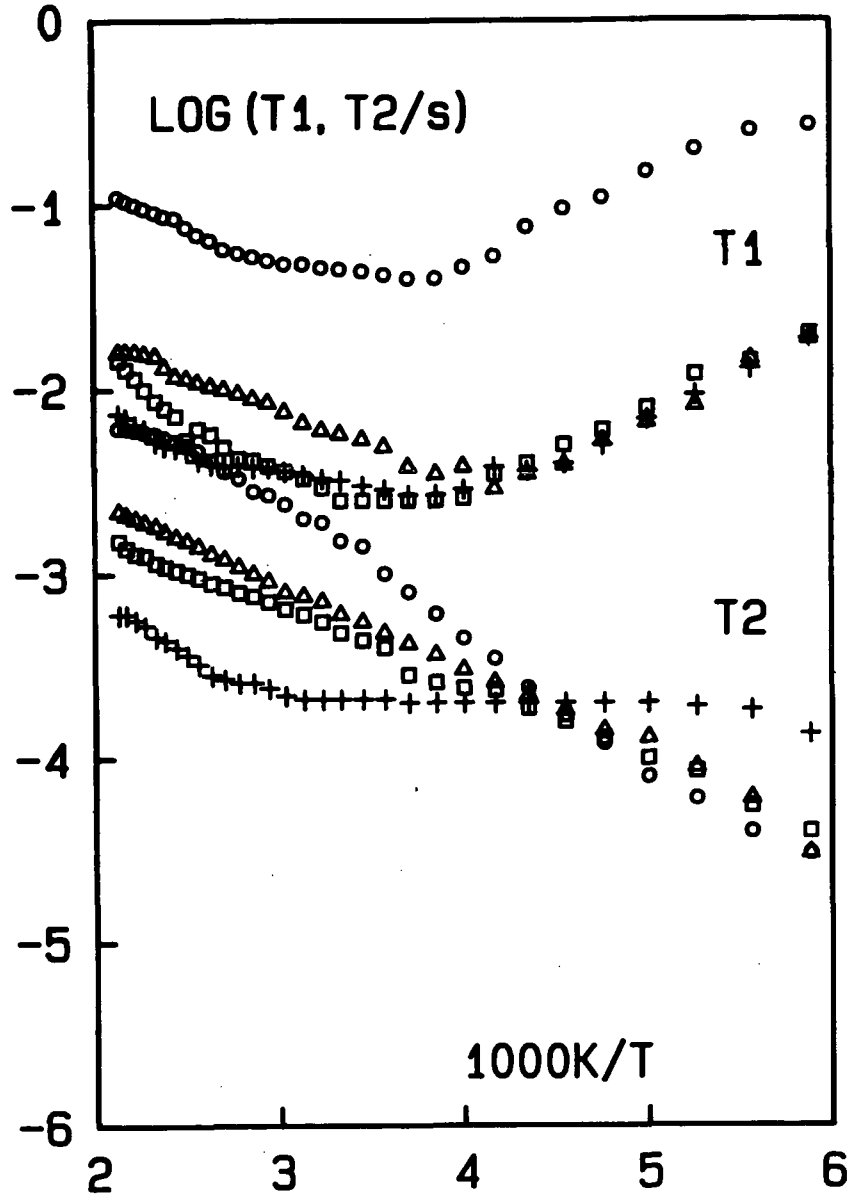

Fig. 3. Temperature dependence of the longitudinal (T_1) and transverse (T_2) proton relaxation times of water and methanol in Na-ZSM 5 with Si/Al = 18 (Z18) and Si/Al = 169 (Z169): ▲ 3.0 mmol water/g Na-Z18, + 4.0 mmol water/g Na-Z169, ○ 4.3 mmol methanol/g Na-Z18, and □ 3.8 mmol methanol/g Na-Z169.

The low temperature values of T_2 of all four substances are well above the expected rigid lattice value of 10 μs. Therefore their correlation time of the molecular reorientation must be shorter than 10^{-5} s at 160 K.

The possible influence of the cations on the sorbate-sorbend-interaction should become apparent comparing silicalite, Z169 and Z18 differing largely in the concentration of Na-ions resp. H-ions. In case of butane no significant difference has been observed for all sorbends, indicating that only non-specific hydrophobic interaction occurs with the zeolite framework.

For butene T_2 = 30 μs is observed up to 470 K, hence there is strong restriction of molecular reorientation in H-Z18, Na-Z18 and also in H-Z169. In Na-Z169 almost no difference between butane and butene can be found (Fig.2). This shows strong interaction between butene and the H-ions. Even the ratio of 1 H-ion to 10 molecules butene in H-Z169 is sufficient to prevent isotropic reorientation.

For Na-Z18 with 1 Na-ions per butene a similar restriction of molecular reorientation takes place but obviously not in Na-Z169. In agreement with these findings the same molecular correlation time of butene in H-Z18, H-Z169 and Na-Z18 is reached at a higher temperature (T_{1min} at 330 K) than in Na-Z169 (T_{1min} at 290 K). Nevertheless, even at the corresponding temperatures of T_{1min} the reorientation is much more anisotropic in the samples with T_2 = 30 μs.

In addition the T_1 and T_2 relaxation times of n-paraffins with C = 6,8,10, and 12 were measured between 120 and 470 K. Low temperature T_2 were about 20 μs. Depending on the chain length, T_2 started increasing at temperatures between 180 and 350 K to a final value of 250 μs. The T_1-minima were broad and situated near 290 K, no systematic variation with C-number could be observed. It can be concluded that the reorientation of n-paraffins with C-number above 6 is severely restricted by the linear channel structure of ZSM 5 whereas butane and probably the shorter n-paraffins may reorient isotropically in the channel intersections.

Finally, the influence of Na-ions on water and methanol was studied by comparing Na-Z18 with Na-Z169 (Fig.3) and silicalite (Fig.1). Going from silicalite to ZSM 5 the T_1-minimum is shifted from 200 to 260 K but no significant difference is observed between Na-Z18 and Na-Z169. Nevertheless, T_2 indicates more isotropic reorientation at low temperatures in Na-Z169 with less Na-ions whereas at higher temperatures a shorter T_2 is caused by the higher Fe-content of Na-Z169.

Like in the case of water the T_1-minimum of methanol is shifted from 230 K in silicalite to about 270 - 290 K in ZSM 5 but no marked difference between Na-Z18 and Na-Z169 can be seen. Evidently already a concentration of 1 Na-ion per 40 molecules of water resp. methanol is sufficient to create the remarkable difference between ion-free silicalite and Na-ZSM 5. Further increase of Na-content seems to be less effective.

The ratio of the T_1 values of Na-Z169 and Na-Z18 is about 10 whereas the ratio of the analytical Fe-contents is 3. This allows the conclusion that not all Fe in ZSM 5 is equally effective in NMR relaxation and hence should be located in sites with different accessibility.

REFERENCES

1. Lechert, H., Schweitzer, W., Proceedings of the Sixth International Zeolite Conference, Eds. D. Olson and A. Bisio, Butterwoths, Guildford, 1984, p. 210.
2. Pfeifer, H. NMR-Basic Priciples and Progress, Vol.7, Eds. P. Diehl, E. Fluck, R. Kosfeld, Springer-Verlag, Berlin 1972, p. 53.
3. Nastro, A., Sand, L.B., Zeolites, 3, 57 (1983).
4. Steijskal, E.O., Tanner, J.E., J.Chem.Phys. 52, 2523 (1970).
5. Flanigen, E.M., Bennett, J.M., Grose, R.W., Cohen, J.P., Patton, R.L., Kirchner, R.M., Smith, J.V., Nature 271, 512 (1978).
6. Kärger, J., Z.phys.Chemie, Leipzig 248, 27 (1971).
7. Kärger, J., Z.phys.Chemie, Leipzig 257, 983 (1976).

FACTORS INFLUENCING SORPTION AND DIFFUSION IN PENTASIL ZEOLITES

V.S. NAYAK and L. RIEKERT
Institut für Chemische Verfahrenstechnik der Universität Karlsruhe, D-7500 Karlsruhe, Germany

ABSTRACT

Pentasil zeolites (Si:Al= 20-50) have been prepared with different templates (TPA, NH_2 $(CH_2)_6$ NH_2, NH_2 $(CH_2)_3$ NH_2, and NH_3 (organic free)) in the hydrogen form; they were characterized by XRD and by chemisorption of pyridine. Equilibrium sorption of hexane, benzene, toluene and p-xylene was studied at 298 K; the uptake of hydrocarbons varies regularly with the nature of the template which had been used in the synthesis of the zeolite. Diffusivities (obtained from sorption rates at 298 K) of aromatic hydrocarbons are independent of the method of preparation of the zeolite. Chemisorbed pyridine does not affect the diffusivity of aromatic hydrocarbons in pentasil zeolite synthesized with TPA as template, whereas it reduces the diffusivities substantially in zeolites prepared with other templates. This observation indicates that the template influences the location of acid sites in the structure of the solid.

INTRODUCTION AND SCOPE

The generic name "pentasil-zeolites", which has been introduced by Meier and Kokotailo (1), covers a family of similar structures with nearly identical lattices containing five-membered rings of tetrahedral silicon or aluminium. The end members of this series are represented by the ideal structures of ZSM-5 (sinusoidal channels) and ZSM-11 (straight channels). Real crystals seem to be an intergrowth of these structures and they also contain stacking faults and disordered domains (2-4). These zeolites are synthesized through crystallisation from silica-rich gels containing nitrogen bases as templates. The classical synthesis relies on tetrapropylammonium for ZSM 5 (5) and tetrabutylammonium for ZSM-11 (6) as templates. It has been found that pentasil zeolites can also be

obtained if the gel contains N-bases other than these, such as 1,6 diaminopropane (8) or no organic template (9). The XRD-patterns of zeolites prepared by different methods are very similar with nearly identical lattice-spacing, whereas sorption of hydrocarbons and catalytic properties have been found to vary with the method of preparation (10, 11). In order to exemplify the influence of the template used for synthesis on the properties of the resulting pentasil zeolites we have prepared pentasil zeolites using 3 different organic templates as well as no organic template. The properties of these zeolites with respect to sorption and diffusion of various hydrocarbons and chemisorption of pyridine are reported here; the catalytic properties of these materials will be the subject of a later publication.

Synthesis and characterization of zeolites. Zeolites were prepared by crystallization from gels at 170°C in a teflon-lined autoclave. The gels were formed by first heating slurries of precipitated silica (Merck) in aqueous solution of NaOH and the template to boiling for 30 minutes and than adding under stirring either a hot solution of $AlCl_3$ (preparation A and B) or a hot slurry of freshly precipitated aluminium hydroxide (preparation D). The molar compositions of the gels were Al_2O_3 -75 SiO_2- x template - 6·2 Na_2O - 870 H_2O, where x = 9·2, 21·0 and 71·6 for TPA-Br, HMD and NH_3, respectively. The crystallization periods were 6 days for TPA- and HMD-zeolites and 12 days for NH_3-zeolite. Sample C (template: 1,3 diaminopropane) was kindly supplied by Dr. Hölderich (BASF Aktiengesellschaft).

The crystalline solids resulting from the gels were filtered, washed several times with distilled water, dried at 120°C and calcined in air at 500°C for 4 h. After cooling to room temperature the zeolites were ionexchanged at 80°C 6 times with 20 ml of 1 m NH_4NO_3 solution per g of zeolites. The ionexchanged solids were dried and deammoniated in air at 500°C for 6 h to obtain the hydrogen forms.

The composition of the resulting zeolites as obtained by wet analysis and AAS and the size of the crystals (which were nearly monodisperse in all preparations as shown by SEM) are given in Table 1.

Table 1

Composition and size of crystals, Sorption capacity for nitrogen, Chemisorption of pyridine

sample designation (template)	Crystal-diameter (µm)	Composition Si/Al	N_2-Sorption at 77 K and p_{N_2} = 1 torr (m mol/g)	Chemisorption of pyridine at 400°C $\frac{m\ mol}{g}$	$\frac{n_{pyridine}}{n_{Al}}$
A (TPA Br)	0.5	36	4.2	0.21	0.48
B ($NH_2(CH_2)_6NH_2$)	0.5	36	3.9	0.26	0.58
C ($NH_2(CH_3)_2NH_2$)	0.8	22	3.6	0.28	0.39
D (NH_3)	0.5	36	2.3	0.28	0.64
ZSM-5 *	1.0	50	-	0.17	0.53

* sample of zeolite ZSM-5 in the hydrogen from, kindly supplied by Mobil Research and Development corporation

Na content in zeolites A, B, C and D $<$ 0.05 wt %.

Chemisorption of pyridine was determined with an electrobalance by evacuating the zeolite at 400°C for 2 h, cooling to room temperature, contacting with pyridine vapour at 13 mbar at this temperature and then evacuating to 10^{-3} mbar at 400°C for 2 h. The amount of pyridine retained thereafter and its ratio to the amount of Al in the zeolite is also listed in Table 1. The main X-ray diffraction reflexes with Cu K_α -radiation and their relative intensities (peak heights) are given in Table 2 as well as the degree of crystallinity which is defined by the ratio of sum of heights of major XRD peaks of test sample to the sum of heights of major XRD peaks of standard (Sample A) multiplied by 100.

Table 2

XRD-data of zeolites in the hydrogen form

Sample:	A	B	C	D	ZSM-5(Mobil)
2θ	100 I/I_o				
7.8	(100)	(100)	(100)	(100)	(100)
8.7	58	56	62	60	56
23.0	49	49	46	78	48
23.8	25	25	26	39	24
24.2	13	14	17	26	13
crystallinity (%)	(100)	98	100	91	99

SORPTION OF HYDROCARBONS INTO THE ZEOLITES IN THE HYDROGEN-FORMS

Sorption equilibria and sorption kinetics were observed gravimetrically with a Cahn RG electrobalance hooked up to a grease-free vacuum system which can be evacuated through a turbomolecular pump to 10^{-3} mbar. Pressure was measured with a capacitance pressure transducer (MKS baratron Type 170 M-6B). The experimental procedure has been described in detail by Doelle and Riekert (12); sorption equilibria were observed on samples weighing about 70 $\pm$ 10 mg, equilibrium being defined by coincidence of isotherms obtained at increasing and decreasing pressures; sorption rates were observed on much smaller samples (about 10 mg each) spread in a monolayer of crystals in order to avoid intercrystalline mass transfer resistance and to minimize the excursion of temperature due to the heat of sorption. Pretreatment of the zeolites consisted in degassing at 400°C for 1 h at p 10^{-3} mbar.

Figure 1 shows the isotherms at 298 K of n-hexane, benzene, toluene and p-xylene on zeolite A and figure 2 shows sorption isotherms of toluene on zeolites A, B, C and D at 198 K. Values of equilibrium-sorption of different hydrocarbons at 298 K and a pressure of 1.33 mbar of the respective hydrocarbon are given in Table 3.

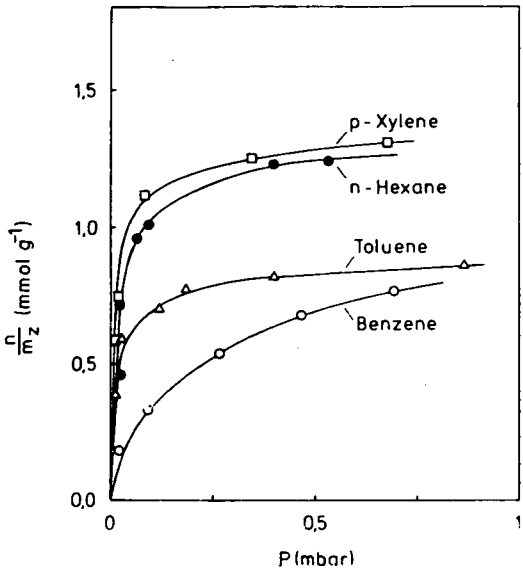

Fig. 1. Equilibrium isotherms of sorption of hydrocarbons in sample A at 298 K

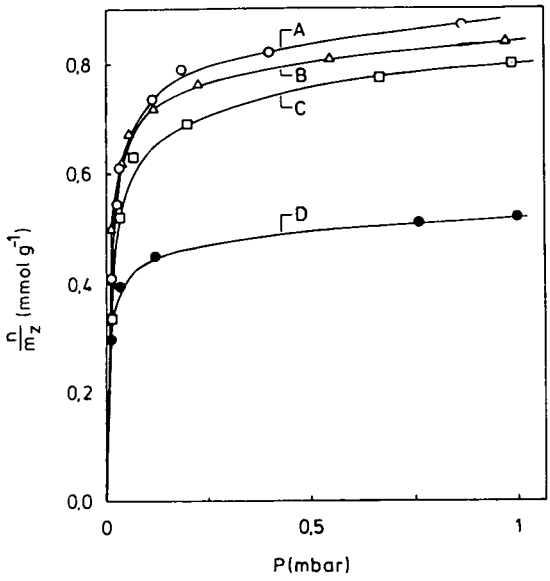

Fig. 2. Equilibrium isotherms for sorption of toluene in samples A,B,C,D at 298 K

Table 3

Equilibrium sorption n_s/m_z in mmol g^{-1} of different hydrocarbons i at 298 K and p_i = 1.33 mbar in different pentasil zeolites

Zeolite / hydrocarbon	A	B	C	D
m-hexane	$\frac{n_s}{m_z}$ = 1.28	1.21	1.12	0.62
benzene	0.91	0.79	0.83	0.42
toluene	0.94	0.87	0.85	0.52
p-xylene	1.33	1.01	0.98	0.67

Sorption of p-xylene at 298 K did show hysteresis on all samples investigated, values in desorption (decreasing p) exceeding the values found in sorption (increasing p). Sorption of o-xylene at 298 K was also investigated on sample A and D where the same loadings are approached as for p-xylene, albeit much more slowly.

The kinetics of sorption of benzene, toluene and p-xylene at 298 K into all zeolites investigated can be described by n/n_∞ (n_∞ = final uptake at equilibrium) being linear in $\sqrt{t}$, up to about n/n_∞ = 0.5 (see fig. 3). In this range the kinetics of sorption is controlled by intracrystalline diffusion under the

conditions of these experiments with monolayers of crystals (12). Assuming diffusion in a homogeneous isotropic medium we have independent of the shape of the crystals for the intial slope of $^{n}/n_{\infty}$ vs. $\sqrt{t}$

$$\lim_{t \to 0} \frac{d(^{n}/n_{\infty})}{d\sqrt{t}} = \frac{2}{\sqrt{\pi}} \cdot \left(\frac{D}{L^2}\right)^{1/2} \qquad (1)$$

where $L = {}^{V}/a$ is the ratio of volume to external surface of the solid; e. g. $L = \frac{d}{6}$ for spherical crystals of diameter d. Intracrystalline diffusion coefficients D of hydrocarbons in the zeolites which were obtained on the basis of eq. (1) are listed in Table 4.

Table 4

Diffusivities (in cm^2/s) of hydrocarbons at 298 K, obtained from initial slopes of $^{n}/n_{\infty}$ vs. $\sqrt{t}$-curves

Sample: (L in µm)	A (0.08)	B (0.08)	C (0.13)	D (0.08)
Hydrocarbon				
Benzene	D= $5.7 \cdot 10^{-12}$	$6.0 \cdot 10^{-12}$	$6.3 \cdot 10^{-12}$	$6.3 \cdot 10^{-12}$
Toluene	$1.6 \cdot 10^{-12}$	$1.8 \cdot 10^{-12}$	$2.0 \cdot 10^{-12}$	$2.2 \cdot 10^{-12}$
p-Xylene	$2.8 \cdot 10^{-11}$	$2.9 \cdot 10^{-11}$	$3.6 \cdot 10^{-11}$	$2.8 \cdot 10^{-11}$

These diffusivities should be considered as rough estimates only, because the characteristic length L obtained from SEM micrographs cannot be considered to be very accurate. Furthermore the patterns of $^{n}/n_{\infty}$ vs. $\sqrt{t}$ at $^{n}/n_{\infty} > 0.8$ seem to indicate that the solids are not always homogeneous, containing disordered domains where diffusivities are lower. The data in Table 4 nevertheless indicate that the order of magnitude of the diffusivity of a given hydrocarbon is the same in all preparations and that p-xylene always diffuses more rapidly into the solid than benzene or toluene. O-xylene on the other hand diffuses much more slowly, in sample A the rate of sorption of o-xylene at 298 K corresponds to $D \approx 6 \cdot 10^{-13}$ cm^2/s.

SORPTION OF HYDROCARBONS INTO ZEOLITES CONTAINING CHEMISORBED PYRIDINE

Equilibria and kinetics of sorption of aromatic hydrocarbons were also investigated in pentasil samples A, B, C and D after these had been modified by chemisorption of pyridine at the acid

sites in the crystal. For this purpose the zeolites where contacted with pyridine-vapour (13 mbar) at 25°C and then degassed at 400°C under vacuum ($p \approx 10^{-3}$ mbar) for 1 h, the amounts of pyridine retained thereafter are given in Table 1. The equilibrium isotherms of hydrocarbons in zeolites modified by chemisorbed pyridine were compared to the isotherms for the unmodified zeolites. It was found throughout that sorption in the modified zeolites at $p > 1$ mbar is reduced by an amount which corresponds roughly to the amount of chemisorbed pyridine. The kinetics of sorption of benzene and p-xylene in the H-forms as well as in the pyridine-modified forms of the same zeolites (A, C and D) is shown in Fig. 3.

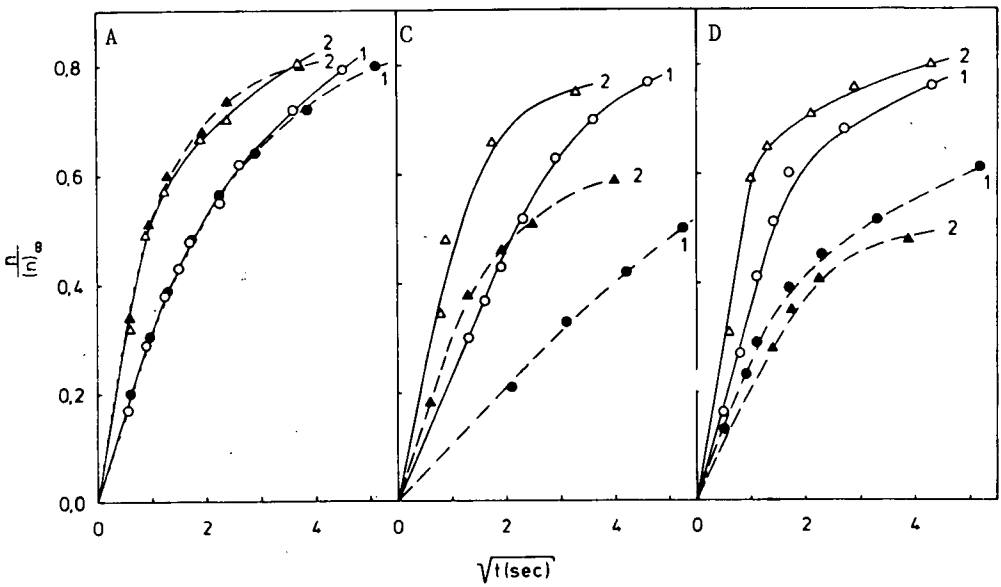

Fig. 3. Kinetics of sorption of benzene (1) and p-xylene (2) into H-forms of zeolites (-o-o-,-Δ-Δ-) and into H-forms containing chemisorbed pyridine (-●-●-,-▲-▲-). T = 298 K.
Initial loading of zeolite $(n_s)_0 = 0$; $\frac{p_\infty}{p_0} \geq 0.9$.

In pentasil A the time-dependence of the dimensionless uptake n/n_∞ is not affected by the presence of chemisorbed pyridine, the diffusivities of the hydrocarbons in this zeolite are the same, whether pyridine is present or not. In zeolites B, C and D, on the other hand, the diffusivities of hydrocarbons are substantially reduced by chemisorption of pyridine. These observations are summarized in Table 5, where the ratio between the diffusivities in the pyridine-modified zeolites and the diffusivities in the

unmodified zeolites at 298 K are listed. These ratios of diffusivities obtained on the basis of eq. (1) do not suffer from incertainities concerning shape and size of the crystals, the morphology being the same when rates of sorption on modified and unmodified crystals are compared for the same zeolite sample.

Table 5

Ratio of diffusivities D in unmodified zeolite and D_{py} in zeolite modified by chemisorbed pyridine at 298 K

Zeolite		A	B	C	D
Diffusing hydrocarbon					
Benzene	$\frac{D}{D_{py}}$ =	1.00	0.3	0.25	0.4
Toluene		1.00	0.55	0.5	0.6
p-Xylene		1.00	0.2	0.4	0.05

DISSCUSION

Zeolites A, B, C and D agree with respect to their crystal-lattice, since x-ray reflexes occur at identical θ-values, characteristic for Pentasil-zeolites. Their chemical composition corresponds essentially to that of silica where between 2 and 5 % of Si-atoms have been replaced by Al. The structures of these zeolites appear not to be identical, however, if the equilibria and kinetics of sorption of hydrocarbons and of pyridine in these solids are considered. Between 40 and 65 % of the Al-atoms are associated with an acidity which gives rise to chemisorption of pyridine at 400°C; the fraction being highest for the zeolite which was prepared without organic template.

The pattern of the equilibrium isotherms for sorption of different hydrocarbons is the same for all 4 zeolites. The amounts of a given hydrocarbon which are incorporated into different zeolites under otherwise identical conditions decrease in the order A > B > C > D, which corresponds to an ordering of the template molecules with their size, decreasing from A (TPA) to D (NH_3). The effect can be due to an increasing degree of disordering in the crystals, as we go from A to D.

The amount of p-xylene which is sorbed at saturation always exceeds the amount of benzene sorbed at saturation; it seems impossible

to explain this result on the basis of space-filling in the structure. The hysteresis observed for p-xylene sorption indicates that a change of the structure of the solid takes place when p-xylene is introduced. A subtle change of the structure of ZSM-5 upon sorption of p-xylene has recently been observed by Fyfe et al. (13) through XRD and NMR spectra. The diffusivity of p-xylene in these zeolites always excedes the diffusivity of benzene by a factor of about 5 (Table 4).

The observation that the diffusivities of benzene, toluene and p-xylene in zeolite A (prepared with TPA as template) are not affected by chemisorbed pyridine shows that in this case the chemisorbed pyridine molecules are located such that they do not obstruct the diffusion pathways of the hydrocarbons. In zeolites B, C, D on the other hand the presence of chemisorbed pyridine entails a substantial reduction of the diffusivities of hydrocarbons in the solid (Table 5). In zeolites B, C and D (prepared with primary amines or ammonia as templates) the chemisorbed pyridine molecules must therefore be located such that they obstruct the diffusion pathways of hydrocarbons in the structure. Theodorou and Wei (14) have shown how observed diffusivities will be reduced, if in a lattice of diffusion pathways a fraction of the pathways in the volume or at the boundary of the system is blocked. This effect is evidently responsible for the decrease of diffusivities in zeolites B, C and D due to chemisorbed pyridine. Since the effect is absent in zeolite A it can be concluded that chemisorbed pyridine occupies different positions in the channel-system of zeolite A than in the case of B, C or D. It follows that the location of framework Al in the lattice is influenced by the template which is used for synthesis.

ACKNOWLEDGEMENTS

We thank Dr. W. Hölderich for providing zeolite C and for helpful discussions. V.S. Nayak thanks the Alexander von Humboldt-Foundation for a fellowship. We are indebted to the Deutsche Forschungs-Gemeinschaft and Fonds der Chemie for financial assistance.

REFERENCES

1. Kokotailo, G.T. and Meier, W.M. in "The Properties and Applications of Zeolites" (R.P. Townsend, Ed.), P. 133, The Chemical Society, London 1979.
2. Thomas, J.M., Milward, G.R., Ramidas, R., Bursill, L.A. and Audier, M., Faraday Discuss. Chem. Soc. 72, 345 (1981).
3. Thomas, J.M., Proc. 8th Internat. Congr. Catalysis I, 31 (1984).
4. Auroux, A., Dexpert, H., Leclercq, C. and Vedrine, J., Applied Cat. 6, 95 (1983).
5. Argauer, R.J. and Landolt, G.R., US Patent 3.702.886 (1972).
6. Chu, P., US Patent 3.209.979 (1973).
7. Marosi, L., Stabenow, J. and Schwarzmann, M., German Pat. DOS 2.830.787 (1980).
8. Marosi, L., Stabenow, J., and Schwarzmann, M., German Pat. DOS 30.06.471 (1981).
9. Grose, R.W. and Flanigen, E.M., Belgian Patent 7.701.115 (1977).
10. Doelle, H.-J., Heering J., Riekert, L. and Marosi, L., J. Catal. 71, 27 (1980).
11. Heering, J., Riekert, L. and Marosi L., Proc. 6th Internat. Conf. on Zeolites (1983), in print.
12. Doelle, H.-J. and Riekert, L., Angew. Chem. Int. Ed. Engl. 18, 266 (1979).
13. Fyfe, C.A., Kennedy, G.J., De Schutter, C.T. and Kokotailo, G.T., J. Chem. Soc., Chem. Commun. 1984, 541.
14. Theodorou, D. and Wei, J., J. Catal. 83, 205 (1983).

TITRATION OF ACTIVE ACID SITES ON H-ZSM-5 BY SELECTIVE POISONING WITH PYRIDINE

V.R. CHOUDHARY AND V.S. NAYAK
Chemical Engineering Division, National Chemical Laboratory, Pune -411 008 India

ABSTRACT

The number and strength of active acid sites on H-ZSM-5 (with different Si/Al ratios) for cumene cracking and o-xylene isomerisation reactions have been determined using the pulse piosoning technique based on selective poisoning of stronger acid sites with pyridine. Only those acid sites which can absorb pyridine irreversibly at $\geq$570K are involved in both the reactions. The number of active acid sites on the zeolite was found to decrease almost linearly with the Si/Al ratio. On the other hand, the number of active acid sites per Al-atom of the zeolite increases with the Si/Al ratio upto the Si/Al ratio of 31.1 and levels-off thereafter.

INTRODUCTION

H-ZSM-5 zeolite has shown considerable promise as a catalyst in the conversion of alcohols to hydrocarbons [1-6], alkylation of aromatics [7,8] and also in a number of hydrocarbon conversions [9-13], and syngas conversion [14]. The acid strength distribution on this zeolite has been found to be broad [15-19]. It is therefore important to know the number of active acid sites which are actually involved in a particular catalytic reaction and also the minimum strength possessed by them. The present investigation was undertaken with the objective of determining the active acid sites on H-ZSM-5 zeolites (with different Si/Al ratios) for the model reactions viz. cumene cracking and o-xylene isomerisation, which are normally employed for studying protonic acid sites on solid catalysts [20]. The poisoning technique [9,21] in which the stronger acid sites are selectively poisoned in the order of their strength has been employed for this purpose.

EXPERIMENTAL

The preparation and characterisation of the H-ZSM-5 zeolites with different Si/Al ratios (varying from 13.6 to 39.7) have been described elsewhere [9].

The catalyst poisoning experiments for measuring the active acid sites

for the cracking and isomerization reactions were carried out in a pulse micro-reactor connected to a gas chromatograph (Perkin Elmer Sigma 3B, with flame ionisation detector) using nitrogen (99.99%) as the carrier gas. The micro reactor consisted of a stainless steel tube (o.d. 6 mm; i.d. 4 mm and length 22 cm) with the zeolite particles (0.2 mm size) packed between the quartz wool plugs. The temperature of the zeolite bed and the injection part of the micro-reactor could be varied independently. The reaction conditions were as follows: amount of catalyst, 0.05 g; N_2-flow rate, 800 min^{-1}; reaction temperature, 573K; pulse size, 0.07 mmol; and pressure, 370 kPa. A part of the reactor effluent was bypassed before it entered the gas chromatograph. The reaction products were analysed in a carbowax 20M (10%) on chromosorb - W column at 343K (carrier gas flow rate: 40 $cm^3.min^{-1}$).

The catalytic titration of the active sites on the zeolite was performed by making the sites with increasing acid strength available for the catalytic reaction by saturating them with pyridine irreversibly adsorbed at 598, 673, 723 and 773K and also by using the zeolite without poisoning. Thus only the acid sites which were weaker than those blocked by the base at the saturation (or poisoning) temperature (Ts) were available for the reaction on the poisoned zeolite. The desorption of the adsorbed pyridine from the poisoned zeolite during the activity test was prevented by carrying out the reaction at a temperature (which was 573K) lower than the lowest temperature at which the acid sites were blocked with irreversibly adsorbed pyridine. A detailed procedure for poisoning the zeolite and measuring its catalytic activity has been described earlier [9].

RESULTS AND DISCUSSION

The results of the catalytic titrations are presented in Fig. 1. For both the cracking and isomerization reactions, the catalytic activity of the zeolite (with the different Si/Al ratios) decreases with the decrease in Ts (i.e. the temperature at which the zeolites are saturated with irreversibly adsorbed pyridine). It can also be noted that the activity vs. Ts curves for both the reactions on zeolites when extrapolated to zero activity meet almost at the same point. This point which corresponds to the temperature Ts required for blocking nearly all the active sites involved in the reactions. These results reveal that the sites having an acid strength of $Td \geq 570K$ (where Td is the temperature at which the irreversibly adsorbed pyridine desorbs) are responsible for both the reactions on the zeolite, or in other words only those acid sites, which can adsorb pyridine irreversibly at or above 570K, catalyse the reactions.

The number of active acid sites taking part in the reaction was obtained

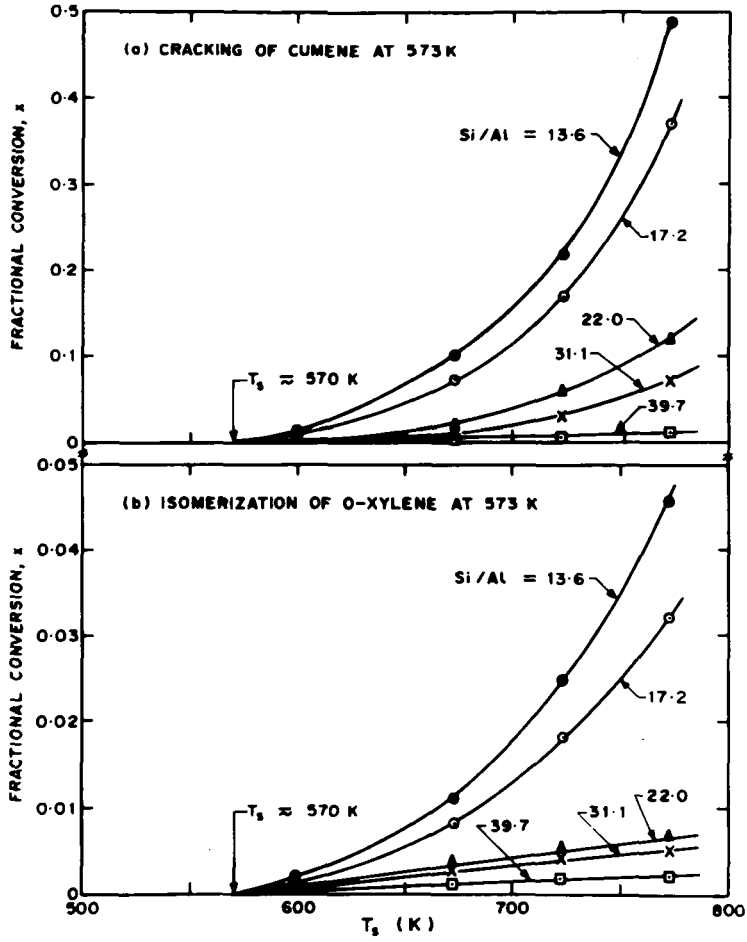

Fig. 1. Dependence of the catalytic activity of H-ZSM-5 (with different Si/Al ratio) on Ts for the cracking and isomerization reactions

in terms of the number of pyridine molecules adsorbed irreversibly at the maximum Ts (570K) required for completely deactivating the zeolite. Figure 2 shows that the number of active acid sites in the zeolite decreases almost linearly with the increase in the Si/Al ratio.

The dependence of the ratio of the active acid sites per unit cell to the Al-atoms per unit cell of the zeolite on the Si/Al ratio is shown in Fig. 2; the active acid sites per Al-atom increases with Si/Al ratio up to the value of 31.1 and levels-off thereafter. This trend in the variation of the active acid sites per Al-atom with the Al-content of the zeolite is expected to be mainly due to the interaction between the structural Al^- anions (which are

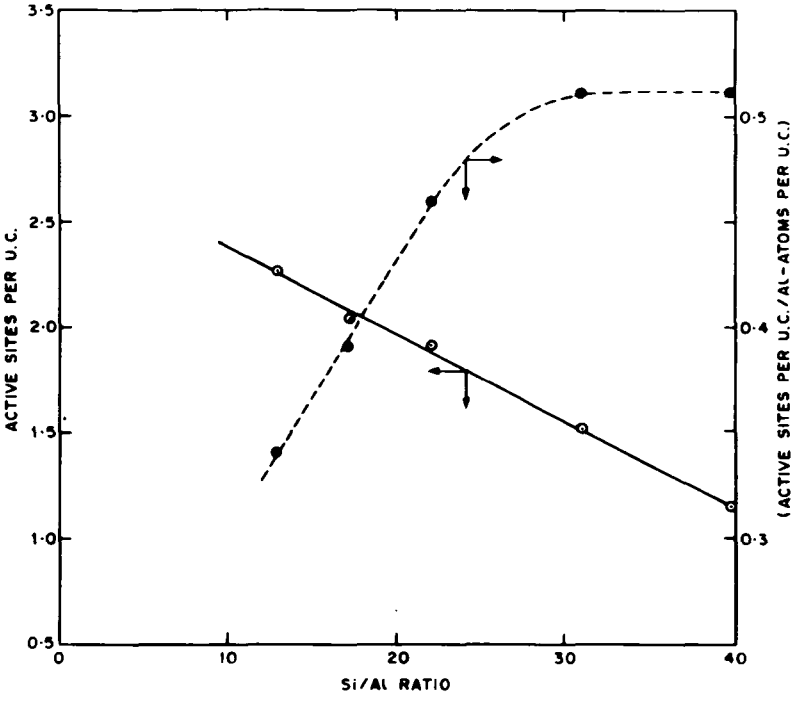

Fig. 2. Dependence of the active sites and the ratio of active sites to Al-atoms on the Si/Al ratio for the cracking and isomerization reactions on H-ZSM-5

responsible for the acid sites). In ZSM-5 zeolite, the structural Al anions are expected to be situated at the channel intersections. Since there are four channel intersections per unit cell of the zeolite [22]; more than one Al^- are present at some of the intersections when the Al-content of the zeolite is more than 4 Al-atoms per unit cell. This situation can also be present in the case of the zeolite containing 4 (or even less than 4) Al-atoms per unit cell when the distribution of the Al-atoms is not uniform. The results (Fig. 2) points to the fact that the number of active acid sites per structural Al-atom on H-ZSM-5 decreases with the increase in the Al-content, the decrease being very pronounced above the Al-content of about 4 Al-atoms per unit cell. The interaction between structural Al^- anions present at the same channel intersection causes a decrease in the strength of the acid sites originating from the Al^- anions, which results in the decrease in the active (or strong) acid sites per structural Al.

The poisoning technique employed in the present study differs from the conventional pulse poisoning technique [23,24] in that the active sites of varying acid strengths are blocked by irreversibly adsorbed pyridine at different temperatures instead of introducing the poison in small doses at the reaction temperature (which does not ensure preferential blockage of active or stronger acid sites), and finding the activity of the catalyst after the introduction of each poison pulse.

The catalyst activity is measured at a temperature lower than the lowest temperature at which the acid sites are blocked by the irreversibly adsorbed poison. The present pulse poisoning technique, therefore, ensures uniform and also preferential blockage of the active acid sites in the order of their strength and eliminates the possibility of the desorption of poison during the activity test. It gives both the number and the minimum strength of the active sites taking part in the catalytic reaction. It can also be employed [9,21,25] for obtaining correlation between the selectivity for the different products and the strength of acid sites involved in the catalytic reactions.

REFERENCES

1. Meisel, S., McCullough, J.P., Lechthaler, C.H.,and Weisz, P.B., Chemtech., 86 (1976).
2. Chang, C.D., and Silvestri, A.J., J. Catal., 47, 249 (1977).
3. Chang, C.D., Kuo, J.C.W., Lang, W.H., Jacob, S.M., Wise J.J. and Silvestri, A., Ind. Eng. Chem. Process Des. Dev., 17, 255 (1978).
4. Derouane, E.G., Nage, J.B., Dejaifve, P., Van Hoof, J.H.C., Spekman, B.P., Vedrine, J.C. and Naccache, C., J. Catal., 53, 40 (1978).
5. Anderson, J.R., Foger,K., Mole, T., Rajadhyaksha, R.A. and Sanders, J.V., J. Catal., 58, 114 (1979).
6. Nayak, V.S. and Choudhary V.R., Appl. Catal., 10, 147 (1984).
7. Lewis, P.J. and Dwyer, F.G., Oil Gas J., Sept. 26 (1976).
8. Kaeding, W.W., Chu, C., Young, L.P., Weinstein, B. and Butter, S.A., J. Catal., 67, 159 (1981).
9. Nayak, V.S. and Choudhary, V.R., Appl. Catal., 4, 333 (1982).
10. Lewis, P.J. and Dwyer, F.G., Oil Gas J., 75 (40), 55 (1977).
11. Chen, N.Y., Kaeding, W.W. and Dwyer, F.G., J. Am. Chem. Soc. 101, 6783 (1979).
12. Kaeding, W.W., Chu, C., Young, L.B., Weinstein, B. and Butter, S.A., J. Catal., 67, 159 (1981).
13. Dejaifve,P., Vedrine, J.C., Bolis, V., and Derouane, E.G., J. Catal., 63, 331 (1980).
14. Chang, C.D., Lang, W.H. and Silvestri, A.J., J. Catal., 56, 268 (1979).

15. Auroux, A., Bolis, V., Weizchowski, P., Gravelle, P.C. and Vedrine, J.C., J. Chem. Soc. Faraday Trans. II, 75, 2544 (1979).
16. Nayak, V.S. and Choudhary, V.R., J. Catal., 81, 26 (1983).
17. Nayak, V.S. and Choudhary, V.R., Appl. Catal., 10, 137 (1984).
18. Choudhary, V.R. and Nayak, V.S., Materials Chem. Phys., 11, 515 (1984).
19. Choudhary, V.R. and Nayak, V.S., Zeolites (in press).
20. Benesi, H.A. and Winguist, B.H.C., Adv. Catal., 27, 97 (1978).
21. Nayak, V.S. and Choudhary, V.R., Appl. Catal., 9, 251 (1984).
22. Flanigen, E.M., Bennett, J.M., Grose, R.W., Cohen, J.P., Patton, R.L. and Kirchner, R.M., Nature, 272, 512 (1978).
23. Turkevich, J., Nozaki, F. and Stamires, D., Proc. Int. Cong. Catal., 3rd Amsterdam, 1964, 1, 586 (1965).
24. Boreskova, E.G., Topchieva, K.V. and Plguzova, L.I., Kinet, Katal. 5, 903(1964).
25. Nayak, V.S. and Choudhary, V.R., Indian J. Technol., 21, 376 (1983).

.....

THE STRENGTH OF OH GROUPS IN NaHZSM-5 ZEOLITES STUDIED BY IR SPECTROSCOPY

J. DATKA, E. Tuźnik
Faculty of Chemistry, Jagiellonian University, 30-060 Cracow, Karasia 3, Poland

ABSTRACT

The acid strength of OH groups in NaHZSM-5 zeolites increases with the cation exchange degree. It has been evidenced by the results of the studies of thermodesorption of pyridine and of the studies of extinction coefficient of OH groups. This effect is rather unexpected because in highly siliceous zeolites like ZSM-5, the concentration of Na^+ and H^+ is very low, the distances between them are long and influence of the exchange $Na^+ - H^+$ on the properties of OH groups should be negligible. Two explanation of this disagreement are proposed.

INTRODUCTION

Acidity is a very important parameter determining the catalytic properties of zeolites. There are numerous methods of modification of acidity of zeolites, such as the modification of cation exchange degree, change of Si/Al molar ratio, partial dehydroxylation, partial poisoning of acid sites etc. The effects of these modifications on the acid and catalytic properties of zeolites are reviewed in the Jacobs' monograph [1].

The present paper concerns the modification of the acid properties of NaHZSM-5 zeolites by the variation of cation exchange degree. In NaHY zeolites the increase of cation exchange degree increased the number of OH groups, their acid strength and also their catalytic activity (for example ref. 1-5).

In ZSM-5 zeolites, the situation is more complicated. T.p.d. studies of NH_3 desorption showed that ΔH_{des} values increase with cation exchange degree [6]. Similar situation was also observed in mordenites [7] in which the temperature of t.p.d. peak of NH_3 desorption does also increase with the cation exchange degree. All these results suggest that in ZSM-5 zeolites and also in mordenites the strength of acid sites increases with the exchange degree (similarly,

as in Y zeolites).

Contrary then in NaHY zeolites, in ZSM-5 the catalytic activity do not show the same trends as the acidity. In n-hexane cracking [6], o-xylene isomerization [8,9], and in dimethylether conversion [9] the rate constant increase linearly with the number of strong acid sites, but no correlation was found b etween the rate of n-hexane cracking and ΔH of NH_3 desorption [6]. Such lack of correlation between the strength of acid sites and their catalytic activity was interpreted assuming the existence of a threshold level for the acid strength [6]. Above this level the acid strength does not influence any more the catalytic activity of zeolites.

The aim of the present study was to follow the dependence the acid strength of OH groups in NaHZSM-5 zeolites on the cation exchange degree. In a previous study [10,11], it has been found that two kinds of Brönsted acid sites exist in NaHZSM-5 zeolites : 3609 cm^{-1} OH group being strong sites and another Brönsted sites of lower acidity.

The concentrations of both kinds of acid sites were determined. In the present study the efforts were made to obtain the information concerning the properties of 3609 cm^{-1} OH groups only. The acid strength of these OH groups was characterized by the i.r. spectroscopic studies of pyridine thermodesorption and by the comparison of extinction coefficients of OH bands.

Two series of NaHZSM-5 zeolites were studied. One of them was obtained by the ion exchange of parent Na form in the HCl solution (HZ series) and another are obtained by the exchange of Na form in NH_4NO_3 solution (NZ series).

EXPERIMENTAL

NaHZSM-5 zeolites were obtained from a parent sodium form ("Utrazet") sample prepared at the Institute of Industrial Chemistry (Warsaw), the composition of which was : $Na_{1.7}H_{0.3}[(AlO_2)_2(SiO_2)_{94}]$ (Si/Al ratio = 47, and Na/Al = 0.85).

Two series of hydrogen forms NaHZSM zeolites were prepared : one by the exchange of Na^+ into NH_4^+ ions in NH_4NO_3 solution and another one by the exchange in HCl solutions. Various exchange degrees were obtained by using various concentrations of NH_4NO_3 and HCl solutions. The highest concentrations of these solutions were 1 m and 0.5 m respectively. After the ionic exchange, the zeolites were washed and dried at 390 K.

In order to calculate the exchange degrees, the zeolites were dissolved in HF solution and sodium content determined by atomic

absorption. The zeolites obtained by the HCl treatment were denoted as : HZ-41, HZ-81, HZ-88 (exchange degree 41, 81, 88 % resp.), and the zeolites obtained by the NH_4NO_3 treatment and further decomposition of NH_4^+ ions as : NZ-43, NZ-83 (exchange degrees 43 and 83 resp.).

For the i.r. spectroscopic studies the zeolites were pressed into thin wafers (3-10 mg/cm^2). The wafers inserted into i.r. cell were pretreated in vacuo at 450°C for 1 h.

At these conditions complete water desorption and decomposition of NH_4^+ ions took place without any appreciable dehydroxylation.

Pyridine (POCh Gliwice, analytical grade was dried over KOH. The i.r. spectra were recorded with a SPECORD 75 IR spectrometer. The accumulation and subtraction of spectra were done with a KSR 4100 minicomputer working on-line with the spectrometer.

RESULTS

Adsorption of pyridine on NaHZSM-5 zeolites. Two distinct OH bands are present in the i.r. spectrum of NaHZSM-5 zeolites : at 3609 and 3738 cm^{-1} . Adsorption of pyridine results in the formation of PyH^+ ions (1545 cm^{-1}), PyL and $PyNa^+$ complexes (1450 and 1444 cm^{-1} bands). First portions of pyridine sorbed in zeolite react with 3609 cm^{-1} OH groups forming PyH^+ ions. The intensity of 3609 cm^{-1} OH band decreases linearly and the intensity of 1545 cm^{-1} PyH^+ bands increases linearly with the amount of pyridine sorbed. After the consumption of all 3609 cm^{-1} OH groups the next introduced pyridine molecules react with weaker Brönsted acid sites forming additionally PyH^+ ions and 1545 cm^{-1} PyH^+ band continues to increase.

The desorption of pyridine removes the molecules bonded with weak sites at first, PyH^+ band diminishes, but 3609 cm^{-1} OH band is still absent. The pyridine molecules neutralizing 3609 cm^{-1} OH groups are removed at higher temperatures. The amount of PyH^+ ions decomposed by the desorption before the 3609 cm^{-1} OH band reappeared was taken as corresponding to the amount of weak Brönsted acid sites, and the remainder of PyH^+ ions as corresponding to the amount of 3609 cm^{-1} OH groups. The concentration of both kinds of Brönsted acid sites was determined in NaHZSM-5 zeolites of various exchange degrees [10,11].

i.r. studies of thermodesorption of pyridine. In order to study the acid strength of 3609 cm^{-1} OH groups the small portions of pyridine were sorbed at 440 K in the zeolite up to the disappearance of this OH band (the excess of pyridine was avoided). The spectrum was then recorded and next the cell was connected to the liquid nitrogen trap and heated to higher temperatures (in the range 620 - 820 K). After each desorption step the cell was cooled down to 440 K and the spectrum recorded. The intensities of 1545 cm^{-1} PyH^+ band were measured after the desorptions of two temperatures : at the temperature at which 3609 cm^{-1} OH band begins to reappear (A_0) and after the desorption at 790 K (A_{790}). The ratio A_{790}/A_0 represents the fraction of 3609 cm^{-1} OH groups which still hold pyridine after the desorption at 790 K. These values which were taken as the measure of the strength of 3609 cm^{-1} OH groups are presented at the Table. In both series of zeolites HZ and NZ the acid strength of 3609 cm^{-1} measured by the pyridine thermodesorption increase with the cation exchange degree.

The calculation of extinction coefficient of 3609 cm^{-1} OH band

In order to calculate the values of integrated extinction coefficient (IEC) at 3609 cm^{-1} OH band, the values of the integrated intensities of these bands were measured in the spectra of freshly activated zeolites. The concentrations of these OH groups were determined by the pyridine adsorption and desorption (as described above). The values of IEC of 3609 cm^{-1} OH bands calculated in such a way are presented in the Table. In both series of zeolites they increase with the exchange degree of zeolites.

Table

A_{790}/A_0 values and integrated extinction coefficients of 3609 cm^{-1} OH groups

Zeolite [x]	A_{790}/A_0	integr. ext. coeff. $cm\ mol^{-1}$
NZ - 43	0.22	1.8
NZ - 83	0.72	2.7
HZ - 41	0.17	2.3
HZ - 81	0.40	2.8
HZ - 88	0.45	2.7

[x] the values of cation exchange degrees are given in the symbols of zeolites.

DISCUSSION

The information concerning the acid strength of 3609 cm^{-1} OH groups was obtained in the studies of pyridine thermodesorption and by the comparison of the values of extinction coefficients.

The results of the studies of pyridine thermodesorption (presented at the Table) show that the acid strength of 3609 cm^{-1} OH groups increases with the cation exchange degree of NaHZSM-5 zeolites. This statement is based on the increase of A_{790}/A_0 values, which represents the fraction of 3609 cm^{-1} OH groups which still hold pyridine after the desorption at 790 K.

The integrated extinction coefficient (IEC) of 3609 cm^{-1} OH band does also increase with the exchange degree, which can be interpreted as the increase of the acid strength of these OH groups. The values of IEC of OH i.r. bands can be successfully used as the measure of the strength of OH groups. Several authors [3,4,12-15] formulated the conclusions on the strength of OH groups by the comparison of the values of extinction coefficients and the results obtained in such a way were consistent with the result obtained by others methods. Recently the quantum-chemical calculations [16] showed that in the clusters $H_3AlOHSiH_3$ where the H atoms were successively substituted by fluorine, the values of dipole moment derivative $(\frac{\partial \mu}{\partial q_{OH}})_0$ increase with the positive charge on hydrogen in OH groups and also with the ionicity of O - H bond.

The results of the studies of both thermodesorption of pyridine and extinction coefficients lead to the same conclusion that acid strength of 3609 cm^{-1} OH groups increase with the cation exchange degree.

Such effect was already observed in NaHY zeolites [2-4] and was interpreted as a consequence of an introduction of more electrophilic protons instead of less electrophilic Na^+ ions. It results in an increase of the polarization in neighbouring OH groups. The same phenomenon can be also explained in the terms of collective model of acidity of zeolites [17]. Hydrogen is more electronegative than sodium (electronegativity 3.55 and 0.70 in the Sanderson scale) ; the increase of cation exchange degree increases the average electronegativity of zeolite and the positive charge on hydrogen in OH groups.

In highly-siliceous zeolites as ZSM-5 the same trends but of much lower extent are expected. In ZSM-5 (Si/Al = 47) the average concentration of Al is much lower than in Y (Si/Al = 2.5). The concentration of Na^+ and of protons is also much lower, the distances

between them much longer, and therefore the exchange $Na^+ - H^+$ should have negligible effect on the properties of OH groups. The same conclusion can be drown if considering the collective model of acidity of zeolites. In ZSM-5, the exchange of all Na^+ to protons results in much lower variation of average electronegativity ($\Delta S_{av} = 0.033$) than in Y zeolite ($\Delta S_{av} = 0.54$).

The results obtained at the present study are not in agreement with such previsions. The increase of the strength of OH groups in NaHZSM-5 zeolites is quite remarkable. Two explanations of this disagreement can be proposed at present :

1. in highly-siliceous zeolites like ZSM-5 the OH groups are stronger acid sites than in Y. The O-H bond is more polarized and is more sensitive to even very weak electrostatic influences.
2. in ZSM-5 zeolites the Al distribution is not homogeneous, there are domaines of lower and of higher Al concentration. In the domaines of higher Al concentration the inductive effects are stronger and the exchange $Na^+ - H^+$ influences the strength of neighbouring OH groups. It should be noticed that several autho reported non-homogeneous Al distribution inside the crystals [18,19] and among the ZSM-5 crystals of various shapes [19].

REFERENCES

1. Jacobs P.A., "Carbohiogenic Activity of Zeolites". Elsevier Sci Publ. Co., Amsterdam, 1977.
2. Barthomeuf D., Beaumont R., J. Catal., 30, 288 (1973).
3. Bieleński A., Datka J., J. Catal., 37, 383 (1975).
4. Datka J., J.C.S. Faraday I, 76, 2437, (1980).
5. Bieleński A., Datka J., Drelinkiewicz A., Małecka A., Acta Physi and Chemica Szegediensis 24, 89, (1978).
6. Post J.G., van Hooff J.H.C., Zeolites, 4, 9, (1984).
7. Hidalgo C.V., Itoh H., Hattori M.N., Morekami Y., J. Catal., 85, 362, (1984).
8. Nayak V.S., Choudhary V.S., J. Catal., 81, 26, (1983).
9. Guisnet M., Cormerais F.X., Chen Y.S., Perot G., Freund E., Zeolites 4, 108, (1984).
10. Datka J., Tużnik E., to be published.
11. Datka J., Wiss. Zeitschrift FEU Jena, in press.
12. Jacobs P., Ballmoos R.V., J. Phys. Chem., 86, 3050, (1982).
13. Datka J., J. Chem. Soc. Faraday I, 76, 705, (1980).
14. Datka J., J. Chem. Soc. Faraday I, 77, 511, (1981).
15. Jacobs P.A., Catal. Rev. Sci. Eng., 24, 3, (1982).

16. Datka J., Geerlings P., Mortier W.J., Jacobs P.A., to be published.
17. Mortier W.J., J. Catal., 55, 138, (1978).
18. Lymen C.E., Betterdge P.W., Morsa E.F., "Intrazeolite Chemistry". ACS Symposium Series 218 G.D. Stucky, F.G. Dwyer Eds., Washington 1983.
19. Auroux A., Dexpert H., Leclercq C., Vedrine J., Appl. Catal., 6, 95, (1983).

ETHYLATION OF TOLUENE ON HZSM-5 ZEOLITES PREPARED WITHOUT ORGANIC COMPOUNDS

XU QINHUA, Zhu Jianhua
Department of Chemistry, Nanjing University, Nanjing, China

ABSTRACT

NK-HZSM-5 (Samples obtained from Nankai University, China) used in this paper were prepared without any organic compound. The ethylation of toluene has been compared over NK-HZSM-5 exchanged with HCl (NK-1) or NH_4NO_3 (NK-2). The factors of increasing the para-selectivity over the sample NK-2 were investigated, including modification of the samples with steam treatment and selective poisoning by 4-methyl-quinoline, and reaction conditions of different temperatures and WHSV of feeds. High para-selectivity in modified samples has been thus achieved. The treatment of modification is considered to have the effects of poisoning the surface acid sites or reducing the pore dimensions. Both these effects determine the product distribution of ethyltoluene. The suppression of external surface strong acid sites is found to be more important than the reduction of pore dimensions.

INTRODUCTION

The alkylation of toluene with ethylene is the determining step in the process of producing poly-para-methylstyrene, which is a new kind of improved polymer with properties superior to polystyrene.[1] High para-selectivity of ethyltoluene has been obtained by Mobil Company utilizing modified ZSM-5 zeolite catalysts.[2-6]

The alkylation of toluene over ZSM-5 catalysts in high para-selectivity has been reported by several papers.[7-12] But they have divergent views on the factors of enhancing para-selectivity.

Instead of ZSM-5 synthesized generally with organic compounds, we used NK-ZSM-5 zeolites prepared without any ammonium, alcohols, amines, quaternary ammonium salts or other organic compounds, to study the shape-selective catalysis of ethylation of toluene and to

examine the main factors of enhancing para-selectivity of ethyltoluene.

EXPERIMENTAL

Samples. Samples NK-HZSM-5 were obtained by the conventional ion exchange method with aqueous solution of HCl (named NK-1) and with solution of NH_4NO_3 (NK-2) for six times. The samples obtained were chatacterized by X-ray diffraction pattern, and found to be consistent with those of literature.[13] Their unit cell compositions were listed in Table 1.

Table 1
The unit cell compositions of NK-HZSM-5 samples

Samples	SiO_2/Al_2O_3 mole%	Unit cell composition
NK-1	45.16	$Na_{0.04}H_{4.03}Al_{4.07}Si_{91.9}O_{192}$
NK-2	43.61	$Na_{0.04}H_{4.17}Al_{4.21}Si_{91.8}O_{192}$

Methods. The activity of catalysts was measured with a fixed-bed continuous-flow microreactor at the temperature of 350°C and atmospheric pressure. All the catalysts were tableted without binder.

The adsorption experiments were made by the gravimetric method and the acidities were measured chromatographically.[14]

RESULTS AND DISCUSSION

Evaluation of the catalytic properties. Alkylation of toluene with ethylene to produce ethyltoluene was carried out, in the presence of the catalysts of NK-1 and NK-2 respectively, at temperature of 350°C and atmospheric pressure. The experiments were made in the presence of hydrogen utilizing a weight hourly space velocity to toluene/ethylene = 1/0.3. The results are listed in Table 2. It is found that the catalytic activity (conversion of toluene, mole%) of NK-1 is greater than that of NK-2, but the selectivity of para-ethyltoluene (mole%) is in reverse order.

The relation between catalytic activity and reaction temperature is shown in Figure 1. From Figure 1 we can see that the sample NK-1 has higher activity above 300°C than NK-2.

Table 2

Comparison of the catalytic properties

Samples	Alkylation		Dealkylation	Isomerization
	conversion mole%	p-selectivity mole%	conversion mole%	conversion mole%
NK-1	42.1	43.9	16.9	45.8
NK-2	28.2	54.2	54.0	27.4

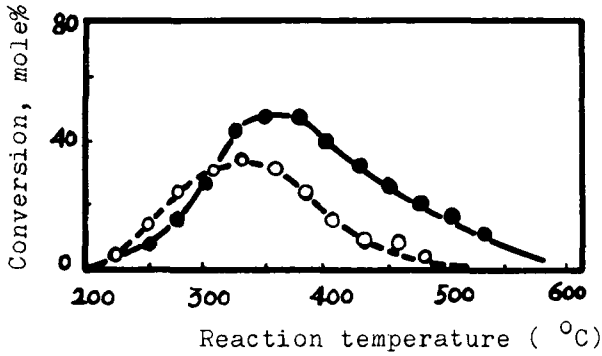

Fig. 1. The relation between activity and reaction temperature for the ethylation of toluene
—●—●— NK-1 --o--o-- NK-2

To determine the difference of these two samples in catalytic properties, we investigated the dealkylation of ethyltoluene and isomerization of p-ethyltoluene (the feed containing 88 mole% of p-ethyltoluene and 12 mole% of m-ethyltoluene). The results are also listed in Table 2, which shows that the activity of isomerization over NK-1 is greater than that of NK-2. According to Jocobs[5] and Verdrine[6], the isomerization reaction requires stronger acid sites than the alkylation and dealkylation reactions. Therefore, there are more the numbers of strong acid sites on the external surface of NK-1. Our experimental results also support this point of view. The acid strength distribution for these samples was determined. The results show that the numbers of acid sites are almost the same, but the amount of strong acid sites of NK-1 is higher than that of NK-2.

The adsorptive rate of m-xylene on NK-1 and NK-2 samples was determined at the temperature of 120°C, the vapor pressure of adsorbate being maintained at 1mmHg. The amounts of adsorption in 10 mins. on these two samples are 8.2 mg/g and 6.0 mg/g respectively. This

demonstrates that the adsorption rate on NK-2 is smaller, and hence its pore size may be smaller too. Thus, the effect of the shape and size of pore on the primary intracrystalline isomer distribution is considerablely important. Therefore, we suggest that the higher para-selectivity of NK-2 may be attributed to its favorable pore size and acid strength distribution on the external surface.

Factors of influence on catalytic properties. We further investigated the factors of enhancing the para-selectivity over the sample NK-2.

1. Steam treatment. The sample NK-2 was subjected to steam treatment for two hours at a flowing rate of 2 $cm^3/g,h$ under a temperature of 600°C. The catalytic activity obtained from the sample after steam treatment was slightly decreased while their para-selectivity increased obviously. The data is listed in Table 3.

Table 3

The catalytic activity and selectivity of NK-2 after steam treatment

Samples	Conversion,mole%	Para-selectivity,mole%
before treatment	28.2	54.2
after treatment	26.2	73.0

2. The ratio of WHSV of toluene/ethylene. The influence of WHSV on the activity and selectivity of the ethylation of toluene was studied. The para-selectivity was plotted against the conversion of toluene under different WHSV, giving a good linear relationship between them, over the sample of NK-2 as shown in Figure 2. The results also show that the conversion of toluene was decreased while para-selectivity was increased with the increase of the ratio of WHSV.

3. Reaction temperature. We have measured the activity of dealkylation of toluene at different temperatures.

The relation of dealkylation conversion to reaction temperature is shown in Figure 3, which shows that the extent of dealkylation rose sharply after 300°C. The reactivity of ethylation of toluene over NK-2 was measured at different temperatures, shown in Figure 4. From Figure 4 it can be seen that there is a maximum in the conversion curve at a temperature of 325°C. It shows clearly that the decrease of activity above 325°C is caused by the fact that the reaction of dealkylation of ethyltoluene is now dominating.

In Figure 4, the para-selectivity lowered at first with the

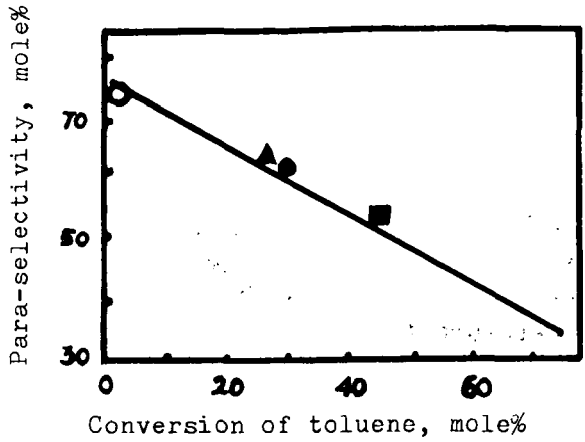

Fig. 2. The influence of ratio of WHSV of toluene/ ethylene, the ratio of WHSV of toluene/ ethylene:
○ 5/0.3, ▲ 5/1, ● 1/0.3, ■ 2/0.7

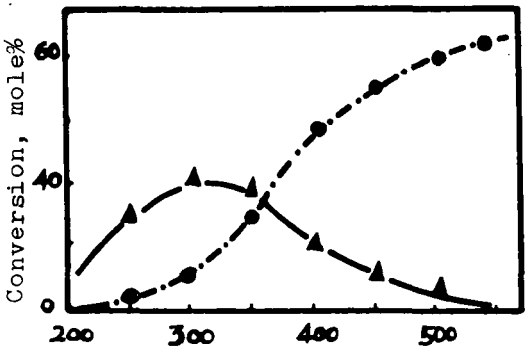

Fig. 3. The relation of activity to reaction temperature
--●--●-- dealkylation
—▲—▲— isomerization

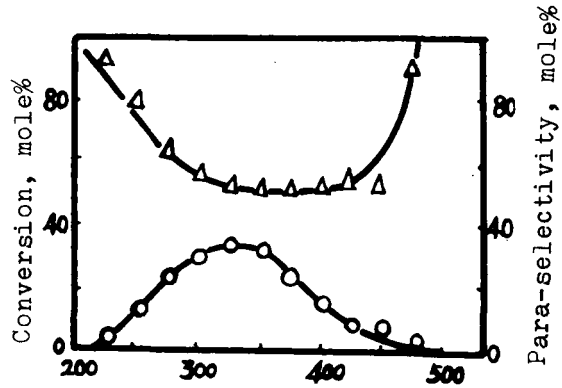

Fig. 4. The relation of reactivity to reaction temperature

increase of the temperature, reaching a lowest level and then going up again. Figures 3 and 4 indicate that the isomerization activity of p-ethyltoluene has the opposite tendency to the para-selectivity of alkylation of toluene with temperature.

4. Modification. To examine the factors controlling the increase of para-selectivity, sample NK-2 was modified with steam treatment as previously described and with selective poisoning by

4-methyl-quinoline respectively.

The adsorption rates were determined on modified samples under the same conditions as described above. The results are shown in Figure 5 and listed in Table 4.

From Table 4 we can see that the adsorption rate of m-xylene on the NK-2 modified with steam treatment drops sharply. It implies that a reduction in effective pore size occurred on the pore openings, which could favor outward diffusion of the para-isomer relative to meta and ortho. Therefore the para-selectivity of ethylation of toluene was increased by 10 units. However, the adsorption rate of m-xylene on the sample modified with selective poisoning was almost unchanged. It means that no change occurred in the pore size

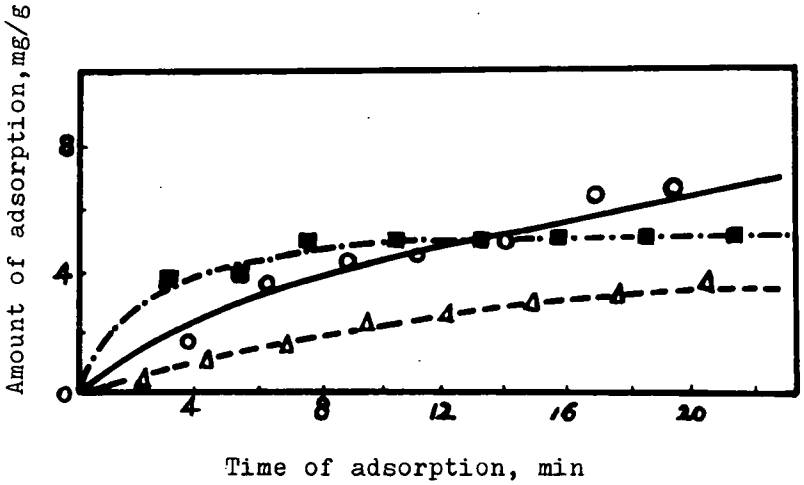

Fig. 5. The adsorption rate on the samples with different treatment

-·-■-·-■-·- without treatment

—o—o— with selective poisoning

---Δ---Δ--- with steam treatment

of the zeolite, but the para-selectivity of this sample was increased by 27 units. It further demonstrates that among the factors of enhancing para-selectivity, the effects of acidity are more important than those of the shape and size of the pore. The strong acid sites on the external surface were reduced by 4-methyl-quinoline, which inhibited the surface isomerization, and consequently the para-selectivity was raised.

The increment of para-selectivity and the decrement of iso-

Table 4

The adsorption rate and para-selectivity of alkylation on the modified samples

Samples	Amount of adsorption of m-xylene in 10 minutes at 120°C, mg/g	Para-selectivity (ratio of WHSV of toluene/ethylene =7/0.5) at 350°C, mole%
NK-2 without treatment	4.8	71.2
NK-2 modified with steam treatment	2.2	81.0
NK-2 modified with selective poisoning	4.6	98.2

merization activity were almost the same with the amount of 4-methylquinoline, as shown in Figure 6. This experiment gives further evidence that high para-selectivity of ethylation of toluene should be attributed mainly to the acidity on the external surface of the catalysts.

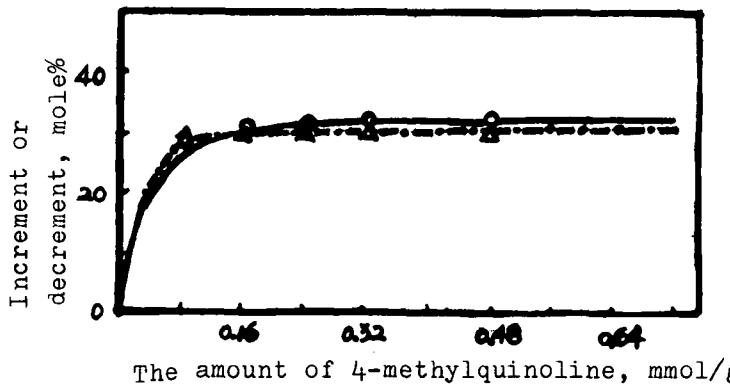

Fig. 6. The increment of para-selectivity (▲) and the decrement of isomerization activity (●) with the amount of 4-methylquinoline

REFERENCES

1. Kaeding, W.W., Young, L.B. and Prapas, A.G., CHEMTECH 556 (1982).
2. Kaeding, W.W., U.S.P. 4, 117, 024 (1978).
3. Kaeding, W.W. and Young, L.B., U.S.P. 4, 094, 921 (1978).
4. Kaeding, W.W. and Young, L.B., U.S.P. 4, 143, 084 (1979).
5. Kaeding, W.W., U.S.P. 4, 128, 592 (1978).
6. Chu, C.C., U.S.P. 4, 420, 418 (1983).
7. Kaeding, W.W., Chu, C.C., Young, L.B., Weinstein, B. and Butter, S.A., Journal of Catalysis, 67, 159 (1981).
8. Young, L.B., Butter, S.A. and Kaeding, W.W., Journal of Catalysis, 76, 418 (1982).
9. Bhat, S.G.T., Journal of Catalysis, 75, 196 (1982).
10. Nunan, J., Cronin, J., and Cunninghan, J., Journal of Catalysis, 82, 77 (1984).
11. Yashima, T., Sakaguchi, Y. and Namba, S., in Proc. 7th Inter. Congress Catal., Tykyo (1980).
12. Kaeding, W.W., Young, L.B. and Chu, C.C., Journal of Catalysis, 269 (1984).
13. Argauer, R.J. and Landolt, R.G., U.S.P. 3, 702, 886 (1972).
14. Misono, M., Saito, Y., Yoneda, Y., Third Inter. Cong. Catal., (Amsterdan) 408 (1964).

ASPECTS OF METAL AND METAL COMPLEX CONTAINING ZEOLITES

N. JAEGER, P. PLATH, G. SCHULZ-EKLOFF
Institut für Angewandte und Physikalische Chemie, Forschungsgruppe Angewandte Katalyse, Universität Bremen, D-2800 Bremen 33, FRG

ABSTRACT

Unambiguous informations on the location and structure of metal particles exceeding super cage size in faujasite matrices are summarized. Current ideas on the possible nucleation and growth mechanisms are presented. The structures of encaged chelates are illustrated by means of the examples nickel dimethylglyoxime and cobalt phthalocyanine with regard to requirements and expections for the catalytic activity of zeolite encapsulated metal complexes. Established applications, prospective uses and promising reactions of metal-containing zeolites in catalysis are regarded exemplarily.

METAL PHASES WITHIN THE ZEOLITE MATRIX

Zeolites, namely X and Y type faujasites are suitable supports for the preparation of well defined monodispersed metal phases, i.e. metal phases located exclusively within the framework of the faujasite matrix.

Narrow particle size distributions can be achieved due to the restrictions imposed by the zeolite channels and cages on the growth of the metal agglomerates. In most cases monodispersed metal phases are found within the supercages [1-6] and a number of excellent tools have been developed and adapted for the study of the physical properties of such highly dispersed metals, of their location and of their interactions with the zeolite support and with suitable probe molecules.

The location of charged clusters of silver atoms [7,8] and of Pd atoms [9,10] on the lattice sites in Y zeolites has been determined from single crystal and powder X-ray diffraction data. Fraissard et al. [11-13] applied the nuclear magnetic resonance of adsorbed Xe to the investigation of Pt dispersions and demonstrated the capability of the method to detect Pt particles consisting of fewer than 10 atoms within the supercages of Y zeolites. Small angle X-ray scattering (SAXS) has been used to determine the size distributions of Pt crystallites in Y zeolites [14,15] and impressive results could be obtained from evaluating the radial electron

distribution from X-ray diffration data, e.g. the changes of interatomic distances in 1 nm Pt particles supported in Y zeolites upon the adsorption of molecules [14, 16, 17]. Mössbauer spectroscopy in combination with measurements of the spontaneous magnetization has been successfully applied to characterize small iron clusters supported in zeolite A [18,19] and to rule out electron transfer from the metal to the support in this case. Electron deficiency has been observed in other cases, e.g. Pd [9] and Pt [20,21]. This is important information with regard to the role of particle size effects in catalysis. The application of static magnetic methods and of ferromagnetic resonance is restricted to ferromagnetic metals and has been applied especially in the case of Ni-loaded zeolites in order to evaluate the size distribution of the metal particles [22-26]. Curve fitting and the interference of Ni^{2+}-ions in partially reduced samples, however, require the application of complementary methods for reliable interpretations of the experimental data. Direct observation of metal agglomerates of and beyond supercage dimension by electron microscopy is the method suited best to determine size, location and distribution of metal agglomerates supported by zeolites. The existence of 2 nm Pd and Pt particles in Y zeolites was demonstrated by this technique [27,28]. In modern electron microscopes the power of the electron beam can be reduced to a point were modifications of the particle size due to overheating the substrate can be avoided [29].

Recently, metal phases with crystallite sizes by far exceeding supercage dimensions were found to exist within a faujasite X framework for a number of metals, namely Pt [30] , Ru [31-33] , Pd [5,34] and Ni [23,35]. Particle sizes ranging from 3 nm for Pd [5] up to 10 nm for Pt and Pd [34,36] and even 15 nm in the case of Ni [37] were determined mainly by electron microscopy. The location inside the zeolite matrix has been confirmed by XPS measurements [38]. It was shown by electron diffraction from selected areas and single particles in the case of Pd, Pt and Ni [34,36,37] that such aggregates are single crystals. Phase contrast imaging and electron diffraction patterns of the zeolite lattice revealed that the structure of the host lattice is maintained in the neighborhood of the metal crystallites. It was proposed that the growth mechanism of the metal single crystals involves atomic rearrangements of the zeolite lattice in analogy to the process of steam stabilization [37]. A variation of the particle size with the Si/Al ratio of the support can be anticipated. The recrystallization of the zeolite lattice during the growth of the metal phase could be inferred from an increase in the temperature of the lattice breakdown and an increase of the N_2 physisorption capacities [36].

The monodispersed metal phases with narrow particle size distributions could be achieved for Ni as well as for Pd and Pt even though the reduction of ion-exchanged samples follows quite different paths. In the case of Ni the dehydrated ion-exchanged samples were reduced by hydrogen, while Pd and Pt metal phases were

formed by autoreduction of the respective exchanged tetrammine complexes in the course of the dehydration process [39,40].

Nucleation in the latter cases must be restricted to the supercages were the big tetrammine complexes are located following the ion-exchange. In the case of platinum a preferred orientation relationship $<100>_{Pt} // <100>_{zeolite}$ has been observed [36]. Relatively high metal loadings were required for these investigations. The existence of a preferred orientation of the Pt crystallites can be explained by assuming an orientated growth of the fcc platinum within the cubic faujasite structure starting from an orientation imposed by the geometry of the supercage on the growing nucleus.

The observed orientation of the platinum crystals can in turn be taken as additional proof that the metal crystals must have been grown in an intact zeolite matrix and not in a priori voids formed under steaming conditions, as is stated repeatedly [41]. Nucleation and growth of the metal phases from atomic dispersions of the reduced metal or from preformed clusters seem to be the decisive steps. According to the theory of nucleation [42] nuclei of critical radius r_c are formed at a rate

$$J = B \cdot \exp(-\Delta G_c / kT) \qquad (1)$$

per unit volume. The free enthalpy of formation ΔG_c of a nucleus of critical size is proportional to $1/(\Delta\mu)^2$. The super saturation $\Delta\mu$ is assumed to be high at least in the case of noble metals under the experimental conditions used in the preparation of the metal phases. In heterogeneous nucleation B is proportional to the coefficient of surface diffusion of single adatoms and to their density on the surface.

According to Wynblatt [43] no barrier exists for the nucleation of 3-dimensional Pt clusters on the surface of an Al_2O_3 substrate. The formation of metal phases preferentially or even exclusively inside the zeolite matrix indicates that a similar favourable situation for the formation of nuclei should exist within the channels and cages of the zeolite. The zeolite lattice offers a number of singular points, where an existing potential barrier for the formation of a critical nucleus could be lowered or where metal atoms could be trapped. Such centers are non-reducible cations, where the agglomeration of metal atoms results in a reduction of the electrostatic energy. Finer dispersions of the metal phase are often observed if non-reducible transition metal ions, e.g. Cr^{3+} [44], Fe^{3+} [45], Ce^{3+} [6] are present in the zeolite framework during the reduction process, operating as preferred nucleation sites. Other centers for nucleation are ions not yet reduced and available for the formation of charged clusters. Nucleation results from the collision of migrating adatoms and of the two alternatives

$$Me^0 + Me^0 = Me_2^0 \qquad (2)$$

$$Me^0 + Me^{n+} = Me_2^{n+} \qquad (3)$$

the initiating step (3) should be favoured.

The free enthalpy of nucleation will be less for charged as compared to uncharged nuclei. The difference in the free enthalpies of nucleation corresponds to the difference in the enthalpies of formation for the two nuclei. The enthalpy of formation for nucleation step (3) will roughly correspond to the difference of the first and the nth ionization potential, i.e. 5-15 eV for n = 2. The formation enthalpy for process (2) will be close to the evaporation enthalpy, i.e. 2-7 eV and is thus smaller.

The nucleation process should therefore be promoted by a high density of transition metal ions populating the migration paths of the metal atoms as collision partners. A nuleus Me_2^{n+}, stabilized in the zeolite framework by electrostatic forces can grow by further collision with Me^0 forming charged clusters, which have been observed in the case of silver exchanged zeolites [46].

In case a barrier of nucleation does not exist [43] singular points will still act as centers for nucleation. The rate of nucleation,however,will not be affected by the exponential term in equation 1. The number of nuclei formed will be proportional to the number of centers and to the number of metal atoms. A high density of nucleation centers exists in calcined platinum exchanged faujasites [5] and a high density of metal atoms can be expected in calcined Ni exchanged faujasites undergoing reduction with atomic hydrogen [47]. High dispersities of the metal within the zeolite matrix were obtained as a consequence. The generally observed bi-dispersities in the case of Ni-loaded faujasites, i.e. large fractions of reduced nickel at the outer surface and another fraction of smaller aggregates inside the zeolite crystal could be due to a relatively low ion density in the migration path of Ni^0 and a small density of metal atoms due to a low rate of reduction.

In the case of the autoreductive decomposition of Pd-tetrammine complexes within a faujasite X an almost linear correlation between the degree of ion exchange and the number of Pd crystallites formed has been established from the evaluation of a large number of electron micrographs (Table 1) [48].

Table 1: Number of Pd crystallites within a faujasite X matrix in dependence on the degree of ion-exchange

Pd content wt%	mean diameter of Pd crystallites (nm)	number of Pd crystallites per g catalyst X 10^{-16}
14,7	10	2,34
4,4	10	0,71
2,4	10	0,38

Under constant experimental conditions the density of metal atoms should be proportional to the degree of ion exchange, determining the rate of nucleation rather than the rate of growth.

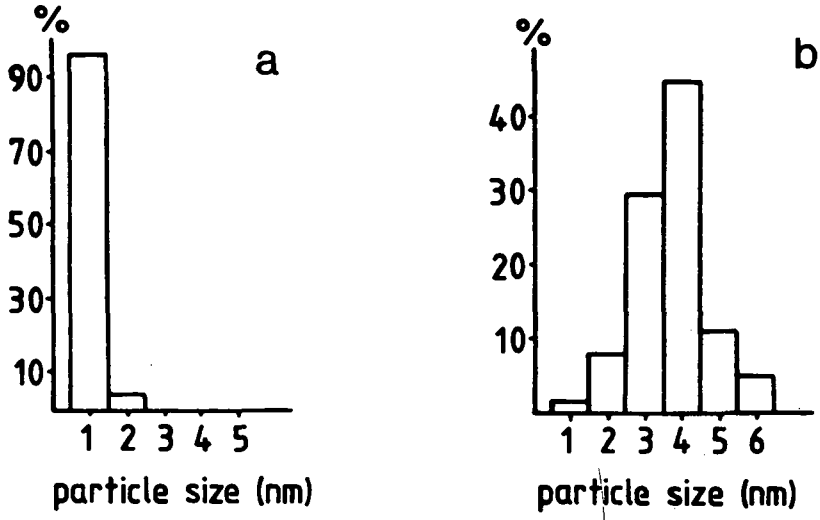

Fig. 1. Platinum particle size distribution by decomposition of $Pt(NH_3)_4X$ in oxygen (a) or in argon (b)

Under precise experimental conditions monodisperse metal phases with narrow particle size distribution can be grown on a zeolite support (Fig. 1). Promising systems can be obtained for the study of the effects of metal particle size and of metal-support interactions on selectivity in catalyzed reactions. The possibility to modify the properties of the crystalline support by controlling the Si/Al ratio, the acidity and by co-exchanging non-reducible cations add another advantage to the system.

On the other hand, fundamental studies regarding the activity of the metal phase are not straightforward due to the catalytic activity of the support itself.

FAUJASITE ENCAGED METAL COMPLEXES

The field of transition metal complexes in zeolite matrices has been reviewed repeatedly [49-52]. The following section will focus on some aspects relevant to the catalytic activity of metal chelates incorporated in a zeolite framework. Limitations in the catalytic application of such complexes with space filling ligands have been pointed out by Lunsford [49].

Howe and Lunsford [53,54] and Schoonheydt and Pelgrims [55] synthesized complexes of Co(II) with ethylenediamine and could demonstrate the formation of the

superoxo adduct, i.e. the catalytic activation of molecular oxygen. The complex exhibited, however, the tendency to form the coordinatively saturated tris-ethylenediamine variant. The ligand ethylenediamine is obviously so strong that the octahedral coordination is favoured and that only a small fraction of the planar low-spin complex is formed. Fully coordinated complexes, however, are of little importance in catalysis and it would therefore be of interest to find and to synthesize complexes exhibiting free coordination sites, which cannot be occupied by the chelate ligands. Furthermore, a distortion of such a stable chelate by partial coordination to zeolite lattice sites [55], which might be favourable for the catalytic activity of the complex, should be expected. These requirements will be met, first of all, by the class of planar complexes. $[CoX_4]^{2+}$ and $[NiX_4]^{2+}$ low-spin compounds with neutral ligand systems, forming planar-quadratic complexes, will be favourable candidates [56,57,58]. Especially the $[CoX_4]^{2+}$ system with D_{4h} symmetry should be of interest, because of its unpaired electron in the ground state. Octahedral complexes with a high tendency for tetrahedral distortion might also be taken into consideration. Such complexes can be formed with the ions Fe^{3+} and Co^{2+}, if different ligands of similar and relatively weak field strength are used.

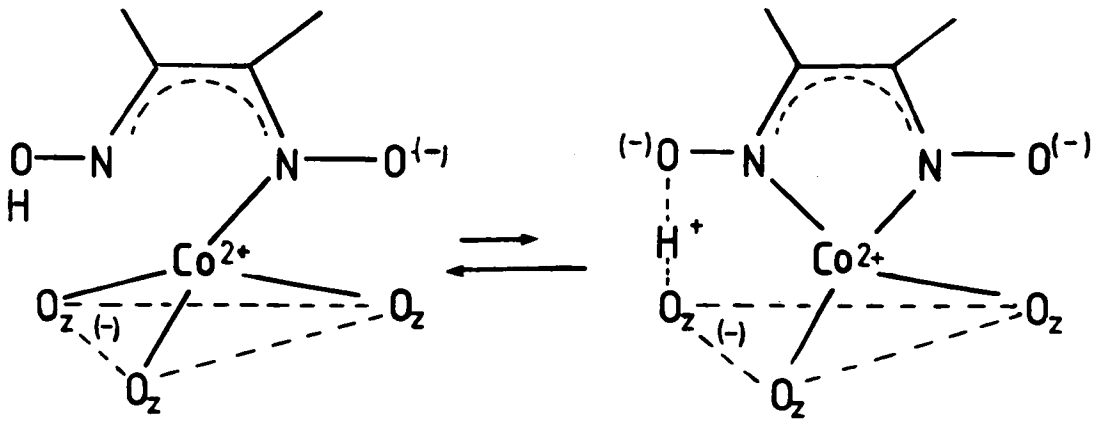

Fig. 2. Possible tetrahedral intermediate in the formation of zeolite encaged cobalt dimethylglyoxime .

The most straightforward way to prepare complexes with planar coordination is the use of four-dentate ligands, like tetrapyridyl, porphyrine or bis-dimethylglyoxime. The large ligands might be incorporated into the zeolite framework either by diffusion or by in situ synthesis from smaller molecules. Charged complexes can be stably fixed to the carrier by strong electrostatic interactions with the zeolite lattice.

Neutral complexes with weak van der Waals interactions with the zeolite can be stably fixed to the carrier only by steric hindrance. This means that the chelate complex should have diameters exceeding those of the super cage window. In this case, the in situ preparation of the ligand within the cavities is the method to be chosen.

Faujasite encaged bis-dimethylglyoximato complexes were obtained by dehydration of Ni^{2+} and Co^{2+} exchanged zeolites and gas phase diffusion of dimethylglyoxime into the cavaties of the support [59-61]. $Ni[dmgH]_2$ is directly formed in this way in the super cages as a planar-quadratic complex. In the cobalt exchanged faujasite, however, intermediate tetrahedral complexes with C_{3v} and C_{2v} distortion are formed (Fig. 2) [61,62].

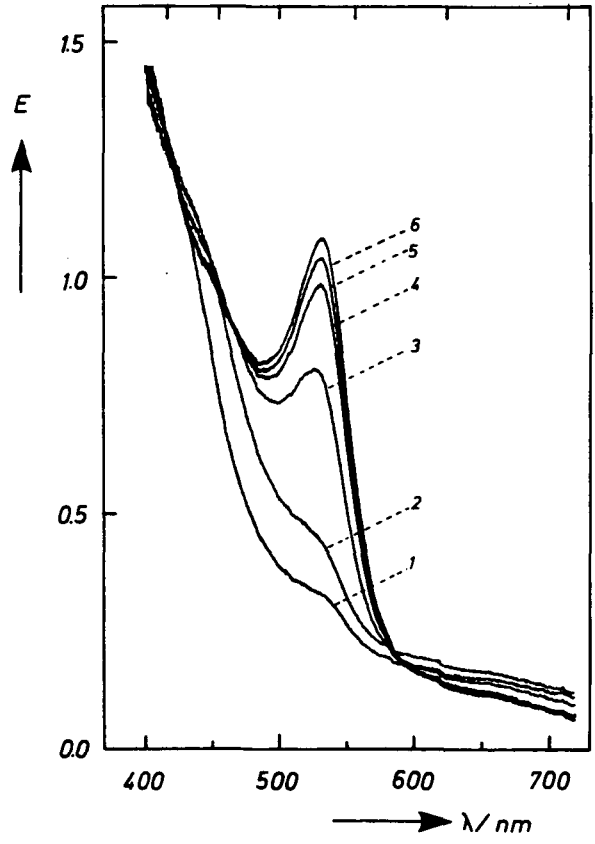

Fig. 3. Bathochromic shift of the 524 nm band of zeolite encaged nickel dimethylglyoxime during the uptake of water

Different coordination properties of the transition metal ions might result in different strengths of interaction between the chelate compounds and the zeolite lattice. Another type of interaction between the faujasite framework and the chelates which is due to the space filling property of the ligand system can be demonstrated in the case of encaged and hydrated nickel bis-dimethylglyoxime. Hydration of the yellow $Ni[dmH]_2X$ leads to a bathochromic shift of the growing and characteristic

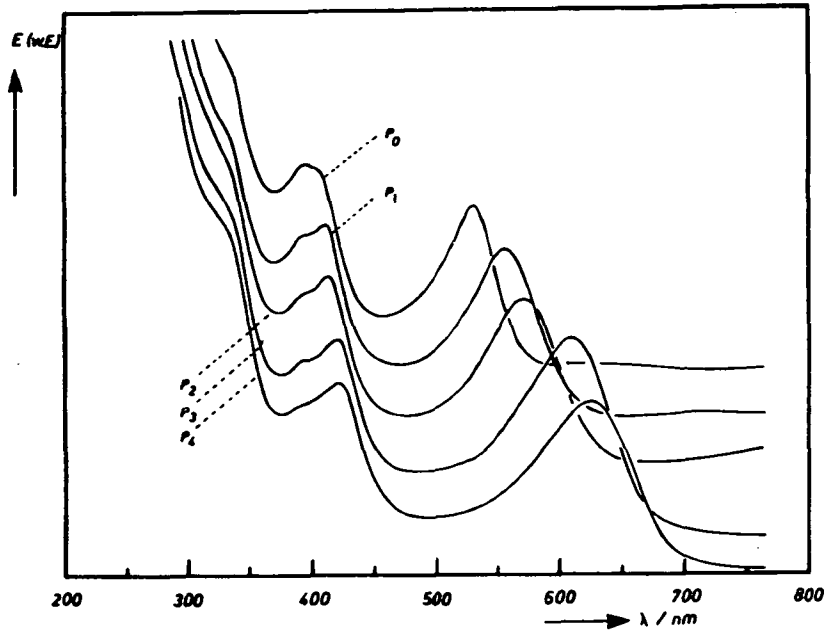

Fig. 4. Bathochromic shift of the 524 nm band of a nickel dimethylglyoxime film in a high pressure diamond-anvil cell (P_0-P_4 ≙ 0.1 MPa - 3.1 GPa)

green band at 524nm which refers to an electron transition perpendicular to the plane of the molecule (Fig.3) [63]. In zeolites a maximum shift of about 10 nm could be observed for the hydrated complex. This shift can be simulated by a pressure of 0.74 Kbar exerted on a film of $Ni[dmgH]_2$ [64] using a high pressure diamond-anvil cell (Fig.4) [65,66]. The spectroscopic properties of the encaged complexes lend support to the conclusion that chemical interactions within the zeolite framework proceed under high pressure. Such a hypothesis was already put forward by Fraissard [67].

The distortion of the symmetry, which chelates incorporated in the zeolite framework can suffer, leads to the expectation that these complexes might exhibit enhanced catalytic activities and selectivities in the cavities of the support. This hypothesis might be studied exemplarily for a class of chelates having rigid

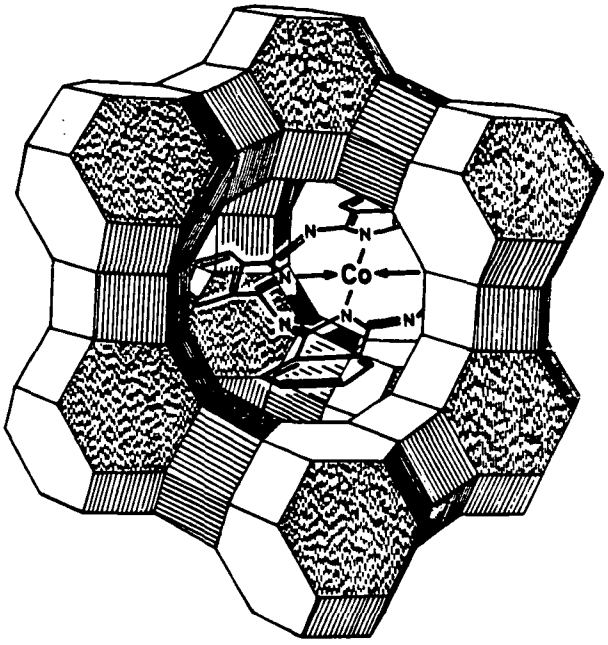

Fig. 5. Scheme of a faujasite encaged cobalt phthalocyanine molecule

planar structures of high stability. The metal phthalocyanines are favourable candidates for such investigations due to the strongly conjugated ¶-electron system of these compounds. The phthalocyanine molecule is larger than the opening of the super cage window, so that it cannot be incorporated by diffusion (Fig. 5). However, the in situ synthesis of these chelates could be achieved [68,69] and their location inside the super cages could be proven [70,71]. The distortion, which the zeolite environment exerts on the electronic structure of the phthalocyanine molecule can be observed by means of the band doublett at about 620 and 660 nm, which corresponds to the electronic vibration transition of the macrocycle [63]. The observed shift of this doublett with respect to the band positions of phthalocyanine in a liquid acid solution corresponds to one obtained by a pressure of about 30 kbar imposed on a metal phthalocyanine film [61,72] and a strong influence of the zeolite cages on the electronic structure of the porphyrine type chelates can be inferred.

Romanovsky and co-workers have shown that faujasite supported phthalocyanines exhibit a variety of marked catalytic properties [68]. The encaged chelates are thermally very stable and, therefore, represent an interesting class of immobilized homogeneous catalysts. Since a large number of variants can be derived for the porphyrine type chelates, the properties of which might be modified by incor-

poration into the zeolite matrix, it is worthwhile to evaluate the potential of this system with regard to its catalytic activity still further.

CATALYSIS BY METAL-LOADED ZEOLITES

Established Applications. The application of transition metal-containing zeolites in petrochemical processes, like e.g. cracking, isomerization, hydrocracking or hydrodewaxing, is of high economic importance and has been reviewed repeatedly [73-76]. Zeolite catalysts, which contain non-reducible metal ions, e.g. rare earth metals or rhenium, or reduced metals, e.g. platinum, palladium or nickel, are used for reforming processes. The catalytic function of the transition metal ions consists in the formation of additional Bronsted acid sites, due to the hydrolysis of water molecules [77-79]. Reduced metal phases supported by acidic carriers like zeolites will strongly increase the hydrogenation and dehydrogenation properties of the catalyst by the enhanced formation of olefin intermediates in the isomerization of paraffins [80]. Since the isomerization reaction proceeds via carbenium ion and carbonium ion intermediates on strong Bronsted sites, it should be favored by an increase of the proton activity [81]. Figure 6 depicts a scheme of the polyfunctional reaction including the suggestions of Weisz for a dual site isomerization [82] and of Olah for carbonium ion intermediates in super acids [83].

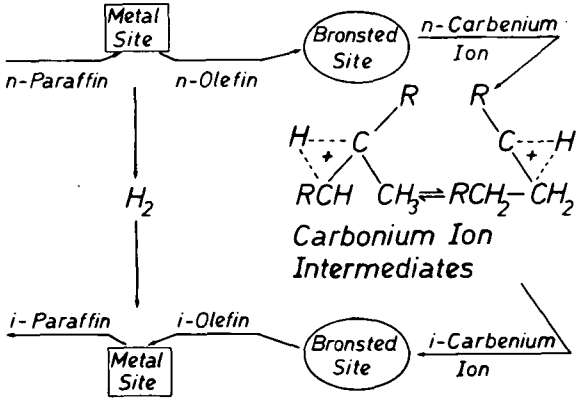

Fig. 6. Scheme of the bifunctional isomerization of paraffins

Zeolite catalysts containing reduced metals generally exhibit reduced rates of deactivation by coke deposition, which might be due to an enhanced hydrogenation of coke precursers, like olefins and aromatics [84]. However, a hydrogenation of hydrocarbons via the activation of molecular hydrogen proceeds on the

strong acid sites of transition metal-free zeolites as well. The non-classical hydronium ion H_3^+, which has been proposed by Olah [85] might be the hydrogen activating intermediate in this reaction. The relatively rapid deactivation of this hydrogenation route is obvious, since the protons of the strong Bronsted sites are constituents of coke precursors.

Prospective Uses. The direct conversion of synthesis gas in a combined process of Fischer-Tropsch synthesis and shape-selective hydrocarbon conversion to gasoline seems to be very promising [86-88]. This two stage reaction proceeds by converting FT products, like olefins and oxygen-containing compounds, to high-grade gasoline, which is rich in isomers and aromatics. The fraction of aromatics can be enhanced by a factor of three if the two catalyst components are mixed in such a way that they can be used in a one-stage process. In this case, the strong acid sites of the zeolite will be located proximate to the FT sites increasing the probability of the formation of carbenium ions from the α-olefins, primarily formed in the FT reaction. Consequently, the fraction of intermediates entering the route of cyclization, aromatization and disproportionation,respectively,is increased resulting in the formation of light aromatics, which are favoured by the restricted transition state-type selectivity of the zeolite [89].

The synthesis gas to gasoline conversion might favorably be carried out by a one-stage process in the liquid phase, i.e. in a slurry reactor, at temperatures below 300°C where the coking rates are low. A regeneration at low temperatures, around 350°C, seems to be successful and not to affect the FT component [90].

The selective FT synthesis, which has repeatedly been reported for different metal-loaded zeolites and which is characterized by deviations from the Schulz-Flory distribution of the products, might in many cases be referred to a variety of secondary effects, caused by long formation periods, keeping the catalyst far from steady states [91]. Such transient states are, presumably, favoured by the zeolite support. The existence of true selectivity effects, which can unambiguously be referred to the geometric or electronic peculiarities of the zeolite matrix, is still open to discussion in view of the large number of factors, which may effect the properties of a zeolite supported metal, e.g. particle size and geometry, metal reducibility, location of metal, pore structure, strength and activity of Bronsted acid sites, nature and strength of Lewis acid sits, nature and location of additional cations, etc.

The aromatization of ethane on a metal-containing shape-selective zeolite is of interest, because it offers a method for obtaining valuable products from a readily available lowcost feedstock. The metal, e.g. platinum, enhances the dehydrogenation of the ethane to ethene, which can enter the route of cyclization and aromatization [92].

The catalytic production of high-grade fuel from biomass compounds by shape-selective catalysis [93] is promising in view of the increasing demand to improve the utilization of rapidly growing amounts of wastes and sewage sludges. Platinum-loaded shape-selective zeolites, which exhibit lower coking rates as compared to the hydrogen forms, might favourably be used, if they are not affected by volatile metals, like Zn, Cd or Hg, which might be evolved in the pyrolysis of the refuse derived biomass.

The use of platinum group metals incorporated in zeolites for the oxidative cleaning of exhaust gases might be expected in the future with respect to the lower amount of precious metals, which is needed for the oxidation of carbon monoxide and hydrocarbons on this type of catalyst. Presumably, the catalytic activity is favourably influenced by the strong Bronsted acidity of the support [94] resulting in a synergistic action of the catalyst.

Promising Reactions. Rhodium and iridium exchanged zeolites were found to show interesting catalytic activities for the carbonylation of methanol to methylacetate [95-100]. The zeolites exhibited more stable activities than other inorganic or polymer type carriers or carbon. Cations in lower oxidation states seem to be the active sites in parallel to the homogeneously catalyzed reaction. Catalyst deactivation by reduction to zero valent metal occurs around 250°C.

Also the hydroformylation of olefins has repeatedly drawn attention [101-103 Presumably, only ethene can be hydroformylated in the pores of the zeolite matrix [103]. A scheme of this metal ion catalysed reaction is depicted in Figure 7.

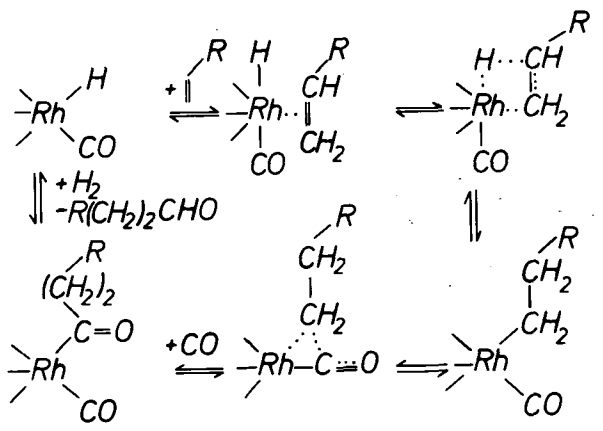

Fig. 7. Scheme of the hydroformylation of olefins by rhodium complexes

The low temperature water gas shift activity of ruthenium zeolites [104] is proposed to proceed on Ru(I) intermediates [105]. The water gas conversion extends to the Kölbel-Engelhardt reaction, if the metal component is reduced to a finely dispersed metal phase, which hydrogenates chemisorbed carbon monoxide [104,106]. The latter reaction requires elevated temperatures (> 330°C), likely, in order to avoid the formation of deactivating surface carbide layers on the metal phase.

Many of the promising reactivities of metal-containing zeolites are based on the property of the microporous matrix to act as a solid solvent for transition metal complexes resulting in heterogenized homogeneous catalysts. Most of these catalysts are based on the faujasite-type zeolites, because of their relatively large internal free space and the three-dimensional pore arrangement. Moreover, the matrix can act as a polydentate ligand and provides discrete domains where distinct steric and electronic configurations can be formed. The zeolite matrix affords the highest metal ion dispersion in comparison with other supports and high stabilization for cations in low oxidation states. The reactions can be carried out at much lower pressures than those required by other homogeneous catalysts in liquid phase. These unique properties will draw continuous future attention to the structures and reactivities of zeolite supported metals and metal complexes.

ACKNOWLEDGEMENT

Financial support by the Deutsche Forschungsgemeinschaft is gratefully acknowledged.

REFERENCES

1. Breck, D.W., in "Zeolite Molecular Sieves - Structure, Chemistry and Use" (Wiley, New York 1974), p. 519..
2. Minachev, Kh., Isakov, Ya. I., in "Zeolite Chemistry and Catalysis", ed. J.A. Rabo (ACS Monograph, Washington 1976), Vol. 171, p. 552.
3. Uytterhoeven, J.B., Acta Phys. et Chem. (Szeged) 24, 53 (1978).
4. Elliott, D.J., Lunsford, J.H., J. Catal. 57, 11 (1979).
5. Gallezot, P., in "Catalysis by Zeolites", ed. B. Imelik et al. (Elsevier, Amsterdam 1980). Stud. Surf. Sci. Catal., vol. 5, p. 227.
6. Delafosse, D., ibid. p. 235.
7. Gellens, L.R., Mortier, W.J., Uytterhoeven, J.B., Zeolites 1, 11 (1981).
8. Gellens, L.R., Mortier, W.J., Uytterhoeven, J.B., ibid., p. 85.
9. Bergeret, G., Gallezot, P., Imelik, B., J. Phys. Chem. 85, 411 (1981).

10. Bergeret, G., Tran Manh Tri, Gallezot, P., J. Phys. Chem. 87, 1160 (1983).
11. Fraissard, J., Ito, T., de Menorval, L.C., Springuel-Huet, M.A., in "Metal Microstructures in Zeolites", ed. P.A. Jacobs et al. (Elsevier, Amsterdam 1982), Stud. Surf. Sci. Catal., vol, 12. p. 179.
12. de Menorval, L.C., Ito, T., Fraissard, J.P., J.C.S. Faraday Trans. I 78, 403 (1982).
13. Ito, T., de Menorval, L.C., Fraissard, J.P., J. Chim. Phys.-Chim. Biol. 80, 573 (1983).
14. Gallezot, P., Bienenstock, A., Boudart, M. ,Nouv. J. Chim. 2, 263 (1978).
15. Gallezot, P., Alarcon-Diaz, A., Dalmon, J.A., Renouprez, A.J., Imelik, B., J. Catal. 39, 334 (1975).
16. Gallezot, P., J. Chem. Phys. 78, 881 (1981).
17. Gallezot, P., Zeolites 2, 103 (1982).
18. Schmidt, F., in "Metal Microstructures in Zeolites", ed. P.A. Jacobs et al. (Elsevier, Amsterdam 1982), Stud. Surf. Sci. Catal., vol. 12, p. 191.
19. Schmidt, F., Gunsser, W., Adolph, J., ACS Symposium Series 40, 291 (1977).
20. Gallezot, P., Catal. Rev. 20, 121 (1979).
21. Tri, T.M., Candy, J.P., Gallezot, P., Massardier, J., Primet, M., Vedrine, J.C., Imelik, B., J. Catal. 79, 396 (1983).
22. Guilleux, M.F., Delafosse, D., Martin, G.A., Dalmon, J.A., J.C.S. Faraday Trans.I., 75, 165 (1979).
23. Jacobs, P.A., Nijs, H., Verdonck, J., Derouane, E., Gilson, J.P., Simoens, A., J.C.S. Faraday Trans. I 75, 1196 (1979).
24. Che, M., Richard, M., Olivier, D., J.C.S. Faraday Trans. I 76, 1526 (1980).
25. Sauvion, G.N., Guilleux, M.F., Tempere, J.F., Delafosse, D., in "Metal Microstructures in Zeolites", ed. P.A. Jacobs et al. (Elsevier, Amsterdam 1982), Stud. Surf. Sci. Catal. vol. 12, p. 229.
26. Romanowski, W., ibid., p. 213.
27. Bergeret, G., Gallezot, P., Imelik, B., J. Phys. Chem. 85, 411 (1981).
28. Gallezot, P., Mutin, I., Dalmai-Imelik, G., Imelik, B., J. Microsc. Spectrosc. Electron. 1,1 (1976).
29. Kleine, A., Ryder, P., Jaeger, N., Schulz-Ekloff, G., in preparation.
30. Exner, D., Jaeger N., Schulz-Ekloff, G., Chem.-Ing.-Techn. 52, 734 (1980).
31. Verdonck, J.J., Jacobs, P.A., Genet, M., Poncelet, P., J.C.S. Faraday Trans. I. 76, 403 (1980).
32. Nijs, H.H., Jacobs, P.A., Verdonck, J.J., Uytterhoeven, J.B., in "Growth and Properties of Metal Clusters", ed. J. Bourdon (Elsevier, Amsterdam 1980), Stud. Surf. Sci. Catal. vol. 4, p. 479.
33. Gustafson, B.L., Lunsford, J.H., J. Catal. 74, 393 (1982).

34. Exner, D., Jaeger, N.I., Möller, K., Nowak, R., Schrübbers, H., Schulz-Ekloff, G., Ryder, P., in "Metal Microstructures in Zeolites", ed. P.A. Jacobs et al. (Elsevier, Amsterdam 1982), Stud. Surf. Sci. Catal., vol. 12, p. 205.
35. Exner, D., Jaeger, N., Nowak, R., Schrübbers, H., Schulz-Ekloff, G., J. Catal. 74, 188 (1982).
36. Jaeger, N.I., Ryder, P., Schulz-Ekloff, G., in "Structure and Reactivity of Modified Zeolites", ed. P.A. Jacobs et al. (Elsevier Amsterdam 1982) Stud. Surf. Sci. Catal., vol. 18, p. 299.
37. Exner, D., Jaeger, N.I., Nowak, R., Schulz-Ekloff, G., Ryder, P., in "Proceedings of the 6th International Zeolite Conference", D. Olson and A. Bisio, Eds., (Butterworths,Guildford 1984) p. 387.
38. Schulz-Ekloff, G., Wright, D., Grunze, M., Zeolites 2, 70 (1982).
39. Reagan, W.J., Chester, A.W., Kerr, G.T., J. Catal. 69, 89 (1981).
40. Exner, D., Jaeger, N., Möller, K., Schulz-Ekloff, G., J.C.S. Faraday Trans. I 78, 3537 (1982).
41. Gallezot,P.in"Proceedings of the 6th International Zeolite Conference", D. Olson and A. Bisio, Eds., (Butterworths, Guildford 1984) p. 352.
42. Chernov, A.A., in "Modern Crystallography", vol. III, (Springer, Berlin 1984) and references quoted therein.
43. Wynblatt, P., in "Growth and Properties of Metal Clusters", ed. J. Bourdon (Elvesier, Amsterdam 1980), Stud. Surf. Sci. Catal., vol. 4, p. 15,
44. Lawson,J.D., Rase, M.F., Ind. Eng. Chem. Prod. Res. Develop. 9, 317 (1970).
45. Winkler, H., Ebert, A., Ebert, W., Riedel, E., Surface Sci. 50, 565 (1975).
46. Beyer, H.K., Jacobs, P.A., Uytterhoeven, J.B., J.C.S. Faraday Trans. I 72, 674 (1976).
47. Olivier, D., Richard, M., Bonneviot, J., Che, M., in "Growth and Properties of Metal Clusters", ed. J. Bourdon (Elsevier, Amsterdam 1980), Stud. Surf. Sci. Catal. Vol. 4, p. 193.
48. Möller, K., Thesis, Universität Bremen 1984.
49. Lunsford, J.H., Catal. Rev. 12, 137 (1975).
50. Lunsford, J.H., ACS Symposium Series 40, 473 (1977).
51. Naccache, C., Ben Taarit, Y., Acta Phys. et Chem. Szeged 24, 23 (1978).
52. Naccache, C., in "Proceedings of the 5th International Conference on Zeolites", ed. L.V.C. Ress (Heyden, London 1980). p. 592.
53. Howe, R.F., Lunsford, J.H., J. Amer. Chem. Soc. 97, 5156 (1975).
54. Howe, R.F., Lunsford, J.H., J. Phys. Chem. 79, 1836 (1975).
55. Schoonheydt, R.A., Pelgrims, J., J. C.S. Dalton Trans. 914 (1981).
56. Schläfer,H., Gliemann, G., Einführung in die Ligandenfeldtheorie (Akadem. Verlagsges., Frankf./M., 1967); references therein

57. Pauling, L., J. Amer. Chem. Soc. 53, 1367 (1931); 54, 988 (1932).
58. Kimball, G.E., J. Chem. Phys. 8, 188 (1940).
59. Diegruber, H., Möseler, R., Plath, P.J., Lubitz, W., Winscom, C.J., in "Recent Progress Reports and Discussion", ed. R. Sersale et al. (Giannini, Napoli 1981) p. 131.
60. Diegruber, H., Plath, P.J., in "Adsorption of Hydrocarbons in Microporous Adsorbents", vol. II. (Akadem. d. Wiss. d. DDR, Berlin 1982), p. 128.
61. Diegruber, H., Thesis, Universität Bremen (1984).
62. Diegruber, H., Plath, P.J., in "Metal Microstructures in Zeolites" ed. by P. Jacobs et al. (Elsevier, Amsterdam, 1982). Stud. Surf. Sci. Catal., vol. 12, p. 23.
63. Edwards, L., Gouterman, M., J. Molec. Spectrosc. 33, 292 (1970).
64. Diegruber, H., Plath, P.J., in preparation.
65. Weir, C.E., Valkenburg, A. van., Lippincott. E.R., in "Modern very high pressure techniques", ed. R.H. Wentorf, jr., (Butterworths, London, 1962) p.51.
66. Whatley, L.S., Valkenburg, A. van., in "Advances in high pressure research", vol. 1, ed. R.S. Bradley, (Academic Press, London, 1966). p. 327.
67. Fraissard, J., in "Catalysis by Zeolites", ed. B. Imelik et al., (Elsevier, Amsterdam, 1980) , vol. 5, p. 343.
68. Romanovsky, B.V., in "Proceedings of the 8th International Congress on Catalysis", vol. IV., Eds. DECHEMA (Verlag Chemie, Weinheim, 1984) p. 657.
69. Meyer, G., Wöhrle, D., Mohl, M., Schulz-Ekloff, G., Zeolites 4, 30 (1984).
70. Diegruber, H., Plath, P.J., Schulz-Ekloff, G., Mohl, M., J. Molecular Catal. 24, 115 (1984).
71. Shpiro, E.S., Antoshin, G.V., Tkachenko, O.P., Gudkov, S.V., Romanovsky, B.V., Minachev, Kh. M., in "Structure and Reactivity of Modified Zeolites", ed. P.A. Jacobs et al. (Elsevier, Amsterdam, 1984), Stud. Surf. Sci. Catal., vol. 18, p. 31.
72. Diegruber, H., Plath, P.J., Z. physik. Chem. (Leipzig), in press
73. Bolton, A.P., in "Zeolite Chemistry and Catalysis", J.A. Rabo, Ed., ACS Monograph 171, (American Chemical Society, Washington 1976). p. 552.
74. Gallei, E., Chem.-Ing.-Techn. 52, 99 (1980).
75. Heinemann, H., in "Catalysis: Science and Technology" J.R. Anderson and M. Boudart, Eds., (Springer, Berlin 1981), vol. 1, p. 1.
76. Guisnet, M., Gnep, N.S., in "Proceedings of the NATO Advanced Study Institute on Zeolites: Science and Technology", F.R. Ribeiro et al., Eds., (Nijhoff Publ., The Hague 1984). p. 571.
77. Venuto, P.B., Hamilton, L.A., Landis, P.S., J. Catal. 5, 484 (1966).
78. Ward, J.W., J. Catal. 10, 34 (1968).
79. Bolton, A.P., J. Catal. 22, 9 (1971).

80. Weitkamp, J., Schulz, H., J. Catal. 29, 361 (1973).
81. Arai, H., Seiyama, T., Harakawa, M., Tominaga , H., in "Catalyst Deactivation" B. Dalmon and G.F. Froment, Eds., (Elsevier, Amsterdam 1980), Stud. Surf. Sci. Catal. vol, 6, p. 167.
82. Weisz, P.B., Adv. Catal. 13, 137 (1962).
83. Olah, G.A., Schlosberg, R.H., J. Amer. Chem. Soc. 90, 2726 (1968).
84. Barbier, J., Marecot, P., Martin, N., Elassad, L., Maurel, R., in "Catalyst Deactivation" B. Dalmon and G.F. Froment, Eds., (Elsevier, Amsterdam 1980), Stud. Surf. Sci. Catal., vol. 6, p. 63.
85. Olah, G.A., Chen, J., Schlosberg, R.H., J. Amer. Chem. Soc. 92, 3831 (1970).
86. Caesar, P.D., Brennan, J.A., Garwood, W.E., Ciric, J., J. Catal.. 47, 249 (1977).
87. Chang, C.D., Silvestri, A.J., J. Catal. 47, 241 (1977).
88. Chang, C.D., Lang, N.A., Silvestri, A.J., J. Catal. 56, 268 (1979).
89. Csicsery, S.M., Zeolites 4, 202 (1984).
90. Nguyen-Ngoc, H., Müller, K., Ralek, M., in "Structure and Reactivity of Modified Zeolites", P.A. Jacobs et al., Eds., (Elsevier, Amsterdam 1984), Stud. Surf. Sci. Catal., vol. 18, p. 291.
91. Jacobs, P.A., van Wouwe, D., J. Mol. Catal. 17, 145 (1982).
92. Bragin, O.V., Vasina, T.-V. Isakov, Ya. I., Palashkina, N.V., Preobrazhensky, A.V., Nefedov, B.K., and Minachev, Kh. M., in "Structure and Reactivity of Modified Zeolites", P.A. Jacobs et al., Eds.,(Elsevier, Amsterdam 1984), Stud. Surf. Sci. Catal., vol. 18, p. 273.
93. Weisz, P.B., Haag, W.O., Rodewald, P.G., Science 206, 57 (1979).
94. Gentry, S.J., Rudham, R., Sanders, M.K., J. Catal. 35, 376 (1974).
95. Nefedov, B.K., Sergeeva, N.S., Zueva, T.V., Shutkina, E.M., Eidus, Ya.T., Izvest. Akad. Nauk. SSSR, Ser. Khim, 582 (1976).
96. Nefedov, B.K., Sergeeva, N.S., Eidus, Ya. T., Izvest. Akad. Nauk, SSSR, Ser. Khim. 2271 (1976).
97. Christensen, B., Scurrell, M.S., J.C.S. Faraday Trans. I 73, 2036 (1977).
98. Anderson, S.L.T., Scurrell, M.S, Zeolites 3, 261 (1983).
99. Yashima, T., Orikasa, Y., Takahashi, N., Hara, N., J. Catal. 59, 53 (1979).
100. Gelin, P., Ben Taarit, Y., Naccache, C., in "New Horizons in Catalysis" T.Seiyama and K. Tanaba, Eds., (Elsevier, Amsterdam 1981). vol. 1, p. 898.
101. Nefedov, B.K., Slinkin, A.A., Kucherov, A.V., Sergeeva, N.S., Eidus, Ya. T., Izvest. Akad. Nauk. SSSR, Ser. Khim, 2119 (1974).
102. Mantovani, E., Palladino, N., Zanobi, A., J. Mol. Catal. 3, 285 (1977/1978).
103. Takahashi, N., Kobayashi, M., J. Catal. 85, 89 (1984).
104. Verdonck, J.J., Jacobs, P.A., Uytterhoeven, J.B. J.C.S. Chem. Commun. 181 (1979)
105. Jacobs, P.A., Chantillon, R., Laet, P. de, Verdonck, J.J., Tielen, M., in "Intrazeolite Chemistry" G.D. Stucky and F.G. Dwyer, Eds., ACS Symp. Ser. 218 (1983), 439(American Chemical Society, Washington 1983)
106. Niwa, M., Izuka, T., Lunsford, J. H,J.C.S. Chem. Commun., 684 (1979).

ESR ON SILVER CLUSTERS IN ZEOLITE A

P.J. GROBET*, H.E. Leeman, R.A. Schoonheydt*
Laboratorium voor Oppervlaktechemie, Katholieke Universiteit Leuven, Leuven, Belgium.

ABSTRACT

The silver cluster formation in zeolite A with different loadings was studied by ESR. Depending on the reduction degree hyperfine spectra with seven and nine lines, a superoxide and a conduction electron spin resonance (CESR) line are observed. These signals could be assigned to the evolution in silver cluster formation in and outside the zeolite structure.

INTRODUCTION

By cation exchange it is possible to incorporate various metals in zeolite structures dispersed as single cations. Reduction by molecular hydrogen leads to highly dispersed metal particles with important catalytic properties [1]. In order to explain the catalytic properties of metal-loaded zeolites it is necessary to know (i) the dimension of the metal clusters, (ii) the location of the metal clusters inside the zeolite structure and (iii) the reduction mechanism and cluster mobility. Metal particles in zeolites have been studied by X-ray diffraction [2], optical diffuse reflectance spectroscopy [3], fluorescence emission excitation [4] and temperature programmed ad- and desorption [5].

In this paper we present ESR measurements on silver particles in zeolite A. There are several reasons to choose this silver-loaded system. Starting from NaA zeolite it is very easy to exchange the sodium cations by silver in any stoeichiometric amount [6]. The reduction of the silver ions is easily performed by reaction with molecular hydrogen; at room temperature the formation of silver particles inside the zeolite structure is expected [7]. Hermerschmidt and Haul [8] confirmed unambiguously the presence of Ag_6^{x+} clusters and submicroscopic silver crystallites by preliminary in-situ ESR measurements on AgA and AgX zeolites during the reduction process.

In zeolite A silver ions are located in the α- and β-cages and after reduction silver clusters are expected inside these cavities. The shaping of metal clusters by the zeolite structure is of interest for the study of the physical and chemical properties of small metal particles. Some theoretical predictions about the quantum size effect [9,10] for instance can be verified.

EXPERIMENTAL

Starting from NaA zeolite (Union Carbide, Linde Division) and by adding the necessary amount of 0.01 molar $AgNO_3$ solutions to the zeolites and exchanging in the dark overnight at room temperature we prepared the following silver samples :

$NaAg_2A$ or $Na_{10}Ag_2(AlO_2)_{12}(SiO_2)_{12}$
$NaAg_6A$ or $Na_6Ag_6(AlO_2)_{12}(SiO_2)_{12}$
AgA or $Ag_{12}(AlO_2)_{12}(SiO_2)_{12}$
$NaAg_3CaA$ or $Na_7Ag_3Ca(AlO_2)_{12}(SiO_2)_{12}$

The sodium-silver-calcium ratios are estimated from synthesis, and the samples were washed and dried. To avoid the ESR lines of Fe^{3+} present in commercial zeolite A we followed a chemical extraction procedure for iron impurities described by Derouane et al. [11]. The dehydration of the samples is done either by heating in vacuum or in a helium and oxygen gas flow at 700 K. The reduction of the samples is performed at room temperature by a pulse method or a flow method. The pulse reduction method consists of the admission of molecular hydrogen (10 p.p.m. O_2) at a certain pressure (3 mbar-1 bar) in the sample holder during a restricted time interval; after this activation the hydrogen gas was pumped off quickly and replaced by 1 bar helium (5 p.p.m. O_2). When severe reduction of the samples was needed a flow of hydrogen gas (1 cm^3/s) was used in the sample holder.

The ESR measurements were performed on a Bruker spectrometer (ER200 D-SRC) at 9.5 GHz and at room temperature.

RESULTS

For the sodium-silver samples the ESR results are independent of the Ag-loading. During the dehydration process the samples change their colour from white to yellow (500 K) and finally to brick red for AgA or yellow-brown for the other compositions. After dehydration we were able to detect in some cases a very weak seven line spectrum similar to that shown in figure 1A and due to Ag_6^{x+}. It is important to notice that these dried powder samples are light insensitive : the treatments and ESR measurements can be performed in day-light.

By gradually reducing the samples at room temperature four kinds of ESR signals are successively seen. In a first stage and under mild reduction conditions (30 mbar H_2 during 60 s) we observe (fig. 1A) a growing seven line spectrum for all sodium-silver samples ($g = 2.025 \pm 0.003$). The observed hyperfine splitting ($a = 6.76 \pm 0.07$ mT) can be assigned to the hyperfine interaction of an unpaired electron with six equivalent silver nuclei ($I = 1/2$). The isotope effect (^{107}Ag, ^{109}Ag) is not resolved due to the small coupling constant and the large line width. This spectrum clearly indicates the presence of charged Ag_6^{x+} clusters; no information on the charge of the clusters is obtained from these ESR measurements ($x = 5,3$ or 1). This result is consistent with the findings of

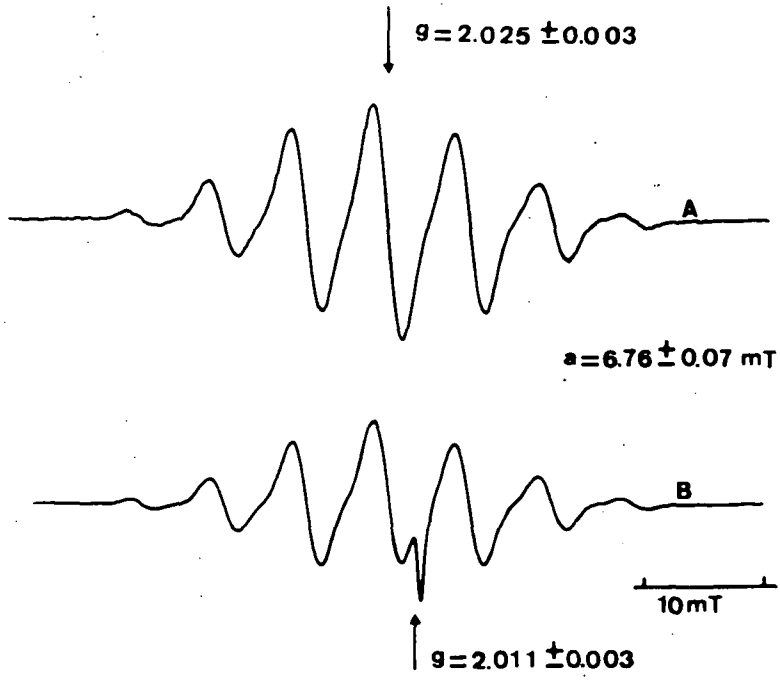

Fig. 1. ESR of Ag_6^{x+} clusters in reduced $NaAg_6A$;
A : mild reduction, B : stronger reduction

Hermerschmidt et al. [8], although some differences in g-factor and hyperfine coupling constant a are found. After one reduction pulse the intensity of the ionic cluster spectrum reaches a constant value only after several hours indicating the mobility of silver atoms and ions during the cluster formation in the zeolite structure. If one applies a stronger reduction (a 60 s pulse of 1 bar H_2) a second ESR signal is superimposed on the ionic cluster signal (fig. 1 B). By further reducing the samples the Ag_6^{x+} spectrum disappears and the second ESR signal is clearly visible (fig. 2 A). This single line ($g = 2.011 \pm 0.003$) has an asymmetric shape and is assigned to O_2^-. This is confirmed by the measurement at 110 K of the anisotropic g-value of O_2^- ($g_{xx} = 2.007$, $g_{yy} = 2.012$ and $g_{zz} = 2.033$). This O_2^- signal grows first and then decreases with further reduction. Superimposed on this signal a weak nine line hyperfine spectrum is sometimes seen in a further reduction stage ($g = 2.025 \pm 0.005$; $a = 5.2 \pm 0.4$ mT; figure 2 B). This nine line spectrum is due to Ag_8^{y+}. The deformed base line in figure 2 B is due to a broad signal which grows by still further reduction at the expense of the other signals. It results into a signal seen in figure 3; this CESR signal has a line width of 10 mT and the g-factor equals 1.981 ± 0.003. It vanishes when the reduction proceeds.

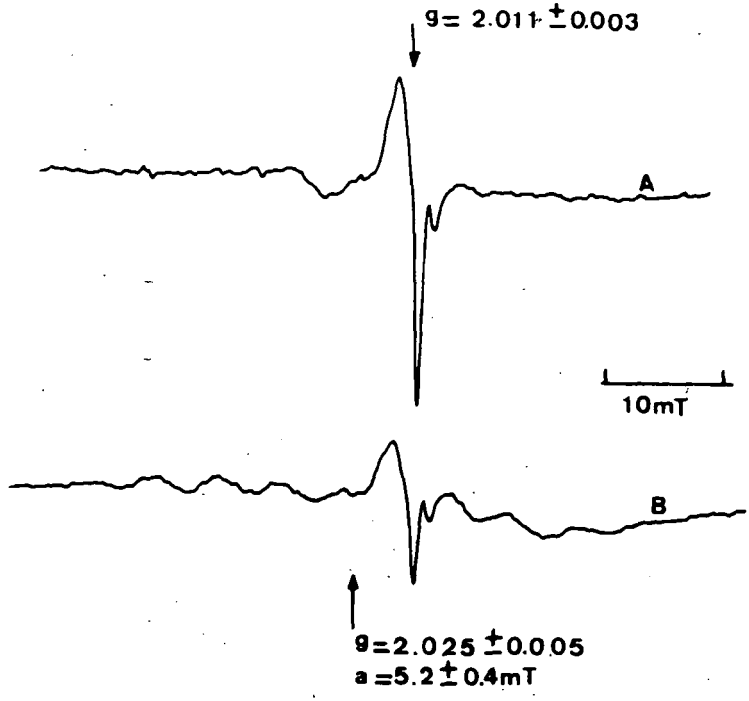

Fig. 2. ESR of O_2^- and Ag_8^{y+} clusters in reduced $NaAg_6A$

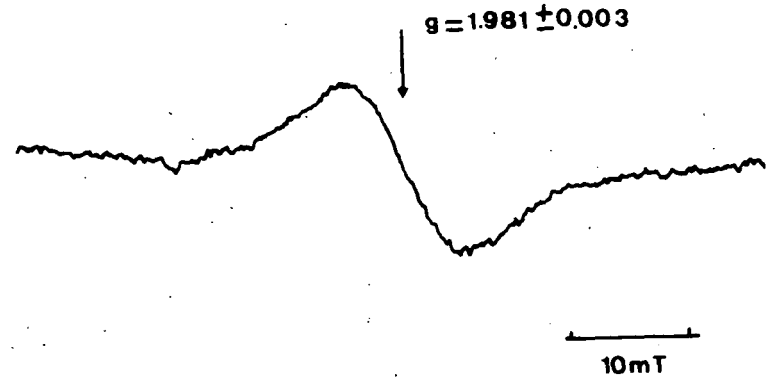

Fig. 3. CESR in severe reduced AgA (1 cm^3/s H_2 flow, 72 h)

This line was also seen by Hermerschmidt et al. but the nine line spectrum not [8]. It is important to notice that the four signals can be stabilized by pumping off the samples and keeping them under helium atmosphere.
In contrast to this, Hermerschmidt et al. detected their signals during a single complete reduction run. The ESR signals are also not affected by an oxygen flow treatment (600 s) at room temperature.

The results on the sodium-calcium-silver sample are somewhat different. Under mild reduction the ionic cluster signals are not observed; only after strong reduction (1 bar during 72 h) the asymmetric O_2^- line (g = 2.014 ± 0.003) is seen (fig. 4A); by further reduction the CESR signal (g = 1.976 ± 0.004; fig. 4 B) becomes apparent.

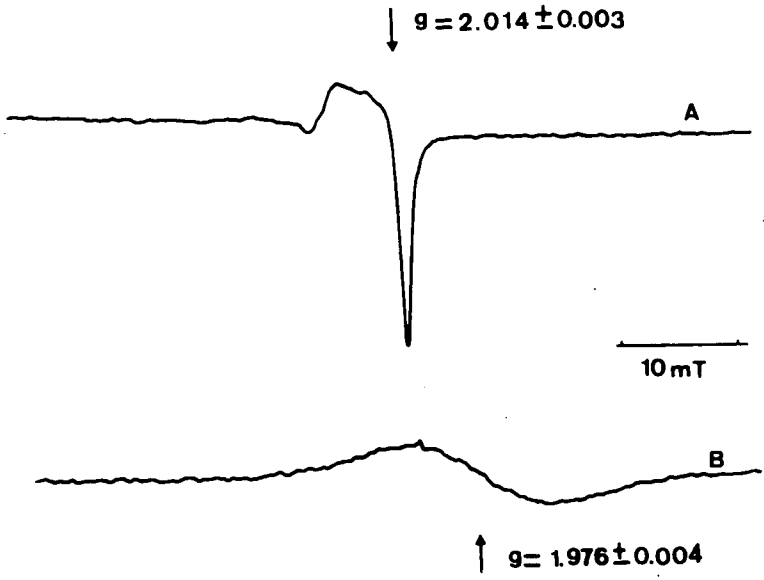

Fig. 4. The O_2^- and CESR line in $NaAg_3CaA$

DISCUSSION

These ESR experiments prove that certain stages of cluster formation in silver-loaded zeolite A can be followed.

First of all, a very weak signal due to Ag_6^{x+} has been found after dehydration. Ag_3^{x+} and Ag_6^{x+} clusters have been found with X-ray diffraction, but the number of clusters detected by ESR is orders of magnitude smaller than the number expected on the basis of the X-ray diffraction data [2].

The comparison of the results of NaAgA zeolites and NaCaAgA allows us to conclude indirectly that the charged clusters, Ag_6^{x+} and Ag_8^{y+}, are located in the sodalite cages. Indeed, according to recent X-ray diffraction studies NaAgA zeolites have part of their Ag^+ ions in the sodalite cages, while NaCaAgA have the Ag^+ ions in the sixrings [2,12]. Thus, in the former case reduction of Ag^+ in the sodalite cages leads to clustering and stabilization of Ag_6^{x+}, and eventually Ag_8^{y+}, inside the cubooctahedron. Reduction of Ag^+ in NaCaAgA gives Ag atoms in the supercages, which agglomerate to metal particles inside the supercages. The dimensions of the supercages are probably too large to stabilize small, well-defined clusters. In NaAgA the charged clusters are decharged by further reduction; the electrostatic interaction with the lattice becomes zero and the Ag atoms migrate inside the supercages and agglomerate into supercage metal particles. The presence of these metal particles are indirectly detected by the appearance of an O_2^- signal. This superoxide line in the spectrum after reduction is coming from adsorbed oxygen on the surface of the very small metal particles located in the α-cage and from the resulting electron transfer from the metal particle surface to the adsorbed oxygen molecules [13]. The relatively narrow signal can not be assigned to the metal particles in the supercages as stated in a previous paper [14]. The O_2 molecules are present as impurities in the H_2 or He gases. Indeed, it is possible to prepare Ag_6^{x+} without the O_2^- by static reduction with H_2, followed by evacuation (instead of He-flushing).

The g-value of the broad CESR line of figure 3 is 1.983, exactly the value of bulk silver [15,16]. We assign this signal and that of figure 4B to larger metal particles in the supercage or on the external surface. The CESR signals exhibit the features of the quantum size effect of small metal particles, for instance the appearance of the signal at room temperature and the Lorentz shape [9,10]. Work is in progress to obtain valuable experimental data concerning the quantum size effect.

* Senior Research Associate of the National Fund for Scientific Research of Belgium.

REFERENCES

1. Uytterhoeven, J.B., Acta Phys. Chem. 24, 53 (1978).
2. Gellens, L.R., Mortier, W.J., Schoonheydt, R.A. and Uytterhoeven, J.B., J. Phys. Chem. 85, 2783 (1981).
3. Kellerman, R. and Texter, J., J. Chem. Phys. 70, 1562 (1979).
4. Ozin, G.A. et al. : Intrazeolite Chemistry. Eds. Stucky G.D. and Dweyer F.G., ACS, Symp. Series 218, 1983, p. 409.

5. Jacobs, P.A., Uytterhoeven, J.B. and Beyer, H.K., J. Chem. Soc. Farad. Trans. 1, 75, 56 (1979).
6. Breck, D.W. : Zeolite Molecular Sieves. John Wiley & Sons, New York, 1973.
7. Jacobs, P.A. : Metal Microstructures in Zeolites. Eds. Jacobs P.A., Jaeger, N.I., Jiru, P. and Schulz-Ekloff, G., Elsevier Sci. Publ. Co., Amsterdam, 1982, p. 71.
8. Hermerschmidt, D. and Haul, R., Ber. Bunsenges. Phys. Chem. 84, 902 (1980).
9. Kawabata, A., J. Phys. Soc. Jpn. 29, 902 (1970).
10. Buttet, J., Car, R. and Myles, C.W., Phys. Rev. B 26, 2414 (1982).
11. Derouane, E.G., Mestdagh, M. and Vielvoye, L., J. Catal. 33, 169 (1974).
12. Schölner, R., Gellens, L.R., Mortier, W.J. and Uytterhoeven, J.B., Zeolites 3, 149 (1983).
13. Hermerschmidt, D. and Haul, R., Ber. Bunsenges. Phys. Chem. 85, 739 (1981).
14. Grobet, P.J. and Schoonheydt, R.A., Surf. Sci., in press.
15. Schultz, S., Shanabarger, M.R. and Platzman, P.M., Phys. Rev. Lett. 19, 749 (1967).
16. Beuner, F. and Monod, P., Phys. Rev. B 13, 3424 (1976).

CATALYSIS BY ZEOLITE INCLUSION COMPOUNDS

B.V.ROMANOVSKY
Moscow State University, Moscow, U.S.S.R.

ABSTRACT

Zeolite-included transition metal complexes constitute a new type of catalysts which offer advantages of both heterogeneous and homogeneous catalytic systems. Main features of intracrystalline synthesis of zeolite inclusion compound as well as their characterization and catalytic properties are discussed.

INTRODUCTION

Zeolite molecular sieves seem to be almost ideal matrices in designing of guest-host catalytic systems. The synthesis of catalitically active species inside the zeolite cavities that might be carried out on molecular scale is of great interest not only for heterogeneous catalysis but also for enzyme modelling. In this context, the complexes of transition metals (TMC) with organic macroligands appear to be of particular interest since they have much in common with biological catalysts.

However, the TMC's with these ligands can be hardly introduced into zeolite pore system by conventional ion-exchange or adsortion procedures. Therefore, only two ways to prepare the inclusion compounds of the type could be used, i.e., (1) capture of the TMC's during liquid phase synthesis of zeolite crystals (ref.1) and (2) in situ synthesis of TMC's inside cavities of zeolite crystals (ref. 2). The first method is obvious to be limited by solubilities of TMC's. The second way of including the TMC's into zeolite host lattices and physico-chemical properties of systems so prepared are surveyed in present paper.

INTRACRYSTALLINE IN SITU SYNTHESIS OF ZEOLITE-INCLUDED TMC's

The framework charge-compensating cations in zeolites are known to have unsaturated coordination geometry and so they can add same more molecules or ions as ligands. Such complexing occurs un-

less the dimensions of entering potential ligands exceed those of zeolite openings. If so, then treatment of corresponding cationic form of zeolite with appropriate complexing agent could result in a formation of TMC's inside zeolitic cavities. By such a way, the complexes of a variety of TM cations with various amines, dipyridil, dimethylglioxime and acetylacetone included into zeolite matrices were obtained (ref.3-6).

Meanwhile, it should be noted that the TMC's mentioned are complex cations and consequently are held electrostatically within zeolite cavities. If it is the case, then the zeolite framework plays a role of macroanion to ensure zero charge of a lattice as a whole. Thus, these systems with complex cations are thought to be hardly referred as inclusion compounds, and this term seems to be more proper for n e u t r a l molecules captured or in situ formed within zeolite cages. If molecular dimension of such a guest are greater than free diameter of zeolite channels, then the molecule turns out to be entrapped inside the cavity, and it is held there rather topologically.

A few examples of neutral guest molecules included into zeolite host lattices are metal carbonyl clusters, Schiff bases, and transition metal phthalocyanines. These latters were synthezised firstly by us (ref.7) and later by Schulz-Ekloff et al.(ref.8). In what follows, the phthalocyanine complexes of transition metals (PcM) are discussed in details.

The planar molecule of PcM is very stable due to a conjugating of 18 electrons in ligand macrocycle. Its dimension is c.a. 1.4 nm as calculated from X-ray data for the crystalline PcM. The Pc complexes may be obtained from both transition metal salts and pure metals as starting materials by treating the first or the second with phthalonitrile. Therefore, their inclusion into zeolites can be carried out by any of following routes: (1) via transition metal cationic forms of a zeolite, and (2) via zero-valent metal containing zeolite. The (3) possible way should be mentioned: via adsorbed volatile carbonyl complexes in which the labile CO ligands would be readily replaced by far more stronger ones, i.e., the phthalonitriles. All these three synthesis of zeolite-included PcM's were carried out by author and co-workers (refs.7,9-11).

Method 1 (refs.7,11). The Co, Ni, Cu, and Ru cationic forms of Y zeolite were placed into one compartment of two- chamber ampoule, another one was loaded with solid phthalonitrile (c.a. 20% in excess)

After evacuation of zeolite at 300-350°C up to 10^{-2} Pa, the ampoule was sealed, and both compartments were heated at 200-300°C for 25-40 hr (depending on the type of metal). After completion of synthesis, excess of phthalonitrile was removed by warm acetone washings. In addition, non-complexed transition metal ions were re-exchanged with NaCl solution.

Method 2 (ref.9). After thorough evacuation of Na form of Y zeolite at 300°C up to 10^{-4} Pa, vapours of $Fe(CO)_5$ were allowed to adsorb at 20°C onto the zeolite, the amount of carbonyl adsorbed being c.a. one molecule of $Fe(CO)_5$ per supercage. Then the zeolite with preadsorbed carbonyl was heated in dry He flow up to 400°C, the CO product releasing being monitored by a catharometer unit. As it was earlier shown by Jacobs et al. (ref.12), under these conditions the adsorbed iron penthacarbonyl transforms quantitatively into metallic iron. Then iron-containing sample was transferred in dry He into one compartment of two-chamber ampoule, and the synthesis of PcFe was carried out at 300°C for 40 hr as described above.

Method 3 (ref.10). On investigating the decomposition of adsorbed $Fe(CO)_5$ within zeolite by temperature-programmed reaction method, we observed that the release of first carbonyl ligands occurs at temperatures 100-150°C lower than that of intracrystalline synthesis of PcM's by methods 1 and 2. The phthalonitrile vapour pressures at these temperatures were, meanwhile, great enough to ensure a reasonable rate of substitution of carbonyl ligands for phthalonitrile ones. Keeping this in mind, we adsorbed Fe or Ni carbonyls onto degassed NaY zeolite (two-chamber ampoule) and heated the sample at 70-115°C for 15-50 hr in phthalonitrile vapours.

All the preparations thus obtained were greenish-blue in color.

CHARACTERIZATION OF IN SITU SYNTHESIZED TMC's

It is obvious that on obtaining the included guest moiety via intracrystalline synthesis, a problem of its identification turns out to be of crucial importance. In the case of zeolite host lattice, the extraction of guest species encapsulated in cavities for subsequent routine identification (e.g., by spectral techniques) is evident to be impossible unless the host lattice were destroyed. Fortunately, when the PcM's are zeolite-included compounds, there is rather unique solvent, i.e., concentrated sulphuric acid which destroys readily the zeolite matrix but only dissolves phthalocyanine component of a cata-

lyst. This method was successfully applied in (refs.8,9) to identify the in situ formed Pc complexes of Fe, Co, Ni, and Cu within zeolites X and Y.

Of course, there were numerous attempts of included TMC identification using spectral (UV, VIS, ESR, ESCA etc.) methods in non-destructive mode, i.e., analysing the guest-host systems as a whole. In some particular cases, identification of in situ formed species as inclusion compounds was well definitive. However, due to the fact that these techniques , in general, do not distinguish between TMC's inside host framework and on external surface of a matrix, the proper assignment of spectral bands appears to be somewhat ambiguous.

DISTRIBUTION OF TMC's IN MATRIX

The problem of the distribution of TMC's between outer surface of zeolite crystallites and their intracrystalline volume is of obvious importance. Indeed, the trend of zeolite exchange cations as well as of metal atoms to migrate onto external surface and to aggregate there is known to be well pronounced. If so, then it would be quite reasonable to assume that complexing agents might facilitate an extraction of metals from zeolite bulk onto its surface and, then, form TMC's on this surface. In this respect, some information can be drawn from our results (ref.11) on ESCA and chemical analysis estimations of transition metal concentration in cationic forms as well as in PcM containing samples of Y zeolites. These data are given in Fig.1. It may be seen that as a rule there is no enrichment of zeolite surface with transition metals when it was treated in phthalonitrile vapours to form Pc complexes (except for one low Ni concentration sample). Here the in situ synthesis via cationic forms of zeolite was used. The same results were obtained also with PcFe/NaY samples which were synthesized via iron carbonyl complexes (refs.9, 10). In this latter case, double extraction, i.e., firstly, with DMFA solvent which dissolves the surface TCM's only and then with H_2SO_4 was used to determine the "outer" and the "inner" phthalocyanines.

It should be mentioned that our conclusions made on the basis of the data just described are not in line with those of Schulz-Ekloff et al. (ref.8) who found only a few percent of zeolite-encaged PcM's as compared to total PcM contents in X and Y zeolites. Although it is not yet fully understood, this difference could be due to a concentration effect of phthalonitrile reactant during a synthesis.

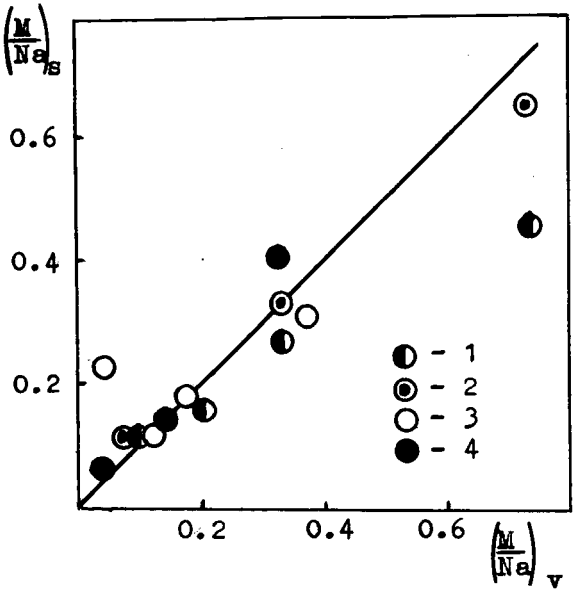

Fig.1. Correlation between relative M to Na concentrations on surface (s) and in volume (v): 1 - NiY, 2 - CoY, 3 - PcNi/NaY, 4 - PcCo/NaY.

A substantial excess of complexing agent (up to two-fold) was applied in (ref.8), the phthalonitrile and zeolite being thoroughly mixed before synthesis. In contrast, we used separate compartments of a reaction vessel to place the reactants as it was described above and thereby the formation of PcM's inside supercages would be favoured by higher concentration of complexing agent within the cavities than at outer surface. In addition, consistent with the notion of preferential formation of the PcM's inside zeolitic supercages is our observation that the adsorption capacities of PcM/NaY samples toward H_2O, O_2, N_2, and CO are linear functions of total PcM contents (M = Cu, Co, and Ni). From all these results, we suggested that the PcM guest molecules do form inside the zeolite host lattice. Thus, these systems could be regarded as a new family of inclusion compounds.

CATALYSIS BY ZEOLITE INCLUSION COMPOUNDS

Zeolite-included TMC's are rather unique heterogeneous catalytic systems with no disadvantages of common catalysts. First of all, there is no question as to what is an active moiety of a catalyst since the nature of it is well known in advance. Moreover, even a concentration of virtually active species in catalysts could be calculated before catalytic experiment and what is far more substantial independently of it. These advantages offered by hetero - genized TMC's would expect to be very useful in solving many important problems of theorical and practical catalysis.

However, on heterogenizing the TMC's two questions arise, i.e., (1) whether they retain the peculiarities characteristic of their homogeneous analogs, and (2) if so, then how do environmental aspects of a matrix influence the TMC molecules as active centers of

catalyst?

For many cases of heterogenized TMC's investigated up to now, the first question could be answered rather positively. In fact, these systems were shown to catalize, for example, H_2O_2 decomposition (ref.3), oxidation of various substrate by molecular O_2 (refs.4, 5, 13), hydrogenation and dehydrogenation (refs.5, 13), dehydration (ref.5), dehydrothiolation (ref.13), hydroformylation (ref.14) etc. which have been well known for homogeneous TMC catalysts.

As to zeolite-included TMC's, they appear to behave very similarly to their analogs in solutions. In particular, they exhibit the most characteristic and important feature of complex catalysts that is the drastic dependence of activity and selectivity on the nature of ligand environment (ref.3). For example, as it was shown in (ref. 5), in cyclohexene epoxide conversion using various zeolite-included chelate of Cu as catalysts the selectivity patterns were strikingly inverse with different ligands, namely, when reacted on PcCu/NaY, the epoxide yields 100% of cyclohexadiene whereas on enCu/NaY (en = ethylenediamine ligand) it forms benzene only.

Fig.2 shows the data obtained for liquid phase oxidation of cystein by molecular O_2 catalyzed by PcCo/NaY (ref.13). The bell - shaped dependence of the reaction rate on pH value of solution which zeolite-included PcCo exhibits is also typical for homogeneous catalysis by transition metal complexes.

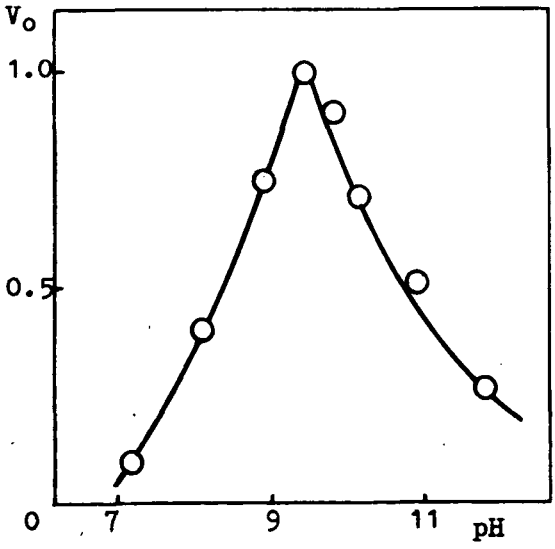

Fig.2. pH dependance of initial rate (arb.units) of cystein oxidation in solution on PcCo/NaY catalyst at 20°C.

Similarly, the pyridine base preadsorbed on the PcM's in zeolite matrices was shown to enhance the ability of metallic centers to fix molecular O_2 as well as their activities in CO oxidation, dehydrogenation of cyclohexane and isopropanol (ref.5).

The most probable explanation for these observations is that Py molecule situated trans to a substrate species may exert a conciderable influence on

the reactivity of latter.

It is noteworthy that the very fact of enhancing influence of preadsorbed Py on the zeolite-included TMC's provides good evidence of molecular or near-molecular dispersity of these in matrix. One should recall that the trans effect is a characteristic feature of homogeneous catalysis by transition metal complexes in solutions.

Finally, even the turn-over numbers (TN) found for supported and not-supported PcM's do not differ substantially as it is seen from the following data:

TN[a] in oxidation by molecular O_2	Individual PcCo	Supported PcCo/NaY
of cystein[b]	7.7	20.7
of carbon monox.[c]	2.8	8.4

a: arbitrary units; b: (ref.13); c: (ref.5).

On the other hand, one might expect that molecular sieve properties of zeolite host lattice could be accounted for some peculiarities of guest species as catalytically active centers. Thus, in liquid phase hydrogenation of olefins using the zeolite-encapsulated Rh complexes as catalyst, rather "anomalous" sequence of reactivities was found (ref.15), i.e., 1-butene > 1-hexene > 1-octene. This series is different from that obtained with SiO_2 matrix where the reaction rates were comparable for the olefins.

At all probabilities, this is due to the strong spatial restrictions imposed by zeolite framework on molecules of olefin entering pores, or of intermediate forming within cavities, or of product leaving supercages.

Another example of specific influence of surroundings on the zeolite-encaplulated TMC's is provided by our findings that the high adsorption potential inside supercages where the complexes reside could promote reagent concentrations and hence higher reaction rates. This effect seems to account for negative temperature coefficient below 0°C of reaction rate in CO oxidation by molecular O_2 on PcM/NaY catalysts (ref.5) as well as for 3-fold increase in TN's on going from individual PcM to included one.

CONCLUSION

The synthesis and the study of zeolite-included guest molecules is a relatively new area of zeolite catalysis. But it is every ground to say that these systems as already outlined could be very promising in the molecular level designing of active centers within

solid matrices and thereby in the building-up of catalysts with foreseen functions. Of course, from a practical viewpoint, there are a number of questions to answer, e.g., the way in which an activity of the TMC's is governed by the environment of the species included what is not yet clear and the diffusional phenomena etc.

REFERENCES

1. Weisz P.B.,Frillette V.J.,Maatman R.W.,Mover E.B.,J.Catal. 1, 307 (1962).
2. Klier K.,Ralek M.J., J.Phys.Chem.Solids, 29, 951 (1968).
3. Mochida J.,Takeshita K., J.Phys.Chem., 76, 1653 (1974).
4. Howe R.F.,Lunsford J.H., J.Am.Chem.Soc., 97, 5156 (1975).
5. Zakharov V.Yu., Cand.Diss., Moscow Univ., 1978.
6. Winskom J.C.,Lubitz W.,Diegruber H.,Möseler R., In Metal Microstructures in Zeolites.Stud. in Surf.and Catal., Elsevier Sci. Publ.Co.,Amsterdam, 1982, p.15.
7. Zakharov V.Yu.,Romanovsky B.V., Vestn.Mosk.Univ.,Ser.Khim., 20, 94 (1979).
8. Meyer G.,Wöhrle D.,Mohl M.,Schulz-Ekloff G., Zeolites, 4, 80 (1984).
9. Korol'kova T.V.,Zakharov A.N.,Romanovsky B.V., Vestn.Mosk.Univ., Ser.Khim., 25, 362 (1984).
10. Zakharov A.N.,Romanovsky B.V., J.Incl.Phen., in press.
11. Gudkov S.V.,Romanovsky B.V.,Shpiro Ye.S., Antoshin G.V.Minachev Kh.M., Izv.Akad.Nauk SSSR,Ser.Khim.,2448 (1980).
12. Bein Th.,Jacobs P.A.,Schmidt F., In Metal Microstructures in Zeolites.Stu. in Surf.and Catal., Elsevier Sci.Publ.Co., Amsterdam, 1982, p.111.
13. Zakharova O.M., Cand.Diss., Moscow Univ., 1982.
14. Céntola P.,Terzaghi G.,Del Rosso R.,Pasquon I., Chim.Ind.(Milano), 54, 775 (1972).
15. Huang Tai.Nang, Schwartz J., J.Am.Chem.Soc., 104, 5244 (1982).

BEHAVIOUR OF Pd^0 PARTICLES IN A MODIFIED AND STABILIZED HY ZEOLITE.

G. Spector, M. BRIEND, R. Monque, D. Delafosse
Laboratoire de Réactivité de surface et structure, Université P. et M. Curie,
4 Place Jussieu, 75230 Paris Cedex 05

ABSTRACT

Palladium has been introduced onto a stabilized HY zeolite by ion exchange with the following complexes : $\left[Pd(NH_3)_4\right] Cl_2$, $\left[Pd(NH_3)_4\right] (OH)_2$ and $PdCl_2$. After activation in flowing air at 773 K and subsequent hydrogen reduction, the catalysts were tested for benzene hydrogenation. The samples exhibit various catalytic behaviours, depending on their preparation and activation treatments. Models are proposed to tentatively explain the apparent structure sensitivity of benzene hydrogenation with these catalysts.

INTRODUCTION

Palladium containing stabilized HY zeolites form a class of bifunctional catalysts very important for the hydrocracking of heavy oils. Hydrothermal treatments suffered by these zeolites lead to a certain heterogeneity and to the formation of neutral or charged alumina species, located inside the zeolitic cavities (1). The location of Pd^{2+} ions introduced on such a carrier, and their subsequent hydrogen reducibility depend largely on the nature of the palladium precursor complex, the pH of the exchange solution and on the activating treatment conditions (2, 3). These catalysts are known to deactivate principally by a slow degradation of the hydrogenating function. In order to determinate the factors influencing the hydrogenating properties of industrial Pd/stabilized HY zeolites and their resistance to poisons, we tested these catalysts in the benzene hydrogenation reaction, before and after poisoning by sulphureous compounds. Benzene hydrogenation is generally assumed to be a structure insensitive reaction. The results of Aben et al. (4), in the case of Pd catalysts, are in agreement with this. They observed a constant specific activity for palladium particles of varying dispersions supported on silica and alumina. However, some authors noted variations in the hydrogenation reaction rate according to the particle size, the nature of the carrier or the reduction temperature of the metallic precursors. In order to explain the increased hydrogenation of benzene with dilution by alumina of a Pd/Al_2O_3 catalyst, Sancier (5) proposed that benzene was reacting with hydrogen spilled over the support. Figueras and co-workers (6) attributed the high activity of palladium dispersed on acidic supports such as protonic

and rare-earth zeolites to its partial electrodeficiency due to electron transfer from the metallic clusters to the carrier. However, such an electronic transfer was not detected by ESCA and esr techniques on Pd loaded Y zeolites (7). Moss et al. (8) admitted that a size effect could occur for benzene hydrogenation on Pd/SiO_2, although no experimental evidence for it was given. Finally, the influence of metal dispersion was demonstrated on the specific hydrogenation activity of Pd/charcoal catalysts by Benedetti et al. (9, 11). It was attributed to the formation or not of a stable palladium hydride phase, according to the particle size. So, the results accumulated up till now, in some cases support and in other cases contradict, the structure insensitivity of benzene hydrogenation. In the present work, we present a new example where small particle sizes seem to favour an increase in the specific activity of this reaction.

EXPERIMENTAL

The initial, stabilized HY zeolite is a Union Carbide synthetic product delivered in the NH_4^+ form with the label LZY82. The overall Si/Al ratio is about 3, but that corresponding to the framework tetrahedra is $\geq$ 4. The unit cell parameter a is 2.455 nm and the weight percentage of sodium is 0.12

Catalyst preparation. Pd^{2+} ions were introduced by ion-exchange with dilute solution of the following salts : (1) $\left[Pd(NH_3)_4\right] Cl_2$: pH $\simeq$ 11 - sample A ; (2) $\left[Pd(NH_3)_4\right] (OH)_2$: pH $\simeq$ 13 - sample B ; (3) $PdCl_2$: pH $\simeq$ 3.5 - sample C. Reducible and non-reducible cations were also added in A and C to give the samples described in Table I.

Catalyst activation and poisoning. After exchange and drying at 393 K, the catalysts were slowly heated (13 K/min) in flowing air up to 773 K, kept for 6 hr and then evacuated at this temperature, in order to avoid preliminary reduction of Pd^{2+} ions by hydroxyls (12) or ammonia (13). The sample reduction was performed at 423 K either in flowing hydrogen (5 l/hr) or in static conditions (hydrogen pressure: 13.3 kPa). In order to simulate the constraints suffered by the catalysts under industrial hydrocracking conditions, the samples were submitted to sintering and poisoning treatments. These consisted either in heating under flowing hydrogen from 423 to 773 K, followed by 6 h at 773 K, or in heating at 673 K under 13.3 kPa H_2S, followed by 15 hr in flowing hydrogen at the same temperature.

Metal Dispersion. Particle sizes were measured by hydrogen chemisorption at 373 K (3) and by electron microscopy.

Catalytic activity. The rates of benzene hydrogenation of sintered and poisoned samples were measured in a conventional flow microreactor. The experimental conditions used were : temperature 353 to 378 K - hydrogen/benzene ratio : 12/1 - atmospheric pressure.

Table 1

Unit cell composition and metallic dispersion of H_2 sintered samples

Exchange complex	Pd % weight	Unit cell composition	Name	Mean particle size (nm)	Dispersion
$Pd(NH_3)_4\ Cl_2$	5.9	$Pd_{6.7}Na_1 (SiO_2)_{148}(AlO_2)_{44}$	PdA	2.8	0.38
$Pd(NH_3)_4\ Cl_2$ then $AgNO_3$	5.74	$Pd_{6.6}Ag_6Na_1 (SiO_2)_{148}(AlO_2)_{44}$	PdAgA	5.0 2.0 to 15	0.21 Heterogeneous
$Pd(NH_3)_4\ Cl_2$ then $Cu(NO_3)_2$	5.80	$Pd_{6.8}Cu_5Na_1 (SiO_2)_{148}(AlO_2)_{44}$	PdCuA	3.2	0.33
$Pd(NH_3)_4\ Cl_2$ then $Ce(NO_3)_3$	4.48	$Pd_5Ce_4Na_1 (SiO_2)_{148}(AlO_2)_{44}$	PdCeA	3.3	0.32
$Pd(NH_3)_4\ Cl_2$ then $La(NO_3)_3$	4.97	$Pd_{5.8}La_6Na_1 (SiO_2)_{148}(AlO_2)_{44}$	PdLaA	2.7	0.39
$La(NO_3)_3$ then $Pd(NH_3)_4\ Cl_2$*	5.25	$La_7Pd_6Na_1 (SiO_2)_{146}(AlO_2)_{46}$	LaPdA	2.4	0.44
$Pd(NH_3)_4\ (OH)_2$	4.8	$Pd_{5.7}Na_{0.8} (SiO_2)_{144}(AlO_2)_{48}$	PdB	2.8	0.38
$PdCl_2$	5.4	$Pd_{6.2}Na_1 (SiO_2)_{147}(AlO_2)_{45}$	PdC	4.6	0.23
$PdCl_2$ then $La(NO_3)_3$	4.57	$Pd_5La_3Na_1 (SiO_2)_{147}(AlO_2)_{45}$	PdLaC	6.4	0.17 Heterogeneous
$PdCl_2$ then $Ca(NO_3)_3$	5.1	$Pd_6Ca_2Na_1 (SiO_2)_{147}(AlO_2)_{45}$	PdCaC	5.6	0.19 Heterogeneous
$PdCl_2$ then $Ca(NO_3)_2$**	5.1	$Pd_6Ca_2Na_1 (SiO_2)_{147}(AlO_2)_{45}$	PdCaC Dyn.	3.8 1.5 to 20	0.28 Heterogeneous

* Part of La^{3+} ions exists as $La_2O_3.CO_3$

** This sample was reduced in dynamic conditions

Table 2

Benzene hydrogenation rates before and after H_2S poisoning.

Sample	Reaction rate at 378K mmole/h/gmetal*	N	E Kcal/mole	Reaction rate at 378K after poisoning	N
PdA	134		15	5.4	1.6
PdB	134		15	6	1.7
PdLaA	112		15	3	0.8
LaPdA	270		15	7	1.7
PdCeA	128		15	2.4	0.7
PdCuA	38		15		0.4
PdAgA	4		15	-	-
PdC	13	6	6	4.4	2
PdLaC	25	16	7	5	2.7
PdCaC	27	1	6	8	4.4
PdCaC-Dyn	63	24	6	4	1.5

* Rate at the steady state for samples C and after one hour reaction for samples A and B.

RESULTS AND DISCUSSION.

Catalysts C. This series of catalysts are characterized by a fairly stable activity. The hydrogenation rates, measured at 378 K at the steady state, are listed in Table 2. The activation energy for the reaction is 6-7 kcal.mole^{-1}, in agreement with previous works.

The presence of additives - La^{3+} or Ca^{2+} ions - results on the one hand in a change in the particle dispersion and on the other hand in a marked increase of the turnover frequency N. As it was previously shown (3), PdLaC and PdCaC catalysts appear heterodispersed, small clusters ($\geqslant$ 1 nm) being observed together with crystallites of up to 20 nm on the microphotographs. This heterogeneity is still more pronounced after a reduction in flowing hydrogen (PdCaC-Dyn sample). Pd particles smaller than 1 nm in size, although not detected by electron microscopy, could exist in the zeolite cavities have an electrodeficient character (14) and thus play a part in the enhancement of the catalytic activity. However, due to the good agreement between particle size determinations both by electron microscopy and hydrogen chemisorption methods, we do not think that clusters smaller than 1 nm are present in our samples. These small particles would exhibit a higher thioresistance than the larger ones. On the contrary, it appears (Table II) that the most highly dispersed C sample - PdCaC-Dyn - is also the most greatly poisoned by sulphur, although it has a population of little aggregates. It is more likely, considering the experimental conditions of this work (378 K and 94 kPa H_2) that both the low specific activity and the apparently greater thioresistance of the largest clusters are related to the formation of a β-hydride phase in the metallic palladium. This phase is known to be less active than the pure metal. Moreover, the dissolved atomic hydrogen is thought to bear a negative charge (15) so that Pd atoms may gain an electrodeficient character. The stability of the palladium β-hydride increases with the particle size (16, 17). In the smallest aggregates, due to the ease of formation and decomposition of this phase, a surface restructuration may also be postulated (10), resulting in an increase of the number of low density planes [111] compared to [100] planes, the former being considered to be the most effective for acetylene hydrogenation (18). In the case of benzene, it is difficult to put forward such a motive. However, the mechanism of hydrogen activation may be modified due to the β-hydride instability in the small crystallites. The decrease in the specific hydrogenating activity and the enhanced thioresistance of coarse Pd aggregates may thus be explained, in agreement with the observations of Benedetti et al. (10).

Catalysts A and B. The initial hydrogenation rate of samples A and B is very high compared to samples C, but it quickly decreases after a few hours and then slowly and continuously diminishes, without reaching a constant value. However, in order to compare the different catalysts A and B, we measured this rate after one hour of reaction and extrapolated to zero time. The rate values so obtained are given in table II. PdCuA and PdAgA samples of this series exhibit the lowest catalytic

activity, presumably due to the formation of bimetallic particles and concomitant dilution of metallic palladium by copper and silver. The most active catalyst appears to be LaPdA which, as well as La^{3+} ions, contains a lanthanum oxycarbonate occluded in the structure. However, the metallic dispersion of this sample differs very little from the others. Moreover, it seems difficult to ascribe the enhanced activity of samples A and B with respect to samples C, to differences in palladium dispersions only, because of the abnormally high activation energy (15 kcal.mole^{-1}) which suggests a new reaction mechanism. We suspect an influence of the support and possibly that of spilled-over hydrogen. No benzene hydrogenation was detected by Angel and co-workers (19) by hydrogen activated on small rhodium clusters and possibly spilled over a mordenite carrier. However, in a previous work (2) we have shown that alumina species - and for the LaPdA sample also a lanthanum oxycarbonate - are found in the LZY-82 cavities. In the reduced samples, metallic particles in the zeolite supercages exist together with these extraframework entities. So, in spite of the low rate of H_2 spillover at 378K, the contribution of hydrogenation sites on the alumina phases inside the zeolite cavities may be postulated, due to their vicinity to the metal. Such an assumption was recently advanced by Vannice et al. (20) to explain the high benzene hydrogenation activity of Pd dispersed on SiO_2-Al_2O_3 and TiO_2 supports, with similar values of activation energies. As a matter of fact, we previously shown that, due to the catalyst preparation conditions (pH $\simeq$ 3.5) the alumina species in samples C are cationic and located in the sodalite cages, i.e. far from the palladium clusters. In that case, hydrogen migration distances are presumably too long to allow the appearance of new hydrogenation sites on the aluminic carrier.

Finally, because of their higher metal dispersion (the β-hydride phase is not stable), A and B catalysts are more poisoned by sulphur than C catalysts.

CONCLUSION

This work was undertaken with the aim of a better understanding of the catalytic behaviour of Pd/stabilized zeolites in the hydrogenation of benzene. Two main factors are assumed to govern the catalyst hydrogenation activity : the existence of extraframework entities in the zeolite cavities and the formation of a β-hydride phase in the metallic palladium which could, too, weaken the Pd-S interaction.

REFERENCES

1. Klinowski, J., Thomas, J., Fyfe, C., Gobbi, G., Nature 296, 533 (1982).
2. Briend-Faure, M., Delafosse, D., Jeanjean, J., Spector, G., Papin, G., submitted to Zeolites.
3. Briend-Faure, M., Delafosse, D., Rocherolles, G., Spector, G., To be published.
4. Aben, P.C., Platteeuw, J.C., Stouthamer, B., in "Proceedings Fourth International Congress on Catalysis, Moscow 1968" Vol. I, p. 395. Akaméiai Jiado, Budapest

1971.
5. Sancier, K.M., J. Catal. 20, 106 (1971).
6. Figueras, F., Gomez, R., Primet, M., Adv. Chem. Ser., 121, 480 (1973).
7. Vedrine, J.C., Dufaux, M., Naccache, C., Imelik, B., J. Chem. Soc., Faraday Trans. I, 74, 440 (1978).
8. Moss, R.L., Pope, D., Davis, B.J., Edwards, D.H., J. Catal. 58, 206 (1979).
9. Benedetti, A., Cocco, G., Enzo, S., Pinna, F., React. Kinet. Catal. Lett. 13(3), 291 (1980).
10. Benedetti, A., Cocco, G., Enzo, S., Piccaluga, G., Schiffini, L., J. chim. phys. 78(11-12), 961(1981).
11. Benedetti, A., Cocco, G., Enzo, S., Pinna, F., Schiffini, G., J. chim. phys. 78(11-12), 876(1981).
12. Spector, G., Briend, M., Delafosse, D., Submitted to J. chim. phys. France.
13. Reagan, W., Chester, A., Kerr, G., J. Catal. 69, 89(1981).
14. Baetzold, R.C., J. Chem. Phys. 55, 4383 (1971).
15. Lewis, F., Plat. Met. Rev. 26, 70 (1982).
16. Aben, P.C., J. Catal. 10, 224 (1968).
17. Boùdart, M., Hwang, H.S., J. Catal. 39, 44 (1975).
18. Janko, A., Palczewska, W., Szymerska, I., J. Catal. 61, 264 (1980).
19. Del Angel, G. Coq, B., Dutartre, R., Fajula, F., Figueras, F., Leclercq, C., in "Spillover of Adsorbed Species" Elsevier, Amsterdam 17, 301 (1983).
20. Vannice, M.A., Chou, P., Proc. VIIIth Congress on Catalysis, Berlin 1984, Vol V, p. 99.

THE STATE OF METALS IN HIGH-SILICA ZEOLITES AND THEIR CATALYTIC ACTIVITY IN ETHANE AROMATIZATION

E.S.SHPIRO , O.V.Bragin , A.V.Preobrazhensky , T.V.Vasina , G.V. Antoshin and Kh.M.Minachev
N.D.Zelinskii Institute of Organic Chemistry of USSR Academy of Sciences , Moscow , USSR

ABSTRACT

The catalytic properties of metal-containing high-silica zeolites in ethane aromatization and XPS spectra of these catalysts have been investigated. Both electronic states of metals (Pt,Rh) and catalytic activity strongly depended upon pretreatment conditions and changed in the course of the reaction. The development of the catalytic activity observed during successive catalytic runs in pulse mode was accompanied by an increasing of positive charge on highly dispersed metallic clusters located in the vicinity of acidic OH-groups of zeolite. The $Me^{\delta+}$- centers in combination with acidic sites are likely to be responsible for ethane transformations into aromatics over metal-containing high-silica zeolites.

INTRODUCTION

As shown earlier by the XPS studies /1-3/ , the interaction of highly dispersed metal particles (Pt,Pd,Ru,and Re) and electron acceptor sites of γ-Al_2O_3 or zeolite Y yields electron deficient metal clusters which display high activity in various reactions. The state of metals can be modified additionally under catalytic reaction conditions /4,5/.

Investigations of ethane and ethylene aromatization in the presence of a number of metal-zeolite catalysts revealed /6/ that in the course of these reactions the Me/H-ZVM (Me=Pt or Pd) catalytic system experiences the so-called activity development effect accompanied by increased yields of aromatics. The causes of the observed phenomenon have so far remained obscure, although an assumption has been put forward as regards the feasibility of metal valent state alternation during the reaction as a result of metal-support and

metal-reagents interactions.

The present study was undertaken with a view to examining by the XPS method how the pretreatment conditions (air,hydrogen or air and then hydrogen) and the reaction medium affect the electronic state of Me(Pt,Rh)-containing pentasil-type high-silica zeolites (H-ZVM). Accordingly,the dependence of Me/H-ZVM catalytic activity in ethane aromatization process on the state of Pt or Rh in corresponding bifunctional system was investigated. In contrast to faujasites,in which the physico-chemical properties of Pt and Rh have been examined in detail /7,8/,practically no data are available in the literature on the valent state of these metals and their migration ability in high-silica zeolites of the ZSM-5 structure. It is further noteworthy that in the majority of investigations /3,5,9-11/ the structure of catalysts was determined prior to the reaction (after carrying out a particular pretreatment procedure) and upon reaction completion. Of greater information value are the data characterizing the catalyst at different reaction steps,which are obtained by the present authors /4/ and refined in the work reported here.

EXPERIMENTAL

Catalysts. In this study use was made of two specimens of Pt catalysts prepared from NH_4-ZVM,viz., 0.48% Pt/H-ZVM (Cat-I) and 1.78% Pt/H-ZVM (Cat-II) as well as of sample ca.2% Rh/H-ZVM (Cat-III) The starting material comprised Na-ZVM obtained by the crystallization of alumosilicagels under hydrothermal conditions in the absence of organic cation /19/,molar ratio of SiO_2/Al_2O_3 =35,content of Na_2O =3%,and of Fe_2O_3=0.12% ; 100% phase purity. The Me-containing zeolites were prepared by treating NH_4-ZVM (after decationation,the residual content of Na_2O was 0.1%) with $[Pt(NH_3)_4]Cl_2$ or $[Rh(NH_3)_5Cl]Cl_2$ aqueous solution under ion-exchange conditions,the degree of exchange being controlled by the residual content of Me in the mother liquor. The resultant powdered specimens were dried and pressed into pellets (without binders). In experiments,0.5-1.0 mm fractions were employed.

For spectral investigations,catalyst samples were subjected to different pretreatment procedures,viz.,1) calcination in a flow of air for 5h (Cat-II at 550°C,Cat-III at 450°C); 2) calcination in air flow at the same temperatures and then in H_2 for 2h(Cat-II at 520°C,Cat-III at 400°C). After above treatments the samples were co-

oled in dry argon to room temperature and transferred into spectrometer (see below).

Catalytic experiments involving ethane were carried out in a pulse microcatalytic unit /20/. The samples of Cat-II or Cat-III were placed in an U-shaped reactor and pretreated according above procedure,followed by replacing H_2 with He (20 ml/min),and in ~20 min starting to feed ethane (0.082 ml). Upon reaction termination and analysis completion (about 30 min),the catalyst was cooled in a stream of He. The XPS spectrum of first sample was recorded after one ethane pulse,of second sample-after two ethane pulses,etc. (see table 2). Each sample consisted of a fresh weighed portion of catalyst.

Spectral investigations. From the catalytic reactor,the samples were transferred into a spectrometer in an inert atmosphere. To do so , the reactor was discharged in a box filled with pure argon, and a sample was pressed into a Pb plate and mounted on a holder followed by connecting the box to the sample insertion lock of the spectrometer and thereafter transferring the sample holder,in an Ar countercurrent,into the spectrometer vacuum system. XPS spectra were recorded with an ES 200B spectrometer using the technique described in /12/. Spectral measurements were carried out at $5x10^{-8}$ Torr using the C 1s (E_b=285.0 eV) and Si 2p (E_b=103.8 eV) lines as reference standards. After the catalytic process,no pronounced distortion of the C 1s line shape was observed. The Me/Al and Si/Al atomic ratios were evaluated using respective integral intensities correlated for the photoionization cross-sections /12/. Since the Pt 4f spin-doublet and the Al 2p line are partially overlapping,determination of spectrum parameters comprised spectrum analysis by the program of deconvolution for the unresolved Gaussian lines using PDP 11/03L minicomputer. The accuracy of E_b determination was 0.2 eV, and that of estimating atomic ratios,20-30%.

RESULTS AND DISCUSSION

Ethane catalytic conversion in the presence of Cat-I was studied in the 300-600°C temperature range in a pulse microreactor (fig.1). Under these conditions ethane undergoes the following principal transformations: hydrogenolysis,formation of C_6-C_8 aromatics,and also the formation of condensation products. Using the same catalyst under flow conditions yields closely allied results.

Next,with Cat-II at 550°C a series of runs (A) was carried out,in which the effect of catalyst activity development became ma-

nifest,activity maximum being attained after 3-5 pulses (fig.2).

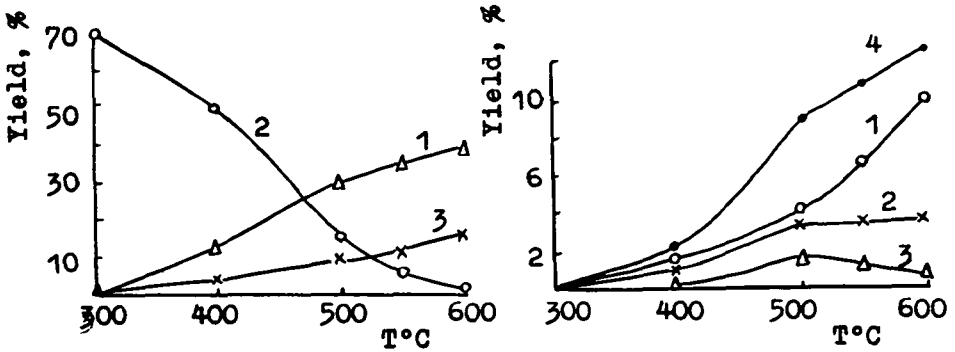

Fig.1. Dependence of the yield of ethane conversion products over 0.5% Pt/H-ZVM on temperature: a) 1-CH_4; 2-unconverted C_2H_6; 3-sum of C_6-C_8 aromatics; b) 1-benzene; 2-toluene; 3-xylene; 4-sum of C_6-C_8 aromatics

With Rh/H-ZVM rather high yields of C_6-C_7 aromatics were succeded at temperature as low as 450°C,similar development of the activity being observed,as in the case of Cat-II (fig.3). In both of cases increasing aromatics yield with pulse number is accompanied by substantial decreasing CH_4 amount which is maximum at the first pulses.

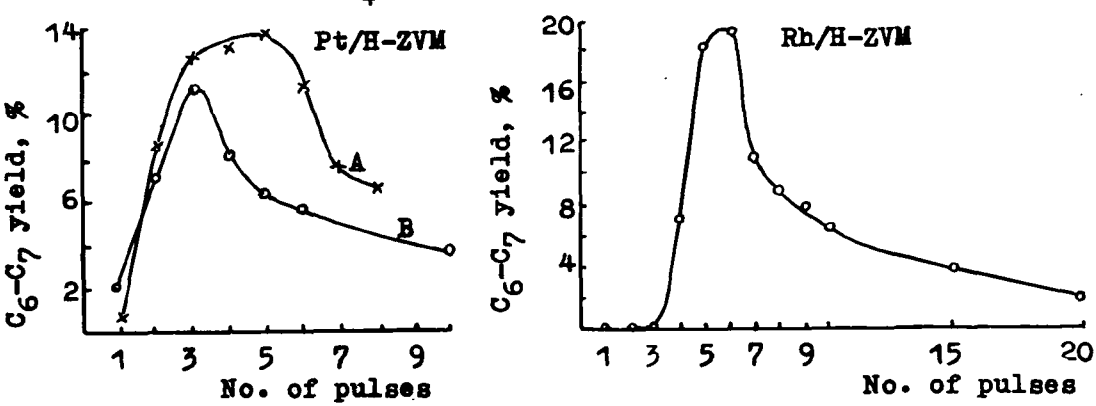

Fig.2. Dependence of C_6-C_7 aromatics yield over 1.8% Pt/H-ZVM pretreated subsequently in air and in H_2 on the number of ethane pulses at 550°C. Series A-sample weight 100 mg; series B-sample weight 70 mg

Fig.3. Dependence of C_6-C_7 aromatics yield over Rh/H-ZVM pretreated subsequently in air and H_2 on the number of ethane pulses at 450°C

It is noteworthy that in the absence of metal (H-ZVM catalyst)

no such effect was observed in the cases of ethane or ethylene, although ethylene aromatization proceeded at an adequately high level /6/. The effect observed is, therefore, due to the presence of a metal in the catalyst and appears to be associated with the variation of metal-support interaction during the reaction. A similar effect was observed by us earlier when comparing the catalytic properties and XPS spectra of alumina supported rhodium catalysts in ethylene cyclotrimerization /4/. During the reaction, the catalyst activity and the electronic state of Rh undergo significant changes with a positive charge (maximum E_b shift for Rh $3d_{5/2}$~0.7 eV) appearing on Rh clusters in the $Rh/Al_2O_3 \cdot F$ catalyst.

Taking this into account, in series of catalytic runs B (fig.2, table 1) investigations of catalytic activity were paralleled by determination of the Pt electronic state during ethane aromatization on seven Cat-II samples. As can be seen from fig.2, in series B the maximum activity falls, as in the case of series A, at third and fourth pulses. Table 2 presents the data on the state of Pt in the Cat-II specimens.

Table 1

Ethane conversions over 1.8% Pt/H-ZVM catalyst at 550°C in pulse mode (Series B)

Pulse No.	Total product yield,%	Gas and liquid products composition, wt.%				
		CH_4	C_2H_4	C_2H_6	benzene	toluene
1	76	35.6	5.4	27.0	1.6	0.4
2	73	57.9	1.6	6.5	6.0	1.0
3	80	56.6	3.2	8.7	9.0	2.3
4	76	32.9	7.1	27.7	6.0	2.2
5	70	24.4	9.2	28.9	4.5	2.0
6	74	10.7	10.3	47.2	3.9	1.8
10	74	26.4	13.6	50.1	2.5	1.4

In the spectra of the starting specimen only the Pt $4d_{5/2}$ line was observed, the Pt 4f doublet being completely masked by the Al 2p line. The value of E_b for Pt $4f_{7/2}$ found by the deconvolution of these spectra is close to that of the starting complex. After air calcination in the spectrum there appears a new line with E_b=72.2 eV. Its position is nearly that observed in the spectra of reduced specimens and can be attributed to the finely dispersed Pt^0 particles /3,12/. The decomposition of Pt complex cations in air appears to

be accompanied by partial reduction of Pt. Pt^0 formation was observed earlier in the oxidative treatment of $[Pt(NH_3)_4]$ -NaY /7,8/.

Although the positions of Pt 4f main peaks for two reduced specimens are close to each other, a significant increase (six-fold) of the Pt/Al atomic ratio was observed for the specimen reduced in H_2 without preliminary treatment in air. This phenomenon results from Pt^0 migration to the external surface of zeolite /8,12/. The data obtained are consistent with the electron microscopy measurements, according to which in the zeolite reduced in H_2 at 500°C there are large metal crystallites from 30 to 150 Å in size along with finely dispersed Pt particles (~10 Å).

Catalytic activity of three types of samples was also different. Maximum activity was displayed by sample calcined in air without subsequent reduction (the highest yield of aromatics was 19.4%) whereas the spicemen reduced directly in H_2 possessed the lowest activity (aromatics yield, 0.4%). To investigate Pt state modification under the action of reaction medium, use was made of the specimen reduced by H_2 after precalcination in the air (maximum aromatics yield, 11.3%), the most pronounced effect of activity development being observed for this catalyst in the pulse reactor (fig.2).

Activity variation was accompanied by definite changes in Pt 4f parameters (table 2). For instance, after the second pulse of C_2H_6 the Pt 4f lines exhibited broadening from 2 to 3 eV and remained so after the third and forth pulses. Subsequently the lines become somewhat narrower but their HWFM exceeds that of the starting sample. An increase in HWFM is likely to be caused by the appearance of several non-equivalent Pt states. Indeed, an analysis of the Pt 4f + Al 2p spectra after the second and third pulses disclosed that they are better approximated by Al 2p singlet and two Pt 4f spin-doublets having the Pt $4f_{7/2}$ E_b of 71.3-71.7 eV and 72.7 eV, respectively. After 10 pulses, Pt 4f spectrum was likewise broadened and resolved into two doublets, but the high-energy doublet parameters being close to thouse observed in initial spectrum (table 2). The spectra of specimens after 4 to 6 pulses could be adequately approximated by one Pt 4f spin-doublet and the Al 2p line.

It is, therefore, evident that Pt state changes occur in the course of catalyst activity development. According to the XPS data, two types of Pt centers could be discriminated which differ in their spectral characteristics: 1) Pt species with the spectra significantly shifted (+1.3 eV) with reference to bulk metal spectrum;

Table 2

XPS spectra parameters of 1.8% Pt/H-ZVM catalysts [a]

Sample No.	Pretreatment conditions	Number of C_2H_6 pulses at 550°C	Binding energy for Pt $4f_{7/2}$, eV	HWFM for Pt $4f_{7/2}$, eV	I (Pt 4f) / I (Al 2p)	Pt / Al	Si / Al
1	starting	-	73.4	2.1	0.9	0.027	
2	air, 550°C	-	73.6(55%) [b] 72.2(45%)	2.4; 1.8	0.6	0.015	22
3	H_2, 520°C	-	72.0	2.4	3.2	0.1	28
4	air, 550°C + H_2, 520°C	-	72.0	2.0	0.5	0.015	18
5	-"-	1	72.2	2.1	0.5	0.015	20
6	-"-	2	72.7(67%); 71.4(33%)	2.4; 1.6	0.8	0.024	18
7	-"-	3	72.7(67%); 71.7(33%)	2.4; 1.6	0.7	0.021	20
8	-"-	4	72.0	2.8	0.8	0.024	19
9	-"-	5	72.2	2.4	0.6	0.018	18
10	-"-	6	72.0	2.6	0.9	0.027	20
11	-"-	10	72.3(67%); 70.7(33%)	1.8; 2.1	0.8	0.024	25

a) E_b for $[Pt(NH_3)_4]Cl_2$ and Pt (metal) are equal to 73.6 and 71.5 eV, respectively

b) The percentage of a given Pt state is shown in parenthesis

2) Pt species characterized by the absence of a positive shift or by a small negative shift (e.g. after ten C_2H_6 pulses). Positive shifts in the spectra of finely dispersed metal can be attributed to a number of factors /1,3,12/,such as a decrease in the extra-atomic relaxation energy,the metal-support interaction, and the inherent electronic structure of fine particles. In compliance with tentative estimates /13/, the relaxation shift for Pt particles from 10 Å to 15 Å in size does not exceed 0.5 eV. Hence,the observed shifts stem, at least in part, from electron density transfer to the acceptor sites of the support. In the course of catalyst activity development, the positive charge on Pt increses and , subsequent to maximum activity passage, undergoes slight diminution, although both in the starting and deactiviated samples a part of Pt centers appear to carry a small positive charge.

As it is shown by XPS a modification of Rh electronic state in Rh-containing zeolite is also observed under reaction conditions. But before reaction (calcination in air at 450°C and then reduction with hydrogen at 400°C) substantial part of Rh is still remained in ionic state (40%). This makes more complicated to follow the changes of Rh state during reaction since some part of ions is additionally reduced to Rh^0 at 450°C. Nevertheless, tha data obtained reveal that, as in the Pt case, some fraction of Rh has a positive charge when maximum activity is reached.

The second type of centers observed for Pt/H-ZVM (~30% after the second and third pulses) is characterized, according to XPS data, either by charge absence or by a small negative charge. Large Pt crystallites disposed, as shown by electron mocroscopy, on the zeolite external surface may be regarded as belonging to such centers. In the case of this size particles the relaxation effects are non-essential and the parameters of spectra should not be different from thouse of bulk metal. For this assignment, a more clearly defined manifestation of the second-type centers after the initial ethane pulses should denote that the reaction is accompanied by an additional sintering of Pt. Although Pt/Al ratio growth observed in the course of the reaction may be due to additional Pt^0 migration to the external surface, this increase is insignificant and remains so during the reaction. The above assumption is further inconsistent with the fact that the catalysts containing a larger fraction of crystallites on the external surface exhibit much lower activity.

The appearence of second-type Pt centers is more likely to be due to the so-called strong metal-support interaction (SMSI) /14/

resulting in the inhibition of the adsorptive capacity of metals towards H_2 and in decreasing their activity in the processes of hydrocarbon hydrogenolysis and hydrogenation /15/. Although the SMSI effect is most typical of metals supported on readily reducible oxides (TiO_2,Nb_2O_5,ZnO),recent data show this effect to be also valid in the case of Pt/Al_2O_3 /16/. It is believed that under severe reaction conditions (550°C,hydrocarbons,and H_2) there occur the formation of oxygen vacancies in the zeolite lattice and the reduction of Al^{3+} ions located in the vicinity of Pt. The interaction of Pt with such electron-donor centers is expected to result in the appearence of electron density excess on Pt,this being indeed the case as demonstrated by XPS data.

In the same manner as with faujasites,the reduction of Pt in high-silica zeolites gives rise the localization of Pt atoms or clusters in the zeolite structure and their partial migration to the external surface. In view of geometric limitations,the localization of large clusters is impossible in the structure of ZSM-5,although formation such clusters in large cavities of zeolite Y has been postulated /6/. In the case of Pt/H-ZVM zeolite a more substantial migration of Pt atoms to the external surface was also observed during direct H_2 reduction. At the same time,preliminary zeolite dehydration (in air) provides for retaining a significant fraction of Pt inside the structure. A positive charge arises on a part of Pt atoms as a result of interaction with the acceptor sites of the zeolite framework (possibly,with Brönsted centers). As with Rh/Al_2O_3 /4/,the charge grows with increase in the degree of ethane or ethylene conversion into aromatics. In addition,a part of Pt centers is in the zerovalent state or has a negative charge due to a strong interaction with the reduced Al atoms. These Pt species may be responsible for a variation in reaction selectivity,in particular for the inhibition of feedstock ethane hydrogenolysis.

Summarizing the data on the state of Pt in Pt/H-ZVM and taking into account catalytic activity variation,it is reasonable to suggest the existence of the Pt form ($Pt^{\delta+}$ with shift of 1.3 eV) that appears to govern the aromatization activity of Cat-II in ethane conversions. Similar conclusion seems to be valid for Rh/H-ZVM. Since the pore sizes of ZSM type zeolites are equal to 5.5-6 Å /17/,the most likely reaction site would apparently be the channel mouths of a zeolite catalyst. It is believed that catalysis takes place on the fraction of Me dispersed to a crystallite size of about 10 Å and lo-

cated in the pore mouths. These are probably the active centers for ethane dehydrogenation to ethylene. The latter,having penetrated into channels,undergoes further conversions into aliphatic oligomers and aromatics,the formation of which involves the participation of bridge acidic OH-groups identified by diffuse reflectance IR /18/.

REFERENCES

1. Antoshin,G.V.,Shpiro,E.S.,Tkachenko,O.P., et al., Proceed. 7th Inter.Congr.Catal.,Tokyo, 1980, prepr. A 18.
2. Minachev,Kh.M., Antoshin,G.V., Shpiro, E.S., Kinetika i kataliz, 23, 1365 (1982).
3. Vedrine,J.C.,Dufaux,M.,Naccache,C.,Imelik,B., J.Chem.Soc.,Faraday Trans.I, 74, 440 (1978).
4. Bragin,O.V.,Shpiro,E.S.,Preobrazhensky,A.V. et al.,Izv.Akad.Nauk SSSR,Ser.Khim., 1980,p.1256.
5. Minachev,Kh.M.,Avaev,V.I.,Ryashenzeva,M.A.,Shpiro,E.S.,Antoshin,G. V., Izv.Akad.Nauk SSSR,Ser.Khim., 1978 ,p.2454.
6. Bragin,O.V.,Vasina,T.V.,Isakov,Ya.I. et al., Izv.Akad.Nauk SSSR, Ser.Khim., 1983, p.2002.
7. Gallezot, P., Catal.Rev., 20, 121 (1979).
8. Minachev,Kh.M., Antoshin,G.V., Shpiro, E.S., Izv.Akad.Nauk SSSR, Ser.Khim., 1974, p.1012.
9. Ng, K.T., Hercules, D.M., J.Phys.Chem., 80, 2094 (1976).
10. Ushakov,V.A.,Moroz,E.M.,Zhdan,P.A. et al.,Kinetika i kataliz, 19, 744 (1978).
11. Bauwman,R., Biloen,P., J.Catal., 48, 209 (1977).
12. Minachev,Kh.M.,Antoshin,G.V.,Shpiro,E.S.: Photoelectron Spectroscopy and its Application in Catalysis.Nauka,Moscow,1981, 214pp.
13. Bahl,M.K.,Tsai,S.C.,Chung,Y.W., Phys.Rev.B.,21, 1344 (1980).
14. Tauster,S.J.,Fung,S.C.,Garten, R.L.,J.Amer.Chem.Soc.,100,170 (1978
15. Meriadean,P., Elestad,O.H.,Dufaux,M.,Naccache,C., J.Catal., 75 , 243 (1982).
16. Kunimori,K.,Ikeda,Y.,Soma,M.,Uchijima,T.,J.Catal., 79 , 185 (1983)
17. Breck,D.W.: Zeolite Molecular Sieves. Willey-Interscience,N.Y.,197
18. Bragin,O.V.,Kustov,L.M.,Borovkov V.Yu. et al.,Kinet.Katal.(in pres
19. Volkov V.Yu.,Kaliko,M.A.,Lipkind,B.A. et al.,Khim. i Tekhnol. Topliv i Masel, 1982,p.8.
20. Bragin,O.V.,Preobrazhensky,A.V.,Liberman,A.L., Izv.Akad.Nauk SSSR, Ser.Khim., 1973, p.2751.

Ni REDOX EQUILIBRIUM IN MORDENITES AT VARIOUS HYDROGEN PRESSURES

C. MIRODATOS

Institut de Recherches sur la Catalyse, Villeurbanne

and

D. BARTHOMEUF

Laboratoire de Chimie des Solides, Université Paris VI

ABSTRACT

The extent of the reduction of nickel supported on sodium, hydrogen and steamed mordenites is different for the bulk and for the surface of the particles. Equilibrium constants for the redox reaction are estimated for both processes. The nickel dispersion, the extent of bulk and surface reductions depend on the balance between the number of sites of suitable acid strength and the reduction hydrogen pressure. The enhanced catalytic properties of steamed mordenites are related to the specific occurence of Ni metal on the outer surface of the particles under high hydrogen pressure.

INTRODUCTION

Applied research has shown the high catalytic performances in acidic catalysis of metal loaded zeolites. Thus, mordenites partly exchanged with transition metals are used in aromatic conversion under specific conditions of activation and reaction (1-3). The specific role played by the metal phase, besides the acid active phase, is not clear, probably in line with the changes in the metal state according to the type of support and pretreatment (4). In this work we have studied among various activation procedures the role and the effect of hydrogen pressure on mordenite supported nickel in close relation with toluene disproportionation data reported in (5).

Besides the interest for catalysis it is also of importance to understand the reduction process of the transition metals supported on acidic carriers in order to control this process (6). Both the gas and the solid phases (reducible ion and support) are involved in the mechanism. The present study is an attempt to point out the respective influence of those parameters.

EXPERIMENTAL

Material. The protonic mordenite catalysts referred to as HM (Si/Al = 5) and

HMD when dealuminated (Si/Al = 9) have been already described in (1,7,8). The sodium-form, Na-M (Si/Al = 5) was provided by Norton (Zeolon 900). Nickel was exchanged in the sodium (1.3 wt % Ni) or decationated (1.45 wt % Ni) forms with 0.5 M nickel nitrate solutions at room temperature to give NiNaM, NiHM and NiHMD zeolites. Each of the Ni samples has been either treated in flowing air (treatment (1)) or steamed (2) prior reduction at 773 K.

Magnetic measurements. The nickel phase was studied by means of magnetic methods as described in (4,9) giving the degree of nickel reduction and the average nickel particles diameters. Magnetic measurements under high H_2 pressure (up to 1.2 MPa) were carried out in a stainless steel cell allowing both a reduction under flowing hydrogen and magnetic measurements using the Weiss extraction method. A typical experiment consists of reducing the sample at 773 K under a flow of hydrogen at the desired pressure (0.1-1.2 MPa), then cooling it down to room temperature without changing H_2 pressure or flow conditions. The cell is then disconnected and isolated from the flow system and the sample internally transfered into the magnetic part of the cell. The magnetic isotherm can be recorded 1) under the reduction pressure (in this case, outer metal atoms with chemisorbed hydrogen do not participate in the collective ferromagnetism), ii) after evacuation - or helium flush - of the cell at 673 K for 1h (in this case all the nickel atoms bulk or surface, which remain in their metallic state in vacuum or neutral atmosphere are taken into account). The comparison between i) and ii) magnetic isotherms allows to determine the amount of stable metallic surface onto the nickel particles. This is also evaluated from the amount of hydrogen chemisorbed onto the sample (volumetry) after its evacuation (or the flush) at 673 K.

Electron microscopy. Electron micrographs were obtained using a JEM 100 CX transmission electron microscope.

RESULTS

Table 1 presents data from magnetic, volumetric and electron microscopy measurements. Let us notefirst that magnetic and electron microscopy informations are quite consistent, although the former are obtained "in situ" and the latter in the open air. The main features of these data are : i) the bulk degree of nickel reduction at 773 K is lower than unity whatever be the reduction procedure for the hydrogen forms of mordenite and very close to unity for the sodium forms. The increase in bulk reduction as a function of temperature (fig. 1) strongly depends on the zeolite, the sodium and steamed forms being the more easily reducible samples. ii) The fraction of nickel metal for hydrogen mordenite is significantly improved when the reduction is carried out at high H_2 pressure (1.2 MPa)instead of atmospheric pres-

Table 1

Magnetic, volumetric and electron microscopy (E.M.) data after reduction at 0.1 (I) and 1.2 MPa (II) hydrogen pressure

Catalysts	Bulk degree reduction [a]		Average particle diameter (nm)				Size heterogeneity				Fraction % of surface with Ni metal (from H_2 adsorption)			
			Magnetic		E.M.		Magnetic [b]		E.M. [c]		Magnetic [d]		Volumetric [e]	
	I	II	I	II	I	II	I	II	I	II	I	II	I	II
NiHM (1)	0.85	0.93	20	20	35	*	0.5	*	1.4	*	0	0	0	0
NiHM (2)	0.9	0.91	14.4	10.4	25	10.0	0.5	0.13	1.0	0.6	0	11	0	4
NiHMD (1)	0.65	0.89	20	20	*	*	0.7	0.5	*	*	0	0	*	*
NiHMD (2)	0.82	0.94	18.0	13.0	*	*	0.6	0.5	*	*	0	5	*	*
NiNaM	1.00	0.98	12.4	10.8	*	*	0.5	0.45	*	*	9	12	10	11

(a) Calculated after outgassing at 673 K the samples reduced at 773 K.

(b) Ratio of the difference between low and high field diameters to the average particle diameter (9).

(c) Ratio of the difference between the highest and the lowest particle size to the average size of the whole distribution.

(d) Ratio of the metallic nickel able to chemisorb hydrogen to the total content of metallic nickel.

(e) Calculated from the adsorption capacity extrapolated at full surface coverage and from average particle diameter (H/Ni = 1 is assumed).

* not determined

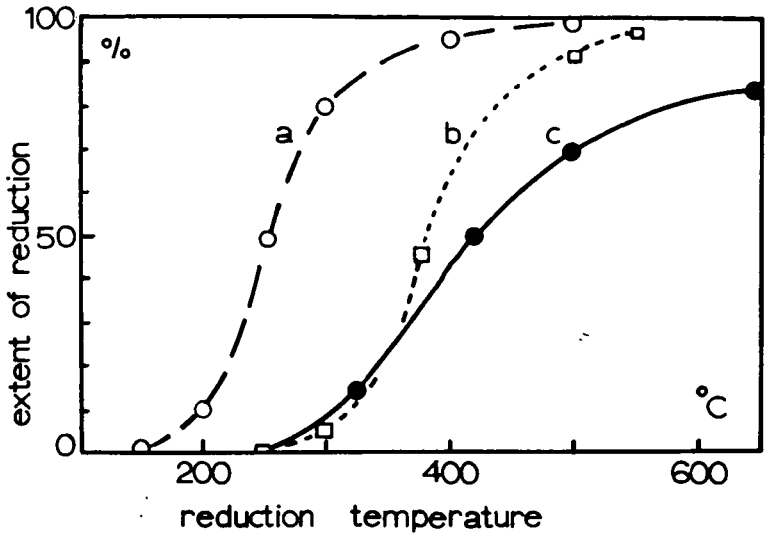

Fig. 1. Change in the degree of reduction at P_{H_2} = 0.1 MPa as a function of reduction remperature. a : NiNaH, b : NiHM (2), c : NiHM (1).

sure.The same holds for nickel dispersion : average particle diameter, particle size distribution and size heterogeneity are shifted towards lower values (Table 1). It can be noted that the average diameter of nickel particles are for any sample larger than the mordenite channels (≃0.7 nm). The nickel particles are then located either outside the framework of the zeolite or entrapped in locally destroyed parts of the framework. iii) Only the sodium nickel samples (NiNaM) and the steamed nickel hydrogen mordenite (NiHM (2) and NiHMD (2)) are able to chemisorb hydrogen, i.e. display particles with metallic surface after evacuation. This coincides with the best nickel dispersion in electron microscope studies. iv) There is no specific effect of mordenite dealumination (i.e. Si/Al ratio) on the state of nickel for hydrogen mordenite material : similar relations between H_2 pressure, steaming treatment, nickel reduction and dispersion are observed, the samples being dealuminated or not.

Catalytic performances. From refs. 5 and 7, table 2 reports some data concerning the effect of pressure in toluene disproportionation carried out on similar H-mordenite samples, exchanged or not with nickel.

The kinetics of the reaction (partial orders vs H_2 or toluene) has been discussed in details in (2,5). It will only be emphasized from Table 2 that the best catalytic performances (activity and selectivity) are obtained at high H_2 pressure with a nickel loaded sample which has been initially steamed (NiHM (2)). In all other cases (dry air pretreated and/or low pressure catalysis), the nickel phase does not play any clear role in the disproportionation process.

Table 2

Catalytic activity in toluene disproportionation at 723 K, $P_{H_2}/P_{Toluene}$ = 4 after 5h on stream (5,7)

Catalyst	$r(10^{-4}$ mole h^{-1} $g^{-1}_{Zeol.})$	
	I	II
HM (1)	ε	20
NiHM (1)	2	15
HM (2)	2	55
NiHM (2)	5	85

I : Total pressure = 0.1 MPa

II: " " = 1.5 MPa

In order to get more information on the state of nickel in catalytic course, some experiments have been performed with the present series of nickel mordenite in CO/H_2 methanation considered as a probe reaction for metallic nickel. Corresponding data are reported in table 3.

Table 3

Catalytic activity in $CO/3H_2$, methanation (P = 0.1 MPa, T = 593 K, microdifferential reactor flow)

Catalysts	CO conversion $(10^{-3}$ mole h^{-1} $g^{-1}_{Ni})$		Fraction of Ni metal accessible [b] (%)	
	I[a]	II	I	II
NiNaM (1)	9	28	9	12
NiHM (1)	0	ε	0	0
NiHM (2)	0	34	0	11

[a] I : activated in flowing H_2, P_{H_2} = 0.1 MPa

II : activated in flowing H_2, P_{H_2} = 1.2 MPa

[b] From table 1

For all samples yielding significant amounts of methane, the apparent activation energy was found around 20 kcal/mole in the 573-623 K range and methane selectivity higher than 90 % which is quite consistent with the values reported for usual supported nickel catalysts (e.g. Ni/SiO_2 (10)). Only nickel loaded on sodium mordenite or on steamed hydrogen mordenite activated under high H_2 pressure is reactive

towards CO/H_2 mixture and so behaves as usual supported metal. The good coincidence noted in table 3 between the CO/H_2 activity and the occurence of stabilized surface metal atoms after evacuation (or the flush) at 673 K for given activation and reduction conditions strongly suggests that the information in table 1 obtained by magnetic and volumetric methods at room temperature (degree of reduction, dispersion, metal/oxide surface) will reflect the state of the nickel phase even when further experimental conditions (T,P) are different from those used for reduction. The reduction step primarily determines the nickel behavior.

DISCUSSION

Correlations with catalytic activity. The toluene disproportionation reaction has been shown to proceed on the Brönsted acid sites of the mordenite, whether hydrogen or nitrogen atmosphere is used (5,7). Yet, a kinetic inhibiting effect of hydrogen pressure has been put forward on the basis of the formation-decomposition equilibrium of the benzylic carbocation, proposed as an intermediate species in the disproportionation mechanism (7). The present study shows an obvious correlation between H_2 pressure activation, good catalytic activity and stability in toluene disproportionation and the occurrence of a metallic surface. The latter is ascertained either from physico chemical characterization (volumetry and magnetism) or from CO/H_2 probe. It is reasonable to admit that this specific property to display a metallic surface under reaction conditions (steamed H-mordenite activated at high H_2 pressure) over-compensates the above mentioned inhibiting effect of H_2 pressure. This role of metallic nickel is very probably in line with coke formation and pore fouling (5). The schematic process would be : hydrogen activation on the Ni particles, then hydrogenation of coke precursor avoiding the very fast deactivation which is noted in (5) for samples reacting at atmospheric pressure. In such a process the migration of activated species from the particles of nickel to the coke deposits is likely to occur. This is consistent with the evidences of hydrogen spillover in partially reduced nickel catalysts provided in (11).

Thermodynamics of reduction. Besides the correlation observed between the impr ved catalytic properties and the presence of nickel metal, the results allow to obtain detailed information on the parameters of importance for nickel reduction. The will be discussed in terms of effect of the OH groups acidity, of hydrogen pressure, of temperature, of steaming and of dealumination. Sample NiNaM does not show any acidity. A $Ni-SiO_2$ sample studied previously (4) and added here for comparison show a large number very weak sites. The steamed NiHM (2) and NiHM (2) mordenites have a small number of strong acid sites and the two samples pretreated in an air flow, NiHM (1) and NiHMD (1), a large number of strong sites (8). For those various samp

rising the hydrogen pressure increases the degree of bulk reduction and decreases the particle size and size heterogeneity. It also gives nickel particles with metal nickel on the outside only when the number of strongly acidic hydroxyls is small (NiNaM, $NiSiO_2$, NiHM (2) and NiHMD (2)). Rising the reduction temperature increases the bulk reduction (fig. 1). Steaming modifies the acidity (decrease in the number of acid sites but not of their strength (8). It also leads to smaller particles and interestingly gives particles with an outer surface of nickel metal only at high ydrogen pressure. By contrast, dealumination alone does not give any specific effect on nickel reduction. This is very likely related to the only small changes in mordenite acidity it produces (8,12).

Average bulk reduction. The increase in bulk reduction with hydrogen pressure, temperature and decrease in strong acid sites concentration is in agrement with the known equilibrium (4,13-15).

$$Ni^{2+} + 2\ O^-_{zeol.} + H_2 \rightleftharpoons Ni^\circ + 2\ OH_{zeol.} \qquad (1)$$

For instance fig. 1 evidences that the extent of reduction at any given temperature higher than about 650 K and at P_{H_2} = 0.1 MPa increases from NiHM (1) to NiHM (2) and then NiNaM following the order of decreasing number of strong acid sites. Except for NiNaM none of the other mordenites reaches the complete reduction even at P_{H_2} = 1.2 MPa. A higher hydrogen pressure is necessary.

The importance of zeolite acidity has been already shown for NiX and Y zeolites at atmospheric pressure (14).

Surface reduction. Uncomplete average bulk reduction may result in heterogeneous particles. It was already shown that for instance a NiHM (1) sample reduced at 773 K and low P_{H_2} (0.1 MPa) consists of nickel particles with a core of metal and a shell of nickel oxide. Other Ni supported oxides such as the $Ni\text{-}SiO_2$ sample are uncompletely reduced in the same conditions but display a metal character at the outer surface of some particles (4). This suggests a heterogeneous distribution of oxide id of the metal particles. The nickel mordenites considered here give results depending on the reduction conditions. Table 4 summarizes the occurence of nickel metal on the particles surface. It can be easily seen that the surface reduction is also governed by the reaction (1) (influence of acidity - number and strength of sites- and of hydrogen pressure). Nevertheless the conditions required for the complete ickel reduction at the surface differ from those in the bulk. For instance the steamed samples (2) show metal on the surface under high hydrogen pressure while the particles average bulk reduction is only 91-94 %. This arises probably from the relative distribution of Ni ions and strong acidic OH groups and from the formation mechanism of the nickel particles, which may give heterogeneity in the phases distribution.

Table 4

Changes in nickel surface state as a function of hydrogen pressure and acidity (number and strength of sites)

Catalyst	Acid sites	Metal nickel on surface particle (a)		$Kp = P_{H_2}$ (a)
		P_{H_2} = 0.1 MPa	P_{H_2} = 1.2 MPa	
NiNaM	no	yes	yes	$Kp < 0.1$
$NiSiO_2$	large number very weak	yes	yes	$Kp < 0.1$
NiHM (2)	small number strong	no	yes	$0.1 < Kp < 1.2$
NiHMD (2)	small number strong	no	yes	$0.1 < Kp < 1.2$
NiHM (1)	large number strong	no	no	$Kp > 1.2$
NiHMD (1)	large number strong	no	no	$Kp > 1.2$

(a) Reduction temperature 773 K

(1) Mordenites pretreated in dry air

(2) Steamed mordenites

Equilibrium constant. An attempt can be made to estimate the equilibrium consta of the reaction (1). It has to be noted that in the experimental conditions used al the water evolved from the zeolite is continuously removed by the hydrogen flow. At equilibrium the only vapor phase left in the system is hydrogen. It is also the onl gas phase involved in reaction (1). The equilibrium constant can then be easily expressed as $Kp = P_{H_2}$. For the surface reduction at 773 K the values estimated from the shift of the equilibrium (1) to the left or to the right are given in table 4.

For the average bulk reduction at 773 K, Kp would be less than 0.1 MPa for the non acidic NiNaM sample and higher than 1.2 MPa for the other mordenites.

Nickel dispersion. The smaller particle sizes (10 to 13 nm) and better homogeneous size distribution are obtained for those samples which have particles with nickel metal on their surface (NiNaM, $Ni-SiO_2$ (4) and steamed mordenites). The thr properties are very likely related to a good balance between the rate of nickel reduction and that of particle growing. The nickel transfer from its initial cationic sites inside the mordenite framework (16) to its final structure of metal particles probably occurs during the reduction treatments via a process of ionic species migration (4,16). No or little particle motion is effectively expected at 773 K (17). The Ni^{2+} migration from one cationic site to another one should be high when the

number of protonic sites, weak or strong is high i.e. for $NiSiO_2$ and NiHM (1), NiHMD (1) mordenites. If the nickel reduction is faster than the migration, i.e. for small number of protonic sites, weak or strong, the final dispersion is high. This occurs already at low hydrogen pressure for NiNaM and Ni SiO_2 (weak acidity) and only at high hydrogen pressure for the steamed mordenites (strong acidity).

CONCLUSION

This study relates the high catalytic activity of some Ni mordenites under high hydrogen pressure to the presence of nickel metal on the outer surface of the particles. This arises from the conjunction of steaming which reduces the concentration of strong protonic sites and the reduction under high pressure. The stabilized metal able to activate hydrogen, associated with a low concentration of strong protons plays a major role in the catalyst life time, limiting the deactivating coke deposition.

The study of nickel reduction under two different hydrogen pressures allows an estimation of the equilibrium constant of the redox reaction to be made. Different behaviors regarding bulk and surface reduction are observed. The final nickel state (dispersion, bulk reduction, occurence of Ni metal on the outer surface of the particles) depends on the relative rates of the migration and of the reduction of nickel ions. A high number of hydroxyls seems to favor the migration rate over the reduction rate while a small number would do the opposite. In addition, for similar OH groups concentration and hydrogen pressure, the higher the acid strength, the lower the reduction degree seems to be. As a consequence the balance between the number of acid sites of suitable strength and the hydrogen pressure determines the nickel particles characteristics.

REFERENCES

1. Marcilly, C., French Patents 75/33.001, 77/01.265.
2. Wu, J.C., Leu, L.J., Applied Catal. 7, 283 (1983).
3. Dimitrova, R.P., Dimitrov, C., Popova, Z., Steinberg, K.H., Applied Catal. 3, 377, (1982).
4. Mirodatos, C., Dalmon, J.A., Garbowski, E.D., Barthomeuf, D., Zeolites, 2, 125 (1982).
5. Gnep, N.S., Martin de Armando, M.L., Marcilly, C., Ha, B.H., Guisnet, H., in "Studies in surface science and Catalysis", "Catalyst Deactivation", Delmon, B. and Froment, G.F. (Eds) Elsevier, Amsterdam 6, 79 (1980).
6. Jaeger, N.I., Ryder, P., Schulz-Ekloff, G., in "Studies in Surface Science and Catalysis", Elsevier, Amsterdam 18, 299 (1984).

7. Gnep, N.S., Guisnet, M., Applied Catalysis 1, 329 (1981).
8. Mirodatos, C., Ha, B.H., Otsuka, K., Barthomeuf, D., Fifth Int. Conf. Zeol., Naples, Heyden, London, 382 (1980).
9. Primet, M., Dalmon, J.A., Martin, G.A., J. Catal., 46, 25 (1977).
10. Dalmon, J.A., Martin, G.A., J. Catal., 84, 45 (1983).
11. Dalmon, J.A., Mirodatos, C., Turlier, P., Martin, G.A., in "Spillover of Adsorbed Species", Pajonk, G.M. et al. (Eds) Elsevier, Amsterdam, 169 (1983).
12. Ha, B.H., Guidot, J., Barthomeuf, D., J.C.S. Far. Trans. I, 75, 245 (1979) : Ha, B.H., Barthomeuf, D., J.C.S. Far. Trans. I, 7, 2366 (1979).
13. Rieckert, L., Ber. Bunsenges. Phys. Chem., 73, 331 (1969).
14. Guilleux, M.F., Delafosse, D., Martin, G.A., Dalmon, J.A., J.C.S. Farad. Trans I, 75, 165 (1979) ; Djemel, S., Guilleux, M.F., Jeanjean, J., Tempère, J.F., Delafosse, D., J.C.S. Far. Trans.I, 78, 835 (1982) ; Sauvion, G.N., Guilleux, M.F., Tempère, J.F., Delafosse, D., in "Studies in Surface Science and Catalysis", Elsevier, Amsterdam, 12, 229 (1982).
15. Suzuki, M., Tsutsumi, K., Takahashi, H., Zeolites, 2, 51 and 87 (1982).
16. Garbowski, E.D., Mirodatos, C., Primet, M., in "Metal Microstructures in Zeolites", Jacobs, P.A. et al. (Eds) Elsevier, Amsterdam, 235 (1982).
17. Baker, R.T.K., Catal. Rev. Sci. Eng., 19, 161 (1979).

PREPARATION AND CHARACTERIZATION OF Mo/Y-ZEOLITE AND ITS CATALYTIC ACTIVITY FOR PROPENE METATHESIS

T. KOMATSU, S. NAMBA, T. YASHIMA
Department of Chemistry, Tokyo Institute of Technology, Ookayama, Meguro-ku, Tokyo 152, Japan

ABSTRACT

The adjustment of the oxidation state of molybdenum in Mo/HNa-Y zeolite and the properties of the catalytically active sites for propene metathesis were investigated.

Mo/HNa-Y zeolite was prepared by the adsorption of $Mo(CO)_6$ vapor on HNa-Y(proton exchange degree; 0 – 74 %) dehydrated at 473 – 873 K, followed by the decomposition of adsorbed $Mo(CO)_6$ at 573 K. We could control the average oxidation number (AON) of molybdenum in the range of 0 – +2 by changing the concentration of proton in Y zeolite.

The catalytic activity for propene metathesis increased with decreasing the AON of molybdenum on HNa-Y. The data of oxygen titration at 97 K and UV diffuse reflectance spectroscopy suggested that the dispersion of Mo species played the important role for the catalytic activity. From these results, it was concluded that the slightly aggregated Mo^0 species showed the highest catalytic activity for propene metathesis.

INTRODUCTION

There have been so many reports in the field of zeolite catalysis in recent years. The major part of them has been related to the solid acid catalysis. On the other hand, the transition metal cations can be supported in a variety of oxidation state on the zeolites by an ion exchange method. These transition metal cations have the high catalytic activities in some organic reactions [1]. We have reported the polymerization of ethene on CrY zeolite [2], the selective dimerization of ethene on NiY and RhY zeolites [3], and the carbonylation of methanol to produce acetic acid on RhY zeolite [4].

Molybdenum oxides and sulfides have been used in chemical industries as catalysts for the hydrodesulfurization of petroleum products, the oxidation, the polymerization and the metathesis of

alkenes. Most of these commercial catalysts are prepared by the impregnation method using oxide supports and ammonium molybdate aqueous solution.

Recently, well-defined molybdenum catalysts were prepared by Yermakov et al. [5] and Iwasawa et al. [6]. Both researchers prepared their catalysts by using $Mo(\pi\text{-}C_3H_5)_4$ and silica or alumina and adjusted the oxidation number of molybdenum to +2, +4 or +6. Bowman et al. [7] have reported that the low oxidation state molybdenum, whose average oxidation number is less than +1, can be prepared by using $Mo(CO)_6$ and highly dehydroxylated alumina.

MoY zeolite cannot be prepared by a conventional cation exchange process, because molybdenum species is not a cation but a molybdic anion as a stable state in aqueous solution. Lunsford et al. [8] have prepared MoY using $MoCl_5$ and HY by means of a solid-solid ion exchange method without solvent. They have reported that their MoY shows the catalytic activity for the oxidation of cyclohexene and that the oxidation number of molybdenum is +6. On the other hand, Gallezot et al. [9] have reported that Mo/HNa-Y zeolite can be prepared by the adsorption of $Mo(CO)_6$ on HNa-Y followed by the thermal decomposition of $Mo(CO)_6$ and the simultaneous oxidation of molybdenum by the protons of HNa-Y.

We have reported [10] that the oxidation state of molybdenum in MoY zeolite derived from $Mo(CO)_6$ and HNa-Y zeolite is changed by the decomposition temperature of $Mo(CO)_6$ and the pretreatment temperature of HNa-Y. Namely, the average oxidation number (AON) of molybdenum increased with increasing the decomposition temperature or with decreasing the pretreatment temperature. We could adjust the AON of molybdenum in the range from +0.6 to +3.8. It has been found that Mo/HNa-Y shows the very high catalytic activity for ethene polymerization at the AON of about +1. It has been pointed out that the dispersion of molybdenum is a very important factor on the catalytic activity.

In this paper, we present a control method of AON of molybdenum by changing the proton exchange degree of HNa-Y and discuss the oxidation states and the dispersion of molybdenum in Mo/HNa-Y catalyst for the propene metathesis.

EXPERIMENTAL

Catalysts preparation. Na-Y zeolites(Toyo Soda Ind. Co., Lot Y-30) were treated with 0.05 N NH_4Cl aqueous solution at room temperature to form NH_4Na-Y. After calcination at 743 K in air, H(x)Na-Y was obtained, where x is the percent degree of proton exchange.

A certain amount of HNa-Y powder set in a quartz tube was heated in vacuo at various temperatures to get dehydrated HNa-Y. The desired amount of $Mo(CO)_6$ was added to the dehydrated HNa-Y in nitrogen or argon atmosphere. After the nitrogen or argon gas was pumped out for 20 s, the tube was put in a thermostated oven at 333 K and allowed to stand for 15 h to adsorb $Mo(CO)_6$ on HNa-Y. Mo/HNa-Y was obtained by heating in vacuo at 573 K.

The content of sodium in HNa-Y and that of molybdenum in Mo/HNa-Y were analyzed by flame emission spectroscopy and atomic absorption spectroscopy, respectively.

Average oxidation number of molybdenum. The average oxidation number (AON) of molybdenum in Mo/HNa-Y after the decomposition of $Mo(CO)_6$ adsorbed on HNa-Y was determined by the O_2 titration method.

Mo/HNa-Y was exposed to oxygen which was introduced into the system at the rate of 20 Torr/min up to 200 Torr at room temperature. Then the sample was heated at 573 K for more than 30 min. The amount of O_2 consumed by the oxidation of molybdenum was measured volumetrically by subtracting the amount of physisorbed O_2. The AON of Mo was calculated by taking account of the observation that all of the Mo species were oxidized to Mo^{6+} [11].

Metathesis of propene. The metathesis of propene on Mo/HNa-Y which was prepared from a certain amount of $Mo(CO)_6$ and 0.2 g of HNa-Y, was carried out at 274 K with a usual closed circulation system of 230 ml dead volume. Propene was purified using a freeze-pump-thaw tequnique. The initial presure of propene was 190 Torr.

The reaction products were analyzed by gas chromatography using a 4 m column of propylene carbonate.

The turnover frequency calculated from the amount of ethene produced for 1 h and the amount of molybdenum in catalyst was used as the catalytic activity of Mo/HNa-Y.

Oxygen chemisorption. The oxygen chemisorption on Mo/HNa-Y was investigated with a static system. First, the amount of oxygen adsorbed at 77 K was measured volumetrically. The pressure of oxygen used was lower than 110 Torr(the vapor pressure of oxygen at 77 K is 156 Torr). After evacuation at 195 K for 30 min, oxygen was readsorbed at 77 K. The amount of chemisorbed oxygen was calculated from the difference between the amounts of oxygen in the first and the second adsorptions.

Ultraviolet spectra. The diffuse reflectance technique was used to obtain the ultraviolet(UV) spectra on a Shimadzu UV-240 spectrometer.

HNa-Y(28 – 60 mesh) was put into a pyrex tube having a branch of

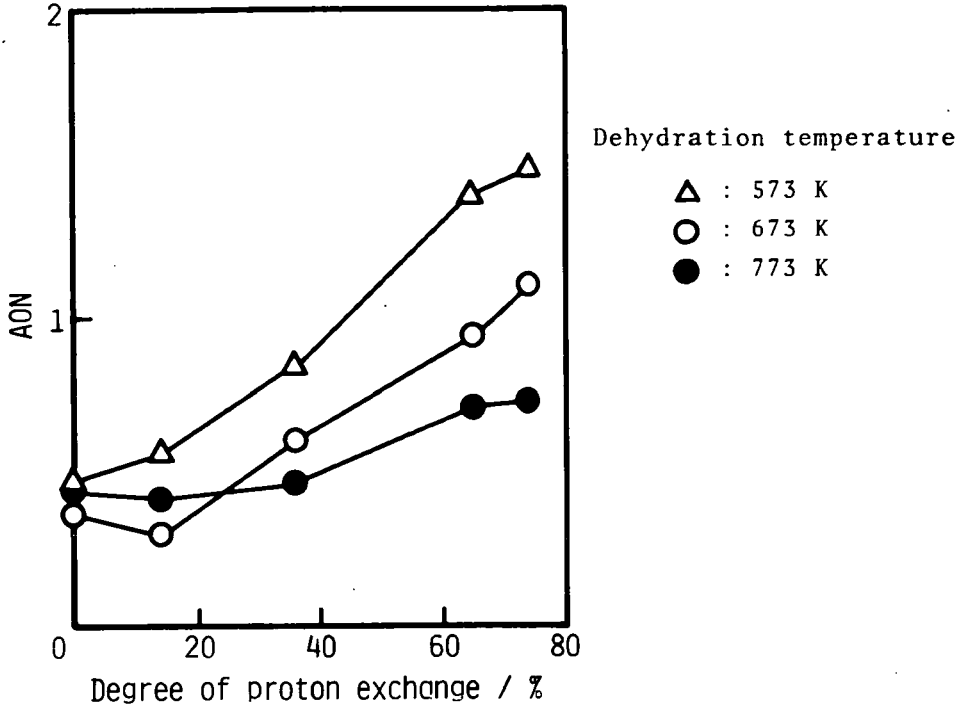

Fig. 1 Effect of degree of proton exchange in HNa-Y on AON of Mo

quartz cell. After Mo/HNa-Y was prepared in the tube, molybdenum was oxidized by O_2 in the same manner as the O_2 titration. Then Mo^{6+}/HNa-Y sample was transferred into the quartz cell in vacuo. The UV-diffuse reflectance spectra were recorded at room temperature in the range of 190 – 700 nm using the parent HNa-Y as a reference.

RESULTS AND DISCUSSION

Oxidation state of supported molybdenum. It has been reported [9 that molybdenum is oxidized by the surface hydroxyl groups of HNa-Y zeolite during the decomposition of $Mo(CO)_6$ adsorbed on the HNa-Y. Therefore, it is expected that the oxidation state of the supported molybdenum is dependent on the concentration of the hydroxyl groups of HNa-Y. We have reported [10] that the average oxidation number (AON) of molybdenum decreases with the increase of the pretreatment temparature of the HNa-Y zeolite. On the other hand, the concentration of the hydroxyl groups of HNa-Y can be varied with the degree of the proton exchange in Na-Y zeolite. In this study, we changed the proton exchang degree from 0 %(parent Na-Y) to 74 % by using the various amounts of NH_4Cl aqueous solutions in the NH_4^+ exchange process.

Fig. 1 shows the AON of molybdenum supported on the HNa-Y

zeolites with various degrees of proton exchange. It was found that the AON of molybdenum increased with increasing the degrees of proton exchange when HNa-Y were dehydrated at the same temperature. It is concluded that the higher content of the hydroxyl groups of HNa-Y causes the higher oxidation degree of molybdenum. In this study, AON of molybdenum was measured by the O_2 titration method. We have evaluated [11] the AON of molybdenum also by the measurement of H_2 formed during the simultaneous oxidation of molybdenum by proton with the decomposition of adsorbed $Mo(CO)_6$. The decomposition and oxidation of $Mo(CO)_6$ was described as follows;

$$Mo(CO)_6 + n(-OH) \longrightarrow (-O-)_n Mo^{n+} + 6CO + \frac{n}{2} H_2 \qquad (1)$$

The AON obtained by this method agreed with that measured by the O_2 titration.

The maximum content of molybdenum for this catalyst system has been reported [9,10] to correspond to one Mo atom per supercage of Y zeolite. However, we found [11] that the maximum content corresponded to two Mo atoms per supercage in the case of H(x)Na-Y (x = 0 – 74 %) supports. The surface area of H(82)Na-Y used as a support in the earlier work [10] was considerably smaller than that of the parent Na-Y. From this result we suggested that the partial destruction of the zeolite crystal structure caused the decrease in the maximum content of molybdenum to some extent. The content of molybdenum used in this study usually corresponded to two Mo atoms per supercage of Y zeolite to avoid the heterogeneous distribution of molybdenum.

In order to prepare Mo/HNa-Y catalysts having various AONs of molybdenum, we varied the dehydration temperature of HNa-Y in addition to the degree of proton exchange. The results are shown in Fig. 2. Less effect of the dehydration temperature on AON was observed in the case of the HNa-Y supports having the lower degrees of proton exchange, because these zeolites have a small amount of protons.

Propene metathesis. The metathesis of propene was carried out at 274 K on Mo/HNa-Y catalysts. Ethene, trans- and cis-2-butenes and a trace amount of 1-butene were detected as reaction products. The amount of ethene formed was larger than that of butenes in every case. We expressed the catalytic activity of Mo/HNa-Y for the propene metathesis in terms of the ternover frequency of the ethene formation.

Fig. 3 shows the relation between the catalytic activity of Mo/HNa-Y and the AON of molybdenum. The catalysts used were Mo/HNa-Y whose AON were controlled by changing the proton exchange degree and the dehydration temperature of HNa-Y zeolites as presented in Fig. 2.

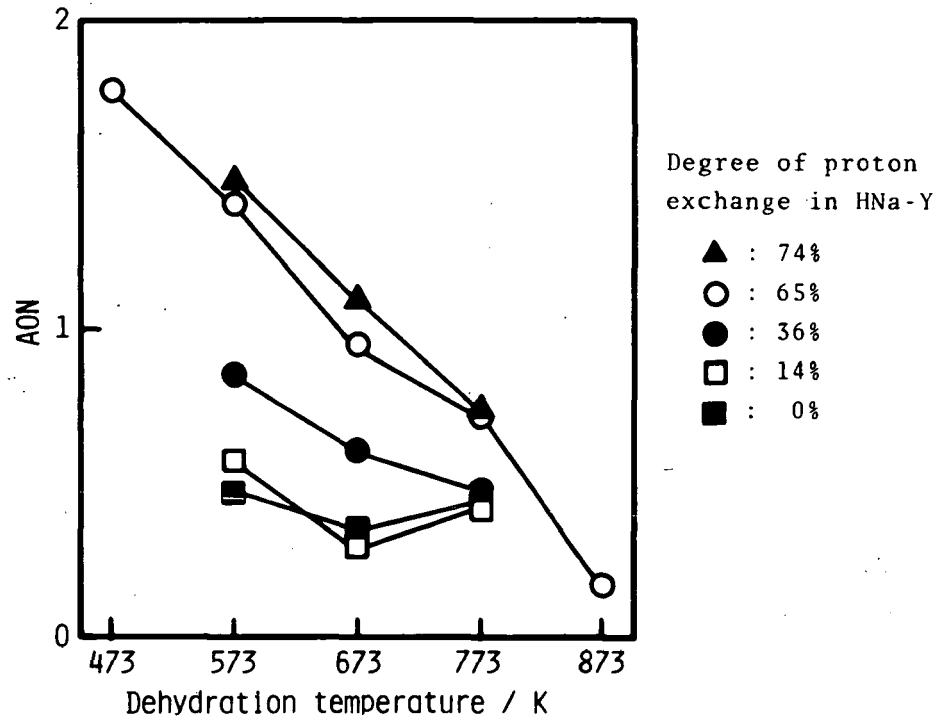

Fig. 2 Effect of dehydration temperature of HNa-Y on AON of Mo

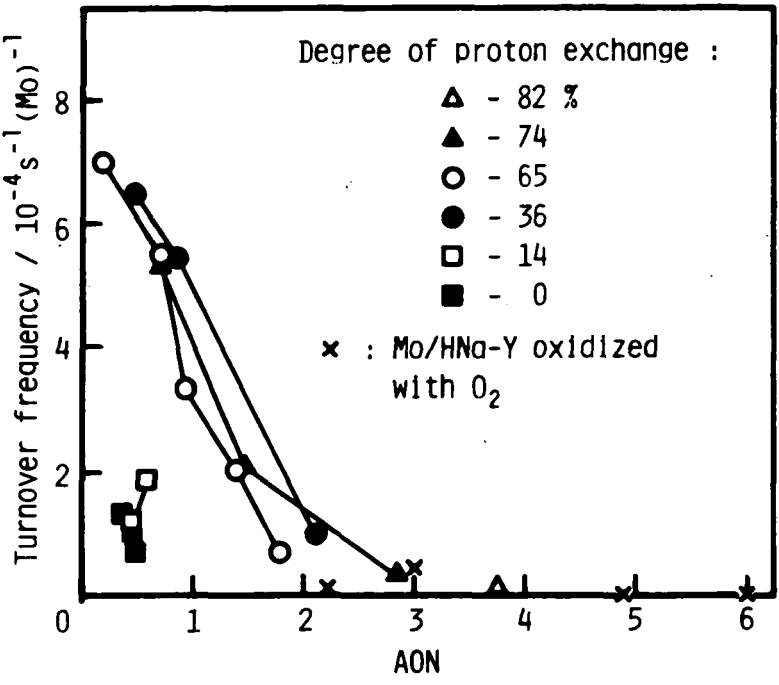

Fig. 3 Change in activity for propene metathesis with AON of Mo

In addition, Mo/H(74)Na-Y(Mo content=0.68 Mo atoms/supercage; AON=2.83), Mo/H(82)Na-Y(Mo content=0.68 Mo atoms/supercage; AON=3.75) and Mo/HNa-Y oxidized with oxygen at room temperature or 573 K were used as catalysts.

In the cases of Mo/H(74)Na-Y, Mo/H(65)Na-Y and Mo/H(36)Na-Y, the catalytic activity increased with decreasing the AON of molybdenum. When Mo/HNa-Y was oxidized with oxygen at room temperature, the AON increased from +1.1 to +3.0, while Mo/HNa-Y oxidized at 573 K had the AON of +6. These oxidized catalysts exhibited very low activities compared with the parent Mo/HNa-Y.

The active Mo species for the propene metathesis have been reported to be Mo^{4+} [12,13] or Mo^{3+} [14] in some supported molybdenum catalysts. In the case of Mo anchored catalysts prepared from Mo(π-$C_3H_5)_4$ and SiO_2 or Al_2O_3, it has been reported [12,13] that the activity was increased by oxygen treatment of Mo^{2+} species at room temperature. Similarly, Brenner et al. [15] have reported that the activity of (σ-$O^-)_2$Mo species was increased by the oxygen treatment at room temperature.

In our catalyst system, however, the activities of the Mo species whose AON were around +4 were much lower than those of Mo species in a low oxidation state for propene metathesis. Besides, the oxygen treatment on the Mo species in the low oxidation states caused the decrease in activity to a considerable extent. Therefore, it is concluded that the oxidation number of the most active Mo species for propene metathesis is not +4 but less than +4, probably 0.

In the case of H(14)Na-Y and Na-Y supports, however, the catalytic activities were relatively low, though the AON of molybdenum in these Mo/HNa-Y were as low as those in more active catalysts using H(36)Na-Y or H(65)Na-Y support. It was suggested that some other differences in the supported Mo species caused the change in activity. We thought that one of these differences consisted in the dispersion of the Mo species. To confirm this speculation, we carried out the oxygen chemisorption studies using some Mo/HNa-Y catalysts.

Dispersion of Mo species. Table 1 shows the turnover frequency and the amount of chemisorbed oxygen in terms of the O/Mo atomic ratio. We have already reported [10] the apparent dispersion of Mo calculated from the amount of irreversibly adsorbed oxygen at 298 K. But at 298 K, the oxygen uptake was gradually increased for more than 40 h. This result suggested that the oxidation of molybdenum in bulk phase occured at 298 K. On the other hand, when oxygen adsorption was carried out at 77 K, the adsorption reached the equilibrium state in 20 min. Therefore, to get the information about the dispersion of Mo species,

Table 1

Oxygen chemisorption on Mo/HNa-Y

Zeolite support	Dehydration temperature /K	Amount of irreversible adsorption of O_2 /O atom(Mo atom)$^{-1}$	Turnover frequency /10^{-4} s^{-1}(Mo)$^{-1}$
Na-Y	573	0.27	0.69
H(36)Na-Y	773	0.58	6.47
H(65)Na-Y	573	1.26	2.00
	773	0.90	5.45

it is better to adsorb oxygen at 77 K. From Table 1 it is clear that the dispersion of molybdenum in Mo/Na-Y is considerably low compared with that in Mo/H(65)Na-Y prepared by a similar procedure. This difference in the dispersion corresponded to the difference in the activities. However, the dispersion of molybdenum in the highly active Mo/H(36)Na-Y pretreated at 773 K was lower than that in the less active Mo/H(65)Na-Y pretreated at 573 K. Similarly in the case of H(65)Na-Y support, the dispersion in the more active catalyst pretreated at 773 K was lower than that in the other pretreated at 573 K. It seems that the Mo^0 species aggregated slightly are the most active for propene metathesis.

We studied the dispersion of Mo species also using ultraviolet diffuse reflectance spectroscopy. It has been reported [16,17] that Mo^{6+} with tetrahedrally and octahedrally coordinated O^{2-} exhibit UV absorption bands at 260 – 280 nm and 300 – 320 nm, respectively. An additional band at 220 – 240 nm is common to tetrahedral and octahedral configurations. The Mo^{6+} species in the tetrahedral configuration were thought to be monomeric species, while those in the octahedral configuration were attributed to polymeric species with bridging O^{2-} [18].

Fig. 4 shows the UV diffuse reflectance spectra of two different Mo/HNa-Y measured after all of the Mo species were oxidized to Mo^{6+}, and the spectra of $Na_2MoO_4 \cdot 2H_2O$ and $(NH_4)_6Mo_7O_{24} \cdot 4H_2O$. The spectrum of Mo^{6+}/H(65)Na-Y had a peak at ca. 255 nm and a shoulder at around 220 nm similarly to the spectrum of $Na_2MoO_4 \cdot 2H_2O$ which consists of tetrahedrally coordinated molybdenum. The spectrum of Mo^{6+}/Na-Y had a peak at ca. 295 nm and three shoulders at around 230, 270 and 320 nm. $(NH_4)_6Mo_7O_{24} \cdot 4H_2O$ which consists of octahedrally coordinated molybdenum exhibited two absorption peaks at ca. 260 and 295 nm and two shoulders at around 220 and 320 nm.

Accordingly it is clear that the Mo species in Mo^{6+}/H(65)Na-Y

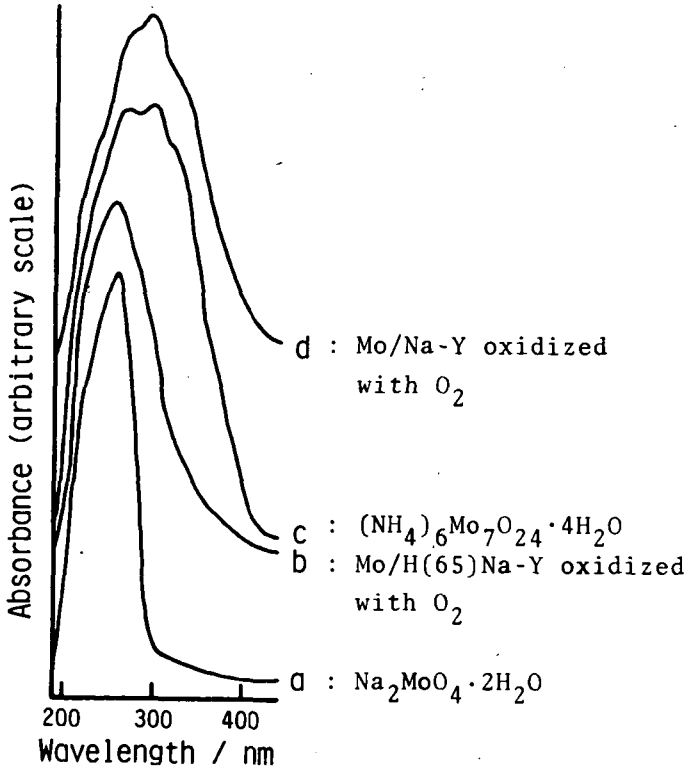

Fig. 4 UV diffuse reflectance spectra

consist almost exclusively of the tetrahedrally coordinated molybdenum. Therefore, the Mo species in this catalyst should be dispersed nearly monomerically in the zeolite. On the other hand, it seems that most of the Mo species in Mo^{6+}/Na-Y have the octahedral coordination, that is, the Mo species are probably aggregated to form bulk oxide. These results are consistent with the results of oxygen chemisorption.

ACKNOWLEDGMENTS

Financial support for this work by the Asahi Glass Foundation for Industrial Technology is gratefully acknowledged.

REFERENCES

1. Maxwell, I.E.: Advances in Catalysis. vol. 31. Academic Press, New York, 1982, p. 1.
2. Yashima, T., Nagata, J., Shimazaki, Y., Hara, N.: Amer. Chem. Soc., Sym. Ser. No. 40, Molecular Sieves II , 1977, p. 626.
3. Yashima, T., Ushida, Y., Ebisawa, M., Hara, N., J. Catal. 36, 320 (1975).
4. Yashima, T., Orikasa, Y., Takahashi, N., Hara, N., J. Catal. 59, 53

(1979); Takahashi, N., Orikasa, Y., Yashima, T., J. Catal. 59, 61 (1979).
5. Yermakov, Yu.I., Kuznetzov, B.N., Prep. 2nd Japan-Soviet Catalysis Seminar (Tokyo), 1973, p. 65.
6. Iwasawa, Y., Nakano, Y., Ogasawara, S., J. Chem. Soc. Faraday Trans I. 74, 2968 (1978).
7. Bowman, R.G., Burwell, R.L.Jr., J. Catal. 63, 463 (1980).
8. Dai, P.-S.E., Lunsford, J.H., J. Catal. 64, 173 (1980); ibid. 64, 184 (1980).
9. Gallezot, P., Coudurier, G., Primet, M., Imelik, B.: Amer. Chem. Soc., Sym. Ser. No. 40, Molecular Sieves II , 1977, p. 144.
10. Yashima, T., Komatsu, T., Namba, S., Proc. 4th Intern. Conf. Chem. Uses Molybdenum. Climax Molybdenum Co. Michigan, 1982, p. 274.
11. Komatsu, T., Namba, S., Yashima, T., Domen, K., Onishi, T., J. Mol. Catal. submitted.
12. Iwasawa, Y., Ichinose, H., Ogasawara, S., J. Chem. Soc. Faraday Trans. I. 77, 1763 (1981).
13. Kuznetzov, B.N., Startsev, A.N., Yermakov, Yu.I., J. Mol. Catal. 8, 135 (1980).
14. Howe, R.F., Kemball, C., J. Chem. Soc., Faraday Trans. I. 70, 1153 (1974).
15. Brenner, A., Burwell, R.L.Jr., J. Catal. 52, 364 (1978).
16. Che, M., Figueras, F., Forissier, M., McAteer, J., Perrin, M., Portefaix, J.L., Praliaud, H., Proc. 6th Intern. Congr. Catal. (London), 1977, vol. 1, p. 261.
17. Giordano, N., Bart, J.C.J., Vachi, A., Castellan, A., Mortinotti, G., J. Catal. 36, 81 (1975).
18. Wang, L., Hall, W.K., J. Catal. 77, 232 (1982).

ISOMERIZATION AND HYDROCRACKING OF ALKANES ON Pt/CeY, Pt/LaY AND Pd/LaY ZEOLITES - BIFUNCTIONAL OR METALLIC CATALYSIS?

J. WEITKAMP[a], W. GERHARDT[a], P.A. JACOBS[b]
Engler-Bunte Institute, Division of Gas, Oil, and Coal, University of Karlsruhe, D-7500 Karlsruhe 1, Federal Republic of Germany (a)
Centrum voor Oppervlaktescheikunde en Colloidale Scheikunde, Katholieke Universiteit Leuven, B-3030 Leuven, Belgium (b)

ABSTRACT

MeNaY zeolites (Me = Ce^{3+} or La^{3+}, degree of exchange = 72 equiv.-%) were loaded with 0.03 to 0.50 wt.-% of Pt or Pd. The resulting Pt/ and Pd/MeY-72 catalysts were tested in isomerization and hydrocracking of n-undecane at P_{H_2} = 2 MPa. Neither the rate nor the selectivity of isomerization depend on the content of noble metal, the selectivity being, moreover, independent of its nature. Hydrocracking typically starts at conversions around 40 %, then leading to large amounts of i-alkanes. Much lower rates of reaction and very different selectivities are encountered on non-acidic 0.50 Pt/NaY and 0.27 Pd/NaY. The detailed discussion of all results strongly suggests that, on Pt/ and Pd/MeY-72, bifunctional isomerization and hydrocracking predominate. However, on the Pt/MeY-72 zeolites, the bifunctional pathways tend to be accompanied by some hydrogenolysis at the noble metal, especially at high Pt loadings.

INTRODUCTION

Catalysts consisting of a large-pore zeolite in a Brönsted acid form and small amounts of a noble metal are used in isomerization of light alkanes and in hydrocracking of heavy petroleum distillates [1]. Since these catalysts possess different kinds of active sites, there is an inherent ambiguity as to mechanisms of reaction [2,3]. In particular, both isomerization and hydrocracking may proceed *via a bifunctional mechanism* or *on the noble metal alone*. In the bifunctional mechanism [3-5], skeletal rearrangement and carbon-carbon bond rupture occur at the level of carbocations chemisorbed at *the acidic sites*, while the main role of the noble metal is to open a fast route for interconversion of alkanes and carbocations via alkenes. In the metal-

lic mechanism [6-8], on the other hand, rearrangement and cleavage take place during chemisorption of the hydrocarbon *at a metal cluster*. On platinum, two different mechanisms of isomerization have been identified [6-8] which are usually referred to as the *bond shift* and the *cyclic* mechanism, respectively. Hydrocracking on metals is often called *hydrogenolysis*.

According to Weisz [3], the bifunctional mechanisms predominate over typical catalysts consisting of platinum on an acidic carrier, provided that the carbon number of the feed is sufficiently high. Indeed, a pronounced shift from bifunctional hydrocracking to hydrogenolysis was observed [9] with a Pt/CaY zeolite catalyst, when the chain length of the feed was lowered from n-octane to n-hexane. Some more recent papers tend to emphasize the importance and to generalize the validity of the metallic mechanisms. Christoffel and Paál even went so far to claim that, with bifunctional catalysts made from platinum on an acidic carrier, *mainly platinum catalyzed reactions contribute to the measured product distributions at temperatures below 350 °C* [10]. Unfortunately, these authors used an ill-defined zeolite catalyst (beside Pt/Al_2O_3 and Pt black) referred to as 0.5 wt.-% Pt/Y, the acidic nature of which was not disclosed.

In the present study, an attempt was undertaken to resolve these contradictions. Series of catalysts were prepared based on zeolite Y. The nature of the noble metal, its content, and the acidity were varied. The catalysts were comparatively tested in the hydroconversion of n-undecane which possesses enough carbon atoms to avoid non-typical side reactions.

EXPERIMENTAL

NaY zeolite with a unit cell composition $Na_{54}Al_{54}Si_{138}O_{384}$ was the starting material for all catalysts. Cerium or lanthanum were introduced by repeated ion exchange at 80 °C using aqueous solutions (0.03 mol-%) of the respective nitrates. After excessive exchange cycles, chemical analyses gave the formulas $Me_{13}Na_{15}Al_{54}Si_{138}O_{384}$ (Me = Ce or La), i.e., the final degrees of Ce and La exchange were 72 equiv.-% (MeY-72). The washed zeolites were dried at 110 °C and then stored at room temperature over the saturated aqueous solution of NH_4Cl. After equilibration, the water content was determined by TGA.

NaY, CeY-72, and LaY-72 were loaded with a noble metal by ion exchange with $[Pt(NH_3)_4]Cl_2$ or $[Pd(NH_3)_4]Cl_2$. A slurry of the zeolite was vigorously stirred at room temperature while the ammine complex,

dissolved in several hundred times its weight of water, was added dropwise over a period of two hours. Afterwards, stirring was continued for 48 h. It was ascertained that under these conditions, the complexes were taken up quantitatively by the zeolites. After drying at 110 °C the zeolite powder was pressed without a binder, the tablets were ground, and the particle size 0.2-0.3 mm was further used.

The ammine complex was decomposed in a purge of O_2 (0.1 MPa, 10 l/h, $T_{max.}$ = 300 °C; for Pt/CeY-72 $T_{max.}$ = 350 °C). The zeolite was then transferred to the fixed bed reactor and dried in flowing N_2 (0.1 MPa, 5 l/h, $T_{max.}$ = 350 °C). Finally, the metal was reduced in a purge of H_2 (0.1 MPa, 5 l/h, $T_{max.}$ = 300 °C, for Pt/CeY-72 $T_{max.}$ = 400 °C). In the catalyst notation used hereinafter the content of noble metal is given in wt.-% on a dry basis. A total of 12 catalysts were prepared, viz. 0.05, 0.10, 0.25, and 0.50 Pt/CeY-72; 0.05, 0.20, and 0.50 Pt/LaY-72; 0.027, 0.055, and 0.27 Pd/LaY-72; 0.50 Pt/NaY; 0.27 Pd/NaY.

The flow-type apparatus with a high-pressure saturator for the feed hydrocarbon has been described earlier [11]. The purities of n-undecane and hydrogen were at least 99.8 wt.-% and 99.99 vol.-%, respectively. The products were analyzed by high-resolution capillary GLC [12] with on-line sampling. Platinum dispersions were determined by conventional H_2 chemisorption techniques.

RESULTS AND DISCUSSION

Activities, isomerization vs. hydrocracking. Fig. 1 shows the conversion of n-undecane along with the yields of isomerized and cracked products for two Pt/CeY-72 catalysts which differ in their content of noble metal. The results are typical for all Pt/ and Pd/MeY-72 zeolites employed in this study and resemble those obtained earlier on 0.5 Pt/CaY [12] or 0.5 Pt/ultrastable Y [13]: Under mild conditions, isomerization predominates. With increasing severity, the yield of isomers passes through a maximum indicating that the i-undecanes formed are consumed by consecutive hydrocracking. The height of this maximum was between 50 and 60 % for all Pt/ and Pd/MeY-72 catalysts.

A closer look at Fig. 1 reveals that, on 0.05 Pt/CeY-72, there is virtually no hydrocracking up to ca. 40 % conversion, whereas on 0.50 Pt/CeY-72 some hydrocracking does occur even at much lower conversions. It will be shown later that this hydrocracking *at low conversions* (as opposed to hydrocracking starting at $X_{n\text{-}Un} \approx 40$ %) is probably due to hydrogenolysis on platinum. In agreement with this interpretation, 0.10 Pt/CeY-72 and 0.25 Pt/CeY-72 gave intermediate extents of

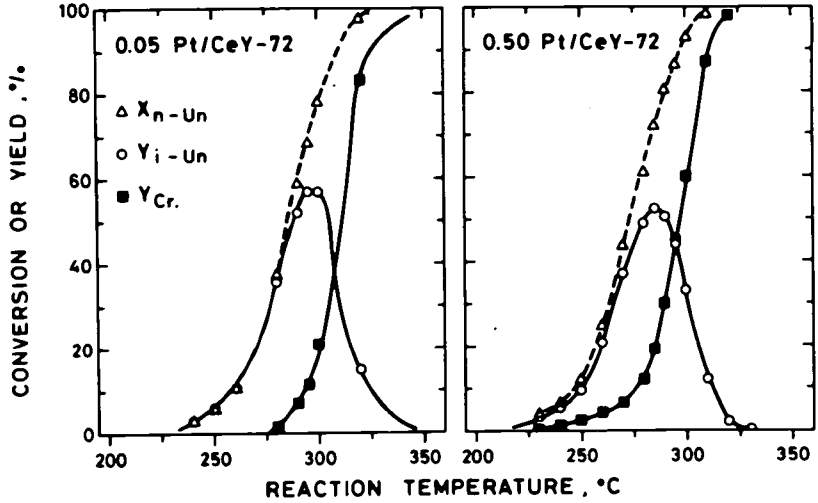

Fig. 1. Conversion of n-undecane, yield of i-undecanes, and yield of cracked products in dependence of reaction temperature (P_{n-Un} = 20 kP P_{H_2} = 2.0 MPa, W/F_{n-Un} = 150 g·h/mol).

hydrocracking at low conversions. Moreover, the same qualitative beha vior was observed on the Pt/LaY-72 series, even though, at comparable conversions below 40 %, the extent of hydrogenolysis over 0.50 Pt/LaY-72 was somewhat lower than on 0.50 Pt/CeY-72. On the Pd/LaY-72 series, there was no hydrocracking at all at $X_{n-Un} \lesssim 40$ %, even not on the ca talyst with the highest Pd loading, i.e., 0.27 Pd/LaY-72. It seems that, in an acidic faujasite, Pd has a lower activity for hydrogenoly sis than Pt.

At this point already, it appears unlikely that, over the Pt/ o Pd/MeY-72 catalyst, *isomerization* occurs on the metals. If it did, the one would expect (based on the results of numerous investigations on the conversion of light alkanes over noble metal catalysts, e.g., [6-8]) that (i) isomerization is *always* accompanied by some hydrogenolysis and (ii) there is only little, if any, isomerization *on palladium*. The same conclusion can be drawn from Fig. 2 in which the rates of iso merization (as determined in the differential reactor regime at $X_{n-Un} \lesssim 20$ %) are plotted versus the metal content of the acidic catalysts. With one exception (0.05 Pt/LaY-72), the rate is practically independent of the metal content. Hence, it is unlikely that isomerization takes place on the metal clusters to any significant extent. One might argue that an increasing metal content could have been counterbalanced by a decreasing dispersion. This, however, was not the case, at least not for the Pt/CeY-72 and Pt/LaY-72 series (Pt dispersions around 40 and 55 %, respectively). The reasons for the relatively low activity

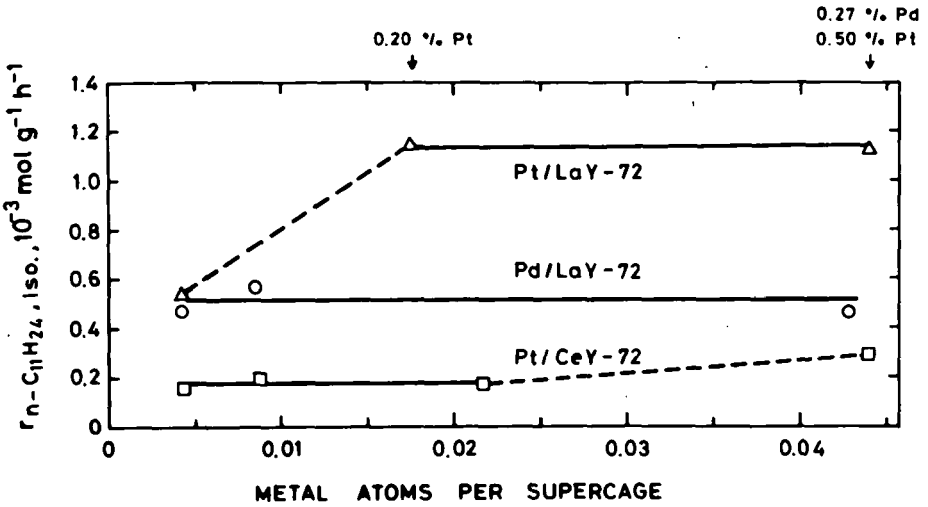

Fig. 2. Influence of the content of noble metal on the rate of n-undecane isomerization (T = 240 °C, P_{n-Un} = 20 kPa, P_{H_2} = 2.0 MPa).

of 0.05 Pt/LaY-72 are not clear, at present. Nor can we explain the different activity levels of the Pt/LaY-72 and Pd/LaY-72 series. Perhaps, the nature of the noble metal influences the acidity somewhat. The relatively low activity level of the Pt/CeY-72 catalysts might be due, at least in part, to the higher pretreatment temperatures (loss of Brönsted acid sites by dehydroxylation).

It must be concluded that, on the Pt/ and Pd/MeY-72 zeolites, isomerization occurs via a bifunctional mechanism. One would then expect that the acidity of the zeolite (number and/or strength of Brönsted sites) has a pronounced influence on its activity. This is, indeed, the case as demonstrated in Table 1: With 0.27 Pd/NaY and 0.50 Pt/NaY (Pt dispersion ≅ 50 %) which are practically non-acidic (except for some few OH groups formed during reduction of the noble metal), there is hardly any conversion even at 300 °C. At this temperature, most or all of the undecane is converted on the acidic zeolites (cf. also Fig. 1).

To arrive at a somewhat higher conversion on 0.50 Pt/NaY, the hydrogen partial pressure was lowered to 0.48 MPa at P_{n-Un} = 20 kPa, T = 300 °C, and W/F_{n-Un} = 150 g·h/mol. The resulting conversion and yields were X_{n-Un} = 4.5 %, Y_{i-Un} = 0.6 %, and $Y_{Cr.}$ = 2.8 % (in addition, there were some unidentified hydrocarbons, presumably C_{11}-naphthenes, with a total yield of 1.1 %).

Selectivities of isomerization. In Table 2, the selectivities of isomerization are compared for 0.5 Pt/NaY and several selected Pt/ and

Table 1

Influence of acidity on conversion and yields (P_{n-Un} = 20 kPa, P_{H_2} = 2.0 MPa, W/F_{n-Un} = 150 g·h/mol).

	non-acidic				acidic			
Catalyst	0.50 Pt/NaY		0.27 Pd/NaY		0.50 Pt/LaY-72		0.27 Pd/LaY-72	
T, °C	260	300	260	300	260	300	260	300
X_{n-Un}, %	0	0.5	0	0.1	58	100	27	95
Y_{i-Un}, %	0	0	0	0	48	0	27	32
$Y_{Cr.}$, %	0	0.5	0	0.1	10	100	0	63

Pd/MeY-72 catalysts at low conversions. All the acidic zeolites give practically identical distributions of i-undecanes, irrespective of the nature and the content of noble metal. This is again strong evidence for a common mechanism of skeletal rearrangement at the acidic sites, i.e., for a bifunctional mechanism. It has been shown [14,15] that ionic rearrangements in which a branching is created are best interpreted in terms of a pathway via protonated cyclopropanes. It has, moreover, been deduced [12] that such a mechanism of branching is expected to result in low rates of formation of 2-methyldecane amounting to about one half of the rates of formation of 3-, 4-, and 5-methyldecane. Table 2 reveals that this is approximately fulfilled on the Pt/ and Pd/MeY-72 catalysts. On 0.50 Pt/NaY, on the other hand, a substantially different isomer distribution is encountered. Its salient feature is the preponderance of 4-methyldecane which has also been found during isomerization of n-undecane over platinum on non-acidic Al_2O_3 [16]. It can be shown [16] that the so-called cyclic mechanism [7,8] indeed predicts 4-methyldecane as a major product. We conclude that isomerization on 0.50 Pt/NaY occurs mainly or totally on the noble metal.

Selectivities of hydrocracking. It is relatively easy to discriminate between bifunctional hydrocracking and hydrogenolysis on metals: Hydrogenolysis inevitably gives a certain amount of methane and ethane [6-8], whereas in β-scission of classical alkylcarbenium ions which is involved in bifunctional hydrocracking [4], C_1- and C_2-moieties are forebidden (besides, an ionic mechanism of bond rupture via non-classical alkylcarbonium ions has been claimed [17] which, however, is unlikely to play an important role under our conditions). Furthermore, starting from a *normal* alkane, the primary products of hydrogenolysis are again n-alkanes, whereas i-alkanes prevail in bifunctional hydro-

Table 2

Selectivities of n-undecane isomerization (moles of i-undecane formed/100 moles of n-undecane isomerized; $P_{n\text{-}Un}$ = 20 kPa, $W/F_{n\text{-}Un}$ = 150 g.h/mol).

Catalyst	0.50 Pt/ NaY	0.50 Pt/ CeY-72	0.05 Pt/ LaY-72	0.20 Pt/ LaY-72	0.50 Pt/ LaY-72	0.27 Pd/ LaY-72
T, °C	300	240	220	220	220	220
P_{H_2}, MPa	0.48	2.0	2.0	2.0	2.0	2.0
$X_{n\text{-}Un}$, %	4.5	5.5	2.6	5.5	5.4	2.5
$Y_{i\text{-}Un}$, %	0.6	4.3	2.6	5.5	5.1	2.5
2-M-De	13	12	12	12	12	11
3-M-De	16	23	23	23	23	23
4-M-De	36	25	25	25	25	25
5-M-De	14	28	29	28	27	30
3-E-No	4	3	3	3	3	3
4-E-No	5	5	5	5	5	5
5-E-No	0	2	2	2	3	2
4-P-Oc	4	2	1	2	2	1
others	8	0	0	0	0	0

cracking because ionic β-scission is preceded by rapid skeletal rearrangements.

Typical selectivities of hydrocracking observed in this study are depicted in Fig. 3. On 0.27 Pd/LaY-72 both the carbon number distribution and the content of i-alkanes are representative for a pure primary cracking via a bifunctional mechanism [4,9,11]. With this catalyst, the selectivity of hydrocracking was found to be virtually independent of $Y_{Cr.}$. Moreover, the results shown for 0.27 Pd/LaY-72 are representative for the whole Pd/LaY-72 series and for the Pt/MeY-72 zeolites with *low* metal loadings.

An entirely different selectivity is encountered on 0.50 Pt/NaY. C_1 and C_2 as well as C_{10} and C_9 now do occur and there are no branched alkanes at all in the cracked products. Without any doubt, they are formed on the noble metal.

On 0.50 Pt/LaY-72, the selectivity of hydrocracking is seen to depend markedly on the yield of cracked products. The cracking reactions which take place at low values of $Y_{Cr.}$ and, hence, *at low con-*

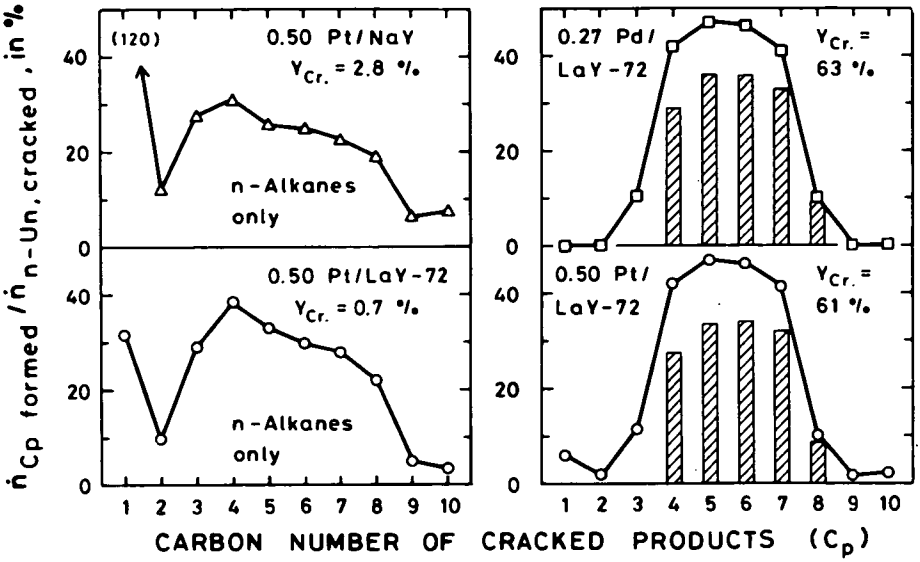

Fig. 3. Selectivities of n-undecane hydrocracking (T = 240 to 300 °C, partial pressures see Table 2, W/F_{n-Un} = 150 g·h/mol). The full curves comprise all products with a given carbon number, the bars are valid for branched alkanes.

versions (cf. also data for 0.50 Pt/CeY-72 in Fig. 1) are best interpreted in terms of a hydrogenolysis which is superimposed to ionic isomerization. This is concluded from a comparison of the selectivities with those found on 0.50 Pt/NaY. At elevated yields of cracked products the selectivities are much more representative for a bifunctional mechanism, i.e., ionic cleavage is much more accelerated than the superimposed hydrogenolysis.

CONCLUSIONS

Several independent results of this study suggest that, on catalysts encompassing a noble metal and a typical Brönsted acid (e.g., Pt/ or Pd/MeY-72), both isomerization and hydrocracking proceed mainly or exclusively via bifunctional mechanisms. This is at least true for (i) elevated conversions, (ii) elevated hydrogen partial pressures, and (iii) a sufficiently high carbon number of the feed, which are all relevant to industrial catalysis. Contrary statements as made in [10] should be considered with great caution.

Of course, the metallic mechanisms always compete with the bifunctional ones and their contributions to the overall hydrocarbon conversion are simply a matter of relative rates. If desired, the

importance of metallic catalysis can be enhanced by several factors, above all by lowering the acidity of the catalyst. On 0.50 Pt/NaY, n-undecane isomerization and hydrocracking probably occur at the noble metal, at least under the conditions applied in this investigation. But even on Pt/MeY-72 zeolites, some hydrogenolysis may be superimposed to the bifunctional pathways. Expectedly, the extent of hydrogenolysis increases as the Pt content is raised. The metal loading of zeolites should, therefore, be carefully optimized for every catalytic application. It can, furthermore, be concluded from this study that Pd is a better catalyst component than Pt, if pure bifunctional reactions of alkanes are aimed at.

ACKNOWLEDGEMENTS

We thank Mr. Stefan Ernst for the dispersion measurements on Pt/LaY-72 and Pt/NaY, and Mr. Wilfried Stober for general assistance with the experiments. Financial support by Deutsche Forschungsgemeinschaft and Fonds der Chemischen Industrie is gratefully acknowledged. P.A. Jacobs acknowledges a research position from N.F.W.O.

SYMBOLS AND ABBREVIATIONS

F_i	feed rate	mol h^{-1}
$\dot{n}$	molar flux	mol h^{-1}
p	carbon number of cracked products	
P_i	partial pressure	Pa
r_i	rate of disappearance	mol $(g \cdot h)^{-1}$
W	mass of dry catalyst	g
X_i	conversion	
Y_i	yield	

M	methyl	Oc	octane	Iso.	isomerization
E	ethyl	No	nonane	Cr.	hydrocracking
P	propyl	De	decane	Me	cerium or lanthanum
		Un	undecane		

REFERENCES

1. Bolton, A.P., in: Zeolite Chemistry and Catalysis (J.A. Rabo, Ed.), ACS Monograph 171, American Chemical Society, Washington, D.C., 1976, pp. 714-779.
2. Myers, C.G., Munns, Jr., G.W., Ind. Eng. Chem. 50, 1727-1732 (1958).
3. Weisz, P.B., Adv. Catal. 13, 137-190 (1962).
4. Weitkamp, J., Erdöl, Kohle - Erdgas - Petrochem. 31, 13-22 (1978).

5. Guisnet, M., Perot, G., in: Zeolites - Science and Technology (F.R. Ribeiro et al., Eds.), Martinus Nijhoff Publishers, The Hague, Boston, Lancaster, 1984, pp. 397-420.
6. Anderson, J.R., Adv. Catal. 23, 1-90 (1973).
7. Gault, F.G., Adv. Catal. 30, 1-95 (1981).
8. Maire, G.L.C., Garin, F.G., in: Catalysis - Science and Technology (J.R. Anderson, M. Boudart, Eds.), Vol. 6, Springer-Verlag, Berlin, Heidelberg, New York, Tokyo, 1984, pp. 161-226.
9. Weitkamp, J., in: Hydrocracking and Hydrotreating (J.W. Ward, S.A. Qader, Eds.), ACS Symp. Ser. 20, American Chemical Society, Washington, D.C., 1975, pp. 1-27.
10. Christoffel, E.G., Paál, Z., J. Catal. 73, 30-44 (1982).
11. Schulz, H.F., Weitkamp, J., Ind. Eng. Chem., Prod. Res. Dev. 11, 46-53 (1972).
12. Weitkamp, J., Ind. Eng. Chem., Prod. Res. Dev. 21, 550-558 (1982).
13. Steijns, M., Froment, G., Jacobs, P.A. Uytterhoeven, J., Weitkamp, J., Erdöl, Kohle - Erdgas - Petrochem. 31, 581 (1978).
14. Brouwer, D.M., Oelderik, J.M., Rec. Trav. Chim. Pays-Bas 87, 721-736 (1968).
15. Chevalier, F., Guisnet, M., Maurel, R., Proc. 6th Intern. Congr. Catalysis (G.C. Bond, P.B. Wells, F.C. Tompkins, Eds.), Vol. 1, The Chemical Society, London, 1977, pp. 478-487.
16. Weitkamp, J., Proc. 9th Iberoamerican Symp. Catalysis, Lisbon, July 16-21, 1984, Vol. 2, pp. 1332-1341.
17. Haag, W.O., Dessau, R.M., Proc. 8th Intern. Congr. Catalysis, Vol. 2, Verlag Chemie, Weinheim, Deerfield Beach, Basel, 1984, pp. 305-316.

ALKYLATION OF HYDROCARBONS WITH ZEOLITE CATALYSTS - COMMERCIAL APPLICATIONS AND MECHANISTIC ASPECTS

J. WEITKAMP
Engler-Bunte Institute, Division of Gas, Oil, and Coal, University of Karlsruhe, D-7500 Karlsruhe 1, Federal Republic of Germany

ABSTRACT

HZSM-5 zeolite is now used commercially in the Mobil-Badger process for alkylation of benzene with ethylene. Due to the relatively high temperature (ca. 400 °C) and the shape selective catalyst, the chemistry and the by-products differ substantially from those in conventional ethylbenzene processes. The shape selective alkylation of toluene with ethylene in modified HZSM-5 gives para-ethyltoluene which is a raw material for poly-para-methylstyrene, a competitor for polystyrene which waits for its acceptance in the polymer industry. Selective side chain alkylation of toluene with methanol on basic faujasites, especially CsX, leads to a mixture of styrene and ethylbenzene. Brönsted acid faujasites in a fresh state are able to catalyze the alkylation of i-butane with light olefins. However, side reactions inevitably lead to carbonaceous deposits which bring about a deterioration of the catalytic performance: After a relatively short time on stream, the zeolite no longer alkylates i-butane; instead, it oligomerizes the olefins.

INTRODUCTION

Alkylation is best defined as the generation of an alkyl group, usually at a C, O, N, or S atom, in an arbitrary substrate. Typical alkylating agents are alkenes, alcohols, alkyl halides, and esters. The new bond may be formed by an addition, insertion, or substitution type of reaction. It is evident that such a definition covers a vast number of organic reactions, the mechanisms of which may differ substantially from each other. Indeed, alkylations may proceed via carbocations, via carbanions, via radicals or via transition metal complexes.

In practice, alkylations via carbocations play by far the most important role. They are catalyzed by acids: In petroleum refining, alkylation of i-butane with light olefins is widely used to produce

high octane gasoline. Since many decades, the commercial processes have been relying on liquid catalyst systems, viz. H_2SO_4 or HF. In petrochemistry, various aromatic raw materials are upgraded by alkylation. In particular, benzene is alkylated with ethylene, propene or a mixture of C_{10} to C_{20} alkenes to manufacture ethylbenzene, cumene, and linear alkylbenzenes, respectively. In almost all these processes, either so-called Friedel-Crafts type catalysts, e.g., $AlCl_3/HCl$, or one of the above-mentioned liquid acids are traditionally employed [1]. However, some years ago, HZSM-5 zeolite has been introduced on a commercial scale as a catalyst for benzene/ethylene alkylation.

Without any doubt, there is additional commercial potential for *acid* zeolite catalysts. Among their principal advantages over conventional acids are (i) the easy recovery of products, (ii) the regenerability, (iii) the lack of corrosiveness, (iv) the absence of noxious or environmentally hazardous streams, and (v) the possibility of shape selective alkylation. Furthermore, *basic* zeolites are attractive catalysts because they enable selective side chain alkylation in alkylaromatics.

In the present article, the industrial use of zeolites as alkylation catalysts will be reviewed. Moreover, mechanistic aspects of alkylation will be discussed with emphasis on zeolites as catalysts. For space reasons, the discussion will be confined to alkylation of hydrocarbons.

ALKYLATION OF AROMATICS

Ethylbenzene, the Mobil-Badger process. Ethylbenzene is the key intermediate in the manufacture of styrene which is one of the most important industrial monomers. Almost all ethylbenzene is synthesized from benzene and ethylene, the worldwide capacity amounting to ca. $10 \cdot 10^6$ t/a.

In the conventional ethylbenzene technology, liquid phase and gas phase processes are usually distinguished. In the liquid phase processes, $AlCl_3/HCl$ is the most widely used catalyst. The temperatures and pressures are 90 to 150 °C and 1 to 10 bar, respectively. In the gas phase processes, solid catalysts such as SiO_2-Al_2O_3 (Koppers), H_3PO_4/SiO_2 (UOP), or BF_3/Al_2O_3 (UOP, Alkar process) are employed. The temperatures are around 300 °C and the pressures above 50 bar.

In 1976, the Mobil-Badger ethylbenzene process was announced [2]. It is based on HZSM-5 zeolite [3] modified, perhaps, by phosphorus [4]. The first commercial unit with a capacity of 500000 t/a went on stream in 1980 at the American Hoechst Corp., Bayport, Tex. Somewhat earlier

the process was implemented at Cosden Oil & Chemical Co., Big Spring, Tex., by revamping an idle Alkar unit [5]. A simplified flow sheet of the Mobil-Badger process is depicted in Fig. 1.

Alkylation is carried out in the gas phase at ca. 400 °C and 20 bar. The molar benzene/ethylene ratio in the feed is 6 to 7. The heat of reaction (ca. 100 kJ/mol) is removed by injection of cold reactants between the catalyst beds. The conversion of ethylene is 100 %. During alkylation, coke deposits slowly onto the catalyst. For regeneration, the deposits are burnt periodically, hence at least two reactors are required for a continuous operation of the plant. The cycle length between successive regenerations is in the order of one to several weeks. In the separation section, excess benzene is first recovered for recycle. Ethylbenzene is then separated from the heavier by-products. In the final column, a diethylbenzene cut is removed from the heavy ends. Upon recycling, the diethylbenzenes undergo transalkylation with benzene, whereby additional ethylbenzene is formed.

Compared to conventional liquid phase processes, the Mobil-Badger process offers all the aforementioned advantages. It is, moreover, energy efficient since the heat of reaction is recovered at a high temperature level. Although hardly any yield data have been published by the licensors, it is known [3] that the nature and concentrations of by-products differ substantially from those encountered in conventional ethylbenzene processes. In the latter, polyethylbenzenes (up to hexaethylbenzene) are typically formed by multiple alkylation. It is very unlikely that, inside the shape selective ZSM-5 catalyst, the bulky

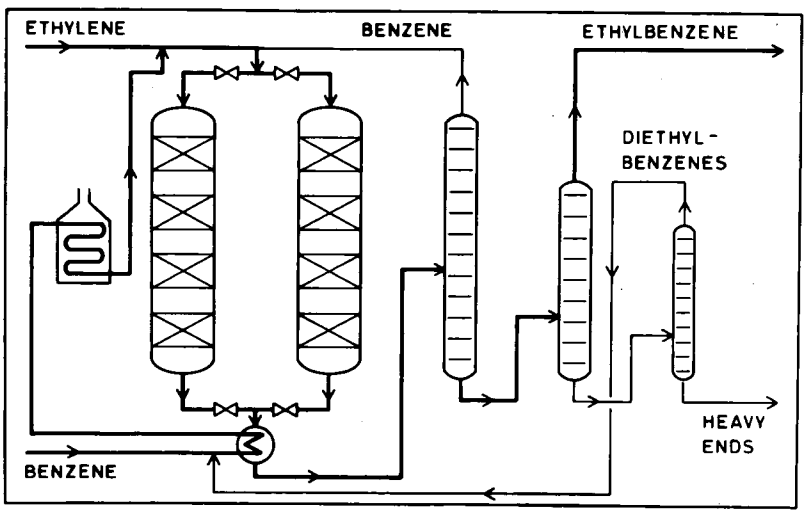

Fig. 1. The Mobil-Badger ethylbenzene process.

polyethylbenzenes with three or more ethyl groups form. Nor could such bulky products diffuse out of the pentasil pore system. On the other hand, certain by-products do occur in the Mobil-Badger process which do not normally play a significant role in the conventional processes, viz. alkylaromatics with side chains other than ethyl groups. Even toluene and xylenes are formed, especially at elevated temperatures [4]. Possible reaction paths which lead to such by-products will be discussed below.

Of utmost importance for the commercial success of HZSM-5 zeolite was its low tendency to build up coke deposits. Probably, the rapid coking of acid faujasites and mordenites, especially when in contact with olefins, prevented such large pore zeolites from attaining commercial acceptance as catalysts in alkylation of aromatics.

Para-ethyltoluene. Toluene is a less expensive raw material than benzene, and the price gap between the two aromatics has been steadily widening over the past decade. Hence, there is an increasing incentive for replacing benzene by toluene. In principle, the whole chemistry from benzene to polystyrene (alkylation with ethylene, dehydrogenation, polymerization) can be based on toluene as well. However, the acid catalyzed alkylation of toluene with ethylene gives a mixture of ortho-, meta-, and para-ethyltoluene. During the subsequent dehydrogenation, part of the ortho isomer undergoes cyclization to indane and indene. These impurities are difficult to remove from the vinyltoluene monomer and deteriorate the final polymer.

All these problems can be avoided by alkylating toluene in a shap selective catalyst which prevents the formation of the bulky ortho-ethyltoluene. Unmodified HZSM-5 zeolite still gives the three isomers, essentially in their equilibrium distribution [6]. However, by modifying HZSM-5 with certain reagents, para-ethyltoluene is formed almost exclusively, together with minor amounts of the meta isomer. Suitable modifyers contain P, Ca/P, Mn/P, B/P, B/Mg, or Si [6]. It has been proposed [7] that they bring about subtle changes in the effective pore width of the zeolite.

Pure para-ethyltoluene can be readily dehydrogenated to para-methylstyrene [8]. Polymerization of the latter gives poly-para-methylstyrene which has been claimed to be superior to conventional polystyrene [8-10], at least for some applications.

In 1982, an idle styrene facility at American Hoechst Corp., Baton Rouge, La., was reactivated for the manufacture of para-methylstyrene [10,11]. Its capacity is low (16000 t/a). It remains to be seen whether poly-para-methylstyrene and, hence, shape selective alkylation

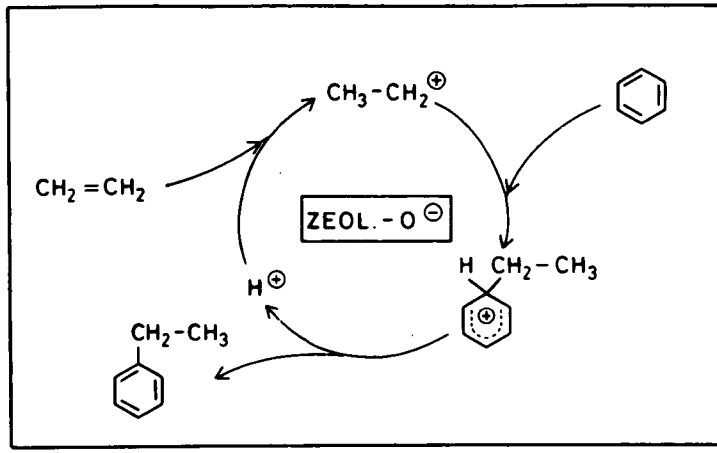

Fig. 2. Mechanism of acid catalyzed alkylation of an aromatic hydrocarbon with an alkene.

of toluene with ethylene will be accepted on a large scale by the polymer industry.

Mechanistic aspects of acid catalyzed alkylation of aromatics. It has been repeatedly demonstrated, e.g. in ref. [12], and re-emphasized recently [13] that Brönsted OH groups are the active sites for hydrocarbon conversion in acid zeolites. The generally accepted mechanism of benzene/ethylene alkylation is shown in Fig. 2. Protonation of the alkene at the acid site gives an alkylcarbenium ion. Its electrophilic attack on the aromatic Π-electrons results in a benzenium cation which re-aromatizes by loss of a proton. While the Brönsted sites is restored, the alkylated hydrocarbon desorbs.

It is clear that, in any ethylbenzene process the monoalkylated product can again enter the catalytic cycle. This way, polyethylbenzenes are formed at high olefin conversions. An alternative pathway for their formation is the acid catalyzed transalkylation, e.g., of ethylbenzene into diethylbenzenes and benzene. In HZSM-5 this reaction has been shown [14] to proceed readily above 250 °C, probably by a pure Streitwieser-Reif mechanism [15] via diphenylmethane type carbocations. This same mechanism then accounts for the reverse reaction, i.e., transalkylation of diethylbenzenes (which are recycled in the Mobil-Badger process, cf. Fig. 1) with benzene into the desired ethylbenzene. Due to steric constraints, very little, if any, polyethylbenzenes with three or more ethyl groups will be formed *inside* the ZSM channel system.

As pointed out earlier, alkylaromatics can be formed in the Mobil-Badger process, which contain C_3, C_4 or even higher side chains. A good

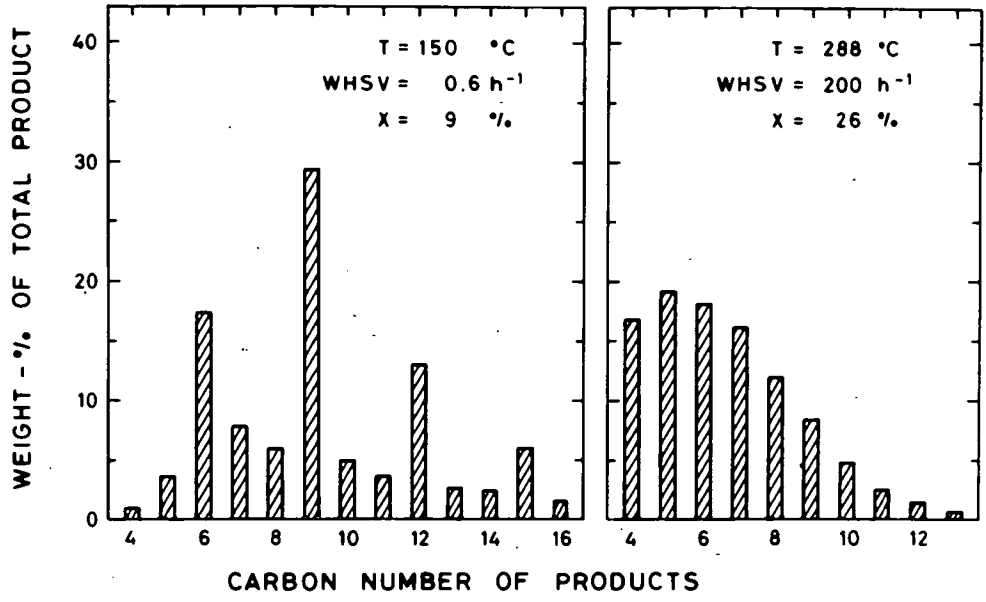

Fig. 3. Products from the conversion of propene in HZSM-5, after [18].

explanation for their occurrence emerged recently from model studies on the conversion of olefins in HZSM-5 [16-18]. Haag [18] published product distributions obtained from propene at different temperatures but comparable conversions (Fig. 3). At 150 °C, true oligomers (C_6H_{12}, C_9H_{18}, $C_{12}H_{24}$, $C_{15}H_{30}$) predominate. At 288 °C, by contrast, there is no indication at all for a common C_3 source. Rather, a pool of olefins is formed with a carbon number distribution governed by a temperature and pressure dependent pseudo-equilibrium [18]. The olefins are interconverted by ionic oligomerization and cracking. Ethylene, though less reactive than propene, gave essentially the same result [17]. Hence, some propene, butenes and, perhaps, even higher alkenes will form in the Mobil-Badger process and eventually take part in the alkylation of aromatics. It appears that the existence of a pool of olefins with different carbon numbers also provides a key to the mechanism of the methanol-to-hydrocarbons conversion in HZSM-5 [18] and related materia [19].

Still other mechanisms must be invoked to account for the formati of *methyl*aromatics in the Mobil-Badger process. It is likely that the methyl groups arise from cracking of C_2, C_3, C_4, or other alkyl chains at elevated temperatures. One possible mechanism is acid catalyzed cra ing via non-classical carbonium ions. For paraffinic substrates, it has recently been claimed [20] that such a mechanism is favored both b

the steric constraints in pentasils and by high temperatures. Alternatively, thermal cracking via free radicals might occur at the zeolite surface [21].

Coke is inevitably formed as a by-product in almost all hydrocarbon reactions on acid catalysts. The low rate of coke formation in HZSM-5 is nowadays interpreted in terms of restricted transition state shape selectivity [22,23]. For a detailed discussion of coke formation and its inhibition in medium pore zeolites, the reader is referred to the excellent reviews by Csicsery [24] and Derouane [25].

Beside olefins, various alcohols have been used in numerous investigations to alkylate aromatic hydrocarbons on acidic zeolites. Methanol as an alkylating agent enables the introduction of a *methyl* group (no olefin is available for this purpose). As with olefins (Fig. 2), the reaction is envisaged [26,27] to proceed via protonation of the alkylating agent followed by electrophilic attack of the resulting cation on the aromatic ring. By use of suitable zeolites, alkylation with alcohols can be conducted in a shape selective manner. For instance, more than 90 mol-% of p-xylene (as compared to ca. 25 mol-% in equilibrium) were obtained from toluene and methanol in HZSM-5 modified with P or B [27,28].

Base catalyzed side chain alkylation of toluene with methanol. On acid catalysts, alkylation inevitably occurs at the aromatic ring which is easily understood in terms of the high electron density at this location (cf. Fig. 2). By contrast, alkylation in the side chain of alkylaromatics can be attained on basic catalysts. In recent years, particular attention has been paid to the side chain alkylation of toluene with methanol which leads to styrene and ethylbenzene (in a rigorous sense, only the formation of ethylbenzene represents a true alkylation). The commercial incentive stems from using toluene, instead of the more expensive benzene, as a raw material for the production of styrene.

Faujasite type zeolites exchanged with large alkali cations, especially RbX and CsX, were found to be the most effective catalysts for toluene/methanol side chain alkylation [29-33]. Special care must be taken during their preparation to eliminate acid sites, otherwise ring alkylation interferes [33]. Boron oxide acts as a promoter [30,32,34] which enhances the selectivity for styrene/ethylbenzene. Typically, the reaction temperatures are around 400 °C.

The precise nature of the basic sites in CsX is not clear. It has been suggested [35] that they consist of Cs_2O and metallic Cs formed by reduction of Cs_2O with carbonaceous residues. Interaction of toluene

with a free basic site gives a carbanion. The new carbon-carbon bond is then generated by addition of this carbanion to formaldehyde which results from dehydrogenation of methanol. The 2-phenylethanol type intermediate is dehydrated to styrene which is either desorbed or hydrogenated to ethylbenzene. An undesirable side reaction is the decomposition of formaldehyde into CO + H_2.

It has been argued [30,32] that the role of the large alkali cations in the supercages of zeolite X is twofold: They strongly interact with the Π electron system of toluene. Moreover, due to their bulkiness and relatively high concentration, they occupy a considerable portion of the free space within the faujasite supercage. In such an environment, toluene is envisaged to be adsorbed with the ring residing between two or more cesium cations. This way, the aromatic portion of the molecule is shielded and the attack of formaldehyde on the side chain is favored. If this picture is correct, then the toluene/methanol reaction in CsX represents a unique example for shape selectivity in faujasites. The boron oxide promoter inhibits the undesired decomposition of formaldehyde.

ALKYLATION OF ISOBUTANE

Its place in petroleum refining, stoichiometry of the reaction. Fluid catalytic cracking (FCC) is used in many refineries to produce gasoline from vacuum distillates. With modern zeolite catalysts, the gasoline yields in FCC are slightly above 50 wt.-%. Besides, some 15 wt.-% of C_3 and C_4 hydrocarbons are formed. The main constituents of this side stream are i-butane, butenes, and propene. Additional high octane gasoline can be manufactured by alkylation of i-butane with the mixed butenes and/or propene. Today, the worldwide capacity for alkylation gasoline amounts to nearly $50 \cdot 10^6$ t/a.

Isobutane/olefin alkylation cannot be described adequately by a simple stoichiometric equation. Alkylate *always* consists of a comple mixture of i-alkanes ranging from C_5 to ca. C_{12}. Typical carbon number distributions are listed in Table 1. It will be shown later that all possible i-alkanes with at least one tertiary carbon atom are usually formed.

The conventional liquid phase processes. In the commercial processes, liquid acids, viz. concentrated H_2SO_4 or anhydrous HF, are used exclusively. Today, the installed capacities of the H_2SO_4 and HF processes are roughly equal, with a trend towards HF alkylation [36].

The reaction is carried out at low temperatures (5 to 10 °C in H_2SO_4, 25 to 40 °C in HF) and moderate pressures, such as to keep the

Table 1

Alkylation of i-butane with butenes. Typical product distributions in wt.-%, after [36].

		H_2SO_4-process	HF-process
"Light ends":	i-C_5H_{12}	8	5
	i-C_6H_{14}	7	4
	i-C_7H_{16}	6	4
	i-C_8H_{18}	64	74
"Heavy ends":	i-C_9H_{20} and higher	15	13

hydrocarbons liquid. The i-butane/olefin ratio in the feed is very high (10 to 20) in order to suppress undesirable side reactions of the olefins. An efficient removal of the heat of reaction is essential. Even under optimum process conditions, some tarry by-products are formed, especially in the H_2SO_4 processes. Propane and n-butane are completely inert.

Although the liquid phase processes have been operated successfully for decades, they are not free from drawbacks and shortcomings. Among these are the corrosiveness and toxicity of HF and the large amounts of tarry by-products formed in H_2SO_4 which are difficult to dispose of in an environmentally acceptable way. A viable and clean process based on a solid catalyst remains highly desirable.

Attempts to use zeolite catalysts. The principal feasibility of i-butane/olefin alkylation on acid faujasites was demonstrated as early as 1968 in the open literature: Mobil researchers published a note on i-butane/ethylene alkylation over deammoniated ammonium/rare earth X zeolite [37]. Much more detailed information was released by the group at Sun Oil Co. [38-42]. They alkylated i-butane with a variety of olefins, mostly on deammoniated ammonium/rare earth Y zeolite. In subsequent years, the fundamentals of the reaction were investigated by a relatively small number of academic groups [43-53]. The contributions of Schöllner et al. [43-46] and the recent papers by Daage and Fajula [52,53] deserve particular attention.

It emerges from all these studies that faujasites in a Brönsted acid form indeed give product distributions with all features of alkylate produced in H_2SO_4 or HF. Typical carbon number distributions of i-butane/n-butene alkylation (1-butene, cis-2-butene, and trans-2-

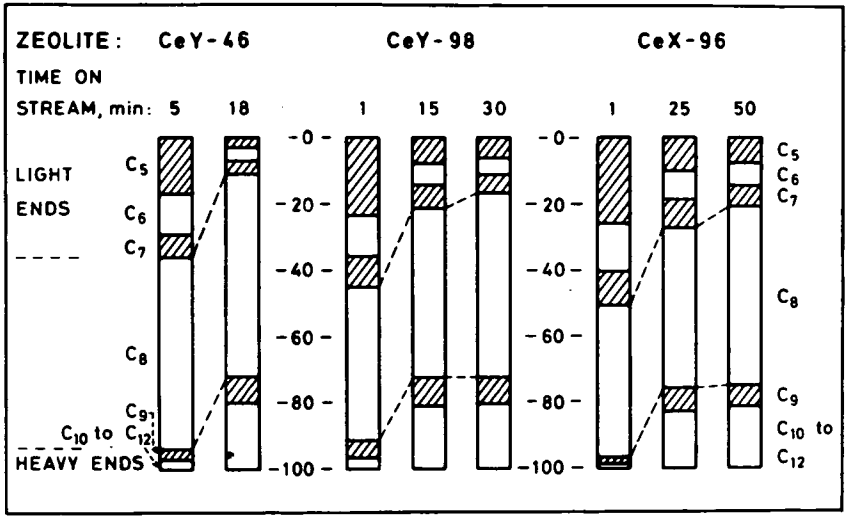

Fig. 4. Alkylation of i-butane with n-butenes on cerium exchanged faujasites ($\dot{n}_{i\text{-butane}} : \dot{n}_{butene} = 11 : 1$, fixed bed reactor, $m_{CeY\text{-}46} = 1.1$ g, $m_{CeY\text{-}98} = 1.4$ g, $m_{CeX\text{-}96} = 1.5$ g, T = 80 °C, P = 3.1 MPa, liquid feed rate = 7.5 cm³/h, [50,51]). Carbon number distributions in wt.-%.

butene give identical results) over cerium exchanged faujasites are shown in Fig. 4. The degree of cerium exchange is given in equiv.-%. All products are i-alkanes. As in H_2SO_4 or HF (cf. Table 1), a complex mixture of i-alkanes with 5 to 12 carbon atoms is formed. In all cases, i-octanes predominate. It is, moreover, seen that the carbon number distributions depend upon the time on stream: As the reaction proceeds, more heavy ends are produced at the expense of the light end (C_5H_{12} to C_7H_{16}).

Distributions of individual isomers in various alkylates are giv in Table 2. The data are limited to the C_5 through C_8 fractions becaus an individual analysis of the C_9 to C_{12} i-alkanes is not feasible, eve with the most powerful GC techniques. The data for the zeolite catalys are considered to be more reliable than those for the liquid acids. As a whole, it is evident that the same hydrocarbons form in H_2SO_4, HF, and acid faujasites: All i-alkanes with at least one tertiary carb atom are present (although sometimes in traces only). Conversely, all alkanes lacking tertiary carbon atoms (e.g., n-alkanes, 2,2-dimethylbu tane, 3-ethyl-3-methylpentane, or 2,2,3,3-tetramethylbutane) are absent Some apparent violations of this rule are probably due to n-pentane im- purities in the feed and analytical difficulties in the experiments with the liquid acids.

Table 2

Alkylation of i-butane with butenes (technical C_4 cut for H_2SO_4 and HF, pure n-butenes for zeolite catalysts). Isomer distributions in mol-%, after [36,50,51].

Catalyst	H_2SO_4	HF	CeY-46	CeY-98			CeX-96
Time on stream, min	-	-	8	1	15	30	25
n-Pn	3	0	0	0	0	0	0
2-M-Bu	97	100	100	100	100	100	100
2,2-DM-Pr	0	0	0	0	0	0	0
n-Hx	0	0	0	0	0	0	0
2-M-Pn	17	25	12	15	19	17	19
3-M-Pn	9	11	45	22	23	27	20
2,2-DM-Bu	0	0	0	0	0	0	0
2,3-DM-Bu	74	64	43	63	58	56	61
n-Hp	0	0	0	0	0	0	0
2-M-Hx	3	6	6	6	8	6	9
3-M-Hx	2	3	15	7	11	11	12
3-E-Pn	0	0	3	1	1	2	1
2,2-DM-Pn	4	4	0	0	0	0	0
2,3-DM-Pn	34	35	60	29	39	42	39
2,4-DM-Pn	57	52	13	51	38	35	36
3,3-DM-Pn	0	0	0	0	0	0	0
2,2,3-TM-Bu	0	0	3	6	3	4	3
n-Oc	0	0	0	0	0	0	0
2-M-Hp	0.1	0.1	0.1	0.2	0.3	0.2	0.5
3-M-Hp + 3-E-Hx	0.4	0.3	0.3	0.4	0.8	0.8	1.1
4-M-Hp	0	0	0.2	0.1	0.2	0.1	0.3
2,2-DM-Hx	0	0	0	0	0	0	0
2,3-DM-Hx	6	7	10	5	13	12	14
2,4-DM-Hx	5	6	4	6	7	5	8
2,5-DM-Hx	8	5	0.3	3	4	2	5
3,3-DM-Hx	0	0	0	0	0	0	0
3,4-DM-Hx*)	0.4	0.8	45	7	14	24	10
3-E-2-M-Pn	0	0	2	1	1	2	1
3-E-3-M-Pn	0	0	0	0	0	0	0
2,2,3-TM-Pn	2	2	4	4	3	3	3
2,2,4-TM-Pn	39	53	4	22	18	12	22
2,3,3-TM-Pn	18	12	16	28	21	20	20
2,3,4-TM-Pn	21	14	14	23	18	19	15
2,2,3,3-TtM-Bu	0	0	0	0	0	0	0

*) both diastereomers

The main constituents of the i-octane fraction are trimethylpentanes (except 2,2,3-trimethylpentane). From a technical point of view, these highly branched isomers are the most desirable products since their octane numbers are very high (around 100). In addition, considerable amounts of dimethylhexanes always occur. Note that the content of 3,4-dimethylhexane may vary over a broad range: In the liquid acids, it is formed in negligible amounts. On CeY-46 (with a low density and, presumably, a low strength of acid sites), by contrast, 3,4-dimethylhexane is by far the most abundant i-octane. The data for CeY-98 further reveal that the content of 3,4-dimethylhexane increases significantly with time on stream. All these results suggest that 3,4-dimethylhexane is a key isomer with a mechanism of formation which deviates from the desirable pathway of alkylate production.

Up to this point, the discussion was restricted to the catalytic behavior of zeolites *in a fresh state*. At low times on stream, alkylation is extremely selective, no olefins, naphthenes or aromatics are formed, even not in traces. During this initial *alkylation stage* the conversion of the feed olefin is always 100 %, regardless of the reaction conditions.

After a certain time on stream, the alkylation stage ends. At this point, butenes begin to appear (Fig. 5), i.e., the olefin conversion drops. Concomitantly, more and more alkenes occur in the C_5 to

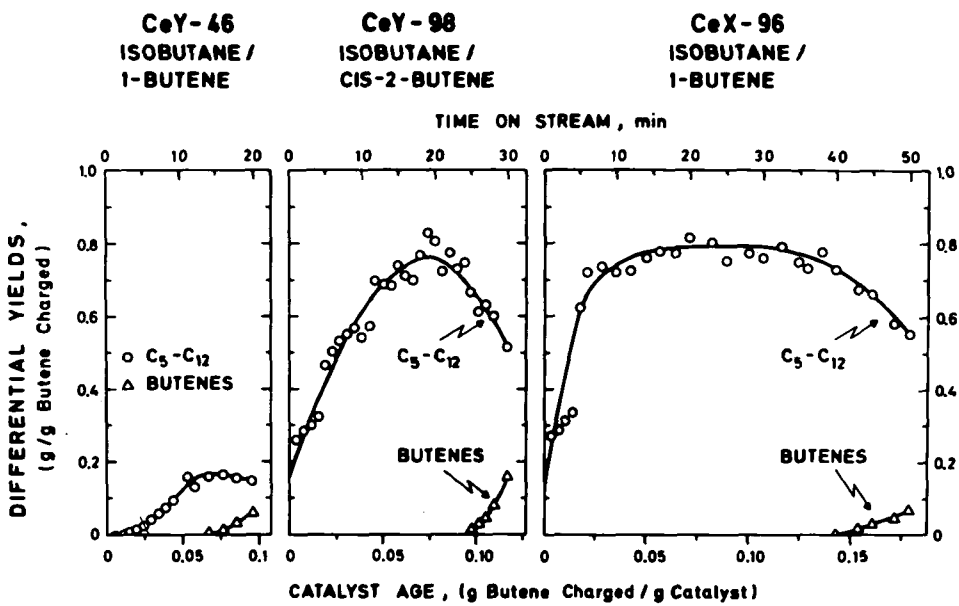

Fig. 5. Differential yields in alkylation of i-butane with n-butenes on Ce faujasites at 80 °C, after [51].

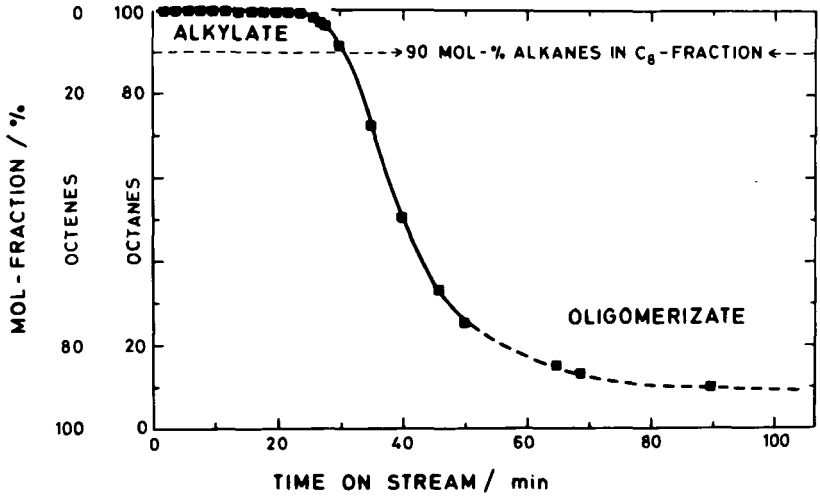

Fig. 6. Isobutane/cis-2-butene conversion on CeY-98. Composition of the C_8 products, after [51].

C_{12} products. This is shown quantitatively in Fig. 6 for the C_8 fraction produced on CeY-98. It can be seen that, late in the run, the C_8 fraction mostly consists of octenes (in this section, the curve is dashed which is to indicate that the analytical accuracy is relatively low). In other words, the reaction is now better described in terms of butene dimerization or oligomerization. The dramatic shift in selectivity is due to catalyst aging. It is convenient to use the composition of the C_8 fraction [51] as a quantitative measure for the duration of the alkylation stage. Arbitrarily, we define the end of the alkylation stage as the particular time on stream at which the content of alkanes in the C_8 fraction has dropped to 90 mol-% (30 min on CeY-98, according to Fig. 6).

A stationary state is never attained in i-alkane/alkene alkylation on faujasite catalysts, at least not in a fixed bed reactor. An adequate investigation of this reaction requires experimental techniques which cope with the simultaneous occurrence of complex product distributions and rapid catalyst decay. One appropriate technique has been described [49-51]. It combines differential (or instantaneous) sampling in glass ampoules with high resolution capillary GLC. If, moreover, an internal standard (such as propane or 2,2-dimethylbutane) is added to the feed mixture in a known concentration, then the analysis of each differential sample can be evaluated for the olefin conversion, the yields of individual products, and other quantities. Differential yields obtained in this manner are plotted in Fig. 5 and Fig. 7 versus

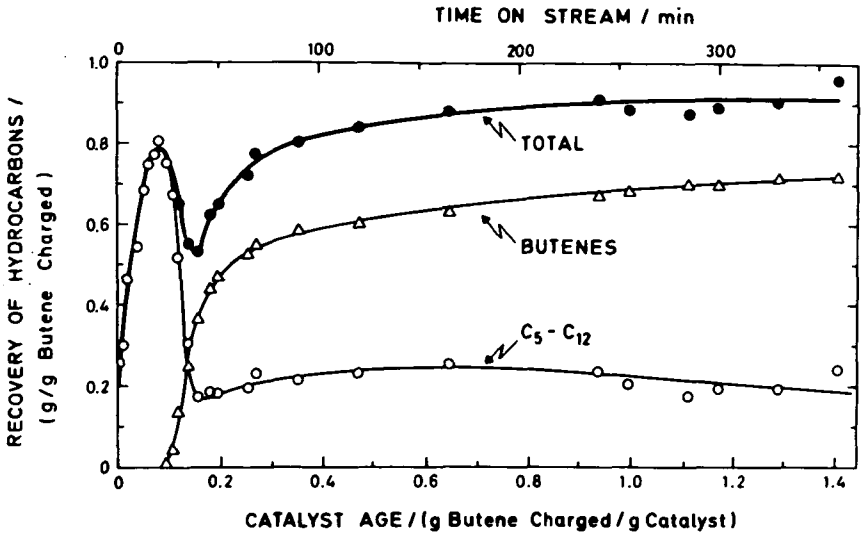

Fig. 7. Isobutane/cis-2-butene conversion on CeY-98. Differential yields of butenes and C_5 to C_{12} hydrocarbons, after [51].

time on stream. In both Figures, a second abscissa referred to as catalyst age [40] is used. It is defined as the cumulative mass of butene fed to the reactor per unit mass of catalyst. Catalyst age is proportional to time on stream. It is seen that the differential yield of C_5 to C_{12} hydrocarbons passes through a maximum. Late in the run, the total yield approaches 1 g/g butene charged.

In Fig. 5, the differential yield curves end at the respective time on stream, at which the content of i-octanes in the C_8 fraction has dropped to 90 mol-%. Integration of the C_5–C_{12} curves gives the following *integrated yields of alkylate*: 9, 70, and 125 mg alkylate/g catalyst for CeY-46, CeY-98, and CeX-96, respectively. For deammoniated ammonium/rare earth Y, the Sun Oil group [40] reported values which are better by one or two orders of magnitude (a continuous stirred tank reactor was employed and a different quality criterion for alkylate was chosen, so a direct comparison of the figures cannot be made). For a commercial process, such yields of alkylate are unacceptably low. The development of acid zeolites with much higher lifetimes in i-butane/olefin alkylation remains a challenge in the field of catalysis.

Mechanistic aspects. Almost always, the mechanism of i-butane/olefin alkylation is interpreted in terms of a chain reaction which is delineated in Fig. 8 for linear butenes. Protonation of the olefin gives the secondary butyl cation. Hydride transfer from i-butane then leads to n-butane and the tertiary butyl cation. These steps are considered

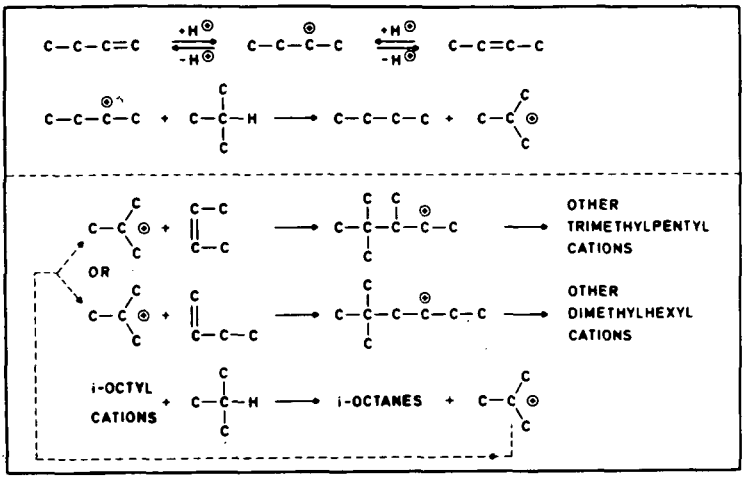

Fig. 8. Classical mechanism of i-butane/n-butene alkylation.

to initiate the kinetic chain only, hence the fact that virtually no n-butane occurs in the product is not a contradiction. Double bond shift in the alkene is considered to be rapid, therefore the tertiary butyl cation can add either 1-butene or 2-butene (which is much more abundant in equilibrium), regardless of which n-butene isomer is used in the feed. The original octyl cations formed in the addition step can rearrange whereby a variety of dimethylhexyl and trimethylpentyl cations are generated. Hydride transfer between the i-octyl cations and i-butane yields a mixture of i-octanes and the tertiary butyl cation which propagates the chain.

One important difference between the alkylation of aromatics and i-butane becomes evident from a comparison of Fig. 2 and Fig. 8: In alkylation of aromatics, the intermediate carbocation stabilizes by *loss of a proton*. By contrast, *transfer of a hydride ion* is required to produce the desired i-alkanes from alkylcarbenium ions. Of course, the latter can also stabilize by loss of a proton, but then olefins are formed, i.e., the overall reaction is olefin oligomerization instead of alkylation. It is likely that, at the relatively low temperatures around 100 °C, strong acid sites are needed to catalyze hydride transfer. These sites are soon deactivated by carbonaceous deposits.

While the classical mechanism (Fig. 8) provides a straightforward interpretation of the events which might lead to i-octanes, it suffers from severe shortcomings. For example, it does not give any explanation for the fact that alkylate always contains i-alkanes with carbon numbers other than the sum of the i-alkane and the olefin used in the feed.

Moreover, the skeletal isomerization steps postulated at the level of trimethylpentyl and dimethylhexyl cations (cf. Fig. 8) are in poor agreement with the knowledge collected in the field of catalytic isomerization of long-chain alkanes. In the first place, it is doubtful whether such isomerization steps are catalyzed at all by zeolites *at the low temperatures* employed. In addition, it is difficult to understand why so little 2,2,3-trimethylpentane is formed from i-butane and n-butanes (cf. Table 2) whereas this particular isomer is predicted to be the primary i-octane (cf. Fig. 8). Compilations of thermodynamic data [54] do not give any indication for an unfavorable equilibrium. To account for these and other inconsistencies, a variety of side reactions have been invoked [55-57]. Among these are the so-called destructive alkylation and self-alkylation of i-butane. Another side reaction which leads from n-butenes to 3,4-dimethylhexane seems to be important in faujasites: If the secondary butyl cation adds 2-butene, then a 3,4-dimethylhexyl cation results. Hydride transfer gives 3,4-dimethylhexane. According to Table 2, this pathway is important on CeY-46 and on CeY-98 at high times on stream.

New insight into the H_2SO_4 catalyzed i-butane/olefin alkylation was gained by Albright et al. in the 1970's. By using sophisticated experimental techniques, these authors showed that the mechanism is extremely complex. The most important ideas were summarized by Albright [58]. Many of these ideas are probably very useful for a better understanding of alkylation in zeolites. In particular, Albright et al. suggest that high molecular weight carbocations and hydrocarbons play a much more important role in the mechanism than hitherto assumed. There is no clear borderline between such species and the carbonaceous residues. The latter are envisaged by Schöllner et al. [43] to consist of highly unsaturated hydrocarbons with cyclic structures.

Daage and Fajula [52,53] introduced the ^{13}C tracer technique to investigate the mechanism of i-butane/propene alkylation on deammoniated ammonium/cerium Y. Either i-butane or the alkene were labelled. A wealth of novel insight into the reaction mechanism was achieved. Among the most interesting conclusions are: There is little, if any, isomerization of tertiary carbocations, because stabilization of a tertiary alkylcarbenium ion by hydride transfer is faster than skeletal rearrangement. The authors divide the constituents of alkylate into four classes. Different mechanisms of formation are sketched for each class. There is no doubt that further application of the ^{13}C tracer technique can contribute to a better understanding of the extremely complex chemistry of i-butane/olefin alkylation, both in liquid acids and in zeolites.

ACKNOWLEDGEMENTS

The contributions of Mr. Wilfried Stober in the experiments on i-butane/olefin alkylation on zeolite catalysts are highly appreciated. Generous financial support of these studies by the German Science Foundation (Deutsche Forschungsgemeinschaft) and Fonds der Chemischen Industrie are gratefully acknowledged.

SYMBOLS AND ABBREVIATIONS

m	mass	kg
$\dot{m}$	mass flux	$kg \cdot h^{-1}$
$\dot{n}$	molar flux	$mol \cdot h^{-1}$
P	pressure	Pa
T	reaction temperature	°C
WHSV	weight hourly space velocity ($\dot{m}_{feed}/m_{catalyst}$)	h^{-1}
X	conversion	

D	di	Pr	propane
T	tri	Bu	butane
Tt	tetra	Pn	pentane
		Hx	hexane
M	methyl	Hp	heptane
E	ethyl	Oc	octane

REFERENCES

1. Keim, W., Röper, M., in: Ullmann's Encyclopedia of Industrial Chemistry, 5th Ed., Vol. A1, VCH Verlagsgesellschaft, Weinheim, Deerfield Beach, Basel, 1985, pp. 185-220.
2. Dwyer, F.G., Lewis, P.J., Schneider, F.H., Chem. Eng. 83 (No. 1, Jan. 5), 90-91 (1976).
3. Dwyer, F.G., in: Catalysis of Organic Reactions (W.R. Moser, Ed.), Marcel Dekker, Inc., New York, Basel, 1981, pp. 39-50.
4. Hölderich, W., Gallei, E., Chem.-Ing.-Tech. 56, 908-915 (1984).
5. Lewis, P.J., Dwyer, F.G., Oil Gas J. 75 (No. 39, Sept. 26), 55-58 (1977).
6. Kaeding, W.W., Young, L.B., Chu, C.-C., J. Catal. 89, 267-273 (1984).
7. Védrine, J.C., Auroux, A., Dejaifve, P., Ducarme, V., Hoser, H., Zhou, S., J. Catal. 73, 147-160 (1982).

8. Kaeding, W.W., Young, L.B., Prapas, A.G., Chemtech 12, 556-563 (1982).
9. Kaeding, W.W., Young, L.B., Prapas, A.G., Preprints, Div. Fuel Chem., Am. Chem. Soc. 28 (No. 2), 158-162 (1983).
10. Anonymous, Chem. Week, Febr. 17, 1982, pp. 42-46.
11. Kaeding, W.W., Phillips, D.D., Preprints, Div. Petr. Chem., Am. Chem. Soc. 28, 1090 (1983).
12. Becker, K.A., Karge, H.G., Streubel, W.-D., J. Catal. 28, 403-413 (1973).
13. Haag, W.O., Lago, R.M., Weisz, P.B., Nature 309, 589-591 (1984).
14. Karge, H.G., Wada, Y., Weitkamp, J., Ernst, S., Girrbach, U., Beyer H.K., in: Catalysis on the Energy Scene (S. Kaliaguine, A. Mahay, Eds.), Studies in Surface Science and Catalysis, Vol. 19, Elsevier, Amsterdam, Oxford, New York, Tokyo, 1984, pp. 101-111.
15. Karge, H.G., Ladebeck, J., Sarbak, Z., Hatada, K., Zeolites 2, 94-102 (1982).
16. Anderson, J.R., Mole, T., Christov, V., J. Catal. 61, 477-484 (1980).
17. Garwood, W.E., in: Intrazeolite Chemistry (G.D. Stucky, F.G. Dwyer, Eds.), ACS Symp. Ser. 218, American Chemical Society, Washington, D.C., 1983, pp. 383-396.
18. Haag, W.O., Proc. 6th Intern. Zeolite Conf. (D. Olson, A. Bisio, Eds.), Butterworths, Guildford, 1984, pp. 466-478.
19. Hölderich, W., Eichhorn, H., Lehnert, R., Marosi, L., Mross, W., Reinke, R., Ruppel, W., Schlimper, H., Proc. 6th Intern. Zeolite Conf. (D. Olson, A. Bisio, Eds.), Butterworths, Guildford, 1984, pp. 545-555.
20. Haag, W.O., Dessau, R.M., Proc. 8th Intern. Congr. Catal., Vol. 2, Verlag Chemie, Weinheim, Deerfield Beach, Basel, 1984, pp. 305-316.
21. Poutsma, M.L., Schaffer, S.R., J. Phys. Chem. 77, 158-166 (1973).
22. Walsh, D.E., Rollmann, L.D., J. Catal. 56, 195-197 (1979).
23. Rollmann, L.D., Walsh, D.E., in: Progress in Catalyst Deactivation (J.L. Figueiredo, Ed.), Martinus Nijhoff Publishers, The Hague, Boston, London, 1982, pp. 81-91.
24. Csicsery, S.M., Zeolites 4, 202-213 (1984).
25. Derouane, E.G., in: Catalysis by Acids and Bases (B. Imelik et al., Eds.), Studies in Surface Science and Catalysis, Vol. 20, Elsevier, Amsterdam, Oxford, New York, Tokyo, 1985, pp. 221-240.
26. Coughlan, B., Carroll, W.M., Nunan, J., J. Chem. Soc., Faraday Trans. 1, 79, 297-309 (1983).
27. Kaeding, W.W., Chu, C., Young, L.B., Weinstein, B., Butter, S.A.,

J. Catal. 67, 159-174 (1981).
28. Nunan, J., Cronin, J., Cunningham, J., J. Catal. 87, 77-85 (1984).
29. Yashima, T., Sato, K., Hayasaka, T., Hara, N., J. Catal. 26, 303-312 (1972).
30. Freeman, J.J., Unland, M.L., J. Catal. 54, 183-196 (1978).
31. Itoh, H., Miyamoto, A., Murakami, Y., J. Catal. 64, 284-294 (1980).
32. Unland, M.L., Barker, G.E., in: Catalysis of Organic Reactions (W.R. Moser, Ed.), Marcel Dekker, Inc., New York, Basel, 1981, pp. 51-71.
33. Engelhardt, J., Szanyi, J., Jóvér, B., Proc. 9th Iberoamerican Symp. Catalysis, Vol. 2, Lisbon, July 16-21, 1984, pp. 1435-1444.
34. Sefcik, M.D., J. Am. Chem. Soc. 101, 2164-2170 (1978).
35. Garces, J.M., Vrieland, G.E., Bates, S.I., Scheidt, F.M., in: Catalysis by Acids and Bases (B. Imelik et al., Eds.), Studies in Surface Science and Catalysis, Vol. 20, Elsevier, Amsterdam, Oxford, New York, Tokyo, 1985, pp. 67-74.
36. Weitkamp, J., Maixner, S., Erdöl, Kohle - Erdgas - Petrochem. 36, 523-529 (1983).
37. Garwood, W.E., Venuto, P.B., J. Catal. 11, 175-177 (1968).
38. Kirsch, F.W., Potts, J.D., Barmby, D.S., Preprints, Div. Petr. Chem., Am. Chem. Soc. 13 (No. 1), 153-164 (1968).
39. Kirsch, F.W., Potts, J.D., Barmby, D.S., Oil Gas J. 66 (No. 29, July 15), 120-127 (1968).
40. Kirsch, F.W., Potts, J.D., Preprints, Div. Petr. Chem., Am. Chem. Soc. 15 (No. 3), A109-A121 (1970).
41. Kirsch, F.W., Lauer, J.L., Potts, J.D., Preprints, Div. Petr. Chem., Am. Chem. Soc. 16 (No. 2), B24-B39 (1971).
42. Kirsch, F.W., Potts, J.D., Barmby, D.S., J. Catal. 27, 142-150 (1972).
43. Schöllner, R., Hölzel, H., Partisch, M., Wiss. Z. Karl-Marx-Univ. Leipzig, Math.-Naturwiss. R. 23, 631-641 (1974).
44. Schöllner, R., Hölzel, H., Aberle, K., Wiss. Z. Karl-Marx-Univ. Leipzig, Math.-Naturwiss. R. 23, 643-652 (1974).
45. Schöllner, R., Hölzel, H., J. prakt. Chemie 317, 694-704 (1975).
46. Schöllner, R., Hölzel, H., Z. Chem. 15, 469-475 (1975).
47. Mortikov, E.S., Zen'kovskii, S.M., Mostovoi, N.V., Kononov, N.F., Golomshtok, L.I., Minachev, Kh.M., Izv. Akad. Nauk SSSR, Ser. Khim. No. 7, 1151-1154 (1974).
48. Mortikov, E.S., Zen'kovskii, S.M., Mostovoi, N.V., Kononov, N.F., Golomshtok, L.I., Izv. Akad. Nauk SSSR, Ser. Khim. No. 10, 2237-2239 (1974).

49. Weitkamp, J., Compendium 78/79, Erdöl, Kohle - Erdgas - Petrochem., Supplementary Vol. 1, 525-550 (1978).
50. Weitkamp, J., Proc. 5th Intern. Conf. Zeolites (L.V.C. Rees, Ed.), Heyden, London, Philadelphia, Rheine, 1980, pp. 858-865.
51. Weitkamp, J., in: Catalysis by Zeolites (B. Imelik et al., Eds.), Studies in Surface Science and Catalysis, Vol. 5, Elsevier Scientific Publishing Co., Amsterdam, Oxford, New York, 1980, pp. 65-75.
52. Daage, M., Fajula, F., Bull. Soc. Chim. Fr., I153-I159 (1984).
53. Daage, M., Fajula, F., Bull. Soc. Chim. Fr., I160-I168 (1984).
54. Stull, D.R., Westrum, Jr., E.F., Sinke, G.C., The Chemical Thermodynamics of Organic Compounds, John Wiley & Sons, New York, London, Sydney, Toronto, 1969, pp. 258-259.
55. Ipatieff, V.N., Schmerling, L., Adv. Catal. 1, 27-64 (1948).
56. Kennedy, R.M., in: Catalysis (P.H. Emmett, Ed.), Vol. 6, Reinhold Publ. Corp., New York, London, 1958, pp. 1-41.
57. Schmerling, L., in: Friedel-Crafts and Related Reactions (G.A. Olah Ed.), Vol. 2, Part 2, Interscience Publishers, New York, London, Sydney, 1964, pp. 1075-1131.
58. Albright, L.F., Preprints, Div. Petr. Chem., Am. Chem. Soc. 22, 391-398 (1977).

ALKYLATION OF THIOPHENE WITH METHANOL OVER SYNTHETIC ZEOLITES

V.SOLINAS[a], R.MONACI[a], G.LONGU[a], L.FORNI[b]
Dipartimento di Scienze Chimiche, Università di Cagliari,
Via Ospedale,72 09100 Cagliari (a)
Dipartimento di Chimica Fisica ed Elettrochimica, Università di Milano
Via C.Golgi,19 20133 Milano, Italy (b)

ABSTRACT

The behaviour of Na-, H-, Ca-, Mg-, K-, La-, totally or partially ion-exchanged X, Y and ZSM5 zeolites and of silicalite in catalysing the methylation of thiophene with methanol was systematically compared and the effect of the most important reaction parameters on catalyst performance was studied, within the 240-300°C temperature range. Interesting selectivity to mono-methyl-thiophenes, coupled with reasonable life, was obtained with partially protonated NaY zeolite, other catalysts giving less satisfactory results. Some correlations were found between physico-chemical properties and activity of the catalyst, which can be easily regenerated.

INTRODUCTION

It is well-known that methanol (M) may be easily converted into hydrocarbons over some zeolite catalysts [1,2]. Furthermore, owing to its particular reactivity [3], thiophene (T) tends to polymerise when put in contact with acidic substances. In spite of this, some data have been published, concerning the alkylation of T with alcohols, including M, on X- and Y-zeolite-based catalysts [4-6]. Unfortunately, these studies were performed in different conditions, so that it is not easy to compare the results and to find correlations between catalyst properties and performance. Therefore, it seemed interesting to carry

out a systematic comparison of the behaviour of catalysts prepared fro
X, Y, ZSM5 zeolites and from silicalite, in promoting the methylation o
T with M. Some preliminary data were recently reported [7]. In the
present work, the comparison has been further extended, in order to pu
in evidence the limitations connected with a process based on such a
reaction.

EXPERIMENTAL

Catalysts. X- and Y-zeolite-based catalysts were prepared from commercially available powder cake (LZY-52, SK-45, SK-500 and Na13X from Union Carbide). ZSM5 and silicalite were prepared in our laboratory, following the well-known procedure [8]. XRD showed that both the latter materials were fully crystalline, their diffraction patterns matching perfecly the corresponding ones reported in the literature. "Analytical grade" pure chemicals were used for the preparation of catalysts and of ion-exchange solutions, as described elsewhere [9]. After ion-exchange, drying and calcination, the powder was pressed (maximum pressure 200 MPa) in ca. 1 mm thick wafers, which were then gently crushed and sieved, collecting the 40-60 mesh fraction. The ion-exchange degree was determined by AA spectrometry. Surface acidity was determined by titration with n-butyl-amine (n-BA) in anhydrous solvent, after pretreatment at 500°C in a slow flow of dry air. The main characteristics of the catalysts employed are summarised in Table 1.

Apparatus, procedure and analysis. Alkylation runs were carried out in a continuous, fixed-bed microreactor, previously described [10]. Hydrogen was used as carrier gas. Before each run, the catalyst was activated "in situ" overnight in a slow flow of nitrogen at 500°C. Standard reaction conditions were as follows: 240°C; molar ratio (R_H) of carrier gas to liquid feed = 3; WHSV (g of liquid feed/g of cat.x h) = 1; feeding T/M molar ratio ($R_{T/M}$) = 2; catalyst weight 1.5 g. Reaction products were collected in traps cooled to -80°C and analysed by GC, on a capillary glass column, 0.3 mm I.D. and 50 m long, coated with Carbowax 20M and kept at 60°C. Usually four samples for analysis, were collected, after 1, 3, 5 and 10 h on-stream, respectively.

Table 1

Main characteristics of catalysts employed and results of activity comparison runs in standard conditions. Data after 1 h on-stream.

Catalyst[a]	Surface acidity (mmol n-BA/g cat.)			y	S_{mT}	$\Delta y/\Delta t$ [b]
	$H_o \leq -1.5$	$-1.5 \leq H_o \leq 3.2$	$3.2 \leq H_o \leq 6.8$	mol%	mol%	mol%/h
NaY [c]	0	0	0	no reaction		
HNaY-17	0	0.03	0.02	2	19	0.05
HNaY-30	0	0.10	0.06	4	65	<0.05
HNaY-55	0	0.65	0.81	32	13	0.5
HNaY-67	0.07	0.87	0.94	75	7	3.1
HNaY-98	0.13	0.87	1.00	82	6	3.6
MgNaY-25	0.01	0.05	0.11	12	6	0.5
MgNaY-55	0.06	0.25	0.92	30	10	0.5
MgNaY-76	0.09	0.57	1.19	50	11	1.9
CaNaY-76	0.05	0.19	0.42	10	12	0.5
CaNaY-91	0.06	0.29	0.76	26	15	2.2
LaNaY-30	0.05	0.12	0.50	29	8	2.0
REY [d]	0.12	0.18	1.53	72	8	2.6
HKY-36 [e]	0	0.08	0.18	22	2	0.3
NaX [f]	0	0	0	no reaction		
HNaX-95	0	0.20	0.07	17	2	0.5
CaNaX-82	0	0.05	0.10	9	13	0.5
CaNaX-98	0.05	0.06	0.57	7	32	0.9
NaZSM5 [g]	0	0	0.02	20	5	1.2
HZSM5 [h]	0.18	0.14	0.56	52	4	3.0
Silicalite	0	0	0	no reaction		

[a]) figures represent the % ion-exchange degree, with respect to the original Na-form; [b]) decay rate relative to the initial 10 h on-stream; [c]) LZY-52 cake, "mother" material of the Y-series, SiO_2/Al_2O_3 wt ratio (s/a) = 2.80; [d]) SK-500 cake, s/a=2.86; [e]) from SK-45 cake, s/a=3.18; [f]) 13X cake, "mother" material of the X-series, s/a=1.73; [g]) "as prepared" ZSM5 cake, s/a=15.0; [h]) from NaZSM5, maximum obtainable ion-exchange degree.

RESULTS AND DISCUSSION

Besides 2- and 3-methyl-thiophene and unreacted M and T, usually some 2,5-dimethyl-thiophene was found in the collected liquid. In higher-temperature (≧270°C) runs, various poly-methyl-thiophenes were also found, especially trimethyl-thiophenes and methyl-ethyl-thiophenes as identified by GC-MS. In any case, the ratio 2- to 3-methyl-thiophene was ca. 2:1.

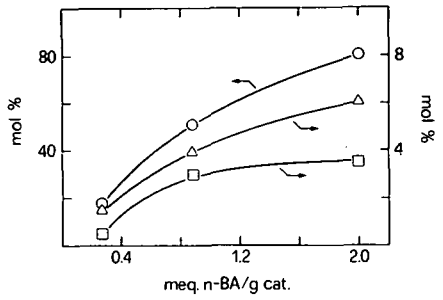

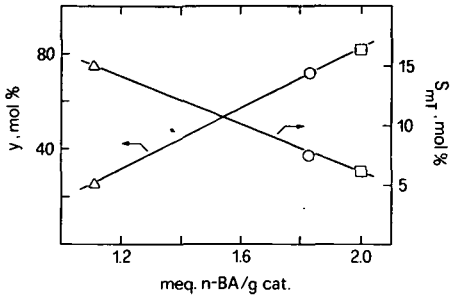

Fig.1. Conversion (O), selectivity (Δ) and decay rate (□, mol%/h) for fully protonated zeolites as a function of surface acidity ($H_o \leqq 6.8$). T=240°C, R_H=3, $R_{T/M}$=2, WHSV=1, time-on-stream=1 h.

Fig.2. Conversion and selectivity vs. surface acidity ($H_o \leqq 6.8$) for CaNaY-91 (Δ), REY (O) and HNaY-98 (□) catalysts. Reaction conditions as for Fig.1.

Results have been expressed in terms of mol % conversion (y) of M and mol % selectivity (S_{mT}) to mono-methyl-thiophenes (mT), defined as follows:

$$y = \left(\frac{\text{reacted}}{\text{fed}}\right)_M 100 \qquad (1)$$

$$S_{mT} = \frac{\text{mT formed}}{\text{M reacted}}\ 100 \qquad (2)$$

The carbon atoms balance, with respect to the feed and referred to liquid products collected within the sampling trap, usually ranged from 94 to 99 %. In two cases this figure was 93% and in only one case it was 91%.

Data from activity comparison runs in standard conditions are

collected in Table 1. These results show that: i) As a general trend, conversion increases with increasing surface acidity, the "as supplied" fully-Na forms and silicalite being completely inactive. The "as prepared" NaZSM5 zeolite cannot be considered as a fully-Na form, due to the presence of protons formed during calcination, by decomposition of residual tetraalkylammonium ions. The latter are trapped within the zeo-

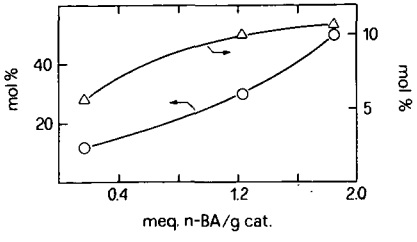

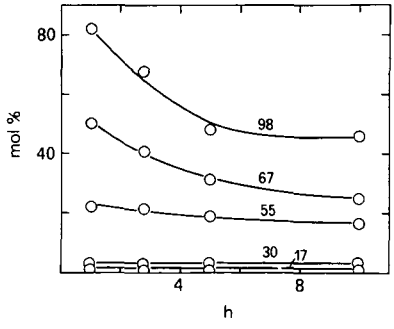

Fig.3. Conversion (O) and selectivity (Δ) vs. surface acidity ($H_o \leq 6.8$) for MgNaY catalysts. Reaction conditions as for Fig.1.

Fig.4. Conversion vs. time-on-stream as a function of ion-exchange degree (figures on the curves). Reaction conditions as for Fig.1. Catalysts: HNaY series.

litic framework during synthesis. ii) When comparing HNa-type catalysts, prepared from different zeolites, one may notice that, in general, both Y- and ZSM5-based catalysts are more active, the former showing also a better selectivity. HNaX catalysts, on the other hand, are less active (see also Figure 1). The different behaviour of HNaY, with respect to HNaX catalysts, seems clearly due to different concentration of surface acid centres. The lower selectivity of ZSM5-based catalysts is very likely connected also with the well-known ability of such a zeolite in catalysing the conversion of M into hydrocarbons [1]. Indeed, some tests, performed by feeding pure M in our standard conditions, confirmed that, with any catalyst based on such a zeolite, no more than 80% of the alcohol could be recovered unconverted, even at temperatures as low as 210°C. iii) A net increase in performance

seems to be conferred by Ca^{2+} ions in the case of X-zeolite. On the other hand, exchange by either Mg, Ca, La or K ions does not change substantially the performance of Y-zeolite catalysts, with respect to the HNaY series. However, some interesting correlations may be found when

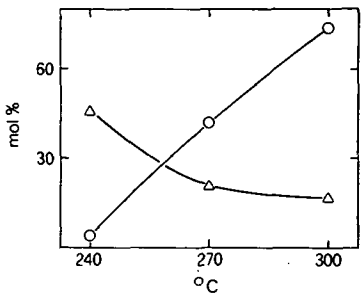

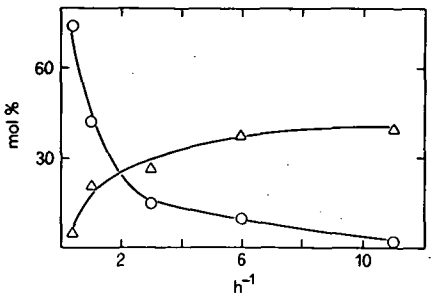

Fig.5. Conversion (O) and selectivity (Δ) vs. reaction temperature. HNaY-30 catalyst.

Fig.6. Effect of WHSV. T=270°C. Catalyst and symbols as for Fig.5.

considering Y-based catalysts. By comparing the results obtained at the highest ion-exchange degree, (HNaY-98, REY and CaNaY-91) one may see (Figure 2) that conversion regularly increases and selectivity decreases with increasing surface acidity, in agreement with an early correlation reported by Venuto [11,12]. Mg- and Ca-exchanged series behave differently: both conversion and selectivity increase with increasing acidity (see e.g. Figure 3). This may be explained when considering that alkylation of T, as well as undesired coking or polymerisation reactions, are catalysed by acid centres, although of different strength. It is known [13] that a different distribution in acid site strength is conferred to the zeolite by bivalent Ca^{2+} and Mg^{2+} ions, with respect to that conferred by H^+, the latter favouring stronger sites. This is confirmed by our data (Table 1): a higher concentration of both stronger ($H_o \leq -1.5$) and medium-strength ($-1.5 \leq H_o \leq 1.5$) sites is usually present in HNaY zeolites, with respect to Ca- or Mg-NaY ones.

Unfortunately, in the present case, the ion-exchange procedure seems unsuccessful in providing selectively only the desired type of centres at any exchange degree and with any of the ions here employed.

In any case, weaker sites, promoting preferentially the alkylation reaction, form first, conferring to the catalyst a higher selectivity at low conversion. However, when attempting to increase conversion, either by increasing the ion-exchange degree or by changing the ion, the unavoidable simultaneous formation of higher-strength centres confers to the catalyst a progressive ability in promoting also unwanted reactions. The result is the simultaneous decrease in selectivity, usually accompanying the increase of conversion.

From a practical point of view, the best compromise seems to be attainable with the catalysts of HNaY series. In this case overall conversion progressively increases, with increasing the ion-exchange degree, while selectivity goes through an interesting maximum (for HNaY-30). In correspondence of the latter, side reactions are still at a reasonable level, as shown by the decay rate (last column in Table 1), which attains the lowest value observed for any of the catalysts tested. Activity decay is shown in Figure 4 for the whole set of HNaY catalysts. Therefore, HNaY-30 catalyst was selected for the following analysis, aiming at the optimisation of reaction conditions.

As expected, conversion increases and selectivity decreases by increasing temperature (Figure 5) or by decreasing WHSV (Figure 6). To enhance the effect of WHSV, Figure 6 data were collected at 270°C.

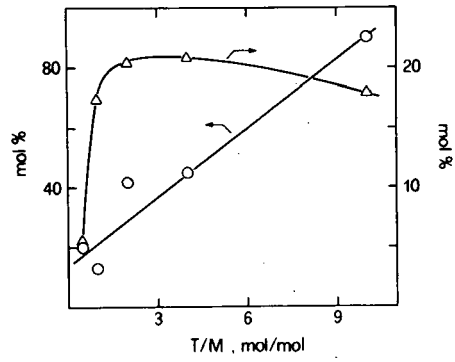

Fig.7. Effect of T/M feeding ratio (mol). T=240°C. Catalyst: HNaY-30. (O) conversion, (Δ) selectivity.

In addition, decay rate increases with temperature, particularly at 300°C, where any reaction stops within a few hours. As for the effect of $R_{T/M}$, an increase of conversion is noticed with increasing such a parameter (Figure 7), while selectivity shows a strong increase for $R_{T/M}$ going from 0.5 to 2, reaching a maximum at $R_{T/M} \sim 4$ and then decreasing slowly for higher $R_{T/M}$ values.

In view of a possible application, since the activity of any of the zeolites tested decays more or less rapidly, it is important to ascertain if the catalyst may be regenerated. This aspect was investigated by performing a series of reaction-regeneration runs on the same sample of HNaY-30 catalyst. To speed up the test, only standard reaction conditions were considered and time-on-stream was limited to 30 h. After regeneration, the reaction was immediately retaken for the next 30 h run. Three reaction-regeneration cycles were carried out, so that the total working time was 90 h. After a short purging with nitrogen, regeneration was performed by simply burning-off carbonaceous deposits in a slow flow of air at 350-500°C. The formation of CO_2 was monitored by bubbling the outcoming gas in $Ba(OH)_2$ solution, that of SO_2 by bubbling in $AgNO_3$ solution. In any reaction cycle conversion remained unchanged during the first 24 h on-stream, then decaying quite slowly. The results showed that regeneration restores completely the activity shown by the fresh catalyst, the behaviour of which was perfectly matched in both the runs following each regeneration.

CONCLUSION

The results of the present work permit to conclude that;

i) Vapour-phase alkylation of T by M may be obtained over zeolites with reasonable selectivity only when acid sites of relatively low strength are present on the catalyst surface.

ii) HNaY-30 catalyst showed the best compromise between activity, selectivity and durability.

iii) Reaction temperature should not exceed 250°C and $R_{T/M}$ should not be lower than 2, to keep within reasonable limits the formation of polymethylates and coking-polymerisation.

iv) The activity decay is essentially due to fouling by carbonaceous

deposits. However, the latter can be easily burned-off with air, so restoring completely the behaviour of fresh catalyst.

ACKNOWLEDGEMENT

This work was done within the Project on Fine Chemistry of CNR (Rome).

REFERENCES

1. Chang, C.D., Catal. Rev. Sci. Eng. 25, 1 (1983).
2. Inui, T., Yamase, O., Fukuda, K., Itoh, A., Tarumoto, J., Morinaga, M., Hagiwara, T., Tagekami, T., Proc. 8th Intern. Congr. on Catalysis, Berlin, 1984, vol. III, p. 569.
3. Appleby, W., Sartor, A., Lee, H., Kapranos, W., J. Amer. Chem. Soc. 70, 1552 (1948).
4. Venuto, P.B., Landis, P.S., Advan. Catal. 18, 259 (1968).
5. Abramovic, V.B., Pankratova, M.F., Masagutov, R.M., Organ. Soed. Sery, Riga 2, 422 (1980).
6. Karahanov, E.A., Filippova, T.I., Isakov, I.I., Minachev, H.M., Bull. Moscow Univ., Chem. Ser. 2, 23, 495 (1982).
7. Solinas, V., Monaci, R., Marongiu, B., Forni, L., Atti XV Congr. Soc. Chim. Ital., Grado, Sept. 1984, p. 332.
8. Argauer, R.J., Landolt, G.R., US Pat. 3,702,886 (1972).
9. Bolton, A.P., in "Experimental Methods in Catalytic Research" (R.B. Anderson, P.T.Dawson, Eds.), Academic Press, New York (1976).
10. Solinas, V., Monaci, R., Marongiu, B., Forni, L., Appl. Catal. 9, 109 (1984).
11. Venuto, P.B., Landis, P.S., Hamilton, L.A., Wise, J.J., J. Catal. 5, 81 (1966).
12. Venuto, P.B., in "Catalysis in Organic Synthesis" (G.V.Smith, Ed.), Academic Press, New York (1977).
13. Barthomeuf, D., in "Zeolites, Science and Technology" (F.Ramoa Ribeiro, E.A.Rodrigues, L.B.Rollmann, C.Naccache, Eds.), NATO ASI Series, no. 80 (1984), p. 317.

THE USE OF LAYERED CLAYS FOR THE PRODUCTION OF PETROCHEMICALS

D.J. Westlake, M.P. Atkins, R. Gregory
BP Research Centre, Sunbury-Upon-Thames, Middlesex, England

ABSTRACT

Some exchanged Wyoming montmorillonite clays are effective catalysts for the alkylation of benzene with propene or ethylene in the liquid phase. Under these conditions the clay catalysts give equilibrium product distributions. In contrast zeolites are generally poor catalysts and do not give equilibrium product distribution under these mild conditions.

INTRODUCTION

The alkylation of benzene by propene and ethylene is widely practised in the petrochemical industry. Cumene has been manufactured on a large scale for more than 40 years, firstly as a high octane component for aviation gasoline and subsequently as an intermediate for the production of phenol. Ethylbenzene is also manufactured on a large scale as a precursor for the production of styrene.

Acidic catalysts are used in the production of both cumene and ethylbenzene. The former is generally manufactured using a supported phosphoric acid catalyst in a fixed bed reactor with the reactants in the liquid phase although aluminium chloride and sulphuric acid catalysts have also been used (1,2). Ethylbenzene is generally produced using either aluminium chloride as catalyst with the reactants in the liquid phase or with a zeolite catalyst and the reactants in the vapour phase (3,4).

There has recently been considerable interest in the application of layered montmorillonite clays as acidic catalysts so it seemed reasonable to examine these materials for the alkylation of benzene. Montmorillonite clays possess both Lewis and Brønsted acid sites which are responsible for the diverse catalytic activity of these materials eg in ether formation from alcohols and alkenes, olefin hydration, ester formation from carboxylic acids and alkenes and many other reactions (5, 6,7).

The detailed structure of montmorillonite minerals is still the subject of debate although it is generally agreed that they are formed from an octahedrally coordinated alumina sheet sandwiched between two tetrahedrally coordinated silicate sheets. The layers carry an overall negative charge which may arise from isomorphous substitution of Al^{3+} by Fe^{2+} or Mg^{2+} in the octahedral sheet and to a lesser extent of Si^{4+} by Al^{3+} in the tetrahedral sheet. These negative charges on the layers are balanced by hydrated cations, usually Na^{+} or Ca^{2+} in the naturally occuring state, which are situated in the interlamellar space and which can be readily ion-exchanged. By suitable choice of cation the acidity and polarisation of coordinated water and other molecules in the interlamellar environment can be varied.

The Bronsted acidity of the cation-exchanged clays can be accounted for by dissociation of coordinated water in the interlamellar space,

$$M(H_2O)_x^{n+} \rightleftharpoons \left[M(OH)(H_2O)_{x-1}\right]^{(n-1)+} + H^+$$

and Lewis acidity may arise from dehydroxylation of the framework hydroxyl groups,

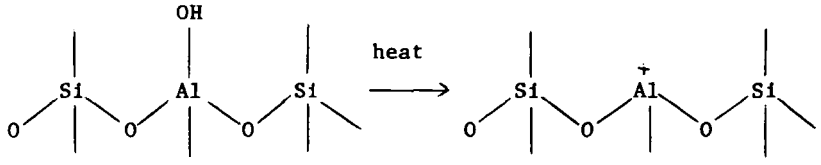

In this paper the performance of montmorillonite clays is compared with zeolite catalysts for the alkylation of benzene with propene and ethylene. The generally accepted mechanism for aromatic alkylation is

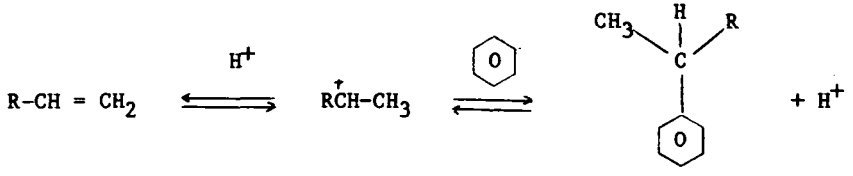

where R = alkyl or H.

Further alkylation of the alkylated product can be reduced, if desired, by the use of large benzene:olefin reactant ratios. Alternatively, lower ratios can be used in commercial processes provided the catalyst chosen is also effective for transalkylation reactions such as

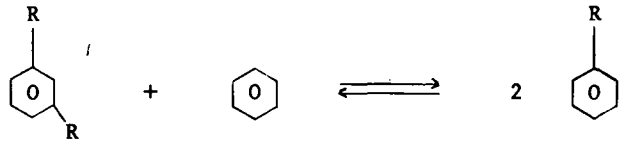

since the unwanted polyalkyl-benzenes can be separated and recycled with fresh feed.

EXPERIMENTAL

Catalyst Preparation. Hydrogen and aluminium exchanged Wyoming montmorillonites were prepared by methods described previously (6,7). The zeolite catalysts were either synthesised by known methods or were commercial samples and converted to the hydrogen form by calcination of the ammonium form. The amorphous aluminosilicate (85.5% SiO_2) was obtained from Strem Chemicals Incorporated.

Apparatus. Alkylation experiments with both ethylene and propene were carried out in stainless steel autoclaves in the normal manner. The autoclaves were heated to the reaction temperature, held for 2.5 hours, and allowed to cool overnight. Continuous experiments were carried out with a premixed feed under pressure in a small continuous unit whose schematic flow diagram has been described previously (6).

Analysis. All reaction products were analysed by capillary gas chromatography using calibration factors derived from authentic standards.

RESULTS AND DISCUSSION

Cumene. The performance of Wyoming montmorillonite clay catalysts is compared with that of a range of zeolite and other catalysts for the alkylation of benzene with propene in Table 1. In these batch reactions the H^+ and Al^{3+} exchanged Wyoming montmorillonite clays gave complete conversion of propene at 150°C with the former giving virtually the same product over the temperature range 125° to 230°C. In contrast none of the other catalysts examined gave more than 65% propene conversion at 150°C. The best result was obtained with the commercial amorphous aluminosilicate and the worst with the large pore size zeolite-Y.

TABLE 1

FORMATION OF CUMENE FROM BENZENE AND PROPENE

Catalyst	Reaction Temp °C	Propene Conversion %	Product Distribution		
			Benzene (Mole%)	Cumene (Mole%)	DIPB[a] (Mole%)
H^+-Montmorillonite	125	100	84.4	14.7	0.9
H^+-Montmorillonite	150	100	84.3	14.7	1.0
H^+-Montmorillonite	230	100	84.3	14.7	1.0
Al^{3+}-Montmorillonite	150	100	85.6	13.9	0.6
H-Y Zeolite	150	5	99.3	0.7	tr
H-Mordenite	150	20	97.8	2.0	0.2
H-MFI	150	25	96.7	3.3	tr
Aluminosilicate	150	65	90.5	8.9	0.6

Reactants:- Benzene 120g, Propene 10g, Catalyst 5g, C_6:C_3 = 6:1
a) DIPB = di-isopropylbenzene

In a second series of experiments the catalysts were compared for the reaction of benzene, propene and meta-di-isopropylbenzene (DIPB) in order to determine how much, if any, of the DIPB was transalkylated to give additional cumene (Table 2). Only H^+-Montmorillonite gave any significant conversion of DIPB under these conditions. The best result with the remaining catalysts was obtained with zeolite-Y whilst the

TABLE 2

FORMATION OF CUMENE FROM BENZENE, PROPENE AND DIPB[a]

Catalyst	Temp °C	DIPB (Prod) / DIPB (React)	Product Distribution		
			Benzene (Mole%)	Cumene (Mole%)	DIPB[a] (Mole%)
H^+-Montmorillonite	230	0.6	72.6	24.7	2.7
H-Y Zeolite	230	0.9	93.9	2.1	4.0
H-MFI	230	1.3	90.2	5.6	4.1
H-MFI	270	1.1	85.3	9.7	4.9
Aluminosilicate	230	1.1	83.5	11.7	4.8

Reactants:- Benzene 120g, Propene 12g, meta-DIPB 12g, Catalyst 5g
a) DIPB = di-isopropylbenzene

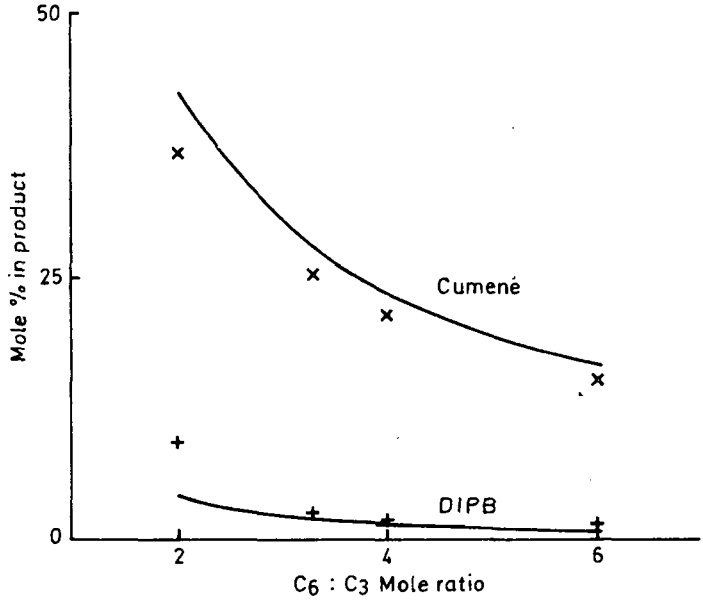

Figure 1. Calculated thermodynamic (solid lines) and experimental (plotted points) product distributions for the formation of cumene.

TABLE 3

CONTINUOUS PRODUCTION OF CUMENE

Catalyst	H^+-Montmorillonite
Temperature (°C)	190
Pressure (bar)	30
LHSV (h^{-1})	2.1
Feed (Mole %)	
benzene	82
Propylene	15
DIPB	2.1
C_6:C_3	5:1
Product (Mole %)	
Benzene	79 ± 1
Cumene	18 ±.1
DIPB	2.3 ± .25

others gave a net production of DIPB. Thus, with the exception of the H^+-Montmorillonite catalysed reaction, the initial DIPB behaves as an inert diluent in these systems.

The reaction product distribution with the Wyoming montmorillonite catalyst in both sets of experiments is close to the calculated thermodynamic equilibrium. In Figure 1 the calculated and experimentally observed product distributions are plotted for a wide range of initial benzene and C_3-alkyl fragment compositions. The experimental points were obtained from reactions using various combinations of propene, benzene and DIPB as the initial reactants and the calculated equilibrium compositions show little variation with temperature over the range 120° to 230°C which is in agreement with the experimental results in Table 1.

The performance of the H^+- Montmorillonite was also examined in the continuous production of cumene using a feed comprising benzene, propene, and DIPB. The product composition shown in Table 3 remained constant over a test period of 50 hours on stream at constant temperature and LHSV. The product composition was also close to the calculated thermodynamic value shown in Figure 1 illustrating that equilibrium is also achieved in continuous reactions with this catalyst and a relatively short contact time.

Ethylbenzene. The performance of Wyoming montmorillonite clay catalysts is compared with the H-MFI zeolite for the alkylation of benzene with ethylene in Table 4. In these batch reactions at 230°C where benzene is in the liquid phase both the H^+ and Al^{3+} Wyoming montmorillonite catalysts gave complete conversion of ethylene compared to only 20% with H-MFI.

As in the earlier experiments with propene only the Wyoming montmorillonite clay catalysts give product distributions which are close to the calculated thermodynamic equilibrium composition. Thus, at a C_6:C_2 ratio of 2.5 :1, the experimentally observed product distribution is ethylbenzene 28.4% and diethylbenzene 5.5% compared to 32.4% and 3.8% respectively for the calculated thermodynamic equilibrium.

Reaction mechanism and catalytic activity. There would seem to be no reason to suggest that the generally accepted mechanism for the acid catalysed addition of an olefin to an aromatic ring should not be extended to reactions catalysed by Wyoming montmorillonite clay, zeolite, or aluminosilicate catalysts. All of these catalysts have acidic sites capable of supplying the necessary proton for formation of the carbonium ion intermediate.

TABLE 4

FORMATION OF ETHYLBENZENE

Catalyst	Temp °C	Ethylene Conv^{n} %	Product Distribution		
			Benzene (Mole%)	Ethyl-benzene (Mole%)	DEB[a] (Mole%)
H^{+}-Montmorillonite[b]	230	100	65.1	28.4	6.4
Al^{3+}-Montmorillonite[b]	230	100	66.1	28.4	5.5
H-MFI[b]	230	20	92.6	6.3	tr
H^{+}-Montmorillonite[c]	250	100	89.6	9.8	0.6

a) DEB = diethylbenzene
b) Reactants:- Benzene 120g, Ethylene to 40bar, Catalyst 5g
c) Reactants:- Benzene 120g, Ethylene to 40bar, DEB 12g, Catalyst 5g

It is proposed that the substantial difference in catalytic activity between the clay and zeolite catalysts is due to the ready accessibility of the acidic sites to the reactants in the former case. In liquid phase reactions diffusional constraints for reactants or products will be greatest for catalysts with rigid microporous structures such as zeolites. The expanding layer structure of the Wyoming montmorillonite clay catalysts allows access to the interlamellar acidic sites with few diffusional constraints and hence these have greater activity. Similarly the acidic sites on the amorphous aluminosilicate are more accessible than those in the zeolite structure.

It is known that zeolite catalysts such as MFI are effective for the vapour-phase alkylation and transalkylation of benzene and ethylene at 425°C (4). Under these conditions the diffusional constraints would probably be much less significant but collapse of the interlamellar space in Wyoming montmorillonite would decrease the activity.

CONCLUSION

It is concluded that Wyoming montmorillonite clays are effective catalysts for the alkylation of benzene with propene or ethylene in liquid phase reactions to give cumene and ethylbenzene respectively. Under these conditions, these catalysts are also effective for transalkylation

reactions thereby allowing recycle of unwanted polyalkylated products to extinction in commercial processes. They are also more effective than zeolite catalysts in these liquid phase reactions.

ACKNOWLEDGEMENTS

We thank the British Petroleum Company plc for permission to publish this paper.

REFERENCES

1. Brayford, D., Encyclopaedia of Chemical Processing and Design, Edited by McKetta, J.J., Dekker 1980, Vol 14.
2. McAllister, S.H., Anderson, J., Ballard, E.F., Chem. Eng. Progress, 1947, 43, 189.
3. MacFarlane, A.C., Oil Gas J,. 1976, 74(6), 99.
4. Hagopian, C.R., Lewis, P.J., McDonald, J.J., Hydroc. Proc., 1983, 62(2), 45.
5. Ballantine, J.A., Purnell, J.H., J. Molec. Catal., 1984, 27, 157.
6. Atkins, M.P., Smith, D.J.H., Westlake, D.J., Clay Miner., 1983, 18, 423.
7. Gregory, R, Smith, D.J.H., Westlake, D.J., Clay Miner., 1983, 18, 431.

CATALYTIC PROPERTIES OF STABILIZED ZEOLITES Y IN THE REACTIONS OF DIMETHYL ETHER AND OF THE TOLUENE DISPROPORTIONATION

V. BOSÁČEK[a], J. JELÍNKOVÁ[a], YA.I. ISAKOV[b], T.A. ISAKOVA[b], K.M. MINACHEV[b]

The J. Heyrovský Institute of Physical Chemistry and Electrochemistry, 121 38 Prague 2, Czechoslovakia (a)

The Zelinsky Institute of Organic Chemistry, Academy of Sciences, Moscow, USSR (b)

ABSTRACT

The catalytic properties of zeolites Y, stabilized under self-steaming conditions, were studied in the reactions of the dimethyl ether decomposition to hydrocarbons and of the toluene disproportionation. It has been found that Cu^{2+} cations introduced into the lattice of a stabilized, partially decationized zeolite enhance the zeolite activity in both the reactions. The favourable effect of the Cu^{2+} cations is mainly due to their easy reducibility leading to additional acidity. The Bronsted acidity form substantially increases the catalyst activity, while the Lewis form decreases the activity.

INTRODUCTION

Stabilized forms of decationized zeolites of the Y type exhibit some properties that differ from those of nonstabilized decationized zeolites /1-5/. The main advantages of stabilized samples involve the material stability in the processes of activation and regeneration at high temperatures. An interesting property, which is important for catalysis, is the localization of exchangeable cations in the large cavities in the crystal structure of these zeolites /4,5/. The possibilities in the use of these zeolites as catalysts in various processes have only rarely been described.

In the present paper, the catalytic conversion of dimethyl ether and the catalytic disproportionation of toluene were studied on H- and Cu-forms of stabilized zeolites Y. This study was stimulated by the fact that Cu^{n+} cations exert positive effects on the activity of zeolitic catalysts in many reactions involving carbonium ions /6,7/.

EXPERIMENTAL

A series of decationized zeolites NH_4Na-Y with varying degree of the Na^+ exchange for NH_4^+ (15-80%) was studied. The materials were subjected to a stabilizing process in the form of powders, in a rotary quartz furnace. The ammonium zeolite form was decomposed in a closed system with a water vapour pressure of ca. 1.8 kPa (13 torr), by increasing the temperature up to 570°C at a rate of 4 degrees per minute. The H,Na-Y zeolite thus obtained and stabilized under hydrothermal conditions was further converted into the Cu^{2+} form in a $CuSO_4$ solution. The samples were washed, dried and their crystallinity was checked by argon adsorption, IR spectra and x-ray diffraction.

The state of the Cu cations in the zeolite was followed using the IR spectra of adsorbed CO and by photoelectron spectroscopy. The IR spectra were measured on a Nicolet MX-1 interferometer, using sample pellets 10-15 mg/cm^2 thick, in the transparent arrangement. The main characteristics of the samples are given in Table 1.

Tab. 1: Characteristics of zeolites Y

Zeolite		Chemical compsition of original zeolite mole					Sorption capacity, Ar mmol/g	
No	Symbol	Na_2O	$NH_4{}_2O$	CuO	Al_2O_3	SiO_2	Unstabilized in vac. 350 °C	Stabilized
1	NaY	0,94	-	-	1	5,4	10,4	-
2	NH_4Y-15	0,78	0,14	-	1	5,9	10,6	9,9
3	NH_4Y-37	0,61	0,35	-	1	5,8	11,1	10,1
4	NH_4Y-53	0,42	0,55	-	1	4,6	11,6	9,5
5	NH_4Y-62	0,31	0,61	-	1	4,3	11,3	10,7
6	NH_4Y-77	0,18	0,75	-	1	4,3	11,1	10,5
7	Cu,HY-St[1/]	0,19	-[2/]	0,11	1	4,5	-	9,1
8	Cu,HY-St[1/]	0,16	-[3/]	0,17	1	4,6	-	9,1

1/ Sample prepared from the stabilized sample No 5
2/ 0,35 H_2O structural OH groups
3/ 0,49 H_2O dtto

The catalytic tests were carried out in flow-through apparatus at atmospheric pressure. Dimethyl ether was injected in a mixture with nitrogen. The products of its conversion were analyzed chromatographically on a column packed with Carbopack-C (Supelco) with 0.02%

picric acid /8/. Chromosorb P with 10% polydiethyleneglycol succinate 78°, helium was used in the analysis of the products of toluene disproportionation. The composition of the isomers of aromatic hydrocarbons was determined on a chromatographic column packed with Benton 245 with a paraffin oil /9/.

The catalysts were activated for 8 hours in a stream of dry nitrogen at 350°C prior to the reaction of dimethyl ether (DME). Before the disproportionation reaction of toluene, the samples were activated for 5 hours at 500 °C in the air stream. The toluene disproportionation was studied without the use of a carrier gas.

RESULTS AND DISCUSSION

1. Conversion of Dimethyl Ether into Hydrocarbons

The dimethyl ether conversion was studied at 300°C and WHSV = 1.2 h^{-1} on a number of NH_4,Na-Y zeolites with various NH_4^+ contents, in nonstabilized form (the ammonium form was decomposed at 350°C in a stream of dry nitrogen) and in stabilized form (decomposition under hydrothermal conditions, 570°C). The DME conversion yielded ca. 45-55% of the C_1 - C_5 aliphatic hydrocarbons; the main reaction products included ethylene and propylene, and saturated hydrocarbons, isobutane, isopentane and n-butane. The time course of the reaction and the composition of the products were analogous to those corresponding to the methanol decomposition on HY zeolites /10/. The catalyst activity is strongly affected by the presence of Bronsted acidic sites. These sites are more acidic in nonstabilized H,Na-Y zeolites than in stabilized zeolites /2,3,11/. In agreement with these facts, a lower DME conversion was found on stabilized zeolites see Fig. 1 . For example, a H,Na-Y St catalyst with a 15% decationization is inactive at 300°C, whereas its nonstabilized form with the same degree of decationization exhibits a 50% conversion of DME into hydrocarbons. The positive effect of Cu^{2+} cations introduced by ion exchange into the stabilized form, H,Na-Y St, with a 70% decationization, is manifested by a substantial increase in the catalyst activity: the conversion reaches 90% and the selectivity remains unchanged /12/.

It should be pointed out that H,Na-Y St zeolites lose their activity much faster than nonstabilized zeolites or stabilized zeolites containing copper cations, apparently because of rapid coking. As all stabilized zeolites contain extra-lattice, nontetrahedrally bonded aluminium that was released from the lattice T-positions during the stabilizing process /13,14/, it can be assumed that this form of aluminium is responsible for the intense formation of polyaromatics and

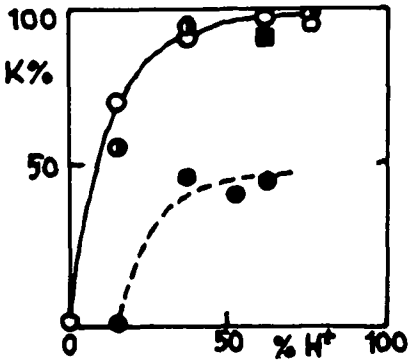

Fig. 1: Dependence of the conversion K of DME 30 min on the decationization degree at 300°C
○... nonstabilized Y zeolites activated at 350°C
◐... nonstabilized Y zeolites dehydroxylated at 500°C
●... stabilized Y
■... Cu, H-Y St, (sample 7)

coke and that it hastens the loss af activity of these catalysts /15/. The presence of these Al species is probably not the only cause of zeolite deactivation, but it is known that these forms of aluminium, which have the character of a Lewis acid, strongly catalyze the oligomarization of ethylene, propylene and other unsaturated compounds /2, 3/. It cannost be excluded that the favourable effect of copper cations is related not only to the formation of additional Bronsted acidity after the reduction of Cu^{2+} to Cu^{+}, but also to the displacement of a certain small fraction of readily exchangeable cationic forms of aluminium Al^{3+}, AlO^{+} that also exhibit the highest Lewis acidity /16/. These readily exchangeable Al species may affect the reaction in the large cavities of a faujasite, while a substantial part of nontetrahedrally bonded aluminium remains in the lattice apparently in the sodalite units or in the form of associates eith a low Lewis electron-acceptor strength /16.17/.

2. Toluene disproportionation

A decationized, stabilized H,Na-Y St zeolite and a Cu,H-Y St zeolite prepared from the former were studied in this reaction at various temperatures see Table 2 and with various methods of activation Table 3. A certain period, during which the activity increased, was observed with both the catalysts. The time after which a maximum toluene conversion and the maximum degree of disproportionation were attained the pertinent values are given in Tables 2 and 3 depended on the zeolite composition and the reaction temperature. This time was usually 2 to 4 hours and decreased at higher reaction temperatures. This phenomenom is apparently connected with the kinetic properties of the process, adsorption-desorption factors and with the effect of the reaction mixture on the formation of catalytically active sites. Toluene demethylation also occured to a very small extent under the reaction conditions and was observable at higher reaction temperatures.

Tab. 2: Results of toluene disproportionation on stabilized Y zeolites

LHSV = 1,2 h^{-1}

T, °C	Conversion of toluene %	Disproportionation degree %	Products w.% from the injected toluene				Composition of the C_8H_{10} fraction %				Composition of ethyltoluenes %		
			Benzene	xylenes	ethyltoluenes	trimethylbenzene	o-xylene	m-xylene	p-xylene	ethylbenzene	o-	m-	p-
Zeolite H,Na-Y 62 St													
350	1,15	0,5	0,28	0,17	0,02	0,05	15	34	40	11	-	-	-
400	7,1	5,85	2,6	3,06	0,17	0,07	16	48	35	1	11	62	27
450	24,4	20,6	10,4	10,6	0,22	0,74	21	51	26,8	1,2	14	59	27
Zeolite Cu,H-Y 62 St (sample 8)													
350	15,0	13,2	5,76	6,81	0,16	0,44	19,0	52	29	traces	24	41	35
400	25,0	21,0	11,8	10,6	0,15	0,96	20	52,5	27	0,5	15	60	25
450	20,0	12,4	9,4	6,5	0,1	0,4	19	52	29	-	5	55	40

Tab. 3: Influence et the treatment on the catalytic properties of Cu,H-Y St /8/ zeolite in the reaction of toluene disproportionation

Temperature of reaction t = 350°C LHSV = 1,2 h^{-1}

Sample No.	Conditions of the sample treatment	Toluene conversion %	Disproportionation degree %	Product in w. % from the injected toluene				Composition et the C_8H_{10} fraction %				Composition of ethyltoluenes		
				benzene	xylenes	ethyltoluenes	trimethylbenzenes	o-xylene	m-xylene	p-xylene	ethylbenzene	o-	m-	p-
1	Air, 500°C, 5h	15,0	13,2	6,73	6,81	0,16	0,44	19	52	29	traces	24	41	35
2	Air, 500°C, 5h and CO, 400°C 5h	11,1	10,1	5,01	5,35	0,12	0,22	17	49	34	-	15	50	35
3	Treatment of sample No 2 after experiment Air, 500°C, 5h	10,8	10,2	4,9	5,45	0,14	0,18	17	52	31	-	13	55	35
4	Air, 500°C, 5h and H_2, 400°C, 5h	25,0	23,5	10,0	10,9	0,83	1,18	18	50,6	27	4,4	14	58	28
5	Treatment of the sample No 4 Air, 500°C, 5h	16,6	14,2	7,0	7,25	0,2	0,5	18	53	28,5	0,5	20	56	24

The fact that ethyltoluenes were formed with both catalysts in addition to sylenes, trimethylbenzenes and benzene is worth attention. This indicates the formation of carbene-type intermediates in the system, whose interaction with the CH_3 groups from xylenes produces ethyltoluenes. The possibility of the formation of ethylene by recombination of carbenes followed by alkylation of toluene cannot be excluded, although it seems that this recombination is less probable than the direct interaction /18/. These considerations are in agreement with the fact that the C_1 - C_4 hydrocarbons were found dissolved in the liquid reaction product.

After treatment of the Cu,H-Y St zeolite with carbon monoxide 400°C, 5 h the zeolite activity decreased by 25%, but the original value was not attained on reoxidation. On the other hand, the catalyst reduction by hydrogen 400°C, 5 h increased the conversion by 70%. The conversion attained the original value on reoxidation. It seems that copper cations have a direct effect on the formation of the zeolite active sites in this reaction.

As can be seen from the above results, the Cu,H-Y St zeolite is more active in the two reactions than the corresponding decationized stabilized zeolite. The increase in the activity is apparently caused by the formation of additional protonic acidity due to the reduction of Cu^{2+} cations to Cu^{+} by hydrogen that is often present in trace amounts in the reaction products. In this way OH groups are formed in the zeolite structure, whose protonic acidity is higher than that of the OH groups in the stabilized H,Na-Y St zeolite from which the Cu,H-Y St zeolite was prepared. The relatively small amount of protons formed in the Cu,N-Y St zeolite can considerably increase the catalyst activity, if the steep dependence of the $(CH_3)_2O$ conversion on the degree of decationization Fig. 1. is taken into consideration.

The infrared spectra of a reduced zeolite given in Fig. 2 confirm certain changes in the spectrum of OH groups after treatment with hydrogen at 400°C. It can be seen that a higher reduction temperature leads to partial dehydroxylation of the sample, which is apparently also the reason of a mild decrease in the toluene conversion at a temperature of 450°C see Table 2, Cu,H-Y St zeolite . It can also be seen from the spectra of adsorbed carbon monoxide given in Fig. 3 that an intense band appears at 2140 cm^{-1} after the reduction with hydrogen; the band is characteristic of the Cu^{+}... CO complex. On the other hand, a zeolite treated with oxygen exhibits an intense band at 2160 cm^{-1}. Easy reducibility self-reducibility of copper ions is well known and has also been confirmed in our zeolites by photoelectronic spectra.

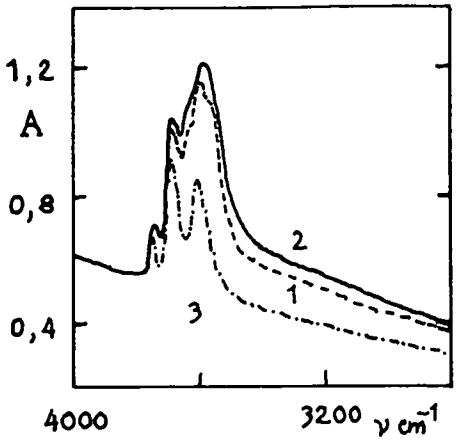

Fig. 2. Infrared spectra of Cu,H-YSt sample 8 in OH stretching region:
1.. Activated in vacuo 350 °, 8h
2.. Reduced with H_2, 350° 8h, vac.1h
3.. Reduced with H_2, 600° 8h, vac. 350°, 1h

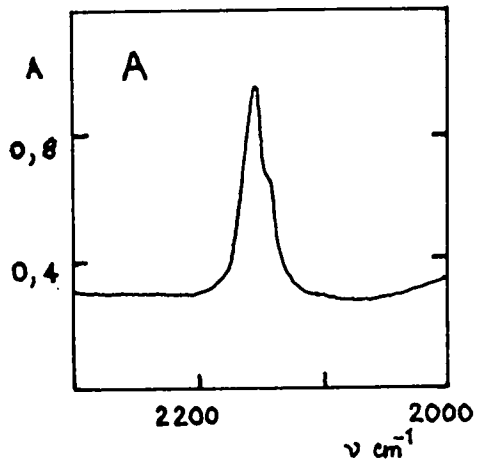

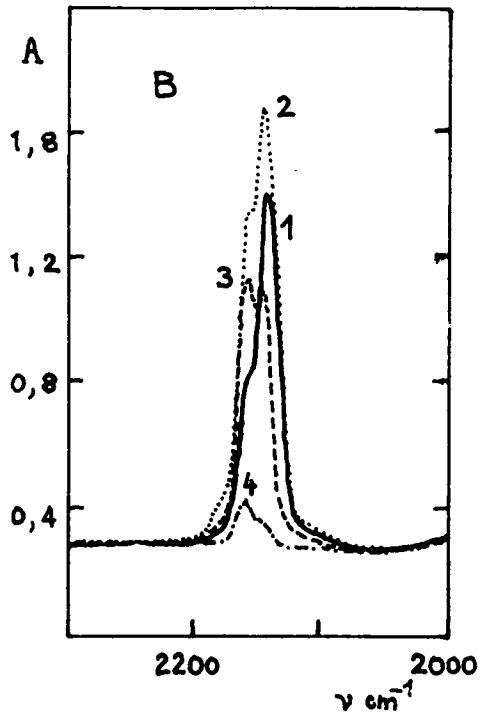

Fig. 3. Infrared spectra of adsorbed carbon monoxide on Cu,H-YSt (sample 8).
A. Sample treated with oxygen, p_{O_2} = 2 Torr, 450°C, 8h in vacuo at 350°, 1h - adsorption of CO, p_{CO} = 1 Torr.
B. Sample treated with hydrogen at 450°C, 4h, p_{H_2} = 250 Torr
CO adsorption: 1.. p_{CO} = 0,1 Torr, 2.. p_{CO} = 1 Torr
CO desorption: 3.. $p_{CO} = 4.10^{-2}$ Torr, 4.. $p_{CO} = 10^{-4}$ Torr.

t should be pointed out that Cu^{2+} was reduced to Cu^{+} very readily in he stabilized forms; at higher temperatures e.g. during the activation in vacuo at 350°C or at higher temperatures the presence of Cu^{2+} ould not be detected using shake-up satellite lines /20/. During the eduction with hydrogen, only the $Cu^{2+} \rightarrow Cu^{+}$ reduction was observed, ut not the reduction to metallic copper. This reduction process was monitored by photoelectron spectroscopy and by the IR spectra of adsored carbon monoxide at 25 °C; absorption bands at 2140, 2160 and, at a O pressure above 25 Torr (3 kPa), also a band at 2180 cm^{-1} were only ound. These bands correspond to valence vibrations of CO in the cordination sphere of copper cations. No absorption band characteristic f CO adsorbed on copper metal Cu^{o} /21/ or of Cu carbonyls /22/ and located at lower wavenumbers was found with the studied zeolites.

The positive effect of Cu^{n+} cations need not be caused only by the formation of additional protonic acidity during the reduction, but ay also be connected with coordination unsaturation of these cations. hese coordination-unsaturated sites can ensure, together with the xistence of protons in the lattice, the optimal configuration of the ctive sites on which active complexes can be formed that take part in the alkylation of the aromatic ring, isomerization and disproportionation /23/.

REFERENCES

1. Scherzer J.; Catalytic Materials - Relationship Between Structure and Reactivity ACS 248, 157 /1984/
2. Tvarůžková Z., Patzelová V., Bosáček V., React. Kinet. Catal. Lett. 6, /4/, 433 /1977/
3. Kubelková L., Nováková J., Bosáček V., Patzelová V., Tvarůžková Z., Acta Phys. et Chem. /Szeged/ 24, 189 /1978/
4. Tvarůžková Z., Bosáček V., Patzelová V., React. Kinet. Catal. Lett. 11, /1/, 71 /1979/
5. Tvarůžková Z., Bosáček V., Coll. Czechoslov. Chem. Commun. 45, 2499 /1980/
6. John Ch.S., Leach H.F., JCHS Faraday Trans.I., 75, 1595 /1977/
7. Maxwell L.E., Downing R.S., van Langen S.A., J.Catal. 61, 485 /1980/
8. Gorcia A.D., Samperi R., J. Chromatogr. 107, 99 /1975/
9. Vigdergauz M.S., Gazovaya Chromatografiya Vol.6., NIITECh. Moscow /1967/, p.30
10. Langner B.E., Appl. Catal. 2, 289 /1982/
11. Kubelková L., Nováková J., Wichterlová B., Jírů P., Coll. Czechoslov. Chem. Commun. 45, 2290 /1980/

12. Jelínková J., Thesis, Charles University Prague 1984
13. Bosáček V., Freude D., Frönlich T., Pfeifer H., Schmiedel H., J. Coll. and Interface Sci., 85, 502 /1982/
14. Engelhardt G., Lohse U., Samoson A., Mägi M., Tarnak M., Lipmaa I., Zeolites 2, 59 /1982, 3, 233 /1983/
15. Ione K.O., Echevskii G.V., Nosyreva G.N., J.Catal. 85, 287 /1984/
16. Beran S., J.Phys. Chem. 85, 1956 /1981/
17. Patzelová V., Bosáček V., Tvarůžková Z., Acta Phys. et Chem. /Szeged/ 24, 257 /1978/
18. Chang C.D., Silvestri A.J., J.Catal. 47, 249 /1977/
19. Jacobs P.A., Beyer H.K., J.Phys. Chem. 83, 1174 /1979/
20. Bastl Z., Bosáček V., Brechlerová D., In preparation
21. Hollins P., Pritchard J., Vibrational Spectroscopy of Adsorbates, Springer-Verlag, Berlin 1980, p.125
22. Huber H., Kundig D.P., Moskovits M., Ozin G.A., J.Am.Chem.Soc. 97, 2097 /1975/
23. Tuen M., Dimitrov Ch., Tyutyulkov N., Kinetika i Kataliz 24, 481 /1982/

AROMATIC SELECTIVITIES FOR LaY ZEOLITE CATALYZED DISPROPORTIONATION REACTIONS

D. J. Collins[a], E. D. Openstone[a], B. H. Davis[b]
Department of Chemical and Environmental Engineering, University of Louisville, Louisville, KY, U.S.A. (a)
Institute for Mining and Minerals Research, University of Kentucky, Lexington, KY 40512, U.S.A. (b)

ABSTRACT

Similar LaY zeolite catalyzed xylene isomerization rates are obtained whether a pure xylene reactant or a mixture of a xylene isomer with either ethylbenzene or toluene is used. Trimethylbenzenes formed from xylene disproportionation are kinetically controlled products that conform to a selectivity determined by the ortho-para directing influence of alkyl substituents. Ethyl containing aromatic disproportionation products, formed in nearly equal concentrations and in parallel with trimethylbenzenes, are present in a nearly equilibrium distribution even at low conversions. In these studies, it appears that shape selectivity and diffusion play a dominant role in determining the product distribution for ethyl containing alkyl aromatics.

INTRODUCTION

Kinetics for the isomerization, and in some cases disproportionation, of xylenes have been obtained for a variety of catalysts [1-6]. In most of the studies, it was concluded that isomerization followed a series of 1,2 methyl shifts. However, other isomerization mechanisms have been reported [7]. In general, the relative rate constants departed from those expected for a series reaction and approached those expected for a coupled reaction system (in effect, both 1,2- and 1,3- methyl shifts are allowed) as catalyst pore size decreased until, with the intermediate pore size zeolite HZSM-5, pore diffusion caused all relative rate constants to approach one [5].

Methyl groups direct ortho-para for electrophilic substitution. Hence, this rule permits a prediction of the initial aromatic products that result from disproportionation. For ortho-xylene the allowed substitution products are 1,2,3-trimethylbenzene and 1,2,4-trimethylbenzene but the 1,3,5-trimethylbenzene isomer is not allowed. With aluminum chloride [1] and LaY [4] catalysts it appears that this rule is obeyed. It also appears to apply for trimethylbenzene disproportionation with a LaY catalyst [4]. Little

attention has been paid to the mechanism for disproportionation of aromatics with alkyl groups larger than methyl. This study examines disproportionations where the larger side, present in chain ethylbenzene, may undergo transalkylation reactions.

EXPERIMENTAL

Catalyst Used. A sodium Y zeolite was multiply exchanged with lanthanum nitrate solutions [4]. The exchanged material was calcined in air at 873°K prior to use. The catalyst particles were very uniform in size and were approximately 80-120 microns in diameter.

Conversion and Analytical Procedures. Conversions were effected in a plug flow reactor containing one gram of catalyst. The catalyst was activated at 775°K prior to use. Reactant, without diluent, was passed over the catalyst at 623°K and 101kPa. The reaction mixture, unless otherwise noted, contained equal molar quantities of each reactant. Samples were collected at intervals and these were analyzed by g.c. using either a DB-5 or Bentone/dissodecylphthalate column to obtain conversion and product compositions [4].

RESULTS

Normalized xylene product data are plotted in figure 1 for the three xylene plus ethylbenzene reaction mixtures. Also included in figure 1 are lines representing earlier data [4] for the isomerization of the pure xylenes. Isomerization data obtained for three xylene plus toluene mixtures are similar to that shown in figure 1 except that the agreement between reference 4 data and the data from the present study is not as good. The experimentally determined straight line intercept in figure 1 corresponds to

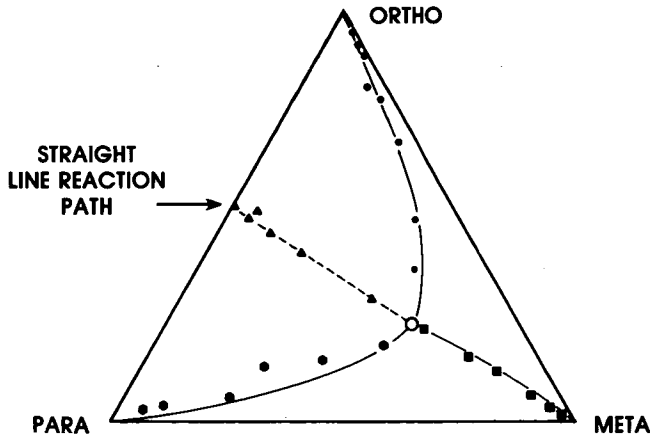

Fig. 1. Wei-Prater plot for xylene products from the conversion of ethylbenzene and xylene mixtures (solid lines from ref. 4).

0.53 fraction of ortho-xylene; this compares to 0.54 (reference 4) and 0.50 (reference 8) for isomerization of pure xylenes. The intercept was the same whether toluene or ethylbenzene was mixed with xylene. The relative rate constants calculated for the pure reactants with $AlCl_3$, LaY and HZSM-5 are presented in Table 1 along with those obtained with the mixed reactants used in the present study. The relative rate constants obtained for the ethylbenzene/xylene reaction mixture using a LaY catalyst are similar to those obtained earlier with the pure xylene reactants using another portion of the same LaY catalyst batch. The constants calculated for xylene plus toluene mixtures are somewhat less indicative of a series isomerization mechanism than when ethylbenzene was used as the diluent.

Table 1

WEI-PRATER RELATIVE RATE CONSTANTS

	LaY			HSZM-5	$AlCl_3$
	This Study				
Rate Constants	Xylene + Ethylbenzene	Xylene + Toluene	Pure Xylene [4]	Pure Xylene [5]	Pure Xylene [1] 60°C
Ortho→Meta, k_{21}	9.50	5.39	10.9	2.13	$2.1(10^5)$
Meta→Ortho, k_{12}	4.18	2.35	4.79	1.12	$5.8(10^4)$
Para→Meta, k_{23}	8.80	4.95	8.08	2.58	$2.8(10^5)$
Meta→Para, k_{32}	3.93	2.21	3.61	0.84	$9.4(10^4)$
Para→Ortho, k_{13}	1.0	1.0	1.0	1.0	1.0
Ortho→Para, k_{31}	1.02	1.02	1.02	1.14	1.2

Ethylbenzene disproportionates to form equal molar amounts of diethylbenzene and benzene. A plot of benzene versus diethylbenzene show that the experimental data fit rather well the straight expected for disproportionation. The normalized diethylbenzene product compisition (figure 2) is constant for a wide range of ethylbenzene conversions. Toluene can disproportionate to form xylene and benzene. At low conversions, xylene formation appears to be controlled by ortho-para directing effects. With increasing toluene conversion the xylenes approach an equilibrium mixture and attain this equilibrium value when about 30% toluene has been converted.

Normalized diethylbenzene distributions for the conversion of an ethylbenzene ortho-xylene mixture are shown in figure 3. The products resemble those obtained for the conversion of ethylbenzene alone except that slightly less of the meta and para isomers, and more of the ortho isomer, are formed. With ortho-xylene present, the equilibrium composition [9] is obtained whereas the one obtained with ethylbenzene alone has more of the meta isomer and less of the ortho isomer than an equilibrium mixture. Similar diethylbenzene distributions were obtained if either meta-xylene or para-xylene was substituted for ortho-xylene in the reaction mixture.

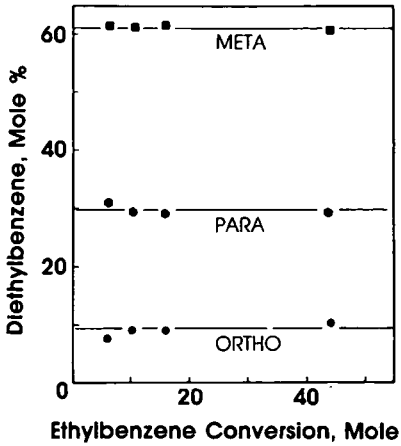

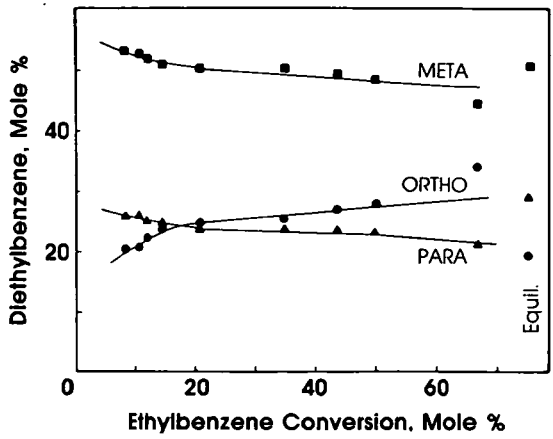

Fig. 2 (left). Disproportionation products from ethylbenzene conversion.

Fig. 3 (right). Diethylbenzenes formed from ortho-xylene/ethylbenzene conversion.

Xylene plus ethylbenzene can disproportionate by two reaction pathways:

(1) xylene + ethylbenzene = toluene + ethyltoluenes, and

(2) xylene + ethylbenzene = benzene + ethyldimethylbenzenes.

Three isomers of ethyltoluene and six isomers of ethyldimethylbenzene may be formed by reactions (1) and (2). Each ethyldimethylbenzene isomer was not related to a g.c. peak due to the small amount of these components and to the lack of suitable standards. Thus, the relative importance of the above two reactions was estimated from the benzene/(benzene plus toluene) fraction; this ratio increases with decreasing conversion and it appears that the transfer of the ethyl group is favored over that of the methyl group by a factor of 3 to 4. Both benzene and toluene can be formed by the disproportionation of ethylbenzene and xylene, respectively; however, correcting for the disproportionation (▲ in figure 4) leads to a similar conclusion. Comparing

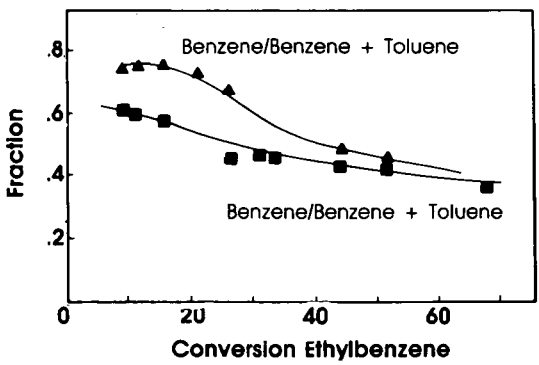

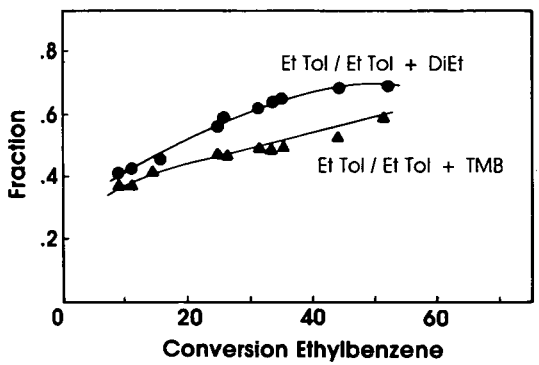

Fig. 4a (left). Fraction of benzene (■) and corrected (see text) fraction of benzene (▲) for ortho-xylene/ethylbenzene conversion.

Fig. 4b (right). Ethyltoluene fraction of C_9 aromatics (▲), and ethyltoluene plus diethylbenzene (●).

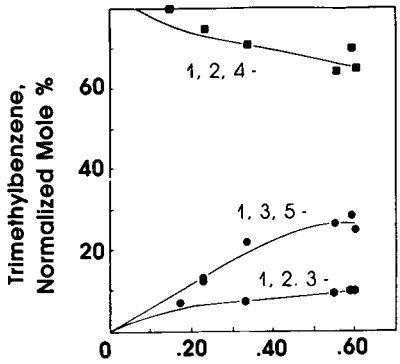

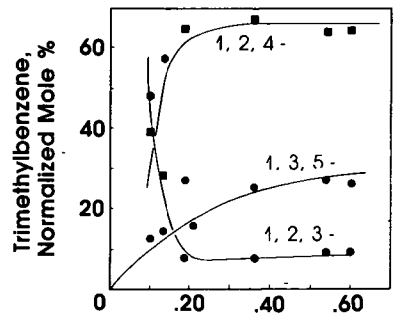

Fig. 5 Trimethylbenzene fraction from <u>para</u>-xylene/ethylbenzene conversion. (left)
Fig. 6. Trimethylbenzene distribution from <u>meta</u>-xylene/ethylbenzene conversion. (right)

the self-disproportionation (i.e. trimethylbenzene from xylene or diethylbenzene from ethylbenzene) to the crossed disproportionation (i.e. ethyltoluene) formation shows: (a) that ethylbenzene and xylene undergo disproportionation at about the same rate and (b) that crossed disproportionation is favored by a factor of 2 over self-disproportionation as expected on a statistical basis for the equal-molar mixture used in this study.

Disproportionatin of xylene to trimethylbenzenes and toluene has been shown to proceed in a one-to-one molar ratio to produce a trimethylbenzene isomer distribution dictated by the ortho/para directing nature of methyl substituents [4]. From methyl group directing effects, it is expected that only 1,2,4-trimethylbenzene should result from <u>para</u>-xylene disproportionation. The trimethylbenzene distribution data obtained with a para-xylene plus ethylbenzene mixture (figure 5) show that 1,2,4-trimethylbenzene is indeed the predominant product and that its fraction increases with decreasing conversion. Both 1,3,5- and 1,2,3-trimethylbenzene decrease with decreasing conversion and appear to approach zero at zero conversions. The data in figure 6 for <u>meta</u>-xylene plus ethylbenzene conversion also agree with the pattern expected for directing effects since the 1,3,5-trimethylbenzene fraction decreases with decreasing conversion so that the lower conversion products are only the two expected isomers; 1,2,4- and 1,2,3-trimethylbenzene. The <u>ortho</u>-xylene plus ethylbenzene reaction mixture also follows the trend expected for ortho-para directing effects. Thus, the selectivity patterns for disproportionation of xylene to trimethylbenzenes in the xylene/ethylbenzene mixtures are very similar to the ones obtained for pure xylene reactants.

Two reactions must be considered for disproportionation of a xylene plus toluene mixture:

(3) xylene + xylene = TMB + toluene, and

and

(4) xylene + toluene = TMB + benzene.

If pathway (4) applies, disproportionation products, trimethylbenzene and benzene, will form in equal molar amounts. However, the amount of TMB produced is much greater than the amount of benzene (figure 7). Consequently, the predominate pathway for trimethylbenzene formation is via xylene-xylene disproportionation.

Figure 8 illustrates the normalized trimethylbenzene isomer distributions versus total trimethylbenzenes formed for para-xylene disproportionation in the presence of toluene. The data indicate that an equilibrium trimethylbenzene mixtures are formed over the entire conversion range. Similar results were obtained when ortho-xylene or meta-xylene was substituted for the ortho-xylene reactant.

Disproportionation of ethylbenzene and ortho-xylene produces ethyltoluene. From 20% to 70% conversion of ethylbenzene the ethyltoluene distribution is essentially constant and contains more than the equilibrium concentration of meta-ethyltoluene and less than the equilibrium concentration of para-ethyltoluene. It appears that the para isomer concentration increases rapidly as the conversion decreases; parallel to this, the concentration of both the ortho- and para- isomers decreases with decreasing conversion (figure 9). The diethylbenzene products, formed along with the ethyltoluenes shown in figure 9, are at a nearly equilibrium composition; however, at low ethylbenzene conversion the ortho-diethylbenzene fraction is greater, and the

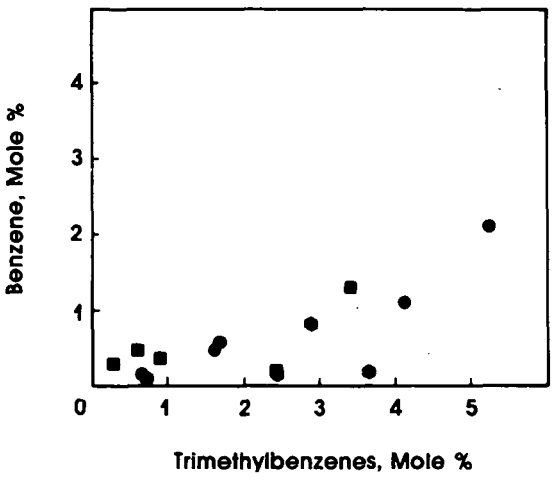

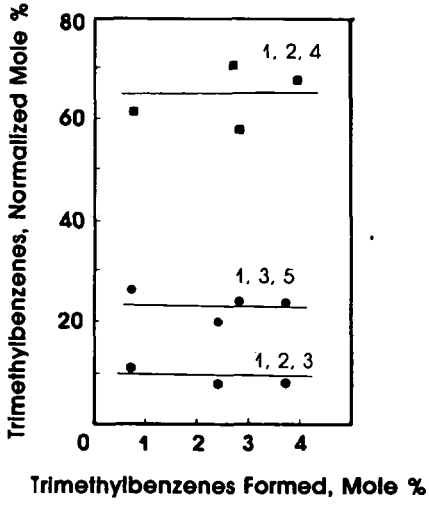

Fig. 7. Disproportionation products from toluene and xylene (ortho, ●; meta, ■ ; para, ◆) conversion.(left)

Fig. 8. Trimethylbenzene distribution from toluene and para-xylene conversion. (right)

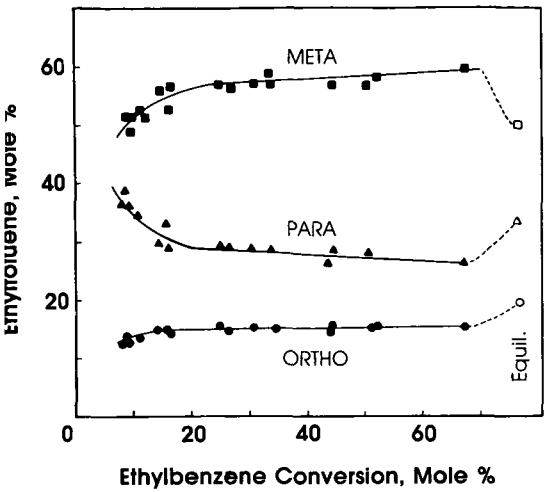

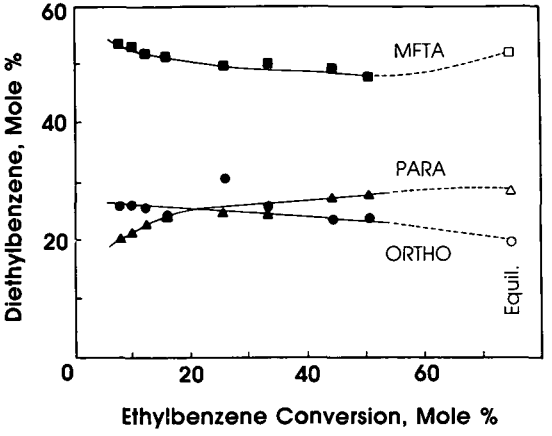

Fig. 9. Ethyltoluene products from the conversion of an ortho-xylene/ethylbenzene mixture.(left)

Fig. 10. Diethylbenzene from the conversion of ortho-xylene/ethylbenzene mixtures.(right)

para-diethylbenzene fraction is less, than the equilibrium amount. Similar results were obtained if either meta- or para-xylene was substituted for ortho-xylene.

The trimethylbenzenes formed in the samples represented in figure 9 and 10 resemble those found earlier [4] with the 1,2,3- and 1,2,4 isomers, both allowed by methyl directing effects, being the dominant, low conversion product (figure 11). 1,3,5-Trimethylbenzene, not allowed by alkyl directing effects, approaches a low, or zero, concentration at low conversions.

An equimolar mixture of toluene and ethylbenzene was also converted over the catalyst at 623°K. With these reactants the meta isomer, both diethylbenzene and ethylbenzene, was in excess of the equilibrium amount while the ortho isomer was lower than the equilibrium amount (figure 12).

DISCUSSION

The relative isomerization rates of xylene are essentially the same whether the reactant is a pure xylene or a xylene isomer in a mixture with ethylbenzene or toluene. This result suggests that the predominant xylene isomerization pathway with LaY is not by a disproportionation mechanism as has been proposed by some [7]. Rather, the isomerization occurs by a series of 1,2 methyl shifts.

Disproportionation is complex. With xylene reactants initial, primary disproportionation products include only those trimethylbenzene isomers that are allowed by alkyl ortho-para directing influences. Also, rate constants for trimethylbenzene isomerization with LaY are very similar to those for

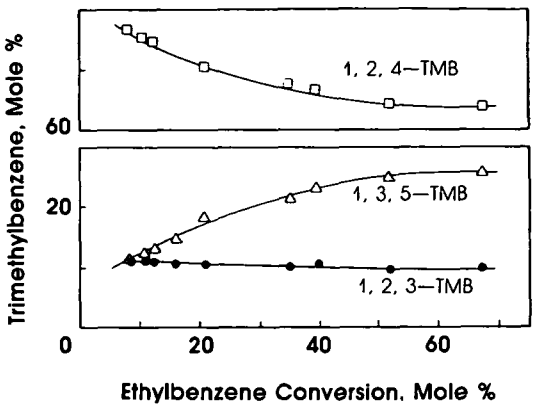

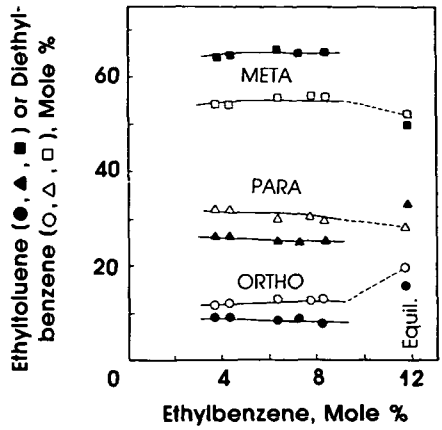

Fig. 11. Trimethylbenzenes formed during the conversion of an ortho-xylene/ethylbenzene mixture. (left)

Fig. 12. Ethyltoluene and diethylbenzene product distribution from the conversion of a toluene/ethylbenzene mixture. (right)

xylene [10]. This is the case whether ethylbenzene is present or not. However, for ethyl containing disproportionation products, diffusion as well as chemical selectivity both appear to play a role in determining reaction products.

Kaeding and co-workers [11] show that shape selectivity will favor the isomer with the minimum dimension with intermediate pore size zeolites such as HZSM-5. With ethyltoluene and diethylbenzene, the para isomer has the smallest minimum dimension, followed by the meta and then the ortho isomer. In our study, the products show evidence for a small degree of shape selectivity. In addition, diffusion of ethyl containing products appears to be considerably slower than for trimethylbenzene products. Thus, initial trimethylbenzene distributions are clearly controlled by chemical selectivity and are far removed from the equilibrium values whereas ethyltoluenes or diethylbenzene isomers are produced, in the bulk liquid, in nearly equilibrium concentrations even at low conversions. This is true even though trimethylbenzene and ethyl containing disproportionation products are formed in nearly equal amounts in the catalyst pores. To learn the extent that ortho-para directing effects influence the disproportionation products for the transfer of ethyl or longer carbon-chain substituents will require the use of much smaller size zeolite catalyst particles than employed in the present study on the use a catalyst with pores much larger than those present in this LaY catalyst.

REFERENCES

1. Collins, D. J., Scharff, R., Davis, B. H., Appl. Catal., 8, 273 (1983).
2. Allen, R., Yats, L., J. Amer. Chem. Soc., 81, 42, 5289 (1959).
3. Sitvestri, A. J., Prater, C. D., J. Phys. Chem., 68, 3268 (1964).
4. Collins, D. J., Mulrooney, K. J., Medina, R. J., Davis, B. H., J. Catal., 75, 291 (1982).
5. Collins, D. J., Medina, R. J., Davis, B. H., Canadian J. Chem. Eng., 61, 29 (1983).
6. McCauley, D. A., Lin, A.. P., J. Amer. Chem. Soc., 74 6246 (1952).
7. Lanewala, M. A., Bolton, A. P., J. Org. Chem., 34, 3107 (1969).
8. Chutoransky, P., Jr., Dwyer, F. G., Advances in Chemistry, 121, pp. 540-552 (1973).
9. Stull, D. R., Westrum, Jr., E. F., Sinke G.C.: The Chemical Thermodynamics of Organic Compounds. John Wiley & Sons, Inc., New York, NY, 1969.
10. Collins, D. J., Quirey, C. B., Fertig, J. E., Davis, B. H., submitted for publication.
11. Kaeding, W. W., Young, L. B., Chu, C.-C., J. Catal., 89, 267 (1984).

CORRELATIONS BETWEEN THE ACIDITY AND CATALYTIC PROPERTIES OF H,Na-MOR

D.Kalló, I.Bankós, J.Papp

Central Research Institute for Chemistry of the Hungarian Academy of Sciences, H-1525 Budapest, P.O.Box 17

ABSTRACT

Acid centres formed by different degrees of decationization have been characterized by the adsorption heat of ammonia and by I.R. spectroscopy. We have established that H,Na-MOR shows a broad acid strength distribution with distinct steps representing different acid strengths. The active sites for m-xylene disproportionation and isomerization can be attributed to centres having adsorption heats for ammonia above 150 kJ/mol, and 120-150 kJ/mol, resp. The disproportionation centres are formed at higher degrees of decationization.

INTRODUCTION

Both isomerization and disproportionation of xylenes take place on acid sites of zeolite catalysts. The ratio of the two transformations i.e. the selectivity depends on the reaction conditions, and on the type and pretreatment of the catalyst [1, 2]. Therefore, different mechanisms have been suggested for the monomolecular isomerization and for the bimolecular disproportionation, which involve different interactions between the acid catalyst and xylene. As a consequence of this difference the selectivity can be expected to be influenced by the strength and the number of acid sites. In addition, steric factors may play an important role in the case of zeolites having pore sizes commensurable with the molecular dimensions of xylenes [2].

The correlation between the catalytic properties and the degree of decationization has been widely investigated for H,Na-Y,FAU [1]. It has been found that active sites of different activities were formed at lower and at higher degrees of decationization [3, 4]. Similar conclusions have been drawn for H,Na-MOR [5-7] but without any detailed correlation with the acidity.

As it is well known acid sites can be studied conveniently by I.R. spectroscopy [8]. The method provides with very important informations on the nature of acid centres, but the quantitative evaluation of the results in rather troublesome. The strength and the number of acid sites can also be determined by titration, the conditions of which differ, however, essentially from those of catalytic reactions.

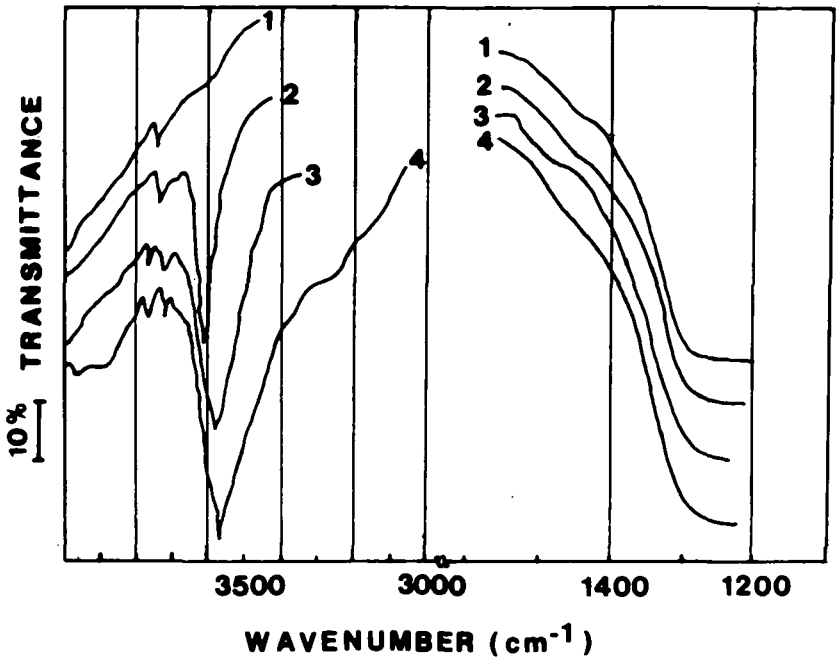

Fig. 1. Infrared spectra of NH_4,Na-MOR samples after evacuation at 823 K for 5 hours. 1.: M-33; 2.: M-46; 3.: M-83; 4.: M-98.

The measurement of the adsorption heat of bases like ammonia seems more promising [9, 10]. The microcalorimetric determination of differential adsorption heat of small doses of ammonia affords to obtain the acid strength distribution of the sites on the catalyst sample.

The aim of the present work was to determine the nature and the acid strengths distribution of active sites in H,Na-MOR, and to correlate them with the catalytic activities for xylene isomerization and disproportionation.

EXPERIMENTAL

Preparation of catalysts

H,Na-MOR samples were prepared from Na-MOR (Zeolon 100, Norton Co., USA) by ion-exchange for ammonium to different degrees in the usual way. Samples of 33, 46, 83 and 98 per cent degree of ion-exchange were produced (M-33, M-46, M-83, M-98). Thereafter they were pelletized without binder. Activation was carried out in the reactor at 823 K for

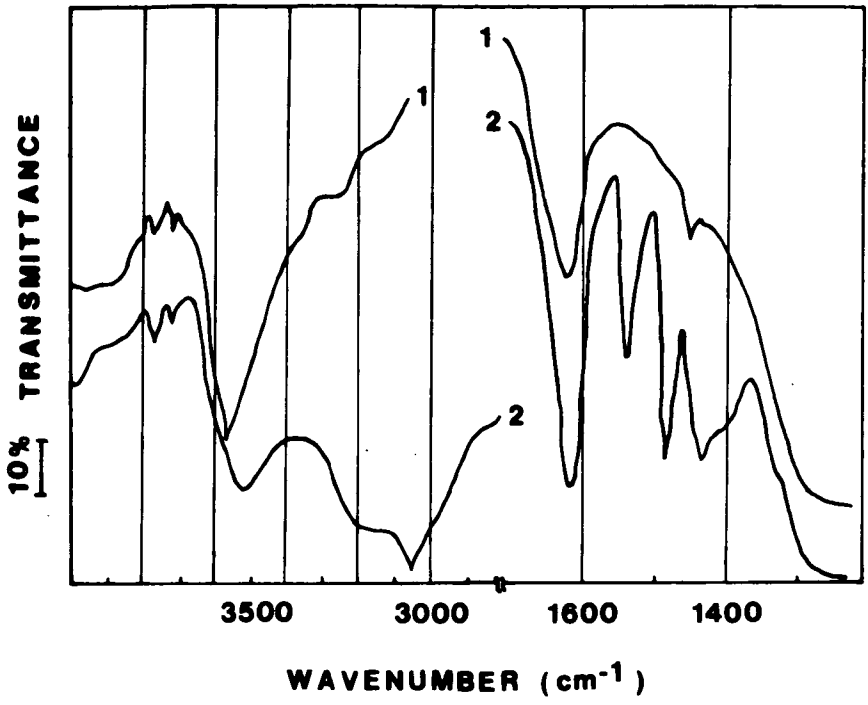

Fig. 2. Infrared spectra of M-98 sample.
1.: after pretreatment at 773 K for 5 hours;
2.: after pyridin adsorbed on the sample at room temperature, at a pressure of 2.66 kPa.

8 hours in a flow of hydrogen.

Catalytic measurements

Transformations of m-xylene were determined in an integral flow reactor at 573 K, at space velocities between 2.5 and 13 hour^{-1}, at 0.5 MPa hydrocarbon pressure and 1.5 MPa hydrogen pressure. Gaseous and liquid products were analyzed with a JEOL 810 gas chromatograph.

I.R. measurements

I.R. measurements were performed in a Perkin Elmer 577 spectrophotometer in the range of 1000-4000 cm^{-1}. The samples were pressed without binder in wafers of a thickness around 10 mg/cm^2.

Calorimetric investigations

Differential adsorption heat was measured in a Calvet calori-

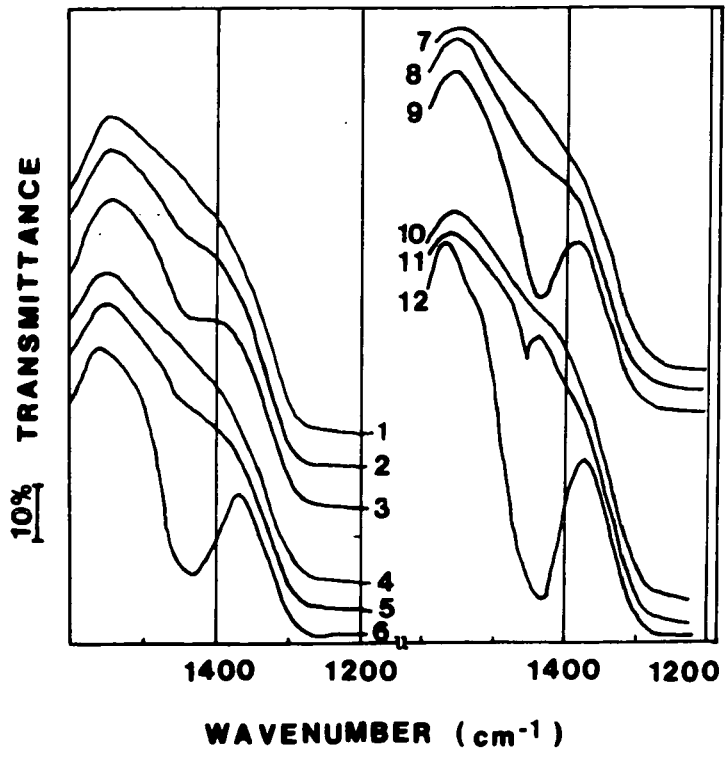

Fig. 3. Infrared spectra of NH_4,Na-MOR samples after evacuation at different temperatures for 5 hours, 1., 2., 3.: at 623, 573, 473 K for the sample M-33; 4., 5., 6.: at 723, 673, 573 K for the sample M-46; 7., 8., 9.: at 773, 723, 673 K for the the sample M-83; 10, 11, 12.: at 823, 773, 673 for the sample M-98.

meter connected to a volumetric adsorption apparatus. Before adsorption samples were pretreated at 753 K for 40 hours at 10^{-3} Pa. Calorimetric measurements were carried out by admitting small doses of ammonia at 573 K. The details of the method are described in [11].

RESULTS AND DISCUSSION

I.R. spectra in Fig. 1 show the intensity changes of acidic OH bands for samples of different degree of decationization. It is striking that practically no OH groups are detectable on the sample having been exchanged for ammonium up to 33 per cent. Dehydroxylation should

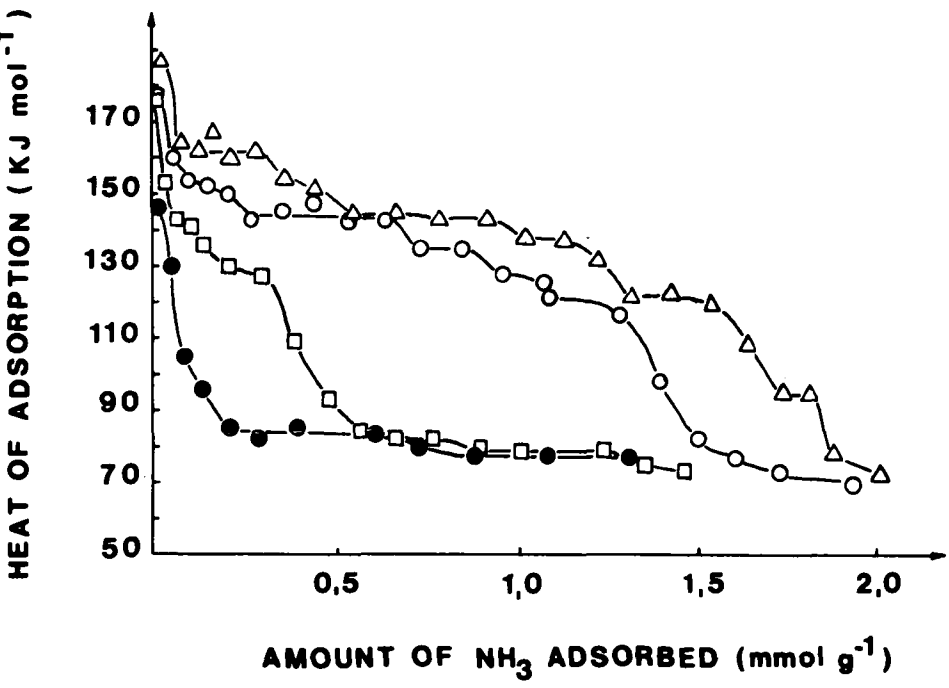

Fig. 4. Differential heat of adsorption as a function of coverage. Adsorption of NH_3 was carried out at 573 K, on M-98 (Δ), on M-83 (o), on M-46 (□), on M-33 (●).

accompany the total deammoniation being very pronounced in the case of low degree of decationization. Dehydroxylation has been traced also for the deeply exchanged sample M-98. Since dehydroxylation results in the formation of Lewis acid sites [12] which can be easily detected by the appearance of the typical absorption bands of pyridin bound to these sites, the pyridin adsorption on sample M-98 pretreated at 773 K was studied by I.R. spectroscopy (Fig. 2). Pyridin adsorption both on Brönsted and on Lewis acid sites can be observed. The presence of Lewis acid sites indicates a significant dehydroxylation Similar measurements were carried out with sample M-33 after pretreatments at 623 and 823 K. Even at 623 K dehydroxylation was detectable, and the ratio of Lewis and Brönsted acid sites was as high 27.7 after a pretreatment at 823 K. This ratio after a pretreatment at 823 K was 3.7 for sample M-98.

It is to be remarked that pyridin adsorption does not result in the total disappearance of acidic OH vibration band (cf. spectra 1 and

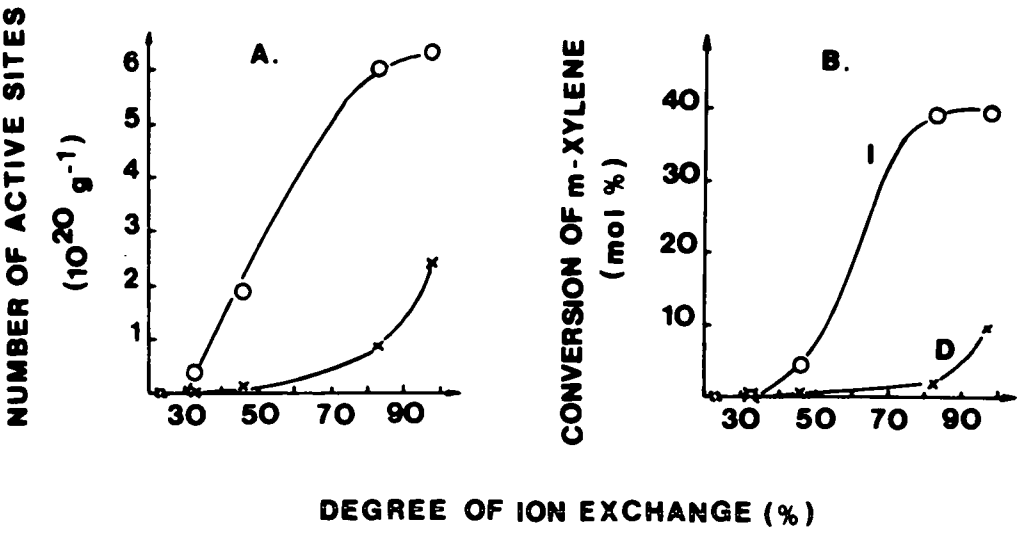

Fig 5. A: number of active sites [$q_{diff}^{NH_3}$ = 120-150 kJ mol^{-1} (o), $q_{diff}^{NH_3}$ > 150 kJ mol^{-1} (x)], B: isomerization (o) and disproportionation (x) conversions as a function of degree of ion-exchange. Adsorption temperature 573 K, reaction temperature 573 K, initial pressures: 0.5 MPa m-xylene, 1.5 MPa hydrogen.

2 in Fig. 2 in the range of 2800-4000 cm^{-1}), which may indicate that a considerable fraction of Brönsted sites is not accessible for pyridin and neither it is for xylene.

The changes of deammoniation of samples M-33, -46, -83, -96 ar illustrated in Fig. 3. The intensities of the bands in the range of am monium deformation vibrations show that the higher the NH_4-ion exchan degree is the higher temperature is needed for the decomposition of th ammonium form under the given conditions. Acid sites of different strength can be concluded: increasing the degree of ion-exchange ammonium occupies stronger acidic sites.

A quantitative correlation between the strength and the number of acid sites can be established by the determination of differential adsorption heat of ammonia as a function of the adsorbed amount of ammonia for samples of different decationization degree (Fig. 4). In thi way all the uncertainities of non-isothermic determination of isosteric adsorption heat can be avoided; i.e. on changing the temperature the

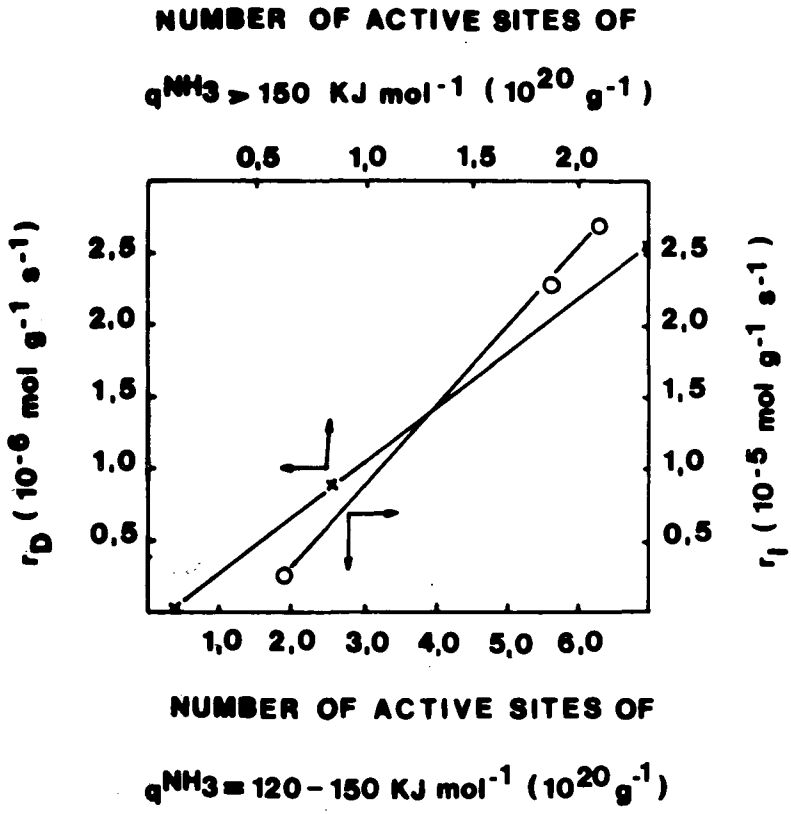

Fig. 6. Initial rates of isomerization (o) and disproportionation (x) as a function of the ion-exchange degree. Reaction conditions are the same as in Fig. 5B.

acid sites can be modified consequently the adsorption heat can change.

The curves in Fig. 4 show that the differential adsorption heat decreases with the coverage.

Being the adsorption heat of ammonia on Na-zeolites around 90 kJ/mol [11], the amount of ammonia bound with a higher energy has to be considered as chemisorbed on decationized sites.

A heterogeneous acid site distribution can be evidenced from the curves in Fig. 4. They are significantly different for the different decationized samples: the lower the degree of decationization by far less the number of stronger acid sites. Well-defined steps at the same heights are often observed on different curves reflecting the existence of distinctly different acid sites.

We tried to find correlation between the acidity and the activity for m-xylene isomerization and disproportionation. Isomerization and disproportionation conversions measured under identical conditions are plotted against the degree of ammonium ion-exchange (Fig. 5.B). As it has been mentioned the two transformation proceed on centres of different acid strength. We looked for acid sites of different strength having a number which shows a similar function of the ammonium ion-exchange as the activities.

The number of acid sites characterized by ammonia adsorption heats between 120 and 150 kJ/mol seems to change similarly with the ammonium ion-exchange (Fig. 5A) as the isomerization conversion, and the number of sites above 150 kJ/mol shows a similar curve (Fig. 5A) as the disproportionation conversion.

If the degree of ammonium ion-exchange is 33 %, no catalytic activities are observable, and the numbers of the corresponding active sites are practically zero.

More accurate and more reliable correlation can be established between the activities and acidities when the initial rates of isomerization and disproportionation are plotted against the number of the above active sites (Fig. 6).

The linear correlation substantiates the existence of distinct active sites responsible for the two transformations. The sections on the abscissa correspond either to the active sites accessible for ammonia but not for xylene (cf. pyridin adsorption in Fig. 2) or to the dehydroxylation which may be suppressed during the low temperature long time pretreatment for calorimetric measurements but takes place to some extent during the activation in the reactor.

These recognitions permit to prepare a decationized mordenite catalyst of high isomerization selectivity and of satisfactory activity: acid sites with more than 150 kJ/mol ammonia adsorption heat must not be formed. This can be attained by partial decationation and/or partial poisoning.

ACKNOWLEDGEMENT

The authors wishes to express their grateful acknowledgement to Dr.A.L.Klyachko and his coworkers (N.D. Zelinsky Institute of Organ Chemistry of USSR Academy of Sciences, Moscow, USSR) for the careful calorimetric measurements, for helpful discussions, and to Mr.J.Papp for the determination of the infrared spectra.

REFERENCES

1. P.A.Jacobs. "Carboniogenic Activity of Zeolites" p. 125. Elsevier, Amsterdam, New York 1977
2. S.M.Csicsery, J.Catal. 19, 394 (1970)
3. K.Tsutsumi, H.Takahashi, J.Catal. 24, 1 (1972)
4. J.W.Ward, R.C.Hansford, J.Catal. 13, 364 (1969)
5. Kh.Minachev, V.Garanin, T.Isakova, V.Kharlamov, V.Bogomolov, in Molecular Sieve Zeolites-II. (eds.: E.M.Flamingen and L.B.Sand) ACS Monograph Ser. 10. 102, Am.Chem.Soc., Washington D.C., 1971, p. 441
6. J.A.Gray, J.T.Cobb, J.Catal. 36, 125 (1975)
7. P.Ratnasamy, S.Sivasankar, S.Vishnoi, J.Catal. 69, 428 (1981)
8. J.W.Ward, in Zeolite Chemistry and Catalysis (ed. J.A.Rabo) ACS Monograph, Ser. 171, Am.Chem.Soc. Washington D.C., 1976, p. 118
9. T.R.Bruera, A.L.Klyachko-Gurvich, A.M.Rubinstein, Izvest. Acad. Nauk S.S.S.R., Ser. Khim. 2807 (1972); 1254 (1974)
10. T.Masuda, H.Taniguchi, K.Tsutsumi, H.Takahashi, Bull. Chem. Soc. Japan, 51, 1965 (1978)
11. G.J.Kapustin, T.R.Brueva, A.L.Klyachko, A.M.Rubinstein, Kinetika i Kataliz, 22, No. 6. 1561 (1981)
12. J.W.Ward, J.Catal. 9, 225 (1967); T.R.Hughes, H.M.White, J. Phys. Chem. 71, 2192 (1967)

CONVERSION OF ALKYLAROMATICS ON HIGH-SILICA MORDENITES

V. Mavrodinova, Ch. Minchev, L. Kozova, V. Penchev
Institute of Organic Chemistry, Bulgarian Academy of Sciences,
Sofia 1040, Bulgaria

ABSTRACT

Comparison is made on the acidity and catalytic behaviours during toluene and o-xylene conversion on silica-rich mordenites with close chemical compositions obtained by direct synthesis or by dealumination with HCl and EDTA. The samples acidity is studied by the TPD of NH_3. The catalytic activity is measured in a flow reactor at temperatures between 453 and 513K and atmospheric presure in presence of H_2 or Ar as carrier gases. It is found, that samples obtained by direct synthesis possess a higher disproportionation activity and are deactivated much more rapidly than the modernites dealuminated with HCl and EDTA. On the basis of the results obtained some differences and peculiarities in the catalytic action of the mordenite samples with nearly the same chemical composition, prepared in various ways were interpreted.

INTRODUCTION

The discovery of the new class of high-silica zeolites of the ZSM-5 type have rekindled the interest in the silica-rich mordenites too. The catalytic activity of these mordenites can be influenced by varying the SiO_2/Al_2O_3 ratio over a very large interval using dealumination with mineral acids or chelating agent /1/. Another possibility to reduce the aluminium content is the direct synthesis, varying the composition of the initial gel /2, 3/. Thus, silica-rich mordenites appear to be a suitable model system for studying the effect of the preparation method on the catalytic performance of zeolites with equal crystalline structures. The increasing interest in these systems is also due to recent data concerning the differences in Al distribution in the zeolite crystal depending on the preparation conditions /4, 5/. In other words, high silica mordenites present a possibility to investigate the effect of both the content

and the distribution of aluminium on its properties. In the literature there are no comperative data on the catalytic behaviour of silica-rich mordenites prepared by direct synthesis and by dealumination excepting the data from the systematic studies of Minachev et al. on o-xylene conversion /5/ and ethylene aromatization /2/.

The catalytic action of the H-forms of mordenites with close chemical composition synthesized in different ways are compared in the present paper with respect to the conversion of toluene and o-xylene. The sample used had a SiO_2/Al_2O_3 ratio ranging from 11 to 18, achieved by direct synthesis (designated as MS) and dealumination of NaM with HCl and EDTA (MD). Special attention was paid to the disproportionation reaction since it is assumed to be especially sensitive to zeolite treatments which modify the acid center concentration /6/. The acidic properties of the samples were also characterized by TPD of ammonia.

EXPERIMENTAL

Table 1
Chemical composition of the catalysts used

Samples	SiO_2/Al_2O_3 mol ratio	NH_3 mmol/g	Mode of preparation
$MS_{11,7}$	11,7	-	Direct Synthesis
$MS_{15,7}$	15,7	0,96	
$MS_{18,2}$	18,2	0,98	
$MD_{14,4}$	14,4	-	2,2M HCl
$MD_{14,7}$	14,7	1,05	6,0M HCl
$MD_{17,4}$	17,4	0,99	6,0M HCl
$MD_{15,3}$	15,3	-	EDTA
$MD_{12,1}$	12,1	0,94	EDTA

Table 1 presents the chemical composition of the samples. The Na-forms of MS were obtained by direct synthesis at 423K in an autoclave with stirring /2/. MD were prepared from NaM with a SiO_2/Al_2O_3 ratio of 10 by dealumination with EDTA or with 2,2 and 6,0 M HCl at 358K /7/. The preparation of the H-forms of MS and MD (dealuminated with EDTA) was achieved by ion exchange with 2M NH_4Cl solution followed by thermal treatment of the ammonium modifications at 723K for 6 h in air. The phase purity and the crystallinity of the samples were controlled with a DRON-1 diffractometer using CuK_α radiation and electron

microscopy /8/.
The samples acidity was determined by TPD of NH_3. The procedure employed was described in /9/. The catalytic studies were carried out in a flow reactor at atmospheric pressure in presence of H_2 and Ar as carrier gases, the gas: hydrocarbon ratio being 10. The temperature varied between 453 and 513K. WHSV of 1,1 h^{-1} was used.

RESULTS

Toluene disproportionation

The H-forms of the mordenite type zeolites are known to possess a high acidity and catalytic activity with respect to the conversion of alkylaromatic hydrocarbons, but are very rapidly deactivated /10, 11/. For this reason, a study of the catalytic performance of samples with practically the same chemical composition, obtained in different ways required selection of the experimental conditions ensuring a correct comparison of their catalytic activities. The reaction temperatures usually applied to toluene disproportionation proved to be inappropriate in this case due to pronounced side reactions. For this reason we used an aproach allowing a study of the activity change with the time on stream at a gradually increase of temperature up to values at which some of the samples showed offset of deactivation (Fig.1).

Comparison of the data on the catalytic activities of the two samples with SiO_2/Al_2O_3 about 18 showed MD to have a lower catalytic activity than MS but to be much more stable at temperatures of 453 - 493K (Fig.1 A). A similar situation was observed with MD (prepared under mild conditions - with 2,2M HCl) having a SiO_2/Al_2O_3 ratio of about 15 in comparison to MS (Fig.1 B).
To check the validity of what was established above, concerning the lower activity of MD than that of MS, we prepared a series of samples dealuminated also with EDTA. The results showed that irrespective of the way of dealumination all the MD probes had a lower activity and a better stability than the MS (with an analogous modulus, (Fig.1 B and C). In addition, it should be noted that due to the rapid ageing of MS samples at higher temperature (513K) the dealuminated materials become more active which could cause some misunderstandings. As the linear relatioship between lnk-1/T in the Arrhenius plot shows, there are no diffusional limitations for all the dealuminated samples investigated. Ea ranges from 14 up to 19 Kkal/mol.

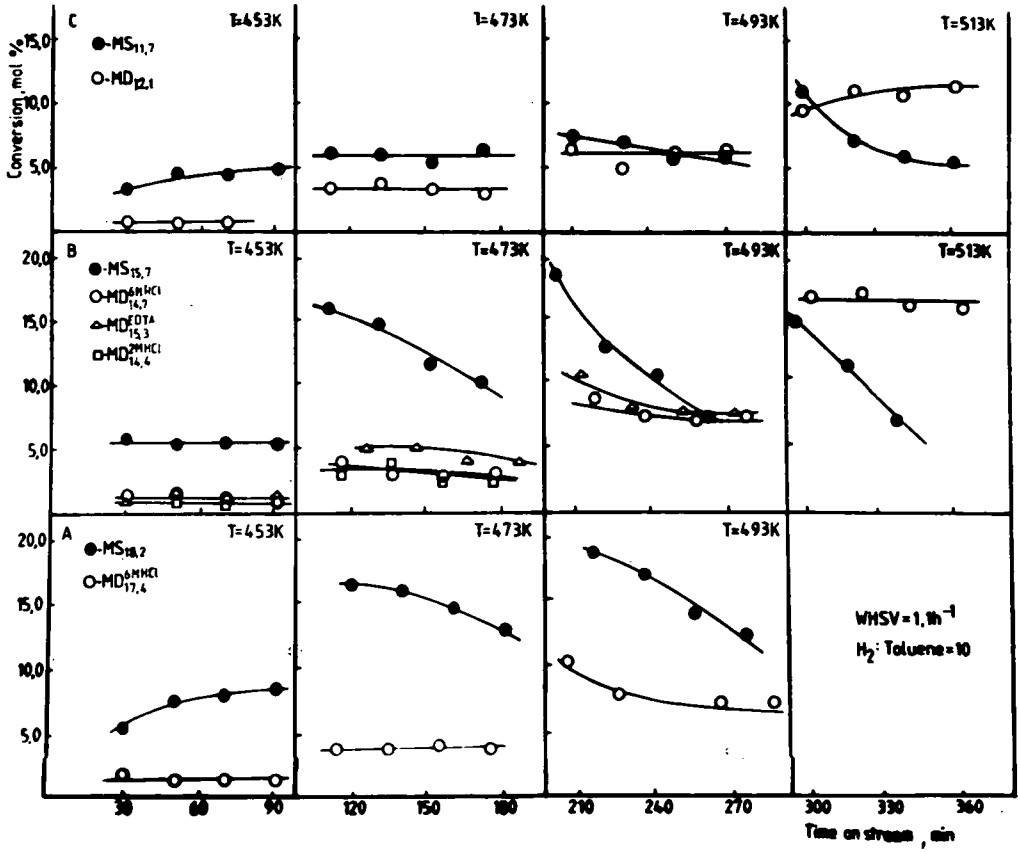

Fig.1. Toluene conversion over differently prepared mordenites with SiO_2/Al_2O_3 ratios about: A-18, B-15 and C-12

Another interesting result from the comparison of the catalytic action of directly synthesized and dealuminated samples is that MD have a considerably higher selectivity with respect to the disproportionation reaction. At higher temperatures the benzene: xylenes ratio is about 0,8 - 0,9 for MD whereas with MS it is considerably lower (0,6 - 0,7). It indicates a higher degree of dealkylation on MS. As far as this result presupposes the presence of more acidic centers in MS, it was of interest to compare the acidity of the series of samples with close SiO_2/Al_2O_3 ratios. Since the couples of mordenites being investigated had nearly the same aluminium contents, differences in the total number of acidic centers were not to be expected. Indeed, NH_3 adsorption at 573K (a temperature at which adsorption is assumed to proceed at the strongly acidic centers) gave practically the same amounts of ammonia adsorbed on the samples

being compared. The shapes of the thermodesorption curves were also analogous (Fig.2). The broad maximum at the thermodesorption curves observed with MS can be indicative of a larger number of strongly acidic centers.

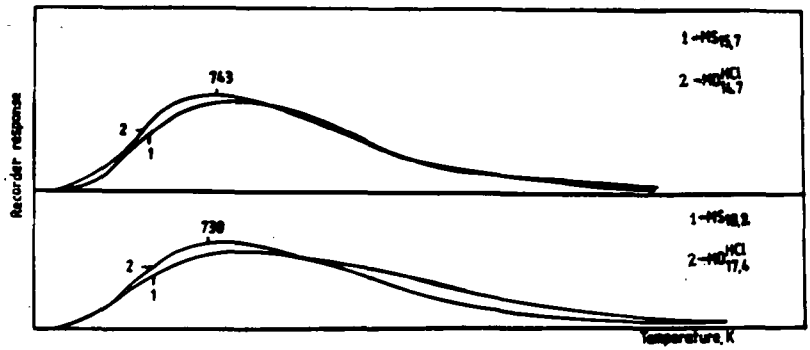

Fig.2. TPD chromatograms of NH_3 adsorbed at 573K

O-xylene conversion

It is known that the o-xylene molecule has a more basic character and a reactivity considerably exeeding that of toluene. This presupposes the proceeding of intensive xylene disproportionation along with isomerization on these strongly acidic catalysts. Hence, the study of o-xylene conversion allowed checking ones more the differences found in the disproportionation activities of MS and MD with respect to a higher - reactive hydrocarbon. On the other hand, comparison and differentation between the performance of the samples in the two competitive reactions: disproportionation and isomerization can be made.

The results indicate a higher o-xylene total conversion in presence of MD at temperatures 443-473K, which was found to be close to that of MS at 503K. However, comparison of the disproportionation and dealkylation activities of MD and MS with SiO_2/Al_2O_3 of about 18 showed a much larger contribution of these side reaction with respect to the total conversion at the very beginning of the experiment in the case of MS than in that of MD (55 and 50% respectively, Fig.3 A, 3 B). After the fast decrease in activity during the first twenty minutes of the experiment and the much more rapid deactivation of MS, MD exhibited higher disproportionation and isomerization ability. This is to be illustrated also by the presence of a maximum in the curves showing the change in the amount of the isomerization products (m- and p- xylenes) for the two samples being compared (Fig.3 C). Therefore, it can be stated that the trend to a very fast

ageing of MS disguises its considerably higher initial activity. In addition, this tendency is more pronounced with MS samples in both disproproportionation (Fig.3 A) and isomerization (Fig.3 C).

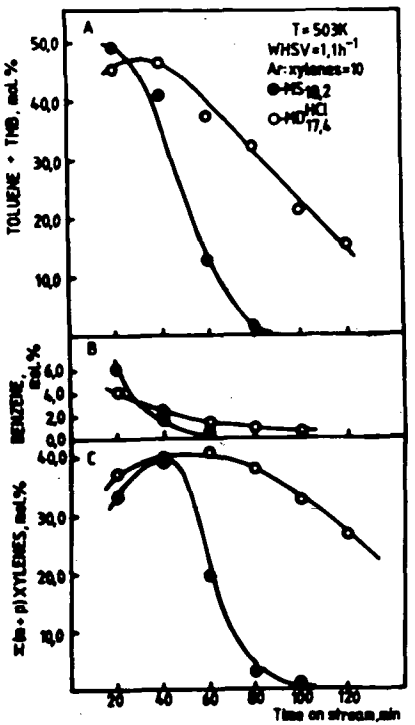

Fig.3. Conversion of o-xylene on dealuminated $MD_{17,4}$ and as-synthesized $MS_{18,2}$ at 503K

DISCUSSION

Comparison of the data obtained during conversion of alkyaromatic hydrocarbons at relatively low temperature (where effects of rapid deactivation are absent) showed that the directly synthesized samples had a higher disproportionation activity but a lower stability than the dealuminated ones. A higher activity of MS compared to MD with a similar chemical composition was also found in other reactions such as C_2H_4 aromatization /2/ and cracking of n-parafines /12/. On the other hand, the studies of Minachev et al. /5/ showed a higher total conversion degree of o-xylene on MD. Therefore, irrespective of the close Si/Al ratio the samples prepared by various methods differed in their behaviours.

It is known that the disproportionation activity of mordenite catalysts is directly associated with their Brønsted acidity /13-15/ or rather /14,15/ with the number of the strongly acidic centers of this type. Our results of TPD of ammonia at 573K showed nearly the same values of the total amount of NH_3 adsorbed for the pairs of samples with a close silicate modulus (Table 1). However, it is difficult to state explicitly that there are different number of centers with diverseing strengths. The data in Fig.2 only indicate this tendency. Obviously, as Jacobs et al. /16/ suggested, some slight differences in the acidity spectrum of samples with close compositions cannot be established by TPD of NH_3. For the present, measurements of the heats of ammonia adsorption /17/ have only permitted to state that there are some differences in acid strength distribution in MS (synthesized in the presence of a TEA-cation) and MD with an identical SiO_2/Al_2O_3 ratios of 20. However these differences alone cannot satisfactorily explaine the effects on the catalytic activities observed by us.

The presence of a gradient in the concenration of the Al atoms and hence, of the active centers (depending on the preparation conditions of the samples) may be an additional reason for the different performance of the mordenites. On the basis of data from the literature, dealumination with mineral acids /1, 4, 5/ and EDTA /1, 18/ leads to preferential elimination of aluminium from the surface layers of the mordenite crystals. In addition, a model proposed by us /19/ have shown that the absolute number of aluminium atoms in the unit cell of the samples obtained by dealumination is lower than that in the corresponding directly synthesized samples with the same silicate modulus. As far as the MS studied by us are concerned, the XPS data /5/ indicate a uniform distribution of Al in the zeolite crystal.

Thus it can be assumed that depending on the method of preparation, zones with active centers differing in number and strength appear in the mordenite crystal. The presence of this microheterogenity should affect the catalytic activity especially in cases when the reacting molecules and products have sizes comparable with those of the mordenite channels. Hence, appropriate variation of the experimental conditions and the kind of substrate used could give additional information on the existance of such a gradient in the concentration of the active centers.

Indeed, our data concerning the distribution of the products of xylene disproportionation - toluene and thrimethylbenzenes (TMB) confirmed this assumption. At relatively low reaction temperatures (443K) in the absence of cracking products, the toluene : TMB molar ratio was to be equal to 1. This was actually observed with the directly synthesized samples only. On the contrary, at practically identical conversion degrees, this ratio was by about one order of magnitude higher for MD and only at 503K it became equal to that for MS. A similar increase in the toluene/TMB ratio was found with rising the contact time. Only at very low conversion degrees, after practically complete deactivation of the MD samples, the toluene : TMB ratio approached unity. It should be noted that the above factors (reaction temperatures, contact time and degree of deactivation) did not affect the value of the toluene : TMB ratio for the MS samples.

On the basis of the results obtained and the hypotheses suggested the different behaviours of MS and MD could be explained as follows. The higher concentration of active centers in the pore mouth of the MS zeolite facilitates its rapid interaction with the reacting molecules and determines the relatively higher initial disproportionation activity of this sample. As some authors proposed, bimolecular disproportionation needs a pair of nearly situated acid sites /13/, which density on the surface of MS probably is greater than on MD.

The faster deactivation compared to that of MD is an additional evidence of the prevailing participation of centers localized near the surface and of the relatively quick blocking of the access to the interior sites. A similar explanation of the effect of the acid center dencity on the stability of the catalytic activity can be found in the literature for highly dealuminated zeolites /18, 20/. With dealuminated samples disproportionation probably proceeds at a larger depth of the mordenite crystal due to the selective denuding of the surface layers and pore mouth sites in the process of dealumination /18/. This can be the reason for the lower disproportionation activity and enhanced toluene : TMB ratio during a reaction proceeding at lower temperatures. The processes of coke precursor formation also concerns a zone inside the zeolite crystal. Moreover, after being formed in the narrow mordenite channels, the large molecules of the polyalkylaromatic hydrocarbons (in which the TMB participate) would hardly be able to desorb out of these channels.

This may be an explanation for the observed higher toluene : TMB ratio. The restricted participation of the surface layers in these reactions in comparison with MS will lead to a much slower fouling rate for MD. Probably, the gradual elimination of the acid sites in the bulk of the crystal by deactivation results in disappearance of the initial inhomogenity of the active centers distribution in MD and the toluene/TMB ratio approaches one, as in the case of MS.

REFERENCES

1. Scherzer, J., ACS Symp. Ser. 248, Amer Chem Soc, 1984, p. 157
2. Mishin, I.V., Vasina, T.V., Palishkina, N.V., Zubkov, A.M., Lipkind, B.A., Senderov, E.E., Bragin, B.V., Izv.Akad.Nauk SSSR, Ser.Khim., 456 (1983)
3. Bodart, P., Nagi, J.B., Derouane, E.G., Gabelica, Z., in P.A.Jacobs et al. (Editors) Structure and Reactivity of Modified Zeolites. Elsevier, Amsterdam, 1984, p. 125
4. Dwyer, J., Fitch, F.R., Machado, F., Oin, G., Smyth, S.M., Vickerman, J.C., J.C.S. Chem. Comm. 422 (1981)
5. Minachev, Kh.M., Shpiro, E.S., Mishin, I.V., Matkhe, T., Antoshin, G.V., Izv.Acad.Nauk SSSR, Ser.Khim., 2682 (1983)
6. Martim de Armando, M.L., Gnep, N.S., Guisnet, M., J. Chem. Research (S), 8 (1981)
7. Penchev, V., Mavrodinova, V., Tamnev, B., Commun. Dept. Chem. Bulg.Acad.Sci, 9, 730 (1976)
8. Tsolovski, I., Minchev, Chr., Senderov, E.E., Penchev, V., Inter.Symp.Zeolites, Portoros, Sept., 1984, in press
9. Kanazirev, V., Borisova, N., Zeolites, 2, 23 (1984)
10. Venuto, P.B., Hamilton, L.A., Landis, P.S., Wise, J.J., J. Cat., 4, 81 (1966)
11. Becker, K.A., Karge, H.G., Streubel, W.D., J. Catal, 28, 403 (1973)
12. Bremer, H., Reschetilowsky, W., Ahmed, A.S., Wendladt, K.P., Nau, P.E., Mishin, I.V., Z.Chem. 23, 381 (1983)
13. Csiesery, S.M., Hickson, D.A., J. Cat., 19, 386 (1970)
14. Karge, H.G., Hatada, K., Zhaug, Y., Fiedorov, R., Zeolites 3, 13 (1983)
15. Karge, H.G., Ladebeck, J., Sarbak, Z., Hatada, K., Zeolites 2, 94 (1982)
16. Jacobs, P.A., Martens, J.A., Weitkamp, J., Beyer, Hr., Farad.

Discuss.Chem.Soc., 72, 353 (1981)
17.Kliachko, A.L., Kapustin, G.I., Glonti, G.O., Brueva, T.P., Rubinshtein, A.M., VI Sov.-Franz. seminar catal., 58 (1983)
18.Seddon, D., Appl.Catal., 7, 327 (1983)
19.Penchev, V., Mavrodinova, V., Acta Phys.Chem., 24, 263 (1978)
20.Bierenbaum, H.S., Partridge, R.D., Weiss, A.H., Adv.Chem.Ser. 121, 605 (1973)

TOLUENE AND XYLENE DISPROPORTIONATION OVER HZSM-5 CRYSTALS OF DIFFERENT SIZE

P.BELTRAME, P.L.BELTRAME, P.CARNITI, L.FORNI, G.ZURETTI
Dipartimento di Chimica fisica ed Elettrochimica, Università di Milano, Via Golgi 19, 20133 Milano, Italy

ABSTRACT

Toluene, xylene (isomer equilibrium mixture) or 1,2,4-trimethylbenzene (1,2,4-TMB) were fed to a fixed-bed reactor in a flow of H_2 or N_2, at 300 to 360°C. The catalyst was HZSM-5, employed as mixed crystals or one of three separate fractions from 2.5 to 7.5 μm average size. A few runs were also carried out after poisoning the catalyst outer surface with 4-methylquinoline.

The catalyst crystal size showed no effect on the disproportionation of toluene and a slight effect on that of xylene. Xylene gave also demethylation, which was the main reaction of 1,2,4-TMB. Poisoning showed a marked effect on selectivity in the case of toluene and on fractional conversion for xylene disproportionation, and deeply affected the reactions of 1,2,4-TMB.

INTRODUCTION

Toluene disproportionation on unmodified HZSM-5 catalysts proceeds usually to an equilibrium mixture of xylene isomers [1]. The para-selectivity could be increased up to 35% by reaction over "large crystals" of catalyst (3 μm size) at 550°C [2]. More impressive results were achieved by using ZSM-5 catalysts modified with Mg, P or B [1,3], or partially deactivated by coking [4].

Xylene reactions over HZSM-5 were studied at 250-300°C, finding a strong selectivity for 1,2,4-trimethylbenzene in the disproportionation, which was accompanied by isomerization [5]. Dealkylation was also found at 370-400°C [6].

We undertook a study of toluene and xylene disproportionation on HZSM-5 crystals of different size, looking for shape-selectivity effects and aiming at discriminating between channel diffusion resistance and transition state steric inhibition as their cause [7]. In order to

get further information on catalyst behaviour, a few runs were also carried out on 1,2,4-trimethylbenzene.

The catalyst employed was the same zeolite, of high and stable activity, previously used for kinetic measurements on toluene disproportionation [8]. However, for the present work, besides using "mixed crystals" (M), three samples with average crystal size 7.5 μm (A), 4 μm (B) and 2.5 μm (C) were separated and tested.

The following reactions were carried out on each catalyst sample in the order given: a) toluene disproportionation (carrier H_2) in standard kinetic conditions; b) toluene disproportionation (carrier H_2) at higher conversion; c) reactions of xylenes, fed as an equilibrium mixture of isomers (carrier H_2); d) (only on catalysts B and M) reactions of 1,2,4-trimethylbenzene (carrier H_2); e) toluene disproportionation (prolonged runs with carrier N_2).

For some reactions over catalyst M, poisoning experiments were also effected, by using 4-methylquinoline, which should inhibit only the acid sites on the outer surface of HZSM-5 [9,10], because of its molecular size.

EXPERIMENTAL

Materials. All reactants and standards were commercial "pure reagents", which gave single peaks by GC analysis, apart from 1,2,4-trimethylbenzene, that contained ca.1% of 1,3,5-isomer.

Catalyst. HZSM-5 was prepared by a standard procedure [11]; it was the same binderless catalyst (SiO_2/Al_2O_3 wt.ratio 15.0) described elsewhere [8] as HZSM-5(HA). Samples A, B and C were separated from it by elutriation in deionized water, leaving behind a small amount of smaller particles. Crystal sizes were evaluated on SEM micrographs. All samples were pressed, crushed and sieved to 40-80 mesh before use. Elemental analysis by A.A. revealed differences between the samples, the content of aluminium (as Al_2O_3) being 4.63% for A and for B, 5.91% for C and 5.06% for the mixed crystals. However, surface acidity, as measured by titration with n-butylamine in anhydrous solvent [12] ($pK_a \leq 1.5$), was found scarcely dependent on Al content: A, 1.0; B, 1.1; C, 1.0 meq/g. When using the bulky tributylamine, the corresponding acidity of the mixed crystals was titrated as 0.075 meq/g.

Apparatus and procedure. A tubular flow reactor with a fixed bed of catalyst (0.5 g), immersed in a thermostatted bath, was employed [8]. Reactants were fed by a glass syringe with PTFE piston and with a carrier to hydrocarbon ratio of 5, at atmospheric pressure (partial pres-

sure of the hydrocarbon in the feed = 17 kPa). The reactor effluent was passed through a condensing trap, kept at ca.-17°C, and liquid products analyzed by GC, using a standard 1:1 Didecylphthalate-Bentone 34 column 4.5 m long.

Selective poisoning experiments were performed following a reported procedure [9], applied to a series of runs on the same catalyst sample. Before each reaction a single dose of 4-methylquinoline was injected (first run, 15 µl; successive runs, 5 µl, to compensate for a possible partial desorption of the poison). Reactions were carried out in the order a, c, d, a.

RESULTS

Products were usually analyzed by gas-chromatography. A more detailed identification, based on GC-MS analyses, was carried out only for runs on the "mixed crystals" catalyst.

The products from a feed of toluene (T) were mainly benzene (B) and the three xylenes (DMB). Small amounts of C9 hydrocarbons were also found, i.e. ethyltoluenes (EMB), not resolved by the standard GC analysis, and trimethylbenzenes (TMB), which were resolved and found to be predominantly represented by the 1,2,4-isomer.

The reaction of xylenes, effected by feeding a mixture close to the isomeric equilibrium, gave toluene and trimethylbenzenes (mostly 1,2,4-TMB) as main products, but also benzene, ethyltoluenes and C10 hydrocarbons in minor amounts. A GC-MS analysis, with a column longer than the standard one, showed that the three isomers of EMB were all present, in the abundance order characteristic of equilibrium (m>p>o). As to the C10 hydrocarbons, they were mainly recognized by GC-MS in two peaks, with M.W. 134 and 132, respectively. The former peak corresponded neither to a tetramethylbenzene nor to a diethylbenzene nor to a propyltoluene; it could reasonably be an ethyldimethylbenzene. The latter peak had a retention time just in the region of the tetramethylbenzenes (TTMB), but it was ascertained that TTMB's were absent or negligible; the relevant compound could be a vinyldimethylbenzene.

When feeding 1,2,4-TMB, the reaction products were mainly xylenes and toluene, with lesser amounts of benzene and C10 hydrocarbons, and a partial isomerization to 1,2,3-TMB. The latter was detected as a shoulder on the peak of the reactant, but sometimes it was not enough for a quantitative integration; in these cases it was only approximately estimated. As to the C10 hydrocarbons, the GC-MS analysis showed

that they were a mixture of isomeric tetramethylbenzenes.

On the basis of the products identified, the chemical behaviour of the system was summarized as follows:

disproportionation

$$2\ T \longrightarrow B + DMB \quad (1)$$

$$2\ DMB \longrightarrow T + C9 \quad (2)$$

$$2\ C9 \longrightarrow DMB + C10 \quad (3)$$

demethylation

$$DMB \longrightarrow T + gas \quad (4)$$

$$1,2,4\text{-TMB} \longrightarrow DMB + gas \quad (5)$$

isomerization

$$1,2,4\text{-TMB} \longrightarrow 1,2,3\text{-TMB} \quad (6)$$

Demethylation reactions, when xylenes or 1,2,4-TMB were fed to the reactor, were evidenced by the sum of the side-chain carbons in the products falling short of the theoretical.

Fractional conversions for disproportionation (y_{dis}), demethylation (y_{dem}), and isomerization (y_{iso}) were therefore defined as follows, for different feed compositions (x_i = molar fraction of component i):

Feed: toluene

$$y_{dis} = x_B + \Sigma x_{DMB} + 2\Sigma x_{C9} \quad (7)$$

Feed: xylenes

$$y_{dis} = 2(\Sigma x_{C9} + 2\Sigma x_{C10}) \quad (8)$$

$$y_{dem} = 2 - x_T - 2\Sigma x_{DMB} - 3\Sigma x_{C9} - 4\Sigma x_{C10} \quad (9)$$

Feed: 1,2,4-TMB

$$y_{iso} = x_{123\text{-TMB}} \quad (10)$$

$$y_{dis} = 2\Sigma x_{C10} \quad (11)$$

$$y_{dem} = 3 - x_T - 2\Sigma x_{DMB} - 3\Sigma x_{C9} - 4\Sigma x_{C10} \quad (12)$$

Reaction selectivities were also evaluated. The isomer distribution within the xylene fraction of products was expressed as S_o, S_m and S_p, defined as $S_o = x_{o\text{-DMB}}/\Sigma x_{DMB}$ and analogously for S_m and S_p. For the reaction of toluene, a further selectivity S_{DMB} was given by the ratio $\Sigma x_{DMB}/(\Sigma x_{DMB} + 2\Sigma x_{C9})$, which represents the fraction of DMB produced by reaction (1) and not entered into further disproportionation. Analogously, for a xylene feed, the ratio $S_{C9}\left[=\Sigma x_{C9}/(\Sigma x_{C9} + 2\Sigma x_{C10})\right]$ represents the fraction of C9 hydrocarbons produced by reaction (2) and not further reacted.

For the reaction of xylenes, the isomer distribution within the C9 fraction was firstly evaluated as the ratio $\Sigma x_{TMB}/\Sigma x_{C9}$ (the differ-

ence to 1 gives the relative weight of the EMB product), and then as the isomer fractions within the TMB product, essentially as S_{124} (the ratio $x_{124\text{-TMB}}/\Sigma x_{TMB}$).

For comparison, it can be mentioned that the equilibrium fractions of isomeric xylenes at 300-360°C are calculated as: ortho, 0.22; meta, 0.54; para, 0.24. The equilibrium fractions of TMB's at 350°C are similarly calculated as: 1,2,3-TMB, 0.07; 1,2,4-TMB, 0.66; 1,3,5--TMB, 0.27 [13].

Experimental results, worked out as described above, are presented in Tables 1-4 and in Figure 1.

Table 1

Disproportionation of toluene in standard runs (carrier H_2; T=300°C; W/F_T^o=164 g h/mol). Average values of measurements.[a]

Catalyst (size)	y_{dis}	S_{DMB}	S_o	S_m	S_p
A (7.5 μm)	0.056	0.95	0.22	0.54	0.24
B (4 μm)	0.064	0.96	0.21	0.53	0.26
C (2.5 μm)	0.050	0.96	0.20	0.55	0.25
M (mixed)	0.052	0.95	0.21	0.53	0.26
M[b]	0.038	0.95	0.09	0.20	0.71

[a] C9 hydrocarbons were exclusively EMB, within the detection limits; [b] sampling 6 h after poisoning by 4-Me-quinoline(15 μl).

Table 2

Disproportionation of toluene at higher conversion (carrier H_2; T=360°C; W/F_T^o=504 g h/mol). Average values of measurements.[a]

Catalyst	y_{dis}	S_{DMB}	S_o	S_m	S_p
A	0.219	0.98	0.22	0.51	0.27
B	0.258	0.97	0.22	0.53	0.25
C	0.213	0.98	0.22	0.54	0.24
M	0.205	0.98	0.22	0.53	0.25

[a] C9 hydrocarbons were EMB and TMB in an approximate ratio of 2:3.

Table 3

Reaction of xylenes[a] (carrier H_2; T=350°C; W/F^{o}_{DMB}=94 g h/mol). Measurements after ca.24 h on-stream.

Catalyst	y_{dis}	y_{dem}	S_{C9}	$\Sigma x_{TMB}/\Sigma x_{C9}$	S_{124}
A	0.099	0.075	0.94	0.98	1.00
B	0.108	0.082	0.92	0.98	1.00
C	0.143	0.063	0.94	0.98	0.97[b]
M	0.134	0.051	0.94	0.99	1.00
M[c]	0.023	0.049	0.92	0.89	1.00

[a] isomers in the feed: o, 0.22; m, 0.54; p, 0.24; unreacted xylenes: o, 0.22-0.24; m, 0.52-0.54; p, 0.24; [b] 1,2,3- and 1,3,5--TMB were both present; [c] after poisoning by 4-Me-quinoline (15+5 µl injected 30 and 3 h, respectively, before sampling).

Table 4

Reaction of 1,2,4-trimethylbenzene (carrier H_2; T=350°C; W/F^{o}_{TMB} = 105 g h/mol). Average values of measurements.

Catalyst	y_{dis}	y_{iso}	y_{dem}	S_o	S_m	S_p
B	0.0030	0.0264	0.0753	0.20	0.52	0.28
M	0.0039	0.01-0.02	0.0721	0.21	0.51	0.28
M[a]	0.0018	nil	0.0253	0.16	0.45	0.39

[a] after poisoning by 4-Me-quinoline (15+5 µl injected 34 and 7h, respectively, before sampling.

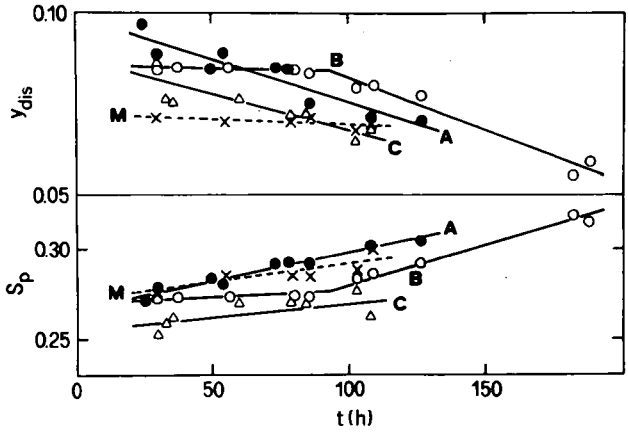

Figure 1. Disproportionation of toluene in prolonged runs with carrier N_2 (T = 300°C; W/F^{o}_{T}=164 g h/mol): y_{dis} (upper plot) and S_p (lower plot) vs. time-on-stream. Catalyst samples: ●,A; o,B; △,C; x,M. Average values of S_{DMB} were in the range 0.97-0.98.

DISCUSSION

According to the measured kinetics [8], for standard runs (a) on toluene a value 0.052 for y_{dis} and an equilibrium xylene isomer distribution were expected. Results in Table 1 show that this was actually found, within experimental error, not only for the mixed crystals of HZSM-5, but even for the largest particles (catalyst A). This evidences that channel diffusion resistance is negligible in this case and that the measured kinetics refers to the reaction under chemical control. Values of y_{dis}, S_o, S_m and S_p appear independent of catalyst crystal size also for runs (b) to higher conversion (Table 2).

Poisoning was effected on runs (a) by injecting a quantity of 4-methylquinoline exceeding by an order of magnitude the amount required to saturate an HZSM-5 catalyst [9], although corresponding to only 1/5 of the theoretical to neutralize all medium-to-high strength ($pK_a \leq 1.5$) acid sites, should the base penetrate the pores. The poison effects on the toluene standard run over M catalyst (Table 1) were a slight decrease of y_{dis} and a substantial change in the xylene selectivities, favouring p-xylene. The former effect proves that toluene disproportionation occurs mainly in the zeolite pores; the latter is very likely due to the fact that the usual isomerization of the preferred primary product on the acid sites at the pore mouth is prevented by the poison.

As to the C9 fraction, EMB was its only component for runs (a) and it was largely present also in runs (b). A side-chain attack is known to occur on X and Y zeolites exchanged with large or medium size alkali cations, from Cs^+ to Na^+, for alkylations of toluene [14], xylene [15] and pyridine [16] by methanol. Perhaps a similar mechanism operates in the present case, due to residual Na^+ ions and favoured also by the smaller pore diameter of the zeolite. TMB, when present, was predominantly the 1,2,4-isomer. It can be noticed that S_{DMB} was close to unity, that is the further reaction of xylenes was a very restricted phenomenon.

Xylene reactions (runs c; Table 3) did not include isomerization, because isomeric equilibrium was present in the feed and was preserved in the unreacted xylene output. The various catalyst samples, while showing slight differences in overall activity ($y_{dis} + y_{dem}$ = 0.174, 0.190, 0.206 and 0.186 for A, B, C and M, respectively), presented more marked differences in the relative weight of the two reactions. Demethylation gained more weight when the catalyst was in larger crystals

(A and B); on the contrary, y_{dis} increased in the order A<B<C. The effect of 4-Me-quinoline was remarkable, the poison scarcely affecting demethylation but heavily depressing disproportionation. It can be suggested that demethylation occurs mainly within the catalyst pores and without intervention of significant diffusive resistance, while disproportionation, in the absence of poison, occurs partly on the outer surface and partly within the zeolite pores, in this case with significant channel diffusion resistance effects (see values of y_{dis}).

Disproportionation gave almost always 1,2,4-TMB as the only trimethylbenzene, independently of the site of reaction; it seems therefore that the predominance of this isomer, which is favoured by electronic as well as by statistical factors, is not clear evidence of shape-selectivity. The fraction of EMB within C9's is a more interesting parameter, since the figures in Table 3 (1-2% EMB on unpoisoned catalysts, 11% after poisoning) show that the rate of formation of EMB was little affected by poisoning, which instead markedly reduced the rate of TMB formation, indicating that the former reaction does not require those acid centres that catalyze the latter one.

Surprisingly, TTMB was practically absent from the C10 fraction of runs (c). Apparently, reaction (3) occurs mainly to C9 molecules just formed within the pores, thus favouring side-chain attack, with the possible formation of ethyldimethylbenzene and vinyldimethylbenzene. In the mentioned cases of side-chain methylation [14-16], formation of both ethyl and vinyl side groups was common.

The main reaction of 1,2,4-TMB (runs d; Table 4) was demethylation. The small amount of disproportionation gave TTMB, as expected, and no EMB was found among the products. Isomerization resulted rather slow, so justifying the very high values of S_{124} of runs (c) at the same temperature. Poisoning depressed demethylation and disproportionation, while preventing isomerization, to the point that the small impurity of 1,3,5-TMB, present in the feed, was found (only in this case) as unreacted. Poisoning slightly favoured p-xylene.

Results of selectively poisoned reactions have been reported up to an overall addition of 20 µl of 4-Me-quinoline and for samples taken up to 34 h after the first poison injection. Results obtained from runs (d) and (a) after further poison additions showed an abrupt decrease of the catalytic activity, so comprimising the reliability of GC analyses.

Prolonged reaction of toluene in N_2 (runs e) gave similar re-

sults for catalysts A, B and C (Figure 1). A "coking" effect was detected, giving decreasing values of y_{dis} and increasing values of S_p (up to 0.32) vs. time-on-stream. Interestingly, the activity of the mixed-crystal sample M was more constant than for samples A-C. This might be connected with slight structural alterations introduced by the elutriation procedure.

REFERENCES

1. Kaeding, W.W., Chu, C., Young, L.B., Butter, S.A., J.Catal. 69, 392 (1981).
2. Chen, N.Y., Kaeding, W.W., Dwyer, F.G., J.Amer.Chem.Soc. 101, 6783 (1979).
3. Young, L.B., Butter, S.A., Kaeding, W.W., J.Catal. 76, 418 (1982).
4. Beltrame, P., Beltrame, P.L., Carniti, P., Forni, L., React.Kinet. Catal.Letters 19, 213 (1982).
5. Collins, D.J., Medina, R.J., Davis, B.H., Can.J.Chem.Eng. 61, 29 (1983).
6. Nayak, V.S., Choudhary, V.R., Appl.Catal. 4, 333 (1982).
7. Haag, W.O., Lago, R.M., Weisz, P.B., Discuss.Farad.Soc. 72, 317 (1981).
8. Beltrame, P., Beltrame, P.L., Carniti, P., Forni, L., Zuretti, G., submitted to Zeolites.
9. Anderson, J.R., Foger, K., Mole, T., Rajadhyaksha, R.A., Sanders, J.V., J.Catal. 58, 114 (1979).
10. Yashima, T., Sakaguchi, Y., Namba, S., in "New Horizons in Catalysis" (Eds.T.Seiyama, K.Tanabe), Elsevier Sci.Publ.Co., Amsterdam, 1981, p.739.
11. Argauer, R.J., Landolt, G.R., U.S.Pat. 3 702 886 (1972).
12. Bertolacini, R.J., Anal.Chem. 35, 599 (1963).
13. Stull, D.R., Westrum, E.F.Jr, Sinke, G.C., "The Chemical Thermodynamics of Organic Compounds", Wiley Inc., New York, 1969.
14. Yashima, T., Sato, K., Hayasaka, T., Hara, N., J.Catal. 26, 303 (1972).
15. Itoh, H., Hattori, T., Suzuki, K., Murakami, Y., J.Catal. 79, 21 (1983).
16. Kashiwagi, H., Enomoto, S., Chem.Pharm.Bull. 30, 404 (1982).

POLYFUNCTIONAL ZEOLITE CATALYSTS IN THE BENZENE-OLEFIN-HYDROGEN SYSTEM

I.I.LISHCHINER, V.A.PLAKHOTNIK, D.Z.LEVIN, E.S.MORTIKOV
Institute for Organic Chemistry of the Academy of Sciences, USSR, Moscow, USSR

ABSTRACT

Benzene alkylation by C_2-C_4 olefins at 537 K and 3MPa over a polyfunctional zeolite catalysts has been studied.

It has been established that the admission of hydrogen to the reaction mixture in case of ethylene and butylene promotes chiefly olefin hydrogenation, while in case of propylene alkylation primarily proceeds. The correlation between acidic and catalytic properties of the catalyst in question has been revealed.

INTRODUCTION

The literature available deals with alkylation and cracking processes able to proceed in hydrogen which promotes a higher zeolite catalysts stability [1,2]. We have found that using polyfunctional zeolite catalysts makes their stability and alkylation selectivity considerably higher if the process occurs in hydrogen [3].

In this paper the alkylating and hydrogenating properties of polyfunctional zeolite catalysts in the benzene-olefin-hydrogen system were studied depending on the olefin nature and the catalyst acidic properties.

EXPERIMENTAL

The experiments were carried out in a 2,5-4,5 cm^3 tubular flow circulation stationary catalyst bed reactor. A mixture of benzene and olefin in the required proportion was pumped into the reactor with simultaneous admission of hydrogen. The amount of the admitted hydrogen was controlled by a highly sensitive flowmeter [4]. An Y-type zeolite, containing La, Ca and Ni-cations and prepared according to the technique [5] was used as a catalyst. A portion of this catalyst was subjected to 100% steam treatment at 873 K. The physicochemical parameters of the zeolite catalysts were determined by X-ray

analysis, IR-spectroscopy [6,7] and TPD of ammonia in chromatographic [8] and thermogravimetric [9] methods.

The action of catalyst pyridine poisoning on the behavior of a polyfunctional catalyst in conditions of competitive processes of alkylation and hydrogenation was investigated. The pyridine adsorbed portion in n-heptane solution was determined by the difference in its concentration before and after its contact with the catalyst.

RESULTS

Fig.1 gives the results on the investigation of CaLaNiY-activity in benzene alkylation by C_2-C_4 olefins depending on the catalyst thermo-steam pretreatment (TST) and hydrogen presence in the reaction mixture.

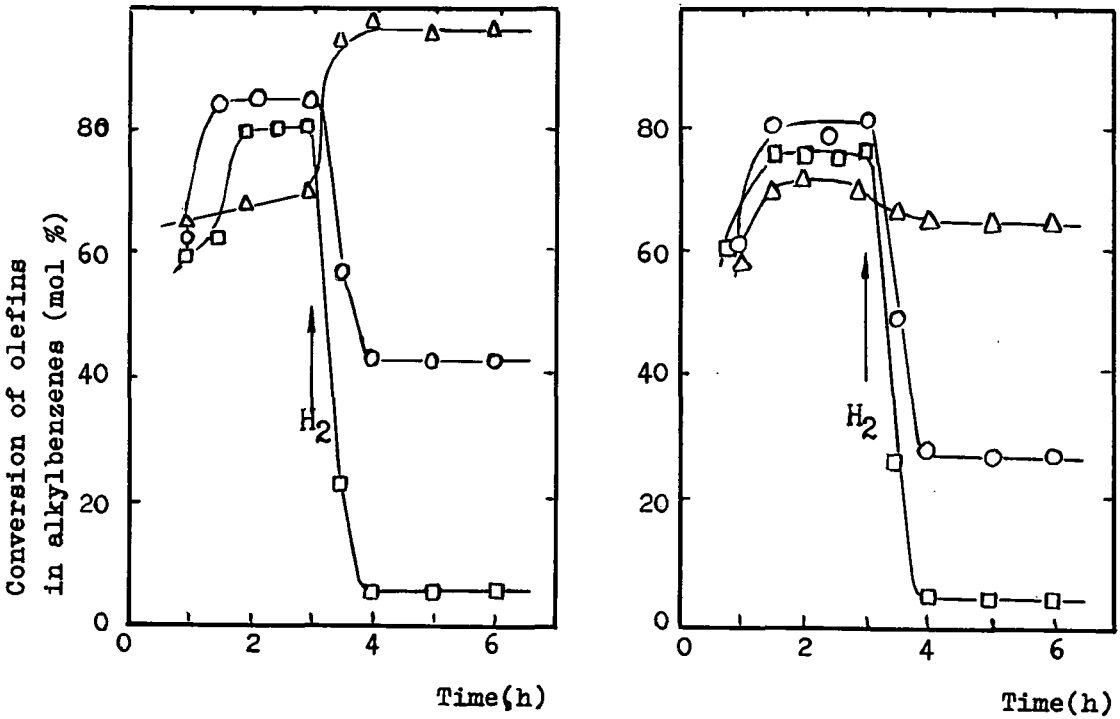

Fig.1. The effect of hydrogen on the activity of CaLaNiY subjected to TST (a) and untreated (b) in benzene alkylation by C_2-C_4 olefins.

O-ethylene, Δ-propylene, □-isobutylene

Conditions: 523 K; 3 MPa; C_6:olefin:H_2= 4,2:1:5; $3h^{-1}$

In case hydrogen is not present the pretreatment of the catalyst does not effect olefins conversion to alkylbenzenes as compared with alkylation in hydrogen. The hydrogen admission into the reaction mix-

ture over the initial (untreaded) catalyst leads to a considerable decrease of olefins conversion to alkylbenzenes due to the competitive olefins hydrogenation to saturated hydrocarbons (fig.1, table 1).

Table 1

The effect of thermo-steam pretreatment on the CaLaNiY activity . Conditions: 523 K; 3 MPa; C_6:olefin:H_2= = 4,2:1:5; 3 h^{-1}

Catalyst	Olefin	Olefin conversion, mol.%	
		to alkylation products	to hydrogenation products
initial sample	ethylene	26,7	67,0
	propylene	65,3	19,6
	isobutylene	1,8	90,0
sample after TST	ethylene	47,9	45,3
	propylene	94,7	1,5
	isobutylene	5,2	78,5

However, if the catalyst undergoes TS-pretreatment and alkylation proceeds in hydrogen, the degree of olefins hydrogenation decreases in the ratio:for ethylene and isobutylene by 1,1-1,4, whereas propylene is not practically hydrogenated in these conditions. Due to the decrease of the olefins hydrogenation degree, the yield of alkylbenzenes increases.

Under conditions unfavourable for alkylation (benzene is replaced by n-heptane) the pretreatment of the catalyst does not affect its hydrogenating activity. For example, the degree of propylene hydrogenation is 82,7% for both the initial and pretreated CaLaNiY - samples.

In order to compare the reactivity of different olefins the benzene alkylation by equimolar ethylene-propylene mixture in hydrogen was carried out (table 2). As is shown, about 90% ethylene used is converted to hydrogenation products whereas 15-20% propylene is converted to propane, and 75-80% - to alkylbenzenes.

The similar dependence is observed in benzene alkylation in hydrogen by propylene-isobutylene mixture. Propylene is almost completely alkylated, while isobutylene is only hydrogenated.

Table 2

Benzene alkylation by ethylene-propylene mixture in the presence of hydrogen over CaLaNiY - catalyst after TST

Conditions: 3MPa, $3h^{-1}$, $C_6:C_2:C_3=2:1:1$; $H_2:C_2+C_3=3:1$

NN	Temperature, K	Ethylene conversion mol.%		Propylene conversion mol.%	
		to alkylbenzenes	to ethane	to alkylbenzenes	to propane
1	453	7,2	87,8	80,4	15,0
2	483	6,3	76,7	74,5	17,1
3	523	7,7	87,3	73,5	19,6

To explain the TST effect on CaLaNiY catalytic properties in the competitive alkylation and hydrogenation processes it was necessary to study the changes which occur in the catalyst during the treatment, i.e. to study its hydroxyl covering, acidity and the crystal structure parameters.

The X-ray analysis data on CaLaNiY-samples before and after TST reveal the relative crystallinity remain unchanged after steam treatment. In determining the adsorption capacity of catalyst samples it was found that the benzene adsorption value as a result of TST does not alter either.

The comparison of IR-spectra of CaLaNiY samples investigated in the range of 450-1450 cm^{-1} showed the frequencies and intensities of typical absorption bands in the range of 570-580 cm^{-1}, 750-800 cm^{-1}, and 1050-1150 cm^{-1} being practically constant.

The nature and concentration of the surface hydroxyl groups of a polyfunctional zeolite catalyst were investigated by diffuse reflectance IR spectroscopy in the range of main valence vibrations of OH-groups at 3000-4000 cm^{-1} [10]. In the spectra of CaLaNiY-samples (fig.2) we observed four absorption bands: the high intensive band at 3540 cm^{-1} attributed to OH-groups and bonded with La-atoms; the weak band at 3680 cm^{-1} which according to [11], is assigned to OH-group, bonded with off-frame Al-atoms; two absorption bands of average intensity at 3645 and 3745 cm^{-1}, respectively. The absorption at 3645 cm^{-1} is referred to structural OH-groups of bridge type [7]. In accordance with [12,13] the bridge hydroxyl groups which have vibration frequency in the range of 3610-3650 cm^{-1}, characterize Brendstad acidity of most zeolites. The frequency at 3745 cm^{-1}

is usually related to Si–OH groups of terminal type on the external zeolite surface or to silane groups of trace amorphous alumosilicate having greater contents of Al_2O_3 [10].

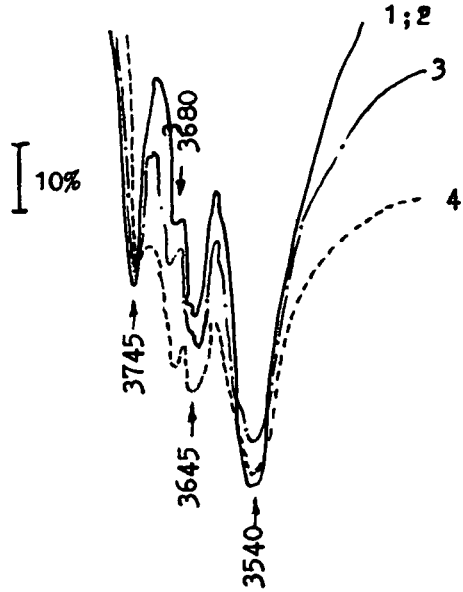

Fig.2. IR-CaLaNiY diffuse reflectance spectra 1-initial sample, 2 - after 2 h TST, 3- after 6 h TST, 4 - after 12 h TST.

The comparison of the spectra shows the spectrum of the initial CaLaNiY samples does not practically differ from those subjected to TST.

Using the programmed ammonia thermodesorption in a chromatographic regime we could investigate the change of CaLaNiY acidity as a result of TST (fig.3).

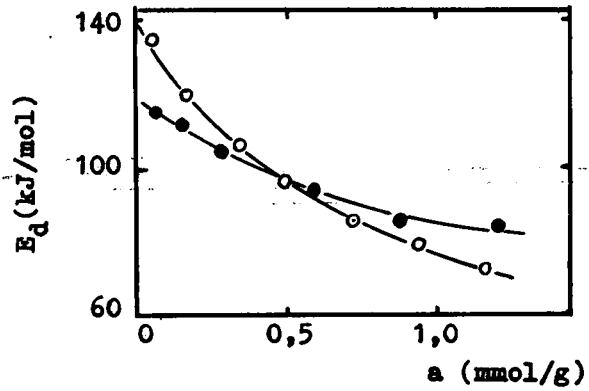

Fig.3. Activation energy of ammonia desorption (E_a) as a function of the amount of chemisorbed ammonium on the LaNiY catalyst: steam-treated (light points) and untreated (dark points)

It is shown that TST leads to the number decrease of strong acidic centres having $Edec_{NH_3}$ > 90 kJ/mol, and the increase of centres with $Edec._{NH_3}$ = 80-90 kJ/mol as compared with the initial catalyst.

These differences become more evident if we consider the dependence of chemisorbed ammonia amount on the temperature obtained by thermogravimetry. The thermograms calculation based on the integral curve (IC) shows that thermo-steam treatment does not influence the total amount of chemisorbed ammonia, i.e. the total CaLaNiY acidity does not alter in various TST conditions (Table 3). For the initial

Table 3

The effect of TST duration on acidic and catalytic properties of CaLaNiY

№	TST time, h	Total acidity, mmol/g	Temperature of ammonia desorption	Conversion of propylene to alkylbenzenes mol.% (A)	Conversion of propylene to propane, mol.% (B)	A/A+B 100%
1	-	2,08	653,853,	68,5	21,8	74,1
2	2	2,05	553,633, 813	71,5	18,5	78,0
3	6	2,05	453,553, 703	95,1	2,9	97,0
4	12	1,98	453,533, 693	96,0	2,5	97,5

catalyst the ammonia chemisorption on the active centres of the surface results in the formation of compounds which have the decomposition temperature 653 and 853 K. The initial catalyst TST, in case it is prolonged, can change DTA-curves. The two hour TST results in the formation of surface centres where the ammonia is desorbed at 553, 633 and 813 K. The six-hour TST provides the formation of centres where the ammonia desorption is observed at lower temperature.

The data of the thermogram calculations based on the conclusions of the paper [14] enable us to make a diagram of distribution the centres according to their acidic level (fig.4) in coordinates $\Delta m/\Delta H_0 - H_0$, where $\Delta m/\Delta H_0$ - the number difference of acidic centres which corresponds to the small interval of change in Hammett acidity function H_0. It is seen that after the catalyst TST the number of centres with H_0~ ranging from -8 to -14 (which corresponds to the ammonia desorption temperature 473-673 K) decreases as compare with the initial catalyst. At the same time the number of centres having H_0 from -6 to -8 (433-473 K) sharply increases and the centres be-

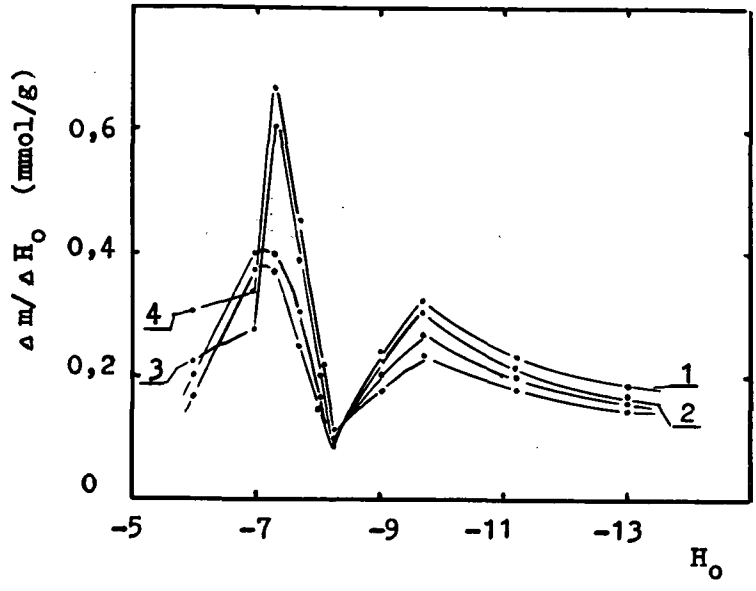

Fig.4. The centres distribution by acidic levels

come more homogeneous by their level with prolonging the TST duration, the number of centres with $H_o < -8$ increases even more at the expense of the number decrease of centres with H_o from -8 to -14.

In order to clear up the correlation of acidic and catalytic properties of a polyfunctional zeolite catalyst the latter was subjected to a subsequent poisoning by pyridine (fig.5).

After the sorption of 0,018 mmol pyridine/g catalyst the alkylating activity of CaLaNiY is lowered half as much as compared to the initial sample, and the hydrogenating activity grows 7 times as much. After the sorption of 0,09 mmol pyridine the conversion of propylene into alkylbenzenes lowers from 75 to 20%, and in case to propane it grows to 64%.

The 0,45 mmol base sorption leads to nearly a complete catalyst deactivation in the alkylation process, hydrogenating activity is remaining as high as in propylene hydrogenation in heptane solution (the conversion to propane 81,5%).

UR - spectra were measured by Kustov L.M. and Borovkov V.Yu.

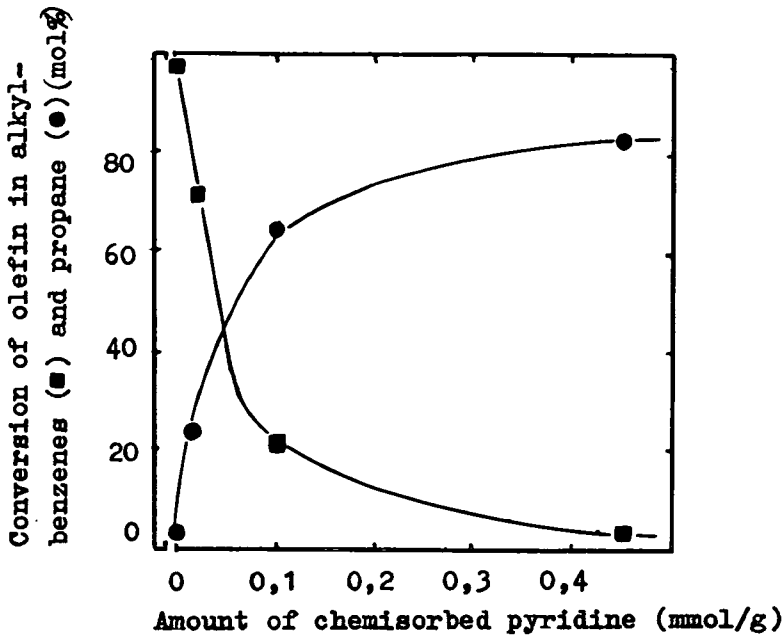

Fig. 5. The dependence of alkylating and hydrogenating activity on the chemisorbed pyridine amount.
Conditions: 523 K; 3MPa; 3 h^{-1}; $C_6:C_3:H_2$=4,2:1:4,2

DISCUSSION

From the data of fig.1 and table 1 it follows that thermo-steam treatment effects a polyfunctional zeolite catalyst activity in alkylation in hydrogen, and promotes a considerable lowering the degree of the C_2-C_4 olefins hydrogenation and increasing the alkylbenzenes yield.

In order to explain the effect of the catalyst TST in the competitive alkylation and hydrogenation reactions it is important to consider the CaLaNiY physico-chemical parameters and their alteration during TST. The X-ray data and IR-spectroscopy, as well as the results of the catalyst sorption capacity determination show that as a result of TST, irrespective of its duration, the crystal catalyst structure, the SiO_2/Al_2O_3 ratio, and also the hydroxyl surface groups nature and concentration do not change while the zeolite acidic properties are altered.

The ammonia thermodesorption data indicate that in the process of TST the redistribution of acidic centres, possessing different levels, is observed. The comparison of CaLaNiY catalytic activity with the change in the catalyst acidity spectra (table 3 and fig.4) shows that TST results in increasing the number of acidic centres

with $H_0 < -8^0$ (as related to the "weak"), and correspondingly, the growth of alkylating activity is observed. After achieving the optimal distribution of acidic centres of different levels at $-6 < H_0 < -8$ and $-8 < H_0 < -14$, CaLaNiY catalytic properties stop changing and as it follows from table 3, the definite ratio between alkylation and hydrogenation reactions is established.

It should be taken into account that a polyfunctional zeolite catalyst hydrogenating activity is determined by presence of a metal while alkylating activity is connected with acidic properties of a catalyst. In favour of this there are data which confirm the change of the alkylating and hydrogenating activity of the catalyst which underwent a subsequent poisoning by pyridine. As poisoning the acidic centres of the catalyst its activity dropped in the alkylation process, while in hydrogenation reaction it rose (fig.5).

Hence, one can assume that the acidic centres of different levels are responsible for the alkylation reaction. However, the advantageous preferred alkylation in the conditions of its competition with hydrogenation over the catalyst, subjected to TST, can be explained by increasing the number of relatively "weak" acidic centres which are apparently determining in alkylation professes.

Thus, thermo-steam treatment allows in the conditions of competitive alkylation and hydrogenation reactions to control purposefully the activity of a polyfunctional zeolite catalyst.

Considering the behaviour of C_2-C_4 olefins in benzene alkylation in hydrogen one can note the following according to [15] , the C_2-C_4 olefins by their reactivity in benzene alkylation over zeolite catalysts can be arranged in the row:ethylene < propylene ~ isobutylene At the same time the hydrogenation rate of individual C_2-C_4 olefins is approximately similar [16]. The results which we have obtained on benzene alkylation by individual olefins and their equimolar mixtures show that in hydrogen media the olefins sequence changes as related to their reactivity in alkylation process over zeolite catalysts:

isobutylene < ethylene < propylene

This change might be due to the difference in hydrogenation and alkylation rates, and also in polymerization,which makes the alkylation process more complicated. According to polymerization, rates over zeolites, containing transition metals cations, the olefins are located [17]: isobutylene > ethylene > propylene

In the presence of hydrogen in the reaction mixture the olefins hydrogenation is suppressed, though for each individual olefin it is

likely to be different, and this effects their reactivity in the alkylation process.

REFERENCES

1. Chen, N.Y., Carwod, W.E., J.Catal.50, № 2, p.252 (1977).
2. Kaeding, Warren, W. Pat USA №4.117.024, 1977.
3. Lishchiner, I.I., Plakhotnik, V.A.,Levin, D.Z., Mortikov, E.S., Neftekhimia, 23, № 3, p.311 (1983).
4. Frenkel, B.A., Automatizatsiya experimentalnych ustanovok. M.: Khimia, 1980, 189p.
5. Baybursky, B.L., Alexandrova, I.L.,Khadziev, S.N.,Leontjev, A.S. et al. Pat. USSR, № 936991, 1980.
6. Kubasov, A.A., Topchieva, K.B. - In: Sb.Sovremenniw problemi fizicheskoi Khimii, 8, p.309 (1975).
7. Kazansky, V.B., Izv.AN SSSR Ser.khim., № 1, p.40 (1984).
8. Yakerson, V.I., Rozanova, V.V. In: Sb.Itogi nauki i tekhniki. Ser. kinetika. - M.: MGU, 3, p.74 (1974).
9. Zadymov, V.V., Lunina, M.I., Kaliko, M.A., Neftekhimia, 21, № 1, p.59 (1981).
10. Kustov, L.M., Andrejev, V.M., Borovkov, V.Yu.,Kazansky, V.B., Kinetika i kataliz., 13, № 4, p.955 (1982).
11. Perc, J.B. In: Catalysis (Ed.Hightover J.W.) - Amsterdam,1973, 1, p.329.
12. Fisenbach, D., Callci, E., J.Catal., 56, № 3, p.377 (1979).
13. Kustov, L.M.,Borovkov, V.Yu.,Kazansjy, V.B., Kinetika i kataliz, 25, № 2, p.471 (1984).
14. Levchuk, V.S-, Kinetika i kataliz, 14, № 2, p.459 (1973).
15. Mortikov, E.S., Marchenko, L.S., Proc.5-th Intern.Conf.Zeolites, Naples, 1980, p.696.
16. Weisz, P.B., Frilette, V.J.,Maatman, P.M., Mower, E.V., J.Catal., 1, p.307 (1962).
17. Nisidzawa, T.,Khashtori, Kh.,Uematsu, T., Siba, T., Osnovi predvidenija katalyticheskogo dejstvija. - M.: Nauka,1970, p.129.

RACKING OF HYDROCARBONS ON ZEOLITE CATALYSTS

. BREMER[a], K.-P. WENDLANDT[a], F. VOGT[a], K. BECKER[b], M. WEBER[b]
Technical University "Carl Schorlemmer" Leuna-Merseburg,
erseburg, GDR (a)
EB Leuna-Werke "Walter Ulbricht", Leuna, GDR (b)

ABSTRACT

Intensive research in connection with the development of industrial zeolite cracking catalysts, contributed towards a better understanding of hydrocarbon cracking reactions and of the factors governing catalyst efficiency. Investigations on FCC catalysts are in progress with the aim of improving selectivity control (gasoline yield, octane number, metal and coke resistance), better pollution control, and the processing of higher boiling feedstocks. Such work includes the simultaneous optimization of both matrix and zeolite properties.

The potential value of partially dealuminated zeolites Y as a highly active and selective catalyst component is demonstrated together with that of ZSM-5 addition, by which the yield of light synthesis olefins can be improved.

NTRODUCTION

Of all the cracking processes in the world petro-chemical industry, catalytic cracking is the most common. 75 percent of cracking is achieved by the catalytic process, whereas the hydrocracking, visbreaking and coking processes occupy only 25 percent.

At present, a total of about 12 percent petroleum in the world and 30 percent in the USA (250 million t/a) are transformed by the FCC process /1, 2/.

In 1979, overall consumption of cracking catalysts was about 205 kt and is continuously increasing. The overall capacity of the firms Akzo, Crosfield, Davison Chemical/W. R. Grace, and Katalistiks International will, it is estimated, reach 85 kt in 1985 /3/. Today, the specific catalyst consumption in the cracking of gas oil amounts to about 0,5 kg/t of feedstock.

Although the first industrial plant for catalytic cracking was in operation as early as 1937, (fixed-bed plant), the revolutionary development of catalytic cracking did not start until 1962, when zeolite catalysts were introduced. The high activity of zeolites led to the introduction of a new process: the riser cracking process. As a result of short contact times between catalyst and feedstock, this form of process permitted optimal utilization of the activity and selectivity of microspherical zeolite catalysts. The first plant for this process was introduced in industry in 1971, and since then riser cracking has been used exclusively in all new FCC units. The chemistry and engineering of catalytic cracking have been reviewed in a large number of publications, e. g. /4-6/.

In the present paper, some problems connected with the development and mode of action of modern catalysts are discussed and analyzed. Special attention is given to partially dealuminated zeolites Y.

MECHANISM AND KINETICS OF HYDROCARBON CRACKING

Hydrocarbon cracking of gas oil involves quite a series of reactions:

Paraffins are cracked to give olefins and highly branched smaller paraffins, the iso/n paraffin ratio often exceeding thermodynamic equilibrium.

Olefins undergo isomerization, cracking into smaller olefins, hydrogen uptake (by transfer from naphthenes or coke), and disproportionation in the case of low molecular weight olefins.

Alkyl aromatics undergo dealkylation, side-chain scission and alkyl group transfer: unsubstituted aromatics are scarcely attacked.

Naphthenes give olefins; cyclohexane is preferentially converted into benzene.

Condensation reactions of aromatics and olefins finally result in coke formation.

Since the work of WHITMORE /7/, THOMAS /8/ and GREENFELDER et al. /9/, the catalytic cracking of the C-C bond has been generally accepted to proceed as an acid catalyzed elimination reaction involving a carbenium ion chain mechanism which consists of a hydride transfer step followed by beta scission. Three possibilities can be considered for the formation of the first carbenium ions, which are responsible for the starting of the carbenium ion chain:

1. Abstraction of a hydride ion from the paraffin molecule by a Lewis site at the catalyst surface.

2. Protonation of the paraffin by a super-acidic Brønsted site, accompanied by the formation of hydrogen and the carbenium ion.
3. Protonation of an olefin at a Brønsted site. The olefin may be contained in traces in the substrate, or may be formed by thermal cracking of the paraffin used. Formation of carbenium ions from olefins is suggested by the strongly protonating action of olefins in the cracking reaction and the direct dependence of the rate of cracking on the olefin content of the substrate /10/.

The role of Lewis sites as catalytic or cocatalytic sites is still a subject of discussion /11, 12/, their role in oligomerization reaction has been demonstrated /13/.

Besides the carbenium ion chain discussed above, some modified mechanisms have been proposed to explain peculiarities observed in product distribution:

i) The catalyst acts as a super acid, and the reaction proceeds via pentacoordinated carbonium ions /14/. However, although some acidic zeolites, e.g. H-mordenites, exhibit a protonating action comparable to that of super acids, it is hard to believe that under reaction conditions and in the presence of a high excess of basic molecules such as olefins, aromatics and coke, they are capable of acting as super acids.

ii) Once the possibility of the formation of cation radicals /15/ and allyl carbenium ions /11/ has been proved, there is still the question of whether or not these entities are relevant to the cracking reaction /16/. The low energetic allylic cation preferentially would take part in oligomerization reactions.

It should be pointed out that any deviation from the product distribution expected to occur in the free-carbonium ion mechanism does not necessarily arise from a different mechanism, but may only be due to the fact that no free ions but ion pairs are available, which are formed by carbocations and nucleophilic sites on the catalyst surface. In this case, variations in selectivity can be described by reactivity-selectivity relationships /17/ as common in organic chemistry. Strong adsorption and diffusion limitations exert a pronounced influence on product distribution. This has to be taken into consideration, e.g. for ZSM-5 as a catalyst.

The simultaneous occurrence of the cracking reactions mentioned above makes mechanistic investigations difficult. In the extreme case, even random isotopic C scrambling is found /18/. Hence individual hydrocarbons have often been used for mechanistic inves-

tigations and for better characterization of the mode of action of the catalyst. To characterize FCC catalysts in the conversion of gas oil feedstocks under conditions close to industrial operation been ditions on a laboratory scale, conventional procedures have been elaborated and widely accepted in recent years /19/.

Besides mechanistic considerations, the kinetics of hydrocarbon cracking is studied to determine the overall conversion rates, and to predict the effect of catalyst variation and modification as well as of refinery operation conditions on the product distribution. Hence, it has become general practice today to provide a process model together with the process license. The most general behaviour of catalytic cracking reactions can be described by a three-lump scheme /20/.

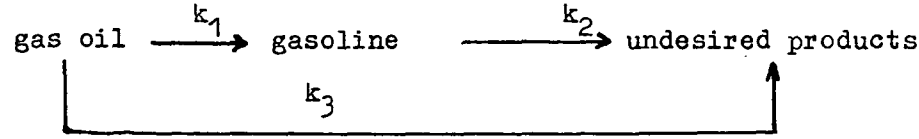

Gasoline cracking (k_2) which produces undesired products, including coke and "overcracked" light compounds, is lower under piston flow conditions. This is one of the advantages of modern riser tube reactors, in which the reaction regime is more closely approximated to the piston flow.

The constants k_1-k_3 being functions of feedstock composition, the three-lump model is inadequate for the case of feedstock changes. JACOB et al. /21/ developed a ten-lump model dividing aromatic rings and alkyl chains into separate species. WEEKMAN /22/ showed this model to be useful for optimizing unit operation.

MODERN FCC CATALYSTS

Conventional zeolite cracking catalysts consist of about 5 to 20 wt.% of zeolite and an X-ray amorphous matrix. Depending on preparation conditions, composition and activation conditions, both components interact in different ways and with different intensities. Both components are subject to definite requirements concerning the access of the hydrocarbon to the zeolite (transport pores > 4,0 nm) and to the active sites in the zeolite (pore openings ~ 0,8 nm), the nature and concentration of active sites in the zeolites and the matrix, the thermal and hydrothermal structural stability of the zeolite, the mechanical stability of the microspherical catalyst particles, and the compatibility of the catalyst with metals.

New trends have appeared in the development and optimization

of the matrix properties for commercial catalysts /22, 23/. Thus, the DA-200 to DA-400 of the Davison Chemical/W. R. Grace are modified as compared with the Super-D Extra as follows: increased Al_2O_3 content up to nearly 50 wt.%, reduced specific surface area and pore volume, nearly doubled mean pore diameter. These changes in composition and texture result in decreased diffusion, "selective" cracking of long-chain hydrocarbons at the matrix, and higher thermal and hydrothermal stability as well as compatibility of the matrix with metals. Similar results were achieved by Katalistiks International with their catalyst series EKZ, SIGMA, BMZ, and CENTURY /24/.

PRODUCTION OF FCC CATALYSTS

Cracking catalysts containing 5 to 20 wt.% of zeolites are mainly produced in two ways: Either the zeolite component is synthesized and modified in a separate step with subsequent dispersion in a synthetic or natural aluminosilicate matrix, or the partial zeolite crystallization is carried out in situ in the natural aluminosilicate matrix. Whereas most firms use the former procedure, others, e.g. Engelhard, synthesize their catalysts from clay or metakaolin by the last-mentioned method.

In most cracking catalysts, the matrix component consists of synthetic, semi-synthetic, or natural clay based aluminosilicate. Sometimes special oxides (e.g. TiO_2) are also added. The matrix must meet the following requirements:

- large pores (>4.0 nm) in order to facilitate mass transfer to the active sites of the zeolite and, if possible, to prevent diffusion limitation. This property is of special importance for the cracking of heavy and residue oils.
- small specific surface area (30 - 50 m^2/g) which is a precondition for high compatibility with metals and hence selectivity.
- small, but selective cracking activity for long-chain hydrocarbons, such that the cracking reaction at the finished catalyst proceeds in the following way:

$$\text{feedstock} \xrightarrow{\text{matrix}} \text{medium cracked products} \xrightarrow{\text{zeolite}} \text{gasoline and light cycle oil}$$

- great thermal, hydrothermal and mechanical stability which is resistent to reaction and regeneration conditions.

The necessary properties of the <u>active zeolite component</u> are the following:

- unidisperse pore structure (pore openings~0,8 nm).
- high activity (10^2 to 10^4 times that of the matrix), and, above all, high selectivity for hydrocarbons within the boiling range of gasoline.
- low tendency for coke formation.
- high thermal and hydrothermal stability and high compatibility with metals.

When the zeolite synthesis is not carried out in situ in the matrix during the preparation of the catalyst, a special binding agent, of which no detailed information is given by the firms, is used to promote homogeneous distribution of the zeolite in the matrix and to increase the mechanical stability of the microspheres. Under the reaction and regeneration conditions of the FCC process, intensive interaction between matrix and zeolite component may be expected to occur which, apart from cation redistribution, leads to structural stabilization of the zeolite in the matrix.

As regards the active zeolite component, X and Y type zeolites in the H^+ and/or RE^{3+} form are used with their alkali content being decreased to 0,3 wt.% Na_2O by the ion exchange. Alkali and alkaline earth metals decrease the activity of the active zeolite component in the order $Na^+ > K^+ > Mg^{2+}$, Ca^{2+}. To prevent overcracking (which is favoured by to many strongly acidic sites) on the fresh catalyst, only a small portion is added to the circulating equilibrium catalyst. Under activation, reaction and regeneration conditions, the fresh catalyst is transformed into the equilibrium catalyst, i.e. the hydrothermal conditions of this treatment affect partial dealumination of the zeolite, along with a change in the acidity spectrum. The properties of the Y zeolite contained in the equilibrium catalyst are comparable to those of a non-extracted, ultra-stable zeolite Y, named US(w). The lattice constant of the starting Y zeolite being 2.46 - 2.47 nm, that of the zeolite in the equilibrium catalyst will range between 2.43 and 2.44 nm, i.e. the SiO_2/Al_2O_3 molar ratio is increased from about 5 to about 20-30. For a priori adjustment of such an acidity spectrum and hence of catalytic activity and selectivity, it appeared reasonable to start from ultrastable Y zeolites.

HYDROTHERMAL TREATMENT OF FCC CATALYSTS

Hydrothermal treatment at temperatures $\geq$ 800 K causes dissolution of aluminium from lattice positions, with simultaneous restoration of the remaining lattice defects. The resulting zeolite lattice,

which is richer in SiO_2, exhibits increased thermal and chemical stability ("ultrastabilization"). The effect of such hydrothermal pretreatment on the catalytic properties of an FCC catalyst containing REY zeolite is demonstrated in Fig. 1.:

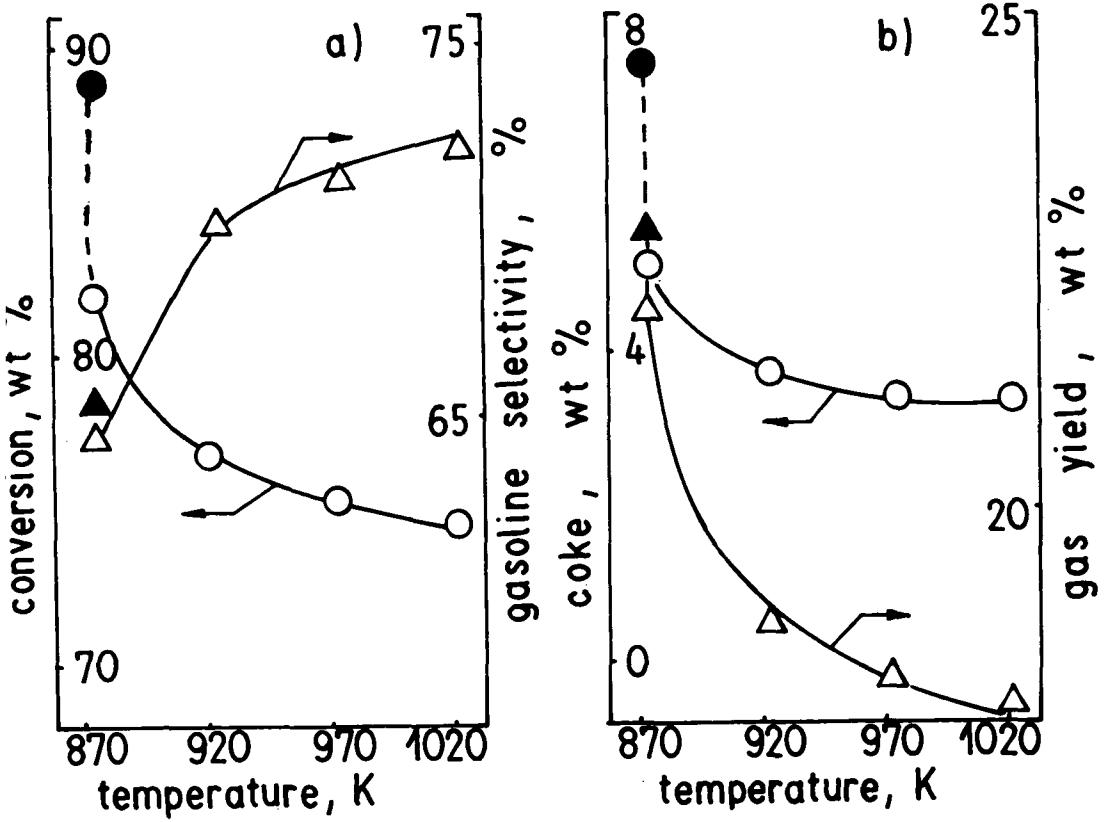

Fig. 1. Effect of hydrothermal pretreatment on the conversion, gasoline selectivity, coke and gas yield in the cracking of gas oil over a FCC catalyst (20 wt.% zeolite HRE-Y in silica-alumina matrix). Davison MAT: 760 K, 5 g catalyst, WHSV 20 h^{-1}
▲, ● - not hydrothermally but only thermally pretreated samples.

Gasoline selectivity is drastically increased, and the formation of coke and gaseous products is suppressed.

As has already been pointed out by Moscou and Moné /25/, gasoline selectivity increases with increasing pretreatment temperatures up to 1020 K. These drastic changes in the catalytical activity of the FCC catalyst suggests that the influence of lattice dealumination should be investigated separately.

HIGH-SILICA ZEOLITES Y

Recently, highly dealuminated ultrastable zeolites Y of good crystallinity with silica to alumina mole ratios up to 350 have been prepared from NH_4-Y zeolites at high temperatures under hydrothermal conditions /26-27/. From the USY samples obtained in this way, the non-framework aluminium can be extracted using diluted mineral acid, which results in USY-ex samples. Structure and adsorption properties have been described in some recent publications /28-30/. The decrease in the concentration of acidic sites, which accompanies the dealumination, leads to a decrease of the cracking activity of the USY-ex zeolites with progressing dealumination /31/. However, the coking velocity is more strongly reduced by dealumination than the cracking activity is: The reduction of site concentration by partial dealumination of the zeolite results in an improvement of the activity-time dependence by decreasing the rate of the coking reaction more rapidly than the cracking reaction rate. This effect can be understood assuming a 2-center mechanism for the coking reaction, whereas cracking follows a 1-center mechanism (equation 1 is derived on this basis).

Table 1

Acidity and catalytic properties of modified Y zeolites in the cracking of gas oil (M = mole ratio SiO_2/Al_2O_3)

	RENa-Y	USY-ex (M=17)	USY-ex (M=350)
Acid strength	$H_o \simeq -8$	$H_o \simeq -12$	$H_o \simeq -8$
Acid site concentration	$5.5 \cdot 10^{-1}$	10^{-1}	about 10^{-2}
Conversion, wt%	82.5	85	82
coke, wt% on catalyst	5.5	3.3	1.7

In Table 1 the acidic and catalytic properties in gas oil cracking over three modified Y zeolites are compared: A Rare Earth NaY zeolite (mole ratio M = SiO_2/Al_2O_3 = 5.2; cation exchange degree = 65 %) and two USY-ex zeolites with M = 17 and 350, respectively. At a comparable conversion degree the most striking feature is the varying amounts of coke formed by the three samples. The sequence of coke formation clearly follows the acid site concentration. At the same acid strength on the RENa-Y and on the USY-ex (M = 350), coke formation is strongly reduced in the case of the USY-ex (M = 350). This effect of acid site concentration even overcompensates an increase in acid strength going from RENaY to USY-ex

(M = 17).

The activity-time dependence in pulse catalytic cracking can be described by a 1-parameter equation:

$$\frac{1}{k(n)} - \frac{1}{k(1)} = B(n-1) \qquad \text{(Equation 1)}$$

in which $k_{(1)}$, $k_{(n)}$ are the rate constants calculated from the first (nth) pulse, and n represents the pulse number. The value of the constant B derived from the slope of the curves obtained by the plot of this function (Fig. 2) reflects the deactivation rate. Deactivation is drastically reduced by dealumination, resulting in an almost time-independent activity at very high dealumination degrees.

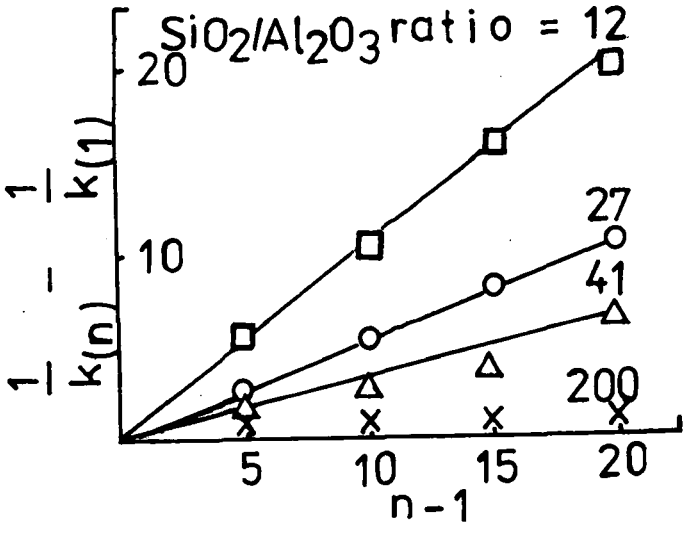

Fig. 2. Deactivation of USY-ex zeolites in hexadecane cracking vs. pulse number n. (k in 10^{-7} mole/ Pa·mg·h)

Besides activity and activity-time dependence, other selectivity parameters of USY-ex zeolites in the paraffin cracking reaction are also influenced by partial dealumination. With an increasing degree of dealumination, the long chain paraffins are more selectively cracked from a mixture with paraffins of lower molecular weight: this is demonstrated in Figure 3 with a mixture of hexadecane/octane. As a consequence, overcracking is reduced, and the gasoline yield in the cracking of gas oil increases. This effect can be made even more pronounced by controlled introduction of cations into such partially dealuminated Y zeolites.

The effect of cation introduction into the partially dealuminated zeolite USY-ex(41) on the acidity and catalytic properties is demonstrated by the results given in Table 2. As a measure of acidi-

ty, the extinction lg (I_o/I) of the 1450 cm^{-1} NH_4^+ band in the ir spectra of ammonia adsorbed on the sample is given. The cracking activity of the fresh, uncoked sample is characterized by the first order reaction rate constant k_1 of n-octane cracking at 473 K (k_1, in mole/Pa·mg·h). The quotient of the rate constants calculated from the first and tenth pulse, respectively, k_{10}/k_1, expresses the deactivation rate. U_{C16} represents the conversion of hexadecane measured in a continuous microtest (725 K, 0.5 g catalyst, 1.5 g feed per 3.5 min.), and Δg the gain in gasoline relative to USY-ex(41) at a level of 40 % conversion, measured in the MAT test.

Table 2

Effect of cation introduction into the partially dealuminated zeolite USY-ex(41) on the acidity and cracking properties.

	USY-ex(41)	$Ca_{0.2}H_{0.6}$USY-ex(41)	$SE_{0.15}H_{0.55}$USY-ex(41)	$Sn_{0.16}H_{0.36}$USY-ex(41)
lg(I_o/I)	0.4	0.05	0.15	0.05
$k_1 \cdot 10^9$	22.3	1.6	5.1	2.4
k_{10}/k_1	0.4	0.9	0.7	0.8
U_{C16}	7.5	7.3	41.7	35.1
Δg		8	16	18

As is evident from the data presented in Table 1, the initial activity (k_1) in n-octane cracking as determined by pulse catalysis decreases along with the Brønsted acidity. Simultaneously, the activity-time behaviour improves (k_{10}/k_1 increases).These samples were used for determining the catalytic properties in a flow reactor in hexadecane conversion, according to the Davison microactivity test (cf. Table 2).

As compared with USY-ex(41) recationized samples give higher or equal conversion, which is obviously due to the different activity-time behaviour. The cracking selectivity (gasoline yield) is strongly affected by the exchange of cations. Whereas USY-ex(41) is characterized by rather nonselective cracking of n-paraffins, gasoline yield is increased by Ca^{2+} exchange. SE^{3+} and Sn^{4+} exchanged USY-ex zeolites exhibit high selectivity despite the high conversion.

Thus, the catalytic properties in paraffin cracking can be varied in a wide range by subsequent recationization of the USY-ex zeolites. The initial activity is decreased, the activity-time behaviour is improved (particularly by exchange of RE^{3+} and Sn^{4+}

cations), and the cracking selectivity is increased.

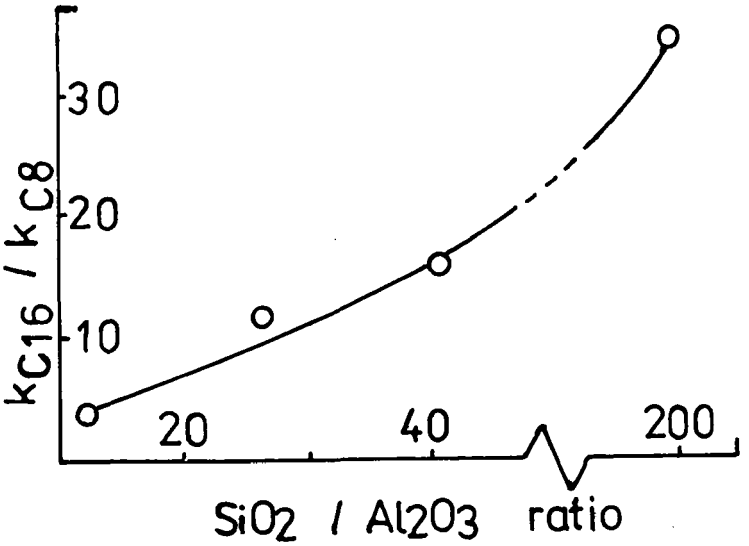

Fig. 3. Selectivity in the simultaneous cracking of hexadecane and octane at 725 K over USY-ex zeolites vs. molar SiO_2/Al_2O_3 ratio.

Very little information is available on the role of extra lattice aluminium in catalysis. SCHEVE et al. /33/ assume the non-framework aluminium to be an inert diluting material, which only decreases the hydrogen transfer reaction. To illustrate the problem, the impact of the extra lattice aluminium on the catalytic cracking of cumene is shown in Figures 4 and 5.

Comparison of Brønsted acidity and catalytic activity of silica-alumina and ion exchanged zeolites Y permit the conclusion that the Brønsted acid sites are the centers which are catalytically active in the cumene cracking reaction. The unusually high activity of the USY sample deserves special explanation, which can only be based on the role of the extra lattice aluminium. This is clearly evident from the fact that after removal of the extra lattice aluminium by acid extraction, the resulting USY-ex(200) sufficiently matches the activity function common to the other samples. This can be interpreted by assuming the extra lattice aluminium to be adsorption sites for the aromatic molecules, which increase the value of the first order reaction rate constant. The effect of extra lattice aluminium depends on its amount, i.e. on the degree of lattice dealumination during the hydrothermal treatment, as is shown in Figure 5a: Cumene cracking activity increases with increasing lattice dealumination, despite the decreasing Brønsted acidity. On the other hand, both, activity and Brønsted acidity of the USY-ex samples decrease with increasing lattice dealumination. Enhanced adsorption on the extra lattice aluminium should be accompanied by a slower

desorption rate of condensed products, which should result in a more rapid deactivation by coking. This is shown to be true by Fig. 5c.

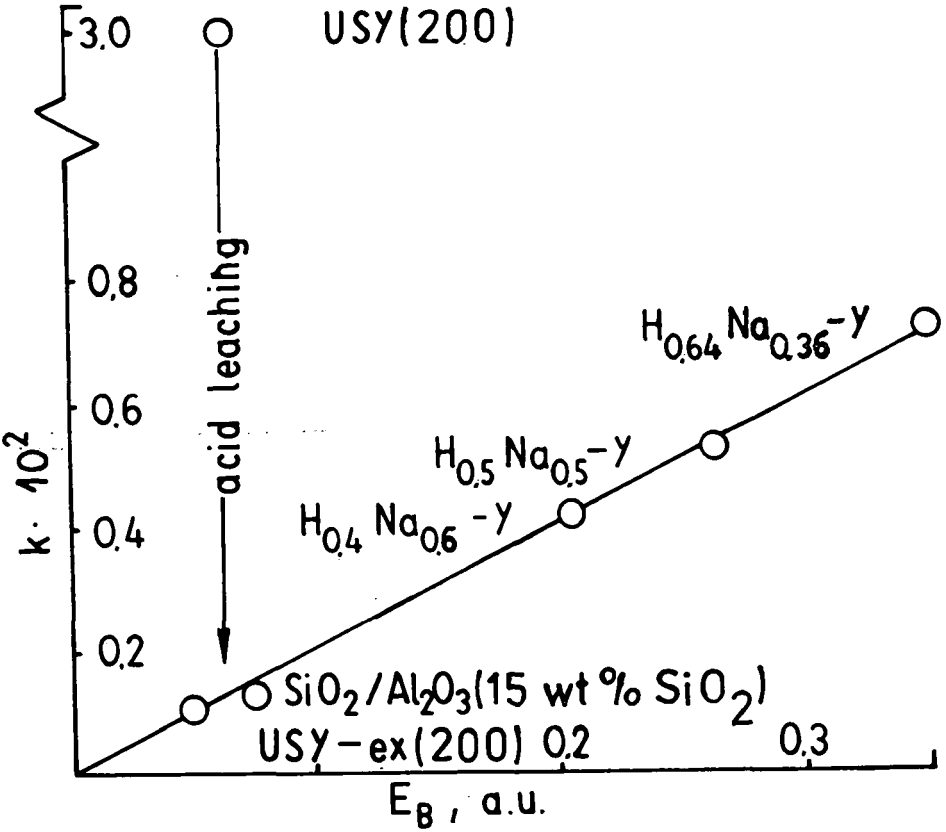

Fig. 4. Brønsted acidity (E_B) and first order reaction rate constant k (mole/MPa · sec · g) of pulse cumene cracking at 575 K /32/. E_B-extinction of pyridinium ion ir band.

The effect of the new secondary pore system (most frequent pore diameter about 1.8 nm) created in the zeolite by the hydrothermal treatment can be evaluated by comparing the catalytic behaviour of USY-ex zeolites with that of high silica HY zeolites not having such a new pore system which can be prepared by the method of BEYER with $SiCl_4$ /34/. There are no differences in the cracking of paraffin based gas oil over the high silica zeolites prepared in both ways. However the cracking of fused multi-ring compounds containing oils, including heavy recycle oil is favoured over the USY-ex samples, due to the new pore system.

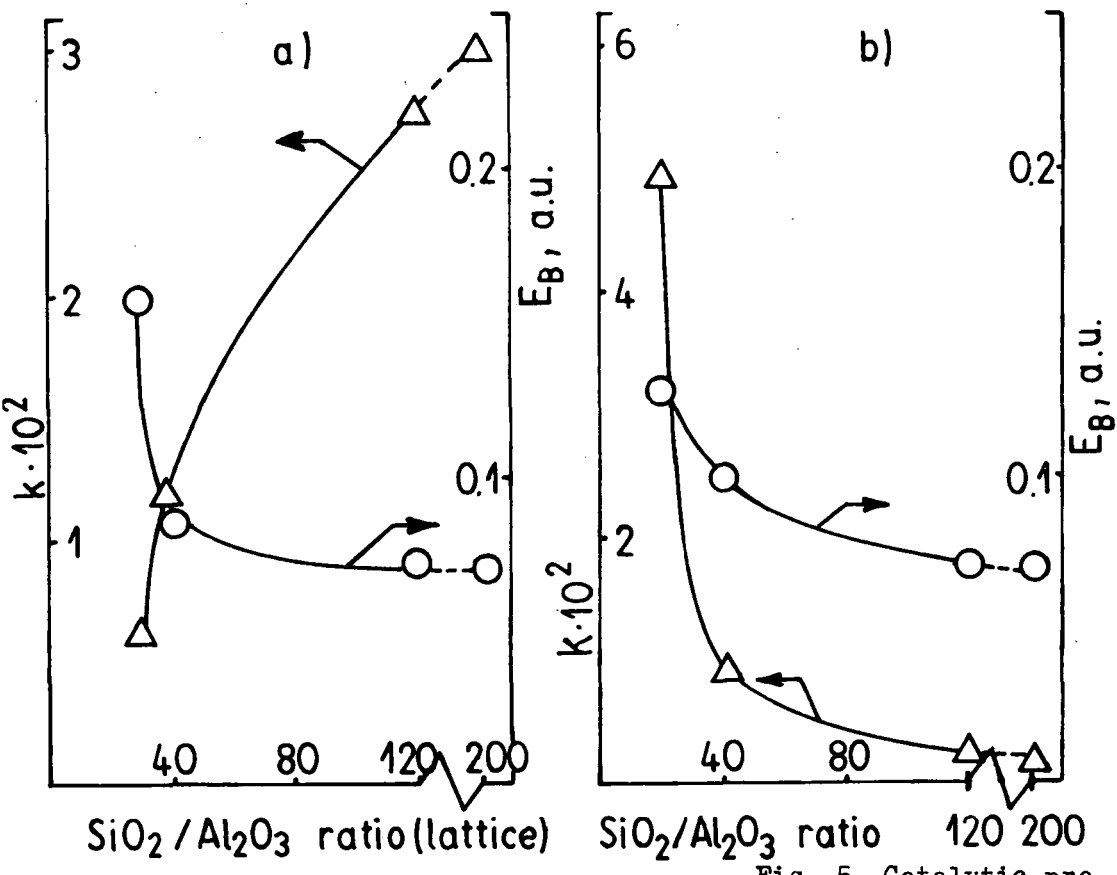

Fig. 5. Catalytic properties (cumene cracking) of hydrothermal pretreated zeolites Y vs. zeolite lattice composition /30/.
a. Extra lattice containing USY zeolites.
b. Samples after extraction of extra lattice aluminium.
c. Activity-time dependency of USY and USY-ex zeolites.
E_B and k cf. fig. 4.
k_{10}/k_1 - quotient of the rate constants derived from pulse 1 and 10.

RAISING THE YIELD OF SYNTHESIS OLEFINS

Under certain conditions, the desired selective cracking with partially dealuminated Y zeolites as the active component in FCC catalysts, may result in the portion of low synthesis olefins formed being smaller than is desired. In such cases, the addition of the zeolite ZSM-5 to the FCC catalyst appears to be advisable.

As demonstrated in Figure 6, 5 wt.% of an REZSM-5 are sufficient for achieving a substantial increase in the yield of propene and butenes. In this way the product distribution commonly obtained in cracking /9/ can be changed to a significant degree. In the extreme case, two maxima can be obtained in the product distribution curve, namely in the gasoline range, and for the C_3/C_4 olefins. Both zeolite components - dealuminated Y zeolites and ZSM-5 - also complement each other excellently, in that coke formation in both cases is very slow. One of the consequences of this fact is that ionic H transfer to the product olefins (with coke as a H donator) is strongly suppressed.

INFLUENCE OF METALS ON THE ACTIVITY AND SELECTIVITY OF ZEOLITE-CONTAINING CATALYSTS

All cracking feedstocks contain traces of metals (which are enriched in the residual oils) in concentrations of about 1 - 1000 weight ppm: vanadium, nickel, iron, copper, sodium, which are fully deposited on the catalyst, and may cause some adverse effects /35, 23/. Whereas vanadium destroys the zeolite crystal lattice, the other metals - in particular nickel - cause undesirable dehydrogenation reactions leading to hydrogen and coke formation at the expense of the desired gasoline. A detailed report on the causes of the poisoning of FCC catalysts by vanadium (action of the V=O species) will be given by OCCELLI et al. /36/ at this conference.

Activity and selectivity losses due to metal contamination can be diminished by using cracking catalysts with increased proportions of zeolite (V tolerances of 1000 ppm and Ni tolerances of 500 ppm on equilibrium catalysts in USA FCC units have already been achieved in 1982), or by metal passivation e.g. by additives containing antimony. This type of passivation is particularly beneficial for nickel-containing catalysts, and the firm Davison has successfully developed and utilized a special vanadium passivator "DVT". To maintain the activity and selectivity of an equilibrium catalyst in practice, a definite limit of contamination by metals has to be set,

which must not be exceeded.

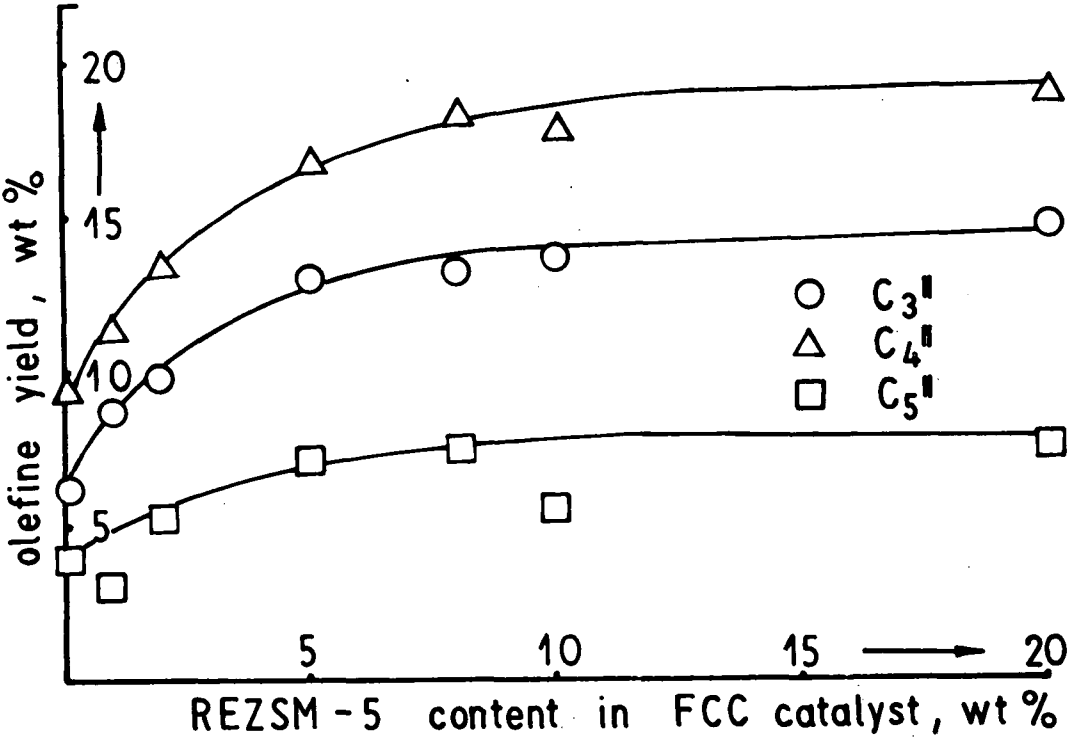

Fig. 6. Influence of the REZSM-5 content on the olefin yield in the cracking of hexadecane under MAT conditions (cf. Fig. 1).

For this reason, the equilibrium catalyst is continuously replaced with fresh catalyst. As is evident from a balance calculation, /2/, the catalyst replacement rate in the cracking of mixtures of vacuum gas oil and residual oil amounts to about 1 kg of catalyst per ton of feed, whereas in the heavy oil cracking process (HOC) 1.9 to 3.7 kg of catalyst per ton of feed are required.

As is evident from experiments on cracking catalysts /37, 38/ which will be presented at this conference by BITTRICH et al. /37/, hydrogen-activating substances (e.g. MoO_3 and WO_3) can increase the activity and selectivity in producing gasoline. Impregnation of a FCC catalyst with these components decreased its activity, whereas a physical mixture results in improved activity. Comparison of the catalytic properties in the cracking of hydrofined vacuum distillates (boiling at 630-820 K) on a commercial catalyst and a catalyst mechanically mixed with SiO_2 (10 wt.%) and WO_3 (0.8 wt.%) is shown

in Table 3 /38/. The effect of the SiO_2/WO_3 additive, which increases the activity and particularly the gasoline yield, is clearly evident. Possible reasons and limits of this effect will be discussed in the announced contribution /37/.

Table 3

Comparison of the catalytic properties of modified cracking catalysts (Davison CAT-A test)

Conditions:			
temperature	753 K	C/O ratio	2.8
catalyst weight	5 g	WHSV	20 g/g·h
particle size	$\geq 63\,\mu m$		
Results:	FCC catalyst	FCC catalyst	(+ SiO_2/WO_3)
(amounts in wt.%)			
conversion	65.5		74.3
liquid products	85.2		84.3
gasoline	51.1		58.5
gas	11.6		13.4
coke	2.9		2.4

PROMOTION OF CO-OXIDATION

Since 1975, promotors have been successfully used for reducing the carbon content on the regenerated catalyst and for minimizing the CO content in the flue gas /39, 40/. In most cases, noble metal additives are used for this purpose (up to about 5 ppm Pt per catalyst weight), which are either fed in together with the catalyst, or are fed into the plant as liquid or solid additives.

The effect of Pt, Pd, Fe, Ni and V salts on the CO oxidation activity in regeneration and their effects on the catalytic cracking activity will be presented in detail by our Hungarian colleagues STEINGASZNER et al. /41/ at this conference.

As is evident from the comparison of the results of conventional regeneration with those of a promoted regeneration, using operational data of an industrial plant /40/, the CO content in the flue gas can be drastically reduced, with the gasoline yield remaining the same. Hence, in the presence of a promoter, a greater amount of heat can be generated in the regenerator, or the catalyst supply can be decreased which will reduce the loss of catalyst by mechanical abrasion. Also, with the use of a promotor, the content of residual coke on the regenerated catalyst can be reduced, enhancing catalyst activity and gasoline yield /39/.

MINIMIZATION OF SO_x POLLUTION

Although intensive work in developing catalyst additives for reducing SO_x emissions in flue gas dates back to the 'seventies, successful industrial application was not achieved until 1979 (Davison additives "S" and "R") /23/.

Table 4 shows that the SO_2/SO_3 content in the flue gas can be considerably reduced. The action of such additives (in most cases catalytically inert oxidic materials) is due to the fact that SO_2 in the presence of excess oxygen oxidizes to give SO_3, which is bound on the catalyst as sulfate. In the reducing atmosphere of a riser, sulphides are formed. These sulphides hydrolyze in the stripping part of the reactor, to give H_2S, which is then removed from the cracking gas. Subsequent H_2S conversion to elementary sulphur might render the whole procedure attractive even from an economic point of view.

Table 4

Results obtained with additive "R" from an FCC plant /23/

Catalyst	DA-400 equilibrium catalyst	DA-400 +4 % additive "R"
S in feed, wt.%	0.56	0.56
excess of O_2, mole %	2-3	2-3
CO, mole %	0-1.5	0-0.1
temperature of regenerator, K	688-704	688-704
SO_2, kg/h	49	20
SO_3, kg/h	9	2

FEEDSTOCK PRETREATMENT

Many difficulties can be overcome by proper pretreatment of the feedstock. RITTER et al. /42/ were the first to point out the advantages of the use of hydrotreated FCC feedstocks, including heavy cycle oil. The benefits of cracking hydrogenated feedstocks are: Improved gasoline output, lower sulphur content in the products, lower SO_2 level in the flue gas, strong reduction of metal contamination, less poisoning and less coking of the FCC catalyst due to previous hydrogenation of heterocompounds and highly unsaturated hydrocarbons.

Excellent experience in all these respects has been gained with the DESUS procedure /43, 44/ in the PCK Schwedt in the GDR. This procedure serves to achieve a 85 to 90 percent desulphurization of middle and vacuum distillates at 650 K, 3.5 MPa H_2, and a LHSV

of 2-2.5 v/vh on a hydrotreating catalyst with optimized shape and pores. It has been developed by the Leuna-Werke "Walter Ulbricht".

Comparison of the most important properties, (gasoline yield and quality, catalyst consumption, and SO_2 emission) in the case of unrefined gas oil and gas oil obtained by hydrotreating according to the DESUS procedure, is presented in Table 5.

Table 5

Influence of DESUS pretreatment on FCC parameters /43/

Parameters of gas oil (725-805 K) cracking	feedstock	
	untreated	DESUS pretreated
Yield, wt.%		
gasoline	46	51
light cycle oil	20	17
heavy cycle oil	8	5
$i\text{-}C_4$	14	16
Quality, ROZ^+ (0.31 g Pb/dm^3)	95	96.5
Catalyst supply,		
kg catalyst/t feed	1.01	0.505
SO_2 pollution, kg/t feed	1.32	0.15

A reduction of the S content from 1.4 to 0.4 wt.% in the oil is associated with increased gasoline yield from 46 to 51 wt.%. This increased gasoline yield is mainly due to selective catalytic conversion of condensed polynuclear aromatics into gasoline derivatives. Simultaneously, the pretreatment of the gas oil results in a decrease of the vanadium content from 2 to 0.2 ppm, and of the nickel content from 0.5 to 0.1 ppm.

TENDENCIES IN FCC CATALYST DEVELOPMENT

Today, intensive work is being carried out to improve the properties of zeolite containing cracking catalysts. The aims of this work are as follows:

- to increase the gasoline yield
- the improvement of gasoline quality (octane number)
- to decrease SO_x and CO emission
- the development of catalysts with high metal compatibility, which also enables heavy feedstocks to be processed.

Increased gasoline yield along (with increased content of aromatics) and reduced coke formation can be achieved when high silica ultrastable zeolites Y are used as active components. However,

due to increased technological expense, production costs of such catalysts are much higher, and their potential use is subject to economical considerations.

When an increased proportion of synthesis olefins is desired in the FCC process, this can be achieved by incorporating an additional proportion of ZSM-5 as a zeolite component into the cracking catalyst.

Other alumosilicate solids, such as dealuminated mordenites and erionites, as well as smektites may be used as active cracking components, little information is however available concerning their application.

ACKNOWLEDGEMENT

The authors are indebted to Dr. U. Lohse from the Central Research Institute for Physical Chemistry of the Academy of Sciences in the GDR, at Berlin, for the preparation of partially dealuminated zeolites Y. We also thank Dr. H.K. Beyer from the Central Research Institute for Chemistry of the Hungarian Academy of Sciences in Budapest, for a high-silica zeolite Y sample prepared in his laboratory.

REFERENCES

/1/ Marcilly, Ch., Revue de l'Institut Français du Pétrole 30, 969 (1975).
/2/ Weitkamp, J., Chemie-Technik 11, 1 (1982).
/3/ European Chem. News 42, 4 (1984).
/4/ Gates, B.C., Katzer, J.R., Schuit, G.C.A., "Chemistry of Catalytic Processes", McGraw-Hill Book Co., 1978, p.1.
/5/ Magee, J.S., Blazek, J.J., Chapter 11 in "Zeolite Chemistry and Catalysis", Ed. Rabo, J.A., ACS Monograph, Washington, D.C.1976.
/6/ Chadzhijev, S.N., "Kreking Neftjanich Frakzii na Zeolitsoderzhasshich Katalizatorach", Chimija, Moskau 1982.
/7/ Whitmore, F.C., J.Amer.Chem.Soc. 54, 3274 (1932); Chem.Eng.News 26, 668 (1948).
/8/ Thomas, C.T., Ind.Eng.Chem. 41, 2564 (1949).
/9/ Greensfelder, B.S., Voge, H.H., Good, G.M., Ind.Eng.Chem. 41, 2573 (1949).
/10/ Weisz, P.B., Chemtech. 8, 498 (1973).
/11/ Fejes, P., Förster, I., Kiricsi, I., Seebode, J., in "Structure and Reactivity of Modified Zeolites", Ed.Jacobs, P.A. et al., Elsevier, Amsterdam 1984, p.91.
/12/ Hall, W.K., Lutinski, F.E., Gerberich, H.R., J.Catal. 3, 512 (1964).
/13/ Kustov, L.M., Borovkov, V.Yu., Kazansky, V.B., loc.cit. 11, p.241.
/14/ Haag, W.O., Dessau, R.M., Proc. 8th Intern.Congr.Catalysis, Berlin (West) 1984, Vol. II, p.305.
/15/ Kutcherov, A.V., Slinkin, A.A., loc.cit. 11, p.77.
/16/ Förster, H., Seebode, J., this symposium.
/17/ Wendlandt, K.-P., Bremer, H., Proc. 8th Intern.Congr.Catalysis, Berlin (West) 1984, Vol. IV, p.507.

/18/ Daage, M., Fajula, F., J.Catal. 81, 394 (1983).
/19/ Wollschlager, L.I., Ritter, R.E., Cracking Catalyst Evaluation, Group Micro Activity Units, W.R. Grace/Davison, Columbia 1975.
/20/ Weekman, V.W. Jr., Ind.Eng.Chem.Process Des. Dev. 7, 90 (1968).
/21/ Jacob, S.M., Gross, B., Voltz, S.E., Weekman, V.W. Jr., A.I.Ch. E.J. 22, 701 (1976).
/22/ Weisz, P.B., Schwartz, A.B., Weekman, V.W. Jr., 10th World Petroleum Congr., Bucharest 1979, RP 5.
/23/ GRACE-DAVISON Seminar Crack-Katalysatoren, Berlin 1984.
/24/ Fachgespräch der Firmen Katalistiks B.V. und Mitsubishi Corp., Berlin 1984.
/25/ Moscou, L., Moné, R., J.Catal. 30, 417 (1973).
/26/ McDaniel, V.C., Maher, P.K., Molecular Sieves, Soc.Chem.Ind., London 1968, p.16.
/27/ Lohse, U., Alsdorf, E., Stach, H., Z.anorg.allg.Chem. 482, 49 (1981).
/28/ Engelhardt, G., Lohse, U., Patzelová, V., Mägi, M., Lipmaa, E., Zeolites 3, 233 (1983).
/29/ Lohse, U., Engelhardt, G., Patzelová, V., Zeolites 4, 163 (1984).
/30/ Gross, Th., Lohse, U., Engelhardt, G., Richter, K.-H., Patzelová, V., Zeolites 4, 25 (1984).
/31/ Bremer, H., Wendlandt, K.-P., Tran Khac Chuong, Lohse, U., Stach, H., Becker, K., Proc. 5th Intern.Symp.Heterogeneous Catalysis, Varna 1983, Part I.
/32/ Jank, J. Thesis, Merseburg, GDR, 1985.
/33/ Burghardt, I., Fichtner, H., Lohse, U., Scheve, J., Schulz, I.W., Illgen. U., this symposium.
/34/ Beyer, H.K., Belen'kaja, I.M., in "Catalysis by Zeolites" Ed. Imelik, B. et al., Elsevier, Amsterdam 1980, p. 203.
/35/ Ritter, R.E., Rheaume, L., Welsh, W.A., Magee, J.S., Oil Gas J. 79, 103 (1981).
/36/ Occelli, M.L., Psaras, D., Suib, S.L., this symposium.
/37/ Bittrich, H.-H., Feldhaus, R., Anders, K., Becker, K., this symposium.
/38/ Becker, K., Vogt, F., Weber, M., Bittrich, H.-H., Zimmermann, G., Anders, K., DD-WP 160 064.
/39/ Chester, A.W., Schwartz, A.B., Stover, W.A., McWilliams, J.P., Chem. Technol. 11, 50 (1981).
/40/ Magee, J.S., Ritter, R.E., Rheaume, L., Hydrocarbon Process. 58, 123 (1979).
/41/ Steingaszner, P., Szücz, A., Dudás, E.L., Mándy, T., this symposium.
/42/ Ritter, R.E., Blazek, J.J., Wallace, D.N., Oil Gas J. 72, 99 (1974).
/43/ Bohlmann, D., Döhler, E., Limmer, H., Schütter, H., Chem. Techn. 33, 358 (1981).
/44/ Becker, K., John, H., Franke, H., Schütter, H., Chem. Techn., 34, 420 (1982).

ÇATALYTIC CUMENE CRACKING ON H-ZSM-5 TYPE ZEOLITES

A. BIELANSKI [a,b], A. MAŁECKA [b]

Department of Chemistry, Jagiellonian University, Cracow, Poland (a)
Institute of Catalysis and Surface Chemistry of the Polish Academy of Sciences, Cracow, Poland (b)

ABSTRACT

The effect of cation exchange degree of H-ZSM-5 type zeolite the mode of its decationation and its granulation on the zeolite catalytic activity in the case of cumene cracking was investigated. Besides benzene and propylene the main products of this reaction butenes and pentenes as well as n-propylbenzene appeared as the products of side reactions. Owing to the shape selectivity no saturated hydrocarbons (except traces of butane) nor ethylbenzene and toluene were forming which are typical products of side reactions on HNaY zeolites. Generally the H-ZSM-5 zeolites decationated by the substitution of Na^+ by NH_4^+ are more active than those decationated by the treatment with hydrochloric acid solution exhibiting comparable content of Brönsted acid sites.However this effect was definitely more distinct in the case of highly exchanged zeolites (cation exchange degree about 90 %).

INTRODUCTION

Despite the fact that cumene cracking belongs to the frequently used catalytic test reactions it has not been more thouroughly studied on the ZSM-5 type zeolites. Nayak and coll. [1] described a series of experiments in which cumene conversion was determined at 673 K on a series of H-ZSM-5 zeolites differing by the cation exchange degree. The present authors [2] compared the behaviour of HNaY and H-ZSM-5 type zeolites as the catalysts of cumene cracking and stated distinct differences in the yield and the composition of the side reactions products. The aim of the present investigation was to study the catalytic cracking of cumene on H-ZSM-5 type zeolites of different cation exchange degree the acid properties of which were well characterized. Simultaneously the effects of the decationation mode and the granulation of the samples were investigated.

EXPERIMENTAL

The samples of ZSM-5 type zeolite (Si/Al molar ratio equal to 47) were obtained at the Institute of Industrial Chemistry, Warsaw, as described in [3]. The decationation was carried out by J. Datka either via substitution of Na^+ ions with NH_4^+ (symbol NZ) or by the treatment with hydrochloric acid solution (symbol HZ). The samples with the highest cation exchange degree were also obtained in the case of which both methods of decationation were applied one after another but in different sequences (symbols HNZ and NHZ). The acid properties of the same samples were investigated in this laboratory by J. Datka and Tużnik and are described by them in full detail in their paper presented at this conference [4] and also in ref. [5] and [6]. The main data characterizing the samples are given in the Table. The numbers in the symbols of samples give the percentage of cation exchange. Strong Brönsted acid centres are formed by OH groups with the stretching frequency 3609 cm^{-1}. Catalytic tests were carried out using either the samples not granulated containing crystallites of $\sim 1\mu m$ or the samples obtained by pressing the same fine crystalline powder, crushing the pellets and selecting the sieve fraction of grains 90-190 μm.

Table

Sample and cation exchange degree %	Apparent activation energy kJ mol^{-1}		Concentration of acid center per unit cell[x]				Rate constant of cumene cracking min^{-1}			
			Brönsted			Lewis	K_{670}		K_{630}	
	powder	granul.	strong	weak	total		powder	granul.	powder	granul.
NZ-31	62	39	0.29	0.30	0.59	0.10	70	100	31	59
NZ-43	54	44	0.47	0.36	0.83	0.15	144	145	85	88
NZ-83	52	30	0.85	0.39	1.24	0.18	238	218	135[xxx]	152
HZ-42	58	49	0.38	0.35	0.73	0.14	143	179	70[xx]	115
HZ-81	35	38	0.82	0.26	1.08	0.18	129	205	77	136
HZ-88	30	37	1.03	0.30	1.33	0.17	168	242	126	167[xx]
HNZ-90	38	35	0.96	0.22	1.18	0.10	115	209	72	140
HNZ-88	55	36	1.04	0.21	1.25	0.13	183	278	115	196

x - Determined by J. Datka and E. Tużnik [5,6] ; xx - Extrapolated ; xxx - Interpolated.

Catalytic tests were carried out in a pulse microreactor connected on line with a gas chromatograph. Helium was used as a carrier gas into the flow of which (1200 cm^3h^{-1}) the doses of 3 μl of cumene were introduced. The samples 0.02 g of catalyst diluted with 0.1 g of powdered quartz were activated "in situ" for 2 h at 720 K in the stream of helium. Analytically pure cumene (POCh Gliwice, Poland) was kept over metallic sodium and distilled before experiments. A Giede 18.6 Gas Chromatograph with programmed heating was used for the analysis of the reaction products applying a chromatographic column (length 2.5 m, diameter 4 mm) filled with Chromosorb W covered with 14 % of silicon oil DC 200. Katharometric detection was applied. The reaction products were identified using Mass Spectrometer LKB 9000 s.

Two series of catalytic tests were carried out. In constant temperature tests the dependence of activity and selectivity on the number of cumene pulses was investigated. In polythermic tests executed usually between 570 and 670 K at each temperature only one pulse was introduced in order to avoid the effects of ageing.

The rate constant of cumene conversion was calculated assuming 1st order of the reaction.

RESULTS AND THEIR DISCUSSION

Reaction products. Besides the main reaction products benzene and propylene some amounts of side reactions products were also detected : butenes, pentenes and n-propylbenzene but only traces of butane. The olefins were the products of the transformations of primary propylene as verified by the separate experiments in which pure propylene was introduced on the catalyst. The fact that olefins were the predominant products of propylene secondary reactions and only traces of alkanes (butane) were present which on the other hand are the main products of propylene secondary reactions on NaHY zeolites [2] is a typical shape selective effect. Presumably it is connected with different properties of propylene oligomer forming in both cases. In ZSM-5 zeolites the narrow pores allow only the formation of linear oligomer which, as it is supposed, decomposes into olefins of various chain length while the threedimensional oligomer forming in large cavities of faujasite type zeolites disproportionates into the hydrogen rich (alkanes) and hydrogen deficient precursor of the coke [7].

Only one aromatic product of side reactions was detected i.e. the n-propylbenzene which is the product of cumene isomerization. According to [8] the latter reaction occurs with the formation of monomolecular

transition complex. No ethylbenzene nor toluene were formed which were observed in the case of NaHY zeolites. They are considered to be formed via bimolecular transition complexes [8] which obviously can not be formed in the narrow pores of H-ZSM-5 zeolite.

Ageing of the catalysts. The ageing of the catalysts was followed at 600 and 670 K. Fig. 1 (full line) shows that the deactivation of the catalyst with the increasing number of cumene pulses was slow being more distinct at lower temperature and in the case of the catalyst exhibiting smaller cation exchange degree. The fact that deactivation was slower at higher temperatures can be explained by a more rapid desorption of precursors of the coke deactivating the catalyst. No influence of the granulation on the ageing of the catalyst (dashed lines on Fig. 1) was observed.

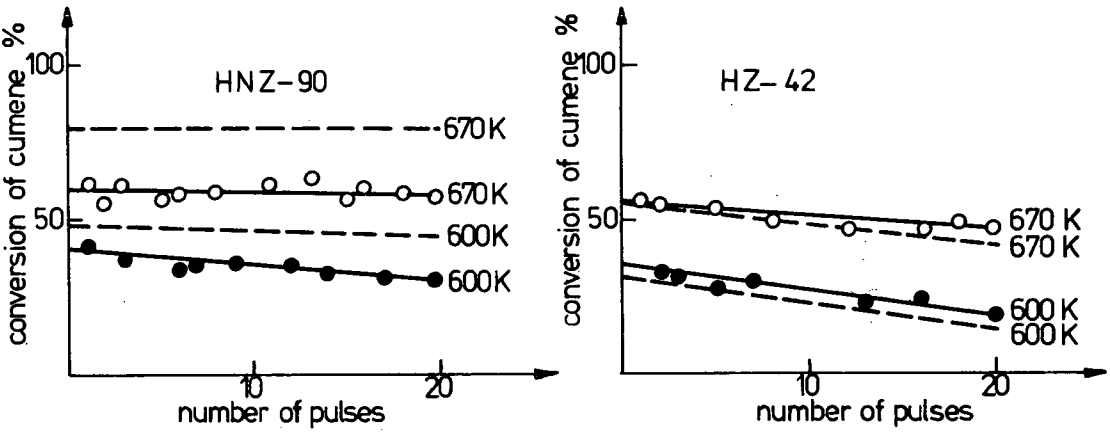

Fig. 1. Conversion of cumene as the function of the number of cumene pulses in the case of HNZ-90 and HZ-42 samples non-granulated (full line) and granulated (dashed line).

Fig. 2 shows on the example of HZ-1 sample the effect of the deactivation on the composition of reaction products. It is seen that the mole % of benzene in the initial pulses exceeded the sum of mole % of propylene unchanged and propylene transformed into butenes. The deficit of propylene must be due at least partially to its irreversible adsorption resulting in the slow catalyst deactivation but also some amounts of it may be only slowly desorbed out of the catalyst and not be included in the pulse of products introduced on the chromatographic column. Similarily as it was observed in [2] catalyst deactivation results in the diminishing of the amounts of side reactions products : increasing the content of propylene, decreasing the content of other olefins. Simultaneously the relative content of benzene with respect to

the total content of propylene is decreasing and slowly approaching the molar ratio 1:1 thus indicating that the deficit of propylene is growing less and the catalyst is becoming more selective in respect to the main cracking reaction. This indicates that the secondary transformations of propylene occur on the acid centres - presumably the strongest ones - which are poisoned at first.

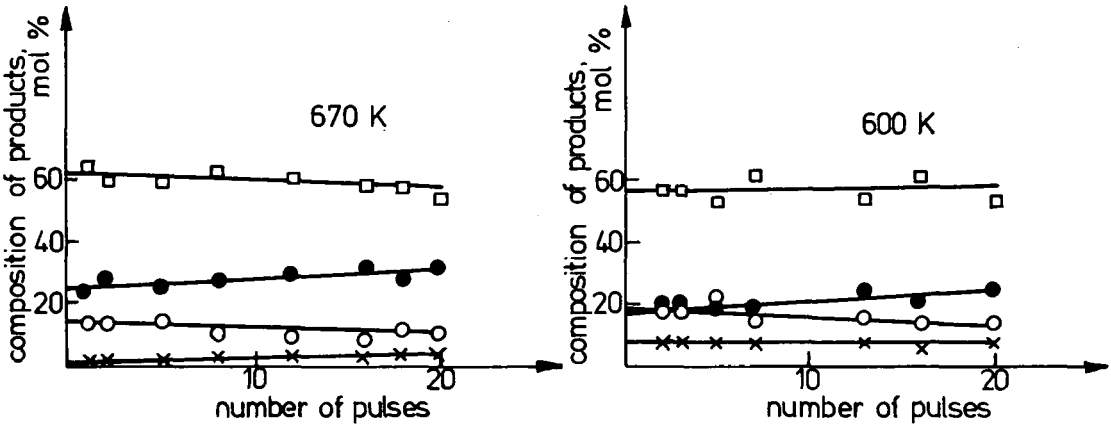

Fig. 2. Composition of the reaction products on the HZ-42 non-granulated at 670 and 600 K as the function of the number of cumene pulses (mol %).

□ benzene
● propylene
○ butenes (expressed as the number of moles of converted propylene)
× n-propylbenzene

The effect of cation exchange degree and the mode of decationation. Fig. 3 shows the dependence of rate constant on the temperature as obtained in polythermic tests carried out with not granulated samples. When comparing the activity of various samples the following statements can be done :

1. Within both series of zeolites NZ and HZ the catalytic activity is increasing with the increasing cation exchange degree and also with the acidity as given by the concentration Brönsted acid centres.
2. The effect of the decationation mode can be followed by comparing samples HZ-42 and NZ-43 with cation exchange degree 42 resp. 43 % and also on the samples HZ-88, HNZ-90 and NHZ-88 with 88-90 % of cation exchange. In the further case the activities of both samples are similar within the whole range of temperature but the sample NZ-43 with higher

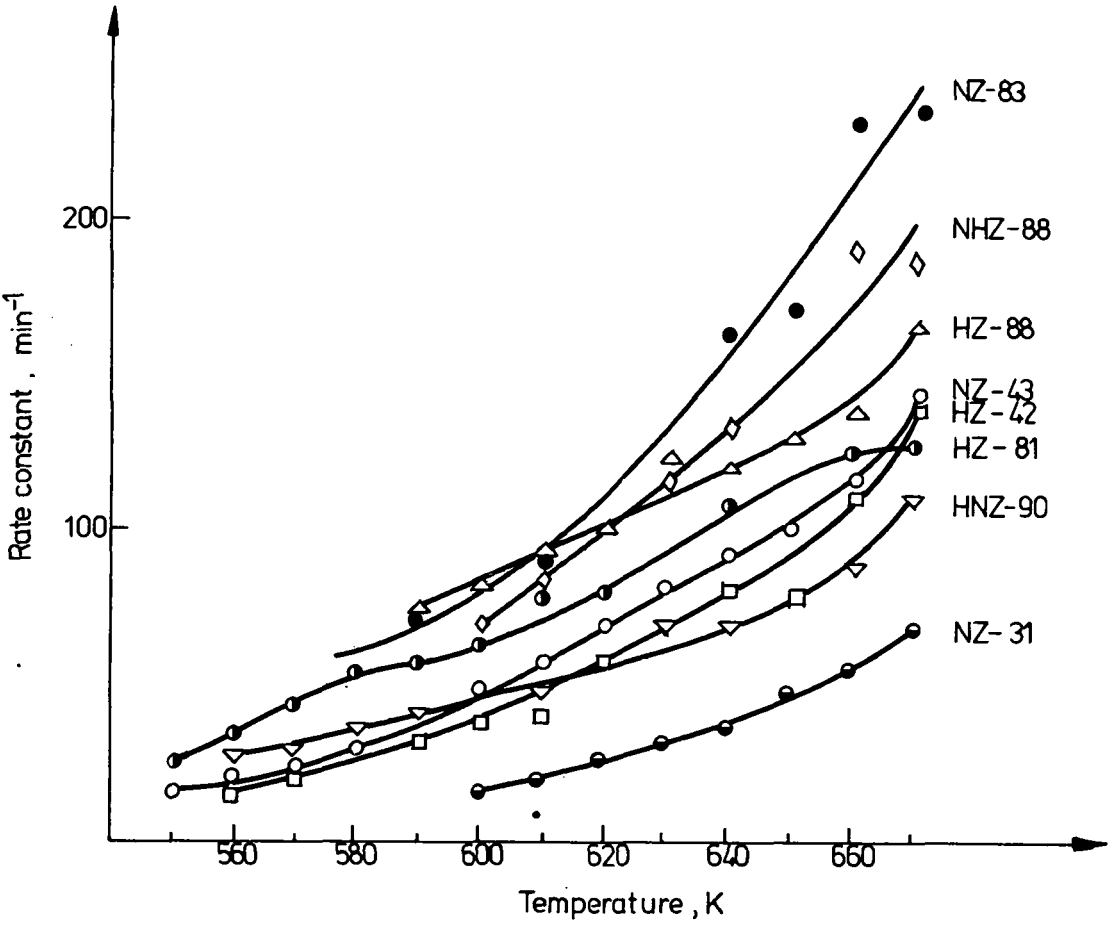

Fig. 3. Rate constant of the non-granulated catalysts as the function of temperature

content of Brönsted acid centres was always more active. In the latter case the discrepancies in the activity are much more pronounced and the sequence of activity HNZ-90 NHZ-88 HZ-88 corresponds well to the sequence of the total concentration of Brönsted acid centres. However it should be observed that the sample NZ-83 with 1.24 Brönsted acid centres per unit cell practically identical with that of the sample NHZ-88 is more active than all the other samples. The apparent activation energies of catalytic reaction of NZ-83 and NHZ-88 are not very much differing but the activation energy in the case of the latter sample is somewhat lower and the observed differences may be attributed to the higher activity of catalytically active Brönsted acid centres. However the second possibility is that in NHZ-88 sample the acid centres although accessible to pyridine molecules in the course of determination of their concentration, are only partially accessible to the cumene molecules. This

might be due to some structural changes in NHZ-88 sample.
3. The apparent activation energy of cumene conversion decreased within both series of samples NZ and HZ with increasing cation exchange degree. With the exception of NHZ-88 sample this rule seems to be also approximately valid for the whole set of the results. The decrease of activation energy with the decreasing cation exchange degree was also observed in some other cases as e.g. in the case of butene isomerisation on NaHY zeolites [9]. There are several possible reasons of such effect. First of all the increasing number of acid centres playing the role of catalytically active sites results in much faster reaction in the zeolite pores and in such situation diffusion becomes a factor influencing the overall rate of the process. Secondly the increased acid strength of the Brönsted acid centres may lower the energy needed for the formation of transition complex. Finally the possible increase of the adsorption heat of the substrate may cause the decrease in the apparent energy of activation even if the true activation energy remains unchanged.

The effect of sample granulation is shown in Fig. 1 in which full lines correspond to the not granulated samples and the dashed lines to the granulated ones. It is seen that in the case of HZ-42 sample exhibiting relatively low activity the effect of granulation is not pronounced. On the other hand in the case of highly active HNZ-90 sample the conversion on the granulated catalyst is definitely higher. This can be attributed to the fact that the reagents penetrating into the pores between particular crystallites remain for a longer period of time in the contact with the catalyst and the effect is similar to that obtained by the prolongation of contact time. The effect of diffusion in the intercrystalline pores of the granules is the obvious reason why granulating the samples lowers the apparent activation energy as it is seen from the data presented in the Table.

REFERENCES

1. Nayak V.S., Choudry V.R., J. Catal., 81, 26 (1983).
2. Bielański A., Małecka A., to be published.
3. PRL Patent 82967 (1973).
4. Datka J., Tużnik E., paper presented at this conference.
5. Datka J., Tużnik E., in print.
6. Datka, J., J.C.S. Faraday I, 76, 2437 (1980).
7. Datka, J., in print.

8. Best, B., Wojciechowski, B.W., J. Catal., 47 (1977).
9. Bielański, A., Datka, J., Drelinkiewicz, A., Małecka, A., Acta Phys. et Chem. Szeged., 24, 89 (1978), Proc. Symposium on Zeolites, Szeged 1978.

EFFECT OF SOME PLATINUM METALS ON THE REGENERATION BEHAVIOUR OF ZEOLITIC CRACKING CATALYSTS

P. Steingaszner[a], A. Szűcs[a], É. L. Dudás[a], T. Mándy[b]
Department of Chemical Technology, Technical University of Budapest, Hungary (a)
Hungarian Hydrocarbon Institute, Százhalombatta, Hungary (b)

ABSTRACT

A simple method is described by which a clear distinction can be made between fluid cracking catalysts, whether they contain oxidation promoters or not. It was shown that by incorporating 1 part per million of platinum into an unpromoted catalysts, its CO-oxidation activity could be improved drastically. Palladium proved about ten times less effective. The regenerability of the catalyst, characterized by the temperature belonging to the CO-conversion of 0.5 changes linearly with the one third power of the platinum concentration. High temperature steam treatment of the platinum metal impregnated catalysts levelled activity differences by decreasing the activity of platinum containing catalysts and increasing that of palladium containing ones.

INTRODUCTION

Synthetic zeolite containing catalysts are used practically exclusively in catalytic cracking units all over the world because of the higher gasoline yield, lower coke make etc. In order to make full use of these advantages a coke level far less than 0.1 % by weight on the recycled catalyst is imperative, since already small amounts of coke left on the catalyst would block the zeolite pores, preventing the molecules to be cracked to enter. The effect of the coke content on cracking yield was shown by Wachtel and coworkers (1).

Highly efficient coke removal can be attained by high temperature regeneration (2), by two-step regeneration (3) and/or by the use of coke oxidation improving agents incorporated into the fluid cracking catalyst (4), or used along with the catalyst in liquid or solid form (5). Using these means, a practically complete oxidation

of the coke to carbon dioxide (and water) with a near-stoichiometric amount of air is possible, that, by decreasing the catalyst-to-oil ratio, brings about higher gasoline yields, more efficient use of the thermal and kinetic energy of the regenerator flue gases in expander turbines, lower carbon monoxide emissions, etc.

Oxidation improvers belong to the class of platinum metals. In spite of the wide-spread use of these so called promoters, no literature is known presenting data on the specific effects of different platinum group metals, how their concentration influences the burning of the coke, how their catalytic effect is influenced by conditions occurring during the cracking/regeneration cycle, etc.

The effectiveness of oxidation improvers is tested either by determining the carbon monoxide/carbon dioxide ratio in the flue gas of a batch regeneration experiment of coked catalysts (2), or by measuring the carbon monoxide conversion of a carbon monoxide containing gas led over the catalyst under specified conditions (6, 7).

The aim of the present work was to investigate how platinum and palladium impregnated zeolitic cracking catalysts behave in carbon monoxide oxidation, what are the metal concentration effects, and how hydrothermal treatment affects their oxidation activity.

EXPERIMENTAL

The apparatus used consisted of an electrically heated upflow isothermal quartz reactor of 20 mm i.d. and 400 mm height with a sintered porous plate in the middle and two thermowells extending from both ends, pressure bottles for compressed air and carbon monoxide, and flow control valve and rotameters for controlling and measuring the flow of gaseous reactants. The temperature inside the reactor was controlled to $\pm$ 1 deg. C by means of temperature controllers.

The carbon monoxide content of the feed gas as well as that of the effluent from the reactor was measured by means of calibrated infrared gas analyzers, type Elkon S-205, operating at a wave-length of 4660 nm.

Measurements were carried out with air containing 2 % by volume of carbon monoxide, at a flow rate of 30 liters/hour, measured at room temperature and atmospheric pressure, using 6.2 ml catalyst samples placed on the porous plate.

Measurements with the same batch of catalyst were carried out at different temperatures. The carbon monoxide content of the effluent was corrected by subtracting the carbon monoxide converted in

the empty (i.e. catalyst not containing) reactor at the same temperature. The correction was negligible at temperatures below 400 deg. C.

Catalyst samples have been stabilized by pretreating the catalyst for 2 hours at 500 deg. C with the same 2 % (volume) CO-containing air used for the activity determination. Industrial fresh and equilibrium fluid cracking catalysts from two different manufacturers have been used, some of them containing promoters of unspecified nature and concentration. Data of the catalysts are summarized in Table 1.

Table 1

Data of the catalysts used

Catalysts	Unpromoted			Promoted		
	Al_F	Al_E	B_F	$A2_{FP}$	$A2_{EP}$	B_{EP}
Chemical composition						
Al_2O_3 %	23.2	21.5	46.8	28.0	26.5	-
Na_2O %	0.24	0.19	0.25	0.20	0.28	-
Fe %	0.01	0.12	0.76	0.08	0.25	-
Coke %	0	0.13	0	0	0.09	0.01
Physical properties						
Apparent Bulk Density (g/ml)	0.46	0.75	0.84	0.53	0.85	0.96
Pore Volume (ml/g)	0.68	0.41	0.27	0.50	0.25	0.23
Surface Area (m^2/g)	565	172	122	390	97	81

-: no data available

Early measurements with these catalysts presented problems as fines leaving the reactor plugged outlet lines. This difficulty was overcome by a previous air elutriation of the catalyst samples, by which about 21-23 % of the original batches have been removed as fines.

In order to test the promoting effect of platinum group metals fresh Al_F catalyst samples were impregnated with aqueous platinum or palladium salt solutions ($H_2(PtCl_6)$ and $PdCl_2$), dried at 120 deg. C for 3 hours and calcined at 600 and 750 deg. C for 3 and 6 hours in air, respectively.

To simulate hydrothermal effects occurring during fluid catalytic cracking, catalyst samples were treated in the laboratory at 750.deg. C for 6 hours with steam.

RESULTS AND DISCUSSION

Figure 1. shows the carbon monoxide conversion vs. temperature curves for commercial fluid cracking catalysts made by manufacturers A and B. The samples tested were the following:

- unpromoted fresh $A1_F$ and B_F,
- unpromoted equilibrium $A1_E$,
- promoted fresh $A2_{FP}$ and B_{FP}, further
- promoted equilibrium $A2_{EP}$ and B_{EP},

where subscripts F, E and P refer to fresh, equilibrium and promoted catalysts, respectively.

Figure 1. clearly shows that the oxidation of carbon monoxide starts and is completed at much lower temperatures with promoted catalysts as in the presence of unpromoted ones. Promoted fresh catalyst $A2_{FP}$ was of lower oxidation activity than its equilibrium counterpart $A2_{EP}$, indicating that one or more of the conditions prevailing during the cracking-regeneration cycle improves carbon monoxide conversion behaviour of certain fluid catalytic cracking catalysts.

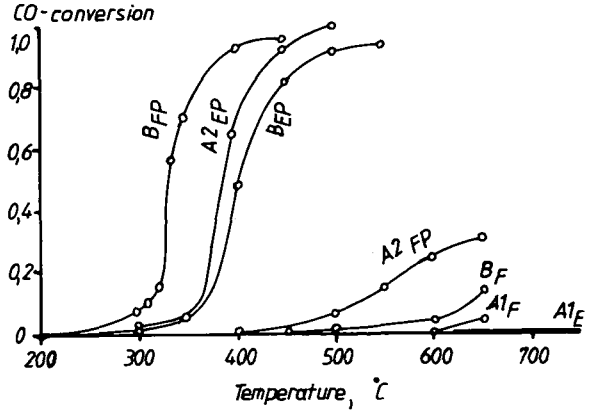

Fig. 1. Carbon monoxide conversion vs. temperature with different commercial cracking catalysts

The carbon monoxide conversion vs. temperature curves for most promoted cracking catalysts were steep, probably because the temperature within catalyst particles was much higher than the

measured bulk gas temperature, due to the heat of combustion of carbon monoxide and the low heat conductivity of the catalyst particles.

Fresh catalyst Al_F was impregnated to different platinum contents of 1 to 200 ppm, with solutions of hexachloroplatinic acid. Data of carbon monoxide conversion vs. temperature for these catalysts, along with those of unpromoted Al_F catalyst are plotted in Figure 2. This figure shows that already the extremely low concentration of 1 part per million of platinum drastically reduces the temperature needed for a given carbon monoxide conversion. Increasing the platinum concentration to 200 ppm further enhances the activity of the catalyst. Reaction temperatures measured at a CO-conversion of 0.5 plotted in function of the one third power of platinum concentration show a linear correlation.

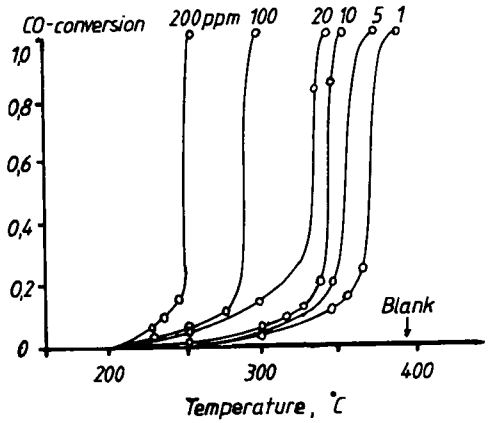

Fig. 2. Effect of platinum concentration

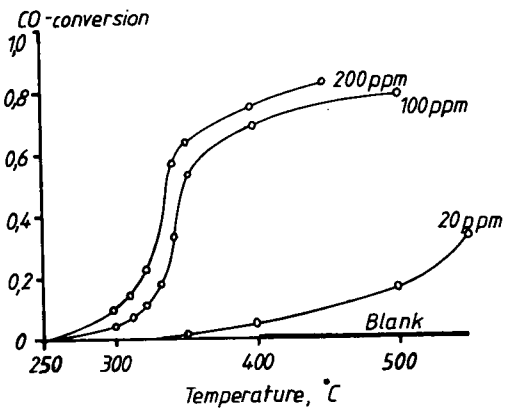

Fig. 3. Effect of palladium concentration

The same fluid cracking catalyst Al_F, when impregnated with solutions of palladium chloride according the procedure previously described, behaved - compared to the platinum impregnated catalysts, as shown in Figure 3. - far less efficiently: e.g. to attain a carbon monoxide conversion of 0.5 about ten times as much of palladium was needed, as of platinum. Additionally, in the higher conversion range, curves flattened out, reaching total carbon monoxide conversion only at very high temperatures.

Preliminary experiments were run to find out if the conditions prevailing within the cracking/regeneration cycle influence the carbon monoxide oxidation activity of cracking catalysts. It has been found that thermal treatment in dry air modified only

slightly the carbon monoxide oxidation activity of the samples tested high temperature hydrothermal treatment, however, brought about considerable changes.

Samples of catalyst Al_F impregnated with hexachloroplatinic acid solutions to 10 and 200 ppm platinum content, along with blank catalyst Al_F were subjected to hydrothermal treatment with steam at 750 deg. C for 6 hours, and subsequently tested for their carbon monoxide oxidation activity.

Results are shown in Figure 4. For comparative purposes, results obtained with the untreated catalysts are also shown. Whereas the oxidation activity of the blank Al_F catalyst increased slightly upon the hydrothermal treatment, catalyst samples containing platinum became less active than they were before hydrothermal treatment.

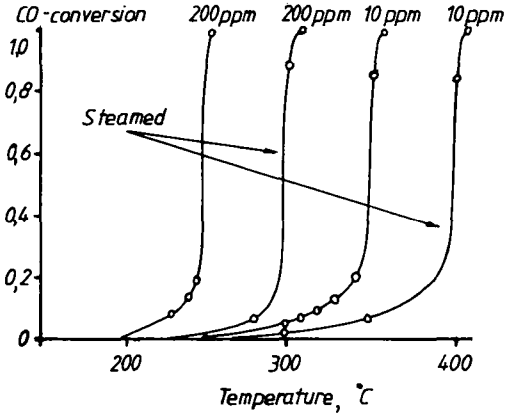

Fig. 4. Effect of hydrothermal treatment on platinum impregnated catalysts

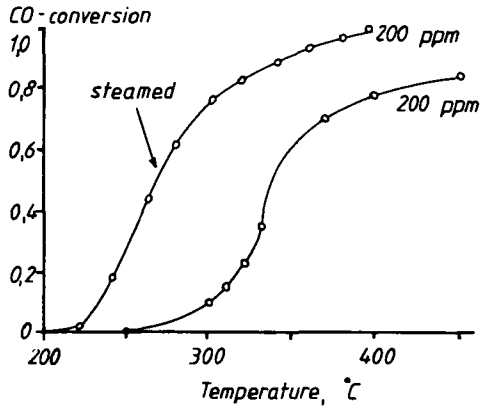

Fig. 5. Effect of hydrothermal treatment on palladium impregnated catalysts

Catalyst Al_F impregnated with palladium chloride solution to contain 200 ppm of palladium, was subjected to the same hydrothermal treatment. The carbon monoxide oxidation activity curve of the treated sample is shown in Figure 5, along with that of the untreated sample. Hydrothermal treatment increased the carbon monoxide oxidation activity of the palladium containing catalyst considerably: comparing this curve with the curve of hydrothermally treated catalyst containing 200 ppm of platinum on Figure 4, it can be seen that hydrothermal treatment brought the two catalysts to about the same oxidation activity level.

ACKNOWLEDGEMENT

The authors express their thanks to Mr. Z. Szerencsés and Mr. Zs. Fazekas for their technical help. This work has been carried out as part of a research project financed by the Hungarian Hydrocarbon Institute.

REFERENCES

1. Wachtel, S.J., Baillie, L.A., Foster, R.L., Jacobs, H.E.: Prepr. Div. Pet. Chem., Am. Chem. Soc., 16 (3), A-55 (1971)
2. Chester, A.W., Schwartz, A.B., Stover, W.A.: CHEMTECH, Jan. 1981. p.50.
3. Murphy, J.R., Soudek, M.: Oil Gas J. Jun. 17, p.70 (1977)
4. USP 4.064.039
5. Hartzell, F.D., Chester, A.W.: Hydrocarbon Processing 58 (7) 137 (1979)
6. Rheaume, L., Ritter, R.E., Blazek, J.J.: Oil Gas J. May 17, p.108 (1976)
7. AKZO Ketjen Technical Information FCC 79/53

ISOMERIZATION OF CYCLOPROPANE OVER Co(II)-EXCHANGED A-TYPE ZEOLITES

P. FEJES, I. Kiricsi, Gy. Tasi, K. Varga
Department of Applied Chemistry, József Attila University, Szeged, Hungary

ABSTRACT

Study of the skeletal isomerization of cyclopropane over Co(Na)A zeolites exchanged to different levels reveals that the reaction takes place irreversibly and follows first-order kinetics. The rate is proportional to the number of accessible Co^{2+} ions in the large cavities. This value is the same as the number of adsorbed propylene molecules at full coverage. In contrast to the situation with Brönsted acids as catalysts, the reaction intermediate is a π-adsorbed complex produced by the interaction of cyclopropane adsorbed "face-on" over Co^{2+} ions. As Co^{2+} ions are inactive in side-reactions such as oligomerization and cracking, the kinetics of isomerization can be studied under "clean" conditions.

INTRODUCTION

It is widely accepted that the skeletal isomerization of cyclopropane on solid acids is one of the most simple catalytic transformations. The reaction takes place irreversibly, following apparent first-order kinetics, and edge-protonated cyclopropane is regarded as the reaction intermediate [1-5]. The product propylene is not stable in contact with Brönsted acids, as it undergoes further reactions leading to different oligomeric and cracking products [6-8]. These undesired side-reactions can be avoided and the kinetic picture is accordingly simplified if alkaline earth or transition metal ion-exchanged zeolites, as Lewis acids, are used as catalysts [9]. With Co(Na)A zeolites, for example, it was possible to follow the kinetics by i.r. spectroscopy, measurements in a static reactor permitting estimation of the relevant rate coefficients of the surface reaction [10]. The i.r. spectroscopic studies revealed that the active centres are Co^{2+} ions interacting with cyclopropane adsorbed in a "face-on" mode [11]. The reactor experiments resulted in a strict correlation between the true kinetic parameters and the number of accessible Co^{2+} ions in the

zeolitic framework.

This paper is intended to shed light on some details of the kinetics of cyclopropane isomerization over Co(Na)A zeolites exchanged to various extents.

EXPERIMENTAL

The Co(Na)A specimens were obtained from binderless Linde 4A zeolite by exchange with $Co(NO_3)_2$ solution. Their compositions are given in Table 1.

Table 1
Unit cell compositions of catalysts used

No	Composition
1	Na_{12} - A (A = $Al_{12}Si_{12}O_{48}$)
2	$Co_{0.24}Na_{11.52}$ - A
3	$Co_{0.85}Na_{10.2}$ - A
4	$Co_{1.38}Na_{9.24}$ - A
5	$Co_{3.6}Na_{4.8}$ - A
6	$Co_{3.7}Na_{4.6}$ - A
7	$Co_{4.02}Na_{3.96}$ - A
8	$Co_{4.55}Na_{1.9}$ - A

The zeolite samples were characterized by XRD, IR spectroscopy and TG.

For adsorption and kinetic studies, the catalyst samples were heat-treated at 673 K, in vacuo, for 4 h. (The final pressure attained was better than 10^{-2} Pa.) A description of the kinetic equipment used and the product GC analysis is to be found in [12].

RESULTS

Adsorption experiments with cyclopropane run into difficulties because the kinetic diameter of the cyclopropane molecule (around 0.52 nm) is larger than the pore openings in NaA. On the other hand, cyclopropane undergoes a quite fast transformation over Co(Na)A, even at ambient temperature. These obstacles are not encountered with propylene as adsorptive.

Figure 1 shows the adsorption isotherms of propylene on NaA zeolite. The isotherms cannot be described correctly by either the Langmuir or the Freundlich isotherm equation: at low temperatures they are rather of the Langmuir type, while at higher temperatures

the Freundlich isotherm equation seems to be valid, with a continuous transition between the two types at intermediate temperatures. Similar results have been obtained with samples with low Co^{2+} contents.

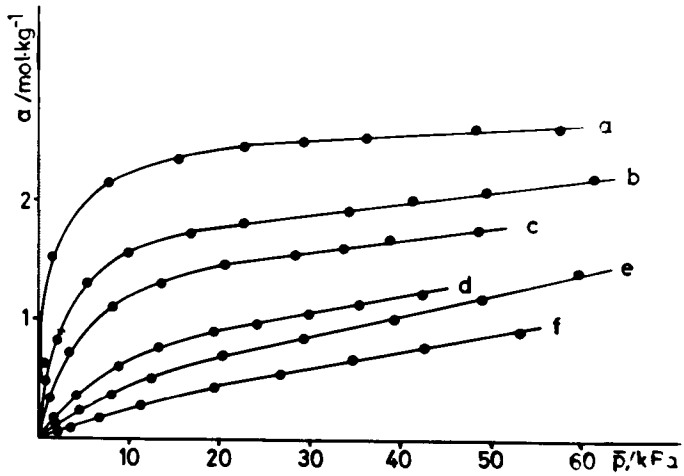

Fig. 1. Adsorption isotherms of propylene on NaA zeolite. (Temperatures: a 332 K; b 377 K; c 398 K; d 438 K; e 453 K; f 473 K.)

Figure 2 depicts the isosteric heats of adsorption at different coverages, as obtained from the isotherms for NaA and a low-level exchanged specimen (No. 2). It is clearly seen that, after some decrease, near $a_s = 0$, the curves level off at the same value (Q_{st} = = 47 kJ mol^{-1}) for the two adsorbents. The quite high value of Q_{st} implies weak chemisorption, as found by Schirmer in the case of Ca(Na)A [13].

With ethylene as adsorptive the character of the curves for a specimen containing 1 Co^{2+} ion/u.c. is similar; nevertheless, the levelling-off occurs at a lower isosteric heat of adsorption (Q_{st} = = 42 kJ mol^{-1} [14]).

At high Co^{2+} ion-exchange levels (see specimens No. 6 and No. 7), the isosteric heat curves are similar to each other (see Fig. 3), but differ markedly from those seen in Fig. 2. At higher coverages a constant value of Q_{st} = 75 kJ mol^{-1} is reached here too.

The adsorption heat curves in Fig. 2 and 3 clearly demonstrate that no simple adsorption model can be valid for the adsorption of propylene on Co^{2+}-exchanged NaA zeolites.

The kinetic curves of cyclopropane isomerization, as measured

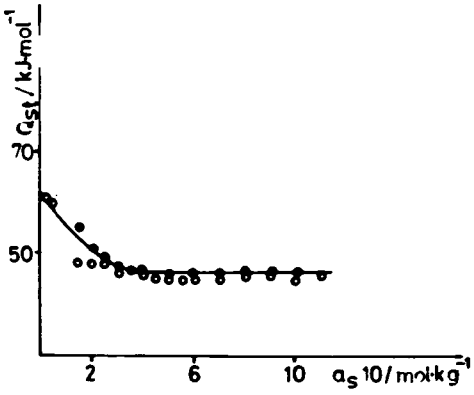

Fig. 2. Isosteric heat of adsorption at different coverages for NaA (o) and sample No. 2 (●).

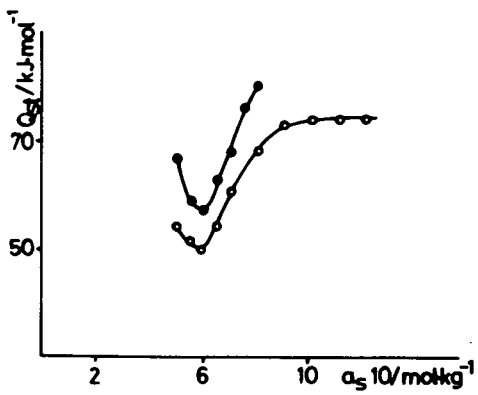

Fig. 3. Isosteric heat of adsorption at different coverages for samples No. 6 (o) and No. 7 (●).

in a recirculatory flow reactor using catalyst samples with varying Co^{2+} contents, are shown in Fig. 4. NaA turns out to be a practically

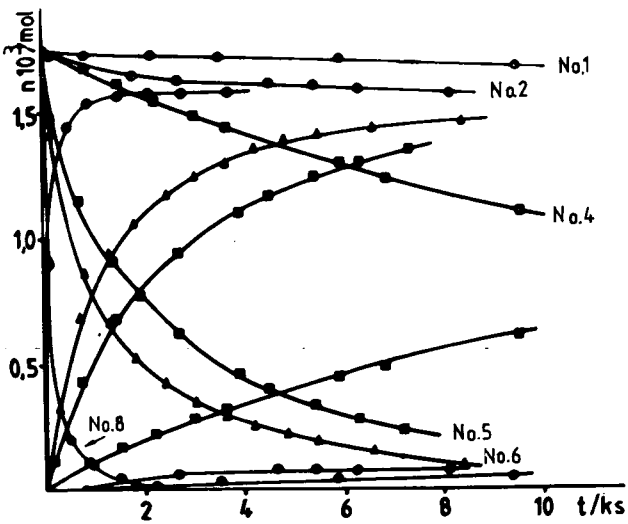

Fig. 4. Kinetic curves of cyclopropane isomerization. (Reaction temperature 473 K; mass of catalyst $2 \cdot 10^{-4}$ kg; reactor volume 0.14 dm^3.)

inactive catalyst, mainly due to sieving effects. The curves reflect a similar change between specific activity and Co^{2+} content. The activation energies computed from the kinetic curves are listed in

Table 2.

Table 2

Activation energies for cyclopropane isomerization

Zeolite samples	No. 4	No. 5	No. 6
Activation energies kJ mol^{-1}	47.2	64.3	65.7

DISCUSSION

The adsorption properties of NaA for different hydrocarbons have been investigated by several authors [15-17]. From the results it could be concluded that through exchange of the bulky Na^+ ions for ions of increasingly smaller size (e.g. Ca^{2+}, Mg^{2+}, Co^{2+}, etc.) the pore openings could be widened (the eight-ring windows are blocked by ions of smaller diameter), permitting the penetration of bulkier hydrocarbon molecules.

Though the amount of propylene adsorbed increases with the degree of Co^{2+} ion-exchange, no direct proportionality can be observed (see Fig. 5). Breck came to a similar conclusion concerning ethylene adsorption on KNaA zeolites [16].

The first-order rate constants for the isomerization reaction can be seen in Fig. 5 too. The similarity of these two sets of data proves that in the chemisorption and in the catalytic reaction the same centres are involved, their number and distribution (accessibility) being identical.

The kinetic curves in Fig. 4 for both cyclopropane consumption and propylene production are apparently first order in the case of high-level exchange. No induction period whatsoever is discernible in the curves, in contrast to NaY and NaCaY zeolites [12], and no oligomeric species or cracking products could be identified by GC. The activation energy for these samples (E_a^+ = 65 kJ mol^{-1}) agrees well with that found previously [18].

At low exchange levels the character of the kinetic curves differs markedly from that found before. The activation energy (for sample No. 4) drops from 65 kJ mol^{-1} to E_a^+ = 47 kJ mol^{-1}, this value being equal to the isosteric heat of adsorption for propylene at high coverages on the same samples.

Propylene preadsorbed on the activated catalyst does <u>not</u> influence the rate of cyclopropane skeletal isomerization. Allene, admit-

ted to the catalyst before commencement of the experiment, causes retardation. This is probable due strong chemisorption, or else is caused by its isomerization product, methylacetylene, rendering the active sites inaccessible for cyclopropane and/or propylene.

These findings are opposite to those found earlier on NaCaY zeolites exhibiting weak Brönsted acidity, where small amounts of presorbed propylene or allene reduced the length of the induction period by creating $C_3H_5^+$ carbocations as ionic chain carriers. This behaviour is characteristic for promoters.

Indirectly, this result suggests that the Co(Na)A samples are free of any Brönsted acidity. Förster and co-workers came to a similar conclusion from their investigation of the i.r. spectra of CoNaA zeolites in the OH region [19].

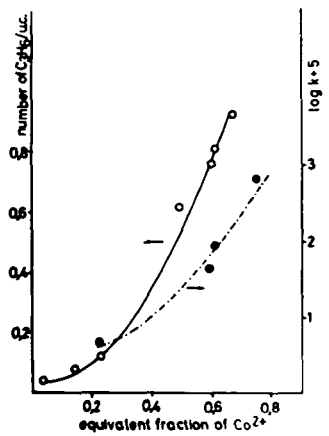

Fig. 5. Comparison of the adsorption and kinetic data

On the basis of what has been stated about the correlation found between specific activity (expressed as the first-order rate constant of the surface reaction) and Co^{2+} content (see Fig. 5), it seems very probable that, starting from NaA, with adsorption practically nil for cyclopropane, the sieving effect diminishes progressively with increasing levels of exchange, permitting access to active sites in the zeolite cavities. This point is stressed, for there are a few cases in the literature where a similar trend was observed with Brönsted acid sites as active centres, which necessitates another explanation [20].

REFERENCES

1. Habgood, H.W., George, Z.M., Molecular Sieves, Soc. Chem. Ind. London, 1968. p. 130.
2. Bassett, D.W., Habgood, H.W., J. Phys. Chem. 64, 769 (1960).
3. George, Z.M., Habgood, H.W., J. Phys. Chem. 72, 1689 (1968), 74, 1502 (1970).
4. Hightower, J.W., Hall, W.K., J. Am. Chem. Soc. 90, 851 (1968), J. Phys. Chem. 72, 4555 (1968).
5. Hall, W.K., Larson, J.G., Gerberich, H.R., J. Am. Chem. Soc. 85, 3711 (1963), 87, 1880 (1965).
6. Kiricsi, I., Hannus, I., Varga, K., Fejes, P., J. Catal. 63, 501 (1980).
7. Tam, N.T., Cooney, R.P., Curthoys, G., J. Catal. 44, 81 (1976).
8. Őrhalmi, O., Fejes, P., Symp. on Mech. of Hydrocarbon Reactions, 1973 Siófok, Hungary, Akadémiai Kiadó, 1973., p. 475.
9. Förster, H., Seebode, J., Zeolites 3, 63 (1983).
10. Fejes, P., Förster, H., Kiricsi, I., Seebode, J., Varga K., Zeolites, to be published
11. Seebode, J., Diplomarbeit Universität Hamburg, 1981.
12. Fejes, P., Hannus, I., Kiricsi, I., Varga, K., Acta Phys. Chem. Szeged 24, 119 (1978).
13. Schirmer, W., Meinert, G., Grossmann, A., Monatsberichte 11, 886 (1969).
14. Klier, K., Kellerman, R., Hutta, P.J., J. Chem. Phys. 61, 4224 (1974).
15. Masahiro Nitta, Shigemi Matsumoto, Kazuo Aomura, J. Chem. Soc. Chem. Comm. 1974, p. 552.
16. Breck, D.W., Eversole, W.G., Milton, R.M., Reed, T.B., Thomas, T.L., J. Am. Chem. Soc. 78, 5963 (1956)
17. Schöllner, R., Ulber, G., Platzdasch, K., Chem. Techn. 34, 583 648 (1982)
18. Fejes, P., Förster, H., Kiricsi, I., Seebode J., Zeolites 4, 259 (1984)
19. Förster, H., Seelemann, R., J. Chem. Soc. Faraday I., 77, 1359 (1981)
20. Jacobs, P.A., "Carboniogenic Activity of Zeolites". Elsevier, Amsterdam, 1977, p. 128.

SPECTROSCOPIC AND KINETIC STUDIES ON THE CYCLOPROPANE ISOMERIZATION OVER MORDENITES OF DIFFERENT ACIDITY

H.FÖRSTER, J.SEEBODE
Institute of Physical Chemistry, University of Hamburg, Laufgraben 24, D-2000 Hamburg 13, Federal Republic of Germany

ABSTRACT

Isomerization of cyclopropane over mordenites of different acidity has been studied by UV-VIS-IR spectroscopy and reactor kinetic measurements.

Apart from the beginning and at high degrees of conversion the kinetics follows the law of a first order irreversible reaction. With increasing proton content of the zeolite the rate of isomerization is enhanced and the activation energy is decreased. The formation of allylic and polyenylic carbocations in Bronsted acidic mordenites responsible for the production of oligomers can be proved by UV-VIS as well as by IR spectroscopy. By-products of this kind are missing on the Na-form, although there is evidence for a low residual surface acidity, the confirmation of which seems to be more likely by kinetic experiments or conversion of selected probe molecules than by vibrational spectroscopy.

INTRODUCTION

In spite of the spectacular transformation of coal or organic waste to hydrocarbons over silica-rich zeolites, there is still much industrial interest and effort in isomerization, which runs parallel to cat-cracking and upgrades the benzine fraction. As this type of reaction is known to be catalyzed by strong acids in homogeneous media, the intermediacy of carbonium ions also with zeolites should be established and their role in parallel or consecutive reaction steps should be explored.

Due to its higher module, mordenite is of greater stability compared to faujasites and seems to be well-suited in the H-exchanged form for fundamental investigations. As the test reaction isomerization of cyclopropane was chosen, details of which are well-established in the literature /1/, stating the rate determining step

being the formation of the non-classical protonated cyclopropane intermediate. The objective of this paper was to examine the dependence of the kinetic parameters for the isomerization of cyclopropane upon the proton content of the zeolite and the influence of other compounds enhancing the allylic ion generation.

EXPERIMENTAL

Materials. The base material was synthetic mordenite Zeolon 100-Na (Norton) designated as Zeolon. A part of this sample was stirred for 16 hours at 350 K in an excess of 1 molar NaCl solution in order to achieve the homo-ionoc Na-form, named NaM. Starting from Zeolon, mordenites of different ammonium content were prepared by stirring with stoichiometric amounts of 0.1 molar solutions of ammonium chloride at 350 K for 16 hours. The compositions were determined by atomic absorption spectrophotometry (AAS) and neutron activation analysis. Samples will be designated as Na_xH_yM, where M denotes $Al_8Si_{40}O_{96}$.

Cyclopropane (Merck, stated purity 99.998%), allene (Matheson, 97%), ammonia (Matheson, 99.998%) and propene (Messer-Griesheim, 99.98%) were used without further purification.

Apparatus. A stainless steel recirculatory flow reactor was used for the kinetic experiments, a more detailed description of which will be given elsewhere /2/. For product analysis the system was connected via a motor-driven sampling valve to a gas chromatograph (VARIAN AEROGRAPH 1520). The FID (flame ionization detector) signal is controlled by an 8-bit microcomputer (COMMODORE CBM 8032) and was stored for further processing on a disk. The FID response was calibrated by known amounts of cyclopropane and propene, respectively. Baseline correction, determination of the rate constants by linear regression and calculation of the apparent activation energies were performed by the aid of computer programs.

The spectra were recorded on a CARY 17, DIGILAB FTS 14 or DIGILAB FTS 20 spectrometer, respectively. Details of the instruments and procedures employed have been described previously /3,4/.

Pretreatment. For reactor measurements 0.5 g of the 0.3-0.5 mm sieve fraction of pelletized zeolites were used and activated in a helium stream of 0.58 ccm/s at 750 K for 13 hours.

For the spectroscopic studies, thin self-supporting wafers were applied and outgassed at 750 K under high vacuum conditions (see also /3,4/).

RESULTS AND DISCUSSION

UV-VIS spectroscopic studies. Isomerization of cyclopropane over Y-type zeolites has been studied by Fejes et al. by means of reactor kinetic measurements /5/. Their kinetic curves showed a pronounced induction period indicating the formation of a reactive intermediate on the catalyst prior to isomerization. Upon pre-adsorption of traces of propene or allene this induction period decreased or disappeared, respectively. Allylic cations were assumed to be these intermediates.

By co-operation, we have studied the formation of carbocations in mordenites of different Bronsted acidity using UV-VIS-NIR spectroscopy. The results are summarized as follows /4/: Upon adsorption of allene, propene, cyclopropane, isopropanol, and acetone, respectively, similar electronic bands in the region 200-600 nm were observed. Their development with time or upon heating up to 370 K decreased in the sequence given above (allene being exceptionally reactive) as well as with decreasing proton content of the zeolites. The bands were divided into four groups and assigned to the π-π^* transitions of mono-, di-, tri-, and tetraenylic carbenium ions. Mechanistically, their formation can be explained by the following steps (see /4/): (i) protonation (and dehydration) of the adsorbates leads to the propyl or allyl ion, respectively; (ii) hydride ion abstraction (by a propyl ion, e.g.) from propene produces the allyl ion; (iii) dienylic carbenium ions are formed by reaction of the allyl ion with allene directly, whereas the reaction of the allyl ion with a mono- or diene to a di- or trienylic carbocation requires consecutive deprotonation and hydride ion abstraction.

In adddition to the published results, we recently investigated the adsorption of allene and cyclopropane on the base material, Zeolon, expecting no formation of carbenium ions, due to the lack of Bronsted acidity. In case of cyclopropane this expectation was proved; no bands were detected even after heating up to 500 K. Surprisingly, upon admission of allene at room temperature very weak absorptions arose immediately, increasing in intensity upon short heating to 400 K. Analysis of this sample by AAS indicated a slight deficiency of Na. Therefore, we assume that this gap is balanced by OH groups, even though they were not detectable by IR spectroscopy. This conclusion agrees with the results and the proposed mechanism of carbocation formation and is supported by further IR spectroscopic and kinetic studies discussed later.

In conclusion, the formation of allylic carbenium ions - even upon adsorption of cyclopropane - in Bronsted acidic mordenites was proved by UV-VIS spectroscopy. But nevertheless, an important question is still open: Is the allylic ion involved in the cyclopropane isomerization or does it produce oligomers via the observed polyenylic carbocations only ?

IR spectroscopic studies. Unfortunately, using the transmission technique, strong lattice vibrational modes of the zeolites obscure bands of adsorbed species in the range below 1300 cm^{-1}. Furthermore, the sharp increase of light scattering at higher wavenumbers leads to spectra of poorer quality in the region above 3000 cm^{-1}. Therefore, and for shortening the discussion, the spectra presented here will be restricted to the region 2300-1300 cm^{-1}. Nevertheless, our conclusions are confirmed by the bands in the range up to 4000 cm^{-1} as well !

The positions and intensities of the bands of propene adsorbed in NaM at room temperature are very similar to those observed on A-type zeolites /3/. The absorptions at 1455 (CH_3 asym. def.) and 1635 cm^{-1} (C=C stretch) are the most intense (very strong) followed by those at 1435, 1382 (strong) and 1417 cm^{-1} (medium) (CH def. modes). As the C=C stretching mode shows a cation-sensitive downscale shift on A-type zeolites /3/ and its position on NaM is identical to that on NaA, sorption of the propene molecules in front of sodium ions is concluded. The spectrum does neither change with time nor does it indicate the formation of any other species.

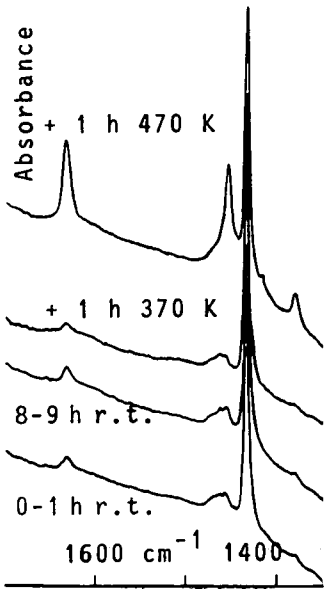

Fig. 1. IR spectra of cyclopropane adsorbed in Zeolon. (r.t. = room temp.)

The spectra of cyclopropane adsorbed in Zeolon at room temperature (Figure 1) prove the slow isomerization on this zeolite, confirmed by the increase of the bands of propene with time and upon short heating of the loaded sample. In the spectral region shown, cyclopropane exhibits only two bands, one of them accidentally at the same position as propene (1435 cm^{-1}) and the other one (1462 cm^{-1}), being a doubly degenerate and only raman active mode of the free molecule, becomes IR active due to symmetry lowering upon

adsorption. As this mode does not split into two bands (parallel to the corresponding absorptions in the CH stretch region) a "face on" interaction of the cyclopropane molecules with sodium ions has to be assumed (compare /3/).

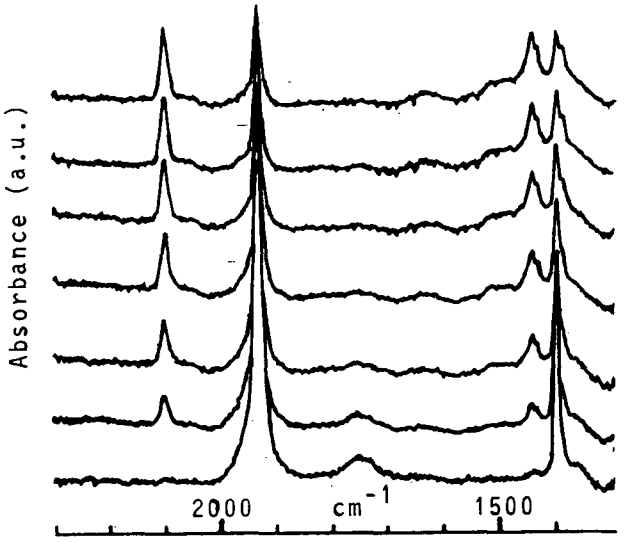

Fig. 2. Dynamic IR spectra of allene adsorbed in Zeolon at room temperature. Sequence from bottom to top (0-10 h after admission).

As allene turned out to be the most reactive substrate concerning the formation of carbenium ions, its adsorption in Zeolon at room temperature was investigated by IR spectroscopy as well (Figure 2). Most of the bands observed in the region 1300-4000 cm^{-1} are unambigously assigned to allene and its isomer, propine. Concerning Figure 2 this is mainly confirmed by the decreasing intensities of the absorptions at 1935, 1750, and 1400 cm^{-1} (C=C stretch, combination of bending modes, and CH def. of allene) and by the increase of the bands at 2102, 1442, and 1388 cm^{-1} (C≡C stretch and CH def. of propine). But in addition a broad absorption at 1510 cm^{-1} arises with time. In agreement with our UV-VIS results and published IR data we assign this band to the CCC stretch of allyl type cations. Deno /6/ and Evans /7/ reported this absorption of monoenylic ions to appear around 1530 cm^{-1}, shifting downscale upon further alkylation and / or conjugation. Furthermore it is generally observed that most of the CH and especially C=C bands of hydrocarbons are shifted to lower wavenumbers upon adsorption in zeolites. So, we conclude that allene isomerizes to propine via the allylic

cation, even though Bronsted acidic hydroxyl groups are not detectable on this sample by IR spectroscopy. But kinetic studies (see below) and recent IR studies on the acidity of our zeolites by adsorption of ammonia /8/ revealed that even the Zeolon exhibits a low residual Bronsted acidity.

The spectra of propene adsorbed in HM ($Na_{0.2}H_{7.8}M$) indicate fast oligomerization. Only during the first 10 minutes after admission propene bands at 1455, 1435 (shoulders, CH def.), and 1613 cm^{-1} (C=C stretch of propene interacting with OH groups) are visible. The assignment of the latter is confirmed by the large shift of the OH stretching band from 3610 to 3480 cm^{-1}. The most intense bands are those of oligomers at 1465, 1385, and 1370 cm^{-1}, which do not vanish upon heat treatment under vacuum. Immediately after adsorption of propene, the CCC stretching mode of allylic cations at 1535 cm^{-1} is present and that of dienylic carbenium ions arises at 1505 cm^{-1} with time. So, the spectra prove the fast oligomerization of propene in HM via allylic and dienylic carbenium ions in agreement with the UV-VIS results.

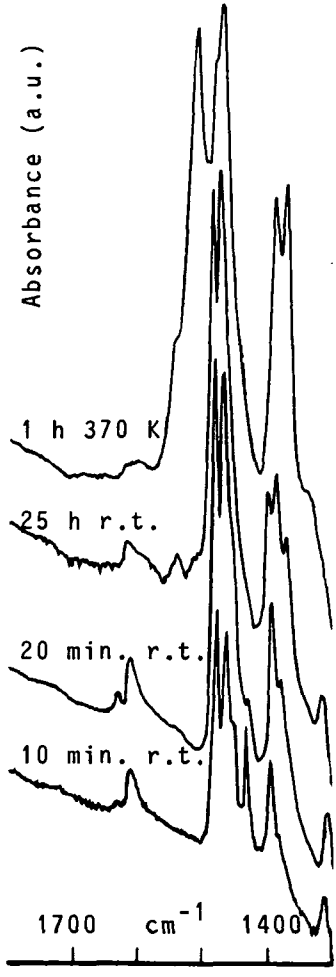

Fig. 3. IR spectra of cyclopropane adsorbed in HM.

Upon adsorption of cyclopropane in HM at room temperature (Figure 3) bands of propene at 1635, 1613, 1455, and 1435 cm^{-1} are detectable only during the first few minutes after admission. In course of time new absorptions at 1535, 1505 cm^{-1} (CCC stretches of mono- and dienylic carbenium ions), and of oligomers in the region below 1450 cm^{-1} arise. After heating the loaded sample to 370 K for one hour even the intense C=C stretching bands of propene totally disappeared and those of the carbocations and the oligomers became the most intense ones. Thus, a fast isomerization of cyclopropane to propene in HM and consecutive (or parallel) oligomerization of propene via allylic and dienylic carbocations is concluded.

Concerning the adsorption of cyclopropane or propene in mordenites of lower proton content, the generation of the bands discussed above is comparable, but the rate of formation of oligomers diminishes with decreasing Bronsted acidity. On samples of small proton content (e.g Na_7H_1M) carbocations are not detectable by IR spectroscopy. Here the bands of the adsorbed species are more clearly assigned to cyclopropane or propene as they are very similar to those observed on NaM.

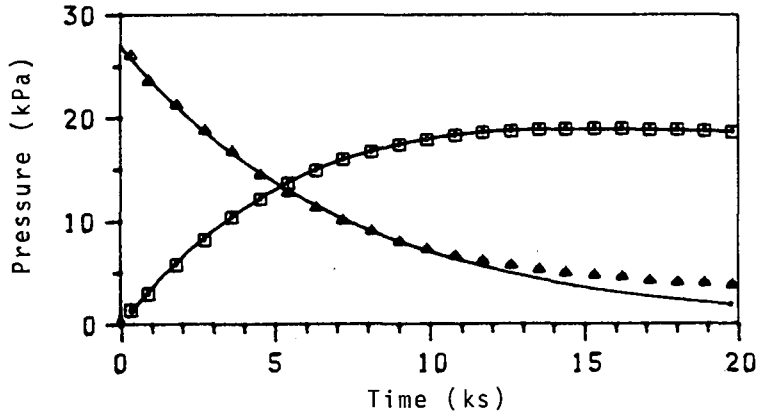

Fig. 4. Kinetic curves (partial pressure vs. time) of the cyclopropane isomerization over Zeolon. (Triangles / squares = experimental cyclopropane / propene data; mass of catalyst 0.5 g)

Kinetic Studies. In Figure 4 a typical set of kinetic curves of the cyclopropane isomerization over Zeolon (reaction temperature: 473 K) is presented. (The cyclopropane curve is calculated by converting ln p(cp) vs. time, obtained by linear regression, to the exponential function, whereas the propene data were fitted by a polynom). In contrast to studies of Fejes et al. on Y-type zeolites /5/ our curves do not indicate any induction period. Deviations from the law of a first order irreversible reaction are detectable at high degrees of conversion only (compare Figure 4: 9 ks = 70% conversion), due to blocking of the active sites by adsorbed propene. At lower reaction temperatures, further small deviations (experimental cyclopropane data higher than the calculated ones) at the very beginning of the reaction (up to 15 minutes) are due to the process of approaching the sorption equilibrium. These features were obtained on A-type zeolites as well /9/.

For convenience all samples were activated overnight (13 hours, exactly) at 750 K. But as the UV-VIS spectra proved the formation of carbenium ions upon adsorption of allene on the starting material, Zeolon, which can be interpreted by Bronsted acidic groups only, the influence of different activation times was investigated. The rate constants of the isomerization measured at 473 K reaction temperature decreased linearly with increasing the activation time from 3 to 18 hours, and a further small decrease was observed upon extending this time to 40 hours. Thus we conclude, that the low residual Bronsted acidity of this sample was reduced by dehydroxylation, even though acidic OH groups were not detectable by IR spectroscopy.

Some kinetic data of the cyclopropane isomerization over mordenites of different Bronsted acidity are summarized in table 1.

Table 1

Rate constants (k) and apparent activation energies (Ea)

Sample	k (443 K) (s-1)	Ea (kJ/mol)	temp. range (K)	number of data
Na_4H_4M	$1.04\ 10^{-3}$	72 +- 4	383 - 443	4
Na_6H_2M	$5.00\ 10^{-4}$	74 +- 10	286 - 443	3
Zeolon	$2.28\ 10^{-5}$	102 +- 2	443 - 473	4
NaM	$1.90\ 10^{-6}$	111 +- 3	443 - 523	5

k values are given for using 0.5 g of zeolite.
Temp. range and number of data refer to calculation of Ea

Table 1 shows that the rate constants are enhanced with increasing Broensted acidity of the samples whereas the apparent activation energies decrease. Whether the rate constants are proportional to the proton content cannot be decided clearly, due to the limitations of the analysis of the samples exhibiting very low acidity, i.e. Zeolon and NaM. Nevertheless, we conclude that the rate determining step of the cyclopropane isomerization over acidic mordenites is the protonation of the adsorbate, leading to a non-classical carbonium ion intermediate.

As UV-VIS and IR spectroscopy prove the formation of oligomers inside the framework of the zeolites, their formation was studied by gas chromatography as well. At a reaction temperature of 403 K in case of NaM there are no by-products detectable even after complete conversion of cyclopropane to propene, whereas in case of Na_6H_2M weak peaks of by-products were detected in the gas phase even at the very beginning of the isomerization, i.e. about 20% conversion. Nevertheless they amount only to less than 0.1% of propene and cyclopropane, respectively. Only after full conversion their amount is remarkably enhanced. So, they do not affect the accuracy of the kinetic measurements.

SUMMARY AND CONCLUSIONS

Isomerization of cyclopropane to propene over mordenites is proved by IR spectroscopy and reactor kinetic measurements. On samples of negligible Bronsted acidity no by-products are detectable by IR spectroscopic and gas chromatographic measurements. The kinetics follows the law of a first order irreversible reaction without any indication of an induction period. On acidic mordenites the rate constants are enhanced and apparent activation energies decrease with increasing proton content of the samples, indicating the rate determining step to be the protonation of cyclopropane to a non-classical carbonium ion. The formation of oligomeric by-products via allylic and polyenylic carbenium ions on acidic mordenites is proved by UV-VIS and IR spectroscopy. Both IR spectroscopy as well as gas chromatographic studies show their generation during isomerization, the rate of their formation being very small compared to the rate of isomerization. Thus, the formation of the by-products is concluded to be a negligible side reaction. The question, whether the proven allylic cation is involved in cyclopropane isomerization is still open, as its formation can be rationalized via small amounts of propene, formed at the very beginning of the isomerization, as well.

ACKNOWLEDGEMENT

The financial support of this work by the Deutsche Forschungsgemeinschaft, the Fonds der Chemischen Industrie, and the Hungarian Academy of Sciences is gratefully acknowledged.

REFERENCES

1. Jacobs, P.A.: Carboniogenic Activity of Zeolites. Elsevier Sci. Publ. Co., Amsterdam, 1977, p. 97
2. Förster, H., Seebode, J., to be published
3. Förster, H., Seebode, J., Zeolites 3, 1983, 63
4. Fejes, P., Förster, H., Kiricsi, I., Seebode, J. in: Structure and Reactivity of Modified Zeolites, Jacobs, P.A. et al. (Eds.), Elsevier Sci. Publ. B.V., Amsterdam, 1984, p. 91
5. Fejes, P., Hannus, I., Kiricsi, I., Varga, K., Acta Phys. Chem. Szeged 24, 1970, 119
6. Deno, N.C. in: Carbonium Ions; Olah, G.A., Schleyer, R.P. (Eds.) Wiley-Interscience, New York, 1970, Vol. II, p. 783
7. Evans, J.C. in: Carbonium Ions; Olah, G.A., Schleyer, R.P., (Eds.), Wiley-Interscience, New York, 1968, Vol. I, p. 223
8. Förster, H., Jacubasch, H., to be published
9. Fejes, P., Kiricsi, I., Förster, H., Seebode, J., Zeolites 4, 1984, 259

OISONING OF FLUID CRACKING ZEOLITE CATALYSTS BY METALS

. L. Occelli[a], D. Psaras[b], S. L. Suib[b]
ulf Research and Development Co., Pittsburgh, PA 15230 (a)
epartment of Chemistry, University of Connecticut, Storrs, CT 06268 (b)

BSTRACT

One of the most important problems facing users of zeolite fluid cracking atalysts is the poisoning of the catalyst by metal deposits such as vanadium and ickel. We have been investigating these poisoned zeolite catalysts with several pectroscopic tools such as luminescence excitation, emission and lifetime spectro-copies. Each of the two main components of these catalysts (the binder and the anthanum faujasitic component) has been independently poisoned by both iron and opper. The decrease in the cracking activity parallels the quenching of the lumi-escence of lanthanum by both metal poisons. From the luminescence data we are able o tell at low loadings (2% by weight) that both copper and iron sinter on streaming. uch metal deposits increase the cracking activity and lead to large coke deposits. atalytic cracking experiments have been carried out in a flow reactor. Correlations etween the spectroscopic data and the cracking data will be discussed.

INTRODUCTION

For a long time it has been known that metals such as Fe, Cu, Ni and V have etrimental effects on the cracking activity of fluid cracking catalysts (FCC). Iron, copper and nickel metal deposits [1,2] cause increasing amounts of coke to orm. On the other hand vanadium is known to destroy the catalytic cracking activity [3,4] of the FCC. It is not well known what the exact surface interactions are in hese systems.

It is believed that these metals (Ni, V, Cu, Fe) which are found in the oil feedstacks are not the only factors which cause deactivation of the cracking catalysts. Partial or total blockage of the pore system of the zeolite component of the FCC can ause the destruction of catalytic cracking activity.

Fluid cracking catalysts are composed of 2 parts. One part is the zeolite cracking component. This is usually a hydrogen or rare earth form of a large pore faujasitic zeolite. The second part of the FCC is the binder or scavenger. The binder is typically a clay such as a dealuminated kaolin. One role that the

scavenger can play is to selectively bind to metal deposits [5] thereby reducing th detrimental effects of these metal deposits.

Another route to control the deactivation of FCC materials is to add a passivating agent such as Sb, Sn, Bi or various combinations of these. [6] For the most part this route has been ignored and not studied in great detail.

The purpose of this paper is to show that both iron and copper deposits on real fluid cracking catalysts can be detected by luminescence emission, excitation and lifetime measurements. Microactivity tests of the cracking activity of the FCC materials were also carried out and correlations between the catalytic and photochemical properties of these catalysts have been made.

EXPERIMENTAL

Sample Preparation. Copper and iron naphthenates were dissolved in benzene and incipient wetness methods were used to impregnate a commercially available fluid cracking catalyst. The naphthanates were obtained from Pfaltz and Bauer and were used without further purification. The catalysts were calcined in air at 540°C for 10 hours and then aged in steam for 10 hours at 730°C in a fluidized bed.

Cracking Activity. The cracking activity of these materials was studied with a flow system which has previously been reported [7]. A Cincinnati feedstock oil with a 260-426°C boiling range was used. About 2.5 grams of 100x325 mesh microspher catalyst particles were used. The catalysts were tested for an 80-second contact time, at 515°C and at 15 WHSV.

Luminescence Methods. All samples were loaded into 2mm path length quartz cells obtained from Precision Cells, Inc., Hicksville, New York. Spectra were recorded using a double Czerny-Turner monochromator Spex Model 1902 fluorometer. Front face detection was used for all samples. Finally, a rhodamine B solution was used as a quantum counter in order to correct for variations in intensity of the excitation source at different wavelengths.

Lifetime experiments were done with a PRA Model 3000 system. A PRA model LN100 nitrogen laser was used as an excitation source. A monochromator was positioned between the sample and the emission photomultiplier tube. The lifetime data were collected by using multichannel scaling methods with a multichannel analyzed an then transferred to a DEC, PDP-1103 computer for data manipulation. All lifetime data were fit to at least 2 exponential decays and usually to 3 decays.

RESULTS

Since these fluid cracking catalysts contain lanthanum Y zeolite as an active component it is essential to know what the photochemical behavior of LaY zeolite is. A luminescence emission spectrum for LaY is given in Figure 1.

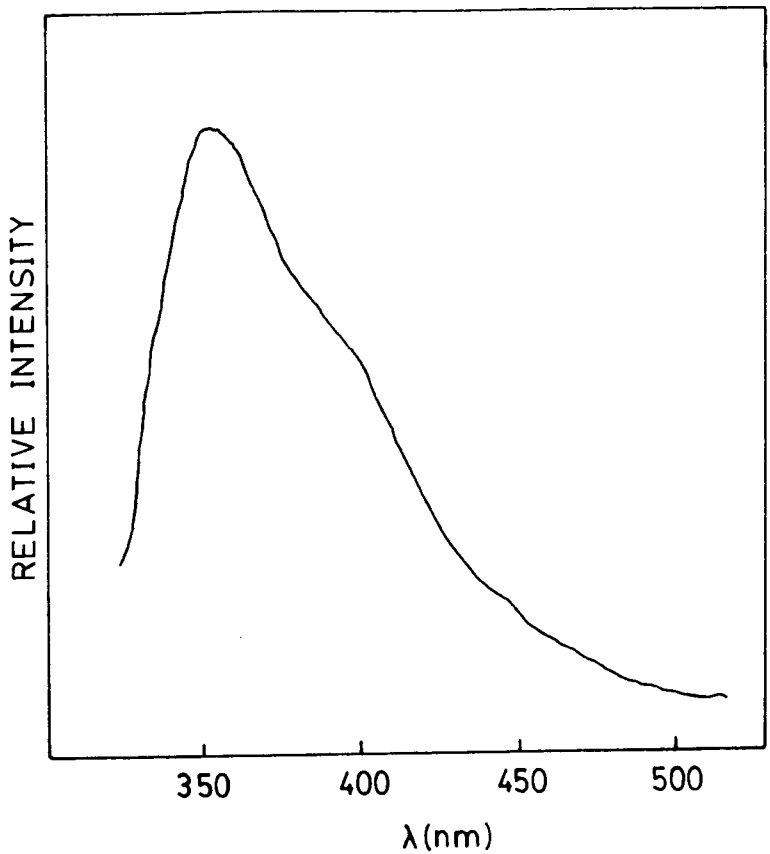

Fig. 1. Luminescence Emission Spectra of LaY.

The luminescence emission spectra of 2% Cu on the fresh catalyst and on the aged catalyst are given in figure 2, as well as the fresh catalyst.

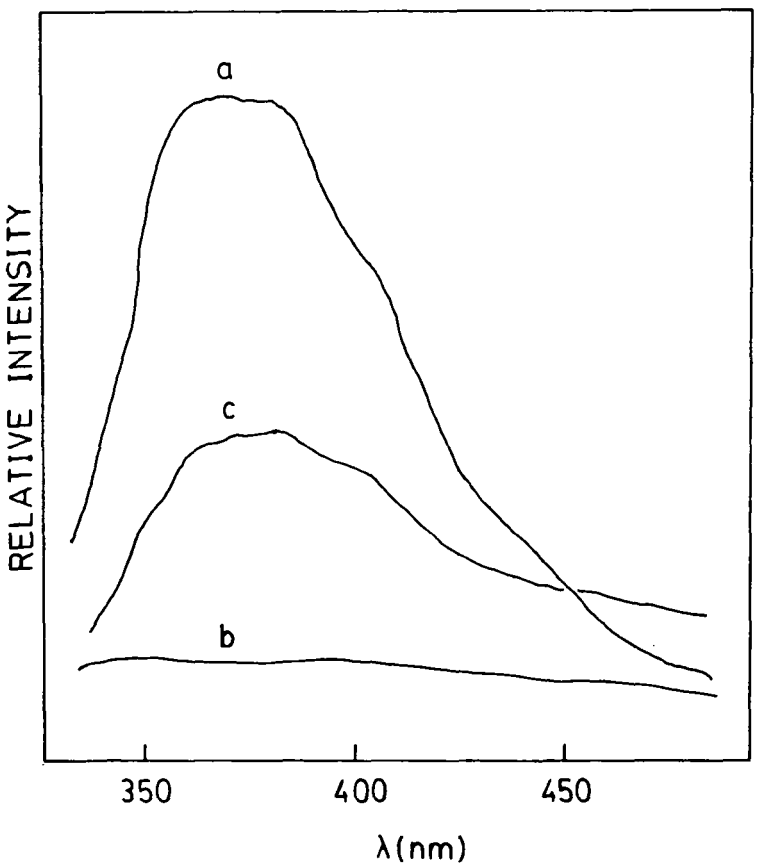

Fig. 2. Luminescence Emission Spectra of (a) fresh catalyst, (b) 2% Cu on fresh catalyst, (c) 2% Cu on aged catalyst.

Similar luminescence emission spectra are given in Figure 3 for 2% Fe on the fresh catalyst, 2% Fe on the aged catalyst, and for the fresh catalyst.

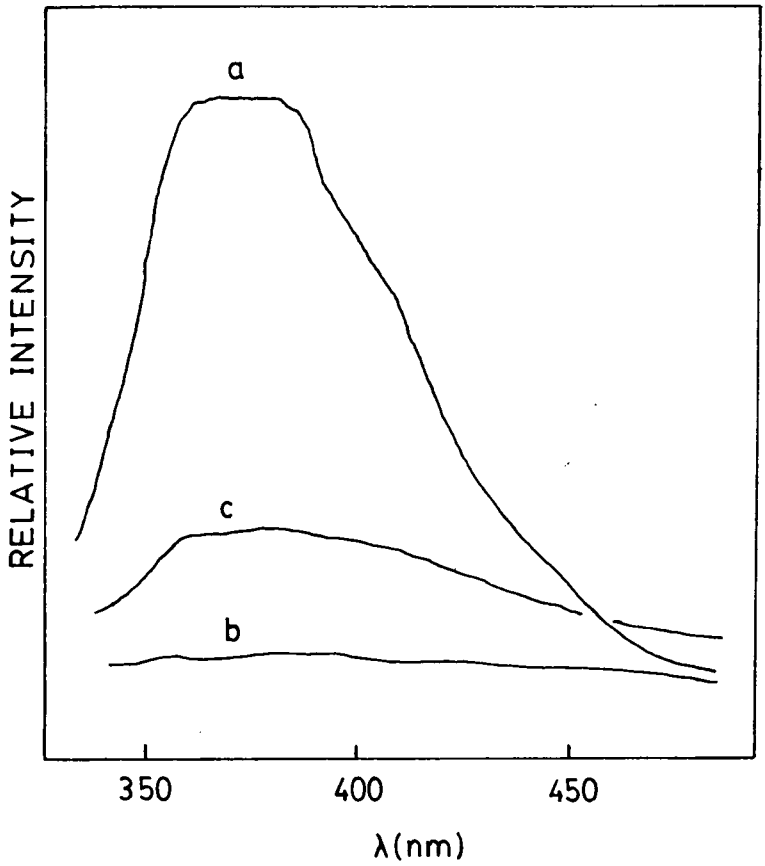

Fig. 3. Luminescence Emission Spectra of (a) fresh catalyst, (b) 2% Fe on fresh catalyst, (c) 2% Fe on aged catalyst.

The effects of increasing amounts of metal, on the cracking conversion are given in Figure 4.

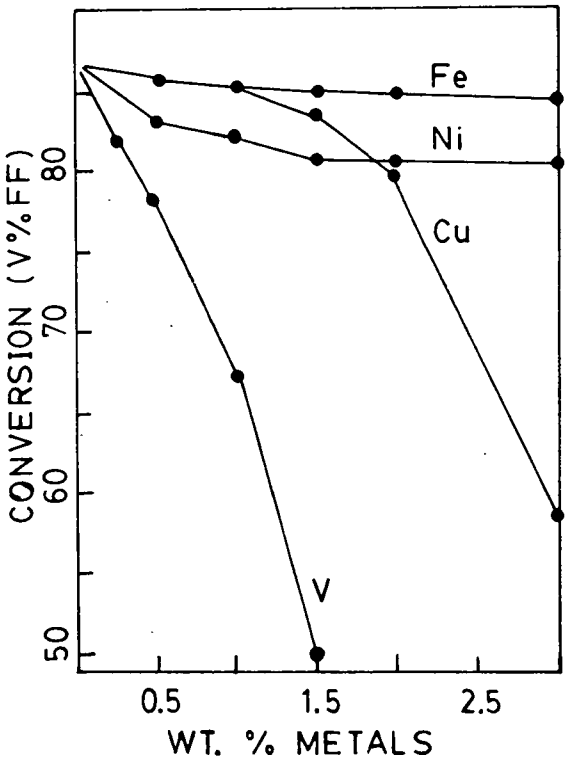

Fig. 4. Effects of Ni, V, Cu and Fe on Cracking Activity.

The effect of metal poisons on the gasoline yield is given in Figure 5.

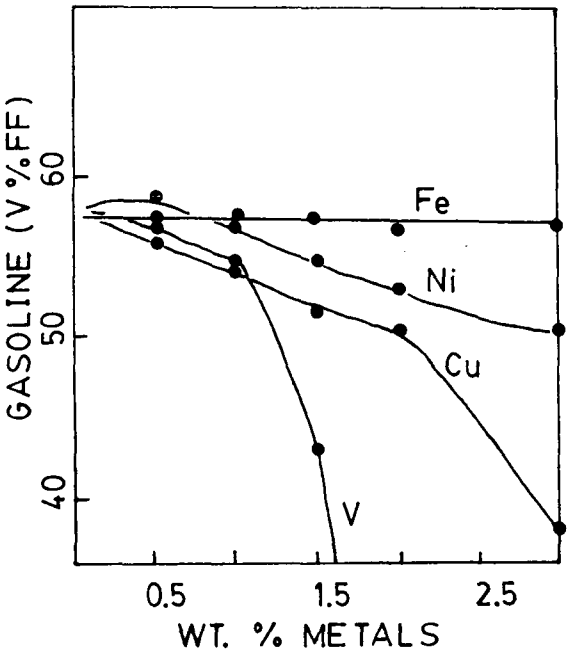

Fig. 5. Effect of Ni, V, Cu, Fe Poisons on Gasoline Yield.

DISCUSSION

The luminescence emission spectra of Figures 1, 2a and 3a show several similarities. This emission is due to the LaY component of the catalyst. On the fresh catalyst the emission is very apparent. As both iron and copper deposits are placed on the fresh catalyst, as in Figures 2c and 3c, the LaY emission is quenched. After steam aging the emission intensity for the LaY component of the FCC increases as shown in Figures 2b and 3b. This indicates that the copper and iron deposits are aggregating on the surface and exposing the LaY.

Similar luminescence results have been found for nickel deposits on FCC materials [9]. Further evidence for sintering of the nickel comes from electron microscopy results.

The catalytic cracking activity for nickel, vanadium, copper and iron deposits changes as a function of the amount of metal poison that is deposited. This is shown in Figure 4. For the most part, nickel and iron show parallel behavior with little decrease in overall activity as the weight % of metal is increased. Vanadium on the other hand shows an abrupt decrease in overall conversion even at relatively low amounts of metal poison. Iron starts to resemble vanadium only at high (>2 weight %) loading.

The gasoline yield also changes as a function of the weight % of metal poison as shown in Figure 5. Note that nickel, copper and vanadium deposits drastically decrease the gasoline yield. Iron deposits on the other hand do not change the gasoline yield too much.

CONCLUSION

It is evident from the data in this paper that luminescence emission spectra can be of great help in the elucidation of poisoning effects of metals on the catalytic activity of fluid cracking catalysts. The luminescence data can be used to determine changes in bond distance [9] during a reaction and as a qualitative tool in the identification of active surface phases. We also point out the good correlation between luminescence emission of the active LaY component and the catalytic cracking activity. Different metal poisons alter the catalysts in various ways depending on the type and amount of metal.

REFERENCES

1. Donaldson, R. E., Rice, T., Murphy, J. R., Ind. and Eng. Chem., 53, 721 (1961).
2. Grane, H. R., Connor, J. E., Masologites, G. P., Petroleum Refiner, 40, 168 (1961).
3. Magee, J. S., Ritter, R. E., Rheaume, L., Hydrocarbon Processing, 123 (1979).
4. Ritter, R. E., Rheaume, L., Welsh, W. A., Magee, J. S., Oil and Gas J., 103 (1981).
5. Occelli, M. L., J. V. Kennedy, U. S. Patent No. 4,465,588 (1983).
6. Briel, R. F., U. S. Patent No. 2,901,419 (1959).
7. Magee, J. S., "Advances in Catalytic Chemistry, II Symposium," Salt Lake City, Utah (1982).
8. Iwamoto, M., Furukawa, H., Matsukami, K., Tekenaka, T., Kakawa, S., J. Am. Chem. Soc., 105, 3719 (1983).
9. Occelli, M. L., Psaras, O., Suib, S. L., J. Am. Chem. Soc., submitted, (1985).

CONTRIBUTION TO REACTOR DESIGN IN A FLUID CATALYTIC CRACKING UNIT. COMPUTATION OF THE ACTIVITY DISTRIBUTION FUNCTION OF THE ZEOLITE ALONG THE RISER.

M. OLAZAR[a], J.M. ARANDES[a], J. BILBAO[a], J. CORELLA[b], R. BILBAO[b]
Department of Technical Chemistry, Universidad del Pais Vasco, Apdo 644, 48080 Bilbao, Spain (a)
Department of Technical Chemistry, Universidad de Zaragoza, Zaragoza, Spain (b)

ABSTRACT

A method based on the population balance model to design the riser in a FCCU is shown. From the deactivation kinetic equation, activity-time on stream, the activity distribution function is evaluated along the riser.

The use of the population balance model to evaluate the average activity, which gives the same results that from the residence time distribution function when the deactivation equation is of first order, avoids the error of this last method when the deactivation order is not the unity.

The design method has been used with experimentally obtained kinetic data in a riser of pilot plant with a MZ-7P zeolite as catalyst. The average activity, temperature, gas oil conversion and gasoline yield have been evaluated along the reactor.

INTRODUCTION

The population balance model is utilized to solve problems that can not be treated by means of models based on mass, momentum and energy balances. These models could range from microscopic models of transport phenomena to macroscopic models [1]. The population balance has been used to represent the age distribution in flow systems, crystal size distributions in steady state, age and size distribution of microbio-

logical cultures, etc.

The population balance was applied before [2] to design fluidized bed catalytic reactors with deactivation and with continuous feed catalyst in order to calculate activity distribution and average activity of particles, in the simplest case in which the deactivation equation, $-da/dt = \psi a^d$, is first order with respect to activity (d=1). However, the traditional method to calculate the average activity is the use of residence time distribution, macrofluid analysis, for any order of deactivation and of the design equation for microfluids, microfluid analysis, when the deactivation equation is firs order [3]. These methods give an accurate value of the average activity when the catalyst is fed continuously with uniform activity. However, this is not so when the activities of the inlet catalysts are distributed [2].

In this work population balance has been applied to the design of a riser in a FCCU in which the activity of the inlet catalyst is distributed because it comes from a fluidized bed regenerator. In Fig 1 it is shown a scheme of the reaction and regeneration sections, where f_1 is the distribution function of catalyst activity at riser inlet and f_2 the distribution function in any point along the riser.

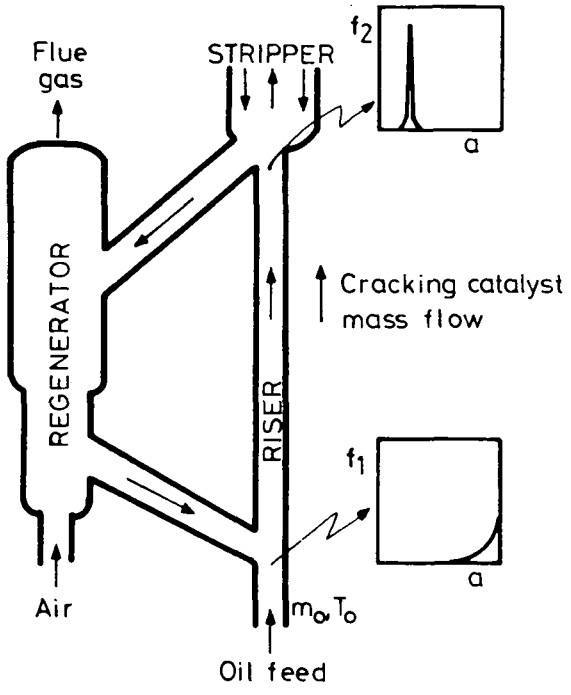

Fig. 1. Scheme of the reaction and regeneration sections in a FCCU.

DESIGN EQUATIONS

In the more advanced methods of riser design the following hypothesis are made [4]: Adiabatic reactor (heat losses below 5%, measured in a commercial unit [5]). Fluid and particles circulating at the same velocity [6,7]. There are not radial gradients of temperature and concentrations. Plug flow if the D/L ratio is small

enough [8].

The general equation of macroscopic population balance with respect to activity is:

$$\frac{df}{dt} + \frac{1}{\tau}\cdot\frac{df}{dz'} + \frac{d}{da}\left(f\frac{da}{dt}\right) = 0 \quad ; \quad dz' = dz/L \tag{1}$$

where f is the activity distribution function and τ the average residence time of the catalyst in the riser.

As it is plug flow, the activity distribution function at outlet can be obtained from the distribution function at inlet. $f_1(a_o)da_o$ represents the fraction of particles that have its activity in the a_o and a_o+da_o range. Later, these particles will have an activity between a and a+da and as the number of particles is the same:

$$f_1(a_o)da_o = f_2(a)da \tag{2}$$

As it is easier, the activity distribution function can be obtained from this equation instead of solving eqn(1).

For kinetic equations of deactivation independents of reactants and/or products concentration:

$$-\frac{da}{dt} = k_d \cdot a^d \tag{3}$$

for d > 1, activity distribution function is given by the equations:

$$f_2(a)=\left[(1-a^{d-1}(d-1)k_d t)^{-d/(d-1)}\right].f_1\left\{\frac{a}{[1-a^{d-1}(d-1)k_d t]^{1/(d-1)}}\right\} \tag{4}$$

for $a<a_e=a_o[1+a_o^{d-1}(d-1)k_d t]^{-1/(d-1)}$

$$f_2(a)=0 \quad \text{for } a>a_e \tag{5}$$

When d=1 the activity distribution function is given by:

$$f_2(a)= \frac{1}{\exp(-k_d t)}.f_1\left(\frac{1}{\exp(-k_d t)}\right) \quad \text{for } a<a_o\exp(-k_d t) \tag{6}$$

$$f_2(a)=0 \quad \text{for} \quad a>a_o\exp(-k_d t) \tag{7}$$

In these equations a_e is the upper value in the range where activity distribution function exists.

After knowing activity distribution function the average activity is given by:

$$\bar{a}= \int_0^{a_e} a\, f(a)da \tag{8}$$

The average activity value along the riser is introduced in the design equations, which will be:

-Mass balance $m_o dX = (-r_o)dW \quad ; W=0, X=0$ (9)

-Heat balance $(-\Delta H_r)(-r_o)dW = (F_s Cp_s + \Sigma m_i Cp_i)dT \quad ; W=0, T=T_o$ (10)

The average reaction heat is 70 Kcal/kg and the specific heats of gas oil and catalyst, supposing them to be constants in the studied temperature range, are 0.80 and 0.24 Kcal/kg K.

The solution of eqns(9) and (10) has been performed by a 4th order Runge-Kutta. The difficult lies in obtaining an average activity for each step. In order to compute it, the value of limit activity from which the distribution function does not exist is calculated in each step along the reactor. Next, the distribution function for lower values than the limit activity is obtained from the distribution function in the previous step. Knowing the distribution function, the average activity in each step can be computed by eqn(8).

THE STUDIED KINETIC SYSTEM

An experimental study of gas oil cracking on a MZ-7P zeolite catalyst supplied by Akzo-Chemie has been carried out in a pilot plant riser. The characteristics of this catalyst are related in Table 1.

Table 1

Characteristics of the MZ-7P catalyst

Chemical composition		Particle size distribution	
Al_2O_3	33	dp (μ)	cumulative weight,%
Na_2O	0.2	0 - 20	5
Fe	0.3	0 - 40	20
SO_4^{2-}	0.3	0 - 80	60
		0 -105	85
Physical properties		0 -150	98
Pore volume	0.28 cm^3/g		
Surface area	140 m^2/g		
Zeolite content	10%		
Bulk density	0.82 g/cm^3		

Zeolite: Faujasite Y rare earth exchanged.

The gas oil used comes from Puertollano refinery (ENPETROL) and it has the properties related in Table 2.

Table 2

Properties of gas oil

Density at 15°C, g/cm^3	0.896
Molecular weight	315
Aniline point	73.5
Ramsbotton carbon residue, % weight	0.17
Conradson carbon residue, % weight	0.14
Hydrogen, % weight	11.9
Sulfur, % weight	2.14
Nitrogen, ppm	562
Melting point, °C	+24
ASTM colour	4.5
Viscosity at 40°C (cs)	11.54

Reaction equipment, which setup and description can be found in a previous work [9], allows work with the following conditions: Temperature: 480-540°C. Time on stream: 0.5-3 s. Catalyst/oil ratio: 2-7 (w/w). Gas oil flow rate: 0.8-120 g/min. Cracking catalyst mass flow: 14-174 g/min.

Vaporized feed is put in contact with the preheated catalyst. Both raise togheter along the reactor and the deactivated catalyst is removed from gas by two cyclones placed at the top. There the catalyst is stripped with steam. Finally, gases are cooled and the gaseous and liquid products are collected and also the catalyst for their posterior analysis.

The reaction model used has been the Weekman's of three lumps[10]

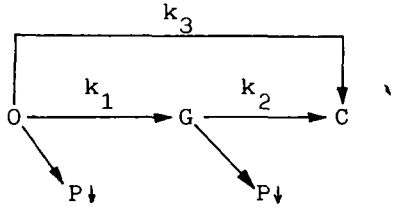

It consists of supposing that there are three characteristics groups of reactants and products: The gas oil, the gasoline and the gases and coke. The gas oil is cracked to give gasoline, coke and gases and the gasoline cracks to coke and gases.The kinetic equations at zero time are:

$$(-r_o)_o = (k_1+k_3)(1-X)^2 = k_o(1-X)^2 \quad (11)$$

$$(r_G)_o = k_1(1-X)^2 - k_2Y_G \quad (12)$$

$$(r_C)_o = k_3(1-X)^2 + k_2Y_G \quad (13)$$

where X is the gas oil conversion and Y_G the gasoline yield.

By kinetic experiments carried out in the before mentioned equipment, the following values have been found for the kinetic constants:

$$k_o(min^{-1}) = 3.5\ 10^4 exp(-12750/RT) \quad (14)$$

$$k_1(min^{-1}) = 1.1\ 10^9 exp(-29700/RT) \quad (15)$$

$$k_2(min^{-1}) = 4.2\ 10^5 exp(-32670/RT) \quad (16)$$

In the deactivation kinetic equation, eqn(3), it has been found that the order d changes throughout the time [11]. For that catalyst and gas oil, it has been found that for contact times shorter than 11 s the deactivation order is 3, for times between 11 and 42 s the order is 2 and for times longer than 42 s it is 1. In a riser the contact time is shorter than 11 s, then the deactivation order will be 3 and the deactivation rate constant is given by:

$$k_d(min^{-1}) = 2.5\ 10^9 exp(-27000/RT) \quad (17)$$

RESULTS

The activity distribution function at the riser inlet has been supposed given by $f_1(a) = 30.a^{29}$, to which corresponds 0.97 average activity. In Figure 2 activity distribution functions have been plotted for different times on stream at inlet temperature 530°C and C/O ratio 5. The area under the curve of all the functions is the unity because distribution function is normalized. It can be noticed the way the

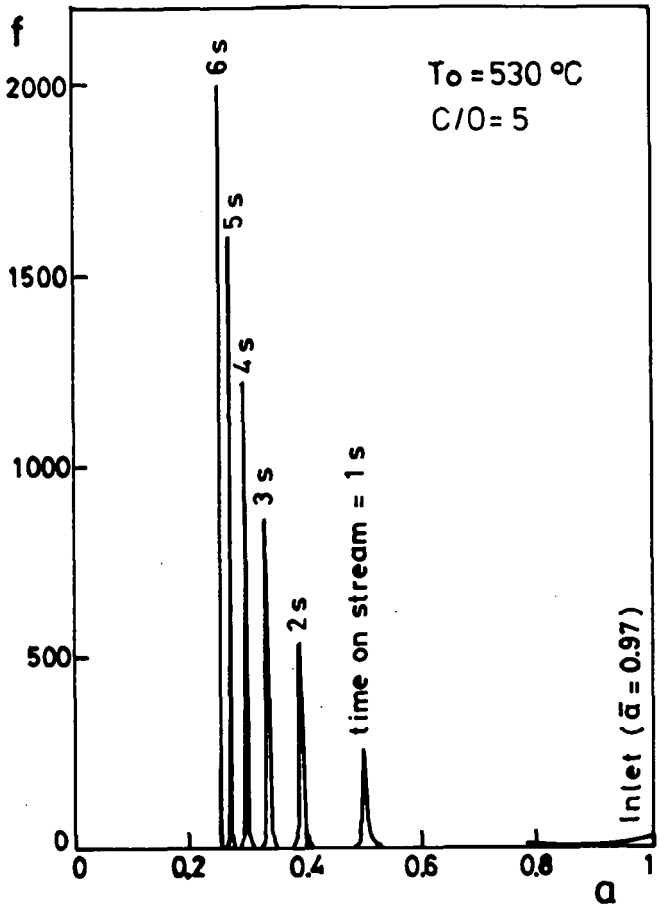

Fig. 2. Activity distribution function for different times on stream.

shape of the distribution function is changing getting more rough because there is plug flow.

The effect of operating variables in the following ranges has been studied:

-catalyst/gas oil ratio (w/w), C/O: 3.7

-temperature of riser inlet, T_o: 520-540°C.

-time on stream: 0-6 s.

In Figure 3 gas oil conversion vs. time on stream has been plotted for different values of C/O: 3, 5 and 7, and temperatures 520, 530 and 540°C. As most interesting result it can be noticed that in very short times, less than 1 s, more than half of the conversion is reached, that is to say, most of the conversion takes place along the initial length of the riser. As temperature increases for the same value of C/O, the conversion increases lightly.

In Figure 4 gasoline yield vs. time on stream has been plotted. Y_G has been evaluated solving the equation:

$$\frac{dY_G}{dX} = \frac{k_1}{k_o} - \frac{k_2 Y_G}{k_o (1-X)^2} \qquad (18)$$

which can be obtained dividing the equations (12) and (11).

In this Figure it can be seen the great impact that has the temperature, so that increasing this, the same gasoline yield as with C/O

ratios a lot of higher, at the same temperature, can be obtained.

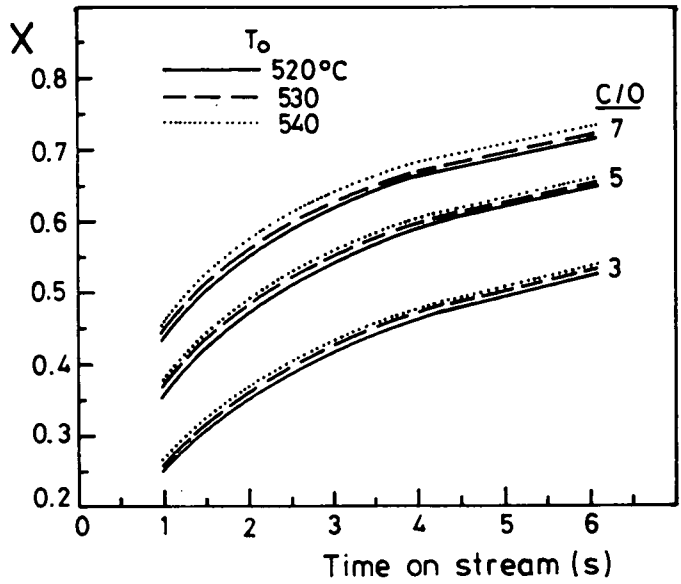

Fig. 3. Gas oil conversion vs time on stream at different inlet temperatures and C/O ratios.

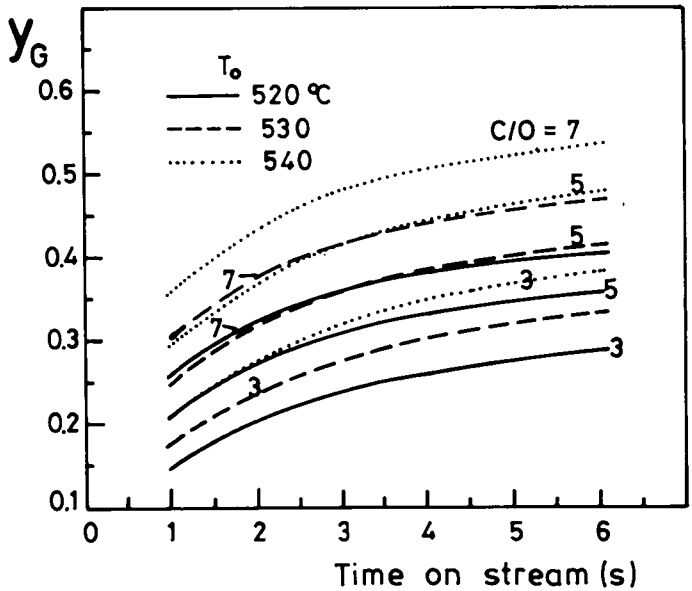

Fig. 4. Gasoline yield vs time on stream at different T_o and C/O.

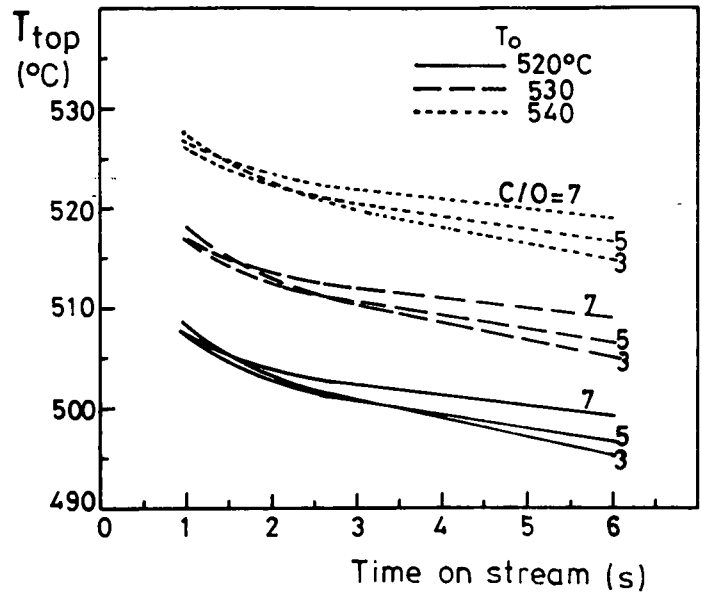

Fig. 5. Temperature vs time on stream at different T_o and C/O ratios.

In the Figure 5, temperature along the riser vs time on stream is drawn. Temperature drops practically in the early instants at the beginning of the riser, and the lower is the C/O ratio the bigger is the temperature drop, since there is less catalyst present.

DISCUSSION

Due to the narrow activity distribution, Figure 2, the results of average activity obtained by application of the population balance are not very different to that obtained using the residence time distribution.

The most interesting innovation in the design method is the use of the activity-time relationship instead of coke-time relationship, the more usual in bibliography. As the coke is not a well defined and stable compound, there is a lot confussion about the existing data.

At the present, in the Dpt. of Technical Chemistry of the Universidad de Zaragoza they are working in finding more accurate deactivation equations for each reaction of three lumps, since the active sites that takes place in each reaction do not have to be the same.

On other hand, in reaction-regeneration systems, it is interesting to know the distribution function of activity. This way, wide

variance in the activity distribution in the reactor could be avoided, since a wide distribution means that there is a catalyst fraction with so low activity that its regeneration is not interesting.

Being clear that in the riser there are deviations from plug flo [12], we are working in designing a riser introducing real data of axial dispersion in the design equations. That will contribute to a more realistic design of the riser of a FCCU.

REFERENCES

1. Himmelblau, D.M., Bischoff, K.B.: Process Analysis and Simulation. Wiley, New York, 1968.
2. Weng, H.S., Chen, T.L., Chem. Eng. Sci. 35, 915 (1980).
3. Corella, J., Bilbao, R., López Peña, J.M., Ing. Quim. 14(158), 127 (1982).
4. De Lasa, H.I., Lat. Am. J. Chem. Eng. Appl. Chem. 12, 171 (1982).
5. Shah, Y.T., Huling, G.P., Paraskos, J.A., McKinney, J.D., Ind. Eng. Chem. Process Des. Dev. 16, 89 (1977).
6. De Lasa, H.I., Errazu, A., Porras, J., Barreiro, E., Lat. Am. J. Chem. Eng. Appl. Chem. 11, 139 (1981).
7. Errazu, A., Porras, J., De Lasa, H.I., X Jornadas de Ing. Química, Santa Fe, Argentina, 1978.
8. De Lasa, H.I., Gau, G., Chem. Eng. Sci. 28, 1875 (1973).
9. Corella, J., Fernández, M., Vidal, J.M., 3rd Mediterranean Congress on Chemical Engineering, Barcelona, 1984, p. 56.
10. Weekman, V.W., Ind. Eng. Chem. Process Des. Dev. 7, 90 (1968) and 8, 385 (1969).
11. Corella, J., Bilbao, R., Artigas, A., Molina, J.A., 3rd Mediterranean Congress on Chemical Engineering, Barcelona, 1984, p. 60.
12. Bernard, J.R., Santos-Cottin, H., Margritta, R., Katalistiks' 5th Annual Fluid Cat Cracking Symposium, Vienna, 1984, ch. 3.

HYDROISOMERIZATION AND HYDROCRACKING OF n-PARAFFINES ON ZEOLITE CATALYSTS

K.-H. STEINBERG[a], K. BECKER[b], K.-H. NESTLER[c]
Karl-Marx-Universität, Leipzig, G.D.R. (a)
VEB Leuna-Werke "Walter Ulbricht", Leuna, G.D.R. (b)
VEB "Otto Grotewohl", Böhlen, G.D.R. (c)

ABSTRACT

In technical gasolines the n-paraffines are the hydrocarbons with the lowest octane number. To convert them into components with higher octane level two different processes are used depending on their C-number: The hydroisomerization of the light gasoline and the shape selective hydrocracking of the n-paraffines of the reformate.

For the development and application of catalysts for both processes two different principles of catalysis on zeolites have been followed. Activity and selectivity of the light petrol isomerization catalyst are based on the formation of BRÖNSTED centres with a specific acid strength in Y zeolites by special ion exchange and activation methods. On the other hand the very shape selective behaviour of H-erionite against n-paraffines even at reforming temperature was used for the development of a zeolite catalyst for the upgrading of reformates.

Details of the zeolite catalysts developed for and applicated in both processes on industrial scale in the G.D.R. are given.

INTRODUCTION

Usually the light gasoline (boiling range about 310 up to 360 K) and the heavy gasoline (boiling range about 370 up to 455 K) are processed separately because of the different potential to get aromatics. However, in the whole gasoline range the n-paraffines are the hydrocarbons with the lowest octane level (see Table 1).

In the light gasoline fraction the aim of processing is the isomerization of the n-paraffines into iso-paraffines. The thermodynamic equilibrium between the n- and iso-paraffines [2] requires

Table 2

Specification of a technical light gasoline to be isomerized

component	mass-%	component	mass-%
$C_3 + C_4$	11.3	benzene	2.4
i-pentane	11.5	toluene	0.3
n-pentane	18.3	RON_{clear}	70.0
dimethylbutanes	1.0	RON_{leaded}	85.5
methylpentanes	20.4	S-content, ppm	5.0
n-hexane	19.0	H_2O-content, ppm	50
naphthenes	8.2		

ming process. The Selectoforming process of Mobil [3] describes the removal of these n-paraffines from the reformate by hydrocracking on metal containing narrow porous zeolites on the basis of the works of Maziuk et al. [4 - 6]. The narrow porous zeolite should possess real shape selective properties for n-paraffines even at the usual reforming temperature, should be highly active and thermostable, should be available, and should stand the reforming catalyst life time at least. For this purpose mordenite, offretite, erionite, and ZSM-type zeolites are to taken into account.

Y ZEOLITE CATALYSTS FOR THE ISOMERIZATION OF LIGHT GASOLINE

In the hydroisomerization of n-pentane and n-hexane the acid Brönsted centres are of essential importance, if the metal function is well established. We took care for this in all our experiments by loading all zeolite catalysts with 0.5 % Pt and by a careful air treatment followed by a slowly reduction with hydrogen. So properties of the zeolite component became determining activity and selectivity, i. e. its acid properties.

Fig. 1 shows the dependence of the Brönsted acid centres concentration on the exchange degree of different cations in Y zeolite. The Brönsted centres concentration has been measured by I.R. spectroscopic determination of the extinction of the pyridinium ion band (1550 cm^{-1}) of the pyridine adsorbed under standard conditions. In all cases the concentration of acid Brönsted centres increases with the exchange degree. The highest concentration was found at the HNaY followed by the CeNaY zeo-

Table 1

Research octane numbers of some hydrocarbons [1]

n-C_4	93.6	i-C_4	99.0	2,2-DMP	80.0
n-C_5	61.5	i-C_5	99.5	benzene	98.5
n-C_6	29.0	2-MP	69.0	toluene	123.5
n-C_7	0.0	3-MP	85.5	m-xylene	120.0
n-C_8	< 0	2,2-DMB	97.0	cyclohexane	109.5

a temperature as low as possible but often the catalyst activity does not meet this demand.

In literature processes for low temperature isomerization using halogen containing catalysts are described. As far we know in all cases a lot of corrosion problems arose due to traces of water in the feedstock as well as other problems. The less sensitive high temperature processes (680 K) use noble metal/alumina catalysts.

The development of catalysts containing zeolites led to milder conditions (520 to 600 K). The required temperature depends on the type of alumosilicate and the process conditions like water, sulphur, and pressure of the recycle gas and on the feedstock composition.

As it is well known by literature, the isomerization of n-paraffines follows the classical mechanism with carbenium ion intermediates. The selectivity for the prefered isomerization depends on the strength of the acid Brönsted centre involved in the carbenium ion formation, if other rate limiting steps are excluded. The problem is how to avoid the nonselective hydrocracking which is also possible under isomerization conditions by a parallel reaction. Especially, this fits in case of the isomerization of a technical light gasoline containing higher hydrocarbons (see specification in Table 2). Therefore we followed in our work of the development of isomerization catalysts the way of creation of enough Brönsted centres of an optimal acid strength by special ion exchange and activation methods of Y zeolites. The pore diameter of Y zeolites allows the fast diffusion of n-paraffines and i-paraffines as well. Furthermore, a lot of details is known of the dependence of the surface chemical properties on the ion exchange.

In reforming products a content of about 5 to 10 % of the low octane level n-paraffines (Table 1) remains after the refor-

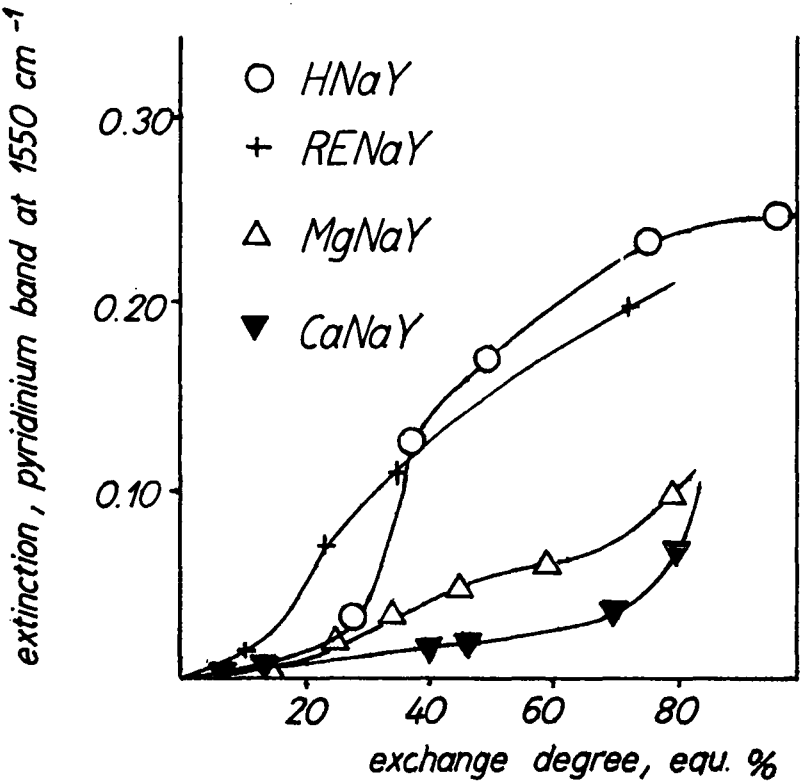

Fig. 1. Dependence of the concentration of Brönsted acid centres on the exchange degree of Y zeolites [7]

lite. One could expect on these results, that the HNaY zeolite would be the most active catalyst in the isomerization. This only refers to the activity but not to the selectivity in the n-hexane isomerization [8]. Due to the parallel hydrocracking of part of the higher hydrocarbons this applies to the hydro-isomerization of a technical gasoline especially.

Therefore we concentrated our efforts on the development of an isomerization catalyst on the basis of RENaY zeolite. We found that a RENaY zeolite catalyst consisting of 0.5 % Pt and with an exchange degree of about 65 equiv. % (specification see Table 3, performance see Table 4) works at satisfactory conditions as working temperature, octane level of the product, and liquid yield. The results are remarkable better than those of the formerly used Pt/Al_2O_3 catalyst (Table 4).

During its technical application the RENaY catalyst was slowly (within a period of about six month) desactivated and its original activity could not be regained by a conventional oxydative regeneration [9]. Investigating the desactivated ca-

Table 3

Specification of Leuna isomerization catalysts with zeolites

	Kt. 8815	Kt. 8850	Kt. 8851	Kt. 8852
composition	Pt/Al_2O_3	Pt/RENaY	Pt/MgCaNaY	Pt/RECaNaY
binder	-	clay	Al_2O_3	Al_2O_3
specific weight, g/l	700	870	580	580
form, diameter, mm	extrudates, 2	cylindric pellets, 5 x 5	extrudates 3	extrudates 3

Table 4

Catalytic performance of Leuna isomerization catalysts with zeolites

Reaction conditions: 2.5 MPa, space velocity 2 v/vh, gas liquid ratio 1000:1, industrial plant, gasoline see Table 2

	Kt. 8815	Kt. 8850	Kt. 8851	Kt. 8852
temperature, K	743	618	603	593
RON_{loaded}	89.5	90.0	90.5	91.0
liquid yield, mass-%	86.5	89.5	90.3	91.5
technical use	up to 1976	1976-1978	1978-1980	since 1980

talyst by means of ion exchange, catalytic and surface chemical methods we found a change in the cation distribution in the zeolite to be the reason. RE^{3+} ions located in the large cavaties and creating there acid Brönsted centres changed their positions with Na^+ ions coming from positions within the small cavaties.

Therefore we looked for a method to fix the cations creating catalytic active centres inside the large cavaties even under the reaction requirements as temperature and life time. At that time our bulgarian colleagues rendered assistance. They found, that it is possible to prevent the Na^+ ion migration into the large cavaties of Y zeolites if all the cation positions inside the hexagonal prisms are blocked by Ca^{2+} ions. This can be reached by simultaneous ion exchange of Ca^{2+} and Mg^{2+} ions at special conditions and cocentrations [10]. A Pt/MgCaNaY zeolite prepared in this manner is a very active and selective catalyst in the n-pentane isomerization [10].

On the basis of these results the Leuna-Kt. 8851 was deve-

loped [11]. Besides the new zeolitic component also the binder was changed. Instead of pilling using a natural clay as binder the Leuna-Kt. 8851 was formed by extrudation with a special activated Al_2O_3 as binder. The main advantages of the changed forming method consist in the lower specific weight (see Table 3), saved platinum and higher porosity. The application of the Pt/MgCaNaY zeolite catalyst in the industrial gasoline isomerization process brought about higher efficiency (see Table 4). Above all no remarkable desactivation could be observed.

Activity, selectivity as well as the altering resistance of the Pt/MgCaNaY zeolite catalyst corroborated the availability of the hypothesis, that it is necessary for good catalytic properties to direct the highly charged cations in positions in the large cavities and to fix them there too. According to this assumption we introduced RE^{3+} ions into a CaNaY zeolite with high exchange degree replacing only part of the Ca^{2+} ions [12]. By this exchange procedure OH groups acting as acid Brönsted centres are additionally formed (see Fig. 2) in comparison with a 0.88CaNaY zeolite and a 0.64 RENaY zeolite too.

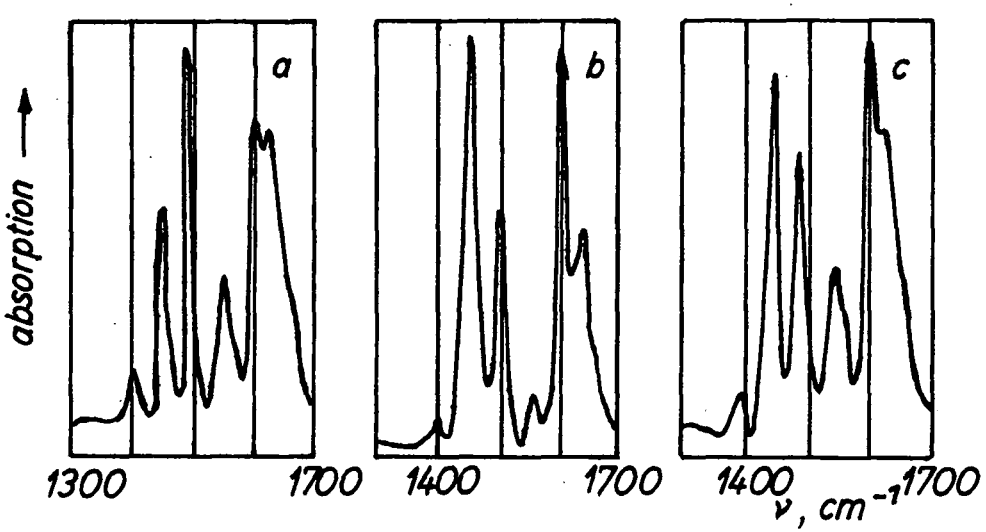

Fig. 2. I.R. spectra of pyridine adsorbed on a) 0.64RENaY b) 0.88CaNaY c)0.28RE0.60CaNaY zeolites
activation temperature 770 K, at 420 K 2.0 kPa pyridine for 10 min, final evacuation at 420 K

The additionally formed Brönsted acid sites in the 0.28RE 0.60CaNaY zeolite possess mainly an acid strength in the region

of pK_a = -8.2 to -5.6 (see Fig. 3). Compared with the 0.88CaNaY zeolite the 0.28REO.60CaNaY zeolite has more and stronger acid centres. In no case the transformation of the used most acid indicator (anthraquinone pK_a = -8.2) has been observed.

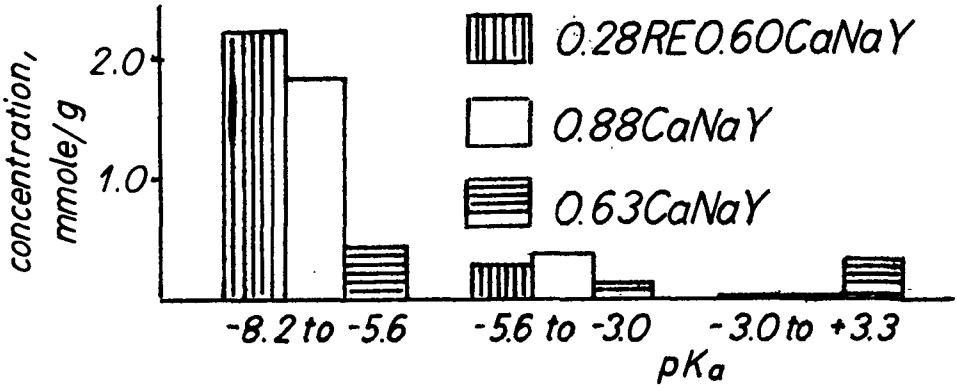

Fig. 3. Results of the titration with n-butylamine according to Benesi [13] using Hammett indicators

Obviously, the formation of more and stronger acid Brönsted sites on the 0.28REO.60CaNaY zeolite is due to the presence and

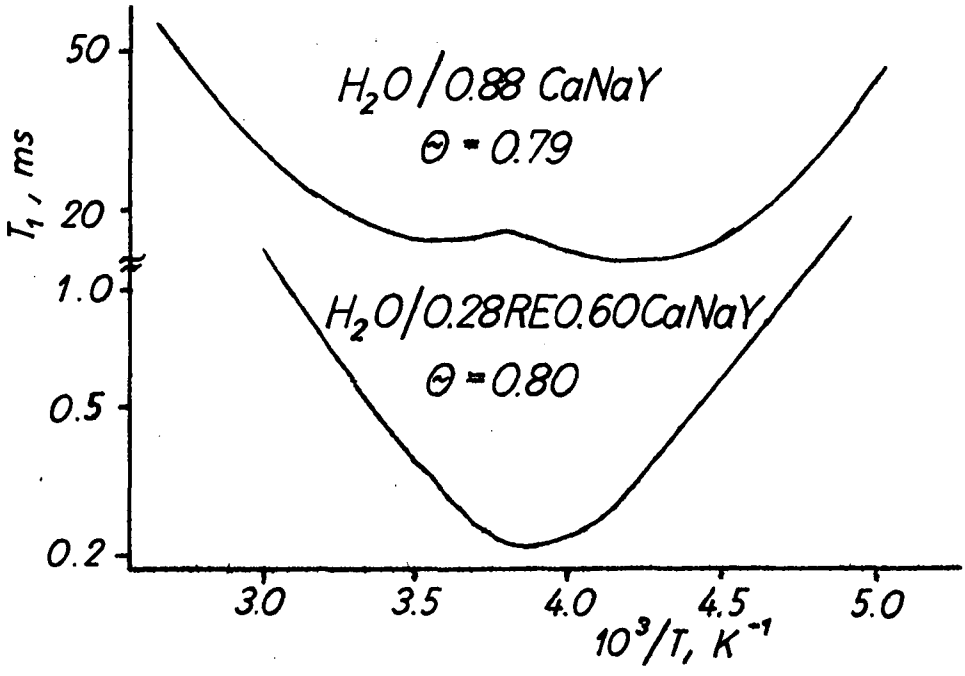

Fig. 4. N.M.R. relaxation of water adsorbed on 0.88CaNaY and 0.28REO.60CaNaY zeolite, longitudinal proton spin relation time T_1 on reciprocal temperature, $\omega_1/2\pi$ = 90 MHz

fixation of part of the RE^{3+} ions within positions in the large cavities (S_{II}). By N.M.R. relaxation measurements (T_1 of adsorbed water, see Fig. 4) [14] and by I.R. measurements in the lattice vibration region [15] (see Fig. 5) it could be shown, that

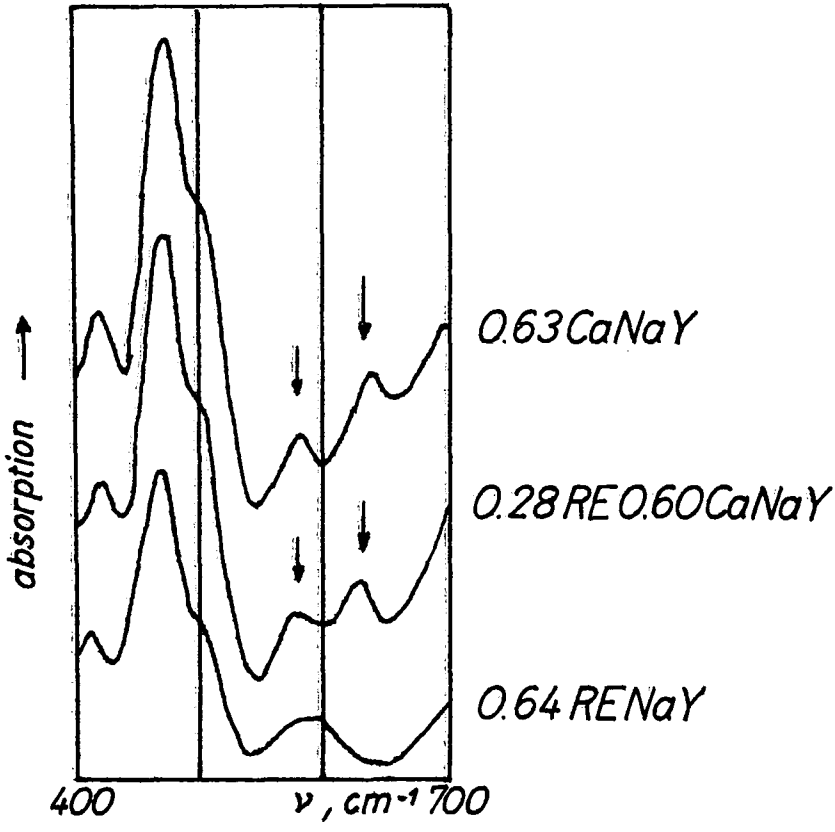

Fig. 5. I.R. spectra of zeolites activated at 770 K, 10^{-2} Pa, 30 min, selfsupporting discs, ⩽0.7 mg/cm^2

the RE^{3+} ions introduced into a 0.88CaNaY zeolite replace part of the Ca^{2+} ions in the S_{II} positions and remain there after thermal pretreatment also. In Fig. 4 it is demonstrated how the longitudinal proton spin relaxation time of adsorbed water decreases, if RE^{3+} ions (paramagnetic) are introduced in a 0.88CaNaY zeolite. This effect is due to the proton paramagnetic ion interaction and a proof of the presence of RE^{3+} ions within the large cavities.

The results shown in Fig. 5 support the N.M.R. data also. The I.R. spectra of unsupported discs (no binder) of the 0.63CaNaY and the 0.28RE0.60CaNaY zeolite [15] are quite similar in the region of the double six ring vibration (550 to 650 cm^{-1}). This

means, the RE^{3+} ions cannot be exchanged preferably into S_I positions (and only part of them may be located in S_I, positions).

The special distribution of the RE^{3+} ions in a RECaNaY zeolite and the outstanding surface chemical properties caused by it are the reasons for the high activity and selectivity of a Pt/0.28REO.60CaNaY zeolite catalyst in the n-hexane isomerization (see Fig. 6). The data given in Fig. 6 show that the highest

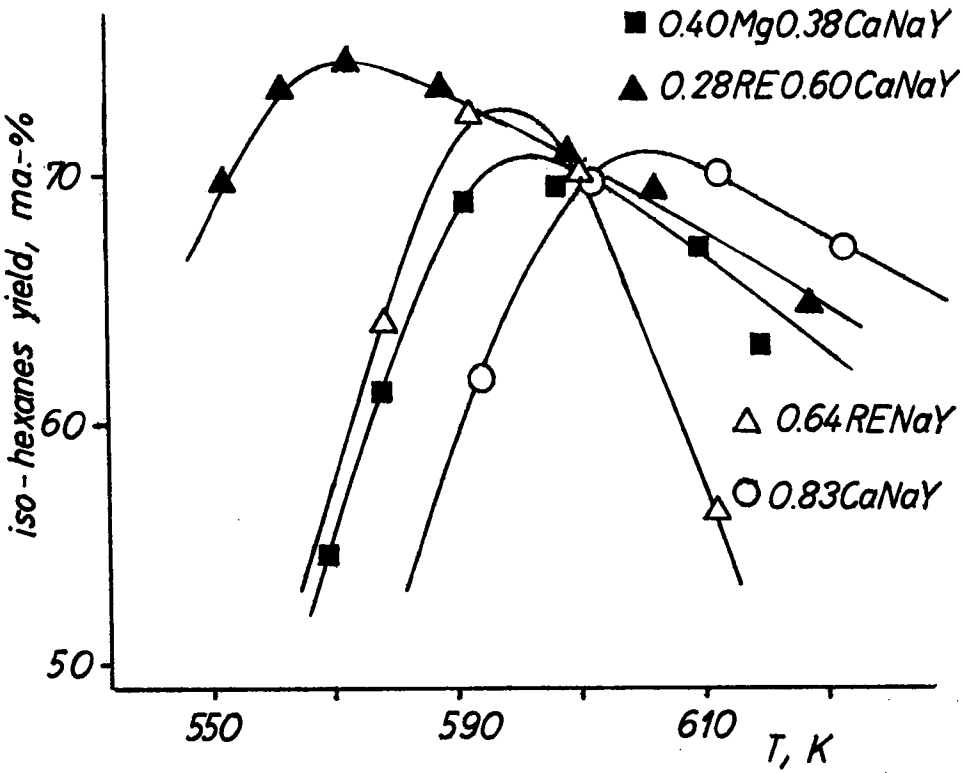

Fig. 6. n-hexane isomerization activity of Y zeolites, dependence on temperature, 2 cm^3 catalyst (0.2 - 0.3 mm) H_2 : n-hexane = 5 : 1 mole/mole, LHSV = 1.5 v/vh, normal pressure, 0.5 % Pt

yield of iso-hexanes at the lowest temperature are obtained on the 0.5%Pt/0.26REO.60CaNaY zeolite catalyst in comparison with catalysts on the basis of 0.64RENaY, 0.83CaNaY, and 0.40Mg0.38 CaNaY zeolites, respectively. Furthermore, the consecutive formation of double branched iso-hexanes is much more higher on the 0.5%Pt/0.28REO.60CaNaY zeolite catalyst [16].

On the basis of these scientific results the industrial catalyst Leuna-Kt. 8852 was developed and applicated. Once again an in -

crease in liquid yield and higher quality at lower temperature could be reached in comparison with its pecursors (see Tab. 4).

MORDENITE CATALYST FOR THE SHAPE SELECTIVE HYDRCRACKING OF n-PARAFFINES

Due to the pores dimensions mordenite, offretite, erionite, and ZSM-5 type zeolites are to taken into account as catalysts for the shape selective hydrocracking of n-paraffines out of a reformate hydrocarbon mixture.

According to the carbenium ion mechanism of cracking and also of hydrocracking of n-paraffines the zeolite must be transformed into an acid form to become actively. In case of mordenite this can be reached by direct acid treatment. By leaching of sodium mordenite with HNO_3 of different concentration it is possible to influence the activity as well as the selectivity of the resulting H-mordenite for the cracking of a 1 : 1 molar mixture of n-octane and iso-octane (see Fig. 7).

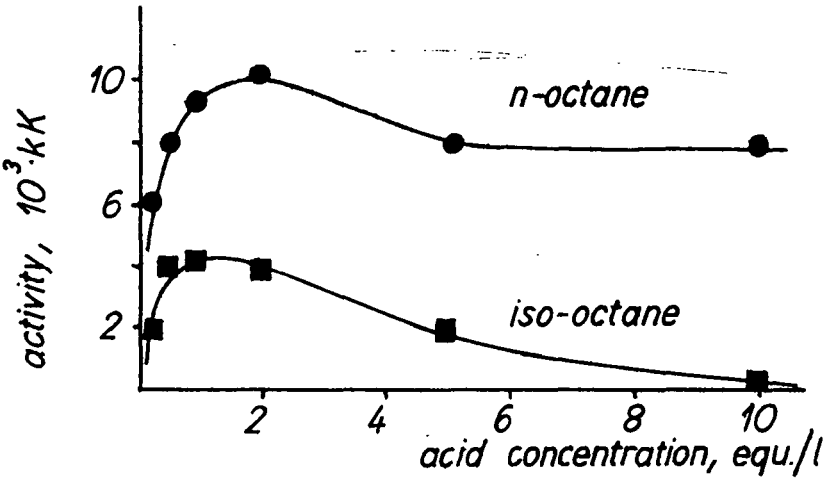

Fig. 7. Activity of Ni/H-mordenite in the hydrocracking of a 1 : 1 molar mixture of n-octane and iso-octane, dependence on the HNO_3 concentration used in the leaching treatment, pulse reactor, 573 K, 3 l/h H_2, 5 μl pulses, 100mg catalyst

The dependence of the selectivity on the acid treatment conditions can be explained by the prefered dealumination of the shells of the mordenite crystallites. The shape selectivity of mordenite for n-paraffines in a mixture with iso-paraffines is only based on the slowlier diffusion of the latter, because iso-paraf-

fines can enter the mordenite channel system too. By the peripherical dealumination the acid centres in the outskirts, where the iso-paraffines could be converted, are removed preferably.

The best results are obtained by leaching with concentrated HNO_3 followed by supporting 5 ma.-% Ni. Investigating the hydrogen reduction process of the Ni^{2+} ions introduced in the H-mordenite by impregnation we found an interesting effect [17]. At temperatures above 770 K we observed a reduction degree of the supported Ni^{2+} of more than 100 percent. A blank test gave the surprising result that even the H-mordenite free of Ni strongly chemisorbs hydrogen at temperatures above 720 K (see Fig. 8).

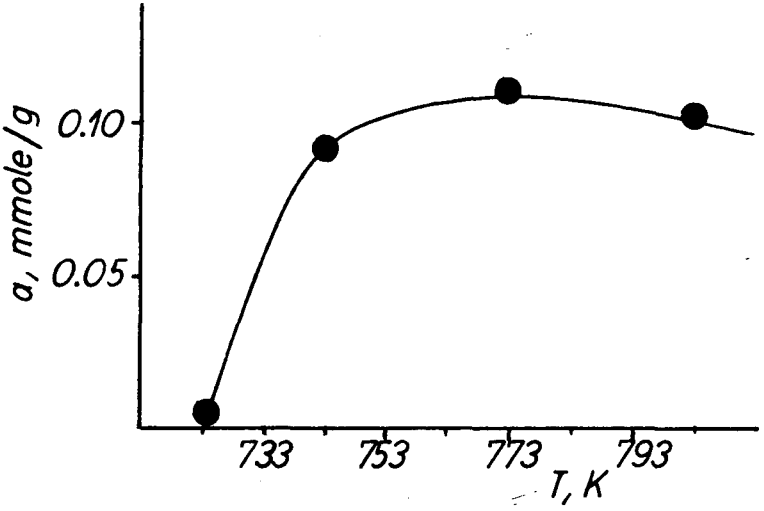

Fig. 8. Hydrogen chemisorption on H-mordenite

These data were obtained by a volumetric method as follows: Activation of the mordenite sample in air for 3 h with 3 l/h at the later reduction temperature, treatment for 2 h with 3 l/h H_2 at the given temperature, treatment for 1 h with 3 l/h Ar at the same temperature, cooling down to room temperature, evacuation to 10^{-2} Pa, adding of outgassed HCl, measurement of the H_2 evolved.

On the basis of such experimental results the Leuna-Kt. 9561 has been developed [18]. Its performance in a pilot reactor is shown in Table 5. The results show, that the Ni/mordenite catalyst is able to improve the octane level by about five units without large loss in liquid yield. The relationship one RON unit

Table 5

Performance of the Leuna-Kt. 9561 in a pilot plant

Reaction conditions: 4.0 MPa, 670 K, LHSV = 3.0, gas liquid ratio = 1000 : 1 m^3/m^3, feed: reformate		
	feedstock	product
density, g/cm^3	0.759	0.748
liquid yield, ma.-%	-	96.5
RON_0	81	86
aromatics, vol.-%	38.0	42.5
naphthenes, vol,-%	7.0	8.5
paraffines, vol.-%	55.0	49.0
sulphur, ppm	3	-
light fraction to 100°C, vol.-%	18.5	23.5

gain per 0.7 ma.-% loss in liquid yield is satisfactory for usual reforming.

Unfortunately the optimal working conditions of mordenite containing shape selective hydrocracking catalysts are about 670 K and a LHSV of about 3 v/vh. This means in case of technical application an additional reactor in the reforming plant is required, in which the special working conditions can be chosen. Especially the working temperature is nontypical of reforming. At higher temperature the selectivity rapidly decreases due to the origin of the shape selectivity of mordenite catalysts and the liquid yield/RON relationship becomes lower than in case of conventional reforming.

ERIONITE CATALYST FOR THE SHAPE SELECTIVE HYDROCRACKING OF n-PARAFFINES

In comparison with mordenite erionite possesses real shape selectivity due to its pores dimensions [19]. From the hydrocarbons contained in a reformate only the n-paraffines are able to diffuse into the erionite structure even at about 770 K.

By repeated ion exchange with ammonium salt solution and thermal decomposition it is possible to prepare a catalytically active form of synthetic erionite. After forming of the H-erionite and supporting 0.5 % Pt for instance by impregnation a very active and selective catalyst is obtained [20]. Similar to this

the Leuna-Kt. 9562 has been produced in 1978 and applicated on industrial scale up today in three refprming plants. Table 6 contains a comparison of usual reforming with a commercial Pt/Al_2O_3 catalyst and a sandwich combination of the same Pt/Al_2O_3 catalyst with the Pt/H-erionite catalyst Kt. 9562 in the same conventional reforming plant consisting of three reactors.

Table 6

Comparison of reforming and reforming/shape selective cracking with Leuna-Kt. 9562, industrial plant, 2.5 MPa, gas product ratio = 1000 : 1 m^3/m^3

	reforming	reforming/selective cracking	
		variant 1	variant 2
results after time on stream, h	4 200	3 900	3 100
inlet temperature, K			
1. reactor	766	743	748
2. reactor	771	747	751
3. reactor	779	725	757
at catalyst Kt. 9562	-	711	735
LHSV, v/vh	2.1	2.1/25.0	2.1/25.0
liquid yield, ma.-%	87.3	87.3	84.4
$RON_{0.04}$	89.6	89.9	94.7
aromatics, ma.-%	39.2	35.1	43.3
naphthenes, ma.-%	6.3	12.8	8.7
paraffines, ma.-%	54.5	52.1	48.0

In case of the combination only 10 % of the reforming catalyst have been replaced by the shape selective hydrocracking catalyst Kt. 9562, that the specific space velocity at the Kt. 9562 is about 25 v/vh.

The results listed in Table 6 show that the application of the catalyst Kt. 9562 in combination with conventional reforming enables

- at unusual low temperature the same reforming result (variant 1), saving of energy and increasing of the life time of the whole catalyst combination up to more than 20 000 h without regeneration

  or

- at lower temperature as it is usually applicated in reforming

plants higher RON level at high liquid yields (variant 2).

These good results are due to the real shape selective hydrocracking of the n-paraffines and an additional formation of aromatics as is shown in Table 7. The data given in Tab. 7 are in accordance to the results of the technical plant listed in Tab. 6.

Table 7

Feedstock and products for reforming and its combination with shape selective hydrocracking, results of capillary chromatography, reaction details see Tab. 6

hydrocarbon	feedstock	reforming	reforming/selective cracking	
			variant 1	variant 2
	ma.-%	ma.-%	ma.-%	ma.-%
n-pentane	0.02	1.3	1.6	1.9
n-hexane	2.0	2.2	1.6	1.3
n-heptane	5.8	4.0	2.3	1.7
n-octane	6.8	2.8	1.9	1.2
n-nonane	4.7	1.3	1.0	0.8
n-decane	2.1	0.4	0.3	0.2
iso-pentanes	0.03	1.8	1.6	2.4
iso-hexanes	0.9	2.9	2.8	2.5
iso-heptanes	6.8	8.7	8.6	7.4
iso-octanes	7.9	8.1	8.6	8.2
iso-nonanes	7.1	5.1	6.6	6.1
benzene	0.4	2.1	1.6	1.9
toluene		9.8	7.6	9.2
C_8 aromatics	2.4	14.6	11.6	17.3
C_{9+} aromatics	5.5	18.2	17.2	21.1

The main advantages of the application of the erionite catalyst are :

- large gain in octane number at only small loss in liquid yield
- mild reforming conditions
- long run without regeneration
- energy economizing
- rationalization of reforming plants without reconstruction.

REFERENCES

1. Anderson, J. of Petr. Inst. 58, 83 (1972)
2. Rossini, F.D., Pitzer, K.S., J. Res. nat. Bur. Standards 27, 529 (1941).
3. Kuchar, P.J., Addison, G.E., The UOP Conference, Budapest 1973
4. Chen, N.Y., Maziuk, J., Schwartz, A.B., Weisz, P.B., Oil & Gas Journal 66, 154 (1966).
5. Burd, S.D., Maziuk, J., 37th Midyear Meeting of the American Petroleum Institutes, Div. of Refining, New York, 9. 5. 1972 .
6. Burd, S.D., Maziuk, J., Hydrocarbon Processing 51, 97 (1972).
7. Steinberg, K.-H., Bremer, H., Hofmann, F. Minachev, CH. M., Dmitriev, R.V., Detjuk, A.N., Z. anorg. allg. Chem. 404, 129 (1974), 404, 142 (1974).
8. Reschetilovski, V., Thesis, TH Carl Schorlemmer Leuna-Merseburg, 1978.
9. Steinberg, K.-H., Becker, K., Bremer, H., Dimitrov, CH., Kanazirev, V., Nestler, K.-H., Minachev, CH.M., Chem. Techn. 33, 296 (1981).
10. Kanazirev, V., Minchev, CH., Penchev, V., Becker, K., Steinberg, K.-H., Hille, J., Reschetilovski, V., Chem. Techn. 31, 275 (1979), Depot 16/79, BG P 24 840, 22. 9. 1977.
11. DD P 151 568, 28. 10. 1981.
12. Steinberg, K.-H., Dombrovski, D., Minachev, CH.M., Dmitriev, R.V., Dimitrov, CH., Popova, Z., Z. anorg. allg. Chem. 467, 34 (1980).
13. Benesi, H.A., J. Amer. Chem. Soc. 78, 5490 (1956).
14. Winkler, H., Steinberg, K.-H., Kapphahn, G., J. Colloid Interface Sci. 98, 144 (1984).
15. Rößner, F., Steinberg, K.-H., Zeolites, sent to the editors, 1985.
16. Dimitrov, CH., Dmitriev, R.V., Dombrovski, D., Minachev, CH. M., Popova, Z., Steinberg, K.-H., Becker, K., Proc. 4th Int. Symp. Het. Cat., Varna 1979, II, 461.
17. Steinberg, K.-H., Becker, K., Bremer, H., Franke, W., Chem. Techn. 29, 269 (1977).
18. DD P 111 091, 10. 10. 1973
19. Breck, D.W., Zeolite Molecular Sieves, Whiley & Sons, N. Y. 1974, p. 143.
20. DD P 136 345, 8. 5. 1978, 136 397, 8. 5. 1978, 151 557, 14.9.79.

HYDROCRACKING OF C_9 THROUGH C_{11} NAPHTHENES ON Pd/LaY AND Pd/HZSM-5 ZEOLITES

S. ERNST, J. WEITKAMP
Engler-Bunte Institute, Division of Gas, Oil, and Coal, University of Karlsruhe, D-7500 Karlsruhe 1, Federal Republic of Germany

ABSTRACT

The pure naphthenes propylcyclohexane, butylcyclohexane, and pentylcyclohexane were comparatively converted on 0.27 Pd/LaY and 0.27 Pd/HZSM-5 zeolite under hydrogen pressure. On the Y type zeolite, the rate of hydrocracking increases sharply as the carbon number of the naphthene is raised from C_9 to C_{11}. Moreover, on this zeolite, the so-called paring reaction takes place if the naphthene contains at least ten carbon atoms. Hydrocracking is then extraordinarily selective. Mechanistically, the paring reaction requires a bulky carbocation intermediate which, expectedly, does not form in Pd/HZSM-5. As a consequence, hydrocracking is much less selective in the medium pore zeolite. This is an interesting example for a *loss of selectivity* under conditions of steric constraints. Hydrocracking of butylcyclohexane is recommended as a potential test reaction for estimating the effective pore width of zeolites with unknown structures.

INTRODUCTION

In the past, valuable insight was gained into the mechanisms of hydrocarbon conversion by model compound studies over bifunctional catalysts. Most of these investigations were conducted with various alkanes. It has been emphasized [1] that such model alkanes should contain at least eight carbon atoms if non-typical side reactions are to be avoided. Recently, the conversion of n-decane in acidic zeolites loaded with a noble metal has been proposed as a test reaction for estimating effective pore widths of zeolites with unknown structures [2].

Much less work has been done with alkyl substituted naphthenes, in spite of the fact that such hydrocarbons represent another major class of petroleum constituents. In this context, the research done at

Chevron more than two decades ago [3] deserves particular attention. These early investigations were performed with non-zeolitic catalysts, e.g., sulfided Ni/SiO_2-Al_2O_3 and a variety of cyclic hydrocarbons. In a recent study, the reactions of C_6 through C_8 naphthenes in bifunctional Y and pentasil type zeolites were compared [4]. These prior investigations are now extended to C_9 through C_{11} naphthenes. An interesting example for a reaction will be presented which proceeds much *less selective* in a zeolite of medium pore width than in large pore catalysts.

EXPERIMENTAL

The pure naphthenes propylcyclohexane (P-CHx, purity >99.9 wt.-%), butylcyclohexane (B-CHx, purity 99.1 wt.-%), and pentylcyclohexane (Pe-CHx, purity 99.4 wt.-%) were comparatively converted on 0.27 Pd/LaY-72 and 0.27 Pd/HZSM-5 zeolite under hydrogen pressure. The flow type apparatus with a fixed bed reactor has been described elsewhere [5].

The Pd content, the molar ratio Si/Al, and the degree of lanthanum exchange of the Pd/LaY zeolite amounted to 0.27 wt.-%, 2.46, and 72 equiv.-%, respectively [4]. HZSM-5 zeolite was prepared according to ref. [6] by first stirring a gel with the molar composition 41.5 SiO_2 : 1 $Al(NO_3)_3$: 10 NaOH : 70 TtPAOH : 11 NH_4OH : 3200 H_2O : 525 glycerol for five days at 200 °C in a stainless steel autoclave. The resulting material was calcined in air at 400 °C for two days, ion exchanged with a 2n solution of NaCl, and then again calcined at 540 °C. It was then ion exchanged with a 2n solution of NH_4Cl at 80 °C and calcined in flowing oxygen, the temperature being 540 °C. In all calcination steps, the heating rate was 20 °C/h. X-Ray diffraction showed that the sample was cristallographically pure. Morphologically, it consisted of rectangular crystallites with a size of about 5 µm. IR spectroscopy indicated OH stretching bands at ca. 3610 and 3745 cm^{-1}. The latter band has been assigned to extra lattice or amorphous material [7]. Chemical analysis gave molar ratios Si/Al and Al/Na of 40 and 38, respectively. To obtain the bifunctional form, HZSM-5 was exchanged with the theoretical amount of $[Pd(NH_3)_4]Cl_2$ in water, such as to achieve a Pd content of 0.27 wt.-%. Both zeolite catalysts were pressed binder-free and used in a particle size between 0.2 and 0.3 mm. They were pretreated successively in a purge of O_2 at 300 °C, a purge of N_2 at 350 °C and a purge of H_2 at 300 °C.

The products formed from the model naphthenes were analyzed by high resolution capillary GLC in the on-line mode. Polypropylene gly-

col was routinely employed as stationary phase. Supplementary off-line analyses were carried out on a different stationary phase, viz. SE 54, using liquid product samples which were condensed at ca. -190 °C from the product stream.

In all catalytic runs, the partial pressures of the feed hydrocarbon and hydrogen at the reactor inlet were 19.4 kPa and 2.0 MPa, respectively. The reaction temperature was varied between 200 and 300 °C. Unless otherwise stated, W/F_{HC} amounted to 140 g·h/mol.

RESULTS AND DISCUSSION

Conversions and yields. During hydroconversion of naphthenes, the following reactions must be distinguished: Skeletal isomerization, aromatization, ring opening to alkanes with the carbon number of the feed, and hydrocracking into products with a lower carbon number. No aromatics were detected under the conditions applied in this study. Typical product yields are shown in Fig. 1. The naphthenes formed by isomerization and the alkanes formed by ring opening were lumped because, at these elevated carbon numbers, they could not be resolved satisfactorily. Conversions can be derived from the data in Fig. 1 by summing up $Y_{Iso.} + Y_{Ro.} + Y_{Cr.}$. It will be noted that both zeolites do not differ too much in their activities. However, marked differences are encountered in the selectivities: On Pd/HZSM-5 there is only little iso-

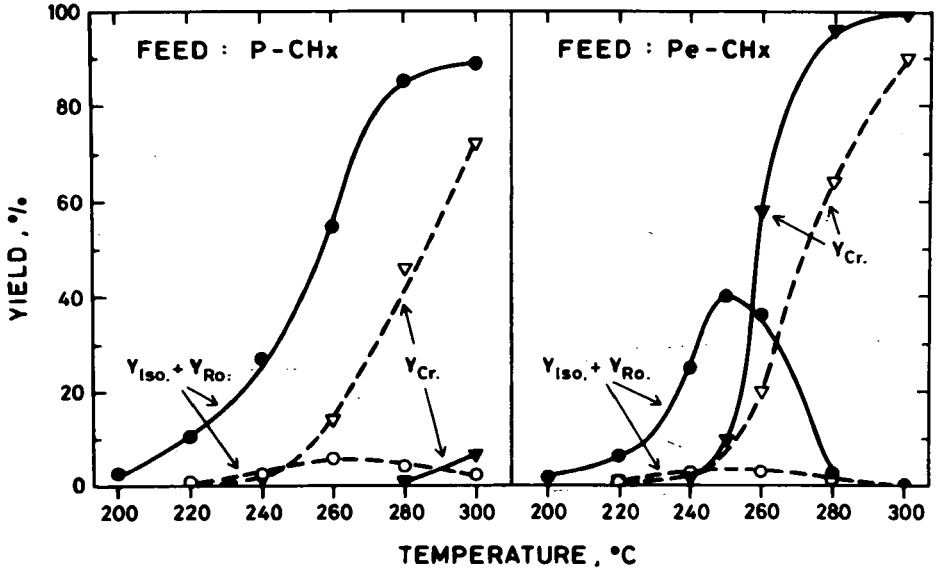

Fig. 1. Yields of products from propylcyclohexane and pentylcyclohexane on Pd/LaY (full curves) and Pd/HZSM-5 (dashed curves).

merization and ring opening, irrespective of the carbon number of the feed and the conversion. On Pd/LaY, by contrast, there is no hydrocracking at all, as long as the conversion is limited to a certain value. It is an important result that, on the large pore zeolite, propylcyclohexane is hydrocracked much more sluggishly than its homologue with two additional carbon atoms.

Fig. 2 clearly demonstrates that, in the homologous series of naphthenes, the rate of hydrocracking in *large pore* zeolite catalysts increases drastically from C_9 to C_{11}. It will be shown below that this is a direct consequence of the mechanism of ionic ß-scission. Earlier experiments with a comparable catalyst revealed [8] that *alkanes* exhibit an analogous jump in the rate of hydrocracking between C_7 and C_9 (see dashed curve in Fig. 2).

Selectivities of hydrocracking in Pd/LaY. Pertinent selectivities of hydrocracking the C_9 through C_{11} naphthenes on the large pore zeolite are depicted in Fig. 3. All curves are nearly symmetrical indicating an essentially pure primary cracking [8]. P-CHx gives mainly $C_4 + C_5$ beside smaller amounts of C_3 and C_6. This carbon number distribution resembles the one which is obtained from n-nonane on, e.g., Pt/CaY zeolite [8]. The occurrence of some C_8 and C_7 as well as the

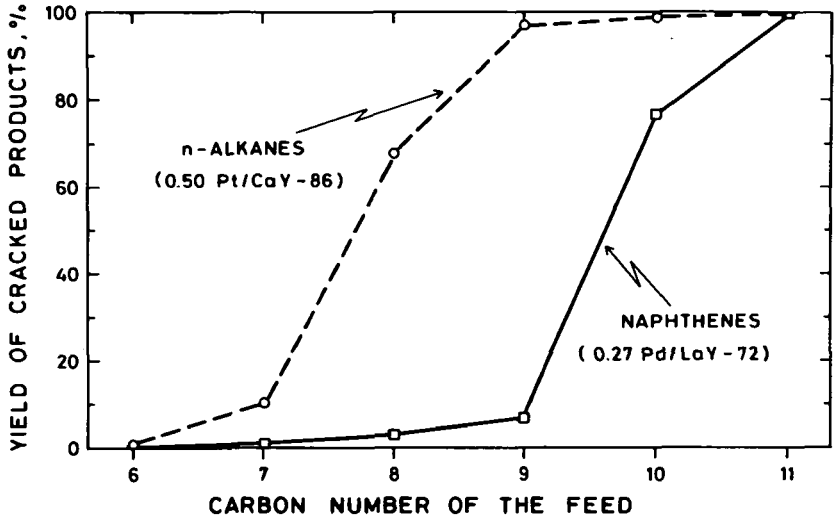

Fig. 2. Hydrocracking reactivities of n-alkanes and naphthenes on comparable Y type zeolite catalysts (n-alkanes: T = 310 °C, P_{HC} = 220 kPa, P_{H_2} = 3.7 MPa, W/F_{HC} = 85 g·h/mol, cf. ref. [8]; naphthenes: T = 300 °C, P_{HC} = 19.4 kPa, P_{H_2} = 2.0 MPa, W/F_{HC} = 140 g·h/mol, M-CPn and M-CHx, unpublished results from this laboratory, E-CHx cf. ref. [4], P-CHx, B-CHx, and Pe-CHx, this study).

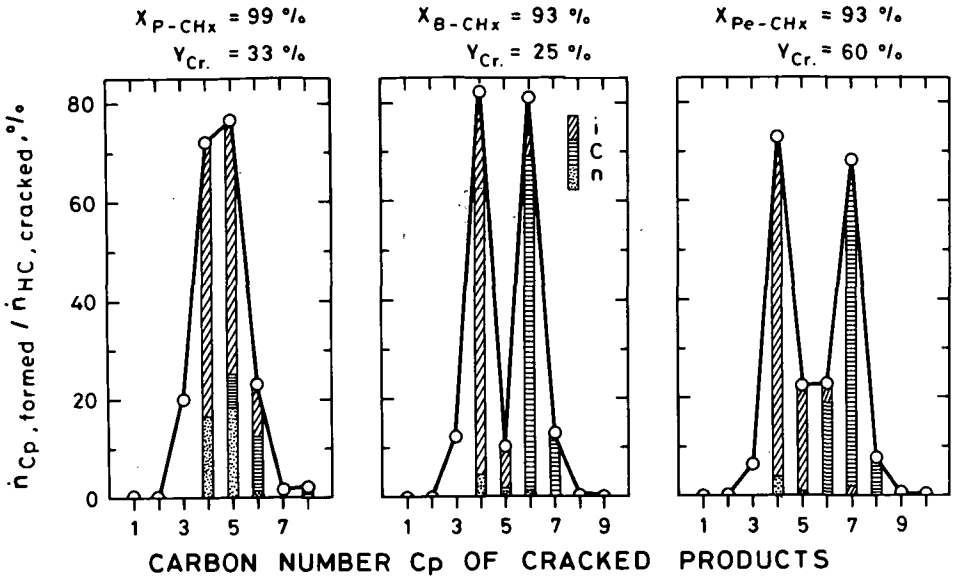

Fig. 3. Selectivities of hydrocracking on Pd/LaY zeolite (P-CHx: T = 300 °C, W/F_{P-CHx} = 570 g·h/mol; B-CHx: T = 280 °C, W/F_{B-CHx} = 140 g·h/mol; Pe-CHx: T = 260 °C, W/F_{Pe-CHx} = 140 g·h/mol).

slight surplus of C_6 and C_5 over C_3 and C_4, respectively, can be attributed to a disproportionation type of side reaction [9]. B-CHx and Pe-CHx give distribution curves which differ extremely from those encountered with paraffinic model hydrocarbons, e.g., n-decane and n-undecane [8]. In particular, very little C_5 or C_5+C_6, respectively, are formed from these naphthenes. Note also that the i-alkanes strongly prevail in the C_4 and C_5 fractions, whereas the C_6 and C_7 moieties consist of naphthenes to a very large extent. All these features of hydrocracking C_{10} and C_{11} naphthenes on large pore catalysts have been reported earlier by Chevron researchers who used a non-zeolitic NiS/SiO_2-Al_2O_3 catalyst and a variety of isomeric C_{10} and C_{11} naphthenes [3,10]. Even tetramethylcyclohexanes gave essentially identical product distributions. In a formal sense, then, the methyl substituents were pared from the naphthenic ring and released as i-butane. Hence, the Chevron group coined the term *paring reaction*.

The mechanism of the paring reaction is easily understood on the basis of bifunctional catalysis and conventional carbocation chemistry. Following a recent nomenclature proposal [11], the naphthenic system tends to undergo *exocyclic type A* ß-scission which requires a minimum of 10 carbon atoms [9]. Precursors of these type A ß-scissions are

α,α,γ-tribranched carbenium ions which are formed by rapid ionic rearrangements from a carbenium ion with the skeleton of the feed. Two exocyclic type A ß-scissions are possible for C_{10} naphthenes. They are shown in Fig. 4 (top). It is evident that, after the usual stabilization steps involved in bifunctional catalysis, they both lead to i-butane and methylcyclopentane as the exclusive products. These are, indeed, strongly favored on Pd/LaY (Fig. 3). In the lower part of Fig 4, some type B [11] ß-scissions are sketched which explain the occurrence of several side products (propane, n-butane, cyclohexane, and C_7 naphthenes).

It is evident from Fig. 4 that type A ß-scissions start from a relatively bulky precursor which carries at least one quaternary carbon atom. It is questionable whether such precursors can be accommodated or formed in a medium pore zeolite such as Pd/HZSM-5 [12] at the temperatures employed in this study. If not, then one would expect that hydrocracking in Pd/HZSM-5 necessarily proceeds via type B (or even type C [11]) ß-scissions. It can be shown that such a route would render hydrocracking of C_{10} or C_{11} naphthenes much *less selective* in Pd/HZSM-5 than in a large pore zeolite.

Selectivities of hydrocracking in Pd/HZSM-5. Selectivities of hydrocracking in Pd/HZSM-5 are shown in Fig. 5. The deviations from symmetry are now much stronger indicating a considerable extent of secondary cracking reactions. It is, moreover, seen that on Pd/HZSM-5,

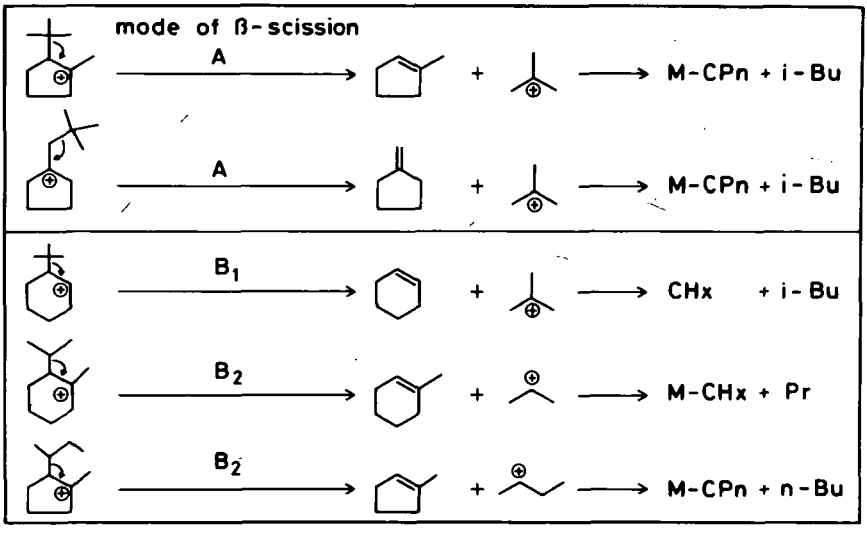

Fig. 4. Exocyclic type A and type B ß-scissions (for nomenclature see ref. [9] or [11]) of cycloalkylcarbenium ions with 10 carbon atoms (probable mechanisms of cleavage in Pd/LaY).

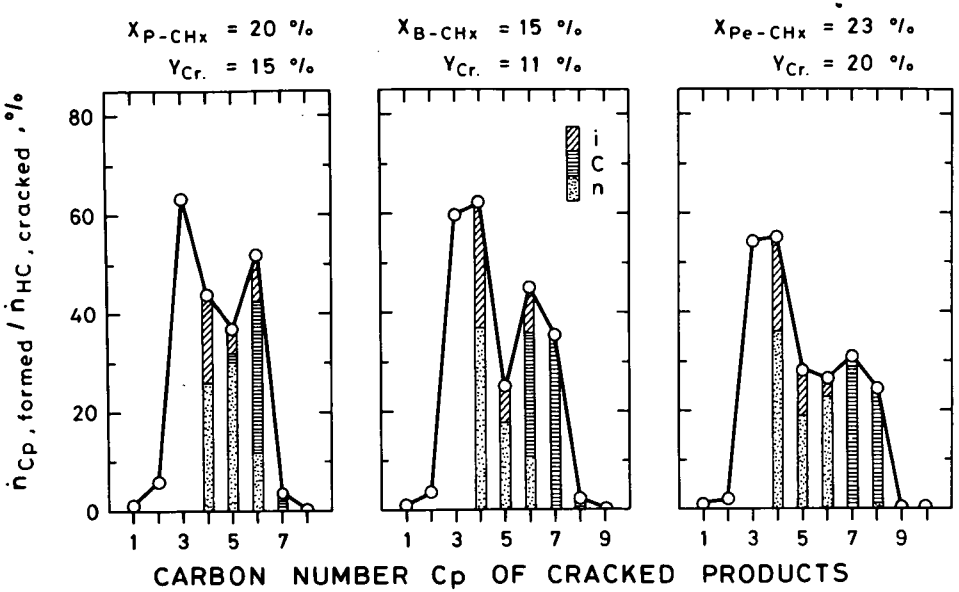

Fig. 5. Selectivities of hydrocracking on Pd/HZSM-5 zeolite (P-CHx: T = 260 °C; B-CHx: T = 250 °C; Pe-CHx: T = 260 °C).

much more C_3 and C_{m-3} are formed than on Pd/LaY. In principle, both these results have been found earlier in hydrocracking of alkanes on Pt/HZSM-5 [11]. Another feature of hydrocracking in 0.27 Pd/HZSM-5 is the formation of some methane and ethane. To account for their occurrence, either hydrogenolysis on Pd or ionic cleavage via non-classical cycloalkylcarbonium ions [13] can be invoked. From the facts that these same products do not form on 0.27 Pd/LaY (Fig. 3) which contains the same amount of Pd, and that there are more moles of C_2 than C_1 [13], one might favor the second possibility.

However, in the present context, the most striking result is that B-CHx and Pe-CHx indeed hydrocrack with a much lower selectivity than on Pd/LaY: Not only are the valleys at C_5 or C_5+C_6 much less pronounced, but many more individual hydrocarbons occur in the cracked products. Note, for example, that starting from B-CHx, the molar i-butane/n-butane ratio is around 0.7 compared to ca. 20 on Pd/LaY. A low i-butane/n-butane ratio of 0.8 has also been reported for hydrocracking of cyclodecane on Pt/HZSM-5 [14]. It is unlikely that the preferred formation of n-butane over i-butane in Pt/ or Pd/HZSM-5 is due to product shape selectivity since the diffusion coefficients of these two isomers in a pentasil type zeolite were shown to differ only slightly from each other [15]. Rather, the loss of selectivity in Pd/HZSM-5 as compared to Pd/LaY (or any other large pore catalyst)

probably results from the fact that the bulky precursors required for type A ß-scissions cannot be formed in the pentasil type channels. Hence, even with B-CHx or Pe-CHx type B and/or type C ß-scissions [11] take place in Pd/HZSM-5 as sketched in Fig. 6. The same principal conclusion was arrived at in a study on hydrocracking C_9 through C_{16} *alkanes* on Pt/HZSM-5. Moreover, this postulated pathway accounts for the independent finding that, in Pd/HZSM-5 (see Fig. 1), P-CHx is hydrocracked essentially as fast as Pe-CHx: C_9 naphthenes, due to their relatively low carbon number, are principally excluded from exocyclic type A ß-scissions. But if this route is forbidden on account of steri constraints, then all C_9 through C_{11} naphthenes are forced to undergo type B and/or type C ß-scissions.

Cleavage of *endocyclic* carbon-carbon bonds is a very slow reaction in large pore zeolites [9]. With C_6 through C_8 naphthenes, this effect was found to be less pronounced in pentasils [4]. It is reasonable, then, to anticipate (Fig. 6, bottom) that ring opening routes contribute to the mechanism of hydrocracking in Pd/HZSM-5. This is one way to explain the formation of, e.g., i-butane and n-hexane (see Fig. 6). Such a pathway is not in contradiction with the low yields of ring opening products (cf. Fig. 1) on Pd/HZSM-5 since the aliphatics formed by ring opening can undergo consecutive cleavage prior to leaving the intracrystalline channel system.

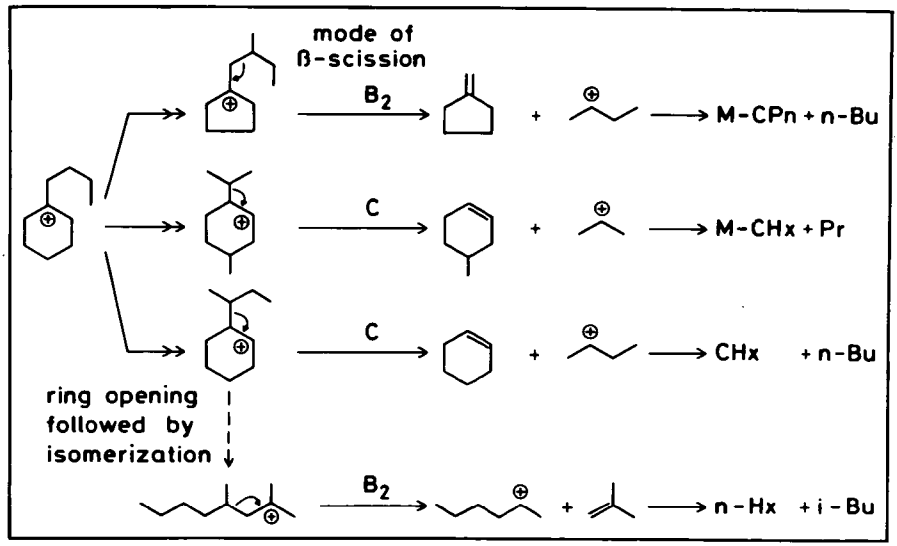

Fig. 6. Exocyclic type B and type C ß-scissions [9,11] of cycloalkylcarbenium ions with 10 carbon atoms and hydrocracking via ionic ring opening (probable mechanisms of cleavage in Pd/HZSM-5).

CONCLUSIONS

This study reveals that catalytic reactions may proceed *less selectively in a medium pore zeolite* as compared to a large pore zeolite. Hydrocracking of butylcyclohexane is an example. The phenomenon can be rationalized if one takes into account that the most selective mode (type A) of ionic ß-scission starts from very bulky intermediates. We propose hydrocracking of butylcyclohexane as another [2] test reaction the selectivity of which might furnish rapid information on the effective pore width of zeolites with unknown structures.

It has been pointed out earlier [1,8] that model *alkanes* with at least eight carbon atoms should be employed to allow for the most favorable ionic pathways of hydrocracking in large pore zeolites. It is now shown that this critical carbon number is even higher for *naphthenes*. For mechanistic studies we recommend model naphthenes with at least ten carbon atoms.

ACKNOWLEDGEMENTS

The authors are indebted to Dr. Hellmut G. Karge, Fritz-Haber-Institut der Max-Planck-Gesellschaft, Berlin, for supplying the IR spectrum of HZSM-5. We further thank Mr. Wilfried Stober for assistance with the experiments. Financial support by Max-Buchner-Forschungsstiftung and Fonds der Chemischen Industrie is gratefully acknowledged.

SYMBOLS AND ABBREVIATIONS

F_i	feed rate	$mol \cdot h^{-1}$
m	carbon number of feed	
$\dot{n}$	molar flux	$mol \cdot h^{-1}$
P_i	partial pressure	Pa
p	carbon number of cracked products	
T	temperature	°C
W	mass of dry catalyst	g
X_i	conversion	
Y_i	yield	

B	butyl	Pe	pentyl	HC	hydrocarbon
Bu	butane	Pn	pentane	i	iso-alkanes
E	ethyl	Pr	propane	Iso.	isomerization
Hx	hexane			n	normal alkane
M	methyl	C	cyclo	Ro.	ring opening
P	propyl	Cr.	hydrocracking	TtPA	tetrapropylammonium

REFERENCES

1. Weitkamp, J., Ind. Eng. Chem., Prod. Res. Dev. 21, 550-558 (1982).
2. Martens, J.A., Tielen, M., Jacobs, P.A., Weitkamp, J., Zeolites 4, 98-107 (1984).
3. Egan, C.J., Langlois, G.E., White, R.J., J. Am. Chem. Soc. 84, 1204-1212 (1962).
4. Weitkamp, J., Jacobs, P.A., Ernst, S., in: Structure and Reactivity of Modified Zeolites (P.A. Jacobs et al., Eds.), Studies in Surface Science and Catalysis, Vol. 18, Elsevier Science Publishers, Amsterdam, 1984, pp. 279-290.
5. Pichler, H., Schulz, H., Reitemeyer, H.O., Weitkamp, J., Erdöl, Kohle - Erdgas - Petrochem. 25, 494-505 (1972).
6. von Ballmoos, R., The ^{18}O-Exchange Method in Zeolite Chemistry, Salle-Sauerländer, Frankfurt, Aarau, 1981, 235 pp.
7. Jacobs, P.A., von Ballmoos, R., J. Phys. Chem. 86, 3050-3052, (1982).
8. Weitkamp, J., in: Hydrocracking and Hydrotreating (J.W. Ward, S.A. Qader, Eds.), ACS Symp. Ser. 20, American Chemical Society, Washington, D.C., 1975, pp. 1-27.
9. Weitkamp, J., Ernst, S., Karge, H.G., Erdöl, Kohle - Erdgas - Petrochem. 37, 457-462 (1984).
10. Sullivan, R.F., Scott, J.W., Heterogeneous Catalysis, Selected American Histories (B.H. Davis, W.P. Hettinger, Jr., Eds.), ACS Symp. Ser. 222, American Chemical Society, Washington, D.C., 1983, pp. 293-313.
11. Weitkamp, J., Jacobs, P.A., Martens, J.A., Appl. Catal. 8, 123-141 (1983).
12. Haag, W.O., Lago, R.M., Weisz, P.B., Faraday Discuss. Chem. Soc. 72, 317-330 (1982).
13. Haag, W.O., Dessau, R.M., Proc. 8th Intern. Congr. Catal., Vol. 2, Verlag Chemie, Weinheim, Deerfield Beach, Basel, 1984, pp. 305-316.
14. Jacobs, P.A., Tielen, M., Proc. 8th Intern. Congr. Catal., Vol. 4, Verlag Chemie, Weinheim, Deerfield Beach, Basel, 1984, pp. 357-369.
15. Paravar, A., Hayhurst, D.T., Proc. 6th Intern. Zeolite Conf. (D. Olson, A. Bisio, Eds.), Butterworths, Guildford, 1984, pp. 217-224.

KINETIC STUDY OF n-HEPTANE HYDROCRACKING OVER HZSM-5 AND Pt-HZSM-5 CATALYSTS

G. GIANNETTO, G. PEROT and M. GUISNET
Unité Associée au CNRS 350, Catalyse Organique, U.E.R. Sciences, 40 avenue du Recteur Pineau, 86022 Poitiers Cedex, France

ABSTRACT

A kinetic study of the n-heptane transformation has been carried out on HZSM-5 and on Pt-HZSM-5 under low pressure (1 bar, pH_2/pnC_7 from 10 to 35) and under high pressure (30 bar, pH_2/pnC_7 from 4 to 15). There are fundamental differences in the distribution of the products in each case. On HZSM-5, cracking is the main reaction ; under low pressure the light products are formed by scission of C_7 carbenium ions and under high pressure by scission of bimolecular intermediates. On Pt-HZSM-5 n-heptane is isomerized into methylhexanes and cracked into isobutane and propane. The formation of these light alkanes results from the scission of tertiary carbenium ions with a 2-methylhexane skeleton. The high rate of this scission is a peculiarity of the porous network of the ZSM-5 zeolite. Moreover the change in reaction rate with n-heptane pressure can only be explained by a concentration effect in the zeolite pores.

INTRODUCTION

The hydroisomerization and hydrocracking of n-alkanes on Pt-HY catalysts have been the subject of numerous studies and we now know the factors which determine the activity, the selectivity and the stability of these catalysts [1-7]. The catalysts in which the noble metal is deposited on a shape-selective zeolite have been studied in much less detail. The main work in this field is that of Weitkamp et al on the transformation of C_9-C_{16} n-alkanes on Pt-HZSM-5 which reveals a variety of shape-selectivity effects [8]. However, no kinetic study has been carried out on these catalysts.

In the kinetic study of the n-heptane transformation on Pt-HZSM-5 and on HZSM-5 reported here, a large range of operating conditions has been explored : pH_2 from 1 to 45 bar, pnC_7 from 0.03 to 7 bar, T from 250°C to 380°C. We shall try to define the factors which govern the activity and the selectivity of these catalysts.

EXPERIMENTAL

Catalysts. HZSM-5 (Si/Al = 40) synthesized according to Mobil Patents [10] was used in extrudates : HZSM-5 (30 wt %) in an alumina binder (70 wt %). Two samples of Pt-HZSM-5 containing respectively 0.4 wt % Pt (0.4 Pt-HZSM-5) and 1 % (1 Pt-HZSM-5).

were prepared by competitive ion exchange of extrudates with a 1/200 $Pt(NH_3)_4Cl_2/NH_4NO_3$ solution. The conditions of calcination under dry air (300°C) and reduction under hydrogen (500°C) are those previously defined as leading to the best dispersion of platinum (H/Pt = 0.7) [11].

Reactions. n-Heptane hydrocracking was studied in dynamic reactors working respectively under normal pressure and under high pressure. The reaction mixtures were analyzed on line using a 100 m Squalane Scot capillary column.

RESULTS

1. Activity and selectivity. The total activities of the three catalysts determined at 260°C, total pressure P_T = 30 bars, pH_2/pnC_7 = 9, are very close. However the influence of P_T (for pH_2/pnC_7 = 9) on the reaction rates is clearly less significant for the bifunctional catalysts : thus under normal pressure the activity of Pt-HZSM-5 is about 25 times higher than that of HZSM-5. The influence of temperature however is more pronounced on the two Pt-HZSM-5 samples : the apparent activation energy is equal to 36 kcal $mole^{-1}$ whereas on ZSM-5 it is only 21.5 kcal $mole^{-1}$.

The selectivities of the HZSM-5 and of the Pt-HZSM-5 catalysts are different (tables 1 and 2) : if the formation of light products is always the main reaction, the isomerization of n-heptane is less significant on HZSM-5 than on Pt-HZSM-5 (table 2). On HZSM-5, C_8-C_{11} alkanes (mainly linear or monobranched) are formed under high pressure. Under normal pressure, these alkanes are no longer observed and the isomerization/cracking rate ratio (I/C) is very small (table 2).

Table 1

Distribution of the products of n-heptane isomerization at 260°C

pH_2 = 27 bar, pnC_7 = 3 bar for a conversion equal to about 5 %.

Catalysts	$2mC_6$	$3mC_6$	$3eC_5$	$2,3dmC_5$	$2,4dmC_5$	$2,2dmC_5$	Other
H ZSM-5	46.2	35.1	4.5	8.3	3.3	2.6	0
0.4 PtHZSM-5	65.7	31.6	1.0	0.6	0.8	0.3	0
1 PtHZSM-5	66.1	32.0	0.9	0.4	0.6	0	0
Equilibrium (9)	21.7	19.8	2.4	28.1	6.5	10.5	11.0

The distribution of isomers and light products differs on HZSM-5 and on Pt-HZSM-5 (tables 1 and 2) :

- thus on the Pt-HZSM-5 catalysts at low conversion the n-heptane isomers are made up of 2- and 3-methylhexanes for 97 % and for more than 95 % at 50 % conversion whereas on HZSM-5 they constitute only 80 % of the n-heptane isomers at low conversion and less than 75 % at 50 % conversion. On all these catalysts the other isomers

formed are, in order of importance 2,3-dimethylpentane, 3-ethylpentane, 2,4-dimethyl pentane and 2,2-dimethylpentane (3,3-dimethylpentane and 2,2,3-trimethylpentane are not found). On Pt-HZSM-5 catalysts, 2-methylhexane is clearly favored at low conversion : the rate ratio of the formation of 2- and 3-methylhexanes is 2.1 for a conversion of 5 % (table 1) ; this ratio approachs its equilibrium value (about 1.2) at very high conversion rates. On HZSM-5, methylhexanes are initially formed in a ratio close to that of equilibrium (1.3 for a 5 % conversion) : curiously this ratio decreases as the conversion rate rises, dropping well below its equilibrium value, e.g. 0.85 for a conversion of about 50 %.

- On Pt-HZSM-5 catalysts, propane and isobutane (in equimolar quantities) are practically the only cracking products, whatever the degree of conversion or the n-heptane pressure (table 2). On HZSM-5, C_3 to C_6 olefinic and saturated hydrocarbons are formed. The iso/n ratio is equal to 1 for C_4 and less than 1 for C_5 and C_6 products. The lower the n-heptane pressure, the higher the quantities of olefins, C_3 and C_4 (table 2).

Table 2

Distribution of the products of n-heptane transformation at 260°C for a conversion equal to about 5 %. I = Isomerization, C = Cracking.

	P_T	PnC_7	C_2	C_3	iC_4	nC_4	iC_5	nC_5	iC_6	nC_6	$iC_4^=/iC_4$	I/C
HZSM-5	30	3	0.3	23.1	20.3	20.4	9.0	14.0	5.8	7.1	0.1	0.15
0.4 PtHZSM-5	30	3	0	50.8	47.7	1.0	0.1	0.3	0	0.1	0	0.55
1 PtHZSM-5	30	3	0	50.5	48.4	0.8	0.1	0.2	0	0	0	0.65
HZSM-5	1	0.03	0	41.6	23.9	19.1	2.6	10.5	0.85	1.85	0.75	0.03
1 PtHZSM-5	1	0.03	0	51.7	47.8	0.4	0	0.05	0	0.1	0	0.45

2. Influence of hydrogen and n-heptane pressure on the reaction rate. On HZSM-5 the reaction rate increases proportionally to n-heptane pressure for low values (< 0.1 bar) and with an order value of 0.6-0.8 for high values (> 10 bar) ; it does not depend on hydrogen pressure (Fig. 1 and 2). On the other hand, on the Pt-HZSM-5 catalysts, the rate is inversely proportional to hydrogen pressure (order value $\simeq -1$) ; it increases with n-heptane pressure for low values, but remains practically constant for high values.

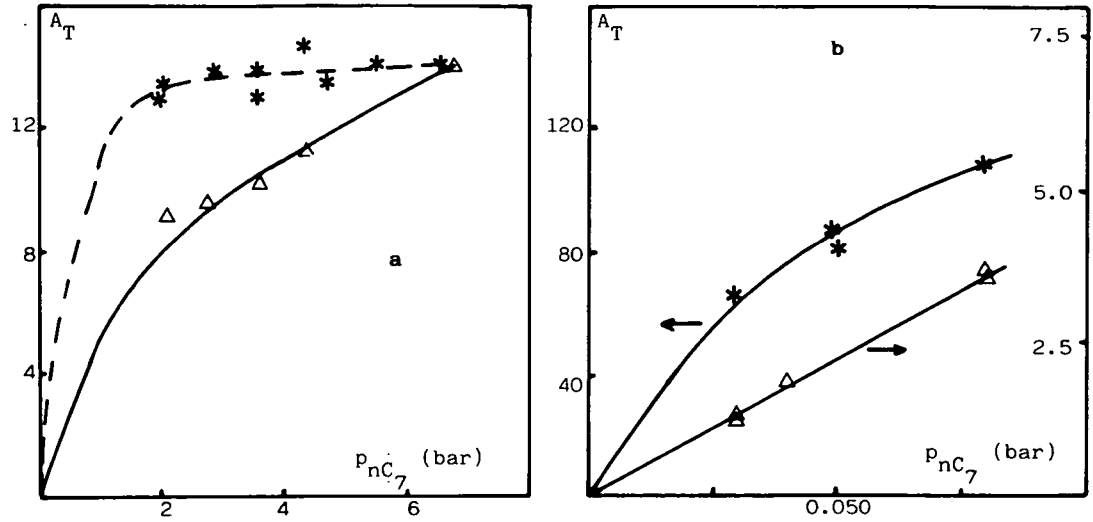

Fig. 1. Influence of n-heptane pressure on the total activities $A_T(10^{-3}$ mole $h^{-1}g^{-1})$ on HZSM-5 (△) and on Pt-HZSM-5 (✱) under high pressure (**a**) and low pressure (**b**).

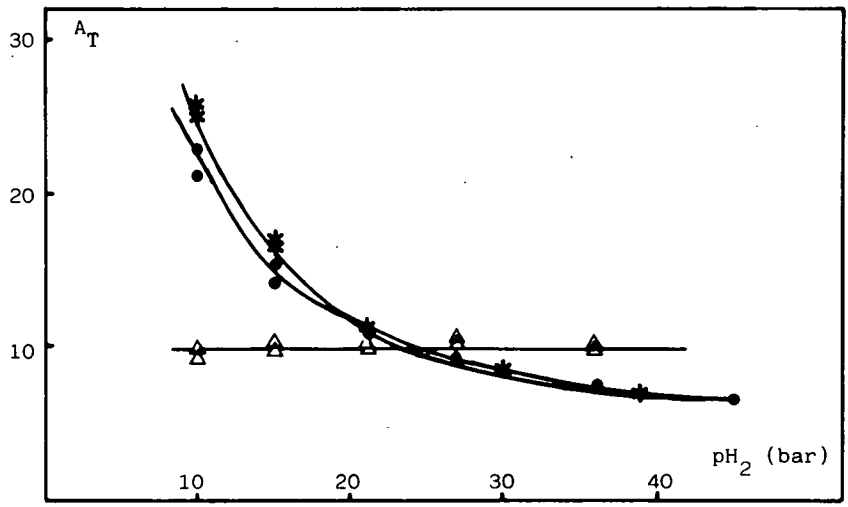

Fig. 2. Influence of hydrogen pressure on the total activities $A_T(10^{-3}$ mole $h^{-1}g^{-1})$ over HZSM-5 (△), 0.4 Pt-HZSM-5 (●) and 1 Pt-HZSM-5 (✱).

DISCUSSION

On catalysts made up of a noble metal deposited on an acid support, three modes of alkane tranformation can be found : the first involves only the metallic sites,

the second only the acid sites and the third successively the metallic and the acid sites (bifunctional mechanism). The relative significance of these three mechanisms depends essentially on the acid strength of the carrier and on the operating conditions [12, 13]. On Pt-HZSM-5 catalysts, C_1 and C_2 hydrocarbons are not formed and transformation on metallic sites (hydrogenolysis...) is probably very slow. The second reactionnal mode can also be excluded since Pt-HZSM-5 and HZSM-5 behave in a completely different way. On the other hand the absence of the bulkier isomers in the products : 3,3-dimethylpentane and 2,2,3-trimethylpentane suggests that the n-heptane transformation occurs inside the ZSM-5 porous system.

1. Factors governing product distribution. On HZSM-5, as on the majority of acid catalysts, cracking is the main reaction. Selectivity depends on n-heptane presssure :

- at low pressure, C_3 and C_4 hydrocarbons (the products expected from a simple scission) constitute more than 80 % of the cracking products and they are formed in equimolar amounts. Their formation can be explained by the scission of mono or bi-branched C_7 carbenium ions formed by rapid isomerization of the linear C_7 carbenium ions (nC_7^+). The formation of these nC_7^+ carbocations by hydride transfer from n-heptane to a preadsorbed carbenium ion is very likely the limiting step of this reaction.

$$nC_7 + R^+ \rightleftharpoons nC_7^+ + RH$$

- At high pressure, C_3 hydrocarbons constitute only 20 % of the cracking products, the formation of C_4, C_5 and C_6 alkanes being highly favoured. Moreover alkanes with more than 7 carbons and n-heptane isomers are formed. All these products can be explained by the reactional scheme proposed for butane disproportionation on mordenite [14]: formation of bimolecular intermediates followed by their rearrangement and scission.

$$2C_7 \overset{\text{slow}}{\rightleftharpoons} C_{14} \overset{\text{rapid}}{\rightleftharpoons} C_{14}' \longrightarrow \begin{cases} C_3 + C_{11} \\ C_4 + C_{10} \\ C_5 + C_9 \\ C_6 + C_8 \end{cases}$$

The formation of the bimolecular intermediates (C_{14} ions carbenium) would be the kinetically limiting reaction [14]. This formation is probably favored by the very high concentration of n-heptane in the vicinity of the active sites as a result of the physical adsorption in the narrow pores of the HZSM-5 zeolite.

On Pt-HZSM-5 catalysts isomerization accompanies the cracking of n-heptane. However, whereas on Pt-HY the n-heptane transformation occurs through the following successive scheme :

$$nC_7 \rightleftharpoons mC_6 \rightleftharpoons dmC_5 \rightleftharpoons \text{cracking products}$$

on Pt-HZSM-5 the reactional scheme is different, i.e. the cracking products are primary products (reaction 2) and isomerization to dimethylpentanes is very slow :

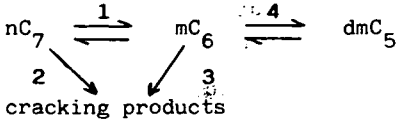

The cracking products being constituted of about 50 % of isobutane and 50 % of propane (table 2), evidently they cannot result from the scission of a carbenium ion with a n-heptane skeleton. The apparent reaction 2 can readily be explained using the classical bifunctional framework [6] if (i) the diffusion of the olefinic intermediates from one hydrogenating site to another is slow in comparison to their reaction on the acid sites or if (ii) these olefinic intermediates remain adsorbed on an acid site long enough to undergo, successively, isomerization and cracking. In both cases the cracking products result from the scission of a carbocation with a mono or bibranched skeleton.

On Pt-HZSM-5 2-methylhexane is clearly privileged in comparison to 3-methylhexane whereas statistically one would have expected the contrary [1]. Since these hydrocarbons diffuse at similar rates, this observation can only be explained by steric constraints in the formation and scission of protonated cyclopropanes [8] (intermediates of the transformation of n-heptane into methylhexanes). The privileged formation of 2-methylhexane found on Pt-HZSM-5 means that the reactions occuring through the protonated cyclopropane **a** are favored.

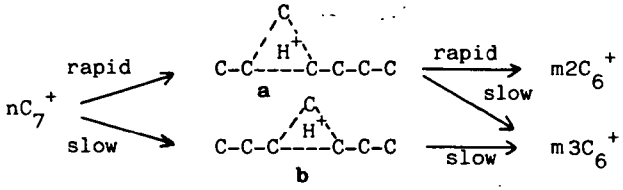

These steric constraints probably also explain why the transformation of methylhexanes into dimethylpentanes is very slow on Pt-HZSM-5. Indeed, this reaction also occurs through protonated cyclopropanes which are moreover bulkier than those invoked in the isomerization of n-heptane into methylhexanes. If such is the case, carbocations with a dimethylpentane skeleton will only be formed in small quanti-

ties and cracking products will thus only result from the scission of carbocations with a monobranched skeleton. It should be noted that this is precisely the conclusion reached by Weitkamp et al in their study of C_9-C_{16} alkane transformation on Pt-HZSM-5 [8]. However, according to the authors, the light products are a result of the scission of secondary carbocations with methylhexane skeletons. Such a mechanism cannot be considered valid here, since it would lead to n-butane rather than to the isobutane observed :

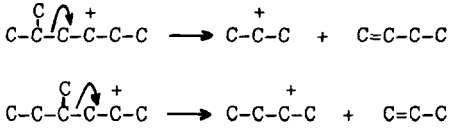

The formation of isobutane can only be explained by concerted β -scission of the tertiary 2-methyl hexane carbocation and hydride transfer [15].

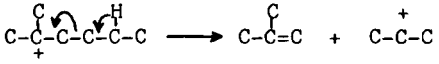

This scission, generally considered to be slow, is certainly favored in the porous structure of ZSM-5 zeolite, for the same reason as protonated cyclopropane **a**.

2. Kinetic models. The influence of hydrogen and hydrocarbon pressures on the n-heptane transformation rate over Pt-HZSM-5 is similar to that reported by Froment et al for n-alkane isomerization on Pt-USY [4,5] : hydrogen order close to -1, hydrocarbon order from 1 to 0 with increasing hydrocarbon pressure. These observations are in agreement with the classical bifunctional mechanism (Fig. 3) provided the concentration of n-alkane in the vicinity of the active sites is taken to be the concentration of physisorbed (and not gas phase) alkane.

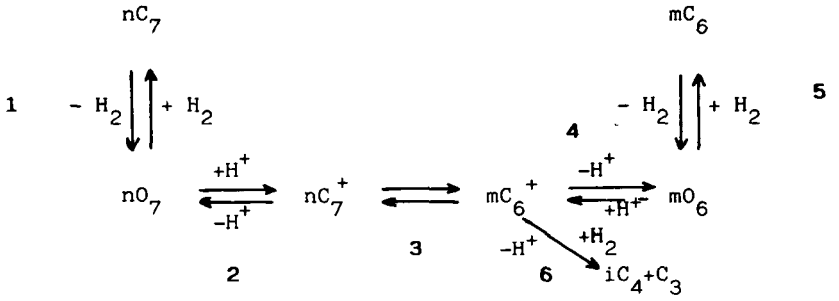

Fig. 3. n-Heptane transformation by the classical bifunctional mechanism : nC_7 : n-heptane ; nO_7 : n-heptenes ; nC_7^+, mC_6^+ : carbenium ions ; mO_6 : methylhexenes ; mC_6 : methylhexanes.

The platinum content of the catalysts is sufficient to consider the reactions on the acid sites as kinetically limiting [11]. The formation of carbocations (step 2) is very rapid, and step 3 is very likely the limiting step in cracking and isomerization. At low conversion (neglecting the reverse reaction and the adsorption of products), the transformation rate of n-heptane can be written :

$$r = \frac{k_3 \, C_m \, K_1 \, K_2 \, C_{nC_7}}{pH_2 + K_1 \, K_2 \, C_{nC_7}}$$

where k_3 is the rate constant of step 3, C_m the concentration of Brönsted sites in the zeolite, K_1 and K_2 respectively the equilibrium constants of the dehydrogenation of n-heptane (reaction 1) and of carbenium ion formation (step 2) and C_{nC_7} the concentration of physisorbed n-heptane. This concentration can be linked to the pressure of n-heptane in gas phase (p_{nC_7}) by the Langmuir-Hinshelwood equation

$$C_{nC_7} = \frac{C_{(nC_7)m} \; K_L \, p_{nC_7}}{1 + K_L \, p_{nC_7}}$$

where $(C_{nC_7})_m$ is the maximum concentration in zeolite pores and K_L the equilibrium constant of n-heptane physisorption.

$$r = \frac{k_3 \, C_m \, K_1 \, K_2 \, (C_{nC_7})_m \, K_L \, p_{nC_7}}{p_{H_2} + K_L \, p_{H_2} p_{nC_7} + K_1 K_2 (C_{nC_7})_m K_L p_{nC_7}} = \frac{a \, p_{nC_7}}{p_{H_2} + b_{pH_2} p_{nC_7} + c_{pnC_7}}$$

This equation accounts for our results : $1/r$ versus pH_2 and versus $1/pnC_7$ are straigth lines. The values of a, b, c are respectively : 3.5, 12.5, 14.

As expected, on HZSM-5 zeolite, the reaction rate does not depend on hydrogen pressure. Hydrocarbon order, equal to 1 at low pressure, remains close to this value under high pressure. This limited change can seem curious compared to the significant change observed on Pt-HZSM-5. But, as shown by the distribution of the products on HZSM-5, the reaction mechanism is not the same at low pressure (monomolecular intermediates) as it is at high pressure (bimolecular intermediates). The latter mechanism could give an alkane order value of 2, as has been observed in butane disproportionation on H mordenite [14]. The value in fact observed (0.7) is much lower, which could be explained ,as on Pt-HZSM-5, by a condensation effect in the narrow pores of HZSM-5 zeolite.

REFERENCES

1. Weitkamp, J., Ind. Eng. Chem. Prod. Res. Dev. 1982, 21, 550.
2. Jacobs, P.A., Uytterhoeven, J.B., Steijns, M., Froment, G., Weitkamp, J., Proc. 5 th Intern. Conf. Zeolites, L.V.C. Rees, Ed., Heyden, London, Philadelphia, Rheine, 1980, P. 607.
3. Steijns, M., Froment, G., Jacobs, P., Uytterhoeven, J., Weitkamp, J., Ind. Eng. Chem. Prod. Res. Dev. 1981, 20, 654.
4. Steijns, M. and Froment, G.F., Ind. Eng. Chem. Prod. Res. Dev. 1981, 20, 660.
5. Vansina, H., Baltanas, M.A. and Froment, G.F., Ind. Eng. Chem. Prod. Res. Dev. 1983, 22, 526 ; ibid 1983, 22, 531.
6. Guisnet, M. and Perot, G. : "Zeolites : Science and Technology" NATO ASI Series, F.R. Ribeiro et al, Ed., Martinus Nijhoff Publishers, The Hague, Boston, Lancaster, 1984, p. 397.
7. Perot, G., Hilaireau, P. and Guisnet, M., Proc. 6th Intern. Zèolite Conf., D. Olson and A. Bisio Eds, Butterworths, 1984, p. 427.
8. Weitkamp, J., Jacobs, P.A. and Martens, J.A., Applied Catalysis 1983, 8, 123.
9. Stull, D.R., Westrum, E.F. Jr., Sinke, G.C. : "The Chemical Thermodynamics of Organic Coumpounds" Wiley, New York, London, Sydney, Toronto, 1969.
10. Argauer, R.J. and Landolt, R.G., USP. 3.702.886/1972 ; Chang, C.D.,Lang, W.H. and Silvestri, A.J., USP. 3.894.106/1975 ; Butter, S.A., Kaeding, W.W. and Jurewicz, USP. 3.894.107/1975 ; Chang, C.D., Silvestri, A.J. and Smith, R.L., USP. 3.928.483/1976.
11. Giannetto, G., Perot, G. and Guisnet, M., "Catalysis by acids and bases", B. Imelik, C. Naccache Eds, Studies in Surface Science and Catalysis, Elsevier, to be published.
12. Ribeiro, F., Marcilly, C. and Guisnet, M., J. Catal. 1982, 78, 267.
13. Christoffel, E.G. and Paal, Z., J. Catal. 1982, 73, 30.
14. Bearez, C., Chevalier, F. and Guisnet, M., React. Kinet. Catal. Lett. 1983, 22, 405.
15. Poutsma, M.L., "Zeolite Chemistry and Catalysis", J.A. Rabo Ed. ACS Monograph 171, American Chemical Society, Washington, D.C., 1976, p. 437.

THE INFLUENCE OF TIN ON THE ACTIVITY AND SELECTIVITY OF Sn-Pd/HY ZEOLITES, IN THE HYDROCRACKING AND HYDROISOMERIZATION OF n-HEPTANE

C. HENRIQUES[a], P. DUFRESNE[b], C. MARCILLY[b], F. RAMÔA RIBEIRO[a]
GRUPO DE ESTUDOS DE CATÁLISE HETEROGÉNEA, Instituto Superior Técnico, Av. Rovisco Pais, 1096 Lisboa Codex, PORTUGAL (a)
INSTITUT FRANÇAIS DU PÉTROLE, B.P.311, 92 506 Rueil-Malmaison Cédex, FRANCE (b)

ABSTRACT

The hydrocracking and hydroisomerization of n-heptane on Sn-Pd/HY zeolites have been studied, in order to understand the influence of tin on the activity and selectivity of these catalysts.

When the tin content increases, we observe a decrease of the global activity, and a change of the selectivity with a decrease of the molar ratios: isomerization/ /cracking and monobranched/dibranched products.

The influence of tin cannot be explained only by the poisoning of the palladium by tin. In fact, the presence of the second metal will probably induce the production of highly active hydrogen species, which diffuse towards the catalyst surface, by a spillover effect, getting in competition with the n-paraffins in the adsorption over palladium. In consequence, there is a change in the balance between the acidic and hydrogenating functions, with a decrease of the hydrogenating activity.

INTRODUCTION

The hydrocracking of different petroleum cuts, from light naphtas to atmospheric vacuum residue, to produce propane, butane, gasoline, jet fuels and diesel oils [1,2] uses bifunctional catalysts, some of them composed of a noble metal (palladium) on a acidic zeolite.

The hydroisomerization of n-alcanes to upgrade the octane number of the light gasoline fractions also use bifunctional catalysts.

The balance between the acidic and the metallic functions has a great influence on the selectivity and activity of the bifunctional catalysts [3,4].

In the last years, the use of bimetallic-acidic catalysts has had a growing interest, namely for the catalytic reforming [5,6]. Consequently, it is important the clarify the role of the second metal [7,8,9] in the behaviour of the bifunctional catalysts.

The purpose of this work is to study the influence of tin on the activity and

selectivity of Sn-Pd/HY zeolites, in the hydrocracking and hydroisomerization of n--heptane.

EXPERIMENTAL

Four tin-palladium HY zeolites were prepared (with different tin contents), according to the following procedure:

- Preparation of the ammonium Y zeolite, by ion exchange of the NaY with ammonium nitrate solutions;
- Dilution of the NH_4Y in an alumina gel (50 wt.%), extrusion and calcination in wet air at 500°C for 2 hrs;
- Introduction of palladium ($Pd(NH_3)_4^{2+}$), by using the technique of ion exchange with competition [10] (the competing ion is NH_4^+);
- Calcination in dry air at 500°C, for 2 hrs, and reduction with hydrogen 2 hrs, at 450°C;
- Introduction of tin, as described in reference [11].

The percentage loadings of tin and palladium on HY zeolite were determined by X-ray fluorescence.

The metallic phase was characterized by electron probe microscopy and transmission electron microscopy.

The n-heptane transformation was carried out in a fix-bed dynamic reactor, under the following conditions: total pressure = 60 bar, molar ratio H_2/nC_7 = 6.2, temperature from 230 to 290°C.

The liquid condensates and the gaseous effluents were analyzed by GLC (100 m squalane capillary column), with a flame-ionization detector.

RESULTS

Characterization of the metallic phase

The metal contents of the catalysts are presented in Table 1:

Table 1

Metal contents of catalysts

Catalyst	Pd (wt.%)	Sn (wt.%)	Sn/Pd (molar ratio)
Pd HY	0.45	-	-
Sn/Pd HY 0.5	0.45	0.25	0.5
Sn/Pd HY 0.8	0.45	0.38	0.8
Sn/Pd HY 2.2	0.45	1.12	2.2

The characterization of the metallic phase, by electron probe microscopy, enable us to conclude that tin remains on the external surface of the catalysts and palladium is well distributed. As shown in Figure 1, with Sn/Pd HY 0.5 tin is locali

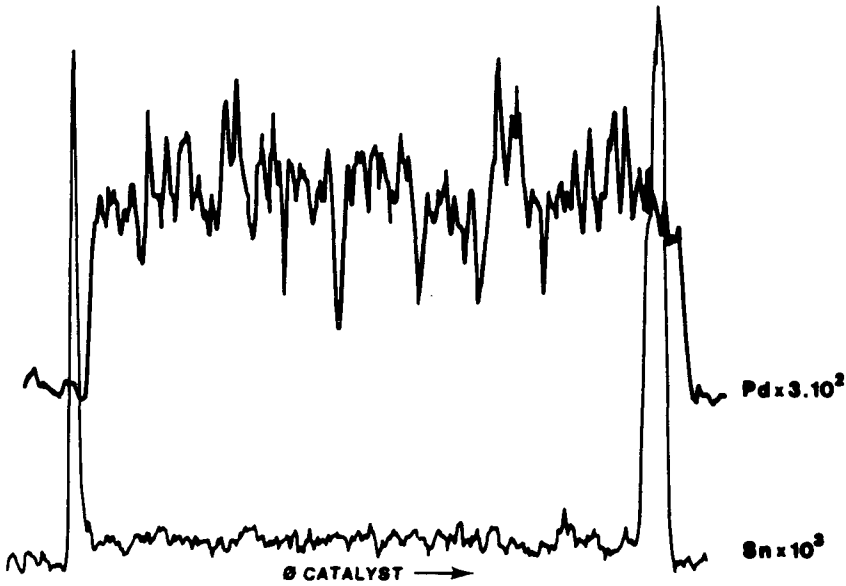

Fig. 1 Distribution of tin and palladium for Sn/Pd HY 0.5, by electron probe microscopy

zed on a thin external layer which represents about 20% of the total surface of the carrier.

Calculated values from electron microscopy of palladium dispersion and average particle size were ~ 30% and 14 A^{o}.

Catalytic Results

(i) Effect of the tin content on the activity

Figure 2 shows, for each catalyst, the n-heptane conversion as a function of the temperature.

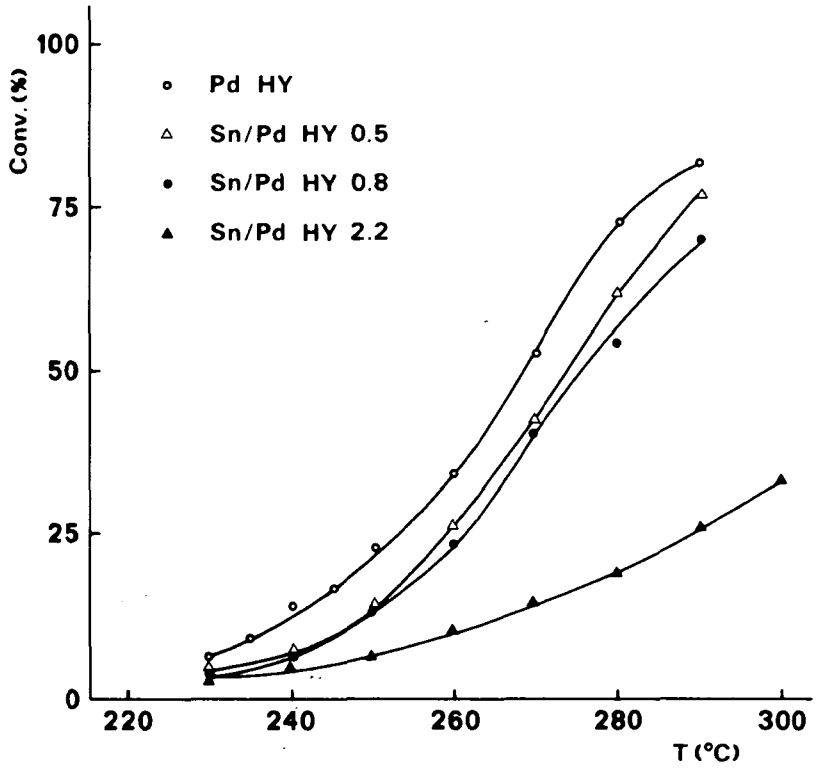

Fig. 2 - n-heptane transformation on Sn/Pd HY zeolites: conversion against temperature

We can conclude that the monometallic catalyst is the most active, and the activity, decreases with the tin content.

(ii) Influcence of the tin content on the selectivity

In Figure 3, it is represented the molar product distribution, of the transformation of n-heptane at the same conversion (30%).

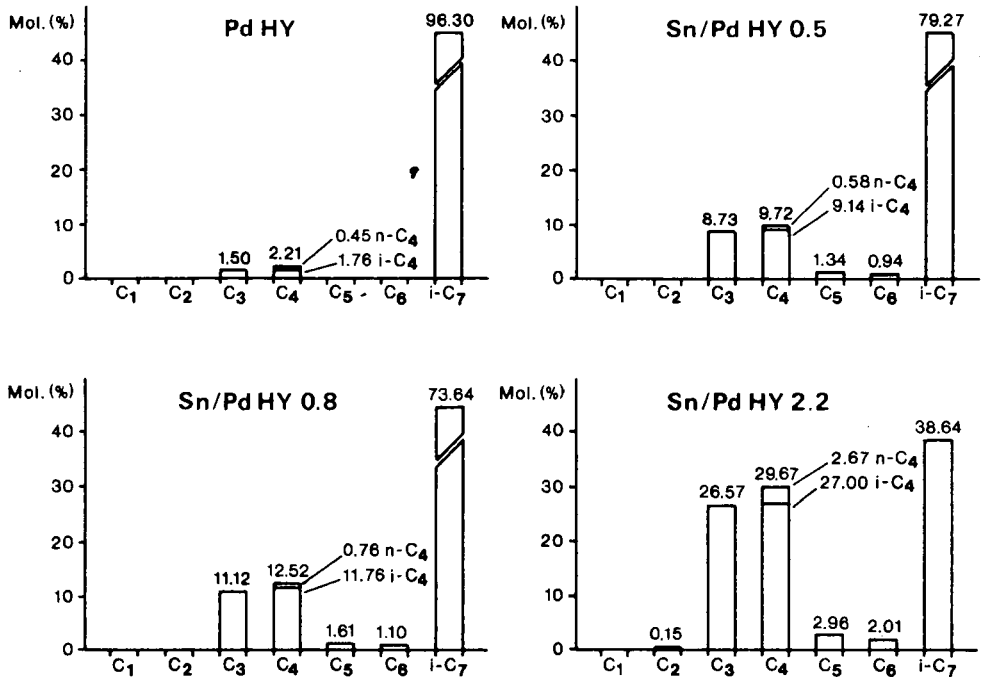

Fig. 3 Distribution of products produced by transformation of n-heptane on Sn/Pd HY zeolites for the same conversion

We can conclude that, as tin content increases, the production of C_7 isomers decreases and that of cracked products increases. For all the catalysts, the main cracking products are butanes and propane in equimolar quantities with a very high isobutane/n-butane ratio. We observe an increase of C_5 and C_6 products without formation of C_1 and C_2, as tin content increases.

Figure 4 shows for each catalyst, the evolution of the molar ratio of the isomerization/cracking products (I/C) with the conversion. It can be remarked that in all the catalysts, there is a decrease of the I/C ratio, as the conversion increases by increasing the temperature. This decreasing is more pronounced for the lowest tin content.

For a given conversion, the I/C molar ratio decreases with the tin content.

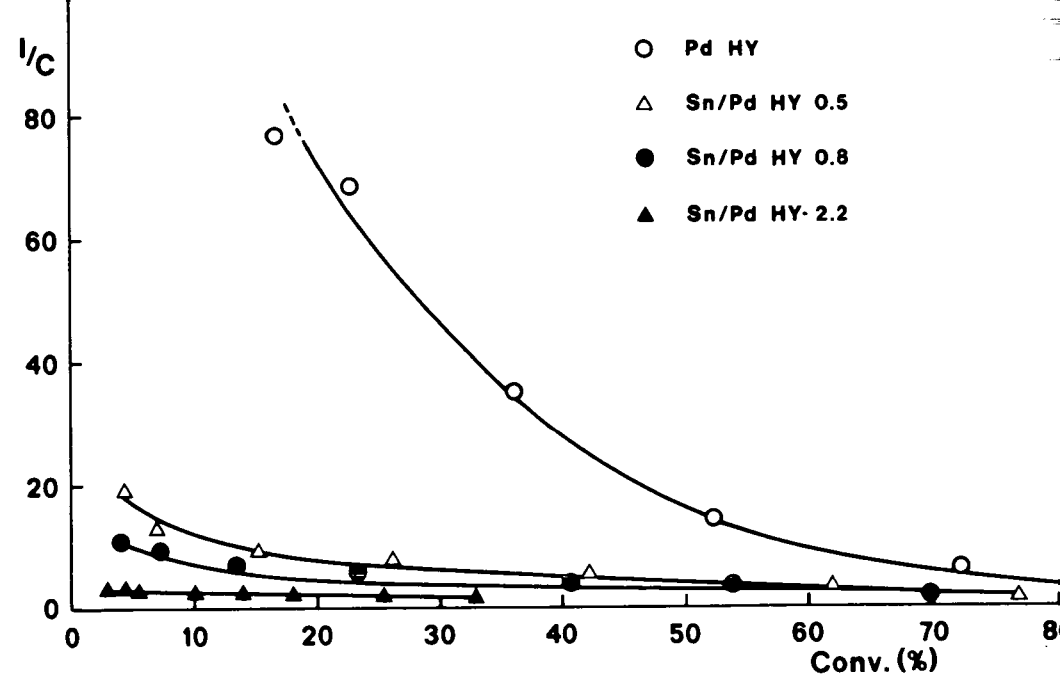

Fig. 4 Isomerization/cracking molar ratio against the conversion for the transformation of n-heptane on Sn/Pd HY zeolites

In respect of the distribution of the hydroisomerization products, Figure 5 shows the evolution of the molar ratio of the monobranched/dibranched isomers (M/D) with the conversion. As the conversion increases, there is a decrease of the M/D ratio, which is more pronounced for the lowest tin content. For a given conversion, the M/D ratio decreases as the tin content increases.

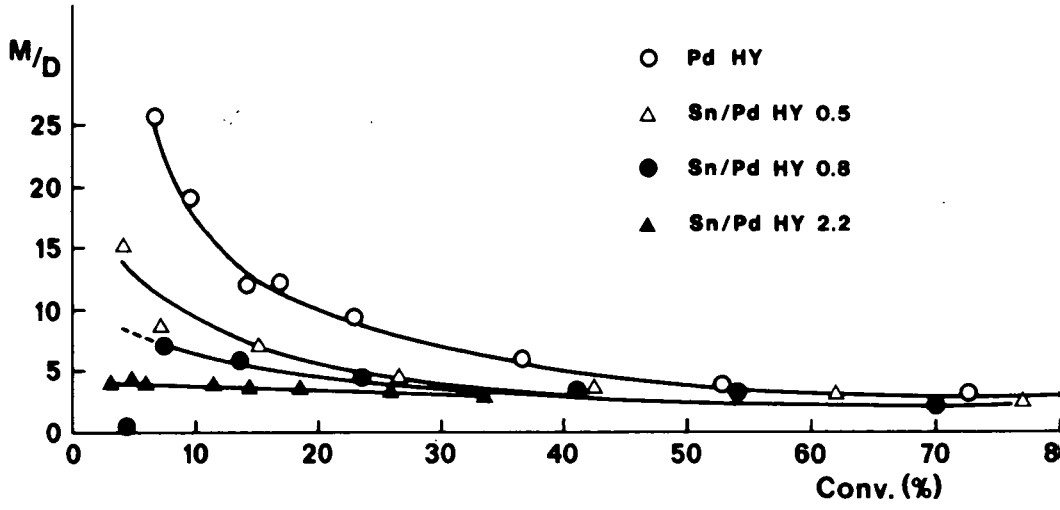

Fig. 5 Monobranched/dibranched isomers molar ratio against the conversion for the transformation of n-heptane on Sn/Pd HY zeolites

ISCUSSION

In order to understand the influence of tin on the activity and selectivity of he bimetallic Sn/Pd HY zeolites, it is important to present the bifunctional mecha- ism [12,13] scheme for the hydroisomerization and hydrocracking of n-heptane, pro- osed by Guisnet [14].

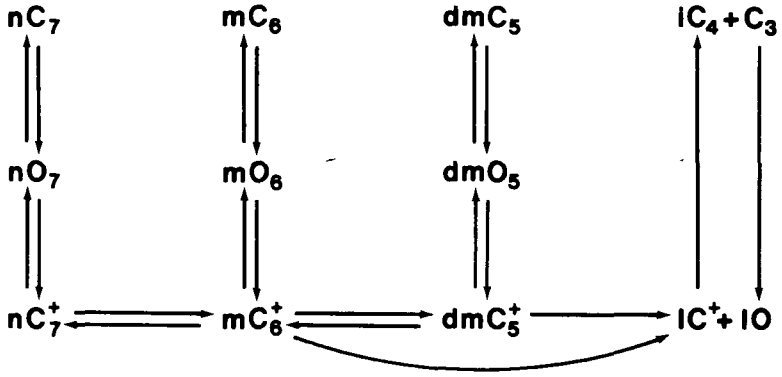

ig.6 Bifunctional transformation of n-heptane (n C_7); m C_6: methylhexanes; d m C_5: dimethylpentanes; C^+: carbocations; O: olefins; ℓ: light products

For high hydrogenating activity, the skeletal isomerization and the cracking of arbocations are, respectively, the rate limiting steps of the hydroisomerization and ydrocracking of n-alcanes [15,16].

For low hydrogenating activity, the dehydrogenation reactions limit the bifun- tional process, and the n-heptane transformation rate is proportional to the metal urface area [16,17].

The evolution of I/C and M/D molar ratios, with the conversion

The decrease of the I/C molar ratio, as the conversion increases by increasing he temperature, can be explained by the fact that the activation energy of cracking eactions is higher than the activation energy of isomerization reactions. So, at igher temperatures, the cracking reactions become more important, and the molar atio I/C decreases.

Moreover, as cracking products are obtained mainly from dibranched carbocations e must wait a similar behaviour for the evolution of I/C and M/D molar ratios as the onversion increases [18].

The evolution of the activity and selectivity of Pd/Sn HY zeolites with the in content

The analysis of Figure 2, indicates that the activity of the catalysts, for he same temperature, decreases, as tin content increases. For the same conversion, he I/C and M/D molar ratios (Figures 4,5) also decrease as tin content increases.

The bifunctional mechanism described above, offers a good explanation for the hange in the activity and selectivity with the tin content: the behaviour of the n/Pd HY zeolites can be explained by a change in the equilibrium of the hydrogena- ing-dehydrogenating/acidic functions, caused by a decrease of the strength of the

metallic function.

In fact, the decrease of the activity of the hydrogenating-dehydrogenating function, in a bifunctional catalyst, will give rise to the decrease of the formation of the intermediate olefins and carbocations and consequently to a decrease of the catalyst activity.

Moreover, we can also explain the decrease of the I/C and M/D molar ratios wi the decrease of the hydrogenating-dehydrogenating function, in agreement with the mechanism of n-heptane transformation on bifunctional catalysts. In fact, with a hi gher hydrogenating activity the rate of carbocation formation will be greater than carbocation skeletal isomerization and/or carbocation cracking; so we will obtain more isomers products and they will be mainly monobranched products [14].

These modifications in the catalytic behaviour of the Sn/Pd HY zeolites,by th presence of tin, cannot be explained only by the poisoning of the palladium by tin. In fact, as referred above, only a small fraction of palladium is recovered by tin. So, we proposed that the presence of tin will induce the production of highly activ hydrogen species, easily desorbed from tin and rapidly adsorbed on palladium particles, displacing the equilibrium (a) to the left:

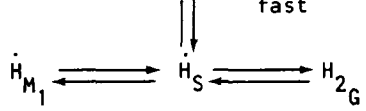

(a)

M_1 - Palladium; M_2 - Tin; S - Support; G - Gaz-phase; $\dot{H}$ - Adsorbed hydrogen species.

So, the concentration of H_{M_1} species will increase, favouring the displacemen of the equilibrated reaction (b) to the left:

$$P_G + M_1 \rightleftharpoons \dot{O}_{M_1} + 2\,\dot{H}_{M_1} \qquad (b)$$

P_G - Paraffins in gaz-phase; O_{M_1} - Olefin adsorbed on Palladium.

Therefore, there will be a decrease of the hydrogenating-dehydrogenating function, induced by the presence of tin. As we have seen above, this explains not only the decrease of the activity of the Pd/Sn HY zeolites, with the tin content,bu also the decrease of the I/C and M/D molar ratios: the occupation of an important number of palladium sites by active hydrogen species, will increase the relative acidity of the bifunctional catalysts.

So, there is a change in the rate limiting step of the bifunctional mechanism and the adsorption of the intermediate iso-olefins on the acidic sites will be favo red, with the consequent increase of the formation of dibranched carbocations and

their consecutive cracking.

This interpretation is also supported by the results of the product distribution in isoconversion conditions (Fig.3): the increasing of C_5 and C_6 products,with the tin content, without formation of C_1 and C_2, are in compliance with a mechanism where the hydrogenation of the intermediate iso-olefins has become the rate limiting step. There is an increase of the carbocations concentration, which can dimerise and, by consecutive cracking, can originate C_5 and C_6 products (without the production of C_1 and C_2).

CONCLUSION

The decrease of the activity and the change of selectivity for the Sn/Pd HY zeolites with the tin content, on the transformation of n-heptane can be explained by a change in the balance between the acidic and metallic functions.

The presence of tin will induce the production of highly active hydrogen species which diffuse towards the catalyst surface, by a spillover effect getting in competition with the n-paraffins in the adsorption over the palladium. In consequence, the hydrogenating-dehydrogenating rate of n-paraffins slows down, becoming the rate limiting step for the bifunctional mechanism.

REFERENCES

1. Marcilly, C., Franck, J.P., in "Catalysis by Zeolites", B.Imelik et al., Eds., Elsevier Sci. Pub. Co., Amsterdam (1980), pg. 93.
2. Jacobs, W.L., Thornton, D.P., Chem. Eng., 77, (25), 79 (1970).
3. Coonradt, M.L., Garwood, W.E., Ind. Eng. Chem., Proc. Res. Dev., 3, (1), 38 (1964).
4. Ribeiro, F., Marcilly, C., Guisnet, M., Proc. 9th Iberoam. Symp. Catalysis, Lisboa (1984), pg. 1237.
5. Rice, R.W., Kang Lu, J. Catal., 24, 367 (1972).
6. Sittig, M., Handbook of Catalysis Manufacture, Noyes Press Ed., Park Ridge N.Y. (1978), pg. 432.
7. Verbeek, H., Sachtler, W.M.H., J. Catal.. 42, 257 (1976).
8. Kuznetzov, B.N., Ermakov, Yu, I., Ryndin, Yu. A., Lorent, J., Duplyakin, V.K., Pentenero, A., Kinet. Katal., 22, (3), 1200 (1981).
9. Burch, R., Mitchell, A.J., Appl. Catal., 6, 121 (1983).
10. Ribeiro, F., Marcilly, C., Rev. Inst. Fr. Pétrole, 34, 405 (1979).
11. US PATENT 4,456,775 (June, 1984).
12. Mills, G.A., Heineman, H., Milliken, T.M., Oblad, A.G., Ind. Eng. Chem., 45, (1), 143 (1953).
13. Sinflet, J.M., Adv. Chem. Eng., 5, 37 (1964).
14. Giannetto, G., Perot, G., Guisnet, M., CNRS International Symposium, Catalysis by Acids and Bases, Sept. 1984, in press.

15. Weisz, P.B., Adv. Catal., 13, 137 (1962).
16. Guisnet, M., Perot, M., in "Zeolites Science and Technology", F. Ramôa Ribeiro et al., Eds., Martinus Nijhoff Publishers, The Hague (1984), pg. 397.
17. Ribeiro, F., Marcilly, C., Guisnet, M., J. Catalysis, 78, 267 (1982).
18. Giannetto, G., Perot, G., Guisnet, M., Proc. 9th Iberoam. Symp. Catalysis, Lisboa (1984), pg. 1661.

ISOMERIZATION AND HYDROCRACKING OF N C10 - N C17 ALKANES ON Pt/H-BETA

J.A. MARTENS, J. Perez-Pariente[a], P.A. Jacobs
Laboratorium voor Oppervlaktechemie, Katholieke Universiteit Leuven,
Kardinaal Mercierlaan 92, B-3030 Leuven, Belgium.

ABSTRACT

Long chain paraffins ranging from decane to heptadecane are hydroconverted over Pt loaded H-BETA. The isomerization-hydrocracking products are analysed using high resolution capillary GLC and compared with those obtained with Pt/H-USY and Pt/H-ZSM-5. Pt/H-BETA behaves as an ideal bifunctional catalyst and its main characteristics are a high selectivity for isomerization, pure primary cracking of the hydrocarbon chain and reduced propane formation. In contrast to zeolite Y, the pores of zeolite-BETA restrict the formation of ethyl- or bulkier side chains in the feed isomers.

INTRODUCTION

During the last decade zeolite research has focussed on the synthesis of high-silica zeolites and the investigation of their properties. Among them the Pentasil family of materials received particular attention. Other high-silica zeolites were known before the advent of the Pentasil zeolites but have been overlooked. Zeolite BETA is such a zeolite.

Zeolite BETA was synthesized in 1967 by Mobil researchers [1] and showed a silica to alumina ratio in the range from 5 to 100 [2]. It is an aluminosilicate crystallised from a gel containing tetra-ethylammonium (TEA) or Na ions [1,2] and eventually Cr, Fe or La [4]. The XRD peaks can be indexed in a cubic unit cell with a_0 = 1.204 nm [1] although Breck [5] contests this. The zeolite has a pore volume of 0.20 ml g^{-1}, sorbs hexane and cyclohexane and can be dealuminated by HCl treatment [3]. Recently it was shown that the void structure was similar to that of zeolite L and consists of pores with 12-membered rings and lobes [6].

---

[a] On leave from : Instituto de Catalisis y Petroleoquimica, Madrid

Only a few industrial applications of this zeolite have been claimed till today. It is able to alkylate benzene with dodecene to prepare phenyldodecanes [8]. In this reaction it has a selectivity similar to that of zeolite L, ZSM-4, ZSM-20, ZSM-38 and mazzite [8]. It can also be used for the formation of diphenylmethane out of benzene and trioxane [7]. High-silica BETA loaded with platinum is an efficient dewaxing catalyst avoiding extensive gas formation [9]. Dealuminated-BETA seems to have potential uses as a catalyst component in the hydrocracking-dewaxing of heavy oils [10].

In the present work, it was aimed to investigate more fundamentally the potential of zeolite BETA in isomerization-hydrocracking reactions of n-paraffins. Its behaviour was compared to that of proven bifunctional catalysts as Pt/H-ZSM-5 and Pt/Ultrastable Y (US-Y).

EXPERIMENTAL

For the synthesis of zeolite BETA a mixture of tetra-ethyl orthosilicate (80 g) and a 40 % aqueous solution of TEA-OH (56.4 g) was stirred for 1 hour to achieve complete hydrolysis of the ester. Then were subsequently added : $Al(NO_3)_3.9H_2O$ (9.5 g), NaOH (1.4 g), TEA-OH solution (56.4 g) and water (8.1 g) under continuous stirring. The gel obtained (with Si/Al = 15) was autoclaved at 393 K. After rotation for 6 days zeolite BETA with Si/Al = 14 was formed in the autoclave. The sample showed the typical XRD-spectrum [2] and a crystal size of 0.2 µm. The H-form of this zeolite was obtained after washing, calcination at 723 K, NH_4-exchange and heating at 673 K.

H-BETA showed a hydroxyl spectrum with bands at 3725 and 3600 cm^{-1}. Similar spectra were reported for H-ZSM-5 samples [11]. The Pt-H-form of BETA was prepared upon impregnating the NH_4-form with aqueous $Pt(NH_3)_4Cl_2$, drying, calcination in oxygen and reduction in hydrogen at 637 K. The latter two treatments were performed in situ in a continuous flow tubular reactor after pelletizing the Pt/NH_4-zeolite into 0.3-0.5 mm grains. The reactor could be operated up to 2 M Pa. Paraffins and hydrogen were mixed in a thermostatted saturator. The whole conversion range was covered by varying the reaction temperature. The reactor outlet was analyzed on-line over a 50 m CPt Sil 5 fused silica column using temperature programming between 283 and 473 K.

The reference zeolite Pt-US-Y was prepared by repeated steaming from NH_4-Y [12]. ZSM-5 with Si/Al = 60 and crystal dimensions of 1-4 µm was synthesized and transformed into a bifunctional catalyst according to published methods [15]. All catalysts contain 1 % by weight of platinum.

RESULTS AND DISCUSSION

1. Isomerization and hydrocracking of tridecane

As a typical example the isomerization of tridecane into mono- and dibranched feed isomers and its hydrocracking is shown in Fig. 1 for the three zeolite frameworks, BETA, ZSM-5 and US-Y. In comparable conditions BETA is more active than ZSM-5 because it contains a higher number of Brønsted sites (the Si/Al ratio of the samples is 14 and 60, respectively). As also found for n-C10 [15], ZSM-5 is more active than US-Y. As far as overall selectivity is considered, BETA behaves as US-Y and from the figure the following reaction sequence is obvious :

tridecane → monobranched C_{13} isomers → dibranched C_{13} isomers → cracked products

As reported for various n-paraffins on Pt loaded US-Y [12], CaY [14] and dealuminated Y [15], very high selectivity for isomerization was also observed for BETA. In terms of a classical bifunctional mechanism, an increase in isomerization selectivity has to be associated with a decrease in average acid strength [14].

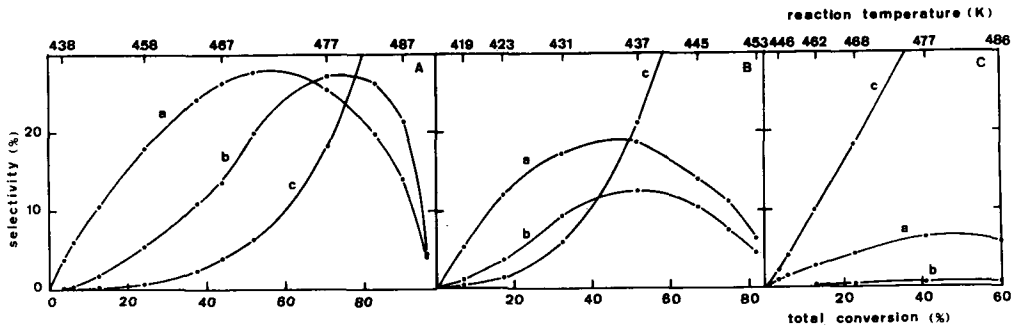

Fig. 1. Conversion of n-C_{13} into mono- (a), dibranched (b) isomers and cracked products (c) against its total conversion; $P_{tridecane}$ = 1.3 k Pa; P_{H2} = 2 M Pa; A, Pt/H-BETA (WHSV = 0.88 h^{-1}); B, Pt/H-US-Y (WHSV = 0.47 h^{-1}); C, Pt/H-ZSM-5 (WHSV = 0.88 h^{-1})

A high selectivity for dibranched isomers is reached on BETA (Fig. 1). The degree of branching of the feed isomers is not determined by acid strength but rather by the size of the zeolite pores [6]. The high yield of dibranched isomers on BETA suggests that this zeolite contains no constraints for the formation of highly branched intermediates. The high overall selectivity for isomerization against hydrocracking also suggests that BETA doesnot possess the very strong acid sites of ZSM-5.

2. Composition of the feed isomers

Starting with n-decane as feed, the distribution of the methyl-branched isomers is shown in Fig. 2.

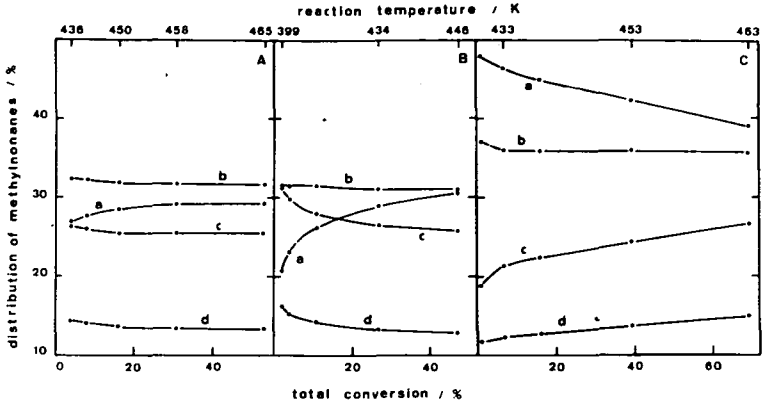

Fig. 2. Distribution of the methylnonanes at increasing total conversion of decane at P_{decane} = 1.1 k Pa, P_{H2} = 0.1 M Pa; A, Pt/H-BETA at WHSV = 0.4 h^{-1}, B, Pt/US-Y at WHSV = 0.2 h^{-1} and C, Pt/H-ZSM-5 at WHSV = 0.3 h^{-1}; a, 2-methylnonane, b, 3-methyl-, c, 4-methyl- and d, 5-methylnonane.

The behaviour of US-Y has already been described at this level [13] : the formation of 2-methylnonane is kinetically hindered since branching occurs via protonated cyclopropane (PCP) intermediates, the rate of formation of which is lower near the end of a hydrocarbon chain [14]. From medium conversion on, thermodynamic equilibrium is reached. In ZSM-5 an excess of 2-methylnonane is found at low conversions, largely at the expense of the 4- and 5-methylisomer. This composition gradually changes to that of equilibrium. Such behaviour is typical for small crystal ZSM-5 [16], while for large crystals the initial composition is not affected by the degree of conversion [15]. Transition state shape selectivity [15] may be responsible for this behaviour.

The distribution of these isomers in BETA is close to that observed on US-Y zeolite, although the kinetic hindrance of 2-methylnonane is less pronounced. This indicates that PCP-type branching is followed by very rapid equilibration via methylshifts. When the Brønsted sites are very diluted in an open zeolite framework, it has been reported that the relative rates of isomerization by alkyl-shifts drops considerably compared to PCP-branching [16]. The behaviour of BETA is explained in this context by its high aluminium content, although secondary isomerization at the external surface cannot be entirely excluded.

The distribution of the isomers at the maximum isomerization conversion in terms of methyl-, ethyl- and propyl-branched products is shown in Table 1. On ZSM-5 only methyl-isomers are formed, which confirms previous reports [15,16] and which can be ascribed to transition and/or product shape selectivity. The product distribution on BETA and US-Y is rather similar, although less propyl- and ethyl-branched isomers are formed on the former zeolite.

Table 1

Distribution of monobranched isomerization products on Pt/H-zeolites at maximum isomerization conversion

Feed	Zeolite	WHSV/ h^{-1}	Temp. K	Isomerization %	Isomer distribution % methyl	ethyl	propyl branched
nC_{10} [a]	BETA	0.4	472	42	88.5	10.2	1.3
	US-Y	0.2	446	34	86.0	12.3	1.7
	ZSM-5	0.3	453	30	98.8	1.2	0.0
nC_{17} [b]	BETA	0.9	472	28	87.6[c]	12.4	-[d]
	US-Y	0.6	431	19	85.1[c]	14.9	-[d]

a, P_{H2} = 0.1 M Pa and P_{C10} = 1.1 k Pa; b, P_{H2} = 2 M Pa and P_{C17} = 0.3 k Pa; C, including 3-ethylpentadecane; d, propyltetradecanes, butyltridecanes and pentyldodecane are not resolved from the dibranched isomers.

This indicates that BETA is a large pore zeolite with cages or lobes slightly smaller than the supercage of the faujasite structure. This is confirmed when other isomer or product fractions are considered. Indeed, the yield of methyl-ethylbranched C_{10} isomers in the dibranched ones amounts to 4.5 and 1 % for US-Y and BETA, respectively.

3. Carbon number distribution of hydrocracked products

On large pore zeolites in the acid form with a well-dispersed metal phase on it, ideal bifunctional cracking is expected. This cracking consists of primary events and consequently the carbon number fractions are distributed symmetrically among their carbon numbers. Central scission is preferred in this type of chemistry and propane abstraction is not very probable [6]. On medium pore zeolites, central scission is less abundant and propane formation has increased [6,15,16]. The carbon number distribution of the hydrocracked products from decane, dodecane and tridecane at low cracking conversions are given in Fig. 3 for the three zeolites to illustrate this.

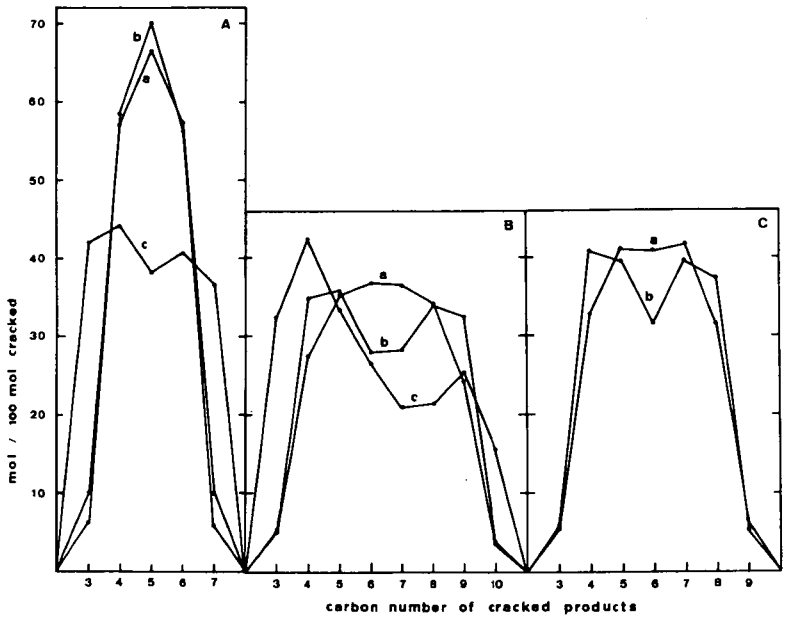

Fig. 3. Carbon number distribution of hydrocracked products from decane (A), dodecane (C) and tridecane (B) at 5 % hydrocracking over a, US-Y, b, BETA and c, ZSM-5 zeolites. Experimental conditions for tridecane and decane are given in Figs. 1 and 2, respectively; for dodecane : P_{C12} = 1.2 k Pa; P_{H2} = 2.0 M Pa; on BETA, WHSV = 0.5 h^{-1} at 465 K, and on US-Y, WHSV = 0.4 h^{-1} at 434 K.

The typical features mentioned are observed for US-Y with each feed molecule. On ZSM-5, much propane is formed, central scission is decreased and secondary cracking of the longer hydrocracked products occurs mainly for the longer feed molecules. This confirms earlier work [6,15,16]. The cracking of decane on BETA shows the ideal pattern. Central scission is even more preferred than over US-Y and propane abstraction is lower. With C_{12} and C_{13} paraffins as feed, however, minor but significant differences between BETA and US-Y appear : the preference of central scission has decreased over BETA. It will be shown elsewhere that mainly A-type cracking of α,α,γ-tri-branched isomers is responsible for this central scission [18]. The absence of dimethylethylisomers in BETA, as a result of shape selective hindrance, can explain that central scission decreases with increasing carbon number of the feed [18]

4. Product distribution in the individual carbon number fractions

The composition of the C6 carbon number fraction is shown in Fig. 4 for feed paraffins with carbon number between 10 and 17. At low cracking conversions it is seen that over US-Y as well as over BETA this composition is the same irrespective of the chain length of the feed hydrocarbon.

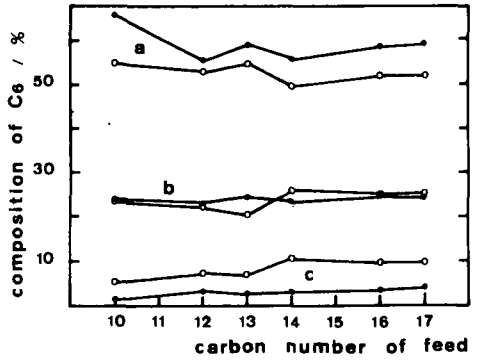

Fig. 4. Composition of the C6 carbon number fraction against the feed carbon number at 5 % hydrocracking conversion over US-Y (full points) and BETA (open points). Experimental conditions : for C10, C12, C13 : Fig. 3; C17 : Table 1; for C14 : P_{H2} = 2M Pa, P_{C14}= 1.1 k Pa, WHSV = 0.6 h^{-1} on BETA at 444 K and 0.4 h^{-1} at 425 K on US-Y; for C16 : pressures as for C14, WHSV = 1.0 h^{-1} at 490 K on BETA and WHSV = 0.5 h^{-1} at 436 K US-Y; a = 2-methylpentane; b = 3-methylpentane; c = 2,3-dimethylbutane.

The figure shows that on both zeolites this composition is not dependent on the chain length of the feedstock. Such a behaviour is only possible when the discrete β-scission mechanisms operate on the parent carbocations at a rate which is not dependent on their chain length. Furthermore, also the relative concentration of these cations with a structure susceptible to an attack by one of the scission mechanisms is independent of the feed. This behaviour will be explained in detail in a later publication. The slight differences in the 2-methylpentane and 2,3-dimethylbutane yields over BETA and US-Y are the result of slight differences in the feed isomer composition mainly at the level of the ethyl- and propyl-branchings.

For the C4 and C5 fractions the same constant composition of the fraction, irrespective of the carbon number of the feed was observed. The yield of isobutane in the C4 fraction varied between 80 and 86 % and between 78 and 83 % for BETA and US-Y, respectively. Isopentane represented always 85 to 89 % of the C5 fraction over BETA and 83 to 87 % over US-Y.

The composition of the C7 fraction hardly changes for feeds longer than C10. The decreased yield in n-fragments in the fraction obtained by propane abstraction is indeed a typical feature of ideal hydrocracking [19] in large pore zeolites and consequently the constant composition is only observed now from C11 on as feed. A typical difference between BETA and US-Y is the decreased yield of ethylpentane on the former zeolite. This component can only be obtained from ethyl-branched parent ions which are less abundant in BETA.

These observations are of key importance for the design of dewaxing and hydrocracking catalysts. It follows that whatever mixture of long chain paraffins is cracked over zeolites as US-Y and BETA always almost identical compositions of the hydrocracked products will be obtained.

CONCLUSIONS

In this work it is shown that zeolite Pt/H-BETA shows all the characteristics of an ideal bifunctional isomerization and hydrocracking catalyst when long chain n-paraffins are used as feed. This material is very active and selective for isomerization of such feeds. Once bulkier than methyl-branchings are formed, sterical restrictions are imposed by the inner structure of this zeolite. This behaviour distinguishes the BETA structure from that of ultrastable Y.

The yields of the carbon number fractions of the hydrocracked products in BETA ressemble those obtained over US-Y. The low yield of ethyl-branchings in the multiply-branched feed isomers causes a somewhat reduced rate of central scission on zeolite BETA. Finally, the distribution of the individual isomers in each carbon number fraction is very similar in BETA and US-Y.

ACKNOWLEDGMENT

J.A.M. and P.A.J. acknowledge a research grant and a research position from N.F.W.O. J.P.P. is grateful to K.U. Leuven for a research grant. The authors acknowledge the Belgian Government (Wetenschapsbeleid) for a grant in the frame of a concerted action on catalysis.

REFERENCES

1. Wadlinger, R.L., Kerr, G.T., Rosinski, E.J., U.S. Pat. 3, 308, 069 (1967), assigned to Mobil Oil Corp.
2. Wadlinger, R.L., Kerr, G.T., Rosinski, E.J., U.S. Pat. 3, 308, 069 (1975), assigned to Mobil Oil Corp.
3. Lapierre, R.B., Wong, S.S.F., Eur. Pat. Appl. 95, 304, (1983), assigned to Mobil Oil Corp.
4. Plank, C.J., Rosinski, E.J., Rubin, M.K., Eur. Pat. Appl. 64, 328, (1982), assigned to Mobil Oil Corp.
5. Breck, D.W. : Zeolite molecular sieves, John Wiley & Sons, New York, London, Sydney, Toronto, 1973, p. 309.
6. Martens, J.A., Tielen, M., Jacobs, P.A., Weitkamp, J., Zeolites 4, (1984) 98.
7. Tobias, M.A., U.S. Pat. 3, 728, 408 (1973), assigned to Mobil Oil Corp.
8. Young, L.B., Eur. Pat. Appl. 30, 084, (1981), assigned to Mobil Oil Corp.
9. Lapierre, R.B., Partridge, R.D., Chen, N.Y., Wong, S.S., Eur. Pat. Appl. 95, 303, (1983), assigned to Mobil Oil Corp.
10. Lapierre, R.B., Partridge, R.D., Eur. Pat. Appl. 94, 827, (1983), assigned to Mobil Oil Corp.
11. Jacobs, P.A., Von Ballmoos, R., J. Phys. Chem. 86, (1982), 3050.
12. Steijns, M., Froment, G., Jacobs, P.A., Uytterhoeven, J.B., Weitkamp, J., Ind. Eng. Chem. Prod. Res. Dev. 20, (1981), 654.
13. Jacobs, P.A., Uytterhoeven, J.B., Steijns, M., Froment, G., Weitkamp, J., Proceed. 5th Conf. Zeolites, 1980, Rees, L.V.C., Ed., Heyden, London, p. 607.
14. Weitkamp, J., Ind. Eng. Chem. Prod. Res. Dev. 21, (1982), 550.
15. Jacobs, P.A., Martens, J.A., Weitkamp, J., Beyer, H.K., Faraday disc. Chem. Soc. 72, (1982), 353.
16. Weitkamp, J., Jacobs, P.A., Martens, J.A., Applied Catal. 8, (1983), 123.
17. Jacobs, P.A., Martens, J.A., Beyer, H.K., Proceed. Symp. "Catalysis by Acids and Bases", Lyon 1984, Stud. Surf. Science and Catal., Elsevier (1985), to be published.
18. Martens, J.A., Jacobs, P.A., Weitkamp, J., to be published.
19. Weitkamp, J., in : "Hydrocracking and Hydrotreating", Waid, J.W. and Quader, G.A., Eds., ACS Symp. Ser. Vol. 20, ACS, Washington, 1975, p. 1.

OXIDATIVE ACETOXYLATION OF PROPYLENE OVER METAL-CONTAINING ZEOLITE CATALYSTS

Kh.M.MINACHEV, V.V.KHARLAMOV
N.D.Zelinsky Institute of Organic Chemistry USSR Academy of Sciences, Moscow

ABSTRACT

The activity and the selectivity of the catalysts on the basis of A, X, Y, chabasite, erionite, mordenite, ZWM and ZWK type zeolites containing VIII group metals have been investigated in the reaction of oxidative acetoxylation of propylene to allylacetate. It was shown that among VIII group metals only Pd-containing catalysts are active in the allylacetate synthesis. The reaction of deep oxidation of propylene takes place in the case of another metal containing catalysts. The effect of transition metals on activity and selectivity of Pd-zeolite catalyst have been studied.

Using ^{18}O labelled acetic acid it was shown that the mechanism of the reaction of propylene oxidative acetoxylation can include the formation of allyl alcohol as an intermediate with its etherization with acetic acid to allylacetate.

INTRODUCTION

As is known the reaction of olefin oxidative acetoxylation can produce many important products such as vinylacetate and allylacetate.

$$CH_2=CH_2 + CH_3COOH + 1/2\ O_2 \longrightarrow CH_3COOCH=CH_2 + H_2O$$

$$CH_2=CHCH_3 + CH_3COOH + 1/2\ O_2 \longrightarrow CH_3COOCH_2CH=CH_2 + H_2O$$

Allylacetate can be used as a starting compound for production of glycerine, glycidol, epichlorhydrine, γ-acetopropylacetate and other useful products [1]. Oxidative acetoxylation of olefins was discovered in 1960 when it was shown [2] that vinylacetate is formed from interaction of ethylene with sodium acetate in the presence of palladium chloride

$$CH_2=CH_2 + 2NaOCOCH_3 + PdCl_2 \longrightarrow CH_3COOCH=CH_2 + 2NaCl + CH_3COOH + Pd$$

Since the process has been improved by using acetic acid instead of sodium acetate and by addition of cupric chloride to the reaction

mixture for palladium reoxidation

$$C_2H_4 + AcOH + PdCl_2 \longrightarrow AcOC_2H_3 + 2HCl + Pd$$
$$Pd + 2CuCl_2 \longrightarrow PdCl_2 + 2CuCl$$
$$2CuCl + 2HCl + 1/2\ O_2 \longrightarrow 2CuCl_2 + H_2O$$

Later it was shown that this reaction could be carried out not only in homogeneous conditions but also in the gas phase using palladium or its compounds together with added different promoters (such as salts of transition metals) supported on alumina, silica gel, silica-aluminas, activated charcoal and other solids [4-11]. Besides palladium alkali acetate added up to 10-15 wt.% is a necessary component of the catalyst. It was suggested that alkali acetate may increase acetic acid adsorption on the catalyst surface, which may result in variation of the reaction kinetic order for acetic acid from 1 to 0 [12,13].

Different olefins, dienes and aromatics are shown to take part in the reaction of oxidative acetoxylation [14-22]

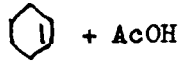

$$CH_2{=}CHCH{=}CH_2 + AcOH + 1/2\ O_2 \longrightarrow AcO{-}CH_2CH{=}CHCH_2OAc + H_2O$$

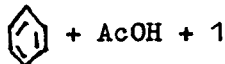

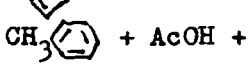

In addition to vinylacetate synthesis another important process is oxidative acetoxylation of propylene to allylacetate. This process is usually carried out in a gas phase at 140-200° under pressures of 1-10 atm 3 . In these conditions together with the main reaction of allylacetate synthesis deep oxidation of propylene proceeds to give carbon dioxide and water but as a rule the selectivity of allylacetate formation is not lower than 90% [3].

The aim of this study is to investigate metal-containing zeolite catalysts in oxidative acetoxylation of propylene to allylacetate and elucidate the kinetics and mechanism of this process.

EXPERIMENTAL

Catalysts were prepared using synthetic zeolites of types A (SiO_2/Al_2O_3=2.0), X(3.0), Y(4.8), K,Na-chabasite (5.0), K,Na-erionite (6.5), mordenite (11.9), ZWM (30-47) and ZWK (68-78). Active components (VIII group metals, promoters) were introduced into the zeolites by both ion exchange and impregnation. After reduction the zeolite catalyst was moulded without any bindings at a pressure of 100 atm The fraction of the catalyst particles of 0.5-1.0 mm was used in the

experiments.

The catalytic experiments were carried aut in a flow reactor at atmospheric pressure, 160-190° and a molar ratio of C_3H_6: CH_3COOH:O_2= = (2-6):1:(0.3-1.0). The amount of the catalyst loaded into the reactor was 1-6 cc. The liquid reaction products were collected into the trap at 0° and analysed by GLC.

Labelled ^{18}O acetic acid was prepared by interaction of CH_3COCl with $H_2{}^{18}O$. The products obtained from propylene oxidative acetoxylation and allyl alcohol etherization with acetic acid- ^{18}O were analysed by chromato-mass-spectrometry with a "Varian MAT-111" and "Kratos MS-70".

The temperature programmed reduction of the oxidized catalyst samples was carried out using chromatographic technique. The weight of the catalyst sample was 0.4 g. The catalyst sample was preoxidized by air or a mixture of air and helium (1:1) at 180 and 500°. The catalyst was reduced in a flow of a N_2 and 10% H_2 mixture at a rate of 30 cc/min. The temperature of the catalyst sample was increased linearly at a rate of 20 K/min. Changes in the hydrogen concentration at the reactor outlet was determined by a catarometer.

RESULTS AND DISCUSSIONS

By analogy with liquid phase olefin oxidation [23] copper is sometimes added to Pd-catalysts for propylene oxidative acetoxylation as a promoter [7]. Therefore, first, we are to discuss the influence of the procedure of Pd,Cu-catalyst preparation on its activity and selectivity in allylacetate synthesis [24]. Results obtained are given in table 1. As is seen the type Y zeolites of Na- and H-forms as well as unreduced PdCuNaY and reduced ones are not active in oxidative acetoxylation of propylene to allylacetate. But over these catalysts acid catalyzed addition of acetic acid to propylene takes place with formation of isopropylacetate. Deep oxidation of propylene also takes place to a small extent over Pd,Cu-catalysts (samples 3 and 4). This is indicated by water formation in an amount of about 2%.

To prevent acetic acid addition to propylene zeolite acidic centers were neutralized in four different ways: 1.catalyst pretreatment with a sodium acetate solution, 2.catalyst pretreatment with a sodium chloride solution, 3.catalyst impregnation with a sodium chloride solution followed by calcination of the catalyst at 500°, 4.catalyst pretreatment with an alkaline solution. Ater pretreatment of the reduced catalyst with a sodium acetate solution (sample 5) the amount of isopropylacetate in the reaction products decreased to 4.3%. At

Table 1

Dependence of the properties of Pd,Cu-catalyst on the basis of NaY zeolite on the preparation procedure (1% Pd and 0.6% Cu were introduced by ion exchange). Process conditions: 180° atmospheric pressure, V_{cat}= 6 cc, V_{CH_3COOH} =0,7h^{-1}, $C_3H_6:CH_3COOH:O_2$ = 6:1:0.5

No	Catalyst and preparation procedure	Product composition, %					Activity $\frac{\text{g-mole}}{\text{g.cat.h}} \times 10^3$	Selectivity %
		acetic acid	water	allyl-acetate	isopropylacetate	isopropyl alcohol		
1.	Starting NaY	98.3	1.2	-	0.5	-	-	-
2.	HY	90.3	0.6	-	9.1	-	-	-
3.	PdCuNaY unreduced	88.4	1.9	-	9.7	-	-	-
4.	PdCuNaY reduced	87.3	2.1	-	10.6	-	-	-
5.	PdCuNaY reduced and pretreated with 0.2 N CH_3COONa (pH=9-10)	93.6	2.1	0.1	4.3	-	-	-
6.	PdCuNaY reduced and pretreated with 0,2 N NaCl(pH= 9-10)	92.7	2.7	2.4	2.2	-	0.25	24.6
7.	PdCuNaY reduced impregnated with 0.2N NaCl and preheated at 500°	86.5	6.2	4.4	0.1	2.9	0.38	29.5
8.	PdCuNaY reduced and pretreated with 0.2 N NaOH	92.1	3.5	4.4	-	-	0.40	39.5

the same time formation of allylacetate as a product was observed. Catalyst pretreatment with a sodium chloride solution is more effective (sample 6). The amount of allylacetate in the reaction products was 2.4 %. This corresponds to catalyst activity of 0.25×10^{-3} g-mole/g.cat-h, with the reaction selectivity of 24.6%. However, with this catalyst pretreatment it is impossible to prevent isopropylacetate formation (2.2%). This suggests incomplete neutralization of zeolite acidic centers. Formation of isopropylacetate was excluded by impregnation of the catalyst with sodium chloride (sample 7), but in this case isopropyl alcohol occured in the reaction products. The rate of allylacetate formation was 0.38×10^{-3} g-mole/g.cat.h, with the reaction selectivity of 29.5%. Catalyst pretreatment with an alkali solution was found to be the best procedure to neutralize the catalyst acidic centers (sample 8). By this method isopropylacetate formation was excluded completely and the catalyst activity and reaction selectivity were 0.40×10^{-3} g-mole/g.cat.h and 39.5%, respectively.

The effect of metal concentration on the catalytic properties of PdCuNaY catalysts have been also investigated (fig.1 and 2).

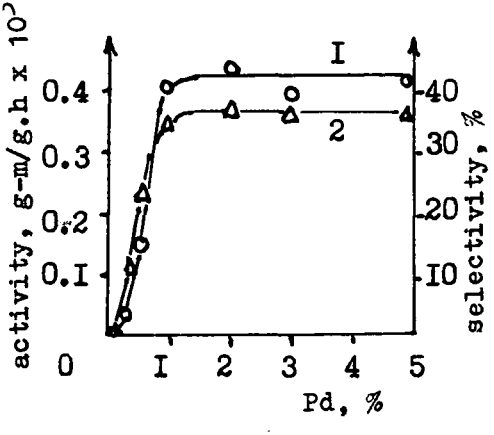

Fig. 1

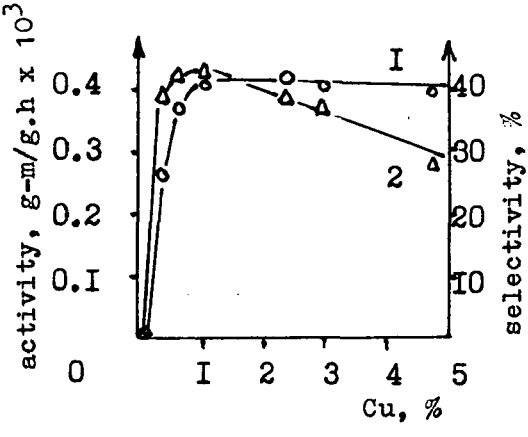

Fig.2

Fig.1. Dependence of the catalytic properties of PdCuNaY on Pd concentration (Cu contents 3%) 1-activity, 2-selectivity.

Fig.2. Dependence of the catalytic properties of PdCuNaY on Cu concentration (Pd contents 1%) 1-activity, 2-selectivity.

As is seen monometallic catalysts containing only Pd or Cu are inactive in propylene oxidative acetoxylation. As the metal concentration increased the catalyst activity and reaction selectivity also increased up to some extent. The catalyst containing 1% Pd and 0.6% Cu is found to be most efficient. This metal content corresponds to

atomic ratio Pd:Cu 1:1.

Next, the effect of different ways of metal introduction into the catalyst was studied. It is shown (table 2) that the most active (0.79×10^{-3} g-mole/g.cat.h) and selective (52.8%) catalyst can be prepared by simultaneous ion exchange introduction of Pd and Cu from a solution of palladium tetraaminochloride and cupric chloride.

The influence of alkali cations on the properties of type Y zeolite based Pd,Cu-catalyst can be seen from the data presented in table 3. The catalytic activity slightly increases with an increase

Table 2

Influence of succession of metals introduction into NaY zeolite on its catalytic properties (1% Pd, 0.6% Cu). Reaction conditions are indicated in table 1

Succession of metals introduction	Activity, $\frac{\text{g-mole}}{\text{g.cat.h}} \times 10^3$	Selectivity %
1. Pd, 2. Cu	0.40	39.5
2. 1.Cu, 2. Pd	0.38	38.1
3. Pd+Cu simultaneously	0.79	52.8

Table 3

Catalytic properties of NaY zeolite with various alkali cations (1% Pd, 0.6% Cu). Reactions conditions are indicated in table 1

No	Zeolite	Activity, $\frac{\text{g-mole}}{\text{g.cat.h}} \times 10^3$	Selectivity, %
1.	LiY	0.34	36.1
2.	NaY	0.40	39.5
3.	KY	0.47	43.2
4.	CsY	0.51	9.6

of the metal atomic number, i.e. with transition from Li to Cs. This is confirmed by the influence of acetates of alkali metals on the Pd catalyst of olefins oxidative acetoxylation [12].

Copper is shown to be a promoter of zeolite NaY based Pd-catalyst only in the case of ion exchange metal introduction. But the c

talyst is also active in the reaction, with no copper involved, provided it is prepared by zeolite impregnation with palladium chloride and alkaline metal acetate after its reduction (table 4). As is seen from the data presented the activity and selectivity of Pd-catalyst depend on the type of zeolite used. The catalysts on the basis of NaA and NaX zeolites are inactive in this reaction. In the case of low silica zeolites of Y, chabazite, erionite and mordenite type the catalyst activity is on the level of $(0.2-0.4)\times 10^{-3}$ $\frac{\text{g-mole}}{\text{g.cat.h}}$

Table 4

The effect of the type of zeolite on the properties of Pd-catalyst (1.5% Pd, 15% AcOK) at 180°, atmospheric pressure, C_3H_6: $CH_3COOH:O_2=2:1:0.5$, V_{cat} = 2 cc, V_{CH_3COOH} = 2 h^{-1}

No	Zeolite	$\frac{SiO_2}{Al_2O_3}$	Activity, $\frac{\text{g-mole}}{\text{g.cat.h}} \times 10^3$	Selectivity, %
1	NaA	2.0	0	0
2	NaX	2.9	0	0
3	NaY	4.8	0.35	35
4	KNa-chabazite	5.0	0.44	34
5	K,Na-erionite	6.5	0.15	100
6	Na-mordenite	11.9	0.19	26
7	ZWM-408	29.6	7.33	96
8	ZWM-364	47	7.43	94.3
9	ZWK-XI	68	5.52	87
10	ZWK-III	78	3.04	89

The catalysts on the basis of high silica zeolites of type ZWM (molar ratio of SiO_2/Al_2O_3= 30-47) are most active. But an increasing in the ratio of silica to alumina in zeolites to 68-78 results in a decrease of the catalyst activity which may be accounted for by structural factors (transition from zeolite of type ZWM to zeolite of type ZWK). The reason for inactivity of Pd-catalysts on the basis of NaA and NaX zeolites is not clear and further investigations are nedeed. The fact that copper is an unnecessary component of the catalyst when it is prepared by impegnation could be explained by a large size of Pd-crystallites resulting from reduction of impegnated catalysts. Consequently the process of Pd reoxidation is facilitated. It is well known [13], that in the case of Pd-catalysts prepared by impegnation of nonzeolite carriers the activity passes through the maximum, which de-

pends on the size of metal crystallites on the surface.

According to the literature data [3-9] Pd with various promoters is usually used as a catalyst for the reaction of propylene oxidative acetoxylation. No information on the catalytic properties of other VIII group metals is available. The data we obtained show (table 5) that among VIII group metals only Pd is active in this reaction.

Table 5

Activity of monometal catalysts on the basis of zeolite of ZWM-408 type (metal content 1,5%, AcOK-15%). Reaction conditions are indicated in table 4

No	Metal	Product composition,%(wt)			Activity, $\frac{\text{g-mole}}{\text{g.cat.h}} \times 10^3$	Selectivity, %
		acetic acid	water	allyl-acetate		
1.	Co	96.2	3.8	-	-	-
2.	Ni	95.2	4.8	-	-	-
3.	Ru	97.4	2.6	-	-	-
4.	Rh	96.6	3.4	-	-	-
5.	Pd	71.5	6.3	22.2	7.33	96
6.	Os	94.1	5.9	-	-	-
7.	Ir	97.1	2.9	-	-	-
8.	Pt	95.1	4.9	-	-	-
9.	Ag	96.5	3.5	-	-	-

Other VIII group metals as well as Ag, a typical catalyst for oxdative reaction, can effect only deep oxidation of propylene. This result is unique because in other oxidative type reactions all VIII group metals are more or less active. The cause of inactivity of VIII group metals, except Pd, in allylacetate synthesis may be either the absence of a necessary intermediate originating from a propylene molecule or a high rate of full oxidation of this intermediate.

Bimetal catalysts on the basis of Pd and a metal of group VIII or another transition metal have been investigated (table 6). As is seen from the table the activity and selectivity of Pd-catalyst depends on the type of the second metal component. In the case of such metals as Rh, Ag the activity of Pd-catalyst decreases up to zero. To explain the effect of transition metals on the activity of Pd-catalyst it is necessary to take into account, on the one hand, possible change in palladium dispersion on the surface of the carrier as well as specific catalytic activity and, on the other hand, possible chan-

Table 6

Activity of bimetal Pd-catalyst on the basis of ZWM-408 zeolite (content of Pd 1.5%, content of second component 1.5% AcOK-15%). Reaction conditions are indicated in table 4

No	Second component	Product composition, (wt) %			Activity, $\frac{\text{g-mole}}{\text{g.cat.h}} \times 10^3$	Selectivity, %
		acetic acid	water	allyl-acetate		
1.	Fe	90.1	3.0	6.9	2.00	71.0
2.	Ni	73.2	17.2	9.6	3.42	26.5
3.	Ru	77.5	17.1	5.4	1.88	16.5
4.	Rh	81.0	19.0	-	-	-
5.	Os	66.2	18.3	15.5	5.75	36.4
6.	Ir	76.9	13.8	9.3	3.20	31.0
7.	Pt	73.7	19.3	7.0	2.52	18.0
8.	Mn	76.8	6.6	16.6	5.35	76.4
9.	Ag	96.8	3.2	-	-	-

ges in the rate of palladium oxidation. To answer the question which of these possibilities is prevailent further investigations are needed.

Studies of bimetal catalysts with copper and a metal of group VIII as its two components has also show that in this case only Pd containing catalyst are active in allylacetate synthesis (table 7).

Table 7

Activity of bimetal Cu-catalyst on the basis of ZWM-408 zeolite (Cu content 1.5%, content of the second component 1.5%, AcOK-15%). Reaction conditions are indicated in table 4

No	Second component	Product composition, (wt.) %			Activity, $\frac{\text{g-mole}}{\text{g.cat.h}} \times 10^3$	Selectivity, %
		acetic acid	water	allyl-acetate		
1.	Co	95.4	4.6	-	-	-
2.	Ni	96.3	3.7	-	-	-
3.	Ru	88.3	11.7	-	-	-
4.	Rh	96,7	3.3	-	-	-
5.	Pd	84.9	6.6	8.5	2.64	52.3
6.	Os	92.9	7.1	-	-	-
7.	Ir	94.9	5.1	-	-	-
8.	Pt	91.5	8.5	-	-	-

Other bimetal Cu-containing catalysts are active only in full oxidation of propylene.

To elucidate the mechanism of the reaction the kinetics of the process has been investigated using Pd,Cu-catalyst on the basis of a mordenite type zeolite [25]. The catalyst was prepared using ion exchange technique. The amounts of palladium and copper in the catalyst were 1.5 wt.% and 2.5 wt.%, respectively. After reduction of the catalyst it was pretreated with an alkaline solution to neutralize the acidic centers,

As is shown the reaction rate is proportional to the oxygen partial pressure (fig.3) and passes through a faint maximum in dependence on the propylene partial pressure (fig.4).

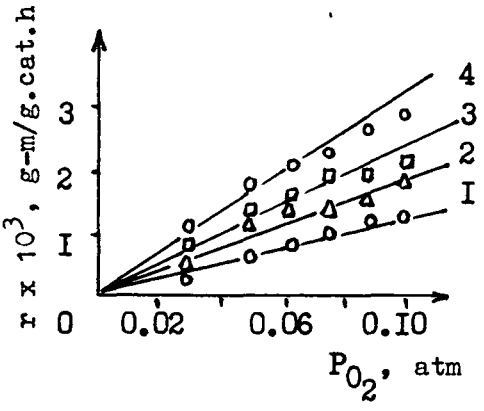

Fig.3

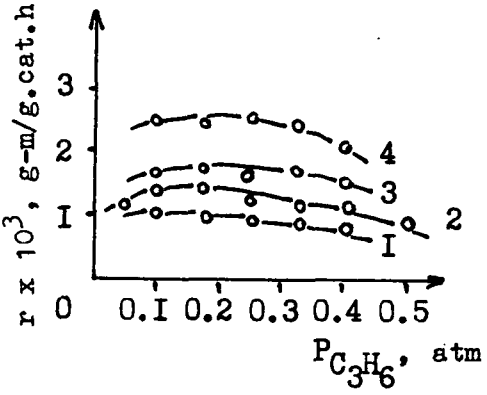

Fig.4

Fig.3. The dependence of allylacetate formation on the oxygen partial pressure at $P_{C_3H_6}$ = 0.25 atm, P_{CH_3COOH} = 0.1 atm and temperatures: 1-160°, 2-170°, 3-180°, 4-190°.

Fig.4. The dependence of allylacetate formation on propylene partial pressure at P_{O_2} = 0.075 atm, P_{CH_3COOH} =0.1 atm and temperatures: 1-160°, 2- 170°, 3-180°, 4- 190°.

Thus, according to the data obtained the following kinetic equation could be proposed

$$r = \frac{k \cdot P_{O_2} \cdot P_{C_3H_6}}{(1 + a \cdot P_{C_3H_6})^2} \qquad (1)$$

The constants "k" and "a" were estimated by the graphical method at various temperatures and the values of the Arrenius parameters of these constants (Ko, E, a_o and Q) were also calculated. Next, using these values as the initial estimates of the parameters the minimization of the function F was done by means of a microcomputer "Iskra-

-1256"

$$F = \sqrt{\frac{1}{n} \sum_{i=i}^{n} \left(\frac{r_{ie} - r_{ic}}{r_{ie}} \right)^2}$$

where n is the number of experiments, r_{ie} and r_{ic} are the experimental and calculated reaction rates. Initial and corrected values of the parameters are presented in table 8.

Table 8

The kinetic parameters corrected with a microcomputer "Iskra-1256"

No	Parameters	K_o	E, $\frac{cal}{mole}$	a_o	Q $\frac{cal}{mole}$	F
1.	initial	89	4090	0.392	2540	0.493
2.	corrected	87.56	4258	0.397	2640	0.177

This table shows that the value of the minimized function decreases from 0.493 to 0.177 but the kinetic parameters vary insignificantly. This is indicative of a rather deep pit over the surface of the minimized function F within the parameters.

To determine the slow stage of the process the catalyst oxidation in air flow at various temperatures followed by temperature programmed reduction has been studied (fig.5). Hydrogen consumption

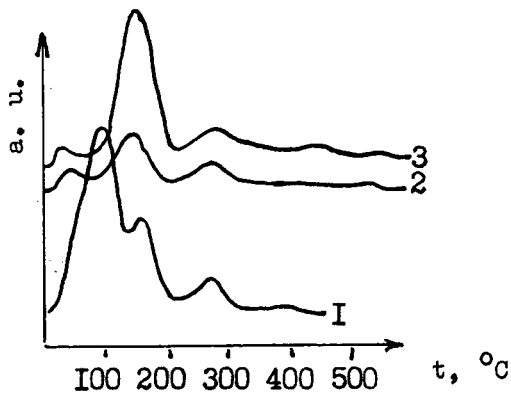

Fig.5. TPR profiles for Pd,Cu-catalysts pretreated at 500° in air flow for 1 hr
1-1.55% Pd, 3.0% Cu
2-0.1% Pd, 1.55% Cu
3-0.1%Pd, 3.0% Cu

takes place in temperature ranges of 40-100°, 100-200° and 200-400°. The first maximum of hydrogen consumption is due to reduction of palladium ions. This conclusion is confirmed by the fact that the area of the first peak increases with an increase in the Pd content in the catalyst from 0.1% (curves 2 and 3) to 1.55% (curve 1). It is well known from the literature data [26,27] that palladium cations are reduced into the atomic state in a temperature range of 20° to 150°.

Two other peaks in temperature ranges of 100-200° and 200-400° are assigned to reduction of copper ions [27,28] since an increase in the copper content of the catalyst results in an increase in the area of these peaks (curves 2 and 3).

As at a temperature as high as 500° metal atoms are oxidized not only on the surface of the metal crystallites but also in their volume the catalyst used to investigate the kinetics of the process was oxidized at the reaction temperature (180°). In this case the oxygen partial pressure in the oxidizing gas (a mixture of air and helium) was equal to 0.1 atm as it was in some catalytic runs (fig.6). As is seen from this figure hydrogen consumption at TPR of the catalyst oxidized at 180° is much lower than that for the catalyst oxidized at

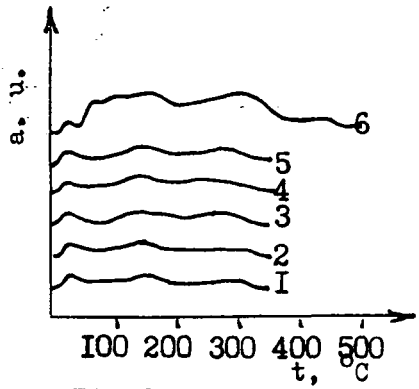

Fig.6

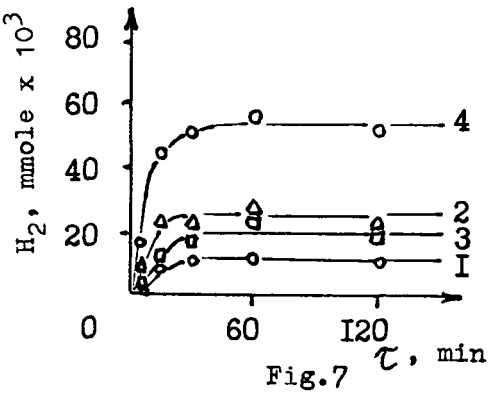

Fig.7

Fig.6. TPR profiles for Pd,Cu-catalyst oxidized at: 1.-180°, Po_2=0.1 atm, τ =5 min; 2-180°, Po_2=0.1 atm, τ =15 min; 3-180°, Po_2 = 0.1 atm, τ =30 min; 4-180°, Po_2=0.1 atm, τ =60min; 5-180°, Po_2 =0.1 atm, τ =120 min; 6-500°, Po_2=0.2 atm, τ =60min.

Fig.7. The amount of hydrogen absorbed by the catalyst at its TPR in temperature ranges of 40-100°(1), 100-200°(2), 200-300° (3) and 40-300° (4) (total amount of H_2) in dependence on the duration of catalyst oxidation at 180° and Po_2= 0.1 atm.

500°. It can be assumed that only atoms on the surface of metal crystallites would be oxidized at 180°.

From the data presented in fig.7 the amount of metal atoms oxidized at 180° could be estimated. For instance, the highest amount of Pd atoms is found to be 20-25% of the total content of Pd in the catalyst. The rate of Pd oxidation as determined by graphical differentiation of the kinetic curve (fig.7, curve 1) is equal to 0.2 x 10^{17} Pd at/g.sec. But the reaction rate of propylene oxidative acetoxylation

at 180° and P_{O_2}=0.1 at, is equal to 5 x 10^{17} molec./g.sec. As Pd oxidation is the first stage of the process of propylene oxidative acetoxylation the rate of metal oxidation could be either higher than that of the overall process or the rates of metal oxidation and those of the process could be equal. It seems likely that a higher rate of the process of propylene oxidative acetoxylation we observed may be indicative of a higher rate of Pd oxidation in the reaction conditions, particularly, in the presence of acetic acid.

Experiments with labelled ^{18}O acetic acid were carried out to identify the intermediate stages of the process of propylene oxidative acetoxylation. It can be assumed that this reaction proceeds through formation of allyl alcohol as intermediate species followed by their etherization with acetic acid to give allylacetate. This conclusion can be made from the fact that acrolein and allylacetate are formed upon propylene oxidation over a Pd,Cu-catalyst prepared on the basis of Na-form zeolite (table 9), whereas only deep oxidation of propylene takes place over a Pd,Cu-catalyst prepared on the basis of H-form zeolite. Acrolein would not form over this catalyst and it would not carry out the reaction of oxidative acetoxylation of propylene to allylacetate. Instead, simple addition of acetic acid to a propylene molecule takes place to form isoproylacetate. One can assume that upon propylene oxidation over Pd,Cu-catalyst on the basis of Na-form zeolite acrolein is formed as a secondary product during oxidation of allylalcohol.

Table 9

Dependence of the products of propylene oxidative conversion on the catalyst composition

Catalyst	Products of propylene oxidative acetoxylation at 180°	Products of propylene oxidation at 200°
PdCu/HM	$CH_3COOCH(CH_3)_2$	CO_2
PdCu/NaM	$CH_3COOCH_2CH=CH_2$	CO_2, $CH_2=CHCHO$ [*] $CH_3COOCH_2CH=CH_2$

[*] Total selectivity of acrolein and allylacetate formation is equal to 40% with propylene conversion up to 10%, but the portion of these products among the products of partial oxidation is equal to 80%.

If the reaction of propylene oxidative acetoxylation proceeds through formation of allyl alcohol followed by its etherization with acetic acid the labelled oxygen of the acetic acid $CH_3CO^{18}OH$ would convert either into molecules of allylacetate or water

$$C_3H_6 + CH_3CO^{18}OH + \frac{1}{2}O_2 \rightarrow \begin{cases} CH_3CO^{18}OC_3H_5 + H_2O & (5) \\ CH_3COOC_3H_5 + H_2{}^{18}O & (6) \end{cases}$$

Which of these processes will take place depends on the mechanism of allyl alcohol etherization over the Pd,Cu-catalyst

$$CH_2{=}CHCH_2OH + CH_3CO^{18}OH \rightarrow \begin{cases} CH_3CO^{18}OCH_2CH{=}CH_2 + H_2O & (7) \\ CH_3COOCH_2CH{=}CH_2 + H_2{}^{18}O & (8) \end{cases}$$

The isotopic composition of the initial acetic acid and that of the acetic acid after the reactions of oxidative acetoxylation and etherization are indicated in table 10.

Table 10

Isotopic composition of acetic acid (%)

Substance	Number of ^{18}O atoms in molecule			Specific concentration of ^{18}O
	0	1	2	
Initial acetic acid	53.4	38.3	8.3	27.5
Acetic acid after oxidative acetoxylation	55.6	37.8	6.6	25.5
Acetic acid after etherization with allyl alcohol	77.7	18.2	4.1	13.2

It can be seen that there are 38.3% of molecules with one ^{18}O atom and 8.3% of molecules, containing two ^{18}O atoms in the initial acetic acid. The specific concentration of ^{18}O in the initial acetic acid is equal to 27.5%. Approximately the same distribution of ^{18}O was observed in the acetic acid after the reaction of propylene oxidative acetoxylation. But the specific concentration of ^{18}O in the acetic acid after the reaction with allyl alcohol decreased approximately twice and was equal to 13.2%.

Masss-spectroscopy of the allylacetate obtained from the reaction of oxidative acetoxylation shows that the specific ^{18}O concen-

tration is equal to ~28% both in acyl and alcoxyl parts of the molecule. This implies that both oxygen atoms in the molecule resulting from this reaction originate from acetic acid and the reaction proceeds according to equation 5.

Allylacetate obtained from the reaction of allyl alcohol etherization with acetic acid on Pd,Cu-catalyst at 180° has been analyzed mass-spectroscopically using chemical ionization. The number of molecules containing no ^{18}O atoms, and one or two ^{18}O atoms is shown to be equal to 79.8, 16.9 and 3.3 %, respectively. Comparison of the isotopic composition of allylacetate obtained from the reaction of allyl alcohol etherization with that of acetic acid after this reaction (table 10) shows their good agreement. Isotopic exchange of oxygen between acetic acid and allyl alcohol makes difficult elucidation of the mechanism of etherization reaction. Calculations made show that the isotopic exchange proceeded up to 83% against the equilibrium. The presence of acetic acid and allyl alcohol with near equilibrium distribution of oxygen ^{18}O will give allylacetate with the same specific ^{18}O concentration independent of the way of its formation (equations 7 or 8). But simple calculations may show that oxygen ^{18}O distribution in allylacetate will depend on the way of the etherization reaction (table 11).

Table 11

Isotopic composition of allylacetate for various mechanisms of allyl alcohol etherization

Number of ^{18}O atoms in allylacetate molecule	Content of isotopic molecules of allylacetate for the etherization scheme (%)	
	$CH_3COOH + HO CH_2CH=CH_2$	$CH_3CO OH + H OCH_2CH=CH_2$
0	77.7	74.4
1	18.2	23.7
2	4.1	1.9
Specific concentration of ^{18}O	13.2	13.7

If a etherization reaction proceeds retaining completely the acetic oxygen in the allylacetate molecule the distribution of ^{18}O in the reaction product will coincide with that in the acetic acid after reaction (table 10). In the case of inclusion of oxygen from allyl alcohol to allylacetate the amount of unlabelled ether molecules and

that with two ^{18}O atoms would decrease but the content of isotopic ether molecules with one ^{18}O atom would increase. Experimentaly observed distribution of ^{18}O in allylacetate molecules indicates that the etherization reaction proceeds according to equation 7, i.e. ether oxygen in allylacetate originates from acetic acid.

Hence, the results obtained do not contradict the mechanism of the reaction of propylene oxidative acetoxylation through allyl alcohol as an intermediate:

$$CH_2=CHCH_3 + \tfrac{1}{2}\,O_2 \longrightarrow CH_2=CHCH_2OH \qquad (9)$$

$$CH_3COOH + CH_2=CHCH_2OH \longrightarrow CH_3COOCH_2CH=CH_2 + H_2O \qquad (10)$$

It can be assumed that allyl alcohol is in a chemisorbed state as a compound with palladium (type B) and scheme of allylacetate formation could be presented as follows:

$$Pd + \tfrac{1}{2}\,O_2 \longrightarrow PdO \qquad (A)$$

$$PdO + CH_3CH=CH_2 \longrightarrow Pd\begin{matrix}OH\\ \diagdown\\ \diagup\\ CH_2CH=CH_2\end{matrix} \qquad (B)$$

$$Pd\begin{matrix}OH\\ \diagdown\\ \diagup\\ CH_2CH=CH_2\end{matrix} + CH_3COOH \longrightarrow Pd\begin{matrix}OCOCH_3\\ \diagdown\\ \diagup\\ CH_2CH=CH_2\end{matrix} + H_2O \qquad (C)$$

$$Pd\begin{matrix}OCOCH_3\\ \diagdown\\ \diagup\\ CH_2CH=CH_2\end{matrix} \longrightarrow CH_3COOCH_2CH=CH_2 + Pd \qquad (D)$$

Thus the reaction of propylene oxidative acetoxylation considered in terms of traditional heterogeneous catalysis has a number of specific features. Firstly, only the catalysts on the basis of alkali forms of zeolites show activity in this reaction. If an H-form of zeolite is used in catalyst preparation addition of acetic acid to propylene with formation of isopropylacetate will take place instead of the reaction of oxidative acetoxylation. The cause is shown to be a change in the selectivity of propylene oxidation in the case of H-form zeolite (table 9). This is likely to be due to the fact that in the case of H-form zeolite catalysts it is not propylene molecules which are oxidized but propyl carbocations emerging on the acidic centers of the zeolite upon their interaction with propylene. Carbocation formation will not take place if zeolites contain alkali cations instead of protons. Another function of alkaline cations in

zeolites may be involvement into formation of alkaline metal acetate in the reaction conditions

$$NaZ + AcOH \longrightarrow AcONa + HZ$$

which in this case will play a role similar to that in the catalysts on the basis of nonzeolites carriers [12,13] . There is some possibility that in the presence of alkaline metal acetate instead of stage (C) in the proposed reaction scheme the following reactions will take place:

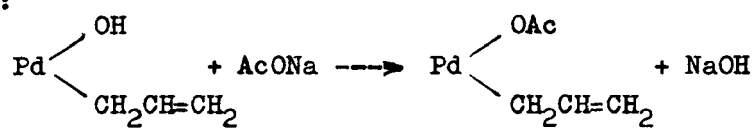

$$NaOH + AcOH \longrightarrow AcONa + H_2O$$

Another specific feature of the reaction of propylene oxidative acetoxylation is that only palladium is active in allylacetate synthesis. In the case of other VIII group metals only the reaction of deep oxidation of propylene takes place. To answer the question what is responsible for this phenomenon further investigations are needed.

REFERENCES

1. Grigoryev,A.A., Katzman, E.A., Khcheyan, Kh.E.,Bobrov,A.F., Markina,N.G., Polkovnikova, A.G., Zavorotov, V.I., Pinkhasik, E.V.,Avrekh, G.L., Chim.promyschlennost, 6, 328 (1982).
2. Moiseev, I.I., Vargaftik, M.N., Syrkin, Ya.K., Dokl.AN SSSR, 133, 377 (1960).
3. Suvorov, B.V., Bukeykhanov, N.R., Oxidative reactions in organic synthesis, Izd."Khimiya", M.,1978, p.111.
4. Svodenk,V., Scharfe, G., Pat. USSR, №353408 (1969).
5. Krönig, V., Scharfe, G., Pat. FRG, №1901289 (1969).
6. Roscher, G., Schmitz, G., Pat.FRG, №2038120 (1970).
7. Heiden, P., Irving, J.V., Brit.pat., №1310225 (1970).
8. Kisaki, H.,Zuzumi, Yu., Takeshigo, K., pat.FRG, №2165738 (1971).
9. Boyadzhan, V.K., Khachatryan, S.S., Stepanyan, G.G., Erisyan,V.K., Agavelyan, E.S.,Nefedov, O.M.,Dolgiy, I.E.,Sisin,M.F.,Kolbasin,A. Ya.,Anikeev, I.I., pat.FRG, №2603550 (1976).
10. Kumigi, T.,Arai, H.,Fujimoto, K., Bull.Jap.Petr.Inst., 12,97 (1970)
11. Politanskiy, S.F.,Shkitov, A.M.,Kharlamov, V.V.,Minachev,Kh.M., Moiseev, I.I.,Nefedov,O.M., Izv.AN SSSR, ser.chim.,7,1479 (1981).
12. Nakamura, S.,Yasui,T.,J.Catal.,17, 366 (1970).
13. Samanos,B., Boutry, P.,Montarnal, R., J.Catal.,23, 19 (1971).
14. Simidsu,T.,Yasui, A., Jap.pat., №49-6303 (1974).

15. Ono,I., Yanagihara, T., Okada,H.,Koga,T.,Kato,T., Jap.pat., № 48-37245 (1973).
16. Take, K.,Mimoun, H., De Roch, I.S., J.Catal., 58, 155 (1979).
17. Kominami, N., Tamura, N., pat.USA, №3772383 (1973).
18. Krönig, V.,Frenz, B., pat.FRG, № 1618364 (1972).
19. Krönig,V.,Frenz,B., pat.Swed., №338768 (1971)
20. Onoda,T.,Vada, K.,Otake, M., pat.USA, № 4016200 (1977).
21. Mazuda, T.,Sirafudsi, T., Jap.pat., №52-151136 (1976)
22. Höring, L.,Arpe, H.-Y., Boldt,M., pat.FRG, № 1593861 (1967).
23. Sheldom, R.A., Kochi, Y.K., Adv.Catal.,25, 274 (1976).
24. Minachev, Kh.M., Nefedov, O.M., Kharlamov, V.V., Panov, S.Yu., Politanskiy, S.F., Izv.AN SSSR, ser.chim.,7, 1490 (1981).
25. Minachev, Kh.M., Nefedov, O.M., Kharlamov, V.V.,Panov, S.Yu., Shkitov, A.M., Trofimov, M.I., Izv.AN SSSR, ser.chim.,12, 2688 (1983).
26. Mahoney, F., Rudham, R.,Summers, J.V., J.Chem.Soc.,Faraday I, 75, 314 (1979).
27. Hurst, N.W., Gentry, S.J., Jones, A., McNicol, B.D., Catal.Rev., 24, № 2, 233 (1982).
28. Gentry, S.J., Hurst, N.W., Jones, A., J.Chem.Soc., Faraday, I, 75, 1688 (1979).

CONVERSION OF METHANOL TO LOWER OLEFINS - APPLICATION STUDIES

L.W.ZATORSKI, P.T.WIERZCHOWSKI, A.A.CICHOWLAS
Institute of Organic Chemistry of the Polish Academy of Sciences, Warszawa, Poland

ABSTRACT

The conversion of methanol to lower olefins over various ZSM5 zeolite catalysts was studied in two-stage fixed bed reactor system. The catalysts containing ZSM5 zeolite with different SiO_2/Al_2O_3 ratios (73 and 183) modified with phosphorus and magnesium were used. Some effects of temperature, space velocity, and water to methanol ratio on the selectivity for C_2-C_4 olefins and product yields were determined. Catalyst deactivation due to coke formation was investigated. The activity loss from coking can be regained by oxidative regeneration. An aging test of over 34.5 hours on stream was performed during which 26.5 g of methanol/g of zeolite catalyst (SiO_2/Al_2O_3 ratio in ZSM5 is 183) was processed, yielding 17.5 g of C_2-C_4 olefins, among of them 5.3 g of propylene was found.

INTRODUCTION

The lower olefins, especially ethylene and propylene, are major raw materials for manufacture of many industrial organic chemicals. The synthesis of lower olefins from methanol, instead of from petroleum naphta, opens a new way to produce hydrocarbons from either natural gas or coal. The discovery that methanol can be converted selectively to hydrocarbons with ZSM5 type zeolite developed by Mobil Oil Corp. was first reported in the middle 1970's. By controlling zeolite structural and methanol conversion process parameters it is possible to enhance the yield of lower olefins. The results of the previous studies [1-4] have showed that to enhance the lower olefins yield the methanol conversion reaction must be run as follows: operate at short contact time, decrease the acidity of the zeolite, and increase the products shape-selectivity by reducing the apparent pore size of zeolite.

This paper describes the results of a process variable study

of the methanol to lower olefins conversion in a fixed bed reactor over various H-ZSM5 zeolite catalysts with different SiO_2/Al_2O_3 ratios. Some effects of temperature, space velocity, time on stream and water to methanol ratio on product yield were determined. The results from an aging test of four zeolite catalysts are described.

EXPERIMENTAL

Catalyst used. ZSM-5 Zeolite (ULTRAZET - designated by the Institute of Industrial Chemistry, Warszawa) in two ranges of SiO_2/Al_2O_3 ratio (73 and 183) was prepared according to the previously described procedure [5] . The zeolite was converted into the hydrogen form by stirring with the solution of hydrochloric acid (0.5 N, 353 K) for six hours. The method of modification of HZSM-5 involved a treatment of the zeolite with trimethyl phosphite as described in Mobil patent [6] . For the catalytic activity tests the zeolites were mixed with magnesium and/or aluminium oxide and tableted (5 x 5 mm tablets were formed) using polyvinyl alcohol (MW=100000) as the binder (binder content - 8 wt %). γ-Alumina (Pechiney-Saint-Gobain Activated Alumina, France) was used as the dehydration catalyst in the first step of the process. Catalyst's composition and characteristics are shown in Table 1.

Table 1

Catalyst's composition and characteristics

No	ZSM-5			Al_2O_3	MgO	Tablets ϕ/h	Compression strength (after reaction)
	[wt %]	$\frac{SiO_2}{Al_2O_3}$	P [wt %]	[wt %]	[wt %]	[mm/mm]	[kg/cm^2]
A	50	73	2.3	50	0	5/5	37
B	50	73	2.3	40	10	5/5	30
C	50	183	0.7	40	10	5/4	45
D	50	183	0.0	40	10	5/4	70

Apparatus and procedure. The experimental studies on process variables were carried out in two-step fixed bed type apparatus with a continuous flow system at atmospheric pressure. Using two reactor system the first reactor contains alumina that promotes only a methanol dehydration reaction to dimethyl ether. Dehydration catalyst in the first reactor can be operated for long period without any significant loss in activity and therefore was

not studied in details.

The studies concerning only the second step of the process have been performed. The special stainless steel tubular reactor (50cm long and 0.5cm in diameter) was developed for these purposes. Three separate electrical heating sections were constructed. The upper part of the reactor was used as a preheater for the gaseous products from the first reactor and for water additionally allowed into the conversion reactor. Six thermocouples connected to a multichannel recorder provided facilities for the controlling of temperature of the gaseous substrates at the inlet to the reactor and to record a profile of the temperature in the catalyst bed. 90 g of HZSM-5 zeolite catalyst was placed on support grid and then calcined at 833 K in a flow of argon/oxygen for six hours. A blend of methanol and water (80/20 w/w) was delivered to the first reactor by a metering pump at a constant feed rate. The hot vapours leaving the first reactor containing a near equilibrium mixture of dimethyl ether, methanol and water were combined with water vapour and fed into the second reactor. Product analysis was provided in a Chrom 4 Chromatograph as described in the details elsewhere [4].

RESULTS

The effects of temperature, space velocity (WHSV), and water to methanol ratio were determined. These parameters were examined over a range of 688-748 K, 0.66-25.0 h^{-1} and 0.25-2.96 g/g, respectively. Representative data are shown in Table 2. Fig. 1 shows the change of activity of the catalyst (A) with the reaction temperature. Changes in aromatics and olefins yield with time on stream on studied catalysts are shown in Fig. 2 - 5. The dependence of C_2-C_4 olefin yield and selectivity in methanol conversion reaction on the water to methanol ratio ilustrates Fig.6.

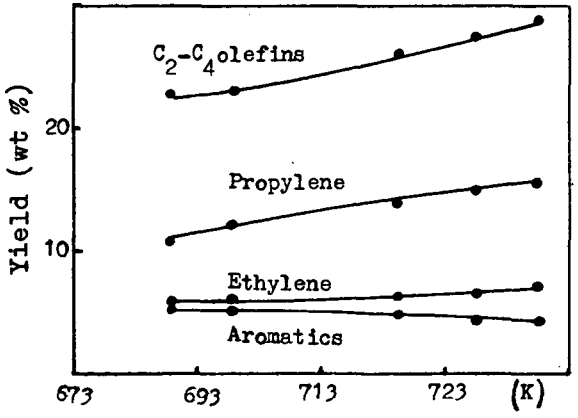

Fig. 1. Effect of temperature on methanol conversion. Catalyst A. WHSV=1.2 h^{-1} H_2O/CH_3OH=2.3

Table 2

Operating conditions and distribution of hydrocarbons in the conversion of methanol

Catalyst No	A	A	A	B	B	B	C	C	C	C	C	C	C	D	D	D	D
Temperature K	703	736	740	740	743	738	748	746	750	748	750	748	746	743	743	745	747
Space velocity gCH_3OH/g cat.h	1.15	1.34	1.41	1.38	1.38	1.37	0.8	0.79	0.79	0.66	0.8	0.8	0.8	2.3	2.28	2.5	2.44
Water/Methanol g/g	2.45	2.19	2.14	2.30	2.30	2.30	0.25	0.97	1.52	1.74	1.80	2.28	2.96	2.15	2.21	2.12	2.16
Conversion %	92.68	97.23	94.29	95.41	96.28	90.74	99.68	98.74	97.92	98.23	97.60	97.18	92.78	94.23	94.05	95.15	95.20
Selectivity %																	
Hydrocarbons	42.41	43.54	43.17	43.45	43.37	42.30	43.74	43.62	43.62	43.65	43.61	43.59	43.07	43.12	43.14	43.47	43.00
Dimethyl Ether	2.15	0.34	0.95	0.49	0.63	2.37	0.00	0.22	0.22	0.17	0.22	0.27	1.12	1.04	1.00	0.39	0.58
Water	55.41	56.12	55.88	56.06	56.00	55.92	56.25	56.17	56.16	56.18	56.18	56.14	55.81	55.84	55.86	56.07	56.48
Hydrocarbons wt %																	
Ethylene	13.24	15.49	15.26	16.57	17.53	14.37	10.90	10.29	10.26	10.59	9.70	9.62	8.71	8.82	8.69	7.33	7.93
Propylene	30.47	35.56	36.58	36.57	35.52	36.48	31.36	40.16	44.08	44.89	43.97	46.80	46.38	47.37	46.69	44.07	48.52
Butenes	13.76	16.81	15.53	15.84	15.11	15.29	22.16	21.86	21.25	21.08	21.66	20.57	20.14	21.00	21.68	20.97	21.12
Methane	0.85	0.88	1.84	0.91	1.34	1.84	2.22	1.82	1.40	1.69	1.13	1.13	1.16	0.97	0.95	0.74	0.84
Ethane + Propane	2.70	2.73	2.19	3.71	4.02	1.57	3.58	2.37	2.05	1.97	1.79	1.51	1.26	0.97	0.96	1.21	1.31
Butanes	9.70	6.34	4.91	5.34	5.10	4.05	4.52	2.82	2.33	2.34	2.73	2.17	2.03	2.91	2.67	2.41	2.35
C_5+ aliphatics	14.83	12.37	12.44	13.18	12.55	16.69	16.61	15.09	14.58	13.46	15.53	14.70	17.38	14.95	14.86	19.03	13.90
C_6+ aromatics	14.53	9.72	11.16	7.79	8.93	9.72	9.16	5.68	4.05	3.88	3.50	3.31	2.83	2.73	3.40	4.24	3.83
C_2-C_4 olefin selectivity %	57.48	67.87	67.36	68.98	68.15	66.13	63.92	72.31	75.59	76.58	75.32	76.89	75.24	78.18	77.06	72.37	77.62
C_2-C_4 olefin Yield %	22.61	28.73	27.42	28.59	28.45	25.39	27.88	31.14	32.28	32.83	32.06	32.61	30.06	31.76	31.27	29.93	32.07
Propylene yield %	12.00	15.10	14.90	15.20	14.84	14.00	13.70	17.30	18.80	19.25	18.70	19.80	18.50	19.20	18.90	18.20	19.90

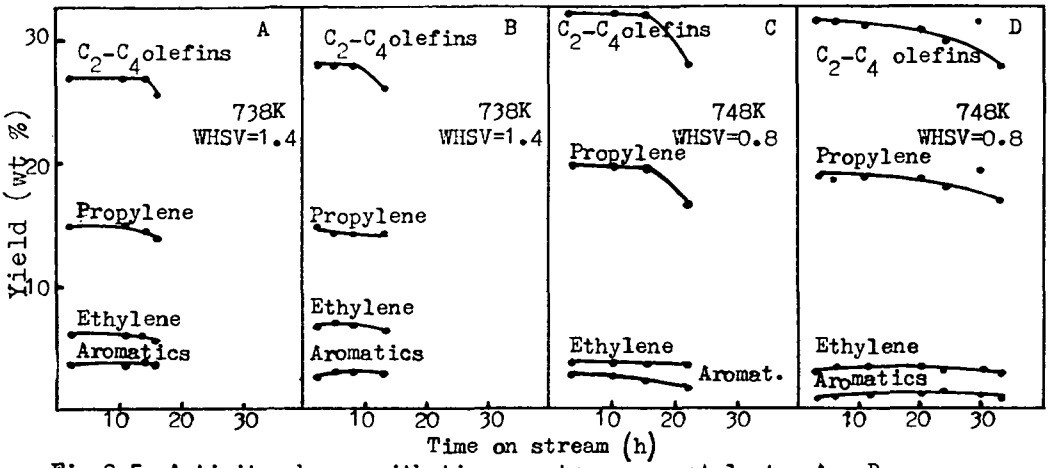

Fig.2-5. Activity change with time on stream on catalysts A - D.

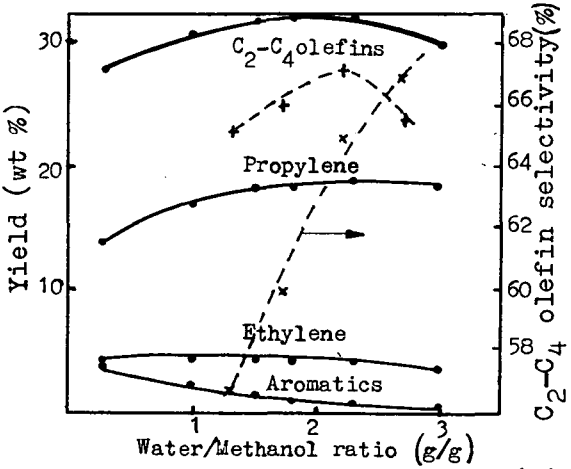

Fig. 6. Effect of water/methanol ratio on methanol conversion. Catalyst A and C.
---- A - 738K; WHSV=1.4 h^{-1}
——— C - 748K; WHSV=0.8 h^{-1}

The performance of the catalyst (D) throughout the 13 successful cycles in the long aging test is shown in Table 3, where the outlet concentrations of products formed from methanol are plotted as function of time on stream in each cycle.

Table 3

Product distribution in long-term aging test. Temp. 733 K; WHSV=1.2; diluent gas - He. I^x - temp. 743 K; WHSV=0.8; H_2O/CH_3OH = 2.7.

Cycle No	1		6			8			10		12		I^x
Time on stream in cycle, h	1	24	1	6	25	5	24	29	1	19	1	22	30
Composition, wt %													
ethylene	7.1	6.2	8.9	9.0	6.9	10.6	6.6	6.7	8.0	7.2	8.5	7.2	8.5
propylene	45.3	42.0	43.9	41.4	38.7	45.5	42.3	40.4	48.0	40.0	46.8	39.5	51.7
butenes	29.4	32.0	29.2	27.0	26.1	28.1	22.2	21.2	27.5	22.2	27.3	21.2	22.2
methane	1.1	1.3	2.4	3.8	8.5	1.7	8.3	10.6	1.5	8.7	1.5	10.1	0.9
ethane/propane	1.3	1.8	1.5	1.4	1.5	0.8	0.2	0.2	0.9	1.0	1.2	0.9	1.4
butanes	2.1	2.7	2.7	3.2	3.5	1.5	0.9	0.8	1.7	1.2	2.0	0.9	2.5
C_5+aliphatics	13.8	18.0	11.4	14.0	20.3	10.7	14.8	12.1	12.3	14.8	12.6	14.0	11.1
dimethyl ether	-	4.0	-	-	10.0	-	4.8	8.0	-	4.9	0.1	5.9	1.3

DISCUSSION

The results from the process variable study previously published [2 - 4] provided basis to select operating conditions for above described experiments. It was found that reaction temperature should be higher than 733 K, and WHSV not be higher than 2.0 h^{-1} and water to methanol ratio at the range 2.0-2.2. Higher space velocity required that the reaction temperature should be so high as 773 K to maintain the conversion level above 90 %. The increasing the temperature above 773 K gave the higher olefin selectivity but simultaneously the amount of methane was increased above 4 %. For these reason WHSV = 1.4 h^{-1} was chosen in further studies.

The next process parameter controlling the formation of olefin which was optimized was water to methanol ratio. The charge stock used in the study was a blend of methanol and water (20 %). This composition simulated the product from the commercial methanol plant. By co-feeding of water to the effluent from the dehydration reactor the contact time of the reactants was shortened resulting in an improvement through the prevention of coke deposition. The relation shown in Fig. 6 allowed one to make a conclusion that the olefin selectivity and yield increases parallely to water/methanol ratio. The optimization of this process parameter is limited because simultaneously with the enhacement of selectivity - conversion and yield of the process are decreased. The maximum C_2-C_4 olefin yield (greater than 28 wt %) and conversion more than 95 % were achieved for water/methanol ratio equals 2.2 over catalysts (A) and (B). The modification of the zeolite with magnesium oxide (B) resulted in the shortening of lifetime of the catalyst (from 17.5 to 13.5 hrs) and the insignificant increasing of the olefins yield.

It is known [7] in the art that the catalytic activity and selectivity for the formation of lower olefins over ZSM-5 catalyst depend on such catalyst parameters as activity and SiO_2/Al_2O_3 ratio. The selectivity to C_2-C_4 olefins increases with diminishing of the strong Bronsted acid sites population, which are probably located at channel intersections [8] as it was observed by Balkrishnam [7]. In general, decreasing of the catalytic activity of the zeolite can be achieved by decreasing of the surface acidity (concentration of all acid sites) parallely with increasing SiO_2/Al_2O_3 ratio. It is also knows [9] that higher yield of olefins can be obtained over phosphorus-modified ZSM-5 zeolite. Therefore, the zeolite catalysts which

contain ZSM-5 with SiO_2/Al_2O_3 ratio equal to 183 and modified with phosphorus and magnesium were prepared. Modification of ZSM-5 zeolite by oxides of magnesium and/or aluminium was aimed to improve the catalyst selectivity towards lower olefins as well as at the preparation of a catalyst with the required mechanical strength. These two features are very important for the catalyst practical application in the industrial process of conversion of methanol to lower olefins. Those modifications of catalysts required us to optimize such a process parameter as the contact time (WHSV). The optimization of this parameter shows that WHSV should be at the level of 0.8 h^{-1} enabling the maintenance of conversion higher than 95 %. Previously [3] we observed the changes of olefin selectivity in dependence to a maximum gradient in the bed. It was noticed that the reducing of temperature gradient gives the increasing of the olefin selectivity. The temperature gradient strongly depends on WHSV and water/methanol ratio. In order to correct these parameters the influence of the dilution of methanol with water on methanol transformation was studied. On comparing C_2-C_4 olefin yields for the zeolite catalyst (A) and (C) (Fig. 6) it is shown that the maximum yield over the range of water/methanol = 1.8 - 2.2 is not so sharply marked for the catalyst (C) as for (A). In order to obtain the high olefin selectivity it is necessary to resolve the problem of such a dilution of substrate at which the conversion will be at the level enabling the recovery and recycling of the unconverted methanol and dimethyl ether to the process. An isolation of these compounds from a big amount of water is difficult technological problem. Therefore the parameters of the process must be checked in a pilot plant and than it will be possible to answer the question to which economical level the conversion can be lowered in order to obtain the best olefin selectivity. Like it was expected the C_2-C_4 olefin yield (Fig.2-5) was increased to more than 30 % using the zeolite catalysts with higher SiO_2/Al_2O_3 ratio. The yield of propylene was also high - about of 20 wt %. The direct comparision of the life-time of the studied catalysts with the various SiO_2/Al_2O_3 ratios was difficult because of the different WHSV used in the experiments. However, refering the life-time of catalyst to the amount of methanol processed on the catalyst it was possible to compare those catalysts.From the results presented in Table 4 it is noticed the prolonged life-time of catalyst (C) and (D) up to 22 and 35 hrs, respectively. It can be also concluded that the best catalyst is that one (D) containing HZSM-5

zeolite with SiO_2/Al_2O_3 = 183 modified with magnesium oxide. During 34.5 hours on stream 26.5 g of methanol/g of catalyst was processed forming 17.5 g of $C_2 - C_4$ olefins, among of them 5.3 g of propylene was found.

Table 4

Comparision of life-time of the catalysts per cycle

Catalyst No	Working time at conversion level above 90 % [hrs]	Methanol processed [g/g cat]	Propylene [g/g cat]
A	17.5	49	7.3
B	13.5	38	5.7
C	22.0	35	7.0
D	34.5	55	10.5

Considerable effort was devoted to the study of catalyst aging which is mainly due to coking. The deactivation is reversible and most of the catalytic activity can be restored by controled coke burning. A noteworthy feature of this process is that a catalyst ages in a band. This was evident from the change of the temperature profil through the catalyst bed. Coke formation which deactivates the catalyst during its time on stream and requires a periodical regeneration determines the cyclic behaviour of the process of methanol conversion to lower olefins.

The results of these studies have demonstrated the feasibility of converting methanol to lower olefins in a fixed bed reactor. These data can be used to develop the design basis for a fixed bed pilot plant.

REFERENCES

1. Zatorski, L.W., Wierzchowski, P.T., Proc. Vth Int.Symp.Heterog. Catalysis, Varna, 1983, part I, p.329
2. Zatorski, L.W., Wierzchowski, P.T., Cichowlas, A.A., Przem.Chem. 62,187 (1984)
3. Zatorski, L.W., Wierzchowski, P.T., Przem.Chem. 62, 242 (1984)
4. Zatorski, L.W., Wierzchowski, P.T., Cichowlas, A.A., Bull. Pol. Acad.Sc., Chemistry, 32, No 3-6, 217 (1984)
5. Berak, J.M., Pieniążek, J., Czerwińska, B., Meisner, J.,Mostowicz, R., Przem.Chem. 61, 85 (1982)
6. US Pat. No 3.911.041
7. Balkrishnan, I.,Rao, B.S., Hedge, S.G., Kotashane, A.N., Kulkarni

S.B., Ratnasamy, P., J.Mol.Cat., 17, 261 (1982)
8. Topsøe, N., Pedersen, K., Deruane, E.G., J. Cat. 56, 169 (1979)
9. Vedrine, J.C., Auroux, A., Dejaivfe, P., Ducarne, V., Hoser, H., Zhou, S., J. Cat. 73, 147 (1982)

This report was prepared as an account of work sponsored by Polish Government; grant designation PR-1.5.2.3.4.

SYNTHESIS OF OLEFINS FROM METHANOL ON ERIONITE AND MORDENITE WITH ISOMORPHOUS SUBSTITUTION OF Si^{4+} CATIONS BY B^{3+}, Ga^{3+} OR Fe^{3+}

N.V. Kljueva, Nguen Duc Tien, K.G. Ione
Institute of Catalysis, Novosibirsk 630090, USSR

ABSTRACT

The peculiarities of erionite and mordenite crystallization in the presence of polycharged cation salts and their catalytic properties in methanol transformation have been studied. It is shown that the capability of zeolites, in which part of Si^{4+} cations are isomorphously substituted by B^{3+}, Ga^{3+} or Fe^{3+}, to accelerate hydrogen redistribution reactions of olefins differs from that of aluminosilicate catalysts of the same crystal structure but without polycharged cations.

INTRODUCTION

As is known, the formation of acid-base centers in zeolites is a result of isomorphous substitution of Si^{4+} by Al^{3+} cations. It was shown earlier [1-3] that introduction of E^{3+} cations, where E^{3+} = B^{3+}, Ga^{3+}, Fe^{3+} into ZSM zeolites changes their catalytic properties in methanol conversion to hydrocarbons due to isomorphous substitutions, $Si^{4+} \rightleftharpoons E^{3+}$ and $Al^{3+} \rightleftharpoons E^{3+}$, and formation of active centers of peculiar compositions. In the present work zeolites with the erionite and mordenite structures were synthesized. Part of Al^{3+} cations in the initial reaction mixture was substituted by the same amount of B^{3+}, Ga^{3+} or Fe^{3+} cations. Crystallization fields in systems Na_2O-K_2O-Al_2O_3-E_2O_3-SiO_2-H_2O and Na_2O-Al_2O_3-E_2O_3-SiO_2-H_2O, where E_2O_3 = B_2O_3, Ga_2O_3 or Fe_2O_3, were studied.

EXPERIMENTAL

The initial reaction mixture for erionite synthesis was prepared by mixing solutions of NaOH, KOH, aluminium, gallium and iron sulphates, boric acid and sodium silicate. Molar ratios of OH/SiO_2 and SiO_2/Al_2O_3 were varied from 0.60 to 0.90 and from 20 to 100, respectively. When thoroughly stirred, the mixture was placed into a steel autoclave in a Teflon tube and was held at 120°C for 1-30 days.

Mordenites were synthesized by crystallization of the initial mixture under hydrothermal conditions at 150°C for 3-7 days. 30% sili-

ca sol, sodium hydroxide, salts of iron, gallium, boron, aluminium were used as reactants, with water and mordenite powder as a seed added in a quantity of 1 wt%. Reactant molar ratios were varied in the range: SiO_2/Al_2O_3 = 30÷80, OH/SiO_2 = 0.25÷0.60, SiO_2/E_2O_3 = 26÷60 at constant $SiO_2/Al_2O_3+E_2O_3$ = 20 and H_2O/SiO_2 = 35.

X-ray spectra were recorded using CuK_α-monochromatic radiation at reflection angles ranging over $2° < \theta < 20°$. The crystalline phase was determined from the comparison of reflex intensities within 10-15° of the resulted product and reference zeolite. This latter was synthesized as described above without addition of inorganic salts.

The efficient specific surface area of silicates (S_{sp}, m^2/g) was calculated from the values of argon adsorption at the temperature of liquid nitrogen.

^{29}Si, ^{27}Al, ^{11}B, ^{71}Ga NMR spectra were recorded* using a Bruker CXP-300 spectrometer. In some cases magic angle spinning was employed Prior to spectra registration, the samples were held in a desiccator over the saturated solution of NH_4Cl at room temperature until the constant weight.

ESR spectra were taken** on a Bruker EP 201 spectrometer. Silica glass with Fe^{3+} admixture ions, whose ESR spectrum was characterized by the line with a g-factor of 4,28, was used as a reference. Relative line intensities were found by comparing peaks of line intensities for the sample under study and the reference.

Experiments were carried out by a pulse method in a fluidized catalyst bed microreactor. The samples were pre-calcined in air flow at 500°C. Methanol conversion was studied in the temperature range 350-450°C at an input methanol concentration of 21 vol%, the rest being helium, and at contact time 1±0.2 s. The reaction mixture at the reactor outlet was chromatographically analyzed using columns filled with polyethylene glycol and sodium-modified γ-Al_2O_3. The selectivity of methanol conversion into i-product was calculated from the formula

$$S_i = \frac{C_i}{\sum_i C_i} \cdot 100\% \text{ , where}$$

C_i is the concentration of i-product in the gas mixture at the reactor outlet in $g \cdot dm^{-3}$. Olefin yield was estimated from the formula

---

* NMR spectra were taken by V.M. Mastikhin

** ESR spectra were taken by V.F. Yudanov

$$W = \frac{V \cdot \sum C_{en}}{m}$$, where

V - space velocity of the gas mixture in $dm^3 \cdot h^{-1}$; C_{en} - olefin concentration in the gas mixture at the reactor outlet, $g \cdot dm^{-3}$; m - catalyst weight in g.

RESULTS

Hydrothermal treatment of bialkaline aluminosilica gels with B^{3+}, Ga^{3+} or Fe^{3+} additives at molar ratios of OH/SiO_2 = 0.70÷0.90, $SiO_2/Al_2O_3+E_2O_3$ = 20 and at 120°C leads to the formation of erionite. Polycharged cations considerably affect the formation rate of a zeolite phase. Thus, crystallization of erionite is markedly accelerated after introduction of B^{3+} and is somewhat slowed down upon addition of a Ga^{3+} source. In the presence of Fe^{3+} the selectivity of the erionite phase formation decreases (Fig. 1).

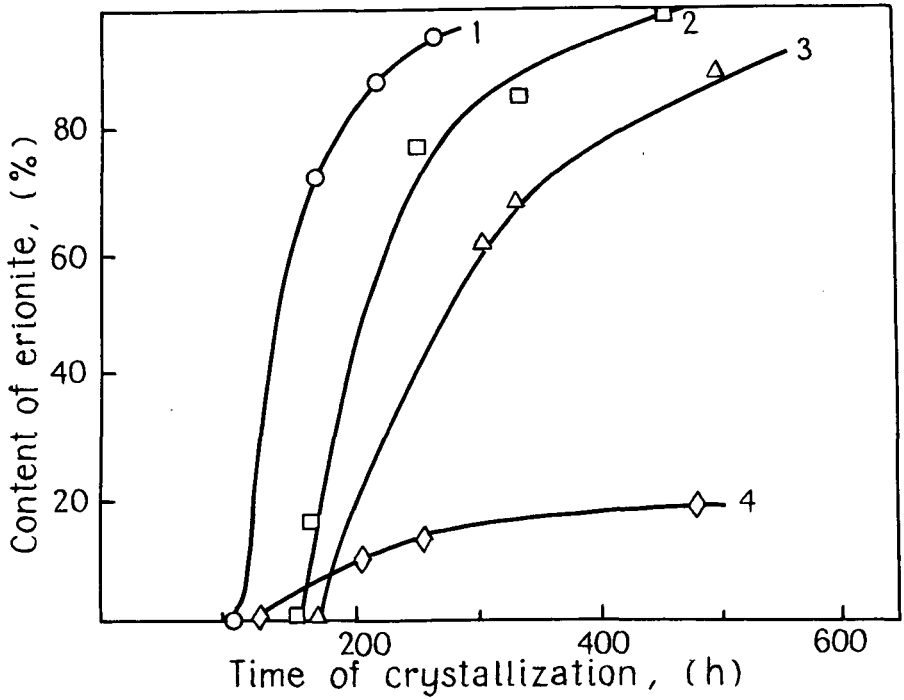

Fig. 1. Content of erionite phase in a solid product versus the time of crystallization in the presence of B^{3+}, Ga^{3+}, Fe^{3+} cations. 1 - BEr, 2 - Er, 3 - GaEr, 4 - FeEr.

In the Na_2O-Al_2O_3-E_2O_3-SiO_2-H_2O system, at OH/SiO_2 = 0.30÷0.60 and $SiO_2/Al_2O_3+E_2O_3$ = 20, crystallization temperature 150°C and 1 wt% of mordenite powder as a seed, crystallization of mordenite is observed. Table 1 shows the effect of the nature of substituting elements introduced into the initial reaction mixture on the content of crystalline phases of erionite and mordenite in crystallization products.

Table 1

Chemical composition of silicates with the structure of erionite (Er) and mordenite (M) synthesized under optimal conditions in the presence of B^{3+}, Ga^{3+}, Fe^{3+} sorces.

Sample	Product composition, mol/mol Al_2O_3						S_{sp}	Content of crystalline phase,%	Crystalline phase composition
	Na_2O	K_2O	B_2O_3	Ga_2O_3	Fe_2O_3	SiO_2	m^2/g		
Er	0.03	0.30	-	-	-	6.7	630	100	erionite
BEr	0.01	0.22	0.29	-	-	7.3	680	95	erionite
GaEr	0.03	0.21	-	0.21	-	8.3	520	100	erionite
FeEr	0.01	0.24	-	-	1.01	12.1	430	80	Er,P,chabasite
M	0.03	-	-	-	-	11.6	600	100	mordenite
BM-1	0.03	-	0.38	-	-	19.0	610	100	mordenite
BM-2	0.04	-	-	-	-	35.0	560	80	mordenite
BM-3	0.04	-	-	-	-	52.0	420	70	mordenite
GaM-1	0.03	-	-	0.59	-	21.3	610	90	mordenite
GaM-2	0.03	-	-	0.79	-	26.0	580	90	mordenite
GaM-3	0.05	-	-	1.33	-	34.4	560	80	mordenite
FeM-1	0.03	-	-	-	0.45	17.3	570	100	mordenite
FeM-2	0.04	-	-	-	1.98	32.5	530	100	mordenite
FeM-3	0.22	-	-	-	2.96	40.6	500	70	mordenite

^{29}Si NMR spectra of the synthesized silicates have signals with chemical shifts (δ) -99, -105, -119 ppm. The line with δ = -113 ppm is attributed [4,5] to silicon cations, having no aluminium cations in the second coordination sphere, and the line with δ = -105 and -99 ppm is attributed to silicon cations with one and two aluminium atoms in the second coordination sphere, respectively. The chemical shifts of the signals in ^{29}Si NMR spectra of the synthesized element-containing silicates are the same, but intensities of signals with δ = -105 and -99 ppm are less than in the spectrum of aluminosili-

cate synthesized without addition of inorganic salts (Fig. 2). This

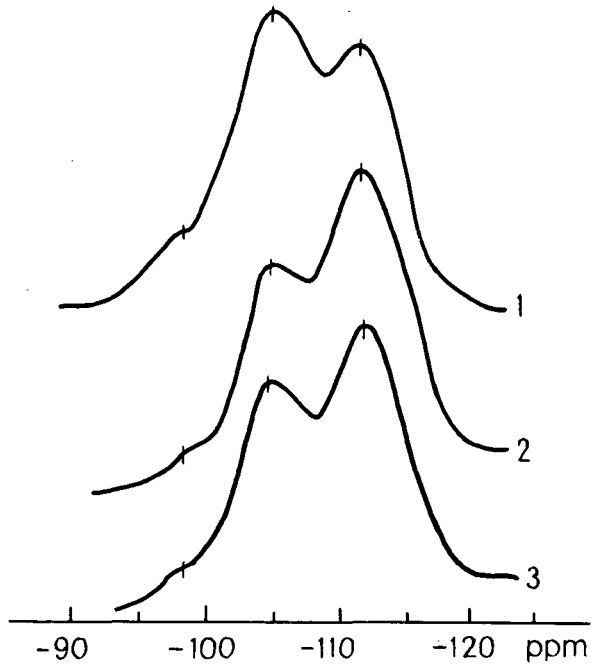

Fig. 2. ^{29}Si NMR spectra of mordenite samples: 1 - M, 2 - BM-1, 3 - GaM-1, compositions of samples are given in Table 1.

indicates that decreasing of the number of aluminium cations in the second coordination sphere of silicon cations has taken place.

In ^{27}Al NMR spectra of all solid samples a line with a chemical shift of δ = 54,3 ppm corresponding to Al^{3+} cations in the tetrahedral coordination is observed [6]. The position of this line and, hence, the state of aluminium cations in the zeolite framework is unaffected by introduction of boron or gallium into the silicates, but the intensity of signal and the content of Al cations decrease. In accordance with the NMR data, the aluminium content in the tetrahedral coordination within the experiment error is consistent with the total concentration of Al^{3+} in a solid product derived from chemical analysis data (Table 2).

^{11}B NMR spectra of mordenite and erionite samples have the line with a chemical shift δ = -23.8 ppm with respect to an aqueous saturated solution of H_3BO_3. This signal is attributed [7] to boron cations in tetrahedral oxygen environment, which appear to enter the zeolite framework. Comparison of NMR and chemical analysis data

Table 2

NMR data on the content of Al^{3+}, B^{3+} and Ga^{3+} cations in tetrahedral coordination in erionite samples.

Sample	$\frac{Al_2O_3^{tetr.}}{Al_2O_3^{com.}}$	$\frac{B_2O_3^{tetr.}}{B_2O_3^{com.}}$	$\frac{Ga_2O_3^{tetr.}}{Ga_2O_3^{com.}}$
Er	0.9	-	-
BEr	0.9	0.1	-
GaEr	1.1	-	0.5

(Table 2) reveals that only small part of B^{3+} cations is fixed in the tetrahedral environment of the zeolite framework.

^{71}Ga NMR spectra possess a broad signal with δ =157 ppm ascribed to gallium cations in tetrahedral coordination, i.e. in the framework [8]. Relative intensities of this signal suggest that only part of the overall amount of gallium cations determined by the chemical analysis are in such state (Table 2).

In ESR spectra of Fe^{3+} cations three signals with g-factors of 2.003, 2.3 and 4.28 are observed. The third signal is the weakest. The presence of the g = 4.28 signal extends an evidence for that part of iron cations is in tetrahedral oxygen environment of the crystalline lattice[9].Relative intensities of signals with g-factors of 2.003 and 4.28 versus the total content of Fe^{3+} in samples are given in Fig. 3. Based on the intensity ratios of these signals one may conclude that the major part of Fe^{3+} are in the oxide phase composition and only little part in zeolite framework.

The main reaction products of methanol conversion are light hydrocarbons, C_2-C_4, paraffins and olefins. Aromatic hydrocarbons, mainly ethyl-benzene, toluene, xylene, are present in the reaction products too. Table 3 shows the effect of Al^{3+} concentration in the zeolites, synthesized in the presence of E^{3+} cations on the selectivity of methanol conversion.

The decreasing of the aluminium content in the erionite, as well as in the mordenite, changes selectivity of methanol transformation to hydrocarbons. Thus, in the case of erionites a decrease in the Al_2O_3 content in the solid product from 15,4 down to 7,5 wt% resulted in the increase of the olefin-to-paraffin ratio in methanol conversion products from 1,6 to 3,8. As for mordenite, the decrease in the Al_2O_3 content from 9,4 down to 5,2 wt% leads to a slight decrease of the olefin-to-paraffin ratio in the reaction product and

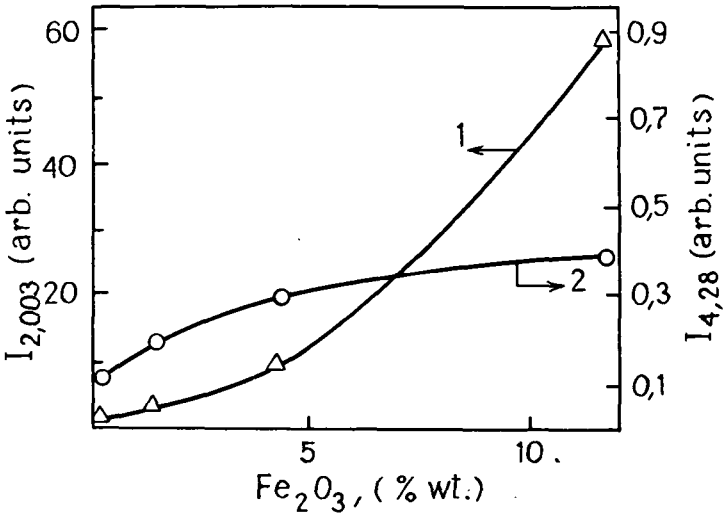

Fig. 3. Relative intensities of signals with g-factors of 2.003 (1) and 4.28 (2) in ESR spectra of Fe-containinf mordenites as a function of the concentration of Fe_2O_3 in the samples.

enhances the selectivity to the formation of aromatic hydrocarbons (Table 3).

Table 3

Selectivity of methanol conversion on silicates synthesized in the presence of B^{3+}, Ga^{3+}, Fe^{3+} sources. Reaction temperature 380°C.

Sample	Content of Al_2O_3 wt%	Selectivity to hydrocarbons, wt%			Yield of olefins $g_{olef}/g_{cat} \cdot h$
		paraffins	olefins	aromat.	
Er	15.4	38.3	61.5	0.2	0.93
BEr	13.9	29.5	69.9	0.6	1.13
GaEr	11.7	20.4	78.0	1.6	0.86
FeEr	7.5	21.4	78.6	0.0	0.07
M	9.4	57.8	41.0	1.0	0.29
BM-1	6.8	64.8	32.6	2.6	0.36
GaM-1	5.2	64.3	27.8	7.9	0.25
FeM-1	6.3	67.0	30.2	2.8	0.12

On further decreasing of Al_2O_3 content down to 2.8 wt% in a solid product the olefin-to-paraffin ratio tends to increase. It is important to note that at the same Al_2O_3 content the lowest selectivi-

ty to olefin formation is observed for B-containing samples and the highest one for Fe-containing mordenites (Fig. 4).

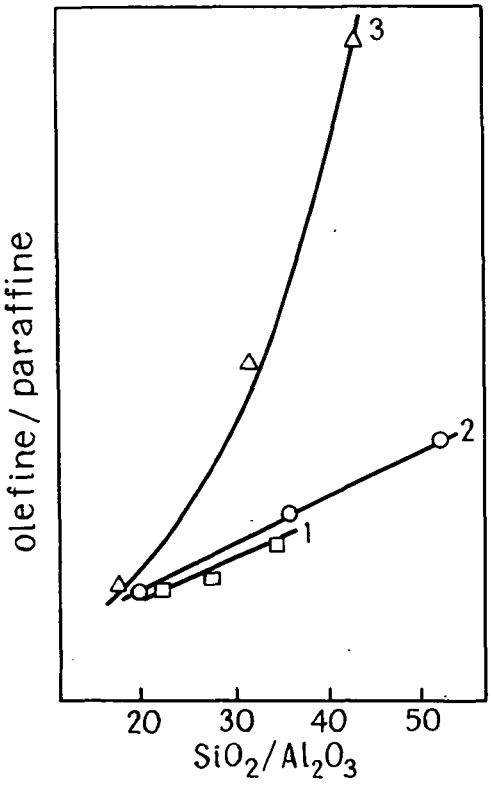

Fig. 4. Olefin-to-paraffin ratios in methanol conversion products at 380°C versus the SiO_2/Al_2O_3 mole ratio in mordenites: 1 - GaM, 2 - BM, 3 - FeM.

The yield of olefins in methanol conversion in the presence of both erionites and mordenites decreases in the order (Table 3):

BEr > Er > GaEr > FeEr

BM > M > GaM > FeM

The yield of olefins is the highest for boron-containing zeolites, and the lowest for ferrozeolites.

The selectivity of methanol conversion to aromatic hydrocarbons is lower on erionites than on mordenites. Different selectivities of erionite and mordenite samples with respect to aromatic hydrocarbons seem to be due to geometric peculiarities of erionite porous structure which prevents the development of hydrogen redistribution reactions [10]. Gallium-containing samples have shown the highest selec-

tivity to the formation of aromatic hydrocarbons.

DISCUSSION

The reported experimental data is an evidence for that the crystallization of erionite and mordenite zeolites with a low content of aluminium cations is possible under hydrothermal synthesis. The crystallization is achieved by introduction of polycharged B^{3+}, Ga^{3+}, Fe^{3+} cations into the initial reaction mixture.

From the character of ^{11}B, ^{71}Ga NMR and Fe^{3+} ESR spectra it may be proposed that during crystallization part of these cations enter the silica-oxygen framework of solid products in isomorphous Si^{4+} positions.

It may be concluded that along with the catalytically active centers of type $[(SiO)_{4-n}Si(OAl)_n]^{n-}$ supposed previously [11], the groups with the composition of $[(SiO)_{4-n}Si(OAl)_{n-m})(OE)_n]^{n-}$ in zeolite structures may also be formed. As reported earlier [11], the ability of zeolites to convert methanol to aromatic hydrocarbons (and coke precursors) depends upon the concentration of the centers of multipoint interaction with reagent molecules $[(SiO)_{4-n}Si(OAl)_{n-1}]^{n-1}$ $\cdot Al^{3+}$. These centers include the framework anions and aluminium cations that have emerged from the framework as a result of hydrolytic rupture of the Si-O-Al bond.

It may be expected that during decationation and thermotreatment procedures of the synthesized element-containing zeolites $[(SiO)_{4-n}Si(OAl)_{n-m-1}(OE)_{m-1}]^{n-2} \cdot Al^{3+} \cdot E^{3+}$ groups may be formed. On the one hand, these groups have a lesser value of "n" in $Si(OAl)_n$ groups and, on the other hand, a lesser concentration of aluminium in cation positions in comparison with zeolites, synthesized without polycharged cations. The appearance of such centers would decrease the rate of secondary reactions of the hydrogen redistribution in olefins and, consequently, change the reaction selectivity. The proposed explanation of variations in the selectivity of zeolite action upon introduction of cations capable of isomorphous substitution of types $Si^{4+} \rightleftharpoons E^{3+}$ and $Al^{3+} \rightleftharpoons E^{3+}$ are consistent with experimental data presented in Table 3 and Fig. 4.

REFERENCES

1. Ione K.G., Vostrikova L.A., Paukshtis E.A., Yurchenko E.N.: Dokl. AN SSSR, 261, 1160 (1981).
2. Ione K.G., Vostrikova L.A., Stepanov V.G.: Certificate of authorship No 1092141, 15.05.84, V.I. No 18.

3. Ione K.G., Vostrikova L.A., Petrova A.V., Mastikhin V M.: Proc. 8th Intern. Congress on Catalysis, v. 4, 519 (1984), W.Berlin.
4. Nagy J.B., Gabelica Z., Debras G., Boudart R., Derouane E.G., Jacobs P.A.: J.Molec.Catal., 20, 327 (1983).
5. Nagy J.B., Gabelica Z., Derouane E.G., Jacobs P.A.: Chem.Lett., 200 (1984).
6. Klinovski J.: Progress in NMR spectroscopy, 16, 237 (1984).
7. Ione K.G., Vostrikova L.A., Petrova A.V., Mastikhin V.M.: Studies in surface science and catalysis, 18, Structure and reactivity of modified zeolites, Elsevier, p. 151-158, 1984 .
8. Akitt J.V.: Ann.Rep.NMR, v. 5, 4 (1973).
9. Dorouane E.G., Mestdaqu M., Vielovye L.: J.Catal., 33, 168 (1974)
10. Weisz P.: Proc. 7th Intern Congress on Catal., Tokyo, 1980, p. 1.
11. Ione K.G., Stepanov V.G., Echevskii G.V., Shubin A.A., Paucshtis E.A., Zeolites, 4, 114 (1984).

STUDIES ON THE INITIAL STAGES OF TRANSFORMATION OF C_1-C_4 ALCOHOLS ON ZSM-5 ZEOLITES

M. DEREWINSKI[a], S. DZWIGAJ[a], J. HABER[a], G. RITTER[b]
Institute of Catalysis and Surface Chemistry, Polish Academy of Sciences, Kraków, Poland (a)
Institut of Physical Chemistry, Technical University, Vienna, Austria (b)

ABSTRACT

Catalytic activity of ZSM-5 zeolite poisoned by adsorption of pyridine was studied in order to elucidate the role of C_2 and C_3 olefins in the transformation of methanol. Consecutive steps in the sequence: alcohol-olefins-oligomers-cyclopolyenes-aromatics/paraffins are catalysed by acid centers of increasing strength, but in case of methanol the initiation of the chain by the formation of the first C-C bond from C_1 species requires the presence of strongest acid centers. Ethylene is the first product in C_1 conversion and its appearance creates a new facile route consisting in methylation and bypassing the formation of C-C bond. Propylene and higher olefins are methylated more readily than ethylene and are responsible for the increasing rate of methanol consumption, but a parallel route to develop the reaction network is operating through oligomerization of propylene.

INTRODUCTION

It is well known that high silica type ZSM-5 zeolites show high catalytic activity in the conversion of alcohols and olefins [1-4]. Reactions of different alcohols in the presence of hydrogen form of ZSM zeolites result in the formation of the whole spectrum of hydrocarbon products containing olefins, cycloolefins, paraffins and aromatics. It is the characteristic feature of these catalysts that the composition of the products obtained is practically independent of the type of alcohols used what hints to the common reaction path of the transformations of all alcohols. The main difficulty in the identification of the elementary steps and in the construction of the

reaction network is due to the very high rate of these transformatio in the presence of the very active hydrogen form of the zeolite. It seems thus of interest to reduce the activity of this catalyst by poisoning the active centers of acid character with appropriate base adsorbed before the catalytic tests in order to study the mechanism of the reactions of C_1-C_4 alcohols and to determine the role of C_2 and C_2 olefins in the transformation of alcohols, in particular of methanol, into higher hydrocarbons.

EXPERIMENTAL

Zeolite Z-79 of the ZSM-5 type was synthesized according to the patent description [5] and its structure was identified as that of ZSM-5 by X-ray analysis. The hydrogen form was obtained by three fold ion exchange in 0.1 M NH_4Cl solution at 363 K and subsequent heating in the stream of nitrogen at 823 K for 5 hr. Preparations with reduced acidity were obtained by adsorption of pyridine, which was introduced into the carrier gas passing through the reactor with catalyst bed heated to the reaction temperature of 673 K until pyridine appeared in the gas at the outlet. Catalytic activity in the reaction of methanol (MeOH), ethanol (EtOH), isopropanol (iso-PrOH) and butanol (n-BuOH) was determined in the pulse microreactor 8 mm in diameter, filled with 0.28 g samples of the catalyst and kept at reaction temperature of 673 K. The flow rate of nitrogen as the carrier gas was 30 ml/min at the atmospheric pressure. Products were analysed using the on-line gas chromatograph with flame ionization detector and a 4 m column filled with Chromosorb W (60/80 mesh) and silicon oil DC 550 with 5 % addition of stearic acid as the active phase. Reagents were of analytical grade and were used without further purification. Pyridine (Fluka) used for poisoning of the catalyst was of spectroscopic grade.

In the Temperature Programmed Desorption (TPD) experiments the sample of 100 mg of the zeolite was first activated at 823 K for 3 hr at the pressure of 5.10^{-3} Torr ($6.63 \cdot 10^{-1}$ N/m^2). After cooling to room temperature 15 μl of alcohol was introduced and its adsorption carried out for 15 min. The sample was then outgassed for 1 hr and TPD experiment was carried out in the temperature range 303-923 K at the heating rate of 10 K/min. Desorbing products were analysed with a mass-spectrometer.

RESULTS AND DISCUSSION

Our earlier studies showed [6] that adsorption of pyridine at

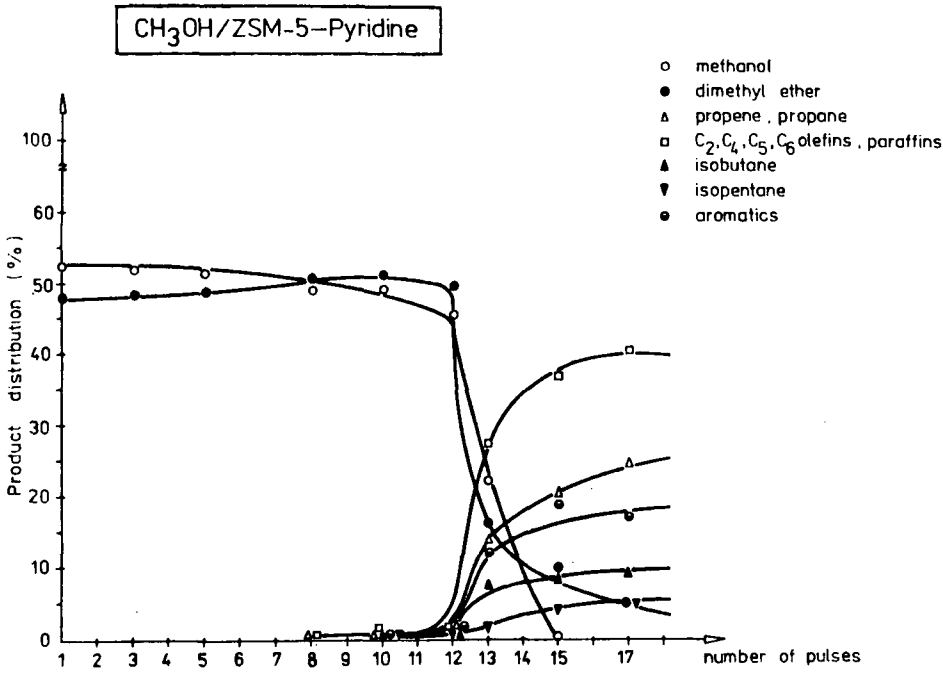

Fig. 1. Product distribution as function of number of pulses of MeOH introduced on ZSM-5 type zeolite poisoned by pyridine.

the surface of ZSM-5 zeolite results in drastic changes of the product distribution of the reaction of alcohols. Fig. 1 shows the changes of the composition of products obtained when pulses of MeOH were consecutively introduced on the initialy poisoned zeolite. In the first pulses dimethylether (DME)is observed as the only product. Only after 10 pulses of MeOH traces of higher hydrocarbons appear. As the first products small amounts of C_2 and C_3 olefins are observed after 8 pulses. When more important amounts of propylene are formed immedietely the whole spectrum of both paraffins and aromatics appears in the products. This is accompanied by the rapid decrease of the amount of unreacted MeOH and DME.

When reaction of EtOH was carried out in identical conditions, 100 % conversion to ethylene was observed already in first pulses, ethylene remaining as the only product through the whole experiment. Zeolite, which after partial removal of pyridine by consecutive pulses of the alcohol due to competitive adsorption of the reaction products and eluating effect of the carrier gas at high temperature developed the activity in the transformation of MeOH not only to DME but also hydrocarbons, remained inactive for the transformation of

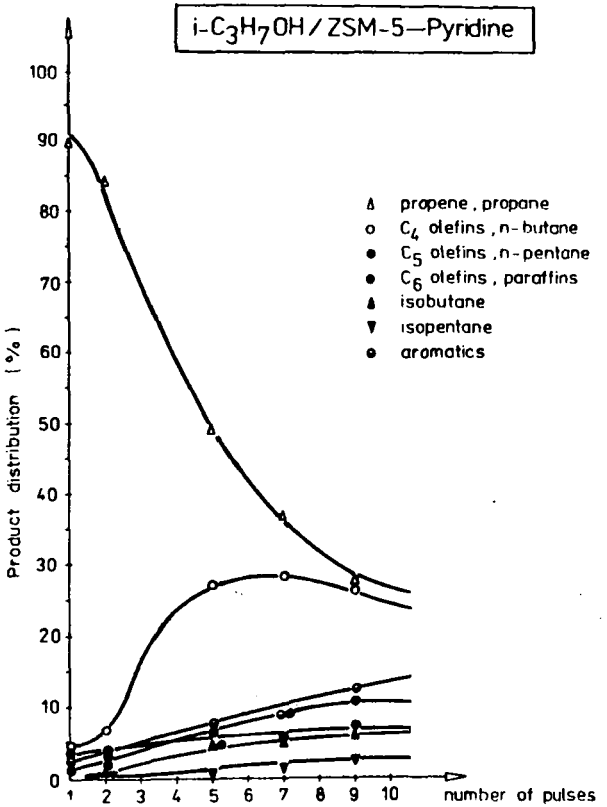

Fig. 2. Product distribution as function of number of pulses of iso-PrOH introduced on ZSM-5 type zeolite poisoned by pyridine.

ethylene. Apparently it still lacks acid centers strong enough to convert ethylene into higher hydrocarbons. Their first trace amounts appeared only in the conditions in which methanol was already transformed into higher hydrocarbons to a considerable degree. After 20 pulses the conversion of ethylene was only 5 % the main product (2 %) being propylene.

Fig. 2 illustrates the results obtained when pulses of iso-PrOH were injected into the reactor with poisoned zeolite. At variance with the behaviour of C_1 and C_2 alcohols already after introduction of the first pulses of iso-PrOH not only propylene as the direct product of the dehydration of this alcohol on weak acid centres, but also the whole spectrum of hydrocarbons including paraffins and aromatics was observed, the conversion of iso-PrOH being 100 %. At the begining mainly propylene, products of its oligomerization and of the oligomer cracking are formed as indicated by high content of C_4-C_6 olefins. It may be mentioned that studies of the adsorption of propylene on HY zeolite [7] revealed the oligomerization of 4 molecules of propylene, and measurements of the adsorption of butene also on HY zeolite [8] indicated the formation of the oligomer from 3 molecules of butene.

Further removal of adsorbed pyridine by pulses of iso-PrOH results in gradual increase of the amount of products of cyclization

and hydride transfer i.e. paraffins and aromatics. It is noteworthy that in the case of iso-PrOH all these products appear in conditions in which in the case of MeOH and EtOH only products of their dehydration to DME and ethylene respectively are observed, but no compounds which require the formation of C-C bonds between C_1 or C_2 species.

Results obtained with n-BuOH were similar to those with iso-PrOH.

Comparison of the behaviour of MeOH and iso-PrOH clearly indicates that formation of the first C-C bond from C_1 species, necessary for further transformations and development of the whole reaction network, requires the presence of acid centers of the catalyst stronger than those, which are involved in the development of this network from propylene. It also shows that transformations of higher alcohols such as iso-PrOH or n-BuOH consist of a series of consecutive steps, catalysed by acid centers of increasing strength:

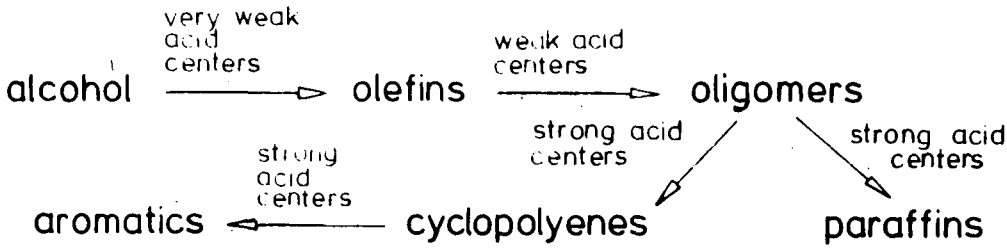

It can be namely concluded from the results presented in Fig. 2 that oligomerization and cracking, which are the first step in the series, require the presence of weaker acid centers and are therefore regenerated in the first instance on pyridine desorption. Further removal of pyridine incovers stronger acid centers of the catalyst responsible for cyclization and hydrogen transfer.

The condition necessary to start the reaction chain in the case of methanol is the removal of pyridine from strongest acid centers required for the formation of the first C-C bond. Appearance of even small amount of such centers makes possible the formation of first portion of ethylene. Once they have been formed they undergo methylation by MeOH, which as shown before [6] procceds with the participation of much weaker acid centers, from which pyridine has already been desorbed earlier. The absence of the products of dimerization or trimerization of ethylene at the early stages with the simultaneous presence of propylene indicates that no oligomerization of C_2H_4 takes

place, but only its methylation with MeOH. It may be concluded, that once small amounts of ethylene have been formed in the reaction of MeOH, the initial step consisting in the formation of C-C bond from C_1 species becomes bypassed by the much easier step of the methylation of the resulting carbon chain. It is obvious that also other products of the reaction sequence, higher olefins, cycloolefins, aromatics may undergo methylation by MeOH.

Thus, in the case of methanol the reaction network may be represented by a following scheme:

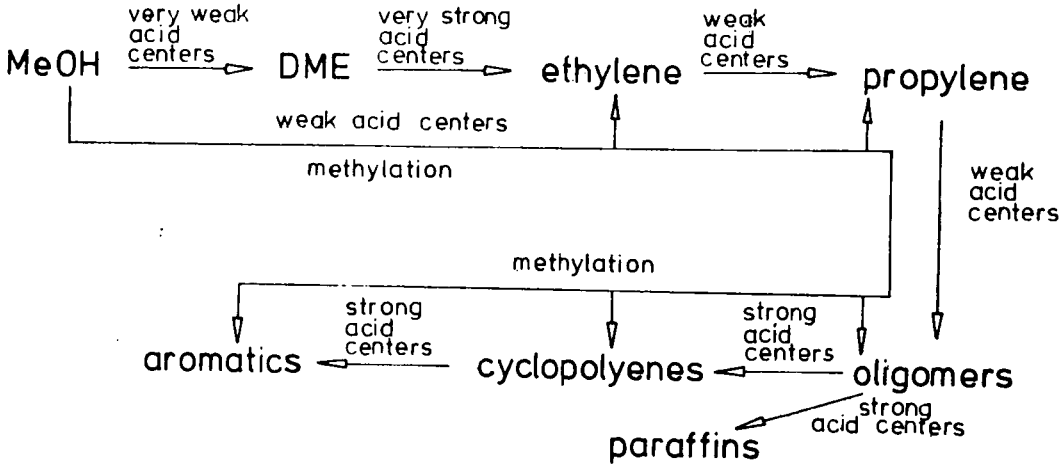

In the absence of MeOH, ethylene remains unreacted and therefore is the only product of the reaction of EtOH on zeolite catalysts which have not available very strong acid centers. The low reactivity of ethyl alcohol and ethylene was also postulated by other authors[3,4,9]

We have noticed that besides the intramolecular dehydration of EtOH also its intermolecular dehydration to diethylether (DEE) is possible in the first stages of the reaction. This is illustrated by Fig. 3, which shows the results of an TPD experiment after adsorption of EtOH on hydrogen form of the ZSM-5 zeolite, which has been previously activated at 823 K in vacuum of ($6.65 \cdot 10^{-1}$ N/m^2) 5.10^{-3} torr. The values in brackets by the TPD curves of different m/e fragments indicate the sensitivity range used by registration. The curve m/e=45 corresponding to the fragment $CH_3CH=\overset{+}{O}H$ with maximum at 395 K represents the desorption of EtOH as confirmed by the appearance of a similar peak on curve m/e=31 ($CH_2=\overset{+}{O}H$), m/e=29 ($H\overset{+}{C}=O$) and m/e=46 ($CH_3CH_2\overset{+}{O}H$). The curve m/e=28 shows two maxima. The first, at 395 K is apparently related to the fragmentation of

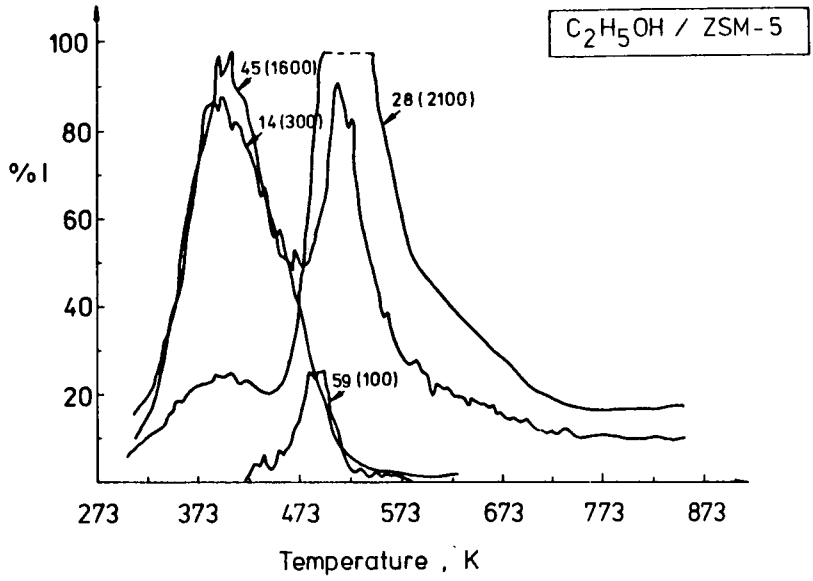

Fig. 3. TPD spectrum obtained after adsorption of EtOH on ZSM-5 zeolite.

desorbed alcohol, whereas the second maximum at 509 K may be assigned to the desorption of ethylene ($CH_2=\overset{+}{C}H_2$ fragment). The presence of other peak characteristic for the mass spectrum of C_2 olefin e.g. e/m=27 ($\overset{+}{C}H=CH_2$) m/e=25 ($CH\equiv\overset{+}{C}$), m/e=14 ($\overset{+}{C}H_2$), confirms the desorption of ethylene at this temperature. The curve illustrating the formation of a fragment with m/e=59 registered at the sensitivity 21 times higher than that of ethylene indicates the presence of diethylether (m/e=59 corresponds to the fragment $CH_2=\overset{+}{O}-CH_2CH_3$). The characteristic fragment m/e=31, which usualy serves for identification of DEE is in our experiment screened by fragments originating from EtOH.

Results of TPD experiment clearly indicate that on the interaction of EtOH with ZSM-5 zeolite not only its intramolecular but also intermolecular dehydration with the formation of DEE takes place.

The studies of catalytic properties of the series of boron and aluminium phosphate of different composition [10] have shown that in the composition range, in which Brönsted acidity is present, only dehydration of EtOH to ethylene takes place, whereas in the composition range, in which pairs of Lewis acid-base centers are generated, ethanol is dehydrated mainly to DEE. It is possible that preactivation of the zeolite sample before the TPD run in comparitively severe conditions resulted in generation of some Lewis acidity. In normal conditions this reaction path is marginal in comparison with intra-

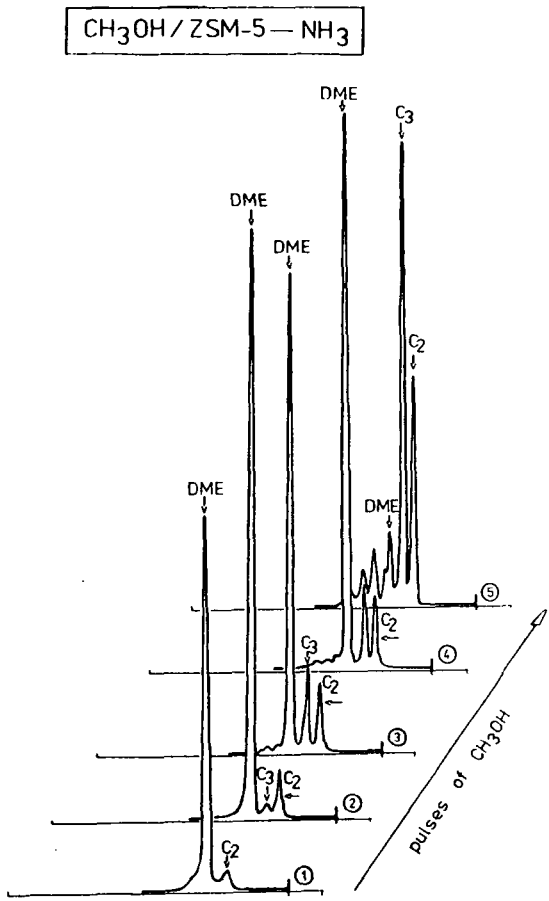

Fig. 4. Results of gas-chromatorgaphic analysis after five consecutive pulses of MeOH introduced on ZSM-5 type zeolite poisoned with ammonia.

molecular dehydration. In order to confirm the role of ethylene as the intermediate which enables the bypassing of the first most difficult step in the transformation of MeOH- the formation of the first C-C bond, a series of experiments was carried out in which the state of the reaction was registered on the zeolite poisoned with ammonia (Fig. 4).

The first product appearing besides the DME at the begining of the reaction is ethylene. The presence of ethylene does not yet lead to the appearance of higher hydrocarbons. The next rapidly growing product is propylene. As already mentioned the absence of C_4 and C_6 hydrocarbons as products of ethylene oligomerization and appearance of propylene indicates that it is methylation of the first portion of ethylene which is responsible for initiation of the reaction sequence. The appearance of propylene results in rapid acceleration of the reaction and increase of the conversion of methanol which is consumed mainly through the methylation of the growing hydrocarbon chains. Simultaneously, as may be concluded from the results obtained with iso-PrOH, propylene alone reacts rapidly, developing through oligomerization and cracking the whole reaction network. This contributes to further consumption of MeOH and results in its total conversion. On studing the influence of various alcohols

and olefins added in small amounts to MeOH on its conversion at the surface of the zeolite catalyst poisoned by pyridine [11] it was found that indeed propylene much easier undergoes methylation than ethylene and therefore accelerates the transformation of MeOH to a much greater extent. In later stages of the reaction ethylene is formed not only by direct formation of C-C bond from C_1 species, which is a difficult step and requires the presence od strong acid centers, but also as the result of cracking of larger olefins.

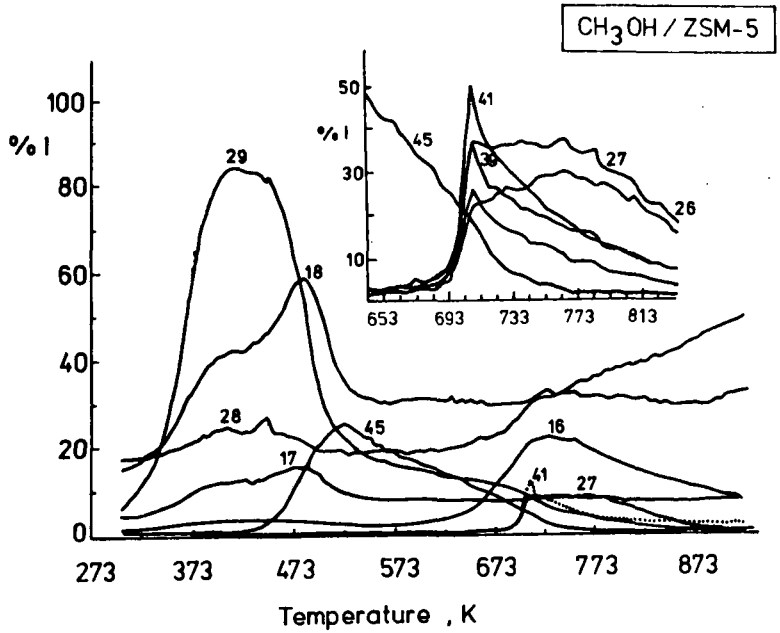

Fig. 5. TPD spectrum obtained after adsorption of MeOH on ZSM-5 type zeolite.

Additional information on the role of lower olefins in the transformation of MeOH was obtained from TPD experiments.

Fig. 5 illustrates the TPD curves registered after adsorption of methanol on active HZSM-5. The curve m/e=29 illustrates the desorption of the unreacted MeOH, curves m/e=18 and m/e=17 - desorption of water. Maximum at 481 K is related to the dehydration of methanol. The curve m/e=45 represents the formation of DME (maximum desorption temperature 523 K) and its disappearance on further heating. The magnified part of the temperature range 643 K - 823 K (shown in the insert) illustrates the desorption of ethylene m/e=27 ($CH_2=\overset{+}{C}H$), m/e=26 ($\overset{+}{C}H\equiv CH$) and propylene m/e=41 ($CH_3-CH=\overset{+}{C}H$) It may be seen that methylation of ethylene is not difficult. On the other hand the very rapid disappearance of propylene at higher

temperatures with simultaneous accumulation of ethylene shows that propylene reacts further more rapidly than ethylene, through methylation and oligomerization. Apparently, the competition from higher olefins and aromatics for methylation results in the accumulation of less reactive ethylene. It is noteworthy that some amount of methane is also formed(curve representing the fragment with m/e=16).

REFERENCES

1. Chang, C.D., Silvestri, A.J., J. Catal., 47, 249 (1977).
2. Derouane, E.G., Nagy, J.B., Dejaifve, P., van Hooff, J.H.C., Spekman, B.P., Vedrine, J.C., Naccache, C., J. Catal., 53, 40 (1978).
3. Anderson, J.R., Foger, K., Mole, T., Rajadhyaksha, R.A., Sanders J.V., J. Catal., 58, 114 (1979).
4. Dejaifve, P., Vedrine, J.C., Bolis, V., Derouane, E.G., J. Catal 63, 331 (1980).
5. Argauer, R.J., Landolt, G.R., US Patent 3 702 886 (1972) Mobil Oil Corp.
6. Derewiński, M., Dźwigaj, S., Haber, J., Zeolites, 4, 214 (1984).
7. Haber, J., Komorek, J., Romotowski, T., prepared for Inter. Symp. on Zeolite Catalysis, Siofok, May 1985.
8. Datka, J., J. Chem. Soc. Faraday I, 76, 2437 (1980).
9. Ahn, B.J., Armando, J., Perst, G., Guisnet, M., C.R. Acad. Sci. Paris 288c, 245 (1979).
10. Haber, J., Szybalska, U., Disc. Faraday Soc., 72, 263 (1981).
11. Dźwigaj, S., Haber, J., Derewiński, M., in press.

HYDRODESULFURIZATION OF THIOPHENE ON H- AND NiH-FAUJASITES X AND Y

N.I. JAEGER, R.NOWAK and G. SCHULZ-EKLOFF
Institut für Angewandte und Physikalische Chemie, Forschungsgruppe Angewandte Katalyse, Universität Bremen, D-2800 Bremen 33, FRG

ABSTRACT

In the hydrodesulfurization of thiophene catalyzed by Ni loaded faujasites two active sites seem to be effective. Besides the Brønsted acidic sites the hydrogenolysis activity of the metal phase is essential for maintaining a stable rate of thiophene conversion and for the prevention of coke deposition. The observed particle size distribution suggests a more effective contribution of the small fraction of larger crystallites (d > 4 nm) to the hydrogenation activity of the catalyst.

INTRODUCTION

The most effective hydrodesulfurization catalysts are based on Co/Mo supported on γ-Al_2O_3. The active phases MoS_2 and Co_9S_8 are responsible for hydrogenation and hydrogenolysis respectively in a model of contact synergism proposed by Delmon [1]. The need for two active sites warrants the study of other groups of bifunctional catalysts, namely metal loaded zeolites in the catalytic hydrodesulfurization reaction. In an extensive study of the properties of transition metal loaded zeolites Brooks [2] demonstrated the capability of Ni loaded faujasites in the hydrodesulfurization of thiophene. In the present study the proposed bifunctionality of the metal loaded zeolite [2], i.e. hydrocracking due to the acidity of the zeolite and minimization of coke formation due to the hydrogenolysis activity of the metal, is tested in more detail.

EXPERIMENTAL

Sodium faujasite X (Si/Al = 1.2; crystal size 5-10 µm) and sodium faujasite Y (Si/Al = 2.8; crystal size 2-3 µm) were prepared by hydrothermal crystallization [3,4]. Ni^{2+}-exchange was carried out in $Ni(CH_3COO)_2$ solutions and for the preparation of H-X, Y samples NH_4CH_3COO-solutions were used. The metal contents were determined by atomic absorption spectroscopy. In the case of NH_4^+ the degree of exchange was determined by backtitration of the solution.

Samples (0.5 g) of the crystalline powders were pressed (0.5 GPa), granulated (0.3 - 0.7 mm), dehydrated in argon (100 ml min^{-1}, 693 K, 16 h,heating rate 5K min^{-1}) NH_4 exchanged samples were converted into the H-form of the zeolite under the same conditions. The NiNaX samples were reduced with hydrogen (80 ml min^{-1}, 573 K, 0.1 MPa 25 h). All reactions were carried out in a fluidized bed reactor.

The crystallinity of the dehydrated and reduced samples was checked by their X-ray pattern as well as their capacities for nitrogen physisorption (77 K, 10 KPa). The particle size distributions were determined by transition electron microscopy (EM 10, Zeiss) following the procedure for sample preparation reported by Nagy et al. [5]. From the approximate degree of reduction (α=0.5 [6]) and the size distribution of the metal crystallites the number of Ni surface atoms could be estimated (Fig. 1).

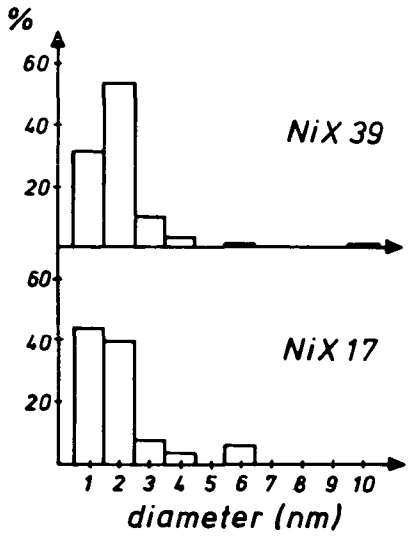

Fig. 1. Particle size distribution for NiX 39 and NiX 17 following reduction of the Ni-exchanged samples

Number and strength of acid sites in the H-X, Y catalysts were determined by titration with n-butylamine solution in the presence of a series of H_0 and H_R indicators [7]. The activities of the samples in the hydrodesulfurization reaction were determined in a fluidized bed reactor (2 ml) containing 0.2 - 0.4 g of the catalyst (60 ml min^{-1}, WHSV: 0.1 h^{-1}, 573 K, 0.1 MPa). The reaction gas mixture consisted of 95 % N_2, 5 % H_2 and 80 vpm thiophene. Thiophene was analyzed by gas chromatography (F 22, Perkin Elmer) using a carbopack column (B-HT-100, Supelco Inc.) and a FID. Hydrocarbons were determined using the same column. The following catalysts were tested: NiX 17, NiX 39 (degree of Ni-exchange 17% and 39% respectively); HX 33 ($H_{27}Na_{57}X$) and HY 100 ($H_{51}Y$).

RESULTS

The distribution of the nickel particle size following reduction is depicted in Figure 1 for the two nickel exchanged zeolites used in the experiments. Table 1 contains the particle size distributions before and after the catalytic reaction (3h time on stream) and an estimation of the number of Ni surface atoms belonging to a selected size range of the Ni particles. Both samples exhibit little sintering. The dispersity of the nickel phase was found to be considerably higher for the NiX 39 sample and only about 25% of the surface atoms belong to crystallites beyond 4 nm in diameter as compared to around 50% in the case of NiX 17.

Table 1

Particle size distribution before and after reaction and related absolute number of Ni surface atoms per gram-unit cell

catalyst	mean diameter nm	following reduction %	following reduction no. of Ni surface atoms per g-u.c.	after 3h time on stream %	after 3h time on stream no. of Ni surface atoms per g-u.c.
NiX 17	1-4	94.3	3.68×10^{23}	89.4	2.17×10^{23}
	5	-	-	2.3	0.37×10^{23}
	6	5.7	2.75×10^{23}	6.1	1.49×10^{23}
	≥ 8	-	-	2.3	1.10×10^{23}
NiX 39	1-4	98.6	11.7×10^{23}	97.4	11.6×10^{23}
	5	-	-	0.5	0.39×10^{23}
	6	0.7	0.88×10^{23}	1.6	1.87×10^{23}
	≥ 8	0.7	2.52×10^{23}	0.5	1.68×10^{23}

The activity of the nickel loaded zeolites are compared in Figure 2 for the first 3 h time on stream. The NiX 39 sample shows a rapid decline in activity starting at high rates of conversion , while NiX 17 starts out at a relatively low value, passes through a maximum and stabilizes at a slightly higher rate of conversion compared to NiX 39. Figure 3 depicts the activities of the hydrogen forms of the faujasites. More than 90% of the acid sites of HY 100 and between 75% - 100% of the acid sites of HX 33 could be titrated. It was found that around 50% of the acidic sites were strong in the case of HY 100 ($pK < -13.3$). In the case of HX 33 around 50% of the acidic sites titrated were of medium strength ($pK > -6.6$). The remaining sites were of lesser acidity. The reactivities of the samples (HY 100 and HX 33) are characterized by rapid deactivation especially in the case of HY 100 having more and stronger acidic sites. Hydrocarbons C_1 - C_4 were formed exclusively in the thiophene conversion.

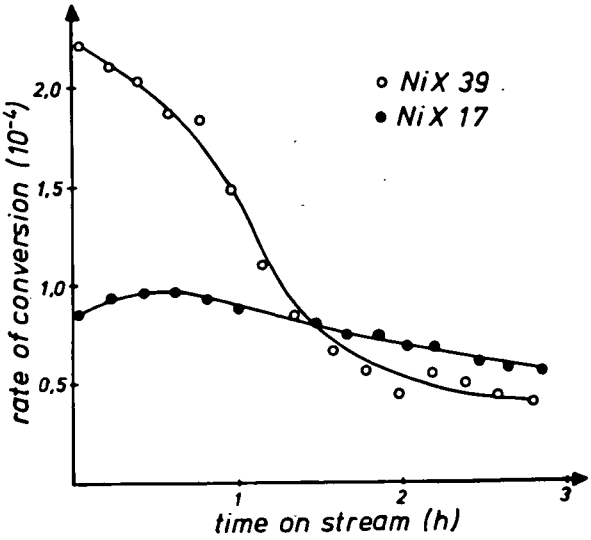

Fig. 2. Rate of conversion (mole thiophene/s·gram-unit cell) vs. time on stream • NiX 17 / o NiX 39

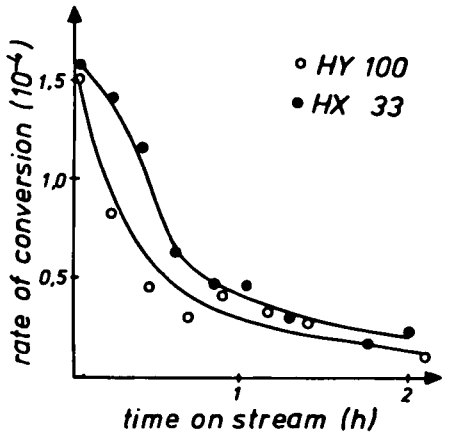

Fig. 3. Rate of conversion (Mole thiophene/s·gram-unit cell) vs. time on stream • HX 33 / o HY 100

DISCUSSION

For thiophene adsorbed on a HY zeolite a strong band was observed in the IR-spectrum, which is due to the S-H vibration. This observation demonstrates the cleavage of the C-S bond, which is assumed to proceed in the presence of Brønsted acidic sites [8]. In the absence of hydrogenolysis activity the high initial activity of the H-X, Y-catalysts decreases rapidly due to coke deposition on strong Brønsted sites.

In the presence of Ni the hydrogenolysis activity of the metal phase may be able to reduce the rate of coke formation on strong acid sites by hydrogenation of coke precursors. The high initial activity of NiX 39 can be attributed to the higher acidity of this zeolite as compared to NiX 17. The activity stabilizes at a value presumably determined by the activity of the metal phase. Both Ni containing catalysts reach about the same stationary level of thiophene hydrodesulfurization.

The estimated number of Ni surface atoms per gram-unit cell is more than twice as large for NiX 39 compared to NiX 17 (Table 1). For metal particles beyond 4 nm in diameter the number is about the same for both catalysts. It is assumed that the larger Ni-crystallites are responsible for the hydrogenation activity of the metal phase in agreement with published results [9,10]. Ni loaded faujasites serve as a model for the study of the bifunctional activity of metal loaded zeolites. Developing the capability of a Ni-faujasite hydrodesulfurization catalyst for the removal of small amounts of thiophene from gases used for synthesis on sulfur sensitive catalysts requires careful consideration of the combined activity of acidic and metal functions.

ACKNOWLEDGEMENT

The authors are grateful to Dr. J. Schweckendiek for the titration of the acid sites.

REFERENCES

1. Hagenbach, G. Courty, Ph., Delmon, B., J. Catal. 31, 264 (1973)
2. Brooks, C.S., Surface Technol. 10, 379 (1980)
3. Charnell, J.F., J. Crystal Growth 8, 291 (1971)
4. Kacirek, H., Lechert, H., J. Phys. Chem. 79, 1589 (1975)
5. Nagy, J.N., Eeno, M. van, Derouane, E.G., J. Catal. 58, 230 (1979)
6. Briese-Gülban, S., Kompa, H., Schrübbers, H., Schulz-Ekloff, G., React. Kinet. Catal. Lett. 20, 7 (1982)
7. Hirschler, E.A., J. Catal. 2, 428 (1963)
8. DeAngelis, B.A., Appierto, G., J. Colloid Interface Sci. 53, 14 (1975)
9. Sauvion, G.N., Djemel, S., Tempere, J.F., Guilleux, M.F., Delafosse, D., in "Catalysis by Zeolites", ed. B. Imelik et al., (Elsevier, Amsterdam 1980), Stud. Surf. Sci. Catal., vol. 5, p. 245
10. Vogt, F., Pitzing, U.-D., Peitzsch, L., Bremer, H., Z. anorg. allg. Chem. 512, 85 (1984)

CATALYTICALLY ACTIVE CENTERS OF ZEOLITES IN THE REACTION BETWEEN H_2S AND CH_3OH

M. ZIÓŁEK[a], J. BRESIŃSKA[a], and H. G. KARGE[b]
Department of Chemistry, A. Mickiewicz University, Poznań, Poland (a)
Fritz-Haber-Institut der Max-Planck-Gesellschaft, Berlin (West) (b)

ABSTRACT

The reaction between methanol and hydrogen sulfide was carried out on HNaY and ZSM-5 type zeolites. Brønsted acid sites are catalytically active centers. In the absence of acidic OH groups, i.e. on NaX and NaY zeolites, sodium cations play the rôle of active sites. The selectivity of this reaction towards $(CH_3)_2S$ and CH_3SH depends on the temperature and the molar ratio H_2S : CH_3OH. Competitive with the reaction of H_2S with CH_3OH is the decomposition of methanol to hydrocarbons.

INTRODUCTION

Results of a study on the reaction between methanol and hydrogen sulfide on HNaY zeolites have been presented in an earlier paper [1]. It was found that the methoxylation of the zeolite surface is the first step of this process. The formation of the methoxyl groups requires Brønsted acid centers to be present on the zeolite surface. It seemed interesting to compare the activity of hydrogen and sodium forms of zeolites, and to find out whether the same catalytically active centers take part in this reaction on both forms of zeolites. It was the aim of this study to elucidate this problem.

EXPERIMENTAL

Catalysts. The following catalysts were used: NaX, Linde Lot No. 1360027, with Si/Al=1.21; NaY, Linde SK-40 Lot No. 3606411, with Si/Al=2.37; HNaY, prepared from NaY *via* ion exchange with 1M solution of CH_3COONH_4 (degree of exchange, δ=60 %); NaZSM-5, Ultraset T-1000/J ($Na_{4.07}Al_{2.45}Si_{93.15}O_{192}$), synthesized in the Institute of Industrial Chemistry in Warsaw, with Si/Al=38; HZSM-5, prepared from NaZSM-5 *via* ion exchange with 0.25 M solution of NH_4Cl (δ =100 %).

Reaction conditions. The continuous flow technique was used to measure the catalytic activity. The apparatus has been described in

Ref. [1]. Portions of 0.2 g of dehydrated zeolite were employed. The zeolite crystallites were tabletted without binder, ground, sieved to a 0.5-1.0 mm diameter range and 4 hours *in-situ* activated in pure and dried helium flow at 673 K.

A mixture containing Merck research grade H_2S (3-12 vol. %, depending on the desired H_2S : CH_3OH ratio), methanol (3 vol. %) and helium as a carrier gas, was passed through the catalyst bed to a gas chromatograph. The flow rate was 2.4×10^{-4} m^3h^{-1}. Each experiment was carried out twice: (i) using GC analysis with a catharometer, (ii) using GC analysis with a flame ionization detector. The first technique was applied in particular for the determination of H_2S conversion. In both analyses a 2 m Porapak Q column was employed at 423 K for separating the products.

The catalytic experiments were conducted at 623 and 673 K, using various H_2S : CH_3OH molar ratios, *viz.* 1:2, 1:1, and 4:1. The reaction between H_2S and CH_3OH was also carried out after poisoning the acidic centers with pyridine at 623 and 673 K.

IR measurements. IR spectra were obtained with a Perkin-Elmer Model 325 spectrometer. Design and operation of the IR cell has been described elsewhere [2]. The zeolite wafers, having a thickness of about 10 $mg \cdot cm^{-2}$, were activated for 12 h at 673 K under high vacuum (10^{-4}Pa). Subsequently, pyridine or water was adsorbed at 623 and 673 K.

RESULTS

Catalytic experiments. The results of the reaction between methanol and hydrogen sulfide on faujasite-type zeolites are presented in Table 1.

The highest conversion of methanol was observed on HNaY, but the selectivity towards CH_3SH and $(CH_3)_2S$ was lower than in the case of the pure sodium forms of faujasite type zeolites. It was observed that on HNaY zeolite a fraction of the methanol underwent decomposition to hydrocarbons. It was possible, however, to increase the selectivity of HNaY towards CH_3SH and $(CH_3)_2S$ by using an excess of H_2S in the feed. In the case of NaX and NaY zeolites, no products of methanol decomposition were observed. NaX zeolite exhibited higher activity than NaY.

The increase of the reaction temperature did not give rise to any significant changes in the activity and selectivity of sodium forms of X and Y type zeolites. However, in the case of HNaY, the selectivity towards $(CH_3)_2S$ increased with increasing reaction temperature. This

Table 1

Methanol conversion and yield of products in the reaction of H_2S and CH_3OH on faujasite-type zeolites (data after 2h time on stream)

Zeolite	$H_2S:CH_3OH$ molar ratio	CH_3OH conv.(%)	CH_3SH yield(%)	$(CH_3)_2S$ yield(%)	After poisoning with pyridine		
					CH_3OH conv.(%)	CH_3SH yield(%)	$(CH_3)_2S$ yield(%)
		Reaction Temperature : 623 K					
NaX	1:2	65	15	40	48	15	30
NaX	1:1	70	40	30	40	30	10
NaX	4:1	85	65	20	50	45	5
NaY	1:2	50	4	18	20	4	-
NaY	1:1	33	13	20	10	10	-
NaY	4:1	50	30	20	25	20	5
HNaY	1:1	98	10	13	25	4	-
HNaY	4:1	100	15	80	50	15	15
		Reaction Temperature : 673 K					
NaY	1:2	50	6	18	20	6	1
NaY	1:1	35	13	20	15	13	2
NaY	4:1	50	30	20	35	30	5
HNaY	1:1	100	5	20	70	5	15
HNaY	4:1	100	15	55	90	6	45

was even more evident in a lower range of reaction temperatures, when no products of methanol decomposition were observed, which was described earlier [1].

Measurements of the effect of the $H_2S:CH_3OH$ molar ratio on the activity and selectivity of the reaction indicated that, on sodium forms of faujasite-type zeolites, an excess of H_2S causes an increase both in methanol conversion and selectivity towards CH_3SH. This seems to be correlated to the reaction between $(CH_3)_2S$ and H_2S. Indeed, inspection of the reaction curves (Figure 1) reveals that at the beginning of the reaction between H_2S and CH_3OH on NaX, the yield of $(CH_3)_2S$ was higher than that of CH_3SH. With increasing reaction time, the yield of $(CH_3)_2S$ decreased and the yield of CH_3SH increased.

Poisoning of the acidic centers on faujasite-type zeolites by pyridine at 623 K resulted in a significant decrease of the $(CH_3)_2S$ yield, and in a smaller one of the CH_3SH yield (see Table 1). At higher temperatures (673 K), the poisoning by pyridine did not change the yield of CH_3SH, but brought about a decrease of the $(CH_3)_2S$ yield. Hence, the formation of either product requires acidic centers, but

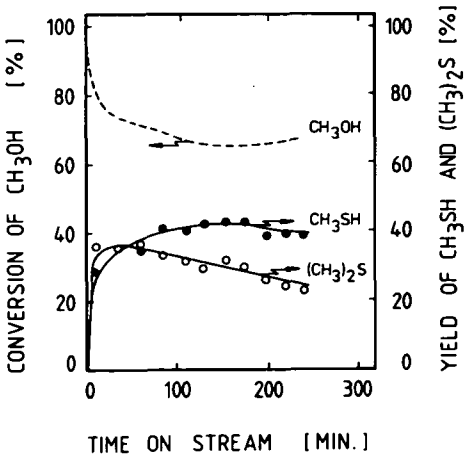

Fig. 1. Conversion of methanol on NaX at 623 K (H_2S:CH_3OH=1:1)

the reaction towards CH_3SH occurs on weaker centers than the reaction towards $(CH_3)_2S$. A fraction of the fed CH_3OH still decomposed when the catalyst was poisoned by pyridine. Again, decomposition of CH_3OH seems to proceed on weaker centers than the reaction with H_2S.

Table 2 shows the results of the reaction between H_2S and CH_3OH over NaZSM-5 and HZSM-5 zeolites. Only in the case of excess of methanol (H_2S:CH_3OH=1:2), were methanol decomposition products observed. ZSM-5 type zeolites exhibited higher activity than faujasite-type zeolites. Similarly, as was found on faujasite-type zeolites, the excess of H_2S caused an increase in selectivity towards CH_3SH. At higher temperature (673 K), the yield of CH_3SH over ZSM-5 is higher than at lower temperature (623 K), in contrast to the behaviour of faujasite-type zeolites. Similar to what was found with faujasite-type zeolites, poisoning of the acidic centers by pyridine resulted in a significant decrease of the $(CH_3)_2S$ yield and a smaller decrease of the CH_3SH yield.

IR measurements. The aim of the infrared study was to clarify which type of acidic centers (Lewis or Brønsted sites) is involved in the reaction between H_2S and CH_3OH and whether water (the product of this reaction) can form acidic hydroxyl groups.

After pyridine adsorption on NaX and NaY zeolites at 623 K for 1 h and evacuation at the same temperature during 15 minutes, weak-to-medium bands at 1442, 1490, and 1598 cm^{-1} appeared (see Figure 2).

According to Parry [3] and Liengme and Hall [4], the band around 1442 cm^{-1} is typical of coordinately bonded pyridine. Liengme and Hall [4] ascribed the band at 1442 cm^{-1} to pyridine coordinated to sodium ions. Therefore, the IR experiments showed that the only centers on the surface of NaX and NaY zeolite which could be poisoned by pyridine were Lewis acid centers (sodium cations); Brønsted or true Lewis sites [4-7] were not present.

Figure 3 presents the spectra obtained after adsorption of pyridine on HNaY zeolite at 623 and 673 K. Bands were observed at the following wavenumbers: 1628 and 1620 cm^{-1}, due to coordinately bonded

Table 2

Methanol conversion and yield of products in the reaction of H_2S and CH_3OH on ZSM-5 type zeolites (data after 2h time on stream)

Zeolite	H_2S:CH_3OH molar ratio	CH_3OH conv.(%)	CH_3SH yield(%)	$(CH_3)_2S$ yield(%)	After poisoning with pyridine		
					CH_3OH conv.(%)	CH_3SH yield(%)	$(CH_3)_2S$ yield(%)
		Reaction Temperature : 623 K					
NaZSM-5	1:2	70	3	50	10	3	-
NaZSM-5	1:1	90	10	80	10	7	-
NaZSM-5	4:1	98	33	65	17	9	-
HZSM-5	1:1	98	5	93	25	3	-
HZSM-5	4:1	100	40	60	20	15	-
		Reaction Temperature : 673 K					
NaZSM-5	1:2	85	-	65	35	-	10
NaZSM-5	1:1	98	15	83	30	15	10
NaZSM-5	4:1	98	43	55	40	25	10
HZSM-5	1:1	100	10	90	40	8	10
HZSM-5	4:1	100	50	50	75	40	35

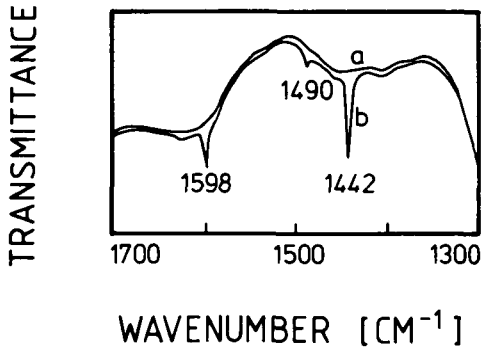

Fig. 2. Adsorption of pyridine on NaY. (a) baseline, after activation at 673 K; (b) after pyridine adsorption and subsequent evacuation, at 623 K

pyridine [4], 1545 cm^{-1} due to pyridinium ions [4], 1488 cm^{-1}, due to pyridine and pyridinium ions [4], 1452 cm^{-1}, due to pyridine coordinately bonded to true Lewis sites [3-7]. After pyridine adsorption at 623 K, a small shoulder around 1442 cm^{-1} appeared (Figure 3, spectrum b), which is assigned to pyridine coordinated to sodium ions. After heating at 673 K this shoulder disappeared (Figure 3, spectrum c). Simultaneously, the intensity of the pyridinium ion band at 1542 cm^{-1} (pyridine adsorbed on Brønsted acid centers) decreased more than the band due to pyridine adsorbed on true Lewis acid sites. The results shown in Figure 3 lead to the following conclusions: (i) After activation at 673 K, HNaY possesses both Brønsted and Lewis acid centers, which are poisoned by pyridine at either reaction temperature (632, 673 K); (ii) pyridine does not

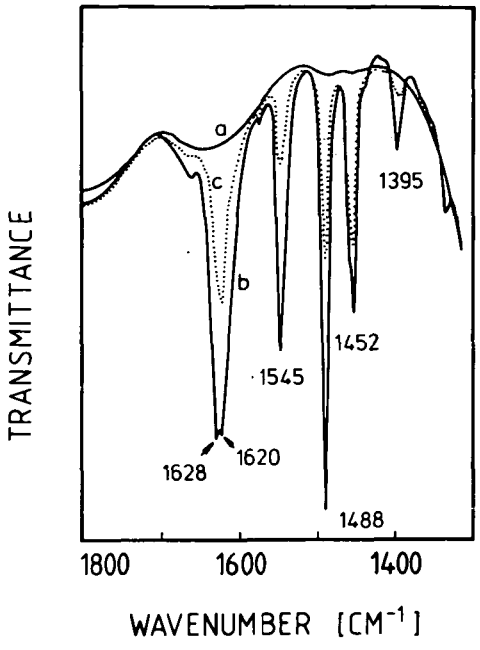

Fig. 3. Adsorption of pyridine on HNaY. (a) baseline after activation at 673 K; (b) after pyridine adsorption and subsequent desorption, at 623 K; (c) after continued evacuation at 673 K

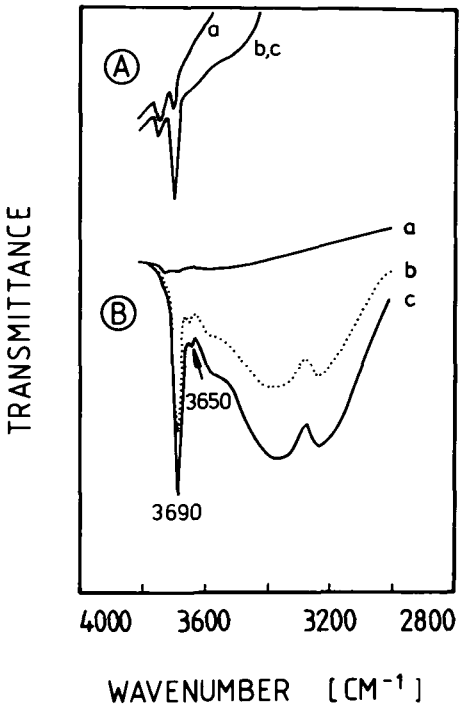

Fig. 4. Adsorption of water on NaY (A) and NaX (B). (a) baseline, after activation at 673 K; (b) after H_2O admission at 623 K (ca. 2 Pa final pressure) and subsequent pumping; (c) after subsequent heating to 673 K (1/2 h) and pumping

poison sodium cations at 673 K.

Adsorption of H_2O on sodium forms of X and Y type zeolites was carried out at 623 and 673 K. Figure 4 presents the IR results. After adsorption of H_2O on NaY zeolite at 623 K no acidic hydroxyl groups were observed. The same was true after heating at 673 K (Figure 4A, spectra b and c). Adsorption of H_2O on NaX zeolite under the same conditions resulted in formation of OH groups, since a very weak band at 3650 cm^{-1} appeared (Figure 4B, spectra b and c). However, this OH band did not disappear after adsorption of pyridine at 623 K. Simultaneously, no bands due to pyridinium ions appeared. This would mean that even if (acidic) OH groups form from the reaction product H_2O under reaction conditions, they are relatively weak, since they cannot be poisoned by pyridine at 623 K.

The results obtained after adsorption of pyridine on NaZSM-5 and

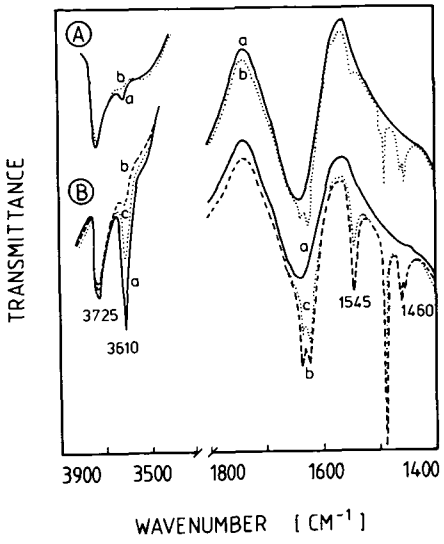

Fig. 5. Adsorption of pyridine on NaZSM-5 (A) and HZSM-5 (B). (a) baseline, after activation at 673 K; (b) after pyridine adsorption and subsequent desorption, at 623 K; (c) after subsequent desorption at 673 K

HZSM-5 zeolites at 623 and 673 K are shown in Figure 5.

After activation at 673 K, two bands at 3610 and 3725 cm^{-1} were present in the infrared spectra of both zeolites (Figure 5, spectra a). Jacobs and Balmoos [8] attributed these bands at 3610 and 3725 cm^{-1} to OH groups of zeolitic Brønsted acid sites and of extrazeolitic material, respectively. Spectra b were obtained after adsorption of pyridine at 623 K on NaZSM-5 and HZSM-5. The intensities of the 3610 cm^{-1} bands were significantly decreased, but the intensities of the OH band at 3725 cm^{-1} were only very little affected. Simultaneously, in the 1400-1800 cm^{-1} region the bands of adsorbed pyridine appeared. Both the bands typical of Brønsted acid (around 1540 cm^{-1}) and Lewis acid sites (around 1452 cm^{-1}) were observed in spectra b. When, subsequent to pyridine adsorption on HZSM-5 at 623 K, the sample was heated to 673 K and evacuated, the band of pyridine coordinatively bonded to true Lewis sites (1460 cm^{-1}) did not change its intensity, but the intensity of the band due to pyridinium ions (1545 cm^{-1}) decreased (spectra c). These IR findings let us conclude that (i) after activation at 673 K both Lewis and Brønsted acid sites exist on the surface of NaZSM-5 and HZSM-5, (ii) pyridine poisons Lewis acid centers equally strongly at 623 and 673 K, but acidic Brønsted sites are poisoned by pyridine to a lesser extent at 673 K than at 623 K.

DISCUSSION

In the previous paper [1], it has been reported that the methoxylation of the zeolite surface is the first step in the reaction between H_2S and CH_3OH on hydrogen forms of Y-type zeolite. It was stated that the Brønsted acid sites of HNaY are the active centers.

After activation at 673 K, sodium forms of X and Y type zeolites do not have any acidic hydroxyl groups (see Figure 4). Nevertheless,

these catalysts, in particular NaX, show high activity for the reaction between H_2S and CH_3OH. Poisoning of the samples with pyridine caused a decrease of the yield of CH_3SH and $(CH_3)_2S$. Infrared measurements indicated that pyridine adsorbs on sodium cations of NaX and NaY which act as Lewis acid centers (Figure 2). These observations allow us to conclude that sodium cations play an important rôle in the reaction of H_2S with CH_3OH when carried out on sodium forms of faujasite-type zeolites. Two possibilities should be considered: Sodium cations might be necessary for chemisorption of H_2S or for chemisorption of methanol. As Karge and Raskó [9] found, the dissociation of H_2S to H^+ and SH^- does not occur on sodium faujasite-type zeolites with Si/Al > 2.21. Thus, dissociative adsorption of H_2S on NaY can be excluded. Therefore, we assume that sodium cations are involved in the chemisorption of methanol, even though Salvador and Kladnig [10] claimed to have ruled out this possibility. However, these authors conducted their experiments at temperatures below 623 K. On the other hand, Unland [11] did find methanol chemisorption on sodium cations of NaX zeolite at 673 K. On the basis of the present knowledge it seems difficult to propose a mechanism for the reaction between H_2S and CH_3OH which makes allowance for the rôle of sodium cations. This problem will be the subject of a subsequent investigation.

In the case of NaX zeolite we have also to take into consideration the dissociative adsorption of H_2S, which occurs on this catalyst [9]. Such a chemisorption of H_2S leads to the formation of acidic hydroxyl groups, which are active sites in the reaction of H_2S with CH_3OH [1]. Formation of acidic OH groups during chemisorption of H_2S may lead to an improved catalytic performance. Indeed, generation of such active centers (acidic OH groups) on the surface of NaX during the reaction appears to be even more favourable than employing hydrogen forms of faujasite-type zeolites. In the case of HNaY, where (strong) acidic hydroxyl groups already exist on the catalyst prior to reaction, methanol is very easily decomposed to hydrocarbons, and the selectivity of the reaction towards organic sulfur compounds is lower than it is on NaX zeolite. This conclusion is supported by the earlier investigations [1], which have shown that HNaY with a lower degree of exchange of Na^+ for H^+, is more active than a catalyst with high degree of ion exchange. Only the increase of the fraction of H_2S in the feed does result in an increase of the selectivity towards CH_3SH and $(CH_3)_2S$ over HNaY (Table 1).

Another possibility of generating OH groups is the chemisorption

of water, which is a product of the reaction between H_2S and CH_3OH. The IR experiments provided evidence that only in the case of NaX dissociative chemisorption of water might occur (see Figure 4). However, after adsorption of H_2O at 623 K on NaX only a very small band at 3650 cm^{-1} appeared. Furthermore, OH groups indicated by that band did not react with pyridine at 623 K. They obviously are very weak sites. Since pyridine adsorbed on NaX at 623 K did indeed reduce the activity of the catalyst *(vide supra)*, it can be excluded that those OH groups, generated *via* chemisorption of H_2O, are active centers for the reaction under study. In the case of NaY, where no acidic OH groups can be formed during the reaction, sodium cations are most probably the only active sites *(vide supra)*.

The infrared spectra obtained after adsorption of pyridine on NaZSM-5 and HZSM-5 catalysts (Figure 5), in correlation with their catalytic activity in the reaction of H_2S with CH_3OH before and after poisoning with pyridine (Table 2), suggest that Brønsted acid sites are the active centers.

The analysis of the results in Table 2 revealed that the selectivity towards CH_3SH increases with the increase of the reaction temperature. This fact can be explained in terms of results which were obtained by Ono and Mori [12], who studied the chemisorption of methanol on ZSM-5. These authors found that the chemisorption of methanol takes place on the acidic hydroxyl groups under formation of methoxyl groups. Methoxyl groups on the zeolite surface may be represented by two resonance structures:

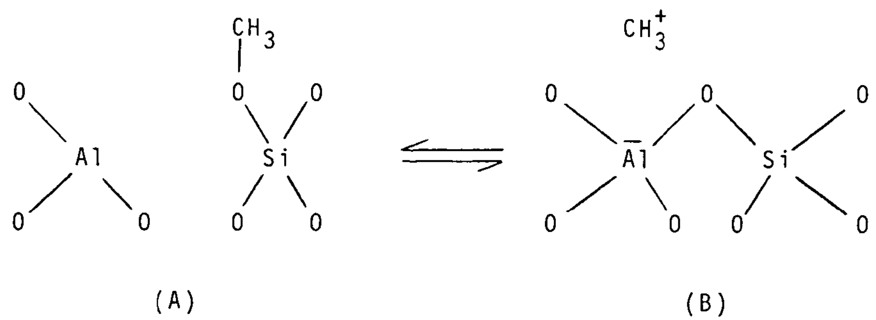

(1)

The CH_3^+ carbenium ion of structure B might react with H_2S to form CH_3SH according to equ. (2)

$$CH_3^+ + H_2S \rightarrow CH_3SH_2^+ \rightarrow CH_3SH + H^+. \qquad (2)$$

Ono and Mori [12] showed that, after chemisorption of methanol, the contribution of structure (B) increases with increasing temperature.

Similarly, the increase of the yield of CH_3SH at higher temperatures, as observed in the current experiments, may be due to a preference of structure B.

CONCLUSIONS

In the case of HNaY and HZSM-5 type zeolites, the Brønsted acid sites play the rôle of active centers in the reaction between methanol and hydrogen sulfide. On the sodium forms of faujasite-type zeolites sodium cations are involved. Competitive with the reaction of H_2S and CH_3OH is the decomposition of methanol. This process predominates on HNaY when $H_2S:CH_3OH=1:1$ and was observed on ZSM-5 for an excess of methanol in the feed. The excess of H_2S leads to an enhancement of the catalytic activity of the zeolite and to an increase of the selectivity towards CH_3SH. A fraction of CH_3SH can form *via* the reaction between the reaction product $(CH_3)_2S$ and H_2S.

ACKNOWLEDGEMENT

The authors thank Mrs. Erika Popović for her valuable assistance in the IR experiments. H.G. Karge gratefully acknowledges the financial support of the Senator für Wirtschaft und Verkehr (ERP Sondervermögen) der Stadt Berlin (West).

REFERENCES

1. Ziółek, M., Bresińska, I., submitted for publication in "Zeolites".
2. Karge, H.G., Z. Phys. Chem. Neue Folge, 122, 103 (1980).
3. Parry, E.P., J. Catal. 2, 371 (1963).
4. Liengme, B.V., Hall, W.K., Trans. Faraday Soc., 62, 3229 (1966).
5. Kühl, G.H., Proc. of the 3rd Int. Conf. on Molecular Sieves, Zürich, Switzerland, 1973 (J.B. Uytterhoeven, Ed.) p. 227.
6. Kühl, G.H., J. Phys. Chem. Solids 38, 1259 (1977).
7. Jacobs, P.A., Beyer, H.K., J. Phys. Chem., 83, 1174 (1979).
8. Jacobs, P.A., von Ballmoos, R., J. Phys. Chem. 86, 3050 (1982).
9. Karge, H.G., Raskó, J., J. Colloid Interface Sci. 64, 522 (1978).
10. Salvador, P., Kladnig, W., J. Chem. Soc. Faraday Trans. I, 73, 1153 (1977).
11. Unland, M., J. Phys. Chem. 82, 580 (1978).
12. Ono, Y., Mori, T., J. Chem. Soc. Faraday Trans. I, 77, 2209 (1981).

A STUDY OF THE INTERACTION OF SOME KETONES WITH HZSM-5 ZEOLITE

J. NOVÁKOVÁ, L. Kubelková, P. Jírů, S. Beran, K. Nedomová
The J. Heyrovský Institute of Physical Chemistry and Electrochemistry, Czechoslovak Academy of Sciences, Máchova 7, 121 38 Prague 2, Czechoslovakia

ABSTRACT

Interaction of several ketones with HZSM-5, NaZSM-5 and HY zeolites was studied. Acetone and methylethylketone on HZSM-5 were investigated in greater detail. IR study of surface complexes remaining in zeolites after treatment at various temperatures in vacuo was used, as well as the temperature-programmed desorption of very small amounts of preadsorbed ketones which was linked directly to the mass spectrometer. It was concluded that acetone transformation proceeds via the decomposition of surface intermediates formed by acid-catalyzed intermolecular acetone condensation. With methylethylketone (and higher ketones) intermolecular dehydration prevails and is enhanced but not conditioned by the presence of zeolitic acid centers.

INTRODUCTION

HZSM-5 zeolite catalyzes the transformation of oxygenated organic compounds such as alcohols, ethers, aldehydes, acids and esters into aliphatic and aromatic hydrocarbons (1). Particular attention has been paid to the conversion of alcohols, especially methanol and numerous theories have been advanced for the reaction mechanism (2). Of the ketones, only acetone has been studied and the reactions on ZSM-5 and faujasites were compared (3). Condensation of acetone to oxygenated products at low temperatures (in some cases up to mesitylene) was assumed to be the first reaction step, followed by cracking to isobutene or -ane and acetic acid. While C_4H_{8-10} hydrocarbons were actually observed on ZSM-5 and rare-earth Y, acetic acid appeared only on the latter zeolite. At higher temperatures, aromatics dominated in the products, with a composition dependent on the zeolite type according to its shape selectivity (1,3).

In order to obtain a deeper insight into the processes occurring during the transformation of carbonyl-group-containing compounds over zeolites, we have focused our study on the comparison of the reaction

of several ketones, mainly acetone and methylethylketone, on HZSM-5. Two experimental methods were used: i) Infrared spectroscopy (IR) of surface compounds which were formed during the adsorption of ketones at room temperature and after their desorption at elevated temperatures. The gaseous products were collected and analyzed mass spectrometrically. ii) Mass spectrometric detection of the products of very small amounts of ketones preadsorbed at room temperature and released during temperature programmed desorption (TPD). In some cases, the catalytic reaction at low-pressure flow conditions was also investigated and the activity of HZSM-5 was compared with that of NaZSM-5 and HNaY.

EXPERIMENTAL

ZSM-5 zeolite with an Si/Al ratio equal to 19 was synthesized in the usual way (4); organic cations were decomposed in an oxygen stream at 870 K. NaZSM-5 was converted to the NH_4 form by ion exchang The sorption capacity measured with Ar was 5.4 mmol g^{-1} (related to the dry sample). The Si/Al ratio of $(NH_4)_{70}Na_{30}Y$ was 2.5 and the sorption capacity equalled 10.6 mmol g^{-1}. Before the measurements, all the samples were dehydrated and deammoniated in vacuo at 670 K for 18 hrs. Ketones (p.a. purity, Lachema) were predistilled in vacuo and degassed by repeated freezing and thawing. Acetone-d_6 (enrichment 99.5 %, Institute of Nuclear Research, Poland) was pretreated in the same way.

The infrared spectra of selfsupporting pellets of zeolites were measured at ambient temperature using a Nicolet MX-1E Fourier transform infrared spectrometer. The spectra presented here correspond to a sample thickness of 7 mg cm^{-2}. Ketones were adsorbed in succesive doses up to 5 mmol g^{-1} at room temperature. The zeolite was then heated (rate, 6 K min^{-1}) and the evolved vapours were collected in the temperature ranges 430 - 530, 530 - 630, and 630 - 730 K by freezing-out into separate bulbs. Up to 430 K, the desorbed gases were pumped off. The collected desorbate was analyzed by a mass spectrometer (MI 1302, USSR). The IR spectra of the zeolites were recorded both during the adsorption and after reaching the temperatures 430, 530, 630 and 730 K, when the samples were rapidly cooled to the ambient temperature.

The TPD was measured on the same mass spectrometer using 0.1 g of the zeolite. After 30 min. adsorption of 5×10^{-2} mmol g^{-1} at room temperature, the zeolite was heated (6 K min^{-1}) with direct pumping of the gaseous products through the spectrometer. A by-pass evacua-

tion was used to ensure that the maximum pressure of the evolved vapours did not exceed 1×10^{-3} Pa. When measuring the catalytic reaction, the zeolite (0.05 g) was placed in a reactor in front of the ionization chamber of the spectrometer and allowed to react with the ketone at inlet and outlet pressures of 10^{-2} and 4×10^{-4} Pa, respectively. The flow under these conditions was about 3×10^{-4} l h^{-1}.

RESULTS

Acetone. Fig. 1a shows the TPD of acetone from HZSM-5: a small amount of acetone is released above 370 K, followed by desorption of butene which exhibits two maxima, at about 570 and 670 K. Between these two maxima, C_{6-7} dienes or most probably cyclohexenes are evolved. Above 570 K aromatics appear with the maximum of toluene. The last observed product above 620 K has the composition C_3H_4, corresponding to allene or methylacetylene. The catalytic reaction under low-pressure flow conditions yields products of very similar composition at the relevant temperatures, as can be seen in Fig. 1b. The TPD of fully deuterated acetone demonstrates that hydrogen from the zeolitic OH groups is incorporated into the products from the very beginning of the reaction. With increasing temperature, the isotopic exchange increases.

In contrast to HZSM-5 almost no conversion of acetone is observed over NaZSM-5; the desorption of physisorbed acetone starts above 520 K and reaches its highest value at about 600 K.

The IR spectra depicted in Fig. 2 show deep changes in the composition of the surface complexes during the desorption of acetone from HZSM-5 between 295 - 530 K. At room temperature, acetone is preferentially adsorbed on the framework OH groups, forming H-bonded complexes with them. This is reflected in the disappearance of the OH band at 3610 cm^{-1} (a, curve 1,2), the appearance of broad OH bands below 3000 cm^{-1} and shifts of the position of bands of adsorbed acetone (b, curve 2) related to the vibrations of molecules in the gas phase. The most pronounced change is that in the C=O vibration adsorbing at 1740 cm^{-1} (gaseous acetone) and at 1670 cm^{-1} (H-bonded acetone) which indicates a partial loss of double bond character. Acetone molecules of further doses are considerably less perturbated as follows from the position of the C=O band at 1720 cm^{-1}. This band is dominant in the spectrum at high pore filling (not shown in Fig. 2). The removal of the adsorbed acetone between 295 - 430 K is accompanied by the formation of new surface species characterized by the bands at 1618 cm^{-1} which can be attributed to

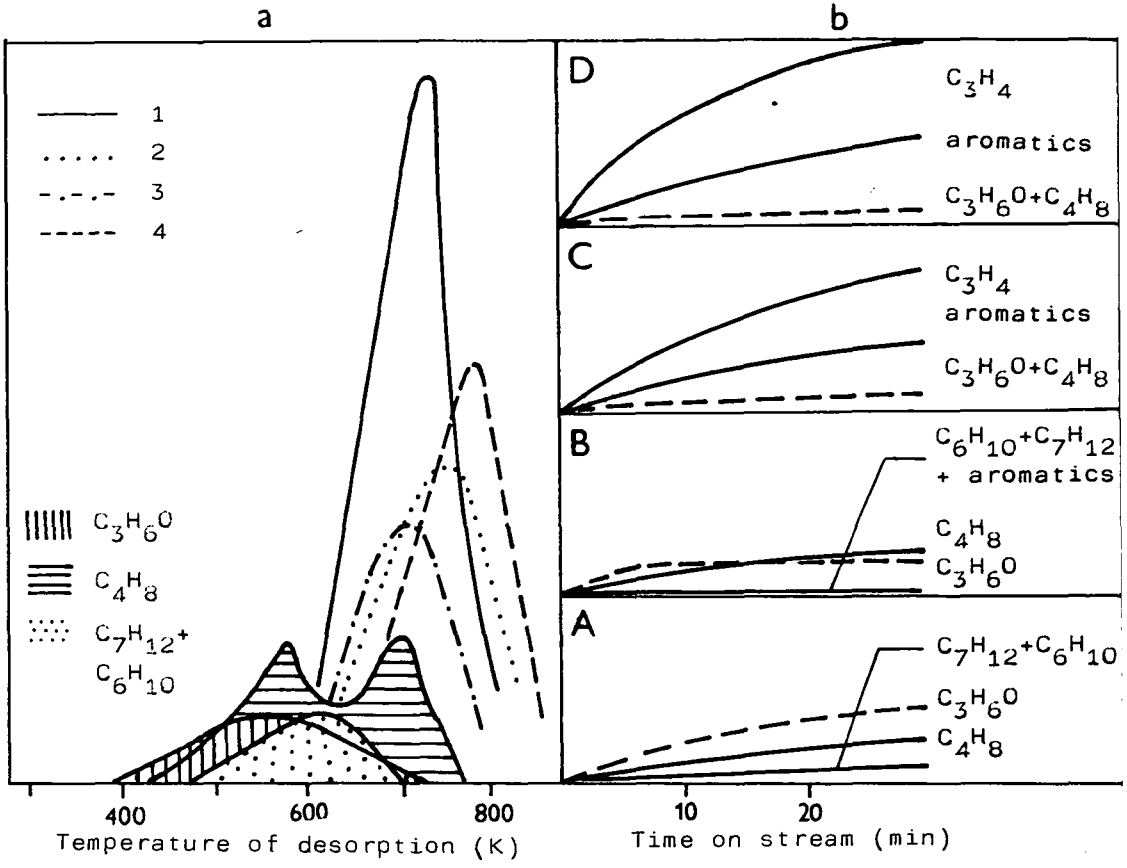

Fig. 1. Acetone (C_3H_6O) reaction with HZSM-5, a) TPD of gas products, b) low-pressure flow conversion at 370, 450, 710 and 790 K, A,B,C,D, respectively

1-C_7 aromatics, 2-benzene, 3-C_{8-9} aromatics, 4-C_3H_4

the C=O and C=C vibrations, respectively, in the products of acetone condensation (b, curve 3). The spectrum of the OH groups (a, curve 3) shows that these products also interact with the framework hydroxyls. Further heating to 530 K leads to a new rearrangement of surface species with simultaneous removal of adsorbed acetone molecules (b, curve 4) and the appearance of isobutene in the gas phase. As this new compound exhibits high thermal stability and the zeolitic OH groups can be restored in the original amount only after complete decomposition during 2 h evacuation at 770 K, it can be assumed that it is bonded directly to the lattice. This together with the prominent bands at 1644, 1543 and 1511 cm^{-1} assigned to the C=O and C=C vibrations support the idea of lattice oxygen bonding with the ketene, e.g.:

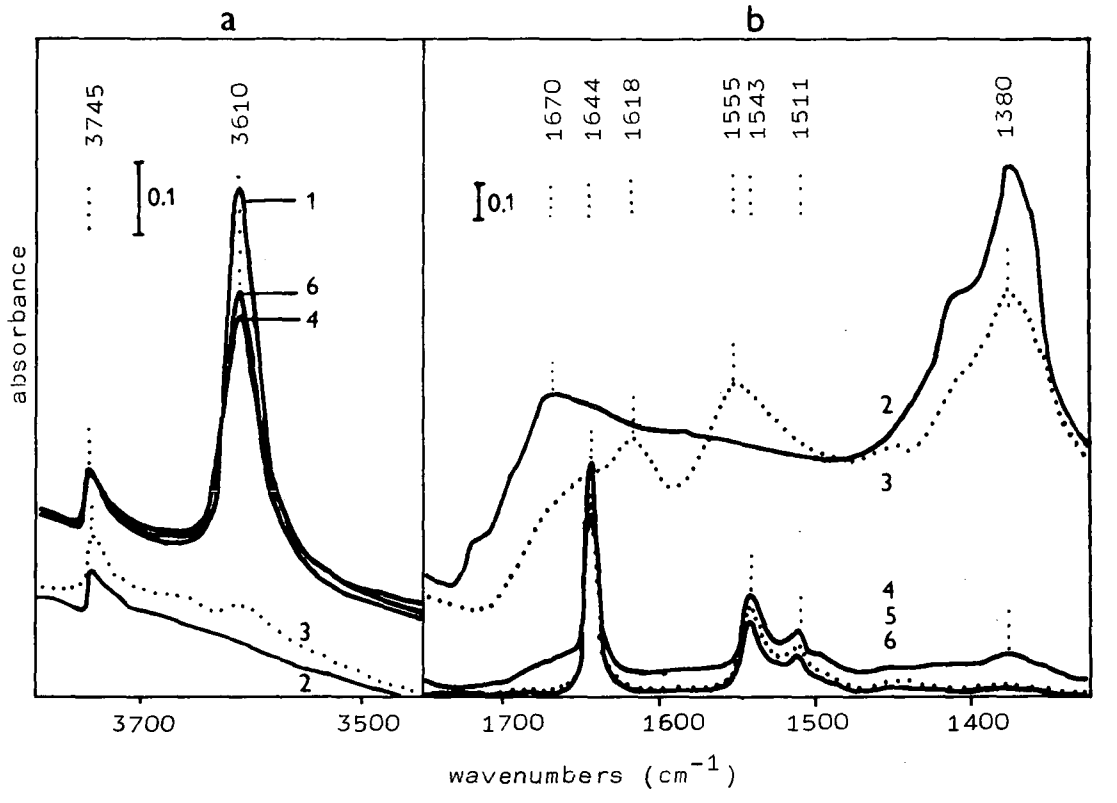

Fig. 2. IR spectra of acetone on HZSM-5, a) OH groups, b) surface complexes
1-original zeolite, 2-after adsorption of 1.1 mmol g^{-1} of acetone, 3-6 after addition of excess acetone and desorption up to 430, 530, 630 and 730 K, respectively

$CH_3-C=CH-C-CH_3$
zeol. O

The formation of a cyclic ketene also cannot be fully excluded. Some of the surface species are removed together with the remaining adsorbed acetone at 530 - 730 K. The collected gas always contains acetone, butene and aromatics. With increasing desorption temperature the aromatics to butene ratio increases.

In agreement with the TPD results, NaZSM-5 strongly differs from HZSM-5. According to the IR spectra shown in Fig. 3a, NaZSM-5 has no acidic OH groups on its lattice and, therefore, no H-bonded acetone complexes appear (Fig. 3b). The C=O bands at 1712 and 1678 cm^{-1} belong to acetone adsorbed most probably on Na^+ and Al electron-accepting sites; the latter are always present on ZSM-5 zeolites. Both these surface species are observed during the adsorption at am-

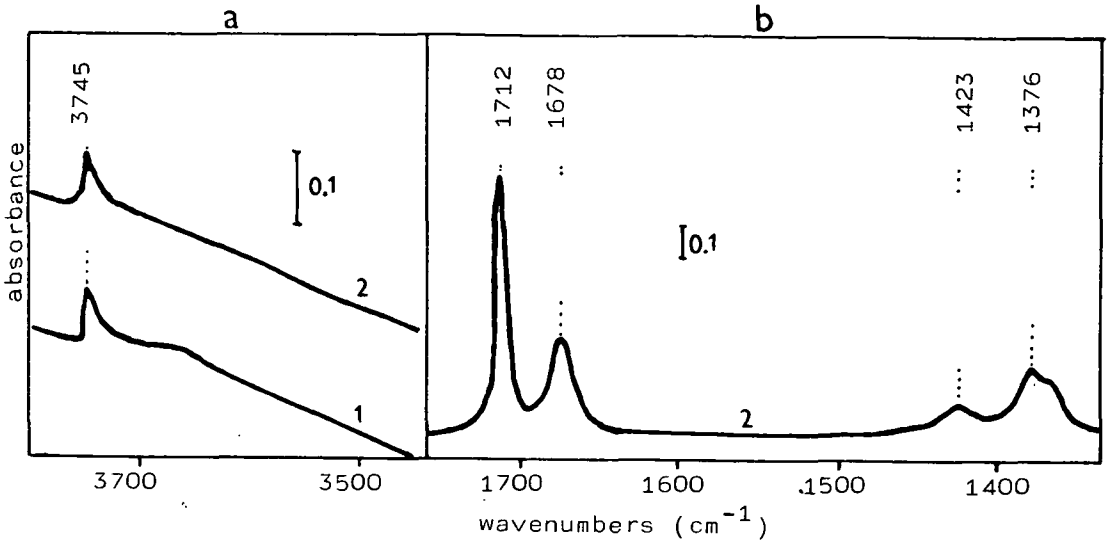

Fig. 3. IR spectra of acetone on NaZSM-5, a) OH groups, b) surface complexes
1-original zeolite, 2-after adsorption of excess acetone and desorption up to 530 K

bient temperature as well as during thermal desorption without any catalytically conditioned changes.

Methylethylketone. The TPD of this ketone is depicted in Fig. 4a,b for HZSM-5 and NaZSM-5, respectively. The conversion is substantially higher with the acid form, where only a very small amount of unreacted ketone appears, preceeded by the evolution of propene and C_{4-7} olefins and cycloalkenes. The amount of these substances is relatively low and is followed above 570 K by a much greater release of propene, C_5H_6 (probably cyclopentadienes) and especially butadiene (dimethylacetylene) and $C_{6,7}$ aromatics. The small maximum of products below 500 K is missing with NaZSM-5 while a large amount of unreacted ketone starts to desorb. This is followed by the release of C_5H_8 (less unsaturated product than with the acid zeolite form), propene and butadiene in almost the same amounts as with HZSM-5. The release of C_{6-8} aromatics is much lower with NaZSM-5 than with HZSM-5.

The IR spectra of adsorbed species on HZSM-5 (Fig. 5b, curve 2) together with spectral changes in the region of OH vibrations (Fig. 5a, curves 1,2) show that, at room temperature, H-bonded complexes of methylethylketone are preferentially formed with framework hydroxyls. The C=O vibration band at 1650 cm^{-1} again indicates an

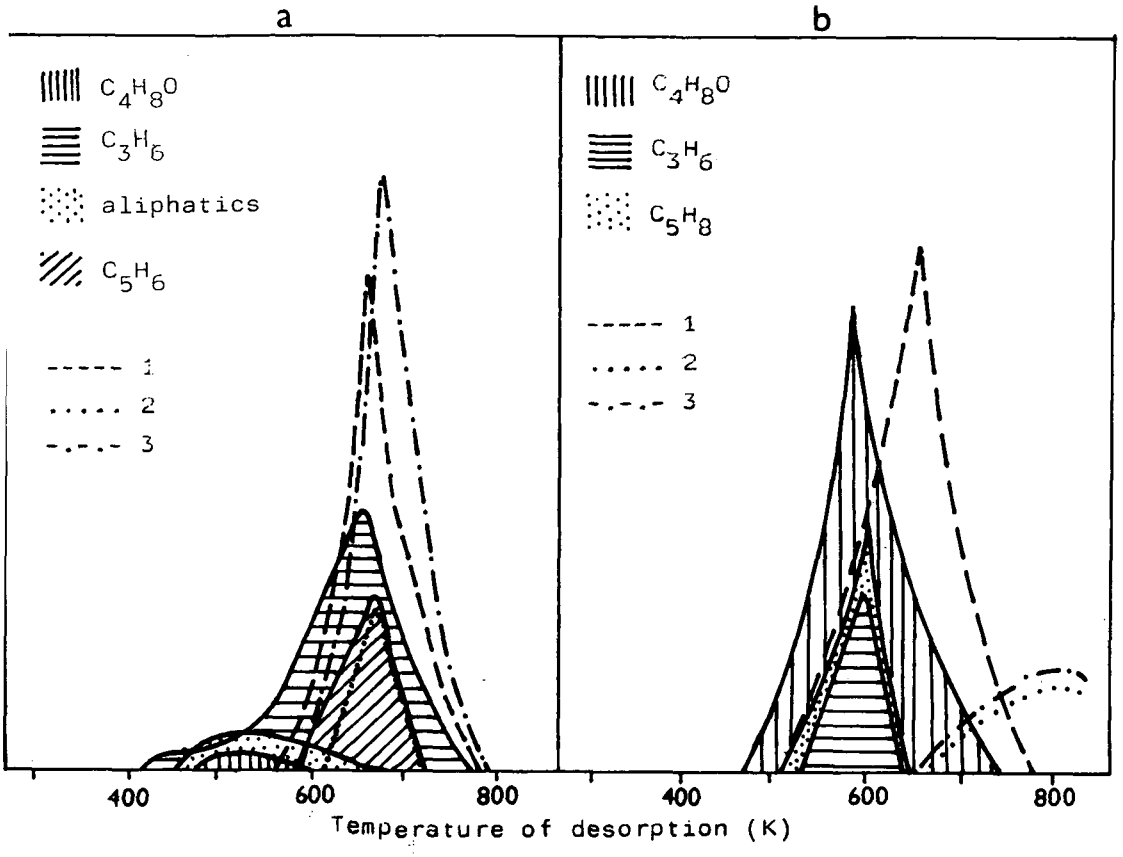

Fig. 4. TPD of methyethylketone, a) from HZSM-5, b) from NaZSM-5
1-C_4H_6, 2-benzene, 3-$C_{7,8}$ aromatics

appreciable weaking of the double bond in comparison with the gas molecule ($\nu_{C=O}$= 1740 cm^{-1}). Thermal desorption leads to the progressive removal of surface species without such pronounced transformations as those observed for the acetone. Only several new weak bands are found in the region 1510 - 1580 cm^{-1}; however, their intensity is changed without any special interrelations. The evolved gas always contains unreacted ketone. Similarly as in TPD, the products of catalytic reaction appear in considerable amounts above 570 K with predominant aromatics. These data support the assumption that the weak band at 1510 - 1570 cm^{-1} which remains in the spectrum of the surface at the relevant temperatures (Fig. 5b, curves 4,5) most probably corresponds to adsorbed aromatics.

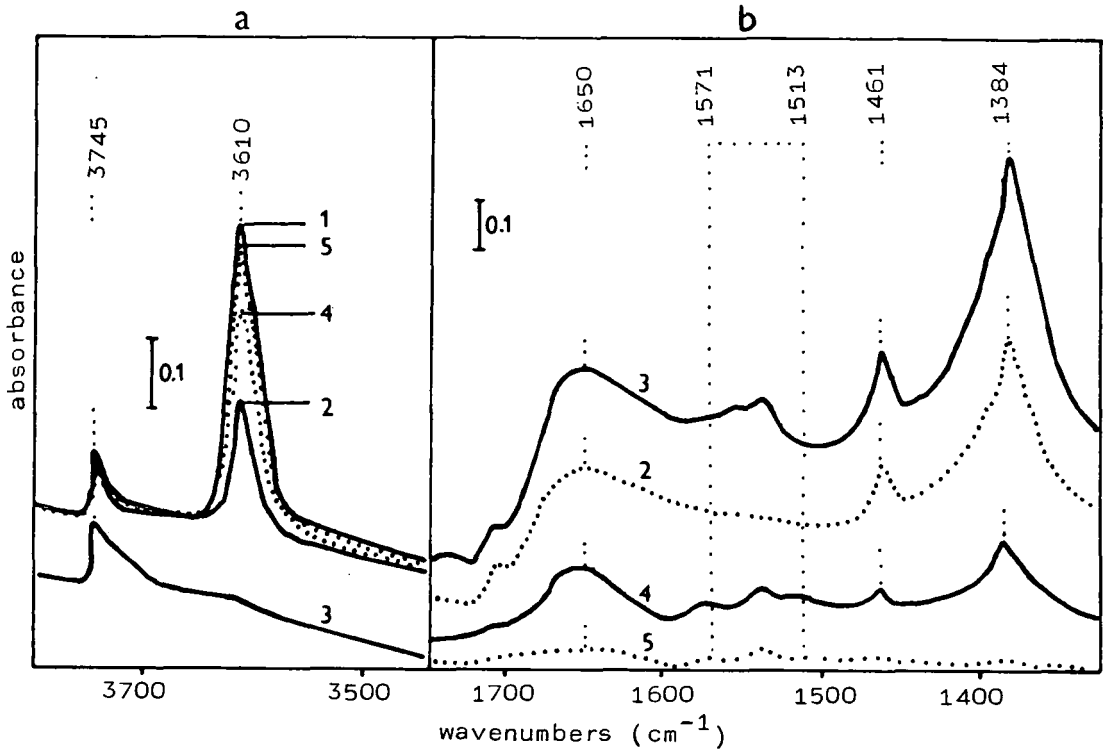

Fig. 5. IR spectra of methylethylketone on HZSM-5, a) OH groups b) surface complexes
1-original zeolite, 2-after adsorption of 0.4 mmol g^{-1} ketone, 3-5- after addition of excess ketone and thermal desorption up to 430, 530 and 630 K, respectively

DISCUSSION

Before discussing the results, it should be mentioned that the interaction of small amounts of reactants with zeolites exhibits special features. This results from the fact that, under these conditions, molecules are preferentially influenced by the most active sites on the surface and mutual interactions among the reactant, intermediates and products are appreciably reduced. The product composition is thus more intimately connected with the first reaction steps and with the presence of various types of surface complexes than for reactions proceeding at higher pressure. Increasing pressure (amount of adsorbed species) naturally changes the product distribution; however,the most characteristic compounds almost always appear (5).

Acetone and methylethylketone are the two simplest compounds in the broad family of ketones. Nevertheless, they can serve as an

example of the substantially changed reaction path in catalytic transformation on the same zeolites. The condensation of ketones in acid media, leading to a series of dehydrated products is well known from organic chemistry. This type of reaction apparently occurs with acetone on HZSM-5 which contains framework hydroxyls of high acid strength, while NaZSM-5 with only Na ions and electron-accepting sites is inactive. The formation of H-bonded complexes, demonstrated by the IR spectra, is probably responsible for the enhanced reactivity of adsorbed acetone because of facilitated splitting off of hydrogens from the methyl groups. The mobility of H^+ between acetone and zeolite follows also from the easy isotopic exchange of deuterated acetone with the hydroxyl hydrogens.

In contrast to (3), oxygen-containing products of acetone condensation were not observed in the gaseous phase, but they were found in the zeolites even below 430 K. As the temperature increased up to 530 K, these condensates were transformed to isobutene, which was released into the gas phase, and to a new carbonyl compound firmly bound to the zeolite lattice. The framework hydroxyls could aid in the cracking of the acetone condensate, e.g. as follows:

$$(CH_3)_2C{=}CH{-}\overset{\overset{CH_3}{|}}{C}{=}CH\overset{\overset{O}{\|}}{C}CH_3 + HO_{zeol} \longrightarrow (CH_3)_2C{=}CH_2 + CH_3\overset{\overset{O}{\|}}{\underset{O_{zeol}}{|}}C{=}CH\overset{\overset{O}{\|}}{C}CH_3 \qquad (I)$$

The new surface species (I) is thermally stable but it can take part in a further reaction when interacting with a compound able to donate a proton for the re-formation of the framework hydroxyls. This most probably occurs at higher temperatures along with cyclization to aromatics which are the prevailing gaseous products. The thermal decomposition of surface ketene (I) might be responsible for the release of C_3H_4 observed in TPD as the last product; however, this compound can also be formed via an intramolecular dehydration.

The interaction of methyethylketone with zeolites is clearly of different character than that of acetone: i) both the acid and the Na form of ZSM-5 catalyzed the transformation, ii) C_4H_6 was formed in an appreciable amount over both zeolites and iii) no firmly bound surface ketene similar to (I) was observed. It can thus be assumed that a simple intramolecular dehydration of methyethylketone to C_4H_6 plays an important role here. This reaction is not apparently conditioned by the formation of H-bonded complexes, as the influence of Al electron accepting sites, Na ions and electrostatic field of zeolites sufficiently activates the ketone molecules.

Butadiene most probably takes part in the formation of aromatics, as follows from their release from NaZSM-5. However, HZSM-5 exhibits much higher activity, reflected in the total conversion and the product composition. This is apparently caused by the participation of the OH groups influencing the transformation and by the contribution of some condensation reactions of ketone, though not as pronounced as with acetone.

Some higher ketones (diethylketone, cyclopentanone and cyclohexanone) were also studied. They released products of intramolecula dehydration which preceeded the evolution of aromatics. 2,4-pentadione behaved in a very similar way to acetone, supporting the conclusion on the dominant role of acetone condensates in its transformation.

The TPD of all these ketones was also investigated with the HY zeolite. The comparison of products released from HZSM-5 and HY reflected the higher acid strength and shape-selective properties of HZSM-5 (6).

REFERENCES

1. Chang, C.D., Silvestri, A.J., J. Catal. 47, 249 (1977).
2. Chang, C.D., Catal. Rev. 25, 1 (1984).
3. Chang, C.D., Lang, W.H., Bell, W.K., Catalysis in Organic Reactions. W.R. Moser, Ed., M. Dekker, N.Y., p. 84-93 (and refs. therein).
4. U.S. Patent 3,702,886.
5. Nováková, J., Kubelková, L., Habersberger, K., Dolejšek, Z., J. Chem. Soc., Faraday Trans. I, 80, 1457 (1984).
6. Nováková, J., Kubelková, L., Jírů, P., to be published.

DEHYDRATION OF DIOLS ON ZEOLITES OF TYPES X AND Y

Á. MOLNÁR, I. Bucsi, M. Bartók
Department of Organic Chemistry, József Attila University, Szeged, Hungary

ABSTRACT

The transformations of 1,2- 1,3- 1,4- and 1,5-diols on NaX, NaHX, NaY and NaHY zeolites were studied in a continuous flow reactor, at atmospheric pressure, at 503-623 K. The acidities of the zeolites were examined by the pyridine adsorption-IR technique, the Me_2Zn-GC method, and titration with n-butylamine. The two main transformations taking place are dehydration and fragmentation. The ratio of the two processes is determined by the structures of the diols, the type of the zeolite and the temperature. The 1,2-diols transform via the pinacol rearrangement; the 1,3-diols give unsaturated compounds via 1,2-elimination while the 1,4- and 1,5-diols undergo stereoselective ring-closure leading to the formation of cyclic ethers.

The activities of the zeolites in the transformations of diols proved similar to their activities in the transformations of alcohols: NaX < NaY < NaHX < NaHY.

INTRODUCTION

Wide-ranging studies have been reported on the catalytic transformations of alcohols on zeolites [1-3]. The acid centres of zeolites are known to catalyse the elimination of water from alcohols. The elimination can lead to the formation of both alkenes and ethers, via intra- or intermolecular dehydration, respectively [4]. Intramolecular dehydration on zeolites involves anti elimination, leading to the formation of alkene mixture with a cis/trans ratio higher than at equilibrium. These observations have been supported by theoretical calculations [5]. The activity of a zeolite in the dehydration process is proportional to the number of its Brönsted acid centres.

On the other hand, only a few data are available on the transformations of dihydroxy compounds (diols) on zeolites. Studies with 2-methyl-2,3-butanediol [6], 1,3-butanediol [7] and 1,4-butanediol [8] have revealed that the characteristic transformation of diols is

intramolecular dehydration, with the formation of carbonyl compounds, dienes and cyclic ethers. Products formed by fragmentation are also detected.

The aim of our investigations was to establish a correlation between the characteristic transformation directions, the structures of the diols (the orders of the carbon atoms bearing the hydroxy groups, and the relative positions of the hydroxy groups) and the acidities of the zeolites.

EXPERIMENTAL

Materials. The following diols (Fluka products) were used after distillation (GC purity: 100%): 1,2-propanediol (I), 2,3-butanediol (II) (1:1 isomeric mixture), 2,3-dimethyl-2,3-butanediol (III), 2,4-pentanediol (IV) (1:1 isomeric mixture), 2,5-hexanediol (V) (1:1 isomeric mixture), 1,5-pentanediol (VII). (±)-2,5-Hexanediol (VI) (isomer purity: 98%) was prepared from V via distillation of the isomeric oxepanes [9].

Catalysts. The NaX and NaY zeolites were commercial products (Strem Chemicals, 011878-G and 042578-G, respectively). The NaHX and NaHY zeolites were prepared by Na^+-NH_4^+ ion-exchange, followed by decomposition of the ammonium form at 673 K for 5h [10].

The acidities of the zeolites were determined by three methods. Method A. The IR absorption bands at 1550 cm^{-1} and 1445 cm^{-1} of pyridine adsorbed on zeolites at 473 K are characteristic of the Brönsted and Lewis acid centres, respectively [11]. The values in Table 1 are the ratios peak height/sample quantity, which are proportional to the number of acid centres. Method B. The number of surface protons was determined with the Me_2Zn-tetrahydrofuran reagent via GC determination of methane formed at 363 K [12]. Method C. After heat treatment at 673 K powdered zeolites were titrated with n-butylamine in benzene, as in [13].

Table 1

Acidities of zeolites used

	adsorption of pyridine		Me_2Zn	n-$BuNH_2$
	Brönsted	Lewis	10^{20}	g^{-1}
NaX	1.5	1.5	2.60	1.35
NaHX	6.4	3.0	7.00	2.31
NaY	2.3	1.3	4.55	1.23
NaHY	14.7	4.3	7.86	3.92

Apparatus. The experiments were carried out in a glass flow reactor (lenght: 160 mm, inner diameter: 20 mm) (Figure 1). The dead space of the reactor tube was filled with glass beads 3 mm in diameter. The liquid products were collected in a condenser (5), while the quantity of gaseous products was measured with a gas burette (9).

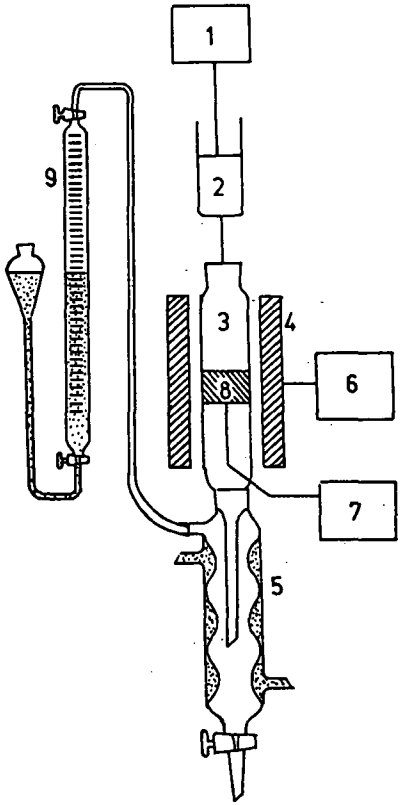

1 Feeding motor
2 Syringe
3 Reactor tube
4 Heating jacket
5 Condenser
6 Temperature controller
7 Temperature meter
8 Catalyst sample
9 Gas burette

Fig. 1. Apparatus

Measurements. The catalyst samples of 2 ml were kept at 673 K for 1 h before use, then cooled to the temperature of the experiment. The diols were fed into the reactor at a feeding rate of 0.6 ml/ml h. After the first 2 ml of diol, a constant catalyst activity was reached, and all the measurements were carried out in this range.

Analysis. The composition of the reaction products was determined by GC. Before analysis, the heterogeneous products (aqueous and organic layers) were homogenized by adding an appropriate amount of diglyme to the mixture. The columns were as follows (length: 1.8 m, solid support: Merck Kieselguhr with a grain size of 0.2-0.3 mm): 10% PEG 20M (for determination of the conversions), 15% Reoplex 400 (for determination of the composition of the liquid products), and 10% squalane (for determination of the composition of the gaseous products). Authentic compounds and calibration curves were used for the identification of products and the calculations, respectively.

RESULTS

Tables 2-5 present data on the transformations of the diols examined.

Table 2

Product compositions (mol %) of 1,2-diols on NaHY zeolite (623 K, 100% conversion)

I		II		III	
Acetaldehyde	4	1,3-Butadiene	28	2,3-Dimethyl-	
Propionaldehyde	67	Acetaldehyde	6	-1,3-butadiene	20
Acetone	13	Acetone	4	3,3-Dimethyl-	
2-Propanol	5	2-Butanone	62	-2-butanone	71
2-Propen-1-ol	5			Unidentified	9
Unidentified	6				

Table 3

Conversions (%) of 2,3-butanediol at 503 K

NaX	NaHX	NaY	NaHY
33	89	36	94

Table 4

Product compositions (mol %), conversions and transformation directions pf 2,4-pentanediol (IV). (X=NaX, HX=NaHX, Y=NaY, HY=NaHY)

	523 K				548 K				573 K			
	X	HX	Y	HY	X	HX	Y	HY	X	HX	Y	HY
Dienes	79	70	37	34	90	53	36	25	95	39	36	11
Propene		4	7	8		2	6	12		6	8	18
Acetaldehyde		4	8	7		2	7	15		7	10	23
Acetone		6	10	8	2	7	11	13	2	14	12	11
Ethanol		3	11	8		4	8	12		12	8	15
2-Pentanone	1	3	4	4	2	1	4	6	2	1	3	6
4-Penten-2-ol	20	3	23	22	6	29	28	10	1	14	20	7
3-Penten-2-one		7		9		2		7		7	3	9
Conversion	53	90	77	95	90	93	93	95	97	98	98	100
Dehydration	100	89	77	81	98	90	80	66	98	75	74	53
Fragmentation	0	11	21	19	2	10	20	34	2	25	26	47

Table 5

Product compositions (mol%) of 2,5-hexanediols (V, VI) and 1,5-pentanediol (VII) (NaHY, 573 K, 100% conversion)

		V	VI		VII
2,5-Dimethyltetrahydrofurans	cis	45	96	Tetrahydropyran	95
	trans	49	4	Unidentified	5
Unidentified		6			

DISCUSSION

The main reaction directions in the transformations of 1,2-diols on zeolites are the two different forms of dehydration (Table 2). The pinacol rearrangement leads to the formation of carbonyl compounds, and 1,2-elimination to an unsaturated alcohol or dienes (Scheme 1).

The carbenium ion formed in the first step may be stabilized in two ways: after 1,2-anionotropic migration of an α-substituent (in the examined 1,2-diols H or Me), carbonyl compounds are formed as a result of proton elimination (pinacol rearrangement); alternatively, unsaturated alcohols may be formed through elimination of an α-proton, and these give the diene end-product through the

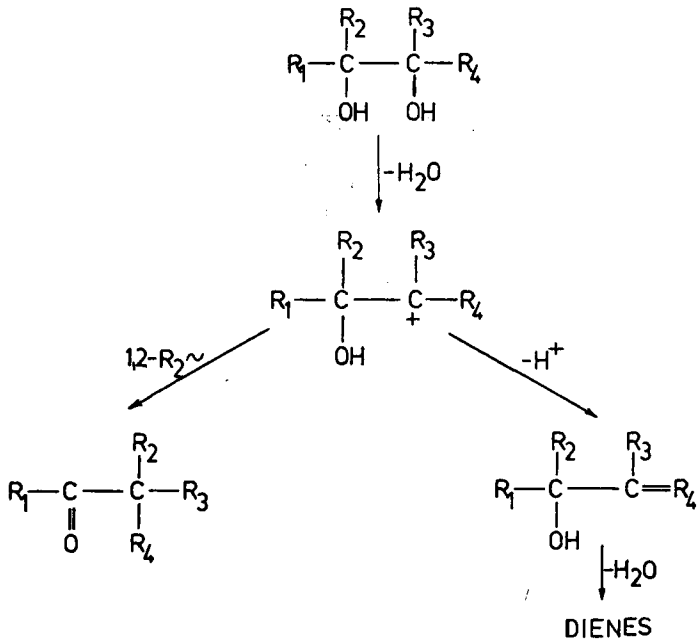

Scheme 1

elimination of a further molecule of water via a similar mechanism.

About 70% of the carbenium ions are stabilized through the pinacol rearrangement, which is in good agreement with the results found on other acid-type catalysts, e.g. Na_2HPO_4 [14] and $Ca_3(PO_4)_3$ [15].

In the case of 1,2-propanediol (I), the results of the pinacol rearrangement can be acetone or propionaldehyde, depending on whether the primary or secondary OH group is eliminated in the first step. Their ratio (acetone:propionaldehyde = 1:5) corresponds to the difference between the rates of decomposition of hydroxonium ions bound to the primary and secondary carbon atoms [16]. Diene formation is not observed in the case of I, for the cumulated diene obtained from it (1,2-propadiene) is thermodynamically unstable under such conditions.

The data in Table 4 show that the main reaction direction for 2,4-propanediol (a typical 1,3-diol) is dehydration through 1,2-elimination, which is accompanied by fragmentation too, depending on the temperature and the zeolite type. The observed transformations are depicted in Scheme 2.

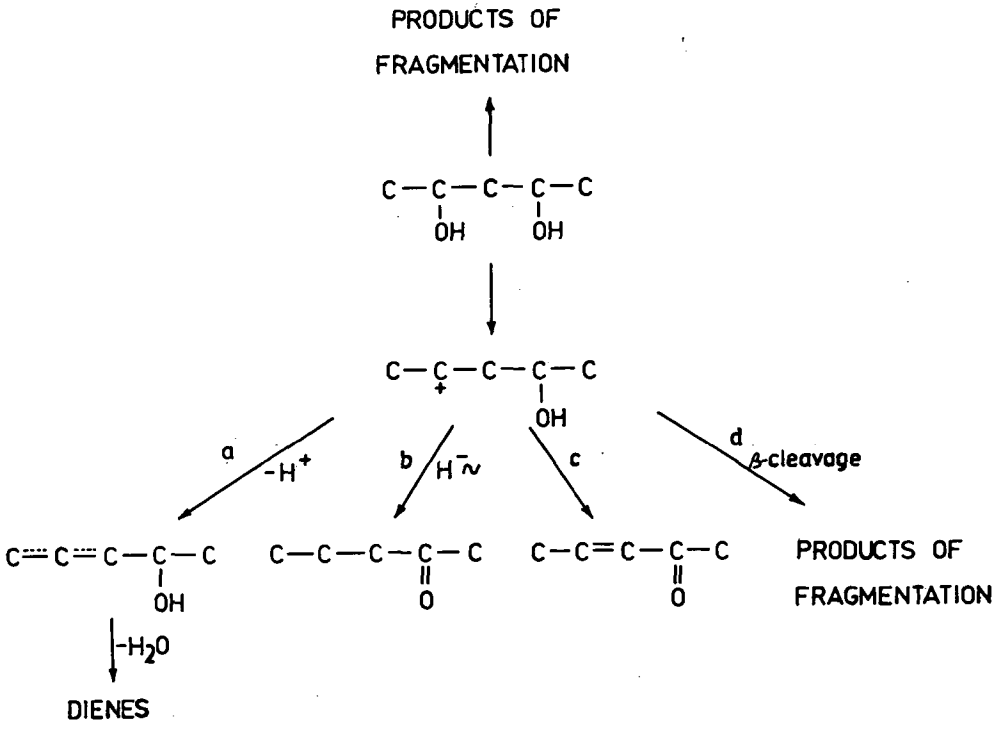

Scheme 2

The secondary carbenium ion formed by elimination of one of the OH groups can react further in four ways:

a) Elimination of an α-proton, with the formation of unsaturated alcohols, which can be further dehydrated to dienes (1,2-elimination);
b) formation of 2-pentanone during hydride ion migration processes;
c) formation of 3-penten-2-one by an unknown route;
d) fragmentation (β-cleavage).

Of these four processes, 1,2-elimination predominates. It may be mentioned that on NaX zeolite, at a conversion of 100%, pentadienes are formed with a yield of 95%. Of the two possible pentadiene isomers, the thermodynamically more stable conjugated 1,3-pentadiene is formed to an extent of nearly 90%.

The large number of fragmentation products to be found in the catalyst demonstrate that, besides the β-cleavage occurring in the carbenium ion, fragmentation also takes place in the diol molecule itself. The latter process was also observed by Mazet et al. [17] during the acid catalysis of 2,2-disubstituted-1,3-propanediols under homogeneous conditions.

It is worth stressing that the 1,2-diols, in contrast with the 1,3-diols, barely undergo fragmentation. The explanation of this may be that the α-OH-containing carbenium ion formed in the first step (Scheme 1) participates much more quickly in 1,2-anionoid migration than in β-cleavage of a C-C bond.

Areshidze et al. [8] found that 1,4-butanediol is converted to tetrahydrofuran on zeolites, i.e. intramolecular ether formation occurs. Our results show that the main reaction for 1,4- and 1,5-diols is cyclodehydration (Table 5). It follows from the tabulated data that, similarly to the cyclodehydration taking place on other heterogeneous catalysts and under homogeneous conditions [9] , the ring closure is stereospecific and is accompanied by inversion. The stereospecific nature of the process permits the conclusion that the

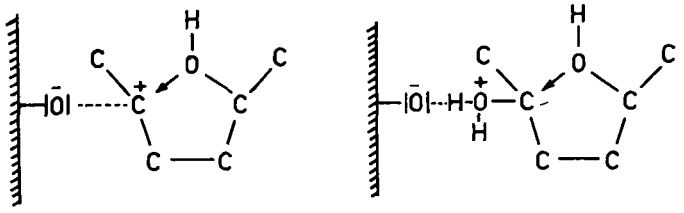

Scheme 3

cation formed in the first step, which may be either a carbenium ion or an oxonium ion, is bound to the surface of the zeolite following intramolecular S_N2 attack by the OH group (Scheme 3), as assumed by other authors for zeolites [18]. This process ensures the occurrence of inversion on one of the asymmetry centres.

The results of measurements of the zeolite acidities (Table 1) and comparisons of the conversions of the diols (Tables 3 and 4) reveal that (as in zeolite-catalysed processes in general) a higher acidity results in a higher activity. Both the activities and the acidities of the zeolites vary in the sequence:

$$NaX < NaY < NaHX < NaHY$$

Apart from this sequence, no more exact correlation can be found between the acidity and the activity, which demonstrates that the activity of a zeolite in the dehydration processes is influenced not only by the acidity, but by other effects too. It can also be seen, however, that the increase of the acidity within the pairs NaX-NaHX and NaY-NaHY results in a higher extent of fragmentation of 2,4-pentanediol (Table 4). It can also be stated that the Y-type zeolites cause more fragmentation than do those of X type. Since stronger electrostatic fields develop in the Y-type zeolites than in those of X type [19], this indicates that the electrostatic fields play some direct role in the occurrence of fragmentation.

REFERENCES

1. Venuto, P.B., Landis, P.S., Adv. Catal. 18, 306 (1968).
2. Rabo, J.A.: Zeolite Chemistry and Catalysis. ACS Monograph Series 171, 505 (1976).
3. Jacobs, P.A.: Carboniogenic Activity of Zeolites. Elsevier, Amsterdam, 1977, p. 100.
4. Gentry, S.J., Rudham, R., J. Chem. Soc. Faraday I 70, 1685 (1974).
5. Sedlacek, J., Coll. Czech. Chem. Comm. 46, 2466 (1981).
6. Gryaznova, Z.V., Nefedova, A.R., Rutman, G.I., Sb. 1-ya Vses. Konf. Primenenie Tseolitov v Katalize, 1976, p. 51; Chem. Abstr. 85, 159280t (1976).
7. Bergk, K.H., Wolf, F., Z. Chem. 18, 67 (1978).
8. Areshidze, Kh.I., Chivadze, G.O., Khim. Geterotsikl. Soed. 195 (1969).
9. Molnár, Á., Felföldi, K., Bartók, M., Tetrahedron 37, 2149 (1981).

10. Ward, J.W., J. Catal. 9, 225 (1967).
11. Ward, J.W., Hansford, R.C., J. Catal. 13, 154 (1969).
12. Nondek, L., React. Kinet. Catal. Lett. 2, 283 (1975).
13. Borodin, V.N., Zh. Fiz. Khim. 51, 928 (1977).
14. Gear, J.L., US Pat. 2,501,042; Chem. Abstr. 44, 5379c (1950).
15. Freidlin, L.Kh., Sharf, V.Z., Izv. Akad. Nauk SSSR, Otd. Khim. Nauk 698 (1962).
16. Gryaznova, Z.V., Ermilova, M.M., Tsitsishvili, G.V., Andronikashvili, T.G., Krupennikova, A.Yu., Kinet. Katal. 11, 147 (1970).
17. Yvernault, T., Mazet, M., Bull. Soc. Chim. France 2755 (1967).
18. Wendlandt, K.-P., Bremer, H., Proc. 8th Internat. Congr. Catal., West Berlin, 1984, IV-507.
19. Pickert, P.E., Rabo, J.A., Demsey, E., Schomaker, V., Proc. 3rd Internat. Congr. Catal., Amsterdam, 1964, 1, 714 (1965).

ACKNOWLEDGMENTS

We gratefully acknowledge financial support for this work by the Hungarian Ministry of Education (Grant No. 40/1981) and the Hungarian Academy of Sciences (Grant No. 319/82/1.3).

HYDRODEOXYGENATION OF FURAN ON H-ZSM-5 AND Pt-ZSM-5

B. KRAUSHAAR, H. KOMPA, H. SCHRÜBBERS, G. SCHULZ-EKLOFF
Institut für Angewandte und Physikalische Chemie, Forschungsgruppe Angewandte Katalyse, Universität Bremen, D-2800 Bremen 33, FRG

ABSTRACT

It is shown that the shape-selective hydrodeoxygenation of furan proceeds on the catalysts H-ZSM-5 and Pt-ZSM-5. The differences in the product spectra obtained on the two zeolite materials and the different coking rates are interpreted with the different hydrogenation capabilities of the two catalysts. The low H/C ratio of furan can be increased to the higher values of the products by activation of added molecular hydrogen or, in the case of Pt-ZSM-5, by hydrogen transfer from added molecules with high H/C ratios. Reaction mechanisms for the furan conversion are discussed, which comprise the observed oxygen eliminations by decarbonylation and dehydration as well as the 2,3-benzofuran formation.

INTRODUCTION

The elimination of the hetero atom from oxygen containing compounds on zeolite catalysts has been studied for a broad class of reactions [1], leading to the discovery of the methanol to gasoline process [2]. Moreover, shape-selective zeolite catalysts have been shown to convert a variety of oxygen containing biomass derived compounds to high-grade fuel [3]. Shape-selective catalysts exhibit the unique property to reconstruct large molecules of quite different type into very similar molecular weight-limited product mixtures. This capability of the pentasil type zeolites can be used to convert the pyrolysis products of the biomass containing municipal wastes and sewage sludges into gasoline. The main classes of organic compounds formed in the decomposition of cellulose, the main constituent of the biomass, i.e. methanol, acetic acid, phenols and furfurals, should undergo shape-selective conversions. For an exemplary clarification of this point, the deoxygenation of the furan, which is readily formed by the decarbonylation of the representative pyrolysis product furfural, is studied on the zeolites H-ZSM-5 and Pt-ZSM-5.

EXPERIMENTAL

Preparation of Catalysts. The sodium form of the ZSM-5 was synthesized according to the recipe example 24 of the patent of Argauer and Landolt [4]. The main variation concerns the manner to achieve the pH value of 11, which we did not adjust by addition of H_2SO_4 but by using colloidal solutions of silica gel (Kieselsol, Bayer, Leverkusen) instead of water glass, leading to lower NaOH portions in the reaction mixture. A teflon vessel equipped autoclave (Berghof, Tübingen) was used. The complete removal of the organic material from the template ion by the calcination procedure was controlled by infrared spectroscopy. No effect of stirring on the crystallinity of the products was observed.

The hydrogen form of the catalyst was obtained by repeated ion exchange in a 5% aqueous NH_4Cl solution (15 ml per g zeolite) at 353 K, subsequent washing, drying at 373 K and calcination at 623 K for 4 hours.

The platinum loaded catalyst was prepared by ion exchange in an aqueous solution of 0.5 % platinum tetrammine chloride at 353 K for 4 hours, using 7 ml solution per 1 g zeolite. After washing and drying the platinum complex was decomposed by temperature programmed heating (5 K min^{-1}) up to 673 K under argon (5 l h^{-1}) and subsequent reduction in hydrogen (1 bar, 5 l h^{-1}) at 673 K. The platinum content of the catalyst was 2.2 wt%.

Characterization. The prepared ZSM-5 exhibited a silicon to aluminum atomic ratio of about 40. The infrared spectra and the X-ray diffraction patterns, typical for the ZSM-5 type zeolite were obtained. A small fraction of amorphous material of about 5% could be detected by X-ray diagrams. The nitrogen physisorption capacities at 77 K and P/P_o = 0.1 were determined by a dynamic method [5] and gave 21 molecules per unit cell, confirming the good crystallinity of the zeolite [6]. From the scanning electron micrographs mean zeolite particle sizes around 1 µm were determined. No platinum lines were found in the X-ray diagram pointing to platinum particles located within the zeolite matrix. Since the amount of platinum corresponds to the aluminium content, a nearly complete ion exchange can be assumed.

Apparatus. The furan conversion was studied in a continuous flow stainless steel microreactor (6 mm inner diameter) with a fixed bed (0.2 g) of the undiluted, pressed (14 MPa) and pelletized (0.35 - 0.5 mm diameter) zeolite catalyst. The reaction was studied at 673 K and at WHSV = 0.5 h^{-1}. Argon and hydrogen were used as carrier gases and were flowing through the catalyst bed until constant reaction temperatures were reached. They were then loaded with furan by streaming through a thermostated saturator. The reaction products were analyzed by gas chromatography (F 22, Perkin Elmer) using a thin film quartz capillary (25 m, OV 101, Perkin Elmer) and temperature programs. Product identifications were made using internal standards.

RESULTS

H-ZSM-5. The catalyst exhibited strong fluctuations in the product distribution during the first minutes, which dissappeared after 10 minutes. The distribution of the hydrocarbon mixture, i.e. without water and carbon monoxide, in dependence on the time on stream of the educt furan is shown in Figure 1. The high fraction of BTX (benzene, toluene and xylenes) aromatics formed in the very beginning decreases rapidly in favour of C_{9+} aromatics, e.g. methylethylbenzenes, mesitylenes, durenes and naphthalenes and especially high fractions of the compound 2,3-benzofuran. The catalyst is deactivated to more than 90% after 1 hour. Its nitrogen physisorption capacity decreases sharply,i.e. by 25%, within the first 10 minutes and then more slightly but continuously.

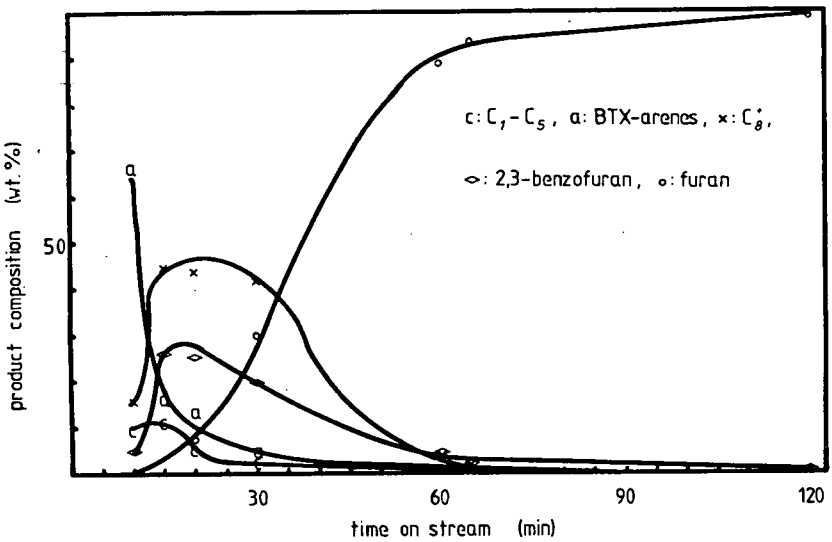

Fig. 1. Product composition (without water and CO) of furan conversion on H-ZSM-5 in hydrogen (673 K, WHSV = 0.5 h^{-1}, 11 kPa furan)

Pt-ZSM-5. Furan was converted to C_1 - C_4 paraffins and BTX aromatics, mainly, without any fluctuations of the product concentrations during the first minutes (Fig. 2). The BTX fraction decreases more slightly as compared to the H-ZSM-5. The fractions of 2,3-benzofuran, the educt furan and the higher aromatics rise slowly

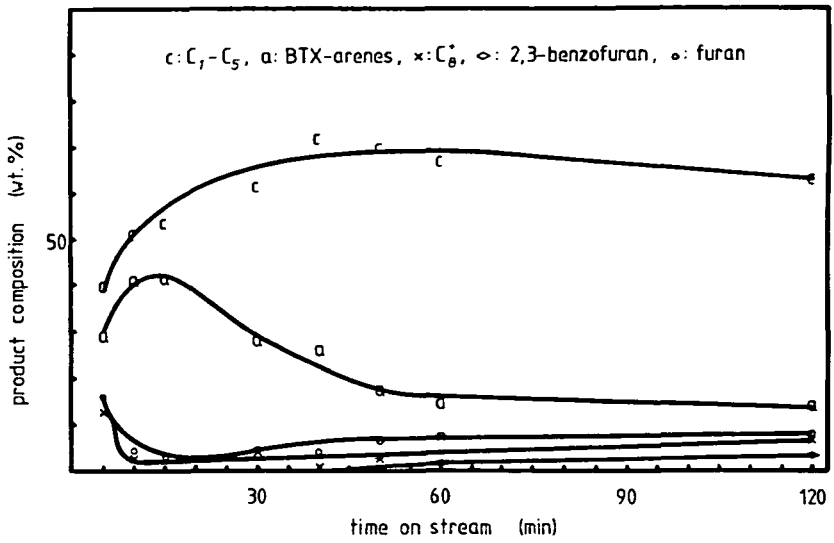

Fig. 2. Product composition (without water) of furan conversion on Pt-ZSM-5 in hydrogen (673 K, WHSV = 0.5 h^{-1}, 11 kPa furan)

in correspondence to the decrease of the nitrogen physisorption capacity (Fig. 3). No decarbonylation is observed, i.e. no CO is found among the gaseous products.

DISCUSSION

Rates of Deactivation. The nitrogen physisorption capacity of the H-ZSM-5 catalyst is decreased by 25% in a time where the catalyst is fed by a number of furan molecules, which is of the order of magnitude of the number of active centers calculated from the aluminum content. This indicates that the conversion proceeds in a relatively thin external shell of the zeolite crystals, leading to a sealing of a fraction of the channels by coke deposition and resulting in the observed strong decrease of the nitrogen physisorption capacity. Pore plugging by coke deposition, which is a general phenomenon in zeolite chemistry and which is found to proceed at reduced rates on the pentasils, is obviously enhanced in the conversion of molecules like furan, which have low hydrogen to carbon ratios.

The relatively low coking rate on the Pt-ZSM-5 catalyst can be referred to the hydrogen activation ability of the platinum metal resulting in an increased hydrogenation rate of potential coke precursors [7].

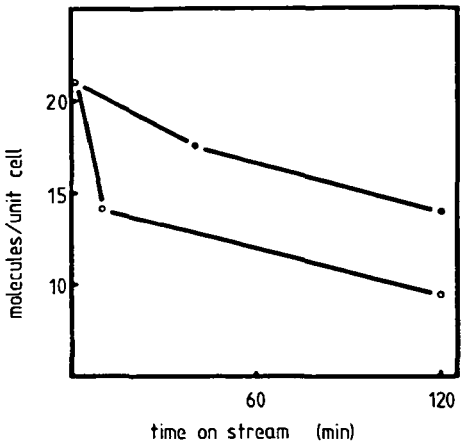

Fig.3 Nitrogen adsorption (77 K, p/p_o=0,1) on H-ZSM-5 (o) and Pt-H-ZSM-5 (•) versus time on stream in furan conversion

Hydrodeoxygenation of furan. The hydrodeoxygenating conversion of furan in acidic media can follow different routes depending on the hydrogenation activity and the strength of the Brönsted acidity. At high hydrogenation rates, which might be realized on the Pt-ZSM-5, the hydrogenation will precede the protonation of the molecule. In this case the reaction routes depicted in the following scheme should be favoured for the formation of primary compounds [8], which can undergo oxygen

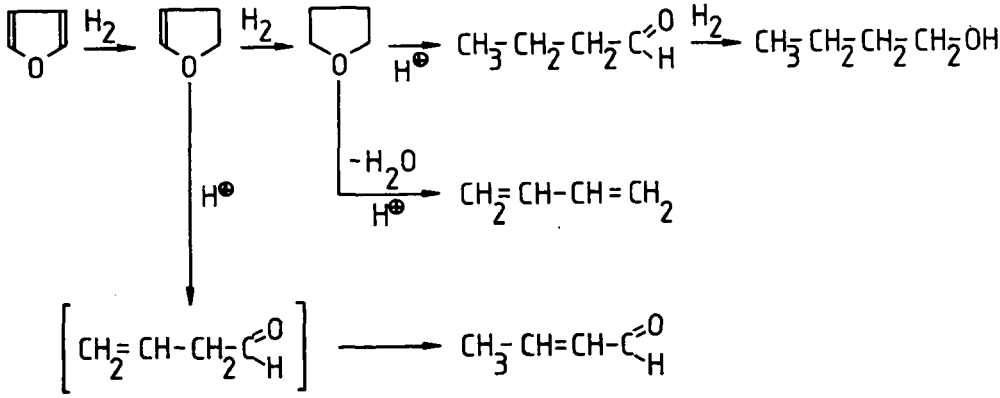

elimination as well as shape-selective cyclization and aromatization reactions via carbenium and carbonium ion intermediates. The high fractions of paraffins and BTX aromatics found on Pt-ZSM-5 support such assumption.

On H-ZSM-5, however, a protonation of the furan followed by ring opening might be an initial step as depicted in the following scheme.

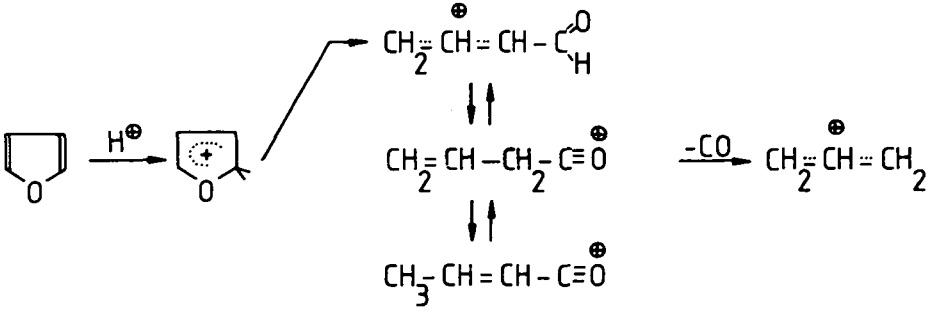

This assumption may find support by the fact that the acylium ion, or crotonylium ion respectively, is stable in super acid media [9]. A subsequent decarbonylation leads to the stable allyl cation, which can be suspected to be a coke precursor due to its low hydrogen to carbon ratio.

With increasing deactivation by coke deposition large fractions of C_{9+} aromatics and of 2,3-benzofuran are found. Since these molecules cannot be formed in the pores of the pentasil zeolites they might originate from alkylation and oligomerization reactions on the external surface of the zeolite crystals. The formation of highly alkylated aromatics might be favoured by an enhanced intermolecular alkyl shift from coke precursors to xylenes.

The 2,3-benzofuran might be formed by a Diels-Alder reaction between two furan molecules, where one furan molecule is activated by the acidic catalyst becoming a dienophil. The bridge oxygen of the dimer ((II)) will be readily eliminated in an acidic medium [10] as is shown in the following scheme.

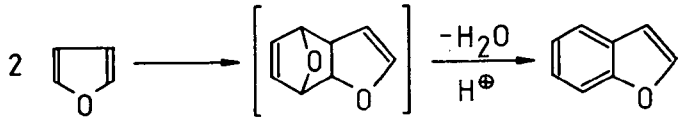

(I) (II)

Using argon as a carrier gas resulted in an increased rate of deactivation of the conversion of furan on H-ZSM-5 and Pt-ZSM-5. The prolonged stability in hydrogen indicates that H-ZSM-5 has considerable hydrogenation activity. The hydrogen molecules are presumably activated via hydronium ions [11]. Addition of propane gave

rapid deactivation for the reaction on H-ZSM-5, but resulted in a prolonged shape-selective conversion of furan on Pt-ZSM-5.

CONCLUSION

Biomass compounds with low H/C ratios, like furan, can undergo shape-selective conversions on pentasil type zeolites better if a hydrogen source is provided to the reaction mixture. The H-ZSM-5 has only a limited hydrogen activation ability, whereas Pt-ZSM-5 can readily transfer hydrogen, even from paraffins, to educts and intermediates, which are deficient in hydrogen.

ACKNOWLEDGEMENT

The authors are indebted to Mr. H. Helms for the determination of the platinum content and for useful discussions. We wish to thank Prof. Jaeger for many helpful and critical comments.

REFERENCES

1. Venuto, P.B., Landis, P.S., Adv. Catalysis 18, 259 (1968).
2. Meisel, S.L., McCullough, J.P., Lechthaler, C.H., Weisz, P.B., Chem. Techn. 6, 86 (1976).
3. Weisz, P.B., Haag, W.O., Rodewald, P.G., Science 206, 57 (1979).
4. Argauer, R.J., Landolt, G.R., U.S. Patent No. 3702 886 (1972).
5. Briese-Gülban, S., Kompa, H., Schrübbers, H., Schulz-Ekloff, G., React. Kinet. Catal. Lett. 20, 7 (1982).
6. Jacobs, P.A., Beyer, H.K., Valyon, J., Zeolites 1, 161 (1981).
7. Barbier, J., Marecot, P., Martin, N., Elassad, L., Maurel, R., in "Catalyst Deactivation" (B. Dalmon and G.F. Froment, Eds.), Elsevier, Amsterdam 1980, Stud. Surf, Sci. Catal., vol. 6, p. 63.
8. Houben-Weyl, Methoden der Organischen Chemie, Band VI/3, Thieme Verlag, Stuttgart 1965; references therein.
9. Olah, G.A., Schleyer, P.v.R., Carbonium Ions, vol. V, Wiley, New York 1976; references therein.
10. Rodd's Chemistry of Carbon Compounds, vol. IV, part A (Ed.: S. Coffey), Elsevier, Amsterdam 1973; references therein.
11. Olah, G.A., Chen, J., Schlosberg, R.M., J. Amer. Chem. Soc. 92, 3831 (1970).

CATALYTIC ACTIVITY OF COBALT AND MOLYBDENUM-CONTAINING Y-TYPE ZEOLITES IN THIOPHENE CONVERSION

A.A.SPOZHAKINA, S.I.Damjanova, N.G.Kostova and D.M.Shopov
Institute of Kinetic and Catalysis of the Bulgarian Academy of Sciences, Sofia 1040, Bulgaria

ABSTRACT

The hydrodesulphurization (HDS) of thiophene on NaY and CaHY zeolites containing 0.7 and 2 wt % cobalt and 7 wt % molybdenum has been studied at atmospheric pressure.

The surface of the samples has been characterized by chemical analysis, I.R. and diffuse reflectance spectra.

It is shown that the conditions of preparation determine the overall activity and selectivity in HDS of thiophene on zeolites.

The silicium and cobaltsilicium heteropoly molybdates (Si HPM and CoSi HPM) along with molybdenum oxide that are formed in the zeolites could be the precursors of the active sites for the HDS reaction.

INTRODUCTION

The catalytic activity of zeolites containing transition metal ions in the reaction of HDS has been studied in a number of papers [1-3]. Although the activity of such zeolites is not very high, the investigation of the CoMo-containing zeolites is interesting because it allows to reveal some aspects of the complex interaction between the catalyst components and its effect on the catalytic activity.

In a previous paper [4] we have shown the existence of a strong interaction between all components in a cobalt and/or molybdenum containing Y-type zeolites and as a result Si HPM and CoSi HPM are formed.

In the present paper we investigate the effect of their preparation conditions on the catalytic properties in the thiophene conversion.

EXPERIMENTAL

Synthetic NaY zeolite (Groz NII,USSR) with SiO_2/Al_2O_3 ratio of 4.2 has been used.Also, a CaHY zeolite (degree of exchange 48 % for each of Ca^{2+} and NH_4^+), obtained from the initial NaY zeolite by con-

ventional ion exchange with calcium nitrate and ammonium chloride. The two initial zeolite samples differ in their acidity as determined by butylamine titration: ΣH_o=1.4 and 0.35 mmol/g for CaHY and NaY, respectively [5]. Cobalt has been introduced in these two samples by ion exchange or by impregnation with cobalt nitrate (CoN). Molybdenum has been introduced in the initial samples by impregnation with ammonium heptamolybdate (AHM). After the introduction of both components the samples are dried at 120°C for 4 hrs and then calcined at 500°C for 2 hrs. This thermal treatment was used after introduction of each component for sample № 8. The preparation conditions are given in Table 1.

Table 1

Conditions of preparation of molybdenum and cobalt-molybdenum containing zeolites

№	Zeolites	Co/Mo	Co content (mg/g)	Conditions of preparation
1	NaY	-	-	AHM*
2	NaY	0.16	6.9	1.CoN exchange.2.AHM
3	NaY	0.16	6.9	1.AHM.2.CoN impregnation
4	NaY	0.48	20.7	1.CoN exchange.2.AHM
5	CaHY	-	-	AHM
6	CaHY	0.16	6.9	1.CoN exchange.2.AHM
7	CaHY	0.16	6.9	1.AHM.2.CoN impregnation
8	CaHY	0.16	6.9	1 AHM.120°C-4h,500°C-2h CoN impregnation

*Impregnation by ammonium heptamolybdate (AHM).

The state of the surface of the samples has beem investigated by IR and diffuse reflectance spectroscopy. The spectra were recorded on an IR - 75 spectrometer (400-2200 cm^{-1}) using pellets in KBr and on a Beekman UV 5270 (280-800 nm) with the initial zeolite as a reference.

The hydrodesulphurization of thiophene has been studied in a flow microreactor (atmospheric pressure, temperature of 400°C, WHSV of 0,6 h^{-1}) loaded with 0,2g catalyst. The temperature is raised upto the reaction temperature within 1,5 hours in hydrogen at flow rate of 40 ml/min. The activity has been expressed in molecular percent of converted into hydrocarbons thiophene or by the amount of released H_2S.

Molybdenum was extracted by treating 0,4 g of sample with 50 ml water for 24 hrs. After the extraction the samples were dried and calcined in conditions analogous to those of the sample synthesis. The content of the active components determined by atomic adsorption spectrometry.

RESULTS

The samples obtained by using NaY zeolite show stable catalytic activity in the HDS of thiophene (Fig.1a). The conditions of preparation effect the initial activity of the samples. Similarly to the con-

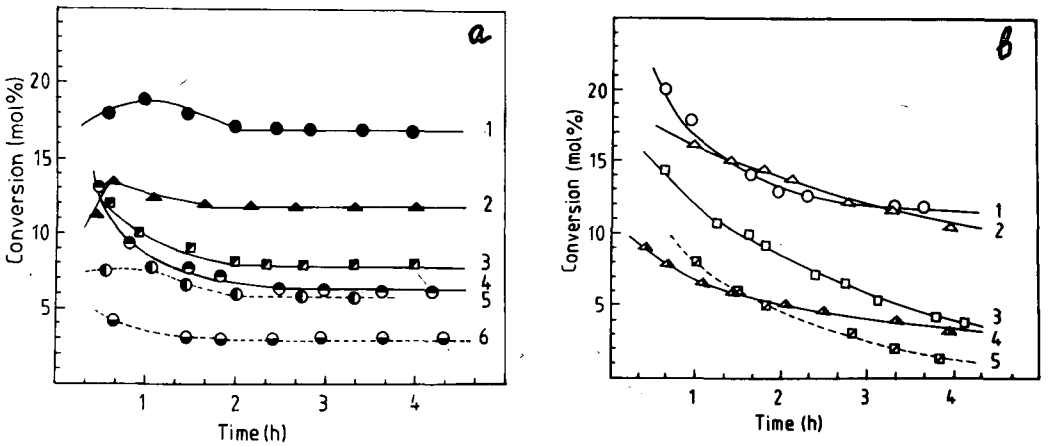

Fig.1. Thiophene conversion in C_4-products vs time for samples (see table 1) on a) NaY: 1-№ 2; 2-№ 3; 3-№ 1; 4-№ 4; 5,6-№2,№ 4 after aquous extraction; b) CaHY: 1-№ 8; 2-№ 7; 3-№ 6; 4-№ 5; 5-№ 6 after aquous extraction.

ventional $CoMo/Al_2O_3$ catalysts, cobalt also shows a synergetics effect in the case of the zeolite catalysts. The steady state conversion at a higher cobalt content (Fig.1a-4) is considerably lower. For sample №4 the activity is even lower in comparison to the activity of sample №1, which does not contain cobalt (Fig.1a-3). The aquous extraction of the samples considerably decreases their catalytic activity (Fig.1a-5,6).

Fig 1b shows changes of the catalytic activity during the run time for the samples prepared by using CaHY zeolite. Decreasing catalytic activity is characteristic for these samples. Here too, the conditions of preparation influence the activity. The samples, obtained by cobalt impregnation manifect higher and more stable activity (Fig.1b-1,2),

For the samples of this series, C_1-C_3 hydrocarbons are revealed among products of the reaction. Even more, for samples № 5 and № 6 (Table 1) the conversion of thiophene proceeds practically as the process of hydrocracking, because the characteristic products of the reaction of HDS (butene isomers) are not observed or their quantity is very small (sample № 6).

The difference in the properties of the two types of samples in the conversion of thiophene is particularly noticeable if their activity is compared by the amount of released H_2S (Fig.2). The amount of H_2S released on NaY samples is much less and it is entirely absorbed

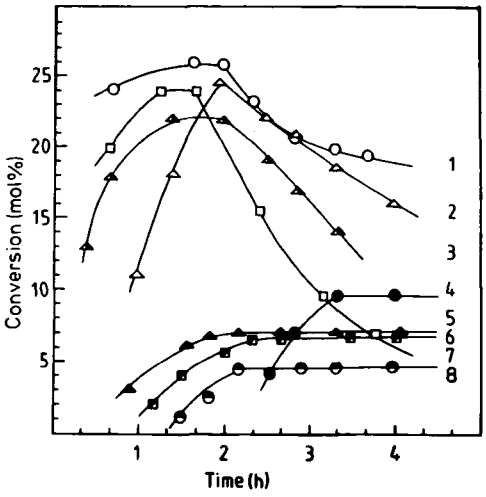

Fig 2. Thiophene conversion in H_2S vs time for samples (see table 1): 1-№ 8; 2-№ 7; 3-№ 5; 4-№ 2; 5-№ 3; 6-№ 1, 7-№ 6, 8-№ 4.

by the catalyst during the first hour of run, then its amount gradually increases (Fig.2-4,5,6,8).

In contrast, the change in the amount of H_2S released with time on the CaHY samples (Fig.2-1,2,3,7) is close to that observed on cracking catalysts [6]. A rapid increase in the amount of the released H_2S is observed for these samples and its highest value considerably exceeds the conversion of thiophene into C_4-products. However, its amount decreases with time similar to that on cracking catalysts.

The diffuse reflectance spectra of the cobalt containg samples show the presence of a cobalt triplet within the 500-630 nm characte-

ric to tetrahedral cobalt |7|. The intensity of this triplet is higher in the NaY samples. The intensity increases with the increase of the cobalt content (Fig.3-1,3). However, the middle peak in the observed triplet is shifted from 570 nm to 585 nm. In our previous work |4| we related this shift to the formation of a CoSi heteropolymolybdate, where cobalt is in an octahedral surrounding.

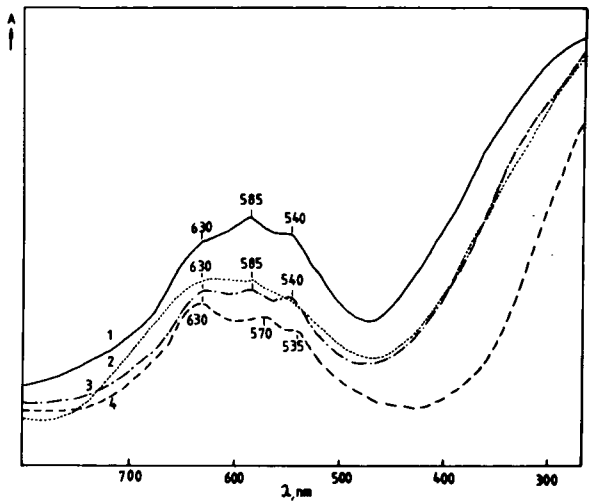

Fig.3. Diffuse reflectance spectra of samples (see table 1): 1-№ 4; 2-№ 6; 3-№ 2; 4- № 2 after aquous extraction.

IR - spectra of the samples with different cobalt content are shown in Fig.4. Both of high and low cobalt contents Si HPM is formed (Fig.4-1,3).

In the spectra are revealed bands at 780, 900, 960 cm^{-1} although the last band is overlapped by intensive absorption of the zeolite itself in the same range.

But in contrast to other samples obtained using NaY zeolites, after calcining of sample № 4 at 500°C, a characteristic band of MoO_3 (at 860 cm^{-1}) appears, along with bands of the HPM. The second characteristic band of MoO_3 at 990 cm^{-1} is not observed due to intensive absorption by the zeolite. It was shown |4|, that MoO_3, along with HPM is present in the samples obtained by using CaHY.

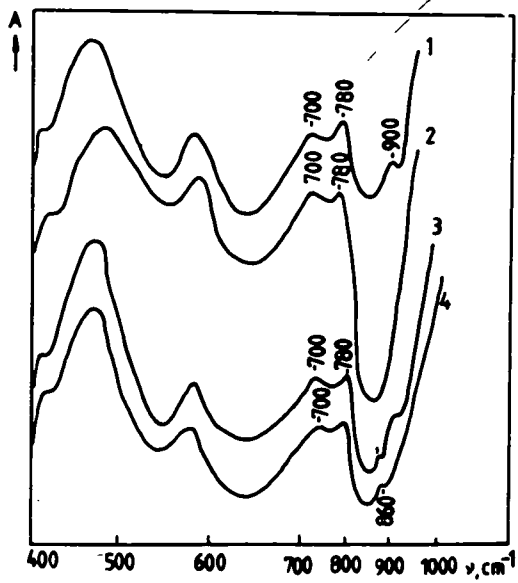

Fig.4. IR- spectra of samples (see table 1): 1-№ 2; 3- № 4;2, 4-№ 2, № 4 after aquous extraction.

DISCUSSION

It is khown that molybdenum increases the acidity and changes the type of acid sites on the surface |8|. The heteropolycompounds formed in the zeolite also manifest acid properties |9|.

Most probaly the overall activity and selectivity depend on the molybdenum content and the acidity of the support.

The CaHY zeolite itself shows very low activity which decreases quckly with time.

The specific interaction between the zeolites and the components is connected with their different acidity and causes the difference in the properties of the two series of samples. Probably the higher acidity of CaHY makes the formation of MoO_3 easier in samples using this carrier. Molybdenum oxide is also found in sample № 4 (on NaY), the acidity of which is probably increased due to the higher cobalt content.

The formation of large amounts of butane on some of the CaHY samples indicates that a hydrocracking processes (or possibly cracking processes without the participation of hydrogen), accompanied by polymerization of some unsaturated products. The decrease of conversion of thiophene into C_4-products and the increase in the amount of H_2S support this conclusion. The amount of H_2S released after two hours of

work for sample № 6 is three times larger than the amount of obtained C_4-products (Fig.1b-3 and Fig.3-7). The formation of coke on the samples after work is confirmed by the presence in the IR-spectra of a band at 1595 cm^{-1} |10|. The last is less strongly expressed for the samples obtained from NaY.

The results show that the activity of the samples in thiophene coversion can be regulated by the order of introducing of the metal components. The activity of the samples obtained using CaHY is increased and stabilized (no matter what the intermediate thermal treatment is) if cobalt is introduced after molybdenum. It is possible that in this case cobalt influences the acid sites. The effect of the support on the activity is not so significant when cobalt is introduced by impregnation (the activity of sample № 8 is close to that of sample № 3) (Fig.1a and Fig.1b).

It should be noted that when cobalt is introduced by ion exchange the activity of the samples in the HDS reaction is higher. This is not so obvious for the samples obtained from CaHY (for example, sample № 6) due to the properties of zeolite itself.

The decrease in thiophene conversion after aquous treatment (Fig.1a-5,6 and Fig.1b-5) correlates with the disapperance in the IR-spectra of the bands characteristic of Si HPM (Fig.4-2,4) and the preservation of bands due to MoO_3. The shift of the band at 585 nm (it was related |4| to the presence of CoSi HPM in CoMo-containing zeolites) to 570 nm in the diffuse reflectance spectra is a result of the aquois treatment. The shift is accompanied by a decrease in the intensity of the absorbtion band at 300 nm which is due to the presence of Mo^{6+}(Oh) (Fig.3). It should be aslo noted that the aquous extracts of samples № 2 and № 6 (with ion exchanged cobalt) do not contain cobalt, while about 40% of molybdenum was extracted. The results obtained allow to suggest that the soluble in water Si HPM and CoSi HPM are the precursors of the catalytically active sites in the thiophene hydrodesulphurization.

The preservation of some activity by the samples after aquous treatment shows that MoO_3 as well as some other unidentified molybdenum compounds could be also precursors of the active sites in thiophene conversion.

The observed correlation between the presence of Si HPM in the zeolites and the catalytic activity is similar to that when SiO_2 is used as a support instead of Y type zeolites |11|. Most probably the precursors of the catalytically active sites are the same on both types of support. The activity of the samples using SiO_2 as a support is

higher that of the samples supported on Y type zeolites. For example the conversion of thiophene on our sample № 2 is 17% while it is 25% on the sample having the same cobalt and molybdenum content but using SiO_2 as a support. This could be explained by the higher concentration of heteropoly compounds in the latter, since 80% of the total amount of molybdenum on SiO_2 is in the form of HPM |11|. This quantity is only 30% for the zeolite sample.

CONCLUSIONS

The observed catalytic conversion of thiophene on the two series of samples shows the strongly expressed bifunctional character of the catalysts, when CaHY is used as a support. The catalytic activity is more steady for samples obtained from NaY zeolites.

The catalytic activity of the zeolite catalysts can be regulated by the order of introducing of the metal components. Cobalt, introduced by ionexchange, leads to an increase in the hydrodesulphyrisation activity.

Si HPM and CoSi HPM, along with MoO_3 could be precursors of catalytically active sites in thiophene conversion on Mo and CoMo-containing zeolite catalysts.

REFERENCES

1. Visotskii, A.V., Chuikova, N.A., Lipovich, V.G., Kinet. Catal. 18, 1345 (1977).
2. Vrinat, M.L., Gachet, C.G., de Mourques, L., Catalysis by Zeolites. Elsevier, Amsterdam, 1980, p.219.
3. Kovacheva, P., Davidova, N., Shopov, D., Zeolites. 3, 92 (1983).
4. Spozhakina, A., Kostova, N., Damyanova, S., Shopov, D., React. Kinet. Catal. Lett., in press.
5. Spozhakina, A., Popova, Z., Dimitrov, Ch., Neftechimia, 22, 64 (1982).
6. Mashkina, A.V., Heterogeneous catalysis in chemistry of sulfur organic compounds, Nauka, Novosibirsk, 1977, p.111.
7. Egerton, T.A., Hagan, A., Stone, F.S., Vickerman, J.C., J.Chem. Soc., Faraday Trans. I. 68, 723 (1972).
8. Ratnasamy, P., Fripiat, J.J., J.Chem. Soc., Faraday. I. 66, 2897 (1970).
9. Misono,M., Proc. Climax Fourth Int. Conference on the Chemistry and Uses of Molybdenum. Climax Molybdenum Company, Ann Arbor, Micigan, 1982, p. 289.

10. Eisenbach, D., Gallei, E., J. Catal. 56, 377 (1978).
11. Spozhakina, A., Kostova, N., Uhchnovskii, I., Shopov, D., Uhrieva, T., Applied Catalysis, in press.

POLYMERIZATION OF BENZYL ALCOHOL IN GASEOUS PHASE ON A Y ZEOLITE

M. OLAZAR, J.M. ARANDES, J. BILBAO, A. ROMERO
Department of Technical Chemistry, Universidad del Pais Vasco,
Apdo. 644, 48080 Bilbao, Spain

ABSTRACT

Polybenzyl polymers obtaining from benzyl alcohol has been studied in a gas phase reaction at atmospheric pressure, using a Y zeolite, in a fluidized bed reactor. Operating conditions to obtain a good fluidization and an isothermal bed have been determined.

It has been proved that the polymerization occurs on the catalyst active sites via Langmuir-Hinshelwood type mechanism, obtaining the following kinetic equation in the 250-310°C range:

$$r_{po} = P_A^2 \frac{K_M^3(k'_d+k'_m)P_A + K_M^2 k'_d}{(1+K_M P_A)^3} \quad (\frac{\text{polymer g}}{\text{g cat.min}})$$

INTRODUCTION

Nowadays there is an increasing interest in obtaining polybenzyl polymers. This interest is due to their high stability at high temperature and to their good electrical properties recently found.

As long ago as 1955, Hass et al [1] determined the tendency of benzyl chloride to polymerize with Friedel-Crafts catalysts. Later [2-6], polymerization studies with different benzyl chloride type monomers have been described, in order to obtain linear structures with high molecular weights.

In spite of a great number of works have been made, the information about the structure, characteristics, properties and aplications of these polymers is very short. To determine the structure, mainly the infrarred spectra [6] and in some cases ultraviolet or NMR have been used. By TGA and DTA it was found that the polymer is thermally

stable up to 300-450°C and that the glass transition region is between 55 and 80°C. The average molecular weights, determined by vapor-pressure osmometry [7], are in the 1000-2500 range.

Polybenzyl polymers were synthesized by means of gas phase reaction on solid catalysts by Jodra et al [8-10] in the dehydrogenation of benzyl alcohol to benzaldehyde on Cu/asbestos catalysts in a fixed bed reactor in the 250-300°C temperature range . Since then, these polymers were synthesized trying other catalysts for the same reaction such as Cu-Cr_2O_3/asbestos [11,12] and Cu/SiO_2[13].

The polymerization in the latest mentioned works is a secondary process by dehydration reaction which takes place in parallel with the main reaction of dehydrogenation and in which the polymer (coproduct) is the main precursor of the coke that deactivates the catalyst.

In this work a study of polybenzyls direct obtaining by benzyl alcohol polymerization has been carried out in gas phase on acidic catalyst, a Y zeolite, for the first time in bibliography. The use of acidic catalysts such as silica-alumina or zeolites in dehydrations is widely admitted [14,15].

Apart from setting up the reaction system and determining the more suitable experimental conditions for the polymerization kinetic study, in this work it has been tried to make up for the absence of methodology for the kinetic study in gas phase on solid catalysts. That was carried out basing on the methodology already developed for contact catalysis.

EXPERIMENTAL

Catalyst

The selection of the MZ-7P catalyst for this reaction has been based on its good behavior (as commercial cracking catalyst) in fluidized systems. This operation regime was determined to be necessary in previous experiments.

The MZ-7P catalyst was supplied by Akzo-Chemie and it has the following characteristics: zeolite containing 10%; zeolite:Y type rare-earth exchanged; chemical composition %: Al_2O_3:33, Na_2O:0.2, Fe:0, SO_4^{2-}:0.3; pore volume:0.28 cm^3/g; surface area: 140 m^2/g.

Equipment and operating conditions

The reaction equipment is basically the same utilised in previous works [10-13] for dehydrogenation of benzyl alcohol. It consists of feeding and measuring system of alcohol and N_2 (as inert), preheater-vaporizer of alcohol, reactor of Pyrex glass of 17 mm inside diameter that is provided with a distributor plate of porous glass and condensers to collect the products.

When trying the fixed bed regime for the catalyst, it was found that the fast deposition of polymer among particles and the exothermicity of the reaction make impossible the isothermicity of the catalytic bed. Due to that, serious problems are originated in the flow which cause the formation of preferential ways to let the reactants go through and the plugging of the reactor.

Working in fluidized bed regime, it has been determined that for particles to be well mixed the following reaction conditions have to be mantained:

Temperature: between 250 and 310°C. The lower limit is fixed to avoid the condensation of alcohol in some point of the reaction system (T_b=210°C). In the other limit, over 330°C the benzyl alcohol cracking is already significative.

Catalyst particle size: +0.15 -0.20 mm

Gas linear velocity: 40 cm/s. Although the minimum fluidizing velocity is 20 cm/s the fact that the catalyst particles size is getting increased outwardly of settled polymer forces to work with higher velocity to keep the fluidization.

Partial pressure of fed alcohol: 0.06-1 atm. At higher pressures the reactor is plugged in very short time making impossible the fluidization.

Catalyst dilution: 10% in silica gel. This way bed isothermicity is favoured and fluidization is maintained longer, in spite of catalyst particles size gets increased progressively.

Space time: 0.4 g cat/h mol.

Experimental results

In order to calculate the length of time of the initiation step and the rate that corresponds to the end of this period, kinetic experiments of different length of time have been made under the conditions above especified. As temperature values they have been chosen: 250, 270 290 and 310°C and for each temperature the following values of partial pressure of alcohol: 0.06, 0.1, 0.2, 0.3, 0.4, 0.5, 0.6, 0.8 and 1.0 at

As the number of experiments was great the weight of polymer on catalyst was measured by combustion of the catalyst mass increased of polymer. It was not made by mechanical removal because it is too laborious for a so great number of samples.

As an example of the obtained experimental results, Figure 1 shows weight of polymer vs. length of time of experiment, for one of the studied temperatures, 250°C. Each curve corresponds to one partial pressure of benzyl alcohol at inlet.

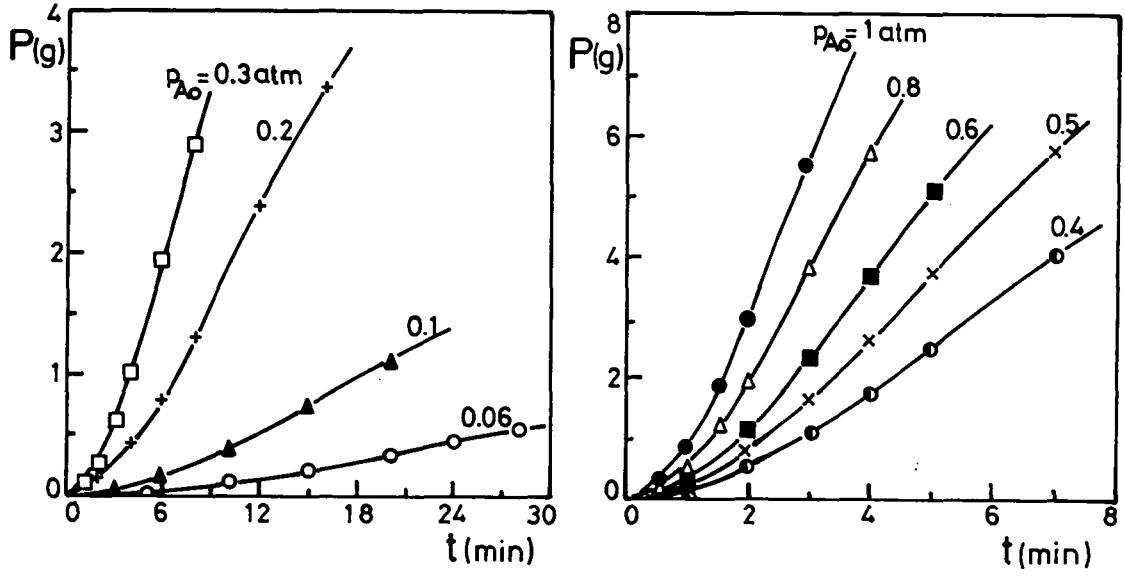

Fig. 1. Weight of deposited polymer vs. time for different partial pressure of benzyl alcohol at reactor inlet. Temperature 250°C.

MECHANISM AND KINETICS OF THE POLYMERIZATION

A Langmuir-Hinshelwood type mechanism has been proposed which is based on Clark and Bailey's theory [16] and enlarged after by Maiti [17].

1. Adsorption and activation step (Initiation)

$$M + L \underset{}{\overset{K_M}{\rightleftharpoons}} M_1 \xrightarrow{k_1} M_1^* \qquad K_M = \frac{[M_1]}{[M][L]} \tag{1}$$

2. Reaction step (Propagation)

$$\left.\begin{array}{l} M_1 + M_1^* \xrightarrow{k_p} M_2^* \\ M_1 + M_2^* \xrightarrow{k_p} M_3^* \\ \vdots \qquad\quad \vdots \qquad\quad \vdots \\ M_1 + M_{n-1}^* \xrightarrow{k_p} M_n^* \end{array}\right\} \qquad (n-1)M_1 + M_1^* \xrightarrow{k_p} M_n^*$$

3. Desorption step (Termination)

3.1. Espontaneous desorption

$$M_n^* \xrightarrow{k_d} P_n + L$$

3.2. Desorption by monomer

$$M_n^* + M_1 \xrightarrow{k_m} P_n + L + M_1$$

Defining the rate of polymerization as total number of monomer units in the polymer that is desorbed from unit catalyst mass per second, it will be calculated as the sum of both termination steps:

$$R = \Delta\left(\sum_{n=2}^{\infty} n[P_n]\right)/\Delta t = k_d \sum_{n=2}^{\infty} n[M_n^*] + k_m \sum_{n=2}^{\infty} n[M_n^*][M_1] \tag{2}$$

Evaluating the summations of eqn(2) it is obtained:

$$R = [M]^2 \left(2k_d\, k_p\, k_1\, K_M^2 [L]^2 + 2k_m\, k_p\, k_1\, K_M^3 [M][L]^3\right) \tag{3}$$

The total concentration of active sites, [N], is:

$$[N] = \sum_{n=2}^{\infty} [M_n^*] + [M_1] + [L] = K_M[M][L] + [L] \tag{4}$$

If the expression for [L], concentration of free active sites, from eqn(4) is substituted in eqn(3) the following expression is obtained:

$$R = [M]^2 \frac{(k_d' K_M^3 + k_m' K_M^3)[M] + k_d' K_M^2}{(1 + K_M[M])^3} \tag{5}$$

where $k_d' = 2k_d\, k_p\, k_1 [N]^2$ and $k_m' = 2k_m\, k_p\, k_1 [N]^3$ (6)

Eqn(5) can be expressed in a way to permit a more direct evaluation from the experimental data of deposition. Expressing the concentration of monomer as partial pressure of benzyl alcohol in the gas flow:

$$r_{po} = P_A^2 \frac{K_M^3(k'_d + k'_m)P_A + K_M^2 k'_d}{(1 + K_M P_A)^3} \quad (\frac{\text{g polymer}}{\text{g cat. min}}) \tag{7}$$

In order to verify the validity of eqn(7) for the studied reaction system and so the proposed mechanism, values of r_{po} have been calculated from experimental data in Figure 1 for 250°C and from the corresponding values at the other temperatures, 270, 290 and 310°C. The computation of r_{po}, maximum rate of polymerization that corresponds to the end of the initiation period, needs the accurate evaluation of the length of this period, t_i.

The experimental data P vs. t have been fitted the following empirical equation:

$$P = a\ln(\frac{t^2+t_i^2}{t_i^2}) = (\frac{dP}{dt})_{t=t_i} \cdot t_i \ln(\frac{t^2+t_i^2}{t_i^2}) \tag{8}$$

where $$(dP/dt)_{t=t_i} = r_{po} W \tag{9}$$

The fitting has been carried out by non linear regression based on the Marquardt method [18]. The results of this fitting are shown in Table 1, where values of initiation time, t_i, and their corresponding polymer deposition rates, r_{po}, are related. The square regression coefficient (r^2) is 0.96 in the worst of the cases.

The r_{po} data related in Table 1 and their corresponding values of average partial pressure between the inlet and the outlet of the reactor have been fitted the eqn(7). The values of the kinetic constants, k'_m, k'_d and K_M evaluated in this way at the different temperatures of reaction have been related in Table 2. The square regression coefficient is 0.97 in the worst of the fittings.

Figure 2 shows the temperature dependency of the kinetic constants in Table 2 by the Arrhenius plot. The following relationships are obtained from fitting these kinetic constants:

$$k'_m = 4.06\ 10^{6}\exp\left(\frac{-11000\pm1000}{T}\right);\quad k'_d = 1.08\ 10^{8}\exp\left(\frac{-12000\pm1000}{T}\right)$$

$$K_M = 1.39\ 10^{-9}\exp\left(\frac{11900\pm900}{T}\right) \qquad (10)$$

Table 1

Calculated values of t_i(min) and their corresponding polymer deposition rates, r_{po}(g polymer/g cat. min).P_{A_o}(atm): At reactor inlet.

T	P_{A_o}	0.06	0.10	0.20	0.30	0.40	0.50	0.60	0.80	1.00
250°C	t_i	23.4	16.2	9.5	7.0	5.6	4.7	4.0	3.3	2.6
	r_{po}	0.16	0.28	0.49	0.63	0.71	0.77	0.82	0.89	0.94
270	t_i	29.8	18.2	9.2	6.4	4.9	3.9	3.2	2.6	2.1
	r_{po}	0.11	0.23	0.54	0.78	0.98	1.13	1.28	1.48	1.61
290	t_i	40.4	22.7	10.4	6.7	4.9	3.9	3.1	2.4	1.8
	r_{po}	0.06	0.15	0.44	0.74	0.99	1.21	1.42	1.79	2.09
310	t_i	61.7	30.0	12.4	7.9	5.6	4.2	3.4	2.5	1.8
	r_{po}	0.03	0.09	0.32	0.55	0.80	1.04	1.28	1.73	2.13

Table 2

Computed values of the kinetic constants

	250°C	270	290	310
k'_m	$2.91\ 10^{-3}$	$6.33\ 10^{-3}$	$1.30\ 10^{-2}$	$2.54\ 10^{-2}$
k'_d	1.16	2.70	5.93	12.3
K_M	9.79	4.25	1.95	0.949

Substituting these values in eqn(7) the kinetic equation for the temperature range between 250 and 310°C is now:

$$r_{po}=P_A^2\left\{\frac{\left[1.39\ 10^{-9}\exp\left(\frac{11900}{T}\right)\right]^3\left[4.06\ 10^{6}\exp\left(\frac{-11000}{T}\right)+1.08\ 10^{8}\exp\left(\frac{-12000}{T}\right)\right]}{\left[1+1.39\ 10^{-9}\exp\left(\frac{11900}{T}\right)P_A\right]^3}+\right.$$

$$\left.+\frac{\left[1.39\ 10^{-9}\exp\left(\frac{11900}{T}\right)\right]^2\left[1.08\ 10^{8}\exp\left(\frac{-12000}{T}\right)\right]}{\left[1+1.39\ 10^{-9}\exp\left(\frac{11900}{T}\right)P_A\right]^3}\right\} \qquad (11)$$

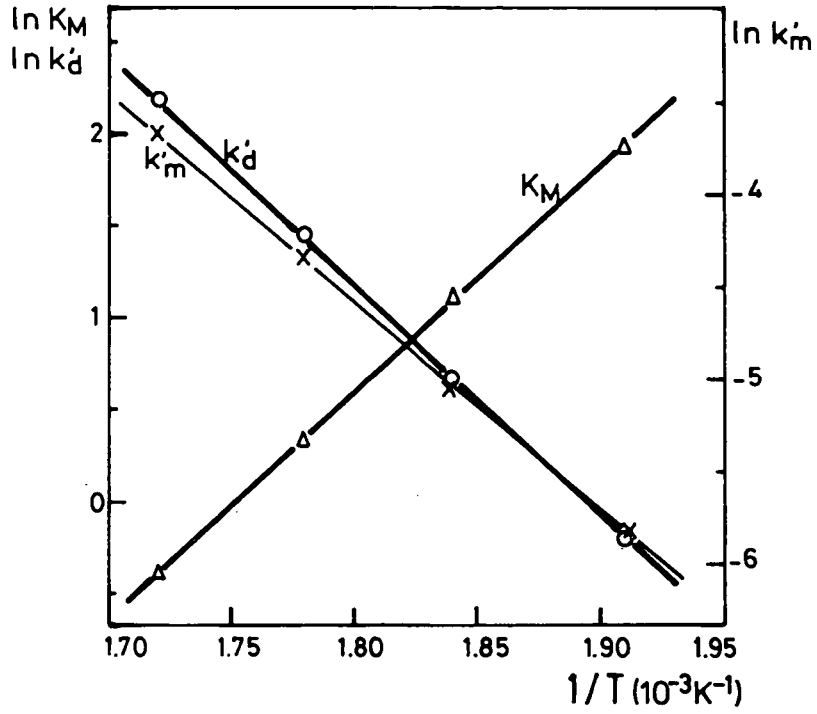

Fig. 2. Temperature dependency of the kinetic constants in eqn(7).

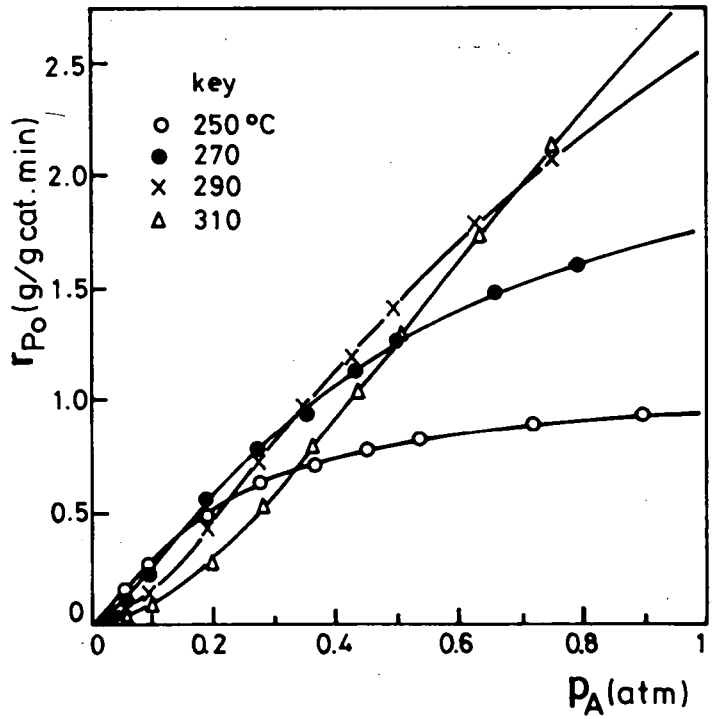

Fig. 3. Kinetic equation checking. Solid lines: computed by eqn(11). Points: experimental.

In Figure 3 is plotted r_{po} vs. P_A. In this Figure curves correspond to the values computed with eqn(11) and points are the experimental data related in Table 1. It can be noticed the fitting goodness in all the studied conditions.

It is remarkable the complexity of the r_{po} vs. P_A curves shape in Figure 3, where curves corresponding to different temperatures cross each other so that the higher reaction rate correspond to a higher temperature as the partial pressure of benzyl alcohol fed to reactor is increased. On the other hand, reaction rate is sensitive to temperature specially at high temperatures.

CONCLUSIONS

It has been determined that this zeolite has a high activity to obtain polybenzyls from benzyl alcohol polymerization in gas phase. Polymer production turned out to be so high by this way that it does not admit comparison with any other obtaining process described up to now in bibliography.

The suitable operating conditions for a MZ-7P zeolite catalyst have been determined in a fluidized bed reactor in order to get an isothermal bed and a good fluidization. In this conditions the polymerization kinetics at zero time follows the eqn(11) for the temperature range 250-310^{o}C and partial pressure of benzyl alcohol at inlet reactor lower than 1 atm. This shows that the polymerization in gas phase on the acidic sites of this zeolite occurs via Langmuir-Hinshelwood type mechanism.

After the initiation period, the curves polymer vs. time in Figure 1 and the homonyms at the other temperatures show a fall in their slopes (rate of polymerization), which can be attributed to the catalyst deactivation. This deactivation can be due to the degradation of polymers in the porous structure towards irreversibly adsorbed species on the acidic sites of the MZ-7P catalyst. It has been proved that the deactivated zeolite can be regenerated by combustion of the carbonaceous material with air, recovering its initial activity and also its physical properties and surface acidity.

REFERENCES

1. Haas, H.C., Livingston, D.I., Saunders, M., J. Polym. Sci. 15, 503 (1955).
2. Iovu, M., Tudorache, E., Dic. Makromol. Chem. 147, 101 (1971).
3. Kuo, J., Lenz, R.W., J. Polym. Sci. Polym. Chem. Ed. 14,2749 (1976
4. Geller, B.A., Khaskin, I.G., Mulik, I.Y., J. Appl. Chem. USSR 50, 1525 (1977).
5. Geller, B.A., Khaskin, I.G., Mulik, I.Y., Zh. Priklad. Khim. 50, 1588 (1977).
6. Pinkus, A.G., Lin, W.H., J. Macromol. Sci. Chem. A13(1), 133 (1979
7. Finocchiaro, P., Passerini, R., Ann. Chim.(Roma) 58, 418 (1968).
8. Jodra, L.G., Romero, A., Katime, I., Corella, J.,An. Quim. 9, 10 (1974).
9. Jodra, L.G., Corella, J., Romero, A., Pat. Esp. 416940 (1975).
10. Jodra, L.G., Corella, J., Romero, A., An. Quim. 72, 829 (1976).
11. Corella, J., Bilbao, J., Sancho, M.H., An. Quim. Supl. 1, 80 (1978)
12. Corella, J., Asúa, J.M., Bilbao, J., Chem. Eng. Sci. 35, 1449 (1980).
13. Romero, A., Bilbao, J., González-Velasco, J.R., Ind. Eng. Chem. Process Des. Dev. 20, 570 (1981).
14. Pines, H., Manassen, J., Adv. Catal. 16, 49 (1966).
15. Licht, E., Schachter, Y., Pines, H., J. Catal. 38, 423 (1975).
16. Clark, A., Bailey, G.C., J. Catal. 2, 230 (1963).
17. Maiti, M.M., J. Catal. 38, 522 (1975).
18. Marquardt, D.W., J. Soc. Ind. Appl. Mat. 2, 431 (1963).

SELECTIVITY IN THE CONVERSION OF ACETIC ACID OVER MFI-TYPE ZEOLITES

Y. Servotte, J. JACOBS, P.A. Jacobs
Laboratorium voor Oppervlaktechemie, Katholieke Universiteit Leuven
Leuven, Belgium.

ABSTRACT

The product selectivity in the conversion of acetic acid over H-ZSM-5 zeolites with different Si/Al ratios was followed at atmospheric pressure in a continuous flow tubular reactor over a wide temperature range.

The primary carbon containing products in this conversion in every case were carbon dioxide and acetone formed via an acid-catalyzed aldolization and a decarboxylation.

The nature of the secondary products was determined mainly by the Si/Al content of the ZSM-5 zeolite, and for a given ratio by the reaction temperature. Isophorone seems to be a key intermediate, which is either cracked to 1,2,4-trimethylbenzene in the very acidic zeolites or transformed into dimethylphenols via a dehydrodemethylation reaction on zeolites with intermediate acidity and Si/Al ratios.

INTRODUCTION

MFI zeolites seem to be able to convert acetic acid into a mixture of hydrocarbons [1]. The distribution of the products of this reaction can be rationalized in terms of a sequence of condensation, decarboxylation and dehydration reactions [2,3]. The primary products of this reaction are acetone and carbon dioxide, formed by a nucleophilic attack of an acyliumion (I) by an acetate anion (II) [4,5] :

$$\underset{\text{I}}{CH_3CO^+} + \underset{\text{II}}{CH_3-C(=O)-O^-} \rightarrow (CH_3)_2CO + CO_2 \qquad (1)$$

Species I may be directly formed by the very acidic ZSM-5 zeolites [3] :

$$CH_3COOH + HO\text{-zeolite} \rightarrow CH_3CO^{+}\ {}^{-}O\text{-zeolite} + H_2O \quad (2)$$

while acetate is formed upon zeolite dehydroxylation [6] :

$$CH_3COOH + HO\text{-zeolite} \rightarrow CH_3COO^{-}\ {}^{+}\text{zeolite} + H_2O \quad (3)$$

Chang et al. [3] associate catalyst deactivation in the acetic acid conversion with the dehydroxylation of the zeolite which is evident from equation (3). This statement tacitly assumes that such a system should not be regenerable in the usual way. It should also be noted that a combination of equations (1) to (3) eventually explains the formation of acetone but doesnot take into account the regeneration of the catalyst Brønsted acidity.

In acid conditions, acetone may undergo further aldolization and subsequent dehydration under formation of diacetone alcohol (III), mesityl oxide (IV) and phorone (V) [7-9] :

$$2(CH_3)_2CO \rightarrow \underset{\text{III}}{CH_3\,\overset{O}{\overset{\|}{C}}\,CH_2\,\overset{OH}{\overset{|}{C}}\,(CH_3)_2} \xrightarrow{-H_2O} \underset{\text{IV}}{CH_3\,\overset{O}{\overset{\|}{C}}\,CH = C(CH_3)_2} \quad (4)$$

$$IV + (CH_3)_2CO \xrightarrow{-H_2O} \underset{\text{V}}{[(CH_3)_2C = CH]_2\,CO} \quad (5)$$

On H-ZSM-5 zeolites, the main products of the acetone condensation were reported to be isobutene and aromatics [1-3]. Isobutene can be formed by acid-catalyzed cracking of diacetone alcohol [2],

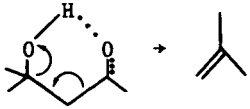

$$+ CH_3COOH \quad (6)$$

and acetic acid reenters the cycle. Mesitylene (1,3,5-trimethylbenzene) is known to be an acid-catalyzed condensation product of acetone [9] :

$$IV + (CH_3)_2CO \xrightarrow{-H_2O} \underset{\text{VI}}{(CH_3)_2C = CH\,\overset{CH_3}{\overset{|}{C}} = CH\,\overset{O}{\overset{\|}{C}}\,CH_3} \rightarrow \underset{\text{VII}}{\text{OH}} \xrightarrow{-H_2O} \quad (7)$$

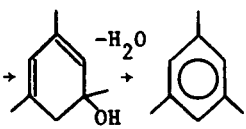

in which the cyclization of the dienone (VI) to an isophorone (VII) is the key step, which at the present time is incompletely understood [2]. Also phorone (V) can be cyclized in acid conditions to an isophorone [10] :

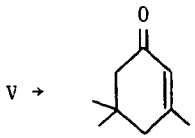

VIII (8)

and gives via classical carbenium ion rearrangements and dehydration 1,2,4-trimethylbenzene :

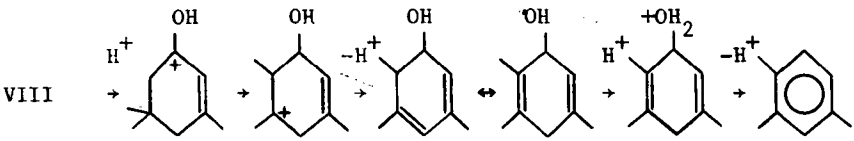

(9)

Since the distribution of aromatics from acetic acid, acetone or methanol over H-ZSM-5 is very similar [1], these aromatics in case of acetic acid or acetone may stem from isobutene condensation-dehydrocyclization reactions rather than from equations (7) or (9).

In the decomposition products of acetic acid small quantities of oxygenated products are observed, not exceeding 4 % by weight [3] and consisting of mainly dimethylphenols. Their formation is explained via the following mechanism [3] :

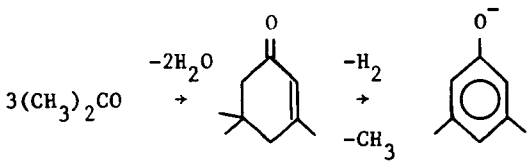

(10)

Puzzeld by this complex chemistry, we decided to investigate over a wide range of reaction temperatures, the influence of the number of acid sites in H-ZSM-5 upon the product distribution from acetic acid by changing the Si/Al ratio of the zeolite.

EXPERIMENTAL

H-ZSM-5 zeolites with different Si/Al ratio were synthesized in the presence of TPA-OH and glycerol and using aerosil as silica source, according to the method published by Von Ballmoos [11]. The Al/Si + Al percentage in the sample is given in brackets after the sample notation. After careful calcination, subsequent ammonium exchange and further deammoniation, as described earlier in detail [12], H-ZSM-5 samples were obtained characterized by a single surface hydroxyl group around 3600 cm^{-1}. X-ray diffraction showed that these samples were highly crystalline and phase pure. Scanning electron microscopy showed that they were devoid of any amorphous material and consisted of large isolated crystals (15 x 20 μm) with an hexagonal shape. Such samples are expected to have an Al-rich rim and silicon-rich core [13,14].

A powder sample of each material was compressed without any binder, crushed and sieved. The 0.25-0.5 mm fraction was used in the continuous flow tubular reactor.

Acetic acid from UCB (99.5 % purity) was vaporized and diluted with helium using a thermostatted saturator and a W/Fo of 2016 $kg.s.mol^{-1}$, W being the amount of catalyst and Fo the acetic acid flow rate at the reactor inlet.

Product analysis was done on-line with a 1 m packed column of Chromosorb 102 (from Johns-Manville) for the separation of CO, CO_2 and C_1 - C_2 hydrocarbons, and with a 50 m fused silica column (CP Sil 5, chemically bound, from Chrompack) with 0.3 mm internal diameter for the heavier products. The latter column was temperature programmed between 338 and 973 K at a rate of 2 K per minute.

RESULTS AND DISCUSSION

Overall reaction rate. For the contact time used, acetic acid could be converted completely in the temperature range from 520 to 700 K. The variation of the initial rate for acetic acid decomposition with the Al content of the ZSM-5 zeolite is shown in Fig. 1.
Surprisingly, and in contrast to what is observed in several other cases [15-17], this particular reaction rate is in no way proportional to the amount of lattice aluminum. This behaviour can only be explained when for the reaction either a particular site strength or site density is needed.

Selectivity for acetone. The selectivity for the supposed primary products from acetic acid, acetone and carbon dioxide, is shown in Fig. 2.

From this figure, two general observations elude :
(i) The initial selectivities for CO_2 are constant, irrespective of the aluminum content of the sample and amount to approximately 45 wt %.

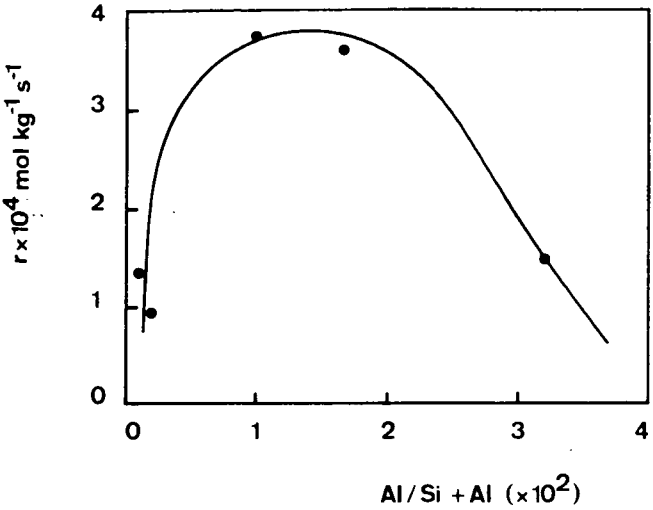

Fig. 1. Initial rate of CH_3COOH decomposition at 550 K for H-ZSM-5 zeolites with different Al content.

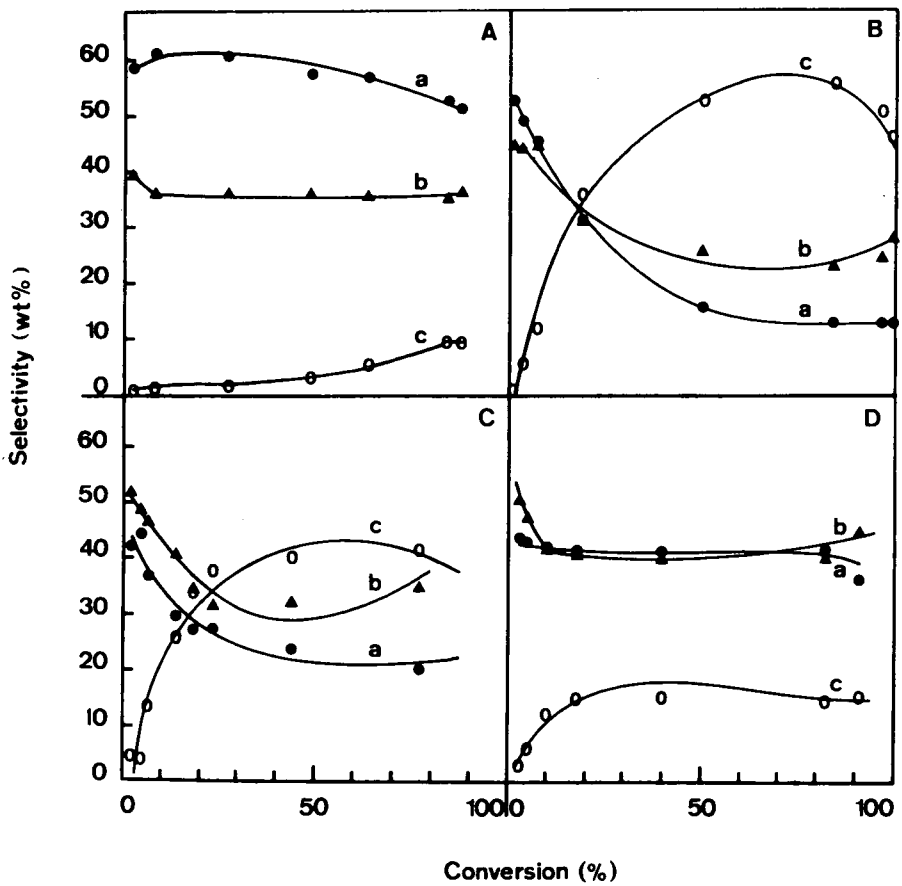

Fig. 2. Reaction selectivity for acetone (a), CO_2 (b) and secondary products (c) from acetic acid, over H-ZSM-5 with different Al/Al + Si fractions = (A) 0.1, (B) 1, (C) 1.6 and (D) 3.2 %.

The theoretical CO_2 selectivity of the bimolecular reaction :

$$2\ CH_3\ COOH \rightarrow (CH_3)_2\ CO + CO_2 + H_2O \qquad (11)$$

is equal to 43 wt % when water is not considered as reaction product.

(ii) The rate at which secondary products are formed is dependent on the Al content of the sample : at intermediate values for the Al content (approximately 1 Al per unit cell), the rate of formation of the secondary products as well as the overall rate of acetic acid decomposition are fastest.

The sequence of events can be kinetically represented as follows :

2 acetic acids $\overset{\rightarrow}{\leftarrow}$ acetone $\rightarrow$ secondary products

In other words, the decomposition of acetone is slower than its formation.

As is evident from the introduction, the presence of catalyst deactivation and the ability to regenerate the system will allow to decide whether the acetone formation can be rationalized by equations (1) to (3). In Fig. 3 time on stream data are plotted using a fresh catalyst.

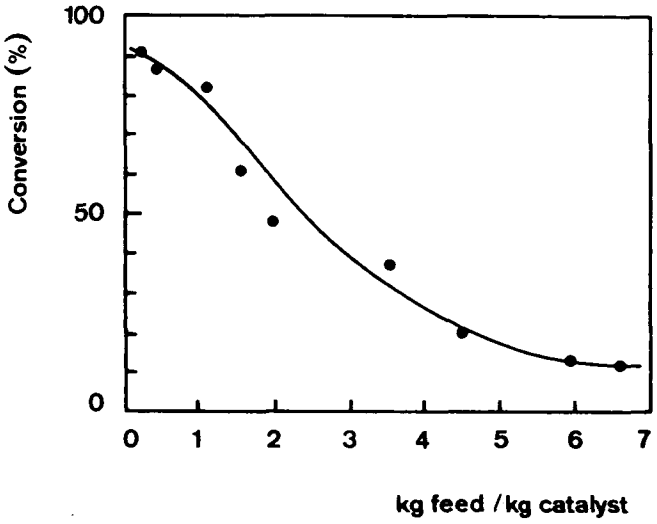

Fig. 3. Catalytic stability of H-ZSM-5 (1) at 633 K.

This catalyst H-ZSM-5 (1), after regeneration (oxygen treatment at reaction temperature), comes back to its original activity.

In agreement with the literature data [3], it is confirmed that all H-ZSM-5 zeolites coke up in a relatively short period, but are easily regenerable. If the mechanism occurs according to equations (1) to (3), the Brønsted acidity of the dehydroxylated zeolite should be restored by H_2O/CO_2 mixtures. Since there is no

direct proof in literature that this is possible for hydrogen zeolites, a alternative explanation for acetic acid activation is advanced using the following transition state :

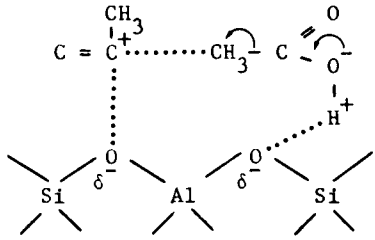

The acylion is formed in the usual way (equation (2)), while the acetic acid is polarized by the diffuse negative charge. In such a way acetate and acyl are formed close to each other (possibly in a channel intersection) and may react upon complete reconstitution of the catalyst in its original state. Such a mechanism doesnot suffer from the drawbacks mentioned for equations (1) to (3).

Distribution of secondary products. The main secondary products formed from acetone are in the order of importance : alkylphenols, isobutene, aromatics and other hydrocarbons. The distribution of these products on the series of ZSM-5 samples is shown in Fig. 4.

This figure indicates that isobutene as well as the alkylphenols are primary products from acetone, while aromatics are only of a secondary origin. Selectivity for the oxygenated products is maximum for the ZSM-5 (1) sample, with intermediate aluminum content.

The formation of isobutene is easily accounted for by cracking of diacetone alcohol (equation (6)). The precursor of alkylphenols can be isophorone (VIII) (equations (8) and (10)). This molecule can be formed from acetone through an acid aldolization followed by dehydration (equations (4),(5),(8)). However, its conversion to dialkylphenols is difficult to explain using Brønsted catalyzed-reactions, since the overall conversion equation represents a dehydrodemethylation reaction. A competitive and Brønsted acid-catalyzed degradation of isophorone (VIII) gives mainly 1,2,4-trimethylbenzene (equation (9)). From the data of Fig. 2 it follows that if too few acid sites are present, the reaction stops when acetone is formed. When too many Brønsted sites are present (i.e. for high Al/Si + Al ratios), it follows from Fig. 4 that more aromatics and much less alkylphenols are formed. This may reflect that reaction (9) becomes fast on such catalysts. This is confirmed when the distribution of the aromatics is considered. The selectivity for 1,2,4-trimethylbenzene decreases with decreasing Al content of the ZSM-5 zeolites and is in any case over 50 wt %. In a given zeolite it increases with the reaction temperature. It can be concluded that reaction (9) is important compared to the formation of aromatics from isobutene and

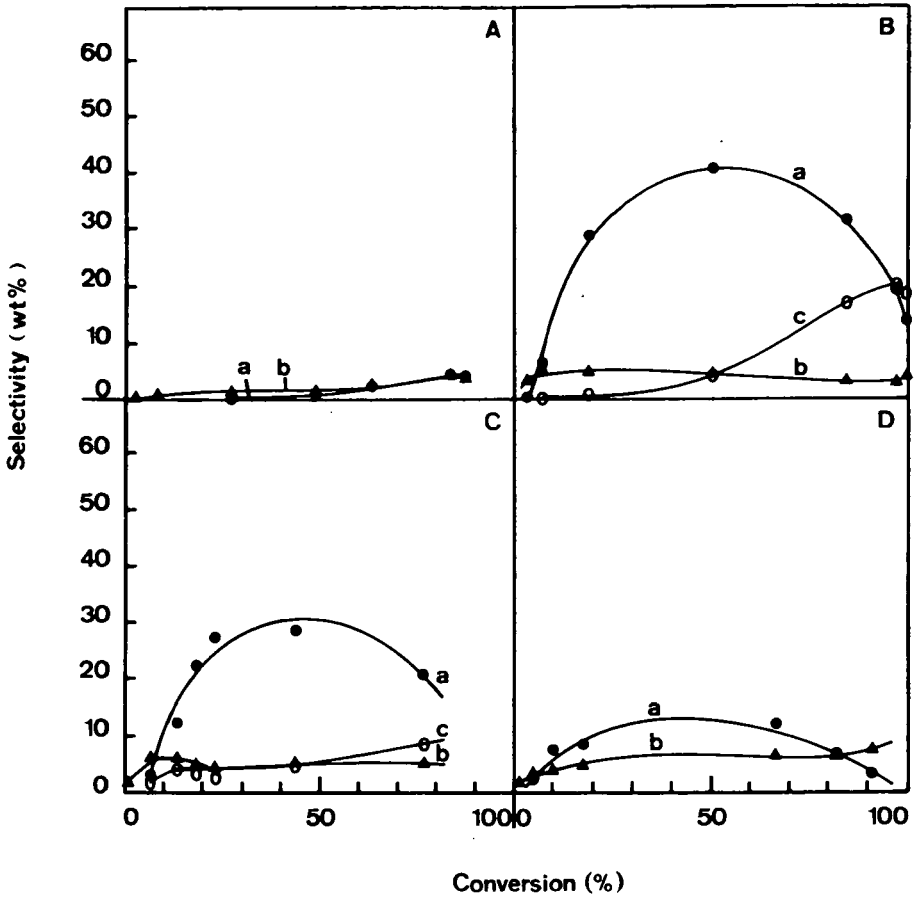

Fig. 4. Distribution of the secondary products from acetic acid : (a) alkylphenols, (b) isobutene and (c) aromatics. The H-ZSM-5 zeolites used contained (A) 0.1, (B) 1, (C) 1.6 and (D) 3.2 % of Al/Al + Si.

competes with the dehydrodemethylation reaction. This would explain the maximum in the yield of alkylphenols (Fig. 4). In the series of ZSM-5 zeolites with different Al content, the right degree of dilution of the Brønsted sites is needed to realize a maximum selectivity to alkylphenols. Whether at this particular dilution a maximum number of Brønsted sites of a given strength is present, is unknown at this time. Neither is known on what kind of site the dehydrodemethylation occurs. A potential active site could be occluded impurity iron.

Although this matter requires further research, at this stage it is believed that rather than by equation (10) the dehydrodemethylation reaction can be best rationalized when it is catalyzed by occluded iron-oxide in the following way :

VIII 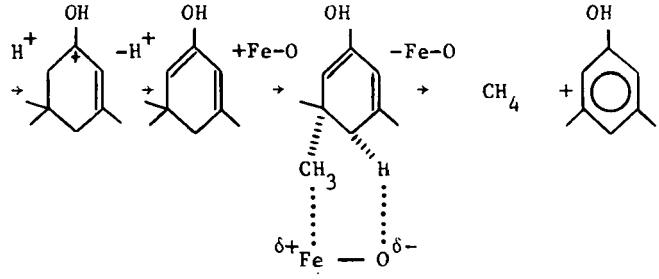 (12)

Distribution of the alkylphenols. The maximum selectivity obtained for alkylphenols when untransformed acetone and CO_2 are not taken into account as products is approximately 80 wt % on H-ZSM-5 (1). The dominating product in this fraction is 2,4-dimethylphenol, with a maximum selectivity of 77 wt %. In analogy to the trimethylbenzenes [3], 2,4-xylenol is expected to be the smallest of the dimethylphenol-isomers. Its formation is therefore governed by product diffusion shape selectivity. At high reaction temperatures, cresol as well as trimethylphenols appear in minor amounts. This represents evidence for a dismutation reaction.

CONCLUSION

Acetic acid is shown to be converted on H-ZSM-5 zeolites into acetone, carbon dioxide and water as primary products. The stoichiometrically expected CO_2 is recovered on all H-ZSM-5 zeolites, irrespective of their Al content. The data can be rationalized in terms of the interaction between a Brønsted acid generated acylium and an acetate ion. In contrast to previously proposed mechanism, no zeolite dehydroxylation has to be invoked.

Acetone is then either converted via a series of Brønsted acid-catalyzed aldolization and dehydration reactions into isophorone or via dimerization and cracking into isobutene. The selectivity for the first reaction is high for H-ZSM-5 samples rich in aluminum. For the high-silica samples, acetone is only cracked at very high reaction temperatures. The key step in the reaction network seems to be the decomposition pathway of isophorone. If this occurs via classical carbenium ion chemistry, 1,2,4-trimethylbenzene is the main product. On H-ZSM-5 zeolites with intermediate Al content (1 %) and at relatively low reaction temperatures, isophorone is via a dehydrodemethylation reaction converted into mainly dimethylphenols, in which fraction 2,4-xylenol as a result of product diffusion shape selectivity is abundantly present.

ACKNOWLEDGMENTS

This research is carried out in the frame of a concerted action on shape selective catalysis, sponsored by the Belgian Government (Diensten Wetenschapsbeleid). P.A.J. is grateful to NFWO for a research position as "Senior Research Associate".

REFERENCES

1. Chang, C.D., Silvestri, A.J., J. Catal., 47 (1977) 249.
2. Chang, C.D., Lang, W.H., Bell, W.K., Catalysis of Organic Reactions, Moser, W.R., ed., Dekker, 1981, p. 73.
3. Chang, C.D., Chen, N-Y., Koenig, L.R., Walsh, D.E., Prep. A.C.S. Div. Fuel Chem., 28(2) (1983).
4. Imanaka, T., Tanemoto, T., Teranishi, S., Catal., Proc. Int. Congr., 5th 1972, 1, 163 (Pub. 1973).
5. Kuriacose, J.C., Jewur, S.S., J. Catal., 50 (1977) 330.
6. Bielanski, A., Datka, J., J. Catal., 32 (1974) 183.
7. Fieser, L.F., Fieser, M., Organic Chemistry, Reinhold Publ., London, 1956, 3rd ed., p. 209.
8. Reichle, W.T., J. Catal., 63 (1980) 295.
9. Whitmore, F.C., Organic Chemistry, Van Nostrand, New York, 1973, p. 253.
10. Szabo, D., Acta Chim. Acad. Sci. Hung., 33 (1962) 425.
11. Von Ballmoos, R., Diss. ETH no. 6765 (1981).
12. Jacobs, P.A., Von Ballmoos, R., J. Phys. Chem., 86 (1982) 3050.
13. Von Ballmoos, R., Gubser, R., Meier, W.M., Proceed. 6th Int. Conf. Zeolites (Reno), Olson, D. and Bisio, A., eds., Butterworths, 1984, p. 803.
14. Von Ballmoos, R., Meier, W.M., Nature, 289 (1981) 783.
15. Olson, D.H., Haag, W.O., Lago, R.M., J. Catal., 61 (1980) 390.
16. Jacobs, P.A., Catal. Rev.-Sci. Eng., 24(3) (1982) 415.
17. Dwyer, J. Fitch, F.R., Qin, G., Vickerman, J.C., J. Phys. Chem., 86 (1982) 4574.

HYDROCONVERSION OF CARBON MONOXIDE IN ZEOLITIC MEDIA - A GENUINE FISCHER-TROPSCH REACTION ?

Y. BEN TAARIT
Institut de Recherches sur la Catalyse, C.N.R.S., 2 Avenue Albert Einstein 69626-Villeurbanne-Cédex.

ABSTRACT

The hydroconversion of Carbon monoxide over multicomponent zeolitic catalysts was reviewed. The Fischer-Tropsch (F.-T.) synthesis, as generally accepted was considered with reference to its obvious limitations : low overall conversion rate, broad product spectrum, and comparatively high methane yields. The design of active catalysts that circumvent the Schulz-Flory (S.-F.) distribution was the aim of most of the litterature disclosed initially. Later composite catalysts were designed to achieve depressed methane yields and narrower distributions : the quest for such catalysts was schematically analyzed : the first association of zeolites to metals known to be active in F.-T. synthesis was aimed at imposing cage and/or size effects so as to by-pass the S.-F. distribution. This idea slowly shifted to the use of intrinsically more selective catalysts for hydroconversion of CO stabilized in the zeolite cavities. These improved the selectivity but did not achieve the long sought higher rates. Composite catalysts including either an F.-T. conventional catalyst or a methanol synthesis catalyst and a shape selective zeolite were the most recent approaches directed at increasing yields and improving selectivites. However questions as to the operating pathways and the unexpected selectivity changes are still pending.

INTRODUCTION

The last decade has witnessed feverish efforts in the search of energy sources alternative to periodically dried up and yet ever lasting oil. Among the possible candidates renewable energy sources enjoyed an immense but fugacious popularity as cheap oil prices reassured the consumer for a new "period". By contrast coal still retains the attention of the professionals. The secret of this new infatuation for coal, in spite of all the heavy toll which traced the coal mining history up to very recently, may lie in the existing coal and coal-derived syn gas conversion

technology. Also the availability of coal in various parts of the world ensured an attractive reliable suplly.

Syn gas conversion is a well known process to methanol and glycol, while Fischer-Tropsch synthesis to produce fuels, though not so popular as it used to be before the oil era regained some luster in recent years. Yet the F.-T. plants remained shut down. Only, in South Africa, probably on political grouns Sasol plants are operating. In order to gain Industrial significance, this process must meet the following conditions : the conversion rate, presently the lowest of all syn gas conversion processes, must be significantly enhanced ; the prevailing broad product distribution must be circumvented and the methane yield must be drastically cut down. Table 1 compares the production rates for methanol synthesis from various technologies and that of the Sasol plants as extract parts of the world ensured an attractive reliable suplly.

Syn gas conversion is a well known process to methanol and glycol, while Fischer-Tropsch synthesis to produce fuels, though not so popular as it used to be before the oil era regained some luster in recent years. Yet the F.-T. plants remained shut down. Only, in South Africa, probably on political grouns Sasol plants are operating. In order to gain Industrial significance, this process must meet the following conditions : the conversion rate, presently the lowest of all syn gas conversion processes, must be significantly enhanced ; the prevailing broad product distribution must be circumvented and the methane yield must be drastically cut down. Table 1 compares the production rates for methanol synthesis from various technologies and that of the Sasol plants as extracted from Dry [1] data.

Table 1

Comparative rates for Methanol and F.-T. synthetisis

Catalyst	temperature centigrades	pressure atmos.	space velocity h^{-1}	yield Kg/Kg/h	source [1,2]
CuO : ZnO : Al_2O_3					
64 : 32 : 4	250	50	10 000	0.3	academic
"	300	50	10 000	0.9	"
CuO : ZnO : Cr_2O_3					Power gas
11 : 70 : 19	270	145	10 000	1.95	corporation
31 : 38 : 5	230	50	10 000	0.755	BAST
33 : 31 : 36	250	150	10 000	1.1	academic
	300	150	10 000	2.2	"
Fe			2 000-3 000	0.01	Sasol

THE FISHCHER TROPSCH SYNTHESIS PRINCIPLES AND LIMITATIONS

The syn-gas conversion occurs formally according to the simplified independent or sequential reactions :

$2n + H_2 + nCO \longrightarrow C_nH_{2n} + nH_2O$ to provide olefins

$(2n + 1)H_2 + nCO \longrightarrow C_nH_{2n+2} + nH_2O$ to yield alkanes

The thermodynamic data [3,4] point to the following predictions :

- the equilibrium conversion will increase with increasing pressure and decrease temperature
- paraffins will be selectively produced in the operating temperature range (150-450°C)
- methane will be the dominant product which is a serious drawback.

But the most obvious limitation of the Fischer-Tropsch synthesis is its product distribution entirely dependent on its reaction mechanism :

Indeed there is a general agreement to ascribe the formation of hydrocarbons in syn-gas conversion to a polymerisation process involving a simple monomeric species. This monomeric species containing one carbon atom adds to the growing chain on the catalyst following the well established polymerisation kinetics with initiation, propagation and termination steps. Such a kinetic has been formulated mathematically [5] as follows

$$W_n = n\,\alpha^{n-1}\,(1 - \alpha)^2$$

W_n indicates the product weight fraction of carbon number n

α indicates the chain groth probability and is constant

α could be determined experimentally from the plot of log W_n/n against n.

Thus the distribution of the Fischer-Tropsch products appears to be predetermined by the chain growth mechanism. This type of product distribution is known as the "Schulz-Flory" distribution. Of course α varies with the nature of the catalyst and other experimental parameters. Nonetheless except where $\alpha = 0$ that is the methanation case, a whole product spectrum must be obtained with the relative concentrations strictly obeying the mathematical equation derived for polymerization schemes.

This is indeed a serious limitation which hinders the use of F.-T. synthesis to the production of a narrow range of chemicals. Though, possibly, parallel and sequential reactions may alter significantly this imposed distribution.

The second limitation is the very low activity of the Fischer-Tropsch catalysts comparaed to methanation and methanol synthesis catalysts (see table 1).

As to the major limitation i.e. broad spectrum of products, the litterature data show that :

a) Higher overall selectivites to lighter hydrocarbons may be reached by increasing either the H_2/CO ratio or the reaction temperature or by decreasing the residence time.

b) As apparently olefins and/or alcohols are the primary products, these are favoured by low conversions achieved by high space velocities and/or low H_2/CO ratios. The selectivity towards these products will obviously depend on the hydrogenation ability of the catalyst. It would seem reasonable that alcohols should be favoured by high total pressures.

c) Higher temperatures would favour olefins with respect to overall hydrocarbon production as increasing temperatures shift the hydrogenation dehydrogenation equilibrium towards olefins.

VIOLATION OF THE S.-F. DISTRIBUTION

Even though modest inflexions of the product selectivities may be achieved as mentioned above or by resorting to the variation in the reactor engineering, these selectivity changes are still achieved within the Shulz-Flory Distribution.

Ways to circumvent the CO hydrogenation were therefore sought in the catalyst design.

As zeolites always appeared as wonder catalysts, it was thought that these solids should be up to the expectation of the many scientists who engaged in the search for means to violate the S.-F. Distribution in order to render to the F.-T. synthesis some of its luster [6-9]. Indeed many reports on the violation of the S.-F. Distribution were issued following the use of zeolitc catalysts.

While this should appear as reasonable goal, a number of reports should be considered with caution.

In effect the following artifacts may well acount four apparently interesting non S.-F. Distributions :

In some cases, for obvious experimental constraints, usually fully mentioned by the authors, only a narrow fraction of products could be analyzed or collected, thus missing a representative picture of the actual distribution.

Analysis of the whole product spectrum may be hindered by a number of reasons from which we single out the following :

fractionation problems and incorrect sampling

condensation of long chain products on the catalyst surface or inside the pores.

preferential adsorption of some products.

Most of these problems may be overcome by running the F.-T. experiment over a long enough period, thus achieving high yields which minimizes the inherent errors to sampling, fractionation and product retention on/in the catalyst.

Alternatively a carefull and accurate material balance would save erroneous and misleading conclusions.

Irrespective of the conclusions following a carefull scrutiny of the available data reporting non Schulz-Flory distributions, several means were employed to circumvent the production of the entire spectrum of hydrocarbons.

The ideas behind the means were inspired by the belief that

(i) metal support interaction may drastically influence both the activity and the selectivity of the supported metal. In particular the acid-base properties of the support were thought to be the most influencial parameters that determine the modifications of the catalytic properties of the metal [10]

(ii) the metal particle size is likely to influence the hydrogenation and hydrogenolysis activity of the metal [11] and possibly have sensitive effects on catalytic steps, such as carbene insertion into M-C bonds etc..., which govern the F.-T. synthesis mechanism.

(iii) the chain growth mechanism may be strongly restricted by steric hindrance which may yield a stereoselective distribution appearing as a sharp cut off at a definite carbon number [12]. This latter way of thinking inevitably brought zeolites into play. The disclosure by Mobil of methanol conversion to hydrocarbons over various shape selective zeolites increased the attractive character of these solids as selective supports or components in F.-T. and F.-T. related synthesis.

(iv) zeolites were well established as acid catalysts which perform cracking and isomerization of hydrocarbons. Therefore hopes were running high to modify the S.-F. distribution in a subsequent conversion step of the hydrocarbons produced on the F.-T. component.

In order to examine the accomplishments achieved by Zeolite "F.-T." synthesis as to the activity and the product distribution we shall consider separatly the following topics which originate from the ideas outlined above as practiced by various groups.

Schematically these ideas inspired the emergence of :

1) bifunctional catalysts associating a metal, known to be F.-T. active, with zeolites

2) bifunctional catalysts associating an active component in hydroconversion of CO (usually a carbonyl complex) with various cage-type zeolites.

3) composite catalysts associating an active F.-T. catalyst with zeolites, which is the procedure used to up-grade F.-T. products.

4) composite catalysts associating an active CO hydrogenating catalyst (usually a methanol synthesis catalyst) with shape selective zeolites.

Roughly three approaches, which sometimes merge, dominated the disclosed data.

(i) upgrading F.-T. products by addition of an acidic component possibly with shape selective properties.

(ii) diverting the CO hydrogenation from the F.-T. mechanism to produce oxygenated species, subsequently converted to hydrocarbons on acid catalys exhibiting(or not) shape selective properties.

While the first approach does not aim in principle at increasing the rate of reaction, the latter is also directed towards improving the yield as well as escaping the Schulz-Flory distribution.

However one more limitation which cannot be lifted upon chosing the first approach consists in unacceptably high methane yields. This feature, combined with low hydrocarbon production rates, and a broad product spectrum, contributed strongly to weight down the F.-T. process.

Therefore it would seem useful to examine the parameters which influence methane formation in order to depress methanation rates whenever possible.

METHANATION

Part of the dilemma in attemps to increase F.-T. synthesis rates is that it is necessary to increase the hydrogenation abilities of the catalyst which almost inevitably results in increased methanation rates as hydrogenolysis activity is also simultaneously increased. Thus both CO hydrogenation intermediates and hydrocarbon products all tend to be ultimatly converted to methane the stable end product.

A well documented investigation by Lunsford and coworkers [13] has elegantly delineated the parameters which play a prominent role in methanation. Recent studies disclosed at this very meeting appear to be in agreement with Lunsford et al. and extend the investigation to the $H_2 + CO_2$ mixture [14].

Rabo and coworkers [15] have shown that supported metallic palladium produced essentially methanol from syn gas under specified pressure and temperature conditions. This result was ascribed to the unique property of palladium to adsorb CO associatively so as preventing methane formation, as this proceeds via dissociation of CO and subsequent hydrogenation of the resulting carbon. Lunsford and Coll. extended this pioneer work to palladium supproted on a number of carriers including zeolites [13].

Large size palladium particles supported on HY and NaY zeolites were compared to similar size particles deposited on neutral silica and acidic silica.

Pd/HY appeared to be the most active methanation catalyst irrespective of t particle size, while only silica-supported palladium exhibited a significan activity in methanol production. Under the same temperature and pressure condition Moreover methane production was shown to proceed by an independent route wi respect to methanol formation and could not be due to sequential hydrogenation methanol. Yet methane did not appear to be formed via CO dissociation. The weakl

adsorbed CO would appear to be the precursor to methanol, while strongly adsorbed CO would favour methanation. Changes in the CO adsorption strength were noticed upon varying the Palladium particle size. Larger particles favoured methanol formation.

The acidity effect seems, on the contrary, to enhance methanation rates (table 2). This was ascribed to an additional and simultaneous interaction of the Oxygen-End of the CO molecule with Brönsted acids, thus considerably affecting the CO bond strength enabling the C-O cleavage in subsequent steps to methanation. In a way, acid sites would provide "oxophile" for CO activation.

Table 2

rates of CH_4 and MeOH production on Pd supported over various acidic and neutral carriers in mmole per metal site per second T = 553 K ± 5 H_2/CO = 2.8 - 2.4 P = 1,51 MPa SV = 1200 ± 200 h^{-1}

Catalyst	support properties	rate CH_4	rate CH_3OH
PdNaY	medium acidity	12 ± 4	-
PdHY	strong acidity	40 ± 3	1
$PdSiO_2$ (01)	acid	2 ± 1	
$PdSiO_2$ (57)	neutral	0.65	18
PdCab-O-Sil	fairly acid	1.2	4 ± 1

A recent report [16] on methanation supported Lunsford et al. [13] conclusions on the absence of any significant charge transfer between the support and the metal. It was suggested in addition that polarization of the chemisorbed CO followed by hydride transfer may enhance the rate of methanation as observed on acid supprots. While it is clearly conceivable that hydride transfer may be favoured in this way, there is no obvious reason that this should be at the exclusive benefit of methanation. As no influence of the acidity was observed on methanol production rate this hypothesis could not be reconciled with experimental data. One would rather favour the acid-assisted CO dissociation mechanism in order to account for methanation rate enhancement.

Qualitative acidity effects were also investigated. It was reproted that the effect varies in the following order HY > HZSM-5 > NaZSM-5 >> NaY > SiO_2 [16]. However too many influencial parameters may have varied simultaneously to infer reliable conclusions. It is almost certain that the palladium particle size, the location of palladium particles and the vicinity of the metallic sites with the acid site may vary substantially from sample to sample.

However there should be no doubt that Brönsted acidity plays a major role in enchancing the methanation rate. Therefore acidic supports for Fischer-Tropsch catalysts should be prohibited on these grounds.

BIFUNCTIONAL F.-T. CATALYSTS

F.-T. Active metals supported on Zeolites. Such catalysts associating mainly ruthenium and iron with cage type zeolites were dealt with in many early investigations [6, 11, 17-19].

Jacobs and coworkers [11, 17] reported that a sharp cut off in chain growth occured around C_9-C_{10} when ruthenium particles were supported on zeolites. Similarly Ballivet et al. [18] showed that iron-Y zeolites and $Fe_3(CO)_{12}$-derived Iron Y zeolites produced C_1-C_{10} hydrocarbons for the latter and C_1-C_{12} hydrocarbons for the former. In both cases the probability in chain growth appeared not to be constant over the entire C_1-C_{12} range. A sharp decrease was observed past the C_9 hydrocarbons. This sharp decrease was attributed to a cage effect, as the $Fe_3(CO)_{12}$-derived iron particles were thought to be located in the Y zeolite supercages.

However as the zeolite cages may have as a primary effect to stabilize metal particles that fit in these cages, it may well be that the interpretation must be considered in terms of particle size effects, regardless of the reason and the means used to develop such particles. Jacobs [6] reported such a drastic effect of the particle size over the hydrocarbon distribution obtained in the case of ruthenium supported on Y zeolites. For example particles sizes of 1.5, 2.5 and 4.0 nm limited the chain length of F.-T. products at 10, 5 and 1 carbon numbers respectively. Thus it would appear sensible to ascribe the observed distribution to particle size effects since the carrier did not change. Additionaly, similar size ruthenium particles deposited on silica also produced similar effects which confirms that the F.-T. distribution is sensitive to the structure of the active component on which the actual chain growth does take place rather than to the porous structure of the matrix, except through secondary effects on the metal particle.

A curious distribution was recently reported where C_1-C_5 hydrocarbons were almost entirely absent from the products using a rod shaped ruthenium oxide supported on Y zeolites and subsequently reduced. However the actual operating catalyst has not been examined [20]. If confirmed this would be the most interesting structrure sensitive example in F.-T. synthesis. This structure sensitivity would imply that only ensembles with as an optimum number of individual metal sites are able to initiate and/or effect the chain growth. It is again interesting to point out that larger particles produced essentially methane while smaller particles produced longer chains. This was further illustrated by investigating the activity and the product distribution exhibited by bimetallic catalyst. For example ruthenium associated with the F.-T. inactive copper in Y zeolite showed an overall decreased activity and additionally a comparitively lower methane yield [6].

A variant of the zeolite effect in F.-T. synthesis was examplified by the addition (mechanical mixing) of HY zeolite to iron and/or ruthenium zeolite [18]. Under such circumstances a narrower range of product distribution was obtained, which was interpreted as the result of cracking of the longer chains. Also iso-products were produced in high yield probably via cracking and isomerization.

Active CO hydroconversion complexes entrapped in zeolites. It appeared that the methane rate depression obtained upon designing small metal particles or alloying F.-T. active elements by an inactive element was unfortunatly accompanied by a depressed overall rate. Therefore another method was sought. Transition metal polynuclear carbonyls either adsorbed into- or synthesized within the zeolite were used. This was inspired by the fact that smaller ensembles may presumably totally inhibit methane formation, while preserving selective CO hydrogenation to higher hydrocarbons via non dissociated CO.

In fact, peculiar distributions were observed by combination of various size-cage zeolites and metals known to form stable polynuclear carbonyls. For example Gates and Coworkers [21] obtained a very narrow distribution in CO hydroconversion over CoII A zeolite subsequently reduced by metallic Cadmium. The narrow (almost C_3 hydrocarbons exclusively) distribution was ascribed to the formation of tiny metal particles in A zeolites as a first step followed by a slow conversion to Cobalt Carbonyl(s), as evident from the significant induction period preceding evolution of products. These results prompted further sutdies [22, 23]. An intersting feature in [22] is the high selectivity to olefins exhibited by Silicalite and concomitant methane rate depression. Silicalite has little (ifany) acid sites which is not only in line with methane suppression (see methanation section), but also with the stability of zerovalent carbonyls, as these are readily oxidized by protons).

These features observed in [21, 22] result from :

- a low dissociation capacity of CO thus depressing methane yields.
- a low CH_2 or CO inserting activity into M-C bonds, which accounts for limited chain growth.
- a low hydrogenation activity as emphasized by the high olefin-to-paraffin ratio.

Diluted metal particles (alloys), as well as small metal particles are well known to possess poor CO dissociation as well as poor hydrogenation activity. Similar properties are also exhibited by metal carbonyl clusters. Such clusters are known to activate molecular hydrogen to form hydrides. Although CO or CH_2 insertion into M-H bond, which constitute the propagation steps in F.-T. synthesis [24] has not been reported for soluble polynuclear carbonyl clusters under normal temperature and pressure conditions, it is not excluded that this might occur under more severe

conditions. Metal formyls have been reported in solution, some of which result from the migratory incertion of CO into a Metal-hydride bond [25-28] in hydrido carbonyl complexes including Ta, Th and more interestingly Rhodium as the central atom. Such a rearrangement would be the initial step to subsequent hydrogenation of undissociated CO to form formaldehyde (either as such or dissociatively coordinated) and ultimately to yield methanol. Alternatively hydrocarbonylation of formaldehyde might lead to higher alcohols and olefins.

Drastic product distribution differences appeared upon reacting syn gas mixture over 20 Å zeolite entrapped rhodium particles and over well characterized $Rh_6(CO)_{16}$ synthesized within Y zeolite cavities. The former catalyst produced essentially methane whereas the latter produced about 60 % methanol + ethanol + C_2-C_5 olefins and paraffins and only ~ 40 % methane.The overall conversion rate was by two orders of magnitude lower than the rate observed for the 20 Å metal particles.

By contrast, 10 Å zeolite-entrapped Rhodium particles exhibited an intermediate behaviour : the initial predominant methane production declined with time on stream, while methanol, and C_2-C_5 hydrocarbon yield increased [29].

Inspection of the catalyst as it reached a steady state activity and selectivity, comparable to those recorderded for $Rh_6(CO)_{16}$-Y catalyst, revealed that the metal particles were indeed converted to the hexarhodium-hexadecacarbonyl cluster [29, 30].

The depressed methane yield as metal particles were progressively converted into $Rh_6(CO)_{16}$, together with the overall CO conversion decline, are indicative of a poor CO dissociation and CO hydrogenation activity of the polynuclear carbonyl. We even feel that methane produced in this case probably originates from a side reaction derived from methanol conversion

$$(2CH_3OH) \text{ or } CH_3OCH_3 \longrightarrow CH_4 + CH_2O + (H_2O)$$

known to proceed over acid zeolites [31-32]

$$CH_3OH + CO \longrightarrow CH_4 + CO_2$$

which may proceed over the rhodium carbonyl [34].

Recent results by Kubelkova and coworkers showed that methanol decomposed at low partial pressure on various zeolites to CH_4 and CH_2O, although it was not suggested that these two compounds were produced via the same pathway [31]. However earlier studies in our laboratory showed a clear correlation between methane and formaldehyde yields when methanol was reacted with a variety of cation exchanged Y zeolites [32]. Recently Chang proposed a concerted mechanism for CH_4 and $[CH_2O]$ formation upon reaction of methanol over adsorbed methoxide species [33].

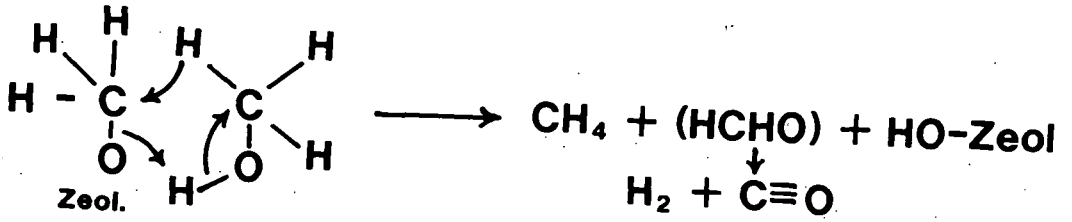

Decomposition of Methanol to produce CO_2 and Methane was shown to occur on Methanol Carbonylation Catalyst via the following mechanism derived by Forster [34].

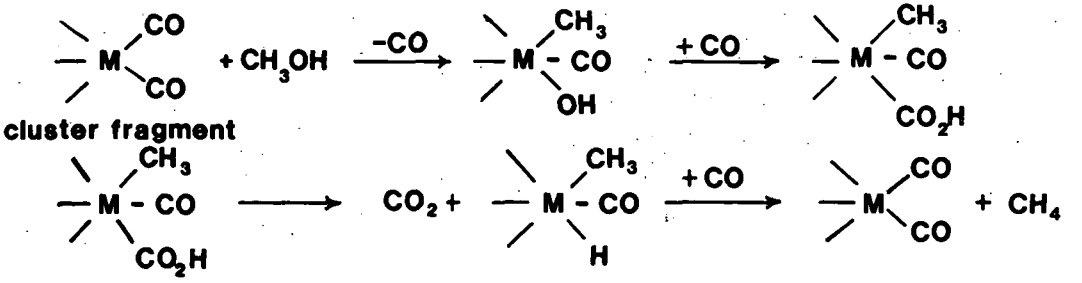

This approach of occluding well defined carbonyls within zeolites either by direct synthesis or via reduction of the active component using a procedure that prevents formation of protons and subsequent conversion to carbonyls by the H_2/CO mixture proved to be efficient in decreasing the methane yield and increasing the olefins and also to circumvent the S.-F. Distribution since the actual reaction pathway deviates substantially from the F.-T. mechanism [24]. Unfortunatly as to the crucial activity problem the answer is not satisfactory as conversion of syn gas over such catalysts is even slower than that observed for conventional F.-T. catalysts already estimated to be rather poor contact masses.

COMPOSITE CATALYSTS

Composites associating a conventional F.-T. catalyst with a zeolitic component

In order to improve the selectivity of conventional F.-T. catalyst whatever its poor activity this approach favoured the adjunction of a zeolitic component meant both to upgrade the F.-T. products and hopefully to prolong the catalyst life time. This idea was first put into practice by Ceaser et al. [35] and by Chang et al. [36]. The results were beyond the initial hope as can be seen from table (3) which shows that a significant improvement is obtained not only considering the product distribution but also in view of the methane yield regression and the enhancement of the conversion rate which practically doubled while little activity improvement was expected.

Table 3

Comparison of the activity and Product distribution of plain F.-T. catalyst an composites F.-T. component + Zeolite component.

Catalyst	T K	P MPa	G HSV h^{-1}	Conversion H_2+CO %	C_1 %	Oxygenates	C_5^+	Ar/C_5^+
ZrO_2	700	9.13	720	7.5	24.8	34.5	24.0	53.1
ZrO_2 + ZSM-5	700	9.13	720	13.8	1.6	0	84.8	99.8

This improvement obtained upon mechanically mixing an F.-T. active component with a pentasil type zeolite should be connected to a rapid migration of mobil intermediates from the F.-T. component to be converted on the zeolite surface.

It is obvious, should this be the case, that profound alterations of the product distribution are to be expected following this diversion ofthe reactio intermediate from an F.-T. pathway to an acid type zeolite catalyzed process. Th extent of such alterations is perfectly illustrated in table 3 and by results reported by Ceasar et al. [35], concerning the liquid fraction using a fused Iron-Zeolite composite. An increased stability against waxing was also observed du to cracking of long chain hydrocarbons. It was also shown that an optimu composition, far in favour of the zeolite, was necessary in order to avoid clogging.

The diversion from simple F.-T. mechanism, which is though to be at the origi of increased life time, was related to the fate of terminal olefins. In a plai F.-T. process these were likely to reenter the propagation cycle and lead to lon chains. If mobile enough, in a composite catalyst, they should be isomerized tc internal olefins which cannot participate in the propagation step any more. Indeed much higher proportion of internal olefins was achieved in composite catalysts witl reference to the simple F.-T. component.

These findings would suggest that higher benefits would be expected if th intimacy of the two components were improved, so as to enhance the migration o F.-T. intermediates to the zeolite surface, thus achieving simultaneously highe rates and narrower distributions.

Also, it was apparent that the best synergetic effect should be achieved whe the "F.-T." intermediate is most likely to be rapidly converted by the zeoliti component. As it is well known that zeolites, particularly those of the pentasi family, are tremendously active is methanol conversion, it was only logical that th next move was to associate a methanol component with a zeolite component.

Composite associating a methanol synthesis catalyst with a zeolitic component

Such catalysts are expected to benefit from the excellent activity of the methanol synthesis component since methanol conversion would not be the limiting step. However no matter how flexible a dual component catalyst might be, its limitations are inherent to its very nature of compromise type catalyst.

Nevertheless the expected benefits from such an association are the following :

(i) as already mentioned a higher overall conversion rate, which would significantly improve the usual F.-T. rates to a level that would compare more favourabley with rates encountered in methanol synthesis.

(ii) a significant decrease in the total pressure. Indeed the usual pressures, employed in methanol synthesis in order to achieve acceptable rates at the most favourable thermodynamic conditions for methanol formation, may be cut down : conversion of the generated methanol would likely result in a significant equilibrium displacement making it possible to achieve reasonable conversion rates at significantly lower pressures.

(iii) narrower product distribution, which should be the end products of methanol conversion under the operating conditions exclusively.

In fact, as already underlined, difficulties may be experienced in setting (adjusting) the optimum conditions to operate both components of the composite simultaneously. In particular the usual temperature range for zeolites to show optimum activity is significantly higher than the optimum range for methanol component.

On the other hand, zeolites used to exhibit an appreciable flexibility in directing the reaction towards the production of olefins or aromatics upon adjusting the experimental conditions (temperature and space velocities) and, to a lesser degree, the acidity of the alumino silicate. In the composite catalyst, however, both the activity and the selectivity pattern of the zeolite may be significantly affected by the presence of the other component and by the ambiant H_2 + CO atmosphere.

The activity of the dual component catalysts

Several components have been selected independently. The usual procedure was to achieve a fine mechanical mixing of a methanol catalyst : Pd/SiO_2 [37], Pd/MgO [38], Pd doped $ZnO-Cr_2O_3$, $Cu-Pd/ZnO-Cr_2O_3$ [39], $CuO-ZnO/Al_2O_3$ [37], CuO ZnO [40] and $ZnO-Cr_2-O_3$ [39] with a zeolite component usually H type zeolites namely HY ; H Mordenites either as prepared or modified, erionite, silicalite and HZSM-5 with various Si/Al ratios, with and without shape selective properties.

In all cases the activity of the composite catalyst was at least an order of magnitude higher than that of the methanol component under the same experimental conditions. This synergetic effect seems to depend on the nature of both components. Although this effect is interpreted in terms of equilibrium displacement by continuous consumption of the methanol produced, little is understood as to the origin of the variation of the extent of this synergetic effect.

Perhaps preparation methods and conditions which would offer the best intimate contact between the two phases, and thus enhance the methanol conversion rate, are not perfectly reproducible. It is not unreasonable, on theother hand, to assume that an intimate enough mixture would enable mobile enough intermediate species, in methanol synthesis, to migrate on the acidic surface of zeolite, to be directly converted into final products, thus bypassing the methanol step and therefore escaping the thermodynamic limitations. This hypothesis seems to be in accordance with the observation that both Pd/SiO_2 and $CuO-ZnO/Al_2O_3$ associated with the same zeolite did not achieve the same conversion, although their independent methanol synthesis rates were comparable under similar experimental conditions [37].

Pd/SiO_2 appeared to achieve a modest synergetic effect under identical conditions [37, 38]. This was ascribed to poisoning of palladium by aromatics [37]. In addition, although, no data is available as to the characterization of the catalysts, it should not be surprising that palladium particles exceed 50 Å in size and would, therefore, provide for a poor interface between the two components. One might expect that migration, over to the zeolite surface, may, permanently and dramatically, alter the final hydrocarbon distribution toward higher methane yields (see methanation section). Such ageing of palladium-zeolite composites has already been observed [37].

The likelyhood of interception of methanol synthesis intermediate(s) which would account for synergetic effects seems to be supported by the steady increase of the yield of hydrocarbons with increasing reaction temperature on the composite catalyst, whereas methanol synthesis rates over the individual "methanol component" passed through a maximum as the reaction temperature increased and then declined drastically.

Also the observation that catalyst composition barely affects the conversion rate is yet another argument in favour of "interface sensitive" reaction than simple trivial multi-step reaction, one would expect that an optimum composition should exist whereby the rate of methanol synthesis on the methanol component should equal the rate of the subsequent conversion on the zeolite. In fact in academic systems the conversion rates achieved were slightly less than those of methanol synthesis though they were obtained under temperature and pressure conditions far away from the optimum thermodynamic conditions for methanol production. As the zeolite component is by far more effective than the other component one would at least

expect that, within a certain composition range, the overall conversion rate should increase linearly with the "methanol component" content in the composite. In fact this was not observed, which suggests that the intermediate migration onto the zeolite is likely to be realistic.

As expected, the nature of the zeolite appeared to be of importance. Silica-rich zeolites exhibited the highest rates, although faujasite type zeolites also exhibited synergetic effects.

By contrast product distributions were drastically dependent upon the nature of the zeolite. Little attention was devoted to the possible mutual influence on the catalyst stability. As already mentioned, the total pressure increase enhanced the yield while increased CO/H_2 ratios slightly depressed the overall production but had marked effects on the composite selectivity.

Selectivity : parameters and trends

Many parameters should affect the selectivity namely the total pressure, the temperature and the feed composition. On the other hand,the nature of the catalyst components and the principal characteristic of each of them : the hydrogenation ability of the MeOH synthesis component, its sensitivity to CO, its dispersion the acidity of the zeolitic component its Si/Al ratio and porous structure should dramatically influence the product distribution.

Too few studies were directed to pinpoint the influence exerted by each of these parameters independently. Rather, studies were directed towards obtaining a hydrocarbon distribution range or simply a desired product. Thus these parameters were optimized to achieve either a narrow spectrum of aromatics [36] or C_2-C_3 paraffin [41] or olefins [38]. However a more detailed study was disclosed by Tominaga and coworkers [37] which investigated the independent influence of a number of these parameters.

The prominent feature of selectivity trends is the total suppression of oxygenates as compared to all F.-T. and MeOH synthesis experiments. This is no surprise since the zeolitic component is usually chosen on the basis of its ability to convert alcohols and analogues at a very high rate.

The other important feature is the methane yield. The composite catalyst was designed to achieve a number of promises among which : increased activity with respect to classical F.-T. synthesis and a depressed methane yield.

The methane production appeared to depend on two main parameters : the temperature and the nature of the MeOH synthesis component and possibly a third parameter under particular circumstances.

The methane production is drastically enhanced by temperature increase this enhancement is well beyond the expected selectivity loss of the methanol synthesis. It probably stems from the subsequent conversion of hydrocarbons produced on the metal (oxide) component which hydrogenating abilities are increased by a temperature increase, as CO poisoning of those properties is partially removed.

The methane production enhancement is even more pronounced when the methanol synthesis component is metallic (usually palladium). It is even more so if one assumes that a temperature increase would result (i) in possible sintering of the metal to produce larger particles which exhibited high hydrogenation and hydrogenolysis activity. (ii) in possible migration from the initial MeOH synthesis carrier to the zeolite carrier which is more acidic and would therefore favour direct conversion of syn gas to methane (see methanation section).

An additional parameter which might influence the methane yield is the nature of the zeolite : while efficient methanol conversion catalyst of the pentasil family produce little methane, medium and large pore catalysts : faujasite, unmodified mordenites produced significant amounts of methane [33] following the reaction

$$CH_3OH + CO \longrightarrow CH_4 + CO_2$$

Thus minimizing the methane yield requires low temperatures, oxide type methanol synthesis and pentasil type zeolites or modified mordenites.

The second feature, with few exceptions, is the increase of the paraffin/olefin ratio as compared to the direct methanol conversion on zeolite catalysts. This phenomenon is even more pronounced when the MeOH component is palladium. This is not surprising as the other component of the composite system has enhanced hydrogenating abilities with respect to the pure zeolite component. The possible way to preserving the higher olefin to paraffin ratio observed with straight forward methanol conversion should be sought through an increase of the CO partial pressure to inhibit subsequent hydrogenation of olefins. This however may result in a lowered overall activity.

The next possible way which has been successfully investigated is the composition shift to a lower proportion of the MeOH synthesis component especially when it is palladium. In that case, it was observed not only that C_1 to C_3 yield in paraffins decreased but also that selectivity towards aromatics increased which is in line with decreasing hydrogenating and hydrogenolysis activity.

The last feature, we select, is the problem of aromatics production and distribution within the aromatic range. Clearly mordenites and pentasil type zeolites produce significantly more aromatics than any F.-T. catalyst, while composite catalyst including Y type faujasite produce almost exclusively aliphatics. This last observation is in line with previous reports concerning the simple

methanol conversion. This itself is a serious proof that the actual mechanism proceeds via methanol or a particular intermediate to methanol then subsequent conversion of the latter or of both.

Aromatic yield would depend on the possibility for olefins to oligomerize, which implies that the "methanol component" must not have a high hydrogenation activity or that the chances for olefins, when formed, to adsorb on the metallic or oxide component should be lowered. The yield in aromatics would become even lower when metallic components are present instead of oxide components.

The aromatic distribution however has been the subject of more concern and it even seemed to shed some doubt on whether syn gas conversion proceeded actually according the two step mechanism

$$CO + H_2 \xrightarrow[\text{catalyst}]{\text{MeOH}} \text{MeOH} \xrightarrow{\text{zeolite}} \text{hydrocarbons}$$

The prominent feature of this distribution is a higher methylation of the aromatic ring, an important shift of aromatic hydrocarbons from the usual C_7, C_8, C_9 with a peak for xylenes to maximum C_{10}-C_{11} production among aromatics on pentasil type composite catalysts and a maximum for aroamtic distribution at C_{11}-C_{12} expanding up to C_{13} on mordenite composite catalysts.

Little has been proposed to account for this commonly recognized effect. Yet it has been observed that increasing CO partial pressure resulted in higher proportion of C_8-C_9 aromatics in the case of the palladium component. This suggests that the palladium component may well be active in the alkylation process (it may also disproportionate substituted aromatics, formed on/in the zeolite, the dealkylated molecules may be subsequently realkylated (by the zeolite) thus progressively shifting the aromatic distribution towards higher carbon numbers.

The alternative is that due to the fact the "methanol component" may only be vicinal to zeolite cristallites the methanol produced in a too low concentration (compared to a methanol feed) could well be converted significantly preferentially at the external surface thus undermining the shape selective property of the zeolite.

PROSPECTS

Too few investigations appeared to be directed at assessing the effect of the preparation method of the composite catalyst. One should think, however, that achieving a more intimate vicinity between centers effecting methanol synthesis or generating intermediate species to methanol and the zeolitic acid sites, would permit a better equilibrium displacement and/or more efficient intermediate interception, to form hydrocarbons, thus greatly improving the overall syn gas conversion rate.

However, in the case of methanol metallic component i.e. Pd the obvious pitfall would be the migration of the metallic component from its appropiate support to the acid zeolite support, which would switch the selectivity towards methane.

As to the selectivity of this process it would be desirable to depress tetra and penta methyl benzene yield. This could, for instance, be achieved by neutralization of the zeolitic external surface or by minimizing this surface using larger zeolite crystals.

In all, this procedure of circumventing the S.-F. Distribution would appear as the most promizing especially that an important flexibility in the choice of the composite components is left at the will of the experimentalist.

As to the overall activity, this procedure also seems to yield the highest rates, as these approach the lower methanol production rates with the advantage over F.-T.-derived procedures of providing directly usable fuels.

ACKOWLEDGEMENTS

Deep gratitude is expressed to Dr. Claude Naccache for fruitfull discussions and encouragements. The cooperation of Mrs. Eliane Vignon in preparing the manuscript is greatly appreciated.

REFERENCES

1. Dry, M.E., Catalysis, Science and Technology. Springer Verlag New-York, 1981, 1, 159.
2. Kung, H.H., Catal. Rev. Sci. Eng. 22, 235 (1980).
3. Stull, D.R., Westrum, E.F., Sinke, G.C. : the chemical thermodynamics of Organic compounds. J. Wiley, N.Y., 1969
4. Christoffel, Von E., Swijo, I., Bears, M., Chem. Zeit. 102, 19 (1978).
5. Henrici-Olivé, G., Olivé, S., Angew. Chem. Int. Ed., 15, 136 (1976).
6. Jacobs, P.A. : Zeolites Elsevier Sci., Publ. Co., Amsterdam, 1980, p. 293.
7. Vannice, M.A. : Catalysis Science and Technology - Springer - Verlag, New-York, 1982, 3, 139.
8. Vannice, M.A., Garten, R.L., J. Catal. 66, 242 (1980).
9. Biloen, P., Sachtler, W.M.H., Adv. Catal., 30, 165 (1981).
10. Bardet, R., Thivolle-Cazat, J. Trambouze, Y., C.R. Acad. Sci., 292, 883 (1981).
11. Nijs, H.H., Jacobs, P.A., Uytterhoeven, J.B., J.C.S. Chem. Comm., 1095 (1979).
12. Vanhove, D., Mucambo, P., Blanchard, M., J.C.S. Chem. Comm., 605 (1979).
13. Fajula, F., Anthony, R.G., Lunsford, J.H., J. Catal. 73, 287 (1982).
14. Rasko, J., Erdohelyi, A., Solymosi, F.

15. Poutsma, M.L., Elek, L.F., Ibarbia, P.A., Risch, A.P., Rabo, J.A., J. Catal. 52, 157 (1978).
16. Saha, N.C., Wolf, E.E., Appl. Catal. 13, 101 (1985).
17. Verdonck, J.J., Jacobs, P.A., Genet, M., Poncelet, G., J.C.S. Faraday I, 76, 403 (1980).
18. Ballivet-Tkatchenko, D., Coudurier, G., Mozzanega H. : Zeolites. Elsevier Sci. Publ. Co., Amsterdam, 1980, p. 309.
19. Chen, Y.W., Wang, H.T., Goodwin, Jr., J.G., J. Catal. 83, 415 (1983).
20. Audier, M., Klinowski, J., Benfield, E., J.C.S. Chem. Comm., 626 (1984).
21. Fraenkel, D., Gates, B.C., J. Am. Chem. Soc., 102, 2478 (1980).
22. Peuckert, M., Linden, G. : Proceedings 8th International Congress on Catalysis II, Dechema. Berlin 1984, 135.
23. Dabrowski, A.J., Solik-Dobrowska, M.,
24. Sachtler, W.M.H. : Proceedings 8th International Congress on Catalysis I, Dechema. Berlin 1984, p. 151.
25. Wayland, B.B., Woods, B.A., J.C.S. Chem. Comm., 700 (1981).
26. Churchill, M.R., Wasserman, H.J., J.C.S. Chem. Comm., 274 (1981).
27. Fagan, P.J., Moloy, K.G., Marks, J.T., J. Am. Chem. Soc. 103, 6959 (1981).
28. Wayland, B.B., Woods, B.A., Pierce, R., J. Am. Chem. Soc., 104, 302 (1982).
29. Lefebvre, F., Gelin, P., Naccache, C., Ben Taârit, Y. : Proceedings of the 6th International Zeolite Conference Butherworths Guildford 1984 p. 435.
30. Bergeret, G., Gallezot, P., Gelin, P., Ben Taârit, Y., Lefebvre, F., Naccache, C., Shannon, R.D., Nouv. J. Chimie in Press (1985).
31. Novakova, J., Kubelkova, L., Habersberger, K., Dolejsek, Z., J.C.S. Faraday Trans. I., 80, 1457 (1984).
32. Chang, C.D., Catal. Rev. Sci. Eng. 25, 1 (1983).
33. Clemençon, J., Memoire, Conservatoire National des Arts et Métiers, LYON, 1979.
34. Forster, D., J.C.S. Dalton Trans., 1639 (1979).
35. Caesar, P.D., Brennan, J.A., Garwood, W.E., Ciric, E., J. Catal. 56, 274 (1979).
36. Chang, C.D., Lang, W.H., Silvestri, A.J., J. Catal. 56, 268 (1979).
37. Fujimoto, K., Kudo, Y., Tominaga, H., J. Catal. 87, 136 (1984).
38. Denise, B., Hamon, C., Sneeden, R.P.A. : Proceeding 8th International Congress on Catalysis II. Dechema Berlin 1984 p. 93.
39. Inui, T., Takegami, Y. : Pan. Pac. Syn. Fuelds Conf., 1, 145 (1982).
40. Chan, T.Y., Report DOE/PC/04 7176, 112 pp.
41. Chang, C.D., Miale, J.N., Socha, R.F., J. Catal. 90, 84 (1984).

STUDIES ON COKE FORMATION ON DEALUMINATED MORDENITES BY IN-SITU IR AND EPR MEASUREMENTS

H.G. KARGE, E.P. BOLDINGH, J.-P. LANGE, A. GUTSZE*
Fritz-Haber-Institut der Max-Planck-Gesellschaft, Berlin (West)

ABSTRACT

Coke formation during dealkylation of ethylbenzene and reaction of ethylene over dealuminated mordenites was followed by simultaneous in-situ IR spectroscopic and conversion measurements as well as by in-situ EPR spectroscopy.

A close correlation emerged between the Si/Al ratio, the number of Brønsted acid sites and the coking tendency of the mordenite catalysts. The rate of deactivation was similar for two catalysts with different Si/Al ratios, in agreement with TPD results according to which these catalysts had sites of similar strength. EPR results suggest that at low reaction temperatures ($T < 373$ K), oligomeric radicals had formed, indicated by a signal at g=2.0028 with hyper-fine structure, whereas at higher temperatures a single coke signal appeared. It cannot be excluded that the oligomeric radicals were precursors of the coke; however, no simple relationship between both species was established. Coke formation seemed to proceed via a carbenium ion rather than a radical mechanism.

INTRODUCTION

With most hydrocarbon reactions catalysed by zeolites, deactivation of the catalyst due to coke deposition is a serious problem. More recently, reinforced efforts were made to elucidate the nature of coke as well as the parameters which influence coke formation (1 - 5). A particularly interesting question is that of the mechanism of coke formation. IR studies on coke formation are particularly useful, since they simultaneously may provide information about changes in the properties of the catalyst (e.g. concentration and involvement of surface OH groups), constituents of the deposited coke (e.g. saturated or aromatic hydrocarbons) and the amount of the carbonaceous deposits present on the surface (measured, e.g., through the intensity of the so-called coke band around 1585 cm^{-1} (3,6)). However, there have been not too many of such investigations, and they generally were designed

*On leave from the Institute of Physics,
Nicholas Copernicus University, Toruń, Poland

for static conditions. Only a very few in-situ experiments have been reported, where the zeolite catalyst was studied under on-stream conditions (4,7 - 9). Similarly, all the EPR experiments which were concerned with deactivation of zeolites via coke deposition seem to be conducted under static conditions. Thus, Kucherov and Slinkin (10-11) recently reported interesting results of olefin adsorption and static interaction with mordenite. Typical EPR signals with remarkable hyper--fine structure (hfs) were observed and their changes with temperature were followed. As is well-known from the literature (12-13), at higher temperatures coking of organic material usually results in the appearance of a typical single EPR line with a g-value close to that of free electrons (2.0023). It seemed worthwhile to investigate both the radicals with hfs, which may or may not be precursors of the coke, and the coke itself in dynamic experiments, i.e. on catalysts under stream. The aim of the current study was to test the in-situ technique and to correlate dynamic IR and EPR results. This paper presents first results of that approach.

EXPERIMENTAL

Materials. Commercial hydrogen mordenite, HM (No.1, Si/Al = 6.8), was purchased from Norton Comp., Mass. Dealuminated hydrogen mordenite was prepared in the laboratory of Professor Fetting, TH Darmstadt, via treatment of sodium mordenite with hydrochloric acid; the sodium mordenite had been supplied by Norton Comp.

Two differently dealuminated HM samples were used (No.2, Si/Al = 12 and No.3, Si/Al = 39). Ethylene (99.95 vol.%) was purchased from Messer-Griesheim, Düsseldorf; ethylbenzene was obtained from Merck, Darmstadt, and carefully purified using a distilling column.

Apparatus and procedure. The IR flow reactor cell, which was integrated into a set-up for catalytic experiments, has been described in detail elsewhere (8). Operation of the cell and experimental procedure were, however, somewhat modified. After activation of the catalyst wafer in high vacuum at 673 K and subsequent cooling to 350 K, a stream of ethylbenzene (0.8 kPa) in He, containing 2 vol-% CH_4 as an internal standard, was passed under normal pressure through the wafer. At such a low temperature, practically no reaction occurred, in particular no coking. When a steady state was reached as shown by the gas chromatograph (constant CH_4 reference peak) the temperature was raised to 550 K within three minutes. Immediately, dealkylation of ethylbenzene started and, as a result of subsequent reaction of ethylene,

leactivation due to coke formation set in. This was followed by GC letermination of the conversion of ethylbenzene (and the yield of enzene and diethylbenzenes). The deactivation was also traced via the R spectra, which were simultaneously scanned in short time intervals y a computerized Perkin-Elmer Model 580B spectrometer.

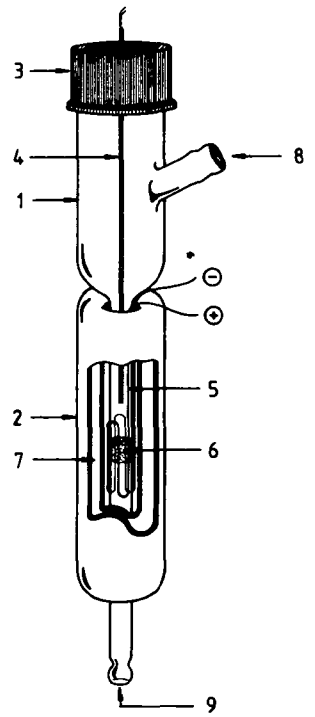

Figure 1.
Flow reactor for EPR in-situ measurements.
(1) reactor tube; (2) Dewar; (3) cap with rubber sealing; (4) thermocouple; (5) heating wire; 0.05 mm diam. Pt; (6) catalyst sample; (7) high vacuum (8) inlet; (9) outlet.

EPR measurements were carried out at X-band frequency with a Varian Model V-4502-15 spectrometer, equipped with a Digital MF-211 computer. A double cavity TE_{104} was employed. Thus, two modulation frequencies (100 kHz and 400 Hz) could be used, which allowed independent measurements of the signal of the sample (e.g. coke, at 100 kHz) and the signal of the reference (e.g. DPPH, at 400 Hz). This arrangement greatly enhanced the accuracy of the measurements of intensities and g-values.

In-situ EPR measurements have been rendered possible by a particularly designed reactor, which could be placed into the resonance avity of the spectrometer. A schematic drawing of the reactor is resented in Figure 1.

The reactor permitted reactions to be carried out within a temerature range from 300 to 800 K. The zeolite catalyst was activated nside the reactor in a flow of N_2. The sample (0.01 g) was heated at a ate of 200 K/hour to 673 K and kept at this temperature for two hours. ubsequently, the reactor was cooled to the reaction temperature and a ixture of 8 vol% ethylene in nitrogen was passed under normal pressure hrough the catalyst bed. EPR spectra were taken at certain time interals, in order to follow the progress of the reaction.

RESULTS AND DISCUSSION

IR in-situ experiments. Figure 2 demonstrates the time on-strea behaviour of two hydrogen mordenite catalysts with significantly dif ferent Si/Al ratios, as measured at 550 K in the IR flow reactor cell.

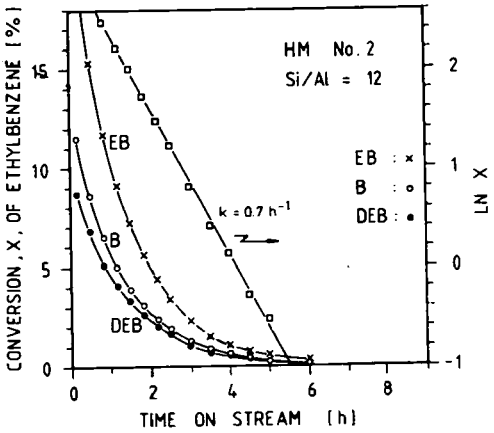

Figure 2A.

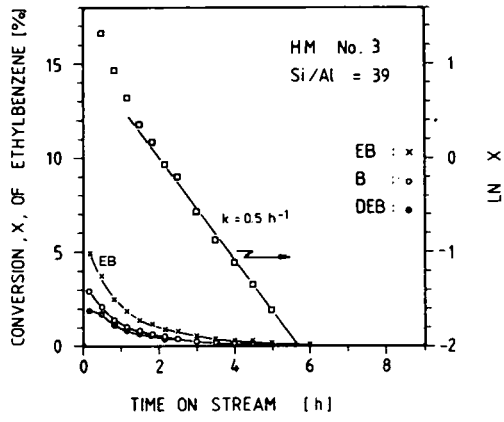

Figure 2B.

Time-on-stream behaviour of two hydrogen mordenite catalysts (HM No. and No.3) upon dealkylation of ethylbenzene at 550 K.

In the case of the higher Si/Al ratio (39, HM No.3) the conver sion-versus-time curve dwells at a substantially lower conversion leve than with Si/Al = 12 (HM No.2). The drop of the conversion, x, wi time on stream, however, proceeds with roughly the same rate, as i both cases plots of ln x vs. time on stream provide straight lines wi slope $k = 0.5 \pm 0.2\ h^{-1}$ (see Figure 2A and 2B). These results sugges that (i) the conversion of ethylbenzene over acidic mordenites i proportional to the number of active sites, N(t), in agreement wit earlier observations (14) and (ii) the deactivation reaction is firs order w.r.t. N(t) according to

$$N(t) = N(t=o) \cdot e^{-k.t} \qquad (1)$$

Since the rate constant k is almost equal for both catalysts, one ha to conclude that the rate of deactivation is not affected by the Si/A ratio. The difference in time-on-stream behaviour is merely due to th fact that the initial numbers of active sites of both catalysts differ they do not differ, however, in strength.

This conclusion is confirmed not only on the simultaneous in-situ IR measurements (see Figure 3), but also by the IR determination of the number of sites and by the TPD experiments evaluating the strength of the Brønsted centers. To start with the latter, TPD of ammonia from both mordenite samples (HM No.2 and No.3), activated at 673 K, produced the TPD peaks due to NH_3 desorption from Brønsted sites (15) at the same desorption temperature, viz. 680± 5 K. This indicated similar strength of the sites of both catalysts. Static IR experiments, which were carried out as described elsewhere (16-17), showed that hydrogen mordenite No.2 exhibited a markedly higher number of Brønsted sites than sample No. 3, as could be expected as a consequence of the lower Si/Al ratio of HM No.2. The maximum absorbances of the OH bands at 3610 cm^{-1} (acidic OH groups (16)), were $A_{max}(OH) = 0.40$ and $A_{max}(OH) = 0.25$ for sample No.2 and No.3, respectively. Correspondingly, the absorbances of the pyridinium ion band at 1542 cm^{-1}, being indicative of acidic Brønsted sites (16) were $A_{max}(HPy^{+}) = 0.20$ and $A_{max}(HPy^{+}) = 0.10$

Figure 3 shows the absorbance of the coke band, A(1585 cm^{-1}), as a function of time on stream. Figure 4 relates the conversion to the amount of deposited coke. These plots again demonstrate that on the catalyst with the higher number of sites(HM No. 2, Si/Al = 12) the amount of coke deposited during dealkylation of ethylbenzene is significantly higher than with the much shorter-lived catalyst HM No.3. This result is supported by the observation that, after almost complete dehydroxylation at 973 K in high vacuum, i.e. after removal of acidic Brønsted sites, hydrogen mordenite exhibited only a very low activity towards coke formation.

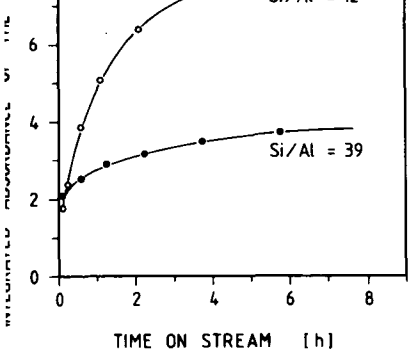

Figure 3.
Coke deposition as measured by the integrated absorbance of the coke band at 1585 cm^{-1}, as a function of time on stream.

It is interesting to note from Figure 4 that over a wide range of coke deposition, the decrease in conversion is directly proportional to the amount of deposited coke. This holds for both catalysts irrespective of the Si/Al ratio. However, a significant and repro-

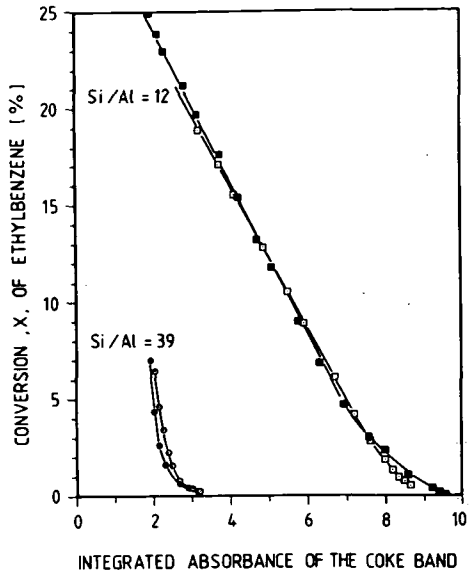

ducible difference in the slopes of the straight lines was observed, i.e. the activity is much more affected in the case of the catalyst with higher Si/Al ratio.

Figure 4.
Conversion of ethylbenzene related to coke deposition, as measured by the integrated absorbance of the band at 1585 cm^{-1}; different experiments are represented by different symbols.

In-situ EPR experiments. EPR spectroscopy provided three contributions to the current investigations into the coke problem, viz. the study of (i) formation of oligomeric radicals upon ethylene interaction with the catalyst at low temperatures (373-423 K), (ii) formation of coke radicals at higher temperatures (T > 423 K), and (iii) annihilation and generation of radicals during oxidative regeneration of coked catalysts.

Oligomeric radicals. When a flow of nitrogen and ethylene was passed through the catalyst sample at room temperature, no EPR signal was observed. At 373 K, however, a weak signal with hyper-fine structure (hfs) appeared. When the reaction temperature was raised to 423 K the signal intensified and exhibited a well-resolved hfs with several lines, the parameters of the spectrum being g = 2.0028 and a = 1.4-1.5 mT (hyper-fine splitting constant). This spectrum differs significantly from the spectrum obtained by Kucherov and Slinkin (10-11) in that the hyper-fine splitting constant is about twice as large as the constant reported by these authors.

Since the spectrum comprises more than five lines, it cannot be due to an ethylene radical. However, ethylene polymerizes on acid mordenites, even at room temperature (2). At higher temperatures subsequent cracking may occur. Thus, the signal is probably indicative of an oligomeric radical generated via polymerization and subsequent homolytic splitting.

In view of the value of the hfs constant, the signal could be ascribed to alkenic or allylic radicals; alkyl radicals appear to be much less likely. A detailed study upon formation of oligomeric radicals due to olefin reaction on zeolites will be published elsewhere (18).

Coke radicals. When the temperature was increased to 453 K, the hfs started to vanish, and in a slow process a symmetrical single line at g = 2.0024 emerged, which is generally ascribed to species generated upon coking of organic material (12-13). Thus, the appearance of this line indicated the onset of coke formation. With increasing temperature, the intensity of the coke signal was markedly enhanced. At 473 K, the hfs had completely disappeared, the intensity of the single line corresponded to ca. 10^{17} spins·(g catalyst)$^{-1}$, the line width was ΔH = 1.0-1.5 mT, and the g-factor still equalled 2.0024. This coke signal with g = 2.0024 immediately developed, i.e. without a preceding oligomeric signal when freshly activated hydrogen mordenite was contacted with ethylene at 473 K. Hence, it seems to be rather unlikely that those oligomers are inevitable precursors of the coke.

The intensity of the coke signal steadily increased, but finally (after 15 hours on stream) approached a constant value, viz. 1.2×10^{19} spins·g^{-1}. The line width was nearly constant, and the g-value remained 2.0024.

The initial rate of coking strongly depended on the reaction temperature. This is demonstrated by Figure 5, where the intensities of the coke signal were plotted versus time on stream for three different reaction temperatures. It is evident from this figure that the initial increase of the intensity of the coke signal is steeper the higher the reaction temperature.

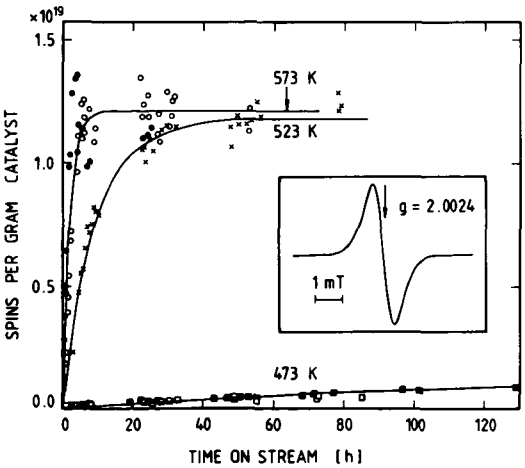

Figure 5.
The intensity of the EPR coke signal at three different reaction temperatures as a function of time on stream (solid lines are calculated curves, eq.3)

After some time, the intensities seem to approach a final level, and the data of Figure 5 may be represented by a first order relationship

$$n(t) = n(t=\infty)\ (1 - e^{-\kappa \cdot t}) \qquad (3)$$

For the experiments at higher temperatures ($T_{react.}$ = 523, 573 K) the final levels coincide (see Table 1)

Table 1 Final intensities of the coke signal at various reaction temperatures (eq.3)

T (K)	n(t = ∞) (spins.g^{-1})	κ (h^{-1})
473	0.20×10^{-19}	0.005
523	1.18×10^{-19}	0.11
573	1.20×10^{-19}	0.50

The results in Figures 3 and 5 indicated that after deposition of a certain amount of coke, which depended on the temperature, all the active sites (acidic Brønsted centers) were poisoned or blocked, and coke formation stopped. Indeed, the IR experiments confirmed that the OH bands at 3610 cm^{-1} had not completely disappeared when the conversion (dealkylation of ethylbenzene) dropped to zero and the coke band at 1585 cm^{-1} had virtually ceased to grow. Therefore, deactivation is not solely caused by poisoning or consumption of acidic OH groups, but also to some extent by pore blocking. Nevertheless, from the IR and EPR results it had become evident that a higher number of acidic OH groups corresponded to a greater amount of coke deposit (vide supra). Hence one would conclude that coke formation requires Brønsted acid sites and proceeds via a carbenium ion mechanism. Coke formation through a radical mechanism, involving the radicals indicated by g=2.0024, is less likely for the following reason.

A high number of radicals due to coke were present on the catalyst at 573 K (see Figure 5) and a fraction of them must have formed on the external surface of the zeolite crystals, where coke species block the openings of the pores. However, in spite of presence and accessibility of these radicals, coke formation levelled off, which was also indicated by the IR and conversion measurements in the IR flow reactor cell.

Coke oxidation and catalyst regeneration. When a stream of oxygen was passed through the catalyst, which had been coked upon ethylene reaction at 573 K, oxidation of the coke at 673 K seemed to occur very rapidly. After about one hour, 90% of the initial intensity of the coke signal was gone. Simultaneously, the g-value shifted from 2.0024 to 2.0035 and the line width decreased from 0.8 to 0.6 mT. After 40 hours of oxidation a very small signal (about 2×10^{17} spins.g^{-1}) was left. The g-value of 2.0035 is similar to that of semiquinones of polyaromatics (19-20). Thus, it may indicate that oxidation of coke results in formation not only of CO_2 but also of oxygen containing molecules with high delocalisation of electrons. However, the present results do not permit an unambiguous identification of the species formed upon coke oxidation.

CONCLUSIONS

(1) Coke formation upon reaction of olefins on acidic mordenites is strongly influenced by the number of Brønsted sites in that a higher density of sites corresponds to a higher yield of coke.
(2) Over a wide range of coke deposition, the decrease in conversion of ethylbenzene on acidic mordenites is directly proportional to the amount of deposited coke.
(3) Coke formation proceeds through a carbenium ion mechanism rather than via radicals.
(4) It is unlikely that oligomeric radicals are necessary precursors of coke. No simple relationship exists between the concentration of such radicals formed at low temperatures and the concentration of coke radicals generated by heating oligomeric radicals at higher temperatures.
(5) As in-situ IR measurements show, deactivation of hydrogen mordenite catalysts due to coke formation upon olefin reaction proceeds not solely through poisoning or consumption of acidic OH groups, but also to a marked extent by pore blocking.

ACKNOWLEDGMENTS

The authors wish to thank Mrs. Erika Popović and Mr. Walter Wachsmann for excellent experimental assistance. They are grateful for financial support by the Bundesminister für Forschung und Technologie (Project No. 03C 111 0)

REFERENCES

(1) Rollmann, L.D., J.Catal.47, 113 (1977)

(2) Karge, H.G., Ladebeck, J., Proc. of the Symp.on Zeolites, Szeged, Hungary, Sept.11-14, 1978 (P.Fejes,Ed.) Acta Phys.et Chem., Nova, Ser.24, 161 (1978)

(3) Rollmann, L.D., Walsh, D.E., J.Catal.56, 139 (1979)

(4) Eisenbach, D., Gallei, E., J.Catal.56, 377 (1979)

(5) Wolf, E.E., Alfani, F., Catalysis Rev.-Sci.Eng.,24, 329 (1982)

(6) Eberly, P.E., Jr., J.Phys.Chem.71, 1717 (1967)

(7) Ward, J., J.Catal.11, 259 (1968)

(8) Karge, H.G., Abke, W., Boldingh, E.P., Łaniecki, M., Proc.of the 9th Iberoamerican Symp.on Catalysis, Lisbon, Portugal, July 16-21, 1984 (M.F. Portela, Ed.) J. Fernandes, Lisbon 1984, p.582

(9) Fetting, F., Gallei, E., Kredel, P., German Chem.Eng.7, 32 (1984)

(10) Kutcherov, A.V., Slinkin, A.A., in: Studies in Surface Science and Catalysis (Structure and Reactivity of Modified Zeolites),Elsevier (P.A. Jacobs et al., Eds.) 18, 77 (1984)

(11) Kucherov, A.V., Slinkin, A.A., Kinetika i Kataliz, 23, 1172 (1982)

(12) Lewis, J.C., Singer, L.S., "Electron Spin Resonance and the Mechanism of Carbonization", in: Chemistry and Physics of Carbon, 17, 1 (P.L. Walker, Jr. and A. Thrower, Ed.) Dekker, New York 1981

(13) Gutsze, A., Orzeszko, S., J. Colloid Interface Sci.,(in press).

(14) Karge, H.G., Ladebeck,J., Sarbak, Z., Hatada, K., Zeolites 2, 93 (1982)

(15) Karge, H.G., Schweckendiek, J., Proc.of the 5th Int.Symp.Heterogeneous Catalysis, Varna, Bulgaria, Oct. 1-6, 1983 (D. Shopov et al., Eds.) Publ. House Bulg. Acad. Sci., Sofia, 1983, p. 429

(16) Karge, H., Z. Phys. Chem. Neue Folge, 76, 133 (1971)

(17) Karge, H.G., Z. Phys. Chem. Neue Folge, 122, 103 (1980)

(18) Karge, H.G., Lange, J.-P., Gutsze A., to be published in "Zeolites"

(19) Bersohn, M., Bair, J.C., "An Introduction to Electron Paramagnetic Resonance; Benjamin Inc., 1966, New York, Amsterdam

(20) Harriman, J.E., "Theoretical Foundations of Electron Spin Resonance; Academic Press, 1978, New York, San Francisco, London

COKE FORMATION ON ZSM-5 AND MODIFIED Y ZEOLITES IN THE REACTION OF ETHYLENE

L. KUBELKOVÁ, J. Nováková, M. Tupá, Z. Tvarůžková
The J. Heyrovský Institute of Physical Chemistry and Electrochemistry, Czechoslovak Academy of Sciences, Máchova 7, 121 38 Prague 2, CS

ABSTRACT

The effect of the acidity and pore size on the coking process in the reaction of ethylene at 670 and 770 K was studied for AlHY, dealuminated Y, HZSM-5 and AlHZSM-5 zeolites using several experimental techniques: gravimetry for kinetic measurements of the surface species formation, mass spectrometry for analysis of the gas phase, infrared spectroscopy for identification of zeolitic OH groups and the composition of coke, temperature programmed desorption of ammonia for determination of acidity. Deactivation effect of coke was tested using oligomerization of ethylene at 300 K. The relation between the nature and strength of the acid sites and conversion of ethylene was found to hold also for the coking rate on the Y zeolites. The ZSM-5 zeolites with the highest activity exhibited the lowest coking tendency, attributed to the effect of the shape selectivity properties. This factor appeared also to be responsible for the composition of the coke and the pathway of the coke formation, which is different in Y and ZSM-5.

INTRODUCTION

The formation of a carbonaceous deposit represents a serious problem in catalysis on zeolites being associated with a decrease in the catalytic activity and with altered selectivity. The role of coke in a catalytic process consists mainly in poisoning of active sites on the zeolites, chocking their channels, reducing the intercrystalline volume and direct involvement in the transformation of the reactants. Numerous studies were devoted to the deactivation of zeolites (1), however, the coking process is still far from being fundamentally understood. Even such questions as the chemical nature of coke, the role of acid sites in coke formation, the poisoning effect of coke and many others still remain to be answered.

In the present paper, we have attempted to contribute to the solution of some of the above problems by studying coke formation in the reaction of ethylene on Y and ZSM-5 zeolites differing not only in their structure and pore size but also in their acidity. Ethylene is a simple molecule with low basicity, whose reactivity is very sensitive to the nature and strength of the acid sites (2,3) and therefore permits study of the effect of both the shape selective factor and the presence of proton-

-donor and electron-acceptor sites. In the studied zeolites, a variation in the acid properties was achieved by a change in the Si/Al ratio in the lattice and by introduction of cationic Al into the cavities.

Several experimental techniques were used in this study: i) gravimetry to monitor the kinetics of zeolite weight-gain, ii) mass spectrometry to analyse the composition of the gas phase, iii) infrared spectroscopy (IR) to determine the nature of surface species and the zeolite OH groups and iv) temperature programmed desorption (TPD) of ammonia to follow changes in acidities. In this paper the term coke refers to compounds which cannot be removed from the zeolites at a temperature of 670 - 730 K.

EXPERIMENTAL

$Al_{12}Na_{25}(NH_4)_{40}Y$ was obtained from $(NH_4)_{70}Na_{30}Y$ using cationic exchange with $Al(NO_3)_3$. The sample denoted as deal Y was prepared from NaY by $SiCl_4$ dealumination at 670 K followed by NH_4^+ exchange (4). ZSM-5 zeolites were synthesized in the usual way (5), calcinated at 870 K and exchanged with NH_4^+. Further exchange with Al^{3+} yielded $AlNH_4$ZSM-5. Good crystallinity of all the samples was evidenced with X-ray diffraction patterns, IR spectra and sorption capacities. The latter values are listed in Tab. 1 together with the Si/Al total value, concerning all respective atoms in the zeolites, and $(Si/Al)_1$ in the lattice (4). Prior to measurements, the zeolites were dehydrated and deammoniated in vacuo at 670 K (Y) and 770 K (ZSM-5) for 18 hrs.

The weight gain resulting from the adsorbed species was measured with a quartz balance within an error $\pm 3 \times 10^{-5}$ g, using a 0.1 g zeolite plate in a reaction volume of 700 cm^3. Oligomerization of ethylene (5.3 kPa) inside the cavities was investigated at 300 K over 30 min. In the high-temperature experiments, 5.3 kPa of ethylene was allowed to react with the Y and ZSM-5 zeolites at 670 and 770 K, respectively, the weight gain was measured at desired time intervals. Small amounts of the gas phase were withdrawn and analyzed using a mass spectrometer (MI 1305, USSR). In some experiments, the sample was filled with oligomers at 350 K prior to the reaction at the high temperature. The amount of coke reported in mg per g of the zeolite was determined from the zeolite weight after 30 min evacuation at 670 and 730 K for Y and ZSM-5 zeolites, respectively.

The IR spectra of the zeolite plates were recorded on a Fourier transform Nicolet MX-1E infrared spectrometer at ambient temperature. Those presented here are related to a sample thickness of 7 mg cm^{-2}. Spectra of the surface species alone and the difference spectra of OH groups were obtained by subtracting the spectrum of the original zeolite form the spectrum after the reaction. The experiments were carried out in the same way and under the same conditions (except the sample weight which equalled 25 - 30 mg) as in the gravimetric studies.

Table 1

Characteristics of zeolites and amounts of coke formed during the transformation of ethylene

Zeolites	$(Si/Al)_l$ lattice	Si/Al total	Capacity (mmol Arg^{-1})	Reaction		
				T(K)	t(hr)	coke ($mg\ g^{-1}$)
AlHY	2.5	2.2	10.5	670	2	4.6
deal Y	10.8	5.7	9.2	670	1	17.4
				670[a]	1	45.7
HZSM-5(a)	13.5	13.5	5.6	770	19	8.5
HZSM-5(b)	19	19	5.5	670	2	<0.5
				770	19	14.1
AlHZSM-5(b)	19	17.5	5.6	770	19	7.5

[a]-before the reaction at 670 K the zeolite was filled with oligomer at 350 K

Ammonia evolved during the TPD measurements (18 μmol of NH_3 preadsorbed at room temperature on 10 mg of the zeolite, either in fresh form or after the coke formation) was pumped through the mass spectrometer. The samples were preheated in vacuo at 670 K for 18 hrs, the heating rate was 6 K min^{-1}.

RESULTS

Zeolite acidity. Various OH groups were found on the studied zeolites, nevertheless, only those located on the framework in positions accessible for the reactant can be considered most important for the reaction, as they possess a high acid strength depending on the $(Si/Al)_l$ (6). Therefore, the ZSM-5 zeolites, with $(Si/Al)_l$ equal to 13.5 and 19 and with hydroxyls characterized by a band at 3610 cm^{-1}, exhibit very high acid strength (6), while the AlHY contains considerably less acidic framework hydroxyls vibrating in large cavities at 3640 cm^{-1}(7). In the deal Y with $(Si/Al)_l$= =10.8, the hydroxyls similar both to those of AlHY and HZSM-5 appear, manifested by

Table 2

Reaction of C_2H_4 - composition of the gas phase (Vol %)

Zeolite	reaction conditions		ethylene	aliphatics	aromatics
	T(K)	t(hr)			
AlHY	670	2	91	9	-
deal Y	670	1	91.7	8.3	-
HZSM-5(b)	670	1	73	16.8	10.2
HZSM-5(b)	770	1	9.8	-	88

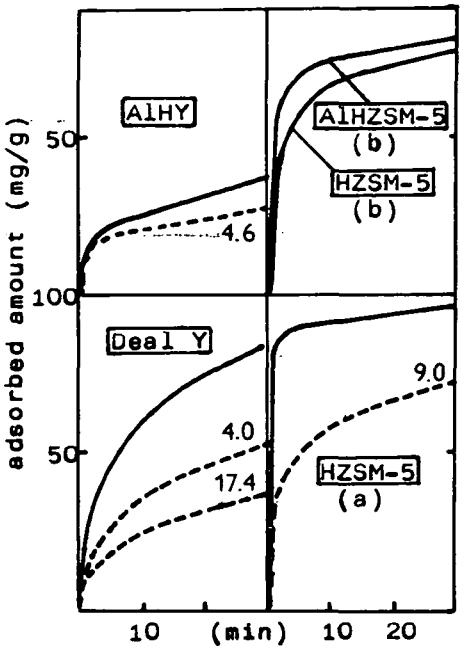

Fig. 1. Ethylene oligomerization on zeolites at 300 K: ——— original zeolit ----- zeolite with coke in mg g^{-1}.

bands at 3630 and 3602 cm^{-1}, respectively, which was recently proved by adsorption o pyridine (7). However, the intensity of the latter band suggests that very strongly acidic hydroxyls are present in a smaller amount than on the HZSM-5 zeolite. The TPD curves of ammonia from fresh zeolites confirm the much higher acid strength of HZSM-5 and deal Y compared with AlHY: the maxima appear at 570, 630 and 450 K, respectively. IR spectra of OH groups and TPD curves of ammonia are depicted in Figs. 2-4, where they represent zeolites before coking. The electron-accepting properties of deal Y, AlHY and AlHZSM-5 zeolites originate from extralattice Al species formed either in the process of dealumination (4) or introduced into the latter two zeolites by ion exchange. The ratio (Al extralattice)/(Al lattice) amounts to 0.84, 0.12 and 0.06, respectively.

Oligomerization of ethylene at 300 K. The kinetic curves for the weight gain reflecting oligomerization activity of zeolites are depicted in Fig. 1. The oligomerization is clearly conditioned by the acidic properties of the individual samples, i.e. by the nature and strenghts of acid sites. Thus, the ZSM-5 zeolites exhibit the highest activity caused by the dominant role of very strongly acidic hydroxyls. The rate of reaction then decreases in the sequence HZSM-5(a)>AlHZSM-5(b)>HZSM-5(b), which can be explained by the effect of the greater number of hydroxyls present on th HZSM-5(a) than on the HZSM-5(b) zeolite and by the participation of Al electron-accepting sites on the AlHZSM-5(b) zeolite. In contrast to HZSM-5, the HY zeolite (not shown here, see ref.(3)) is almost inactive. However, after the addition of cationic Al, oligomerization occurs, as demonstrated with AlHY, even though the rate is still low due to the relatively weak acid strength of the hydroxyls. This supports

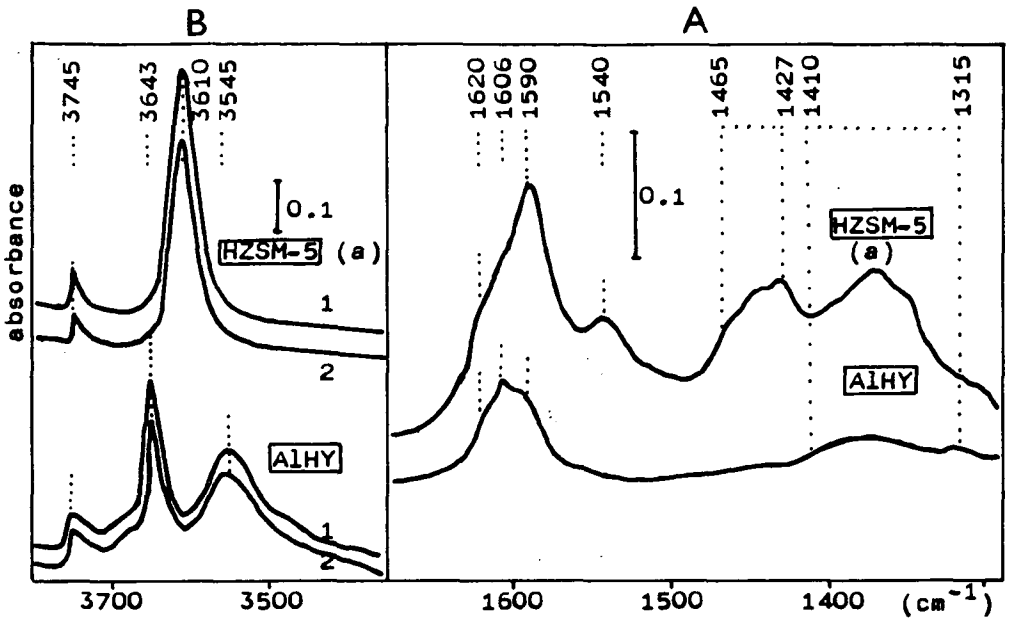

Fig. 2. IR spectra of the coke (A) and OH groups (B) of the HZSM-5 and AlHY zeolites: 1- original zeolite, 2- after coke formation caused by the reaction of ethylene, HZSM-5: 19 hr, 770 K, AlHY: 2 hr, 670 K.

the suggestion (3) of direct involvement of Al electron-accepting sites in the activation of ethylene. An appreciable increase in the oligomerization rate found for the deal Y zeolite can then be attributed to the presence of both very strongly acidic hydroxyls and Al electron-accepting sites.

Oligomers on Y and ZSM-5 zeolites differ in their composition consisting of saturated branched and straight-chain hydrocarbons, respectively (2,3). On heating to 670 K, oligomers on Y zeolites yield coke (see below and ref. (8)) while on ZSM-5 zeolites are completely decomposed.

Fig. 1 also demonstrates the deactivation effect of coke. It can be seen that the presence of coke even in amounts below 10 mg g^{-1} considerably decreases the oligomerization rate on both Y and ZSM-5 zeolites. This decrease is most pronounced with very small amounts of coke as is evident from the activity of deal Y.

Reaction of ethylene at high temperatures. Coke formation. The gravimetric experiments indicate a continous increase in the sample weight when ethylene reacts over the Y zeolites at 670 K. They point to coke formation at a rate appreciably higher on deal Y than on AlHY as is demonstrated in Tab. 1 with the amount of coke formed after 1 and 2 hrs. During this period, ethylene also yields aliphatics C_3-C_5, which are the main gas products at the ethylene conversion level of about 10 % (Tab. 2). ZSM zeolites exhibit the highest activity, however, coking does not proceed at a measurable rate. Even at 770 K, when ethylene is rapidly converted, mainly to

C_6-C_8 aromatics (Tab. 2), coking is a very slow process: coke appears after 19 hrs of reaction in amounts comparable with those reported above for the Y zeolites at 670 K after 1 and 2 hrs (Tab. 1).

It follows from the IR spectra in Figs. 2 and 3 that the composition of coke on Y zeolites is different from that of HZSM-5. It is also apparent from these data that coke formation leeds to removal of part of the framework hydroxyls, namely those vibrating at 3640, 3602 and 3610 cm^{-1} on the AlHY, deal Y and ZSM-5 zeolites, respectively.

The coke on Y zeolites is characterized by bands in the regions 1640 - 1590 and 1410 - 1315 cm^{-1} which can be assigned to C=C and CH vibrations, respectively, of the unsaturated compounds, while the bands near 1460 and at 3000 - 2800 cm^{-1} representing paraffinic CH_3 and CH_2 groups are very weak. In addition, the typical bands of aromatics, which should appear near 1500 cm^{-1}, are hardly visible in our spectra. It thus follows that the coke consists mainly of hydrogen-deficient polyene species. The band of the C=C vibration is composed of several components, of which the most prominent ones appear at 1595 and near 1610 cm^{-1}. A specific increase in the intensity of the latter band is observed when deal Y is filled with the oligomer at 350 K

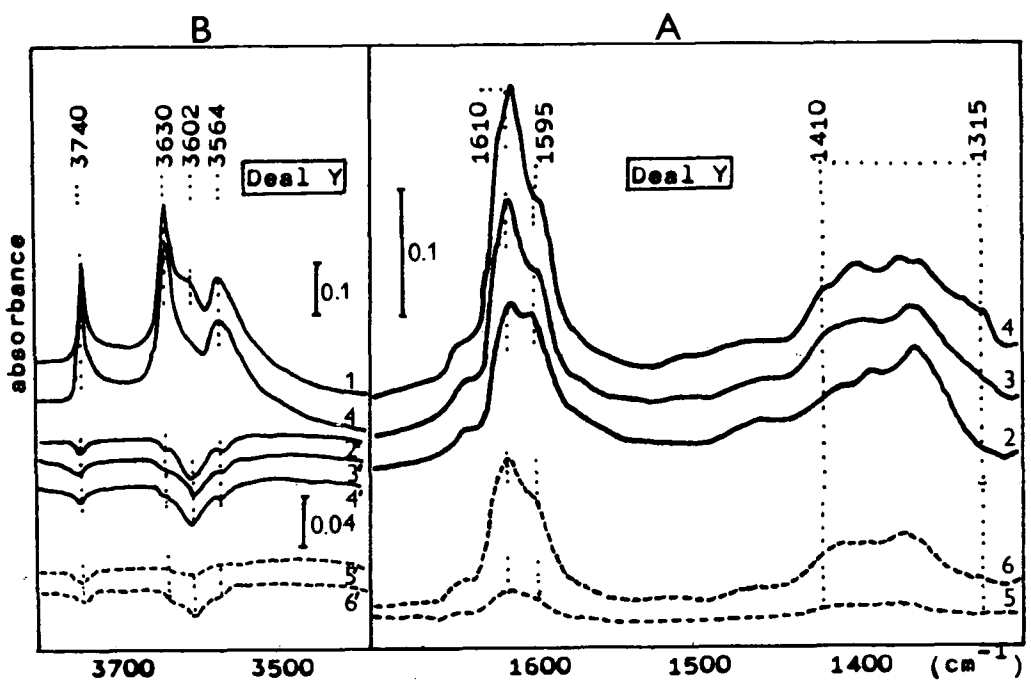

Fig. 3. IR spectra of coke (A) and OH groups (B) of the deal Y zeolite.
1- original zeolite, 2,3,4- after transformation of low-temperature oligomers and reaction of ethylene at 670 K for 15, 30 and 60 min., respectively, 5,6- after reaction of ethylene with fresh zeolite at 670 K for 15 and 60 min., respectively; 2'-6'. difference spectra of OH groups.

prior the reaction of ethylene at 670 K. Then the coke formed at the expense of the oligomer substitutes the most acidic hydroxyls at 3602 cm^{-1} giving rise to the appearandce of both the 1595 and 1610 cm^{-1} bands. Further coking is not associated with changes in the composition of the OH groups, but leads to the most pronounced increase in the intensity of 1610 cm^{-1} band (Fig. 3). Thus it can be assumed that the 1595 cm^{-1} band represents polyene species in an intimate contact with the lattice, while the band at 1610 cm^{-1} corresponds to the component of the coke which might be responsible for the pore chocking. Fig. 3 also shows that the reaction of ethylene with the fresh sample at 670 K is accompanied by a simultaneous increase in intensity of both the bands of coke and a decrease of the 3602 cm^{-1} band of most acidic hydroxyls. This result should be interpreted as implying continuous poisoning of the acid sites and pore chocking from the beginning of reaction.

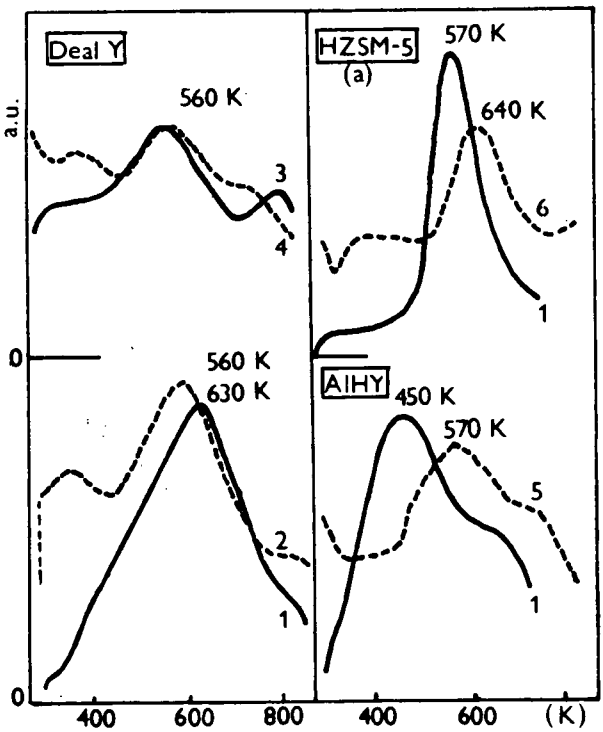

Fig. 4. Effect of coke on the TPD of ammonia from the deal Y, AlHZSM-5 and AlHY zeolites. 1- original zeolite, 2,3,4,5,6- zeolites with coke in amount of 3, 9.7, 19.2, 6.7 and 7.4 mg g^{-1}, respectively.

In contrast to Y zeolites, the ZSM-5 zeolites contain coke consisting apparently of polyene chains and bulky aromatics and exhibiting a higher H/C ratio. This is evidenced by bands at 1590, 1540 and 1465 - 1315 cm^{-1} (Fig. 2) representing vibrations of C=C, the aromatic ring and CH_n groups, respectively.

TPD of ammonia. The TPD curves of ammonia evolved from AlHY, deal Y and HZSM-5 are depicted in Fig. 4. It can be seen that the presence of coke substantially changes the shape of the curves; the maximum effect is again reserved for the lowest amount of the coke. The original zeolites consume almost all the ammonia dosed at 295 K. Coked samples do not adsorb all the ammonia from the gas phase and the peak

heights are lower, indicating poisoning of the acid sites. For AlHY and HZSM-5, the peaks are shifted to higher temperatures. As it is hardly possible that this could be caused by increased acid strength, hindered ammonia desorption due to pore blocking could explain this shift. With deal Y, the maximum is shifted to lower temperatures, reflecting the poisoning of most of the acid sites. In addition, the desorption curves are also influenced by the limited diffusion caused by the coke.

DISCUSSION

In the course of a catalytic reaction, several types of compounds can be found in the zeolite cavities. Some of them act as reaction intermediates and some represe reaction products with restricted diffusibility hindering their removal from cavitie the remaining species which are stable towards desorption at high temperatures and c be removed only by burning represent the actual coke considered in this paper.

It follows from the above results that the acidic properties of zeolites condi the conversion of ethylene both in the low-temperature oligomerization and in the catalytic reaction at high temperatures: the higher the acid strength of the framework hydroxyls the higher is the reactivity of ethylene and the lower this acid strength the more important the role played by Al electron-accepting sites. Nevertheless, the catalytic power of the latter centres is much less than that of the strongly acidic hydroxyls of ZSM-5 and deal Y zeolites. The same factors were found to govern the coking of Y zeolites. However, ZSM-5 with the highest catalytic activity exhibited substantially lower coking tendency. This distinction supports the suggestion (1) that coking reactions are spatially demanding.

The typical features of this process, occuring on the Y and ZSM-5 zeolites, an reflecting a shape selectivity effect , can be characterized as follows:
i) For Y zeolites at 670 K, ethylene yields C_3-C_5 aliphatics in the gas phase while predominantly polyene species with low hydrogen content appear in zeolite. These species also can be obtained via direct transformation of low-temperature oligomer through heating. In addition, the coking tendency of the samples parallels their low-temperature oligomerization activity. Therefore, coking apparently proceeds via oligomerization, isomerization, hydrogen transfer and cracking steps, of which the first is most probably the rate determining one. ii)In contrast to Y zeolites, the oligomer formed from ethylene on ZSM-5 zeolites at a low temperature is decomposed at 670 K. Coking on ZSM-5 zeolite occurs at a measurable rate at 770 K, when ethylen is rapidly converted to C_6-C_8 monoaromatics, so that the deposit increases in an atmosphere of these substances. This ability to provide monoaromatics probably via rapid condensation of ethylene is apparently closely connected with the high coking tolerance of ZSM-5, as these products can diffuse out of the pores. Nevertheless, further reactions of aromatics can be considered to be responsible for coking. No special relationship was found between the amount of coke on various ZSM-5 samples and their low-temperature oligomerization activity. According to the IR spectra,

the carbonaceous residue is composed of bulky aromatics together with polyene- type structures.

It can thus be concluded that the shape-selectivity factor governs not only the coking tendency of zeolites but also the composition of carbonaceous residues as well as the pathway of their formation. This pathway probably proceeds through oligomer precursors on Y zeolites and through aromatics ones on ZSM-5.

The deactivation effect of even low amount of coke (below 10 mg g^{-1}), tested by the oligomerization of ethylene at 300 K, consists of both the poisoning of acid sites and the blocking of pores near the surface. This is reflected in the loss of part of framework hydroxyls and in the increased resistance to mass transfer (IR spectra, TPD of ammonia). For Y zeolites, two types of polyene coke species were found using IR spectroscopy. The first one, characterized by the band at 1595 cm^{-1}, is supposed to act in the poisoning of the acid sites while the second one, represented with the band at 1610 cm^{-1}, in the chocking of the pores. In the ethylene reaction at 670 K, the formation of both coke species proceeds simultaneously.

REFERENCES

1. Rollmann, L.D., Walsh, D.E., in Progress in Catalyst Deactivation, Ed. Figueiredo, J.L., Martinus Nijhoff Publishers, The Hague, 1982, p. 97 (and refs. therein).
2. Vedrine, J.C., Dejaifve, P., Naccache, C., Derouane, E.G., in New Horizonts in Catalysis, Ed. Seiyama, T., Tanabe, K., Konansha, Tokyo, 1981, Part A, p. 724.
3. Kubelková, L., Nováková, J., Wichterlová, B., Jírů, P., Coll. Czech. Chem. Commun. 45, 2290 (1980).
4. Kubelková, L., Seidl, V., Nováková, J., Bednářová, S., Jírů, P., J. Chem. Soc. Faraday 1, 80, 1367 (1984).
5. U.S. Patent 3, 702, 886.
6. Jacobs, P.A., Catal. Rev. Sci. Eng. 24, 415 (1982).
7. Kubelková, L., Nováková, J., Zeolites, submitted.
8. Datka, J., Zeolites 1, 145 (1981).

INVESTIGATION OF THE DEACTIVATION OF MORDENITE CATALYSTS BY COKE DEPOSITION AND THEIR REGENERATION

J. HAAS[a], F. Fetting[a], L. Gubicza[b]
Institut für Chemische Technologie, TH Darmstadt, Bundesrepublik Deutschland (a)
Department of Technical Chemistry, Hungarian Academy of Science, Veszprem, Hungary (b)

ABSTRACT

Reaction parameter and pretreatment of zeolite catalysts used in this investigation were varied in order to obtain information about the possibilities to reduce deactivation by coke formation. Hydroisomerisation of n-hexane was used as a test reaction to study activity and deactivation of various synthetic and natural mordenites. Improvement of conversion and time on stream could be achieved for the synthetic mordenites by steaming at 450°C and by strong dealumination using HCl to get SiO_2/Al_2O_3 ratios up to 77. These zeolites could be regenerated several times without losing activity. Natural mordenites from the Tokaj-mountains (Hungary) gave satisfying results only after doping with platinum. Indications were obtained that the isomerisation reaction and the coking reaction proceed independently.

INTRODUCTION

Today zeolite catalysts are mainly applied for acid catalytic cracking and isomerisation reactions because of their strong acidity and their shape selectivity. However, during these reactions coke is formed by undesired side reactions. Coke, according to Venuto and Habib [1], is a high polymer deposition on the catalyst surface with a high carbon content. The nature and the chemistry of formation of these deposits are hitherto largely unknown. For this reason deactivation of a zeolite catalyst by coke deposition was studied using the hydroisomerisation of n-hexane on various modified mordenites as an example.

The mordenite which is rich in silicon exhibits a comparatively

high stability at high temperature and when treated with acid. Therefore it can be modified by various means without losing cristallinity. The mordenites used in this investigation were modified by exchange with Pt-complex compounds, by acid treatment and following calcination or by ammonia exchange and following defined steaming.

Isomerisation of n-hexane was chosen because this reaction can easily be handled and is almost isothermal. At the same time this reaction exhibits all features necessary to study the capabilities of zeolite catalysts. Publications about kinetics and mechanism of this reaction are available [2,3,4], yet little has been published about deactivation by coking during this reaction. Therefore, this investigation aims to prolong the time on stream by modifying natural and synthetic mordenites and by adjustment of the reaction parameters. At the same time the yield of branched hexane isomers should be as high as possible. Furthermore, these catalysts were tested with respect to their stability for regeneration by burning off the coke.

EXPERIMENTAL

Reactions were performed in an isothermal differential tube reactor. Products were analysed by gaschromatography. The regeneration of the coked catalysts was possible "in situ" by burning the coke in a stream of 5% oxygen in nitrogen at 550°C. Amounts of CO and CO_2 produced by this were determined by an infrared analyser. From this the original amount of coke could be calculated.

3 g mordenite were used for each run; when applying the natural Tokaj-mordenite a larger amount was used corresponding to the impurities. The reaction conditions held constant for all runs are shown in table 1.

Table 1
Reaction conditions for all runs

Flow of n-hexane	0.2 ml/min
Flow of hydrogen	200 ml/min
Total pressure	25 bar
Temperature	280°C
Time on stream	4 or 4.5 h
WHSV	2.64 g/g·h

The catalysts were activated inside the reactor by a hydrogen flow at 350°C for 1.5 hours.

Synthetic mordenite "Zeolon 100 H" from Norton and natural mordenite from the Tokaj-mountains (Hungary) were the basic materials from which modifications were obtained. Part of this material was treated with 1 N or 6 N HCl under reflux for various lengths of time. This was followed by "deep bed" calcination at 550°C for 16 hours. Another part of Zeolon 100 H was exchanged by ammonium nitrate and thereupon hydrothermally treated between 300 and 600°C whereupon the H-form was rebuilt. This steaming was performed in a special quartz tube with heaters through which air (55 l/h) loaded with water vapor was passed [5]. The partial pressure of the water was 306 Torr. 8 g of NH_4-mordenite were steamed for 4 hours at a time.

A part of the acid treated Tokaj-mordenite was afterwards doped with platinum in the following way: The mordenite was stirred for 24 hours in a cold water solution of $Pt(NH_3)_4CL_2$ corresponding to 0.5 w.% whereby the exchange resulted quantitatively. Reduction in a stream of hydrogen at 200 and 400°C followed. The catalyst material was pelletized to pellets with a mean diameter of 2.5 mm. Table 2 summarizes all used catalyst modifications.

Table 2

Modifications of mordenites used

H-mordenite	modulus[×] 23.3, 34.1, 59.2, 68.6, 77.8
NH_4-mordenite	steamed at 300, 400, 450, 500, 600°C
Tokaj-H-mordenite	modulus 23, 34
0.5 w.% Pt-Tokaj-mordenite	modulus 23, 34

[×] Modulus is defined as molar ratio SiO_2/Al_2O_3

RESULTS AND DISCUSSION

Synthetic H-mordenites

Typical Features of Deactivation

A typical example of rapid deactivation is shown in fig. 1.

Activity of the H-mordenite with a modulus of 23.3 decreases to 50% after 30 minutes and to 25% after 2 hours. The exponential falling-off of the conversion is accompanied by an increase of the formed amount of coke. Strong coking at the beginning of the reaction is striking. So, after 10 minutes 50% of the final amount of coke is formed. Only little increase of the amount of coke can be observed after 2 hours because conversion has already reached a low level. A similar course of coke production was obtained by Shiring et al. [6].

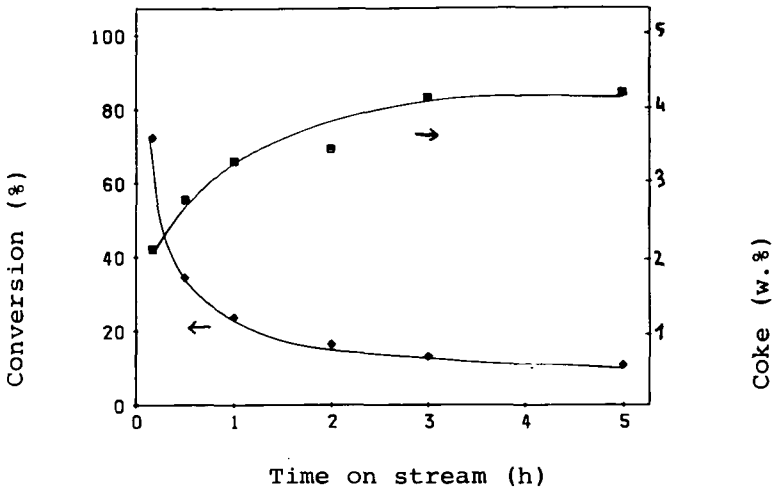

Fig. 1. Conversion and amount of coke vs. time on stream

It seems to be plausible that initially certain active centers of the catalyst are blocked. This effects cracking- and isomerisation processes quite differently as can be seen in fig. 2 which shows product yields of cracking and isomerisation. Coke deposition during the first hour of reaction causes a very strong decrease of cracking activity of the catalyst. Isomerisation conversion even shows a little increase during this time but it is usually only slightly influenced by coke formation. Yet, a strong correlation between coke formation and cracking activity is to be noted. It can therefore be assumed that by decrease of cracking activity less coke will be produced and at the same time the deactivation will be lowered. By this the selecti-

vities of hexane isomers will be raised.

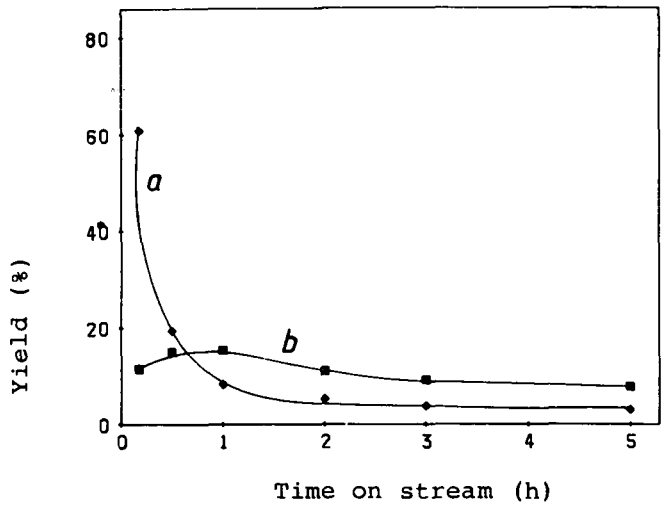

Fig. 2. Yields of cracking (a) and isomerisation (b) vs. time on stream

Influence of reaction parameters on deactivation

Much suppression of the cracking reaction can be achieved by lowering the reaction temperature. This can be seen in fig. 3 in which the ratio of hexane isomers to cracking products is drawn against time on stream. The modulus and reaction temperature were varied. The effects are so drastic that a logarithmic ordinate has to be chosen. The ratio of hexane isomers to cracking products covers the region between 0.1 and 100 for high temperatures as well as high initial conversions and for 250°C-reaction temperature as well as strong dealumination respectively. The four curves in fig. 3 nicely demonstrate the synergistic effect between reaction temperature and modulus. The mentioned ratio always decreases with increasing temperature; the decrease can partly be compensated by an increase of the modulus.

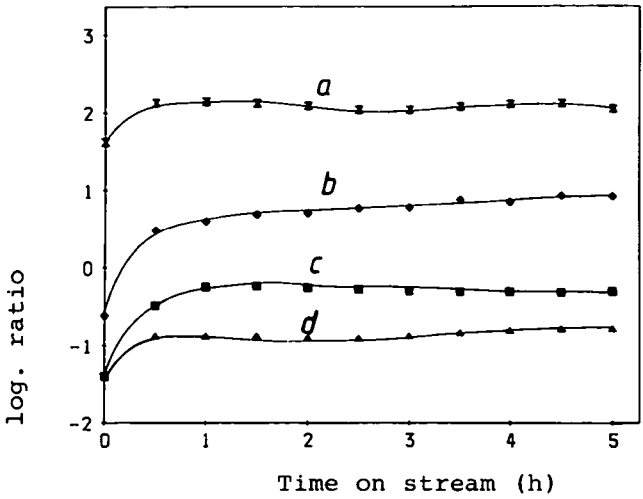

Fig. 3. Dependence of the ratio of n-hexane isomers/cracking products on modulus, reaction temperature and time on stream: a) modulus 77.8, 250°C, b) modulus 34.1, 250°C, c) modulus 77.8, 350°C, d) modulus 34.1, 350°C.

Suppression of cracking reactions by lowering the reaction temperature,however, causes a strong decline of conversion. Conversion can again be improved by an increase of total pressure and of the hydrogen partial pressure. Deactivation is also diminished by this. Optimization with respect to activity and time on stream can only be achieved in a limited way by variation of the reaction parameters. A real improvement can only be gained by modification of the zeolite structure. This is shown next with the example of hydrothermal treatment.

Influence of the modifications of the catalyst

In fig. 4 is shown how conversion and yields of cracking products and branched hexane isomers depend on steam temperature for an ammonia mordenite after 2 h time on stream. A distinct maximum can be seen at 450°C for all curves. The decrease of conversion at low temperatures is assumed to be due to the fact that ammonia is not completely decom-

posed and still blocks active centers. The decrease of conversion at higher steam temperatures on the other hand is caused by AlO^{+}-cations occupying active centers which are produced by the dealumination process. It is interesting to note that all three curves are more or less parallel. The strong influence of the AlO^{+}-cations should be mentioned; they cause the cracking reactions to stop because they apparently preferably block those centers that produce cracking products.

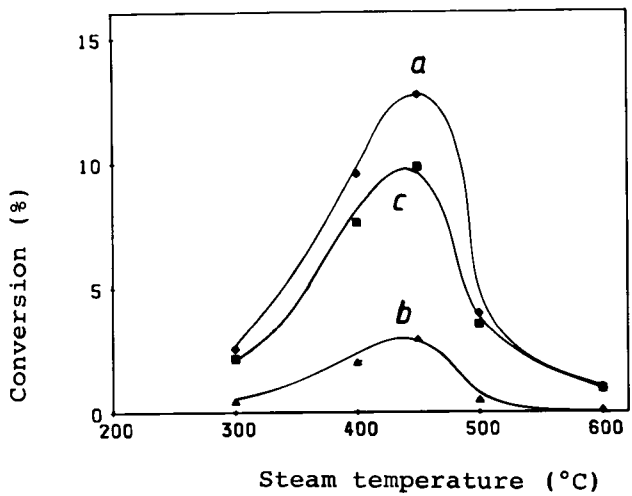

Fig. 4. Dependence of conversion (a) and yields of cracking (b) and isomerisation (c) on steam temperature

An increase of n-hexane isomer yields in connection with diminishing deactivation can also be achieved by strong dealumination of the mordenite by HCl. This treatment causes an increase of strong Broensted acid sites while the total number of OH-groups decreases [7]. Fig. 5 shows the yields of cracking products and branched hexane isomers and the conversion in dependence of the modulus after 2 h time on stream. Conversion and yields decrease slightly with increasing degree of dealumination for lower values of the modulus. However, for strong dealunination yields for branched hexane isomers increase, this in turn causes conversion to increase in spite of decreasing cracking activity. If the modulus is larger than 68 the catalyst exhibits a substantially

smaller tendency to coke and the amount of coke produced is essentially less. So, the mordenite with a modulus of 68.6 still shows a conversion of 14% even after 4 h time on stream. For the two most dealuminated mordenites even after 4 h the yields for n-hexane isomers are still between 10 and 11%.

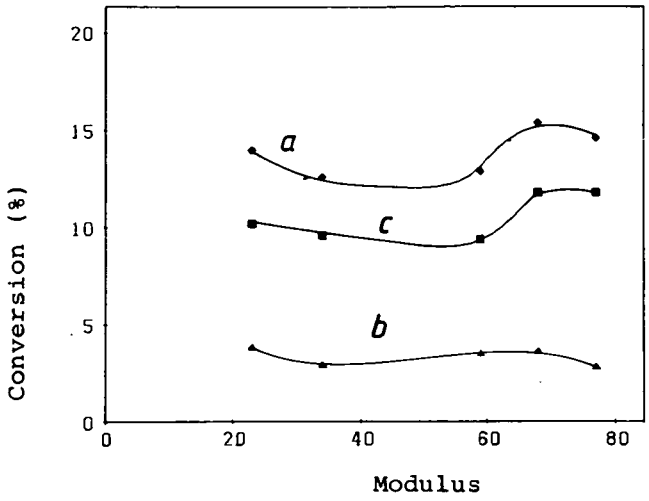

Fig. 5. Dependence of conversion (a) and yields of cracking (b) and isomerisation (c) on modulus.

Natural Tokaj-mordenite

While in the case of synthetic mordenites even small dealumination results in a decrease of conversion, the activity of natural Tokaj mordenites can be increased by raising the modulus from 23 to 34. This is probably due to a slight widening of the pores by acid treatment which is not observed with the synthetic mordenite. However, the activity of the Tokaj-mordenite is substantially lower than the synthetic mordenite. It can be increased by addition of platinum to a degreee that is comparable with strongly dealuminated synthetic mordenites. This treatment almost completely suppresses the cracking activity and conversion is more stable. However, even with this catalyst constant conversion for a longer period could not be achieved.

Comparison of the various catalyst modifications

For the final discussion of the catalyst modifications the selectitivies after 1.5 h time on stream of five selected mordenites are compared in fig. 6 . It can be seen, that the selectivities of hexane isomers can be improved by stronger dealumination as well as be steaming at 450°C when compared with a catalyst of a low modulus of 23. It can also be noticed that of the catalysts tested the Tokaj-mordenite shows the lowest selectivities in spite of low conversion-rates. However, the selectivity is better than that of a steamed synthetic catalist when the Tokaj-mordenite is doped with platinum. The trend of these selectivities is also reflected by the deactivation behaviour. The three catalysts with the lowest cracking selectivities exhibit the highest stability of conversion while mordenites with high cracking activity distinctly deactivate faster.

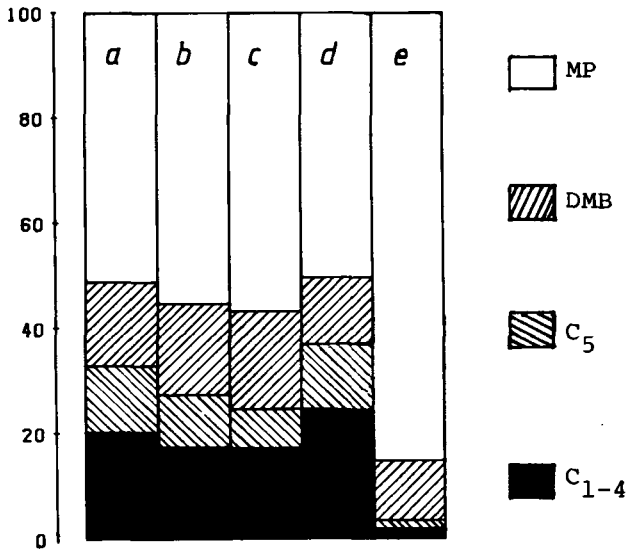

Fig. 6 . Selectivities of five selected mordenites after 1.5 h time on stream: a) H-mordenite modulus 23.3, b) H-mordenite modulus 68.6, c) NH_4-mordenite steamed at 450°C, d) Tokaj-mordenite modulus 23, e) Pt-Tokaj-mordenite modulus 23.

Behaviour on repeated regeneration

Final runs were undertaken to test the activity after repeated

regeneration. Furthermore the influence of residual amounts of coke on the initial activity of the catalyst was investigated. Residual amounts of coke could be realized by variation of the regeneration temperature between 450 and 550°C.

Fig. 7 shows the conversion after 1 h time on stream in dependence of the number of cycles and on the residual amount of coke. Furthermore the ratio methylpentanes/dimethylbutanes is shown which is related to the pore width of the catalyst at the beginning of each reaction period. Initially a pore widening is observed after the first cycle which also causes an increase of conversion. Regeneration was performed at 550°C for this first cycle. The regeneration temperature was lowered by 25°C after each of the following cycles. A distinct decrease of conversion - accompanied by a pore narrowing by residual coke - is only observed after the fifth cycle before which regeneration took place at 475°C. Before this cycle the initial activity was again attained. This proves that H-mordenite can repeatedly be regenerated without losing its activity.

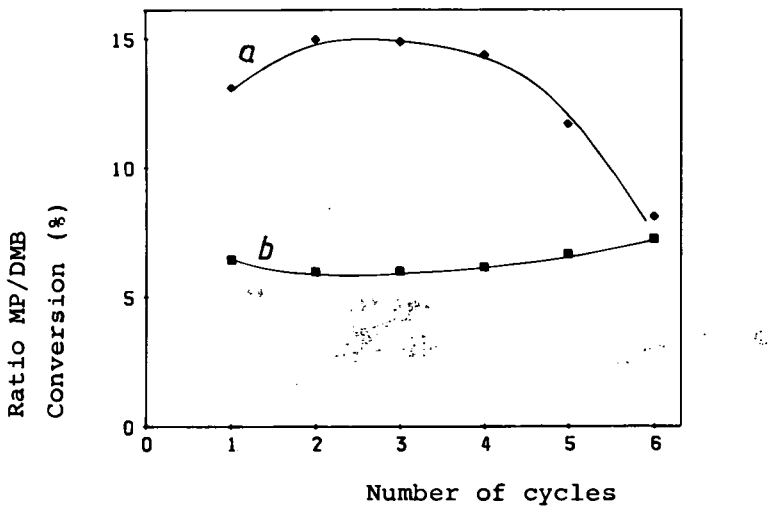

Fig. 7. Dependence of conversion (a) and MP/DMB ratio (b) on the number of cycles and the residual amount of coke.

FORMATION OF DEPOSIT AND AROMATICS ON HNaY ZEOLITE

J.HABER, J.KOMOREK, T.ROMOTOWSKI
Institute of Catalysis and Surface Chemistry of Polish Academy of Sciences, Cracow, Poland

ABSTRACT

Formation of deposit /i.r. band 1600 cm^{-1}/ and aromatics or their precursors such as cyclic oligomer /1500 cm^{-1}/ through a common oligomer on HNaY zeolite was studied using i.r. spectroscopy. Olefins, isopropanol, aromatics and unsaturated aliphatic cyclo-compounds were used as adsorbates in the range 301-673 K. Deposit formation preceded aromatics, which were never observed before appearing of deposit. Aromatics were not formed from deposit but always in the presence of it and were not necessary for deposit formation. There are two paths of oligomer transformation: one to deposit and the second, after a suitable modification of HNaY zeolite by deposit, to aromatics. The two processes can be separated at relatively low temperature but they occur very fast at 673 K before the full deactivation of HNaY zeolite.

INTRODUCTION

Our earlier investigations of the adsorption of alcohols, ethers and olefins on ZSM-5 and HNaY zeolites showed that olefins play an important role in transformations of alcohols and ethers into hydrocarbons /1/.

Olefins are transformed into desorbable species characterized by i.r. absorption band about 1500-1518 cm^{-1} and to carbonaceous deposit called also coke /i.r. band about 1600 cm^{-1}/.

Formation of oligomers and deposits from olefins and others molecules on decationized zeolites was studied in many papers /2-14/ and different hypothesis were advanced as to the nature of the deposit. It was described as aliphatic /polyens/ or /and, at least at higher temperatures, aromatic/ hydrogen-poor condensed aromatics or alkylaromatics non desorbable species/, which could be removed from a zeolite only by burning with air or oxygen.

We assumed earlier that the band about 1500 cm^{-1} is due to a shift of double bond in an olefin and we assigned this band to an electron-deficient double bond or even to stabilized carbenium ion /15,16/.

An olefin adsorbed on decationized zeolite forms a carbo-cation and transforms into an oligomer /1,2/, clearly visible in the case of ethylene. This oligomer seems to be present in the form of stabilized carbo-cation /6/. The spectrum of a saturated species after adsorption of an olefin on decationized zeolite is then the spectrum of a stabilized alkyl carbo-cation without any i.r. bands about 1500 cm^{-1} /6/.

The results described in /1/ made us to conclude that the oligomer transforms into another species, the appearance of the 1500 cm^{-1} band being not due to the shift of double band, because diminishing intensities of oligomer bands indicated that some cyclization might take place. The region of 1430-1600 cm^{-1} is characteristic for the group frequencies of aromatic compounds which show the bands of the breathing vibrations at 1430-1500 and 1580-1600 cm^{-1}. Taking in to account that some authors /17,18/ assigned the band at 1500 cm^{-1} to aromatics and that the same band appears also at higher temperatures /without evacuation/, we assumed its appearance indicates the formation of aromatic species or at least their adsorbed precursors such as cyclic oligomers /possibly in form carbo-cations/, though the temperature is very low. In this connection we may quote /19/ the existence of an alkenyl carbo-cation with an intense band at 1533 cm^{-1}, the only band between 2850 and 1450 cm^{-1}. The 1500 cm^{-1} band and bands of oligomer disappear after evacuation and heating to about 523 K /in many cases oligomer is more strongly adsorbed than species with 1500 cm^{-1}/, but up to this temperature aromatics are not appearing in the products /7/. It could be supposed that species characterized by the band about 1500 cm^{-1} is at least an intermediate or precursor of aromatics which at higher temperature desorbs in form of aromatics. We shall thus call it "aromatics" although its nature is not yet fully known.

Propertions of aromatics and deposit depend on the type of zeolite. In preliminary experiments on HZSM-5 zeolite only the formation of aromatics was observed, whereas on HNaY zeolite mainly the deposit and only a small amount of "aromatics" were formed.

The mechanism of formation of deposit and "aromatics" on HNaY zeolite is not yet fully understood and it seemed of interest to

study this mechanism by monitoring the transformations of some molecules on HNaY zeolite with i.r. spectroscopy.

EXPERIMENTAL

The decationized form of HNaY zeolite was obtained from the NaY parent zeolite of the composition: 0.87 $Na_2O \cdot Al_2O_3 \cdot 5.05\ SiO_2 \times H_2O$ by exchange of ammonium ions /degree of exchange 71 %/. Samples were pressed into self-supported plates and placed in the high temperature vacuum cell /20/, connected to conventional vacuum apparatus. Adsorption and desorption of adsorbates were carried out at temperatures from 301 - 318 to 673 K and from several Torr to 10^{-1} - 10^{-5} Torr.

All the adsorbates were of pure grade: propene, but-1-ene, dec-1-ene, isopropanol, benzene, toluene, p-xylene, ethylbenzene, cumene, cyclohexene, cyclohexadienen /1,3/, methyl-1-cyclohexe-1-ene, methyl-1-cyclohexadiene /1,3/ and cyclopentene.

I.r. spectra were recorded on a double beam spectrophotometer UR-20 /Zeiss/.

RESULTS AND DISCUSSION

Adsorption of olefins on HNaY Zeolite

After adsorption of propene on HNaY zeolite, beside the i.r. absorption bands of the oligomer /1470 cm^{-1} and 2880-3000 cm^{-1}/ the band of deposit /1600 cm^{-1}/ /Fig.1/ was observed already at 301 or 318 K. On heating the i.r. bands of oligomer diminished and that of deposit increased. It is noteworthy that the band of the deposit appeared before the i.r. shoulder or band of "aromatics" /1500 cm^{-1}/ were formed in the range of 343-373 K. In the range of 348-423 K new i.r. bands about 1350 cm^{-1} appeared, which could be connected with isomerization of oligomer yielding more branched structures, containing tertiary groups. At 623 K "aromatics" desorbed, but oligomer remained in the zeolite. I.r. bands of OH groups were rebuilt after heating but they did not reach their initial intensities. After oligomer desorption a new band between 1350 and 1400 cm^{-1} developed which was earlier tentatively assigned by us as symmetric vibration of carboxylate species /1/.

On HNaY zeolite "aromatics" were never formed before appearing of the deposit. It may be thus concluded that deposit modifies the system of cages and channels of HNaY zeolite making possible the formation of small molecules, which can then desorb.

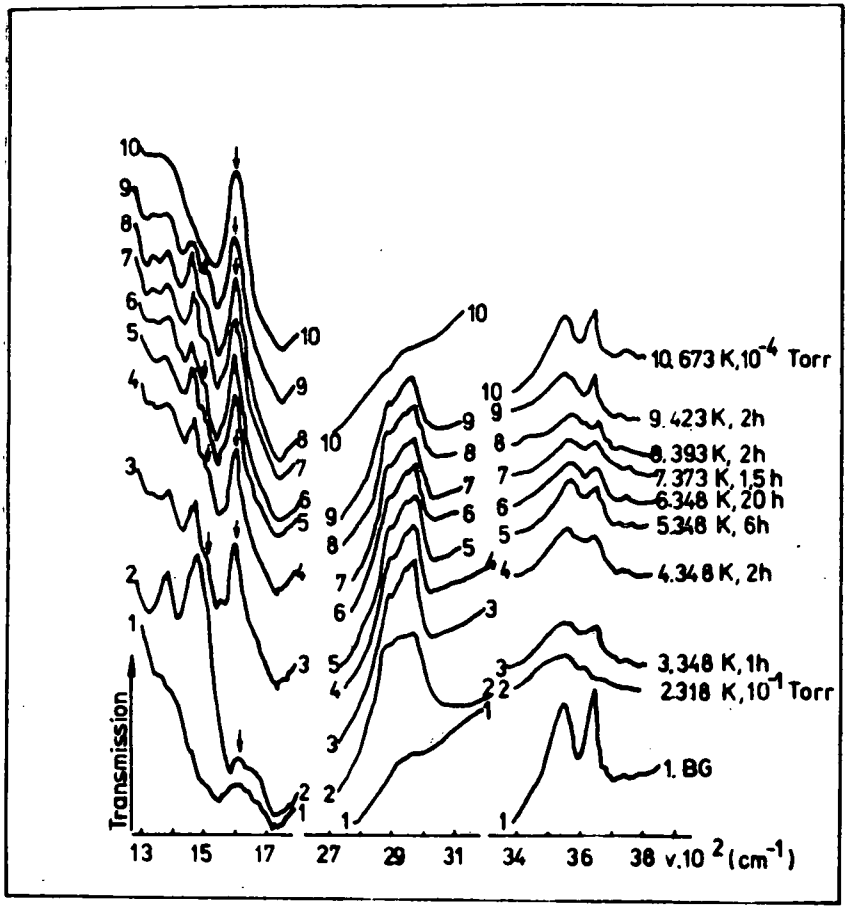

Fig. 1. Spectra of propene adsorbed on HNaY zeolite

When small portions of propene were consecutively adsorbed on HNaY zeolite it was found that adsorption of about 31 molecules of propene per unit cell resulted in the complete disappearance of HF OH groups at 3650 cm^{-1}. It may be concluded that the oligomer contains on an average 12 carbon atoms, the same as that found in /2/ after adsorption of butene.

In the case of but-1-ene and dec-1-ene on HNaY zeolite, similarly as in case of propene the deposit appeared at 301 and 318 K and "aromatics" at 398 and 363 K respectively.

In the case of dec-1-ene the oligomer was formed instantaneously because dec-1-ene could directly form stabilized carbo-cation.

Adsorption of aromatics and alkylaromatics on HNaY zeolite

No i.r. band of deposit were observed in spectra after adsorption of benzene and toluene on HNaY up to 673 K, what rules out the

possibility that aromatics and alkylaromatics form deposit in this temperature range.

Spectra recorded during adsorption of p-xylene on HNaY zeolite showed that deposit band appeared from 533 K as a result of p-xylene dealkylation and formation of reactive species as e.g. olefins.

Adsorption of ethylbenzene was carried out in such a way that before every registration of spectrum with a change of temperature, the sample was outpumped in order to expose deposit band screened by the spectrum of ethylbenzene. The band of deposit /most probably formed from ethylene/ was observed at 533 K, its intensity increasing with temperature.

The procedure by adsorption of cumene was the same as for ethylbenzene in order to expose the band of deposit which was observed at 423 K. Some changes in the spectra after heating of cumene were connected with its decomposition to benzene and propene. A shoulder appearing at 533 K at 1500 cm^{-1} could be assigned to the band of "aromatics" originating from propene.

It may be thus concluded that in the case of alkylaromatics the deposit appears first at such a temperature, whereat decomposition of alkylaromatics begins, resulting in the formation of reactive species such as olefins.

Adsorption of isopropanol on HNaY zeolite

Bands of isopropanol, water and deposit were present in the spectrum of adsorbed isopropanol /318 K/, which after heating to 353 K resembled the spectrum from olefins. At 373 K the intensity of deposit band increased, whereas that of oligomer bands diminished and a new band about 1350 cm^{-1} appeared. At 403 K a shoulder appeared about 1500 cm^{-1}, becoming more pronounced at 443 K, the band at 1350 cm^{-1} also increased in intensity and changed its shape. Evacuation at 318 K caused disappearance of the band of water and exposure of the big band of deposit. The band of "aromatics" was clearly visible and reappearance of OH groups began. After heating to 673 K following bands were only left: deposit, weakened OH groups and the band about 1350 cm^{-1}.

Adsorption of isopropanol on HNaY zeolite resembles thus that of olefins /oligomerization goes fast at 353 K/ but presence of water hinders the formation of "aromatics" which become visible in the spectrum only at 403 K.

Adsorption of unsaturated aliphatic cyclocompounds on HNaY

It seemed interesting to investigate adsorption of some unsatu-

rated aliphatic cyclocompounds on HNaY zeolite to explain their role as possible precursors of aromatics in the reaction sequence: cyclohexene → cyclohexadiene → benzene.

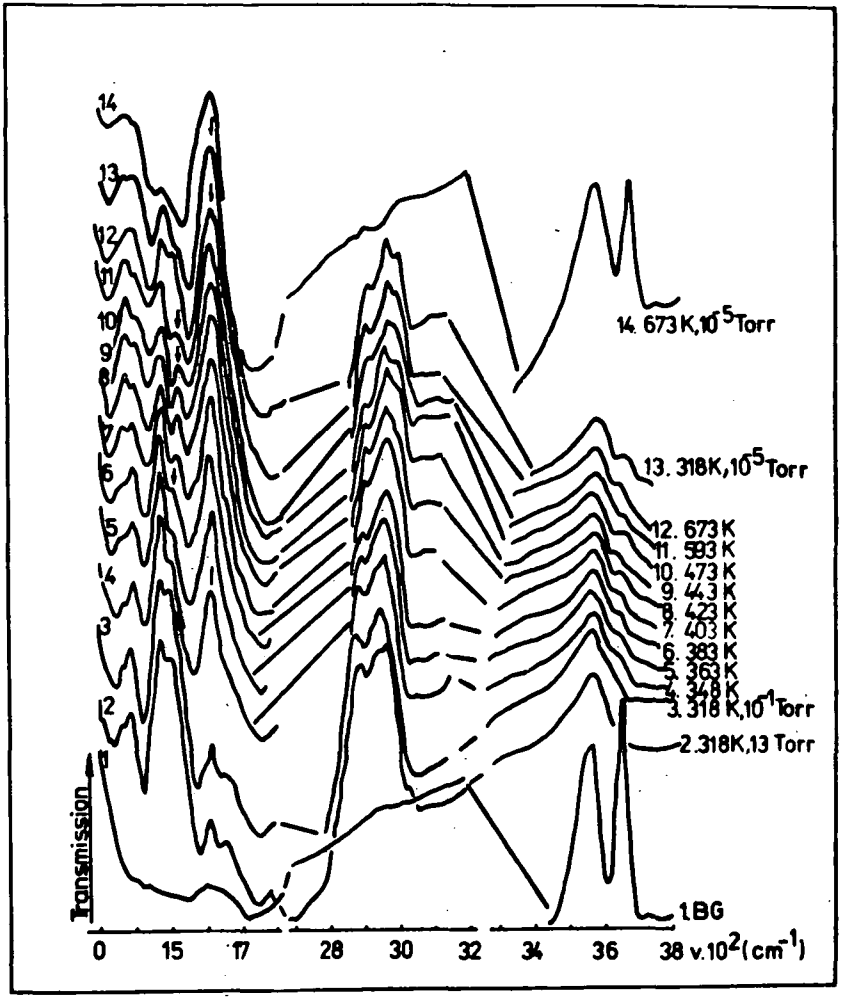

Fig. 2. Spectra of methyl-1-cyclohex-1-ene adsorbed on HNaY Zeolite

The set of i.r. bands characteristic for adsorbed methyl-1-cyclohex-1-ene is very similar to that of an oligomer formed from an olefin on HNaY /Fig.2/ and behavee in a way similar to that of an oligomer, revealing that deposit and "aromatics" are formed on heating. It may be thus concluded that after adsorption of methyl-1-cyclohex-1-ene an appropriate type of oligomer is formed. The band at 1490 cm^{-1} not observed before could belong to this type of oligomer, but its intensity diminished much faster that those of

other bands of oligomer and disappeared below 373 K, "aromatics" beginning to appear above this temperature.

Heating to 348 and 363 K caused the decrease of all oligomer bands /the band at 1490 cm^{-1} most rapidly/ and considerable growth of deposit band. At 373 K the band of "aromatics" appeared at 1503 cm^{-1}, its intensity increasing at 403 K. The oligomer bands diminished, that of deposit grew and a group of bands at 1360 cm^{-1} increased and changed its pattern. After heating to 423 K the band of "aromatics" /1510 cm^{-1}/ and that at 1360 cm^{-1} increased, the former reaching its maximum at 443 K. The group of bands at 1360 cm^{-1} was at its maximum at 473 K. After evacuation at 673 K only following bands remained: strong deposit, one at 1350 cm^{-1} and weakened OH groups.

The sequence given above resembles that obtained after adsorption of an olefin on HNaY zeolite: deposit is formed first, "aromatics" later.

Adsorption of cyclohexene on HNaY was quite similar to the case of methyl-1-cyclohex-1-ene. Deposit started to form at 318 and "aromatics" at 383 K.

Adsorption of cyclopentene is also similar to that of methyl-1-cyclohex-1-ene: deposit at 318 K and the band about 1500 cm^{-1} at 403 K. It is necessary to stress that the difference in the ring structure of the adsorptive does not influence the results.

Adsorption of methyl-1-cyclohexadiene /1,3/ on HNaY resembles that of methyl-1-cyclohex-1-ene: deposit is formed at 318 and "aromatics" from 383 K. Similarly cyclohexadiene /1,3/ gives deposit at 318 and "aromatics" at 363 K.

Results described above enable following conclusions to be formulated:

1. appearance of the deposit /the characteristic band at about 1500 cm^{-1}/ from the oligomer, formed earlier from: propene, but-1-ene, dec-1-ene, isopropanol, cyclohexene, cyclohexadiene /1,3/ methyl-1-cyclohex-1-ene, methyl-1-cyclohexadiene /1,3/ and cyclopentene on HNaY zeolite occurs in the temperature range 301-318 K and always precedes the formation of "aromatics" /the characteristic band about 1500 cm^{-1}/,

2. "aromatics" were formed at relatively low temperatures: from olefins at 348-363 K, from isopropanol at 403 K and from investigated unsaturated aliphatic cyclocompounds at 363-403 K,

3. "aromatics" were not observed before the appearance of the deposit, what indicates that "aromatics" were not the source

for deposit formation,

4. formation of "aromatics" from deposit was not detected,

5. deposit was not formed from benzene or toluene /up to 673 K/ but it was generated by adsorption of p-xylene and ethylbenzene at 533 K and cumene at 423 K, i.e. at temperatures higher than those necessary for the formation of deposit and aromatics from olefins and unsaturated aliphatic cyclocompounds; it may be concluded that deposit was obtained from alkylaromatics only after their dealkylation and appearance of some reactive species as e.g. olefins,

6. only two central members of the sequence: cyclohexane → cyclohexene → cyclohexadiene → benzene can transform into deposit in mild conditions /at 318 K/,

7. in the case of unsaturated aliphatic cyclocompounds the ring structure does not influence their transformations,

8. a new band at 1350 cm^{-1} was observed at higher temperatures and its assignment is not clear; it may be assigned to carboxylate species though the appropriate asymmetric vibration band with few exception was not observed; it could be screened by very strong deposit band,

9. intensities of OH group diminish after deposit formation,

10. "aromatics" appear on HNaY zeolite always in the presence of deposit,

11. it can be assumed that at the beginning favourable conditions exist in supercages of HNaY zeolite for the formation of big molecules of deposit from the oligomer and these molecules have no possibility to leave the zeolit; by formation of the deposit the system of cages and channels of the HNaY zeolite is modified and in some regions conditions arise for oligomer transformation to small aromatic species which are able to desorb from the system.

This modyfication may consist e.g. in such distribution of the deposit that the resulting geometry of cages and channels resembles that existing in ZSM-5 zeolite. Thus, two paths of oligomer transformation exist: the first /especially fovoured in fresh samples/ to deposit and the second, after a suitable modification of supercages by the deposit earlier formed, to some desorbable species of aromatic character; these processes can be separated at relatively low temperature under nonstationary conditions when the coverage by the deposit has not yet caused the complete deactivation of HNaY zeolite, but they proceed very fast at 673 K.

REFERENCES

1. Haber, J., Komorek-Hłodzik, J., Romotowski, T., Zeolites 2, 179 /1982/.
2. Datka, J., J. Chem. Soc. Faraday Trans. I, 76, 2437 /1980/.
3. Datka, J., J. Chem. Soc. Faraday Trans. I, 77, 391 /1981/.
4. Datka, J., J. Chem. Soc. Faraday Trans. I, 77, 511 /1981/.
5. Datka, J., Bull. Acad. Polon. Sci. Ser. Sci. Chim. 28, 669 /1980/.
6. Datka, J., Zeolites 1, 113 /1981/.
7. Datka, J., Zeolites 1, 145 /1981/.
8. Langer, B.E., J. Catal. 65, 16 /1980/.
9. Dejaife, P., Auroux, A., Gravelle, P.C., Vedrine, J.C., Gabelica, Z., Derouane, E.G., J. Catal. 70, 123 /1981/.
10. Samoilov, N.A., React. Kinet. Catal. Lett. 19, 5 /1982/.
11. Blackmond, D.G., Goodwin, J.G., Lester, J.E., J. Catal. 78, 34 /1982/.
12. Blackmond, D.G., Goodwin, J.G., Lester, J.E., J. Catal. 78, 247 /1982/.
13. Dźwigaj, S., Haber, J., Romotowski, T., Zeolites 4, 147 /1984/.
14. Karge, H.G., Abke, W., Boldingh, E.P., Łaniecki, M., Proc. 9th Iberoamerican Symp. on Catal., Lisbon, 582 /1984/.
15. Bezuhanova, C.P., Lechert, H.T., Dimitrov, C., Nenova, V.V., J. Mol. Struct. 11, 301 /1984/.
16. Dimitrov, C., Bezuhanova, C.P., Nenova, V.V., J. Catal. 80, 457 /1983/.
17. Novaková, J., Kubelková, L., Dolejšěk, Z., Jirů, P., Collection Czechoslov. Chem. Comm. 44, 3341 /1979/.
18. Bolis, V., Vedrine, J.C., Van den Berg, J.P., Wolthuizen, J.P., Derouane, E.G., J. Chem. Soc. Faraday Trans. I, 76, 1606 /1980/.
19. Deno, N.C., Richey, H.G., Hodge, J.D., Wisotsky, M.J., J. Amer. Chem. Soc. 8, 1498 /1962/.
20. Haber, J., Piekarska-Sadowska, H., Romotowski, T., Bull. Acad. Polon. Sci. Ser. Sci. Chim. 26, 967 /1978/.

EFFECT OF COKE ON Y ZEOLITE ACTIVITY FOR CUMENE CRACKING

W.J. HATCHER, JR.

Department of Chemical Engineering, The University of Alabama, University, AL 35486 USA.

ABSTRACT

Carbonaceous deposits on a lanthanum-exchanged Y zeolite results in an exponential relationship with catalytic activity for cumene cracking. The observed relationship can be attributed to several possible mechanisms. One mechanism that fits the experimental data involves multilayer coke formation. Parameters from this model suggest that the rate of coke chain growth or polymerization increases rapidly with increasing temperature. Titration experiments show that active sites for cumene cracking have approximately equal strengths since initial catalyst activity was found to decrease in direct proportion to the amount of sorbed pyridine. Diffusivities measured by a chromatographic technique indicate no significant difference in values between fresh catalyst and catalyst with 5 percent coke. Therefore, pore blockage does not appear significant.

INTRODUCTION

The activity of cracking catalysts declines rapidly because of the accumulation of carbonaceous deposits on the catalyst surface. This phenomenon has very significant economic importance and, therefore, has been the subject of a number of studies over the years. Experimental studies on lanthanum-exchanged Y zeolite for isopropylbenzene (cumene) cracking in our laboratory demonstrated an exponential relationship between total coke deposited on the catalyst and catalyst activity decline [1,2]. The observed relationship between coke level and catalyst activity can be attributed to several possible mechanisms.

For example, if the catalytically active sites have a distribution of strengths and the strongest sites were deactivated first, a exponential coke-activity relationship would be found. Another explanation, outlined by Beeckman and Froment [3], is that a pore blockage mechanism, for certain parameter values, provides an exponential relationship between catalyst activity and coke content. A third possibility, proposed by Nam and Kittrell

[4], is that both monolayer and multilayers of coke form on the surface. This model can predict linear, hyperbolic, or exponential activity-coke relationships depending on parameter values.

Acid catalysts such as zeolites can be readily poisoned by basic organic compounds. One of the earlier studies of the deactivation of amorphous silica-alumina cracking catalysts by organic compounds such as quinoline, quinaldine, pyrrole, piperidine, decylamine, and aniline was done by Mills et al [5]. A poisoning study by titration of quinoline on zeolite catalyst was investigated by Goldstein and Morgan [6]. They concluded that the amount of quinoline required to completely poison the zeolite was equal to the number of supercages in its structure.

EXPERIMENTAL

The lanthanum-exchanged Y zeolite (La Y) was made by contacting an ammonium Y (Linde type 31-200 powder) with an aqueous solution of lanthanum chloride. Approximately 60-70 percent of the ammonium ions were exchanged in the procedure. The resulting La Y powder was pressed into tablets without binder, crushed and sieved to -60+80 mesh.

A thermogravimetric analyzer was used as the reactor in this study. Coke on catalyst was measured by weight change of the catalyst and cumene conversion by chromatographic analysis of product gases. For the coking study cumene was continuously introduced into the reactor by passing helium through a sparger containing cumene. Additional details of the equipment has been previously reported [1].

For the titration study a certain amount of pyridine was injected into a stream of heated helium. After adsorption of pyridine, helium flow was continued to purge the remaining pyridine from the system and to desorb physically adsorbed pyridine from the catalyst. This purge was for 30 minutes. The final amount of pyridine loading was determined by the catalyst weight change. Then cumene was introduced to test the cracking activity of partially poisoned catalyst.

Diffusivities in fresh and coked catalysts were measured by a chromatographic technique. Chromatographic curves were measured using a constant-temperature gas chromatograph (Perkin-Elmer Model 820) with a thermal conductivity detector. Helium was used as the carrier gas, and measurements were made by injecting a small pulse of adsorbable component plus helium into the pure helium carrier. A four way, two position sampling valve was used to inject the pulse. The adsorbable component stream was prepared by passing a pure helium stream through a sparger containing the hydrocarbon. The column was 34 cm long by 0.483 cm inside diameter.

RESULTS

Cumene conversion at the low cumene partial pressures studied resulted in the formation of benzene, propylene and coke. No secondary reaction gaseous products were found. Reaction rates (r) for the differential conversion data were calculated from:

$$r = F_A X_A / W \quad (1)$$

where F_A is the moles/s of cumene flowing, X_A the fractional conversion of cumene and W the catalyst mass. The initial reaction rates (r_o, at zero coke) fit a first order model with respect to cumene partial pressure:

$$r_o = k\, pA \quad (2)$$

where k is the reaction rate coefficient and P_A the cumene partial pressure. Figure 1 shows an example of this relationship at 430° C.

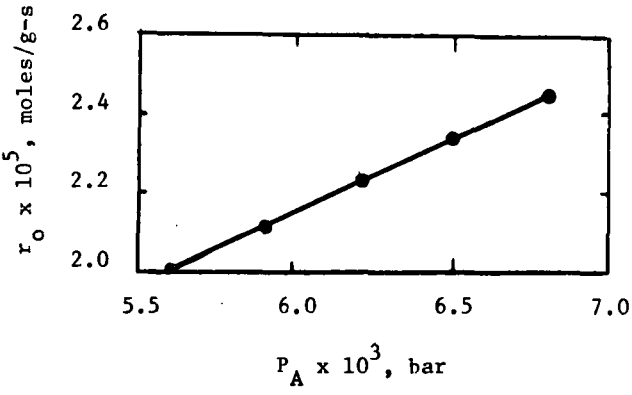

Fig. 1. Cumene cracking rate with uncoked catalyst vs. cumene partial pressure. 430°

Then the relative catalyst activity (ø) was calculated from:

$$ø = r/r_o \quad (3)$$

Figure 2 illustrates the effect of total coke (q) on catalyst activity.

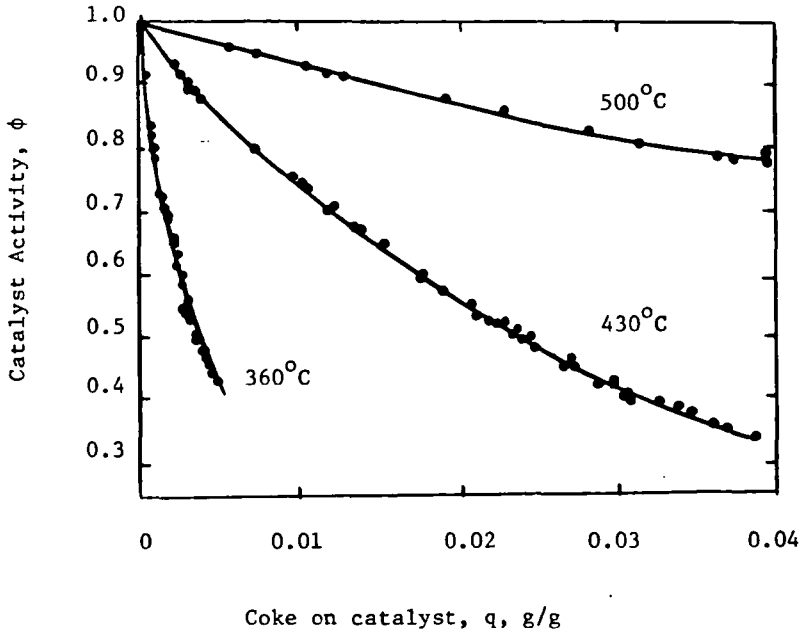

Fig. 2. Relative catalyst activity vs. total coke on catalyst. Cumene cracking over LaY

In describing deactivation processes due to coking, it is common to assume two independent reactions occur, the primary reaction and the coke formation reaction [4]. Following Nam and Kittrell's deactivation model [4] with cumene cracking kinetics [1-2], the following individual steps may be written:

$$A + 1 = A1 \tag{4}$$

$$A1 = R1 + S \tag{5}$$

$$R1 = R + 1 \tag{6}$$

$$R1 \rightarrow \text{coke} \tag{7}$$

In eq 4-7, A, R and S represent gaseous cumene, propylene and benzene respectively, 1 represents an active site and A1 and R1 represent adsorbed A and R. The total number of active sites is the sum of the vacant sites, the sites covered by adsorbed A or R and the sites inactivated due to coke coverage:

$$L_c = C_v + C_{A1} + C_{R1} + C_{c1} \tag{8}$$

the relative activity is defined by the fraction of sites not inactivated by coke:

$$\phi = \frac{L_c - C_{cl}}{L_c} \tag{9}$$

The rate of coke formation on the active surface is assumed to be proportional to the surface concentration of the coke precursor.

$$\frac{\delta C_c}{\delta t} = \frac{k_D C_{Rl}}{\rho_c} = \frac{k_D K_R p_R C_v}{\rho_c} \tag{10}$$

The parameter ρ_c is used to represent the stoichrometric coefficient to convert the weight of coke on the surface to the number of sites deactivated, $C_{cl} = \rho_c C_c$, k_D is the surface coke rate coefficient, K_R propylene adsorption coefficient, P_R the propylene partial pressure, and t time. By substitution of eq 8 and 9 into 10:

$$\frac{\delta C_c}{\delta t} = \frac{k_D K_R p_R \phi L_c}{\rho_c (1 + K_A p_A + K_R p_R)} \simeq \frac{k_D K_R p_R \phi L_c}{\rho_c} \tag{11}$$

K_A and p_A are the cumene adsorption coefficient and partial pressure respectively. It must be noted that C_c is the coke in direct proximity to the catalyst surface. The balance of the total measured coke is described as multilayer coke. It can be envisioned as growing on top of the monolayer coke by an Eley-Rideal mechanism. The multilayer coke (C_L) forms as:

$$\frac{\delta C_L}{\delta t} = k_L C_c p_R \tag{12}$$

where k_L is the multilayer coke rate coefficient.

The total measured coke content of the catalyst becomes

$$q = C_c + C_L \tag{13}$$

and

$$\frac{\delta q}{\delta t} = \frac{k_D K_R p_R \phi L_c}{\rho_c} + \frac{k_L L_c (1-\phi) p_R}{\rho_c} \tag{14}$$

Eq 9 can be differentiated and combined with eq 11 to yield

$$\frac{\delta \phi}{\delta t} = -k_D K_R p_R \phi \tag{15}$$

Dividing eq 15 by 14 yields the relationship between catalyst activity and total coke

$$\frac{\delta\phi}{\delta q} = \frac{-\rho_c k_D K_R \phi}{k_D K_R \phi L_c + k_L L_c (1-\phi)} \tag{16}$$

Eq 16 can be integrated to yield

$$\frac{q}{1-\phi} = \frac{L_c}{\rho_c} - \alpha - \alpha \frac{\ln\phi}{1-\phi} \tag{17}$$

where

$$\alpha = \frac{k_L L_c}{\rho_c k_D K_R} \tag{18}$$

Total coke versus catalyst activity data from cumene cracking in the thermobalance reactor are plotted in the form of eq 17 in Fig. 3. Note that α should exhibit an Arrhenius temperature dependence. This effect is shown in Fig. 4.

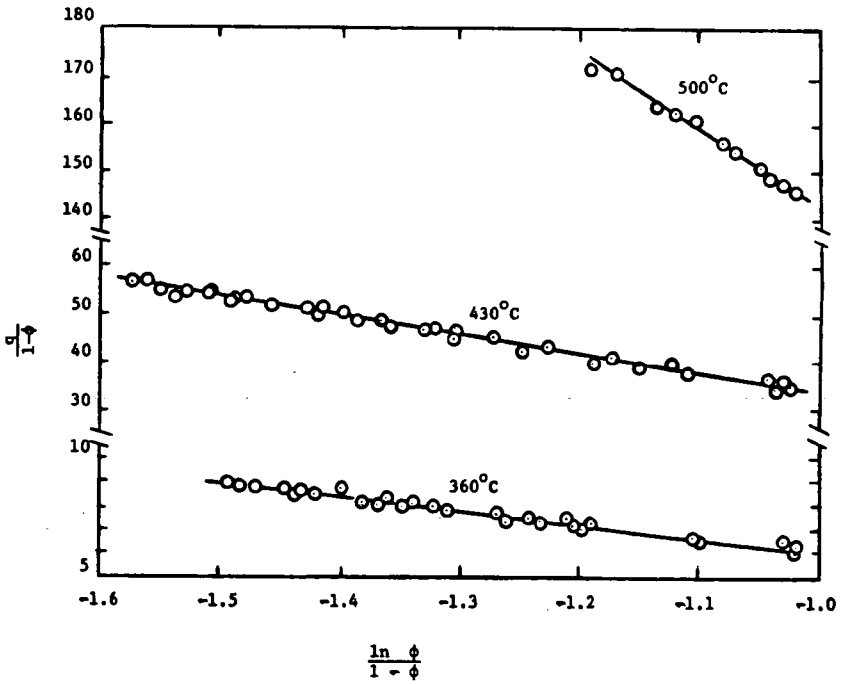

Fig. 3. Test of multilayer coke model. Plot of data in form of eq 17.

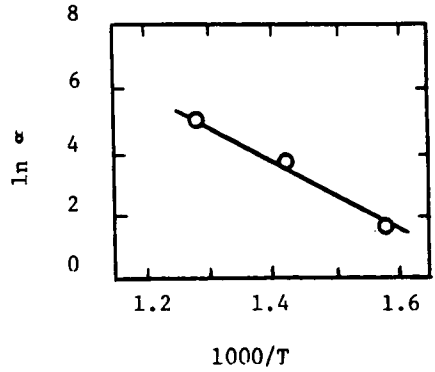

Fig. 4. Arrhenius dependence of α. Multilayer coke model.

Results of the pyridine titration study is shown in Fig. 5.

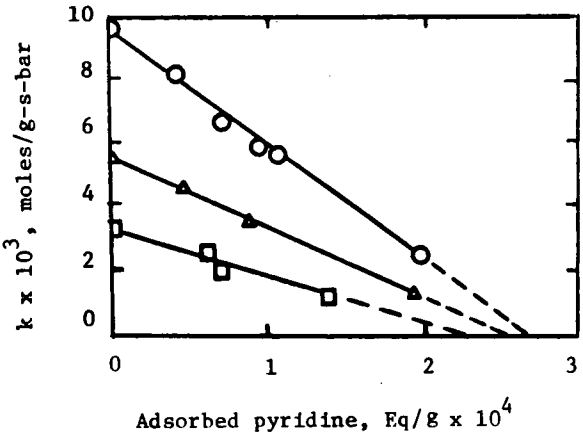

Fig. 5. Pyridine loading on La-Y . Effect on cumene cracking rate coefficient. Key: o 300°C, Δ 250°, □200°.

Zeolitic diffusivity was calculated from measurements of the variance and mean of experimental chromatographic curves. Shah and Ruthven [7] modified equations for the variance and mean for the situation in which Reynolds number is low, macrotransport is predominately by molecular diffusion, and the sorption equilibrium constant is greater than one. The modified equations yield:

$$\frac{\sigma^2}{2\mu^2}\left(\frac{L}{U}\right) = \frac{D_L}{U^2} + \left(\frac{\varepsilon}{1-\varepsilon}\right)\left(\frac{1}{3} + \frac{t}{15\theta}\right)\frac{R_p^2}{D_m} + \frac{\varepsilon}{1-\varepsilon}\,\frac{r_c^2}{15K_pD_c} \qquad (19)$$

The terms on the left hand side are σ^2 the variance and μ the mean of the chromatographic curve, L the bed length and U the interstitial velocity. The terms on the right hand side represent the respective contributions of axial diffusion, film-plus-macropore resistance, and zeolitic diffusion resistance. The axial dispersion coefficient (D_L), molecular diffusivity (D_m), and tortuosity factor (t) can be estimated [7]. Therefore, the axial dispersion resistance can be calculated. Parameter ϵ is the bed porosity, θ the pellet porosity, R_p the pellet radius, r_c the zeolite crystal radius, D_c the zeolitic diffusivity and K_p the hydrocarbon sorption equilibrium constant. Since the left hand side of eq 19 can be calculated from experimentally measured quantities, the resistance due to zeolitic diffusion can be calculated by difference. A comparison of resistances for benzene diffusion in LaY with and without 5 percent coke at 30°C shown in Table 1.

Table 1

Comparison of Resistances for Benzene Diffusion in LaY

$\frac{\sigma^2}{2\mu^2}(\frac{L}{U})\times 10^3$, s	$\frac{D_L}{U^2}\times 10^3$, s	$(\frac{\epsilon}{1-\epsilon})(\frac{1}{3}+\frac{t}{15\theta})\frac{R_p^2}{D_m}\times 10^3$, s	$\frac{D_c}{r_c^2}$, s^{-1}
Coked Catalyst			
53.79	36.47	0.44	2.15
41.10	21.30	0.44	1.84
33.94	13.87	0.44	1.82
31.95	8.77	0.44	1.57
17.45	5.87	0.44	3.20
18.19	3.97	0.44	2.59
		Average =	2.2
Uncoked Catalyst			
42.69	25.92	0.44	1.80
23.29	10.33	0.44	2.35
20.93	5.90	0.44	2.02
18.12	3.20	0.44	2.03
14.35	2.03	0.44	2.48
		Average =	2.2

DISCUSSION

The kinetics of cumene cracking over LaY, as measured in the thermobalance reactor, can be modeled by a mechanism based on the formation of both monolayer and multilayer coke. At the low cumene partial pressures employed, the reaction rate with fresh catalyst (no coke on the catalyst) is directly proportional to the cumene partial pressure as shown in Fig 1 and the

slope of this plot yields an intrinsic reaction rate coefficient. Then the relative catalyst activity can be determined experimentally by the ratio of the reaction rate at any coke level to the reaction rate with fresh catalyst. The relative catalyst activity has an exponential relationship with the total coke on the catalyst as shown in Fig 2. The effect of coke level decreases with increasing temperature. The experimental data are well represented by the multilayer coke model as illustrated by Fig 3. The slopes of the lines give values of α at each temperature. The parameter α has an Arrhenius temperature dependence:

$$\ln \alpha = \ln \frac{A_L L_C}{\rho_C A_D A_R} - \frac{E_L - E_D + \Delta H_R}{RT} \qquad (20)$$

The parameters A_L, A_D and A_R are the frequency factors for the multilayer coke reaction, surface coke reaction and adsorption of R respectively, E_L and E_D the activation energies for the multilayer coke and surface coke formation, ΔH_R the heat of adsorption of propylene, R the gas constant and T absolute temperature.

The slope of the line in Fig 4 yields a value of 92.5 KJ/mole. This suggests that the activation energy of the multilayer or polymerization coking reaction is greater than the monolayer coke formation. Apparently more of the total coke is in the multilayer form at higher temperatures.

The effect of pyridine poisoning on cumene cracking activity is shown in Fig 5. This linear relationship suggests uniform catalytic site strength. The total number of active sites estimated by extrapolation to zero activity is approximately 1.5×10^{20} sites/g.

The zeolitic diffusivities, as measured by the gas chromatographic technique, indicated no significant difference in the values for fresh LaY and LaY with 5 percent coke. The calculated values of diffusivity included a large degree of error because axial dispersion accounted for much of the variance in the residence time distribution curves, and the calculation method involved taking the difference of two large numbers. Nevertheless, the actual residence time distribution curves were essentially identical for coked and fresh catalyst. Therefore, coke appeared to have little effect on the diffusivity. The fact that coke has little effect could be reasonable if coking occurred uniformly throughout the zeolite because the three dimensional nature of the supercages and the large number of windows into the interconnected supercages would minimize pore plugging possibilities.

REFERENCES

1. Lin, C.C., Park, S.W., Hatcher, W.J., Ind. Eng. Chem. Process Des. Dev. 22, 609 (1983).
2. Lin, C.C., Hatcher, W.J., ACS Symp. Ser. 196, 249 (1982).
3. Beeckman, J.W., Froment, G.F., Ind. Eng. Chem. Process Des. Dev. 15, 291 (1976).
4. Nam, I.S., Kittrell, J.R., Ind. Eng. Chem. Process Des. Dev. 23, 237 (1984).
5. Mills, G.A., Boedeker, E.R., Oblad, A.G., J. Amer. Chem. Soc. 72, 1554 (1950).
6. Goldstein, M.S., Morgan, T.R., J. Catal. 16, 232 (1970).
7. Shah, D.B., Ruthven, D.M., AICHE J. 23, 804 (1977).

ACKNOWLEDGMENT

The author gratefully acknowledges the contributions of S.W. Park, C.C. Lin and J.W. Potter in obtaining the experimental data.

AUTHOR INDEX

Information for Contributors

1. Manuscripts should be submitted to Prof. Pál Fejes, Institute of Applied Chemistry, József Attila University, Szeged, Rerrich tér 1, Hungary, H-6720.
2. The manuscripts must not exceed in any case 32 pages (Figures, legends, Tables and Summary included). Manuscripts should be submitted in duplicate.
3. The format of the text: A/4, double spaced, 25 lines per page and 50 characters per line. Title: all capital characters; underlined twice. Subtitle(s) should be written in new line(s) in normal writing, underlined also twice, first characters: capital. (See the following example).

STEREOCHEMICAL STUDIES

Studies on Cyclic-2-Hydroxycarboxylic Acids

By

PÁL KISS

Research Institute for Industrial Chemistry, Budapest
(Received.....)

4. After these comes the summary, which is followed by the text proper. If the parts of the paper are separated by secondary titles like: Introduction. Experimental etc., the following rule holds: secondary titles of equal rank are to be written in new lines, the first word with capital letter, otherwise running text underlined once.
   Example:
   Introduction
   Experimental part
5. The names of the authors in the running text are written in capital letters. Exceptions are the names in connection with scientific instruments, etc. where only the first letter should be capital.
6. Citations in the text with reference to selected literature at the end of the paper are to be made with squared brackets, like: [5], [4, 9], [4—9].
7. To make printing easier, mathematical formulas are to be simplified as much as possible. Reference to mathematical equations is made by numbers in parenthesis, like: (16).
8. Tables should be typed on separate pages. Please supply numbers and titles for all tables (Numbering occurs with Roman numerals: Table I).
   Throughout the whole text the IUPAC nomenclature should be used.
   Insert of Tables in the text will be indicated at the appropriate place of the margin, like this: Table I.
9. Figures must be drawn clearly with Chinese ink on oily drawing paper, the thickness of lines as well as size of letters and symbols should be selected with care, the minimum size is nearly 0.3 cm.
   The maximum width of Figures is 24 cm, however, Figures of width equal or less than 12 cm are preferred.
   Please, use upwright on the Figures.
   In the case of real numbers points are used instead of commas.
   The place of Figures in the text is indicated on the margin like this: Figure 13.
   Please supply legends for all figures and compile these on separate sheets. Indicate only the number of the Figures in the original drawing, for this purpose use blue pencil.
10. Literature will be given under the heading References, like this: (on a separate sheet at the end of the manuscript).
    [1] Allinger, N. L., M. T. Tribble: J. Phys. Chem. 33, 1565 (1976).
    [2] Abraham, J. K., H. S. Hoover: Principles of Competitive Oxidation. Mc Graw-Hill, New York, 1977, p. 133.

A kiadásért felelős: Dr. Bartók Mihály
1985
A kézirat nyomdába érkezett 1985. márc. 15. Megjelenés 1985. május
Példányszám: 800. Ábrák száma: 246. Terjedelem: 22 (A/5) ív
Petőfi Nyomda, Kecskemét — F.v.: Ablaka István igazgató